NUREG/IA-0211
IRSN 2005-194
NSI RRC KI 3188

International Agreement Report

Experimental Study of Embrittlement of Zr-1%Nb VVER Cladding under LOCA-Relevant Conditions

Prepared by
L. Yegorova, K. Lioutov, N. Jouravkova, A. Konobeev
Nuclear Safety Institute of Russian Research Centre "Kurchatov Institute"
Kurchatov Square 1, Moscow 123182, Russian Federation

V. Smirnov, V. Chesanov, A. Goryachev
State Research Centre "Research Institute of Atomic Reactors"
Dimitrovgrad 433510, Russian Federation

Office of Nuclear Regulatory Research
U.S. Nuclear Regulatory Commission
Washington, DC 20555-0001

March 2005

Prepared for
U.S. Nuclear Regulatory Commission (United States),
Institute for Radiological Protection and Nuclear Safety (France),
and Joint Stock Company "TVEL" (Russian Federation)

Published by
U.S. Nuclear Regulatory Commission

AVAILABILITY OF REFERENCE MATERIALS IN NRC PUBLICATIONS

NRC Reference Material

As of November 1999, you may electronically access NUREG-series publications and other NRC records at NRC's Public Electronic Reading Room at http://www.nrc.gov/reading-rm.html. Publicly released records include, to name a few, NUREG-series publications; *Federal Register* notices; applicant, licensee, and vendor documents and correspondence; NRC correspondence and internal memoranda; bulletins and information notices; inspection and investigative reports; licensee event reports; and Commission papers and their attachments.

NRC publications in the NUREG series, NRC regulations, and *Title 10, Energy*, in the Code of *Federal Regulations* may also be purchased from one of these two sources.

1. The Superintendent of Documents
   U.S. Government Printing Office
   Mail Stop SSOP
   Washington, DC 20402–0001
   Internet: bookstore.gpo.gov
   Telephone: 202-512-1800
   Fax: 202-512-2250
2. The National Technical Information Service
   Springfield, VA 22161–0002
   www.ntis.gov
   1–800–553–6847 or, locally, 703–605–6000

A single copy of each NRC draft report for comment is available free, to the extent of supply, upon written request as follows:

Address: Office of the Chief Information Officer,
Reproduction and Distribution
Services Section
U.S. Nuclear Regulatory Commission
Washington, DC 20555-0001
E-mail: DISTRIBUTION@nrc.gov
Facsimile: 301–415–2289

Some publications in the NUREG series that are posted at NRC's Web site address http://www.nrc.gov/reading-rm/doc-collections/nuregs are updated periodically and may differ from the last printed version. Although references to material found on a Web site bear the date the material was accessed, the material available on the date cited may subsequently be removed from the site.

Non-NRC Reference Material

Documents available from public and special technical libraries include all open literature items, such as books, journal articles, and transactions, *Federal Register* notices, Federal and State legislation, and congressional reports. Such documents as theses, dissertations, foreign reports and translations, and non-NRC conference proceedings may be purchased from their sponsoring organization.

Copies of industry codes and standards used in a substantive manner in the NRC regulatory process are maintained at—

The NRC Technical Library
Two White Flint North
11545 Rockville Pike
Rockville, MD 20852–2738

These standards are available in the library for reference use by the public. Codes and standards are usually copyrighted and may be purchased from the originating organization or, if they are American National Standards, from—

American National Standards Institute
11 West 42nd Street
New York, NY 10036–8002
www.ansi.org
212–642–4900

Legally binding regulatory requirements are stated only in laws; NRC regulations; licenses, including technical specifications; or orders, not in NUREG-series publications. The views expressed in contractor-prepared publications in this series are not necessarily those of the NRC.

The NUREG series comprises (1) technical and administrative reports and books prepared by the staff (NUREG–XXXX) or agency contractors (NUREG/CR–XXXX), (2) proceedings of conferences (NUREG/CP–XXXX), (3) reports resulting from international agreements (NUREG/IA–XXXX), (4) brochures (NUREG/BR–XXXX), and (5) compilations of legal decisions and orders of the Commission and Atomic and Safety Licensing Boards and of Directors' decisions under Section 2.206 of NRC's regulations (NUREG–0750).

NUREG/IA-0211
IRSN 2005-194
NSI RRC KI 3188

International Agreement Report

Experimental Study of Embrittlement of Zr-1%Nb VVER Cladding under LOCA-Relevant Conditions

Prepared by
L. Yegorova, K. Lioutov, N. Jouravkova, A. Konobeev
Nuclear Safety Institute of Russian Research Centre "Kurchatov Institute"
Kurchatov Square 1, Moscow 123182, Russian Federation

V. Smirnov, V. Chesanov, A. Goryachev
State Research Centre "Research Institute of Atomic Reactors"
Dimitrovgrad 433510, Russian Federation

Office of Nuclear Regulatory Research
U.S. Nuclear Regulatory Commission
Washington, DC 20555-0001

March 2005

Prepared for
U.S. Nuclear Regulatory Commission (United States),
Institute for Radiological Protection and Nuclear Safety (France),
and Joint Stock Company "TVEL" (Russian Federation)

Published by
U.S. Nuclear Regulatory Commission

ABSTRACT

During 2001-2004, research was performed to develop test data on the embrittlement of niobium-bearing (Zr-1%Nb) cladding of the VVER type under loss-of-coolant accident (LOCA) conditions. Procedures were developed and validated to determine the zero ductility threshold. Pre-test and post-test examinations included weight gain and hydrogen content measurements, preparation of metallographic samples, and examination of samples using optical microscopy, scanning electron microscopy and transmission electron microscopy. Sensitivity of the zero ductility threshold to heating and cooling rates was determined. Oxidation kinetics and ductility threshold were measured for the standard E110 alloy, six variants with different impurities, Zircaloy, and irradiated E110. Oxidation temperatures were varied from 800-1200 C, and mechanical (ring compression) testing temperatures were varied from 20-300 C. It was concluded that (a) the current type of E110 cladding has an optimal microstructure, (b) oxidation and ductility of the oxidized cladding are very sensitive to microchemical composition and surface finish, (c) the use of sponge zirconium for fabrication of cladding tubes provides a significant reduction of the oxidation rate and an increase in the zero ductility threshold, and (d) additional improvement in oxidation and ductility can be achieved by polishing the cladding surface.

FOREWORD

A world-wide trend to substantially increase nuclear fuel burnup to higher levels has led fuel manufacturers in the U.S. and France to develop niobium-bearing cladding alloys that are similar in composition to Russian cladding alloys. These alloys, E-110, E-635, ZIRLO, and M5, all have greatly improved corrosion resistance compared with Zircaloy during normal operation, especially at higher burnup levels. However, in early 2001, it was realized that the Russian alloys and the Western niobium-bearing alloys behaved somewhat differently under conditions of a loss-of-coolant accident (LOCA), during which the cladding is exposed to steam at high temperatures.

At that time, a research program was already underway at Argonne National Laboratory in the U.S. to investigate the effects of high-burnup on cladding behavior under LOCA conditions. Further, a cooperative research effort on fuel behavior was also underway at the Russian Research Center (Kurchatov Institute) with partial sponsorship by the French Institute for Radiological Protection and Nuclear Safety and the U.S. Nuclear Regulatory Commission; additional funding was being provided by the Russian fuel vendor, TVEL. It was then decided to investigate the underlying phenomena that governed cladding behavior of niobium-bearing alloys — particularly the Russian cladding — in this Russian program. By closely coordinating this research with the work underway at Argonne National Laboratory on similar Western alloys, it was hoped that a fuller understanding could be obtained. Coordination between laboratories was further enhanced by including some Zircaloy cladding specimens in the Russian program and including some E110 cladding specimens in the program at Argonne National Laboratory.

After several years of research at both laboratories, the general cause of differences in behavior under LOCA conditions has been isolated to the ore reduction process and the surface finish of the cladding tubing. This understanding is helping to improve licensing criteria that can be applied to new and different cladding alloys. The extensive work performed by the Russian Research Center (Kurchatov Institute) and their collaborating laboratory at the State Research Center (Research Institute of Atomic Reactors) is documented in the following report.

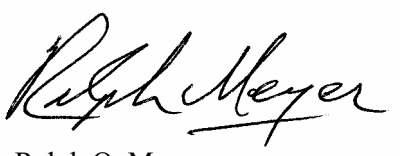

Ralph O. Meyer
Senior Technical Advisor
Office of Nuclear Regulatory Research
U.S. Nuclear Regulatory Commission

Carl J. Paperiello
Director
Office of Nuclear Regulatory Research
U.S. Nuclear Regulatory Commission

TABLE OF CONTENTS

LIST OF FIGURES

LIST OF TABLES

LIST OF APPENDICES

ACKNOWLEDGEMENTS

The authors of the report are pleased to acknowledge that this research program was initiated and implemented with the intellectual support of the following key persons from the sponsoring organizations: P. Lavrenyuk (Joint Stock Company "TVEL", Russia), V. Asmolov (Russian Research Centre "Kurchatov Institute", Russia), R.O. Meyer (U.S. Nuclear Regulatory Commission, USA), J. Papin and G. Hache (Institute for Radiological Protection and Nuclear Safety, France).

We express our profound appreciation to these persons as due to their efforts the motivated balance was achieved between the investigations performed in width and in depth.

The major goal of this research was to understand the effect of niobium on the embrittlement of zirconium-based alloys and in particular the unique embrittlement behavior of the E110 alloy under LOCA conditions. Achievement of this goal would have been impossible without the appropriate test data base developed in the investigations performed by the following specialists:

- Kosvintsev Yu.Yu., Leshchenko A.Yu. (State Research Centre "Research Institute of Atomic Reactors", Russia): development of the oxidation facility and of special computer system for the test data measurement and processing;
- Prokhorov V.I., Makarov O.Yu. (State Research Centre "Research Institute of Atomic Reactors", Russia): performance of mechanical tests of oxidized claddings;
- Shishalova G.V. (State Research Centre "Research Institute of Atomic Reactors", Russia): hydrogen content measurements;
- Stupina L.N., Svyatkin A.M., Zvir E.A., Ivanova I.A. (State Research Centre "Research Institute of Atomic Reactors", Russia): metallographic examinations and computer processing of the cladding images;
- Novoselov A.E., Shishin V.Yu., Ostrovskiy Z.E., Yakovlev V.V., Kuzmin S.V., Obukhov A.V. (State Research Centre "Research Institute of Atomic Reactors", Russia): SEM and TEM examinations of the cladding material;
- Panchenko V.L., Averin S.A. (Institute of Reactor Materials, Russia): TEM examinations of the cladding microstructure;
- Pylev S.S., Shestopalov A.A., Abyshov G.N. (Russia Research Centre "Kurchatov Institute", Russia): analytical and calculation investigations, development of the computer data base;
- Kaplar Ye.P. (Russian Resarch Centre "Kurchatov Institute", Russia): development of the program principles and the preliminary analysis of test results during the research first stage.

The authors express their sincere gratitude to all these specialists for their outstanding contribution into this work. Besides, the authors thank individually the above listed specialists for the permission to use the results of their special investigations in this report.

Many scientific and practical aspects of this work were clarified by discussions and the exchange of views with several experts involved in this problem. In this connection, we would like to express our profound appreciation to the following experts:

- Pimenov Yu.V. (Joint Stock Company "TVEL", Russia);
- Bibilashvili Yu.K., Nikulina A.V., Novikov V.V. (All-Russian Institute of Inorganic Materials – VNIINM – Russia);
- Billone M., Chung H. (Argonne National Laboratory, USA).

1. INTRODUCTION

To study the oxidation behavior and embrittlement threshold of Zr-1%Nb cladding under loss-of-coolant accident (LOCA) conditions, a research program was developed and implemented by the Russian Research Center "Kurchatov Institute" (RRC KI) in cooperation with the Research Institute of Atomic Reactors (RIAR). The program was performed during the period of 2001–2004 and sponsored by (a) Joint Stock Company "TVEL" (JSC "TVEL", Russia), (b) U.S. Nuclear Regulatory Commission (U.S. NRC, USA), and (c) Institute for the Radiological Protection and Nuclear Safety (IRSN, France).

The incentive to begin this work was directly related the increase of fuel burnup in light-water reactors (LWRs) to 60–70 MW d/kg U and higher. Substantial corrosion is experienced with Zircaloy claddings at fuel burnup higher than 50 MW d/kg U, whereas much less corrosion occurs with Zr-1%Nb cladding during the commercial operation in the Russian type of pressurized-water reactors (VVERs) and with niobium-bearing claddings manufactured from the M5 and Zirlo alloys after operations in the pressurized-water reactors (PWRs). Experimental studies performed with the VVER type of Zr-1%Nb claddings refabricated from commercial fuel rods with burnup up to 60 MW d/kg U have shown that this cladding has a high safety margin under reactivity-initiated accident (RIA) conditions. But the preliminary consideration of safety aspects associated with niobium-bearing claddings under LOCA conditions raised the following issues:

- several investigations performed with Zr-1%Nb cladding of the VVER type in different countries in the 1990s have shown that the niobium-bearing cladding has somewhat different oxidation and embrittlement behavior in comparison with the zircaloy cladding;
- the same general requirements concerning the prevention of the embrittled cladding fragmentation are applied in the LOCA safety analysis of the VVER and PWR reactors, but different approaches are used for this goal.

Taking into account these and other issues, it was decided to perform a special research program including the following main parts of investigations:

- the reassessment of published data concerning the PWR and VVER cladding embrittlement under LOCA conditions;
- the development and validation of test apparatus and test procedures;
- the performance of sensitivity studies and the determination of key factors which must be studied during this program;
- the performance of oxidation, mechanical tests and different pre-test and post-test examinations;
- the analysis and interpretation of obtained results.

The major focus of investigations performed in the frame of this work was concentrated on the characterization of Zr-1%Nb (E110) oxidation and mechanical behavior as a function of such parameters as:

- oxidation conditions (single-sided or double-sided, heating and cooling rates, oxidation temperatures from 800–1200 C, and weight gain);
- mechanical test conditions (ring tensile tests, ring compression tests, three-point bending tests) and test temperature (20–300 C);
- cladding irradiation (as-received and refabricated claddings from the commercial fuel rods with the burnup about 50 MW d/kg U);
- cladding surface conditions (as-received tubes, as-received claddings, polished as-received tubes, ground as-received tubes);
- impurity compositions in the cladding.

In addition to oxidation and mechanical tests with Zr-1%Nb (E110) cladding, several reference tests were performed with the Zircaloy-4 (zirconium-tin) and E635 (zirconium-niobium-tin) claddings. The research program results are presented in this report.

2. BACKGROUND

The prevention of cladding fragmentation in LWR-type reactors under the LOCA conditions is one of the basic principles of the current safety philosophy. The reason for this is related to the following physical phenomena:

- significant increase of the cladding temperature during the LOCA accident caused by the coolant blowdown and degradation of heat transfer;
- high temperature cladding steam oxidation accompanied by cladding embrittlement;
- possible fracture of the embrittled cladding caused by post-LOCA forces during quenching and post-quenching actions.

In accordance with the current world practice, the prevention of the cladding fragmentation under LOCA conditions is assured by special safety criteria. Thus, the main Russian regulatory document contains two special requirements concerning this problem: for the Zr-1%Nb (E110) cladding [1]:

- the peak cladding temperature (PCT) must not exceed 1200 C;
- the local oxidation depth (Equivalent Cladding Reacted layer, ECR) must not exceed 18% of the initial wall thickness.

Similar criteria are contained in the regulatory documents of other countries for the zircaloy cladding (1200 C, 15–17% ECR). It should be noted that the concept for the use of fragmentation criteria of these types was developed by the NRC (USA) with respect to the zircaloy claddings [2]. The motivation for the choice of this approach for the safety fragmentation criteria was reconstructed in the recent paper prepared by H.Chung and G.Hache [3].

The first research to determine the zero ductility threshold of oxidized Zry-4 claddings after the quench cooling was performed by D.O. Hobson at the beginning of 1970s [4, 5]. In accordance with results of a slow compression of Zry-4 oxidized samples, he revealed the relationship between the critical relative thickness of the prior β-phase and zero ductility threshold at 135 C (the saturation temperature during the reflood stage). This relationship was used to develop the following embrittlement criterion [6]:

$$\frac{\xi_T}{W_o} \le 0.44 ,$$

where ξ_T – the thickness of the oxygen-rich cladding layers (ZrO_2 and α-ZrO);

W_o – the initial thickness of the unoxidized cladding.

Further, it was revealed that the cladding ductility margin at low temperatures (150 C or less) was a function of not only the prior β-phase thickness but also of the oxygen concentration in this layer. The appropriate analysis of Hobson's test has shown that:

- the maximum oxygen concentration in the prior β-phase is a function of the oxygen solubility in the β-phase under high temperature oxidation conditions;
- the zero ductility threshold (at 20 - 150 C) is associated with 0.7% (by weight) oxygen concentration in the prior β-phase. This critical oxygen concentration is achieved very fast if the oxidation temperature is higher than 1204 C (2200 F).

Taking into account these test results, the embrittlement criterion was added with the Peak Cladding Temperature (PCT) criterion. The PCT criterion was estimated as 1204 C [6].

The final evolution of these criteria involved the following:

- the extension of the test data base needed to validate criteria [7, 8, 9];
- the introduction of the reasonable conservative principle into the safety analysis procedure.

As for the conservatism, it was decided to organize the results of different tests into the unified system using the Baker–Just equation allowing to calculate the Zry-4 high temperature kinetics with the conservative margin [10]. This equation was used to determine the oxygen weight uptake with each tested sample. Besides, to

improve the physical interpretation of calculated results, the concept of the Equivalent Cladding Reacted (ECR) layer was introduced:

$$ECR = \frac{\delta_e}{\delta_o},$$

where δ_l – oxidation equivalent layer determined using the following condition: the all uptaken oxygen are used for the formation of the stoichiometric zirconium dioxide (ZrO_2);

δ_o – the initial cladding thickness.

The practical implementation of this approach allowed the development of a test data base with the following list of test parameters:

- ECR calculated with the Baker–Just;
- oxidation time and temperature;
- tested cladding sample characterization: intact, failed.

The analysis of this data base presented in Reference 3 shows that:

- at an oxidation temperature less than 1204 C, the brittle fracture of oxidized claddings was not observed under ring compression test conditions (at 135 C and higher) if the ECR calculated with the Baker–Just correlation was less than 17%;
- at an oxidation temperature less than 1600 C, the brittle fracture of oxidation claddings was not observed under thermal-shock during direct quenching conditions if the ECR calculated with the Baker–Just correlation was less than 19%.

Thus, the results of two different types of tests (the comparison of mechanical tests and thermal–shock tests) demonstrated the similarity in the evaluation of the critical oxidized thickness (17–19% ECR) although there was a significant discrepancy in the estimation of the permissible peak cladding temperature. These results led the experts responsible for the development of the proposal on safety criteria to the formulation of their position concerning the choice of the permissible peak temperature [11]. This position may be characterized by the following general provisions:

- the practical application of thermal–shock test results requires such a detailed knowledge of physical processes during the LOCA which cannot be provided;
- to prevent the fragmentation, the oxidized cladding must retain some margin of ductility;
- the choice of 1204 C (2200 F) PCT limit based on results of compression mechanical tests provides the conservative margin in comparison with the thermal–shock test results.

In 1973, this position was used to formulate the NRC criteria [2]: 1204 C, 17% ECR (calculated using the Baker–Just equation). During the period of 1974–1990, experimental investigations with zircaloy claddings were continued to understand the sensitivity of fragmentation threshold to such factors as:

- the cladding ballooning and burst;
- the mechanical interaction of the oxidized cladding in the fuel bundle caused by ballooning and bending;
- the axial mechanical constraint of ballooned cladding by the grid spacers.

A brief description of this cycle of Zry-4 investigations is presented in Table 2.1. The main outcomes of these investigations may be characterized in the following way:

1. The thermal–shock tests performed with the original geometry of the oxidized cladding (without axial constraint or ballooning and burst) or with the original geometry of fuel rod simulators have shown that the current safety criteria (1204 C, 17% ECR) have a margin of about 100% in ECR. The margin in PCT does not exceed 150 C.
2. Thermal–shock studies performed to check the constraining effect of the grids when using deformed cladding (ballooning and burst) have shown that the fragmentation threshold decreased significantly with axial constraint, but the test fragmentation threshold did not exceed the safety criteria.

3. Special impact tests performed with the simulation of potential impact fracture energy (estimated as 0.3 J) have shown that:

- the oxidized cladding with the original geometry had a high margin before fracture;
- the fragmentation threshold of the deformed cladding (after ballooning and burst) was in agreement with the safety criteria. Some claddings were fragmented at values lower than 17% (safety criterion), and the increase in hydrogen content in local parts of the oxidized claddings (local cladding hydriding) was the cause of this effect, but the peak cladding temperature was higher than 1204 C (safety criterion).

4. Additional studies of the hydriding effect performed with compression tests demonstrated that the zero ductility threshold of hydrided cladding corresponded to 700 ppm of hydrogen in the prior β-phase.
5. The axial tensile and ring compression tests confirmed that the zero ductility threshold was reached when the average oxygen concentration in the prior β-phase increased from 0.6% by weight up to 0.8% by weight.

Taking into account results of all these tests and understanding of the fact that the ductility margin of the oxidized cladding is a function of oxygen and hydrogen concentration in the prior β phase, several investigators proposed to change the current safety criteria (1204 C, 17% ECR) into criteria based on the oxygen and hydrogen concentrations in the oxidized claddings. But these suggestions were not apparently implemented due to the fact that:

- the introduction of these criteria must be accompanied by the use of computer codes for the safety analysis which are able to calculate the appropriate parameters with the required accuracy;
- numerous additional experimental programs would be needed to develop and validate the integral criterion based on the oxygen and hydrogen content in the prior β-phase of the oxidized cladding.

In accordance with these considerations, improvement of the safety criteria was postponed for the time being.

Table 2.1. The list of major investigations performed during 1974–1990 to study the fragmentation threshold of unirradiated Zircaloy claddings

Test type	Test characterization	Test results
1. Thermal shock tests performed by H.Chung and T.Kassner, USA, 1980 [12]	The double-sided oxidation of Zry-4 claddings at 1000–1500 C with slow cooling though phase transition followed by quench type cooling	The cladding fragmentation threshold was 28% ECR (measured) at 1500 C and 33% ECR at 1200 C
2. Thermal shock tests performed by H.Uetsuka et. al., Japan, 1983 [13]	The double-sided oxidation of Zry-4 claddings at 950–1350 C with the quench cooling	The cladding fragmentation was not noted in this temperature range at 17% ECR (as-calculated using Baker-Just correlation)
		The cladding fragmentation threshold was higher than 35% ECR (as-calculated using Baker-Just correlation) at 1200 C
3. Thermal shock tests with the cladding axial mechanical constrain performed by H.Uetsuka et. al., Japan, 1983 [13]	The double-sided oxidation of Zry-4 cladding with the strong fixation of one cladding end at 900–1300 C. The fixation of the second cladding end at the beginning of the quench cooling	The cladding fragmentation was not observed in this temperature range at 17% ECR (as-calculated using Baker-Just correlation)
		The cladding fragmentation threshold was 20% ECR (as-calculated using Baker-Just correlation) at 1200 C

Test type	Test characterization	Test results
4. The in-pile tests (PHEBUS research reactor) of the tests fuel bundle performed by M.Reocreux and E. Scott de Martinville, France, 1990 [14]	The LOCA-type test (#219) without the quench mode with Zry-4 claddings: the cladding ballooning and burst at high temperature, the cladding oxidation	The cladding fragmentation of one fuel rod occurred at the following parameters: • 16% ECR • 1330 C
		The reason of the fragmentation was assessed as the mechanical constrain of the temperature-induced cladding replacement
5. Impact tests of oxidized claddings of original geometry performed by H.Chung and T.Kassner, USA, 1980 [12]	The double-sided oxidation of Zry-4 claddings at 1100–1400 C and the cooling rate 5 C/s. The impact tests of oxidized claddings	The failure impact energy was higher than 0.8 J* [15], if the oxidation temperature did not exceed 1315 C and the ECR did not exceed 17% (as-measured using the metallographic method)
6. Impact tests of deformed (after the ballooning and burst) and oxidized claddings performed by H.Chung and T.Kassner, USA, 1980 [12]	Fuel rods with the Zry-4 cladding and fuel pellet simulators were pressurized at the high temperature up to the ballooning and burst. After that, fuel rods were oxidized (under isothermal conditions) and quenched. The impact tests of these fuel rods were performed at the fixed impact energy 0.3 J	A good correlation between the cladding fragmentation threshold and 17% ECR (as-measured with the use of metallographic method), 1204 C was observed for the most tested fuel rods.
		A special analysis has shown that: • some parts of the inner surface of deformed claddings are characterized by the formation of a thick spalled oxide • it is revealed that stagnant steam/water conditions are responsible for the initiation of the breakaway oxidation on these parts of the cladding • the high hydrogen uptake up to 2200 ppm was noted in these specific zones • it is observed that the cladding fragmentation threshold sharply decreases at the cladding hydrogen content 700 ppm and higher
7. The compression tests of oxidized and hydrating claddings performed by H.Chung and T.Kassner, USA, 1980 [12]	The mechanical compression tests were performed with fuel rods (Zry-4 cladding, fuel pellet simulators) after the pressurization of the fuel cladding up to the burst and high temperature oxidation	These scoping tests have shown that the residual ductility of the oxidized cladding is a strong function of oxygen and hydrogen content in the prior β-phase
8. The ring compression tests of deformed and oxidized claddings performed by H.Uetsuka et. al., Japan 1981–1982 [16, 17]	Zry-4 claddings were heated, pressurized up to the burst, oxidized and quenched. The compression tests were performed at 100 C with ring samples which were cut off from oxidized claddings	A strong correlation between the hydrogen content in the prior β-phase and cladding residual ductility was developed
		It was shown that the cladding was fully embrittled at 700 ppm of hydrogen content

* The expert estimations of possible loads in the commercial fuel bundle during late stages of LOCA have shown that the impact energy may achieve 0.3 J

Test type	Test characterization	Test results
9. The tensile mechanical tests of the oxidized performed by A.Sawatzky, UK, 1978 [18]	The Zircaloy claddings were oxidized in the water steam at 1000–1600 c. After that, the tensile tests were performed at room temperature. the test data base was added with the microhardness measurements across the cladding thickness	It was revealed that the oxygen in the prior β-phase was distributed nonuniformely
		It was shown that the oxidized cladding had some ductility margin if the average oxygen content in the prior β-phase did not exceed 0.6% by weight
		It was determined that the zero ductility threshold of the oxidized cladding corresponded to 0.8% averaged oxygen content (the appropriate ECR was 16%)
10. The in-pile tests of fuel rods performed in the PBF research reactor, USA, 1982 [19]	The single pressurized fuel rods with the Zry-4 cladding were oxidized at the temperature transient mode	Several fuel rods which failed after the tests at the post-test manipulations had the following parameters: • the fuel rod with the burst at 1100 C oxidized up to 12% ECR (as-measured) at the equivalent temperature 1262 C • three fuel rods oxidized at equivalent temperature 1300 C up to 5–11% ECR (as-measured) • fuel rods oxidized at equivalent temperature up to 7–8% ECR (as measured) were not fragmented

New attempts to resume this activity were made in the middle of 1990s in the context of the increase in fuel burnup up to 60 MW d/kg U and higher in the LWRs. An important aspect of this new stage of investigations was connected with the fact that zircaloy cladding has a tendency towards the breakaway oxidation and cladding hydriding at the high burnup (55 MW d/kg U and higher) under normal operation conditions. These effects result in a decrease of cladding ductility and lead to questions concerning the mechanical behavior of these claddings under accident conditions. The importance of this problem was shown practically in the experiments with the Zry-4 irradiated cladding under reactivity-initiated accident (RIA) conditions [20, 21, 22].

Taking into account the revealed problems, extended investigations were initiated to study the irradiation effects in zircaloy claddings under LOCA conditions [23, 24, 25, 26, 27]. The important direction of these investigations was connected with advanced cladding materials including the niobium-bearing alloys. In this context, it should be noted that a niobium-bearing alloy E110 (Zr-1%Nb) had been used as the VVER cladding material for several decades. Moreover, special investigations performed in 1990s showed that this alloy demonstrated a very high corrosion resistance under normal operation conditions up to 60 MW d/kg U [28].

Further, special investigations devoted to measurements of mechanical properties of E110 irradiated claddings under accident conditions [29, 30, 31, 32] and experimental studies of VVER high burnup fuel rods (50–60 MW d/kg U) under RIA conditions [30, 33, 34, 35] have demonstrated that fuel rods with the Zr-1%Nb (E110) cladding have good prospects in respect to the increase of the fuel burnup in VVERs. But it is obvious that the final analysis of this situation cannot be made without the consideration of experimental results characterizing the ductility margin of E110 claddings after the high temperature oxidation and quenching under LOCA-relevant conditions.

The official history of such investigations with the E110 alloy was initiated in Russia goes back to the beginning of the 1980s. Previous investigations used for the development of the second design limit of fuel rod damage (1200 C, 18% ECR) in the first national regulatory document on LWR safety issues [36] were not described in the open publications. The outline of main Russian research programs performed during the 1990s to develop an experimental data base characterizing the oxidation and mechanical behavior of the E110 cladding is presented in Table 2.2.

Table 2.2. Results of Russian investigations performed during 1980–2001 to study the oxidation and mechanical behavior of unirradiated Zr-1%Nb (E110) claddings

Test type	Test characterization	Test results
1. High temperature oxidation tests performed in VNIINM* and VTE** [37, 38, 39, 40]	The double-sided oxidation of E110 claddings at 700–1500 C under isothermal and transient conditions	The test data base needed to develop the E110 oxidation kinetics correlations was obtained
		The effect of ZrO_2 spallation was revealed in the temperature range 900–1100 C on achieving the critical oxide thickness (~25 μm)
		A significant change of the cladding geometrical sizes was revealed for some transient modes
2. Ring tensile tests of oxidized claddings performed in VNIINM, 1990 [41]	The double-sided oxidation of E110 claddings at 1000–1200 C with the direct current heating and fast air cooling. Ring tensile tests of oxidized samples at 20–1000 C	The zero ductility threshold was associated with the weight gain 450 mg/cm^2 (~6% as-measured ECR) at 20 C
		The reasonable margin of residual ductility in fully brittle samples was revealed at temperatures higher than 500 C
3. Impact tests of oxidized claddings performed in VNIINM, 1990 [41]	The double-sided oxidation of E110 claddings at 1000–1200 C with the direct current heating and cooling rate 10–20 C/s. The impact tests of oxidized claddings at 20 C	The brittle fracture occurred at the weight gain higher than 600 mg/dm^2 (7% ECR)
		The relationship between the failure specific impact energy of the unoxidized sample and brittle oxidized sample (500 mg/dm^2) was assessed as 100 J/cm^3 and 5 J/cm^2, respectively
4. Development of the E110 conservative oxidation kinetics performed in VNIINM, 1990 [42, 43]	The test data base obtained due to investigations stated in item 1 was used	The following correlation was developed: $\Delta m = 920 \exp\left(-\frac{10410}{T}\right)\cdot\sqrt{\tau}$, where Δm–oxygen weight gain (mg/dm^2) T–temperature (K) τ–time (s)
5. High temperature oxidation tests of deformed claddings performed in VNIINM and VTE, 1990–91 [42, 43]	The oxidation tests of pressurized (Ar) cladding samples at 700–850 C. The measurement of the cladding hoop strain in the ballooning area (the variation of the outer diameter relative increment was 0–85 % ($\Delta D/D_o$)	The systematic increase of the oxygen weight gain was observed as a function of $\Delta D/D_o$ increase. The dependence of the weight gain on the cladding surface in the ballooning area was estimated
6. Thermal shock tests of oxidized claddings performed in VNIINM and VTE, 1990–91 [42, 43, 44]	The double-sided oxidation of E110 claddings at 800–1200 C and water quench cooling	The fragmentation did not occur for all claddings with the ECR less than 18% (as-measured)
7. Ring compression tests performed in VNIINM and VTE, 1990 [42, 43]	The double-sided oxidation of E110 and Zry-4 (French and SANDVIK zircaloy) claddings at 800–1200 C and water quench cooling. (Reference tests with slowly cooled samples). Reference tests with the air oxidation of E110 claddings. Ring compression tests of 30 mm oxidized claddings at 20 C	Ring compression tests showed that: • a sharp decrease of the E110 ductility occurred after the achievement of some criterial ECR • this criterial ECR was a function of the oxidation temperature • the worst studied temperature was 1000 C • the best studied temperature was 800 C • the range of the E110 zero ductility threshold may be estimated as 3–4% (as-measured)

* All-Russian Research Institute of Inorganic Materials

** All-Russian Heat Engineering Institute

Test type	Test characterization	Test results
		• the Zry-4 oxidized cladding had the monotonic character of ductility reduction at the ECR increase. The zero ductility threshold of Zry-4 cladding was not higher than 15% ECR (as-measured)
		The visual observations of oxidized samples allowed to reveal that: • at ECRs close to the criterial value (3–4%) the white spalled oxide appeared on the E110 cladding surface • Zry-4 oxidized samples were covered with the black bright oxide
		The comparative analysis of results of hydrogen content measurements showed that E110 claddings unlike Zry-4 had the tendency towards the high hydrogen absorption at 1000–1100 C. Reference tests with air oxidation confirmed that the E110 residual ductility increased significantly in this case (without the cladding hydriding effect)
		The comparative data characterizing the sensitivity threshold to the cooling rate showed that this effect was insignificant
		The metallographic studies of the E110 oxidized cladding allowed to note that: • the following difference in the E110 and Zry-4 α-Zr(O) phase morphology was revealed: – the α-Zr(O) phase in the Zry-4 cladding consisted of equiaxed grains; – the α-Zr(O) phase in the E110 cladding consisted of thin plates • taking into account the difference in the phase transition temperatures for E110 and Zry-4 alloys, the E110 β-phase must dissolve more oxygen than the Zry-4 one to provide the α-Zr(O) phase initiation condition. This effect led to the difference in the α-Zr(O) thickness in E110 and Zry-4 claddings
8. Thermal shock tests of VVER fuel rod simulators performed in VNIINM and RIAR*, 1998–2001 [45, 46, 47, 48]	The oxidation of unpressurized fuel rod simulators with the E110 cladding at 900–1200 C, after that water quenching of oxidized simulators. Two types of simulators are used: • with Al_2O_3 fuel pellets and radiant heating of the fuel rod • with UO_2 fuel pellets and W-heaters installed inside the fuel stack One end of the fuel rod was open for the steam penetration	Both types of VVER fuel rod simulators were not fragmented during and after thermal shock tests in the following range of test parameters: • 900–1200 C • as-calculated ECR (using the E110 conservative correlation) less or equal to 18%
		The different margin for the safety fragmentation threshold (18% ECR) was demonstrated as a function of the oxidation temperature and simulator type

* State Research Center "Research Institute of Atomic Reactors"

Test type	Test characterization	Test results
9. Impact tests of oxidized VVER fuel rod simulators performed in VNIINM, 1998–2001 [45–48]	The E110 oxidized cladding after investigations performed as stated in the item 8 were tested in accordance with the following requirements	The reference tests with the unoxidized cladding shown that the impact-toughness fracture was of 64–89 J/cm^2
	• claddings removed from the first type of fuel rod simulators were used • the circamferel notch 1–1.5 mm deep and 0.5 mm wide was made on each 100 mm oxidized cladding • the impact tests were performed at 20 C	Impact tests with the oxidized cladding demonstrated that: • the impact-toughness fracture was reduced down to 2.5 J/cm^2 at 5% ECR (as-calculated using the E110 conservative correlation) • the impact-toughness fracture at 10–15% ECR (as-calculated) was about 1 J/cm^2 • the tough type of the cladding fracture was observed up to the 5% ECR • the brittle fracture occurred at 7% ECR
10. Compression tests of E110 oxidized claddings performed in VNIINM, 1998–2001 [45–48]	The double-sided oxidation of E110 claddings at 800–1200 C with water quenching. The compression tests of oxidized samples 30, 50 mm long at 20–900 C	Test data in general confirmed the results of previous tests: • the oxidation at 800 C was much better than the oxidation at 1000 C
	The compression tests (at 20 C) of oxidized claddings (18% as-calculated ECR) taken from type two simulators tested in accordance with requirements given in the item 8	• the relative displacement at failure was 4% at the following combinations of as-calculated ECR and the oxidation temperature: – 800 C: 10% ECR – 1000 C: 5% ECR • no new effects were revealed in the tests of claddings taken from the fuel rod simulators
		The following effects of the mechanical test temperature were noted: • the ductility of E110 oxidized at 200 C occurred if the ECR was less than 5% • at 18% ECR, the temperature effect in the range 20–500 C was insignificant

It should be noted that intensive studies with the E110 irradiated cladding were started in the middle of 1990s in addition to the test program presented in Table 2.2. The first results of investigations performed with the E110 irradiated claddings refabricated from VVER high burnup fuel rods (50 MW d/kg U) under LOCA conditions are presented in References 46–48.

The analysis of the whole scope of obtained results allowed to conclude that:

1. Numerous thermal–shock tests performed with different E110 samples (unirradiated and irradiated oxidized claddings and fuel rod simulators) showed that the E110 fragmentation threshold was higher than 18% ECR (calculated with the VNIINM conservative correlation) in the temperature range 800–1200 C.
2. The effect of breakaway oxidation accompanied by the hydrogen uptake was revealed in E110 claddings oxidized at temperatures higher than 800 C and relatively low ECRs.
3. Mechanical tests (tensile, compression, impact) demonstrated that a sharp decrease in residual ductility of the E110 oxidized cladding occurred in the measured ECR* range 4–7%.

* The measured ECR should not be compared with the safety criterion (18%) because (as it was noted earlier) the calculated ECR was used for the safety and analysis. That ECR was calculated using the conservative oxidation kinetics.

During 1990s several research programs devoted to the high temperature oxidation behavior of the E110 cladding were initiated in Germany, Hungary and the Czech Republic. Major findings of these test programs obtained by 2001 are presented in Table 2.3.

Table 2.3. Major results of mechanical tests with the E110 unirradiated oxidized claddings performed in Germany, Hungary and Czech Republic during 1990–2000

Test type	Test characterization	Test results
1. Ring compression tests performed by J.Böhmert in Germany (NC Rossendorf), 1992 [49, 50]	The double-sided oxidation of E110 and Zry-4 (SANDVIK) in water steam at 800–1100 C with the water quench cooling. Ring compression tests at 20 C	Results of mechanical tests showed that: • the ductility of the E110 oxidized cladding (850–1100 C) decreased sharply down to the zero ductility threshold in 2(3)-4(5,6)% range of the as-measured ECR • the ductility of E110 claddings oxidized at 800 C was high up to the 8% ECR (the maximum value was achieved under this test conditions) • the Zry-4 ductility decreased monotonically as a function of ECR, relative displacement at failure was 8% at 18.5% ECR (as-measured)
		The visual observations showed that: • the white porous spalled oxide covered the E110 cladding sample at the relatively low ECRs • the black bright oxide covered the Zry samples
		The comparative measurements of hydrogen content in the oxidized claddings demonstrated that E110 had the tendency towards the high hydrogen absorption in contrast to the Zry-4 cladding (especially at 1000 C). So, the maximum hydrogen content at the ECR of about 18% (as-measured) was: • 2050 ppm in E110 • 130 ppm in Zry-4
		The microhardness measurements allowed to reveal that the microhardness (oxygen concentration) in the prior β-phase was significantly higher in the E110 cladding at the following test parameters: • temperature oxidation: 900–1100 C • oxidation time: 30 min
2. Thermal shock tests performed in Hungary [51]	The oxidation of 50 mm fuel rods simulators (E110 cladding, Al_2O_3 pellet) at 1000–1250 C with the water quench cooling	The cladding fragmentation did not occur if the ECR (calculated using the VNIINM conservative correlation) was less than 30%
3. Ring compression tests performed in Hungary [51, 52]	The double-sided oxidation of E110 and Zry-4 samples at 900–1200 C. Ring compression tests at 20 C	Visual observations showed that: • the black bright oxide covered the Zry-4 samples in most cases • the white spalled oxide covered E110 samples at relatively low ECRs
		The mechanical tests allowed to reveal that: • the Zry-4 ductility decreased monotonically at the ECR increase • the E110 ductility decreased sharply in the ECR range (as-measured) 1.6–5%

Test type	Test characterization	Test results
		The hydrogen content measurement showed that the Zry-4 hydrogen uptake was very low, the E110 hydrogen content achieved 600–800 ppm at the 5% ECR in the temperature range 900–1100 C. The E110 hydrogen absorption rate was somewhat slowed down at 1200 C
4. Thermal shock tests performed in Czech Republic [53, 54]	The double-sided oxidation of 30 mm E110 cladding samples at 800–1200 C with the water quench cooling	The E110 cladding fragmentation threshold was observed at ECRs higher than 30% (as-measured)
5. Ring compression tests performed in Czech Republic [53, 54]	The double-sided oxidation (argon and steam mixture) of 30 mm E110 cladding samples at 800–1200 C with the water quench cooling. Ring compression tests at 20 C	The visual observations showed that: • the E110 steam oxidation at temperatures higher than 800 C led to the formation of the light color oxide and flaking-off effect (but without nodular corrosion effects) • the E110 heating in the argon atmosphere up to the isothermal oxidation temperature led to the formation of the black lustrous oxide on the E110 surface
		The ring compression tests and hydrogen content measurements allowed to reveal the following: • the zero ductility threshold of the E110 cladding was associated with 5% ECR (as-measured) • besides, the zero ductility condition was accompanied by the hydrogen content 500–700 ppm in the prior β-phase • the further ECR increase led to the oxide spallation and the increase of hydrogen content up to 2000 ppm

The experimental data organized in Table 2.3 confirmed that:

- the tested E110 claddings had a tendency towards breakaway oxidation and the hydrogen uptake at temperatures 850–1200 C;
- a sharp decrease in E110 ductility occurred at measured ECRs of 4–6%;
- fragmentation of E110 oxidized cladding was not observed at a calculated ECR less than 18% (1200 C) in accordance with the thermal–shock tests.

Analysis of results of experimental investigations with the E110 cladding performed in Russia and abroad lead to the following observations:

1. All investigations presented in Table 2.2 and Table 2.3 were performed with as-received E110 tubes manufactured during 1980s. But numerous improvements and changes were made during the 1990s in procedures for producing Zr ingots and fabricating E110 cladding.
2. The first published results characterizing the oxidation and mechanical behavior of other Zr-1%Nb cladding (French M5 alloy) showed that earlier breakaway oxidation and high hydrogen uptake were not observed in these tests with niobium-bearing cladding [55].
3. Procedures of many oxidation tests (including the oxidation history, heating and cooling rates, temperature and weight gain measurements, steam flow rate value, etc.) were not validated and documented along with the published data. The nature of cladding material used in investigations performed outside of Russia was not documented also. Procedures of mechanical tests, parameters of cladding samples and processing of obtained results were quite different in some cases and often unknown in other cases.

4. Taking into account that niobium-bearing alloys are of a high priority with respect to the increase of LWR fuel burnup, an understanding of physical phenomena defining the mechanical behavior of these claddings under accident conditions is an important international research task.

These considerations have led to the decision to perform the special research program concerning the experimental study of embrittlement of Zr-1%Nb (E110) cladding under LOCA–relevant conditions.

REFERENCES FOR SECTION 2

[1] Nuclear Safety Rules for Reactor Installations of Nuclear Power Plants, PBYa RU AS-89/97, Gosatomnadzor, Moscow, 1997.

[2] New Acceptance Criteria for Emergency Core-Cooling Systems of Light-Water Cooled Nuclear Power Reactors, Nuclear Safety 15 (1974).

[3] Hache G., Chung H. "The History of LOCA Embrittlement Criteria", *Proc. of the 28th Water Reactor Safety Information Meeting*, NUREG/CP-0172, 2000.

[4] Hobson D.O. and Rittenhouse P.L. "Embrittlement of Zircaloy Clad Fuel Rods by Steam During LOCA Transient", ORNL-4758, Oak Ridge National Laboratory, 1972.

[5] Hobson D.O. "Ductile-Brittle Behavior of Zircaloy Fuel Cladding", *Proc. of ANS Topical Mtg. on Water Reactor Safety*, Salt Lake City, 26 March, 1973.

[6] Atomic Energy Commission Rule-Making Hearing, Supplemental Testimony of the Regulatory Staff Docket RM-50-1, 26 October, 1972.

[7] Lorenz R.A. "Fuel Rod Failure under Loss-of-Coolant Conditions in TREAT", *Nucl. Tech*. 11(1971).

[8] Hesson J.C. et al. "Laboratory Simulations of Cladding-Steam Reactions Following Loss-of-Coolant Accidents in Water-Cooled Power Reactors", ANL 7609, 1970.

[9] Pawel R.E. "Oxygen Diffusion in beta Zircaloy during Steam Oxidation", *J. Nuclear Mater.*, 50, 1973.

[10] Baker L., Just L.C. "Studies of Metal Water Reactions at High Temperatures", Technical report of ANL-6548, 1962.

[11] Atomic Energy Commission Rule-Making Hearing, Opinion of the Commission, Docket RM-50-1, 28 December, 1973.

[12] Chung H.M. and Kassner T.F. "Embrittlement Criteria for Zircaloy Fuel Cladding Applicable to Accident Situations in Light-Water-Reactors", NUREG/CR-1344, January 1980.

[13] Uetsuka H. et.al. "Failure-Bearing Capability of Oxidized Zircaloy-4 Cladding under Simulated Loss-of-Coolant Conditions", *J. Nucl. Sci.* Tech. 20 (1983).

[14] Reocreux M. and Scott de Martinville E. "A Study of Fuel Behavior in PWR Design Basis Accident: An Analysis of Results from the PHEBUS and EDGAR experiments", *Nucl. Eng. Design* 124 (1990).

[15] Parsons P.D. et.al. "The Deformation, Oxidation and Embrittlement of PWR Fuel Cladding in a Loss-of-Coolant Accident: a State-of-the Art Report", CSNI Report 129, December 1986.

[16] Uetsuka H. et.al. "Zircaloy-4 Cladding Embrittlement due to Inner Surface Oxidation under Simulated Loss-of-Coolant Conditions", *J. Nucl. Sci. Tech.* 18 (1981).

[17] Uetsuka H. et.al. "Embrittlement of Zircaloy-4 due to Oxidation in Environment of Stagnant Steam", *J. Nucl. Sci. Tech.* 19 (1982).

[18] Sawatzky A. "Proposed Criterion for the Oxygen Embrittlement of Zircaloy-4 Fuel Cladding", *Proc. 4th Symp. on "Zirconium in the Nuclear Industry"*, Statford-on-Avon, UK, 27-29 June, 1978.

[19] Haggag F.M. "Zircaloy-Cladding-Embrittlement Criteria: Comparison of In-pile and Out-of-pile Results", NUREG/CR-2757, July 1982.

[20] Meyer R.O., McCardell R.K., Chung H.M., Diamond D.J., Scott H.H. "A Regulatory Assessment of Test Data for Reactivity-Initiated Accidents", *Nuclear Safety*, Vol. 37, No4, 1996.

[21] Papin J., Balourdet M., Lemoine F., Lamare F., Frizonett J.M., and Schmitz F. "French Studies on High-Burnup Fuel Transient Behavior Under RIA Conditions", *Nuclear safety*, Vol.37, No.4, 1996.

[22] Fuketa T., Nagase F., Ishijima K., and Fujishiro T. "NSRR/RIA Experiments with High-Burnup PWR Fuels", *Nuclear safety*, Vol.37, No.4, 1996.

[23] Yang R.L., Waeckel N., Montgomery R., Rosenbaum H.S. "Regulatory-Related Activities in the Robust Fuel Program", *Proc. of Top Fuel-2001*, Stockholm, May 27-30, 2001.

[24] Grandjean C., Mailliat A., Hache G. "IPSN Considerations on Prospective LOCA Testing with High Burnup Fuel", *OECD Topical Meeting on "LOCA Fuel Safety Criteria"*, Aix-en-Provence, France, March 22-23, 2001.

[25] Meyer R.O. "NRC Program for Addressing Effects of High Burnup and Cladding Alloy on LOCA Safety Assessment", *Proc. of OECD Topical Meeting on "LOCA Fuel Safety Criteria"*, Aix-en-Provence, France, March 22-23, 2001.

[26] Meyer R.O. "NRC Assessment of High Burnup Fuel Issues", *Proc. of Enlarged Halden Programme Group Meeting on "High Burnup Fuel Performance, Safety and Reliability, and Degradation of In-Core Materials, and Water Chemistry Effects, and Man-Machine System Research"*, Loen, Norway, May 19-24, 1996.

[27] Nagase F. et.al. "Experiments on High Burnup Fuel Behavior under LOCA Conditions at JAERI", *Proc. of ANS Topical Meeting on LWR Fuel Performance*, Park City, USA, April 10-13, 2000.

[28] Smirnov A.V., Smirnov V.P., Beck A.G., Panushkin A.K., Enin A.A., Rozhkov V.V. "Characteristics of VVER Fuel after the Operation under Normal and Transient Conditions: Forecasts for the Overnight Burnup", *Proc. of an International Conference "Atomic Energy in the XXI Century"*, Electrostal, Russia, June 8–10, 2000.

[29] Asmolov V., Yegorova L., Kaplar E., Lioutov K., Smirnov V., Prokhorov V., Goryachev A. "Development of Data Base with Mechanical Properties of Un- and Preirradiated VVER Cladding", *Proc. of Twenty-Fifth Water Reactor Safety Information Meeting*, NUREG/CP-0162 Vol.1, 1998.

[30] Yegorova L., Asmolov V., Abyshov G., Malofeev V., Avvakumov A., Kaplar E., Lioutov K., Shestopalov A., Bortash A., Maiorov L., Mikitiouk K., Polvanov V., Smirnov V., Goryachev A., Prokhorov V., and Vurim A. “Data Base on the Behavior of High Burnup Fuel Rods with Zr-1%Nb Cladding and UO_2 Fuel (VVER Type) under Reactivity Accident Conditions”, RRC "Kurchatov Institute" report NSI RRC 2179, Vol.1-3, 1999 (also USNRC report NUREG/IA-0156 and IPSN report IPSN 99/08–2).

[31] Lioutov K., Yegorova L., Kaplar E., Konobeyev A., Smirnov V., Goryachev A., Prokhorov V., Yeremin S. "Mechanical Properties of Unirradiated and Irradiated Zr-1%Nb Cladding under Accident Conditions", *Proc. of Twenty-Seventh Water Reactor Safety Information Meeting*, NUREG/CP-0169, 2000.

[32] Kaplar E., Yegorova L., Lioutov K., Konobeyev A., Jouravkova N., Smirnov V., Goryachev A., Prokhorov V., Yeremin S., Svyatkin A. "Mechanical Properties of Unirradiated and Irradiated Zr-1%Nb Cladding", RRC "Kurchatov Institute" report NSI RRC 2241, 2001 (also USNRC report NUREG/IA-0199 and IPSN report IPSN 01-16).

[33] Asmolov V., Yegorova L. "The Russian RIA Research Program: Motivation, Definition, Execution, and Results", *Nuclear safety*, Vol.37, No.4, 1996.

[34] Bibilashvili Yu., Sokolov N., Nechaeva O., Salatov A., Asmolov V., Yegorova L., Kaplar E., Trutnev Yu., Smirnov I., Ustinenko V., Sazhnov V., Smirnov V., Goryachev A. “Experimental Study of VVER High Burnup Fuel Rods at the BIGR Reactor under Narrow Pulse Conditions”, *Proc. of an International Topical Meeting on Light–Water–Reactor–Fuel–Performance*, Park City, Utah, USA, April 10-13, 2000.

[35] Bibilashvili Yu. et. al. “Study of High Burnup VVER Fuel Rods Behavior at the BIGR Reactor under RIA Conditions: Experimental Results”, *Proc. of the Topical Meeting on RIA Fuel Safety Criteria*, Aix-en-Provence, France, May 2002 (NEA/CSNI/R(2003) 8/Vol.2).

[36] General Regulations for Nuclear Power Plant Safety (OPB-82), Atomnaya Energia, v.54, N2, 1983 (rus).

[37] Solyany V.I., Bibilashvili Yu.K., Tonkov V.Yu. "High Temperature Oxidation and Deformation of Zr-1%Nb alloy of VVER Fuels", *Proc. of OECD-NEA-CSNI/IAEA Specialists' Meet. on "Water Reactor Fuel Safety and Fission Product Release in Off-Normal and Accident Conditions"*, Riso (Denmark), 16-20 May, 1983.

[38] Solyany V.I. et. al. "Steam Oxidation of Zr-1%Nb Clads of VVER Fuels at High Temperature", *Proc. of IAEA Specialists' Meet. on "Water Reactor Fuel Element Performance Computer Modeling"*, Bouness-on-Windermere (UK), 9-13 April, 1984.

[39] Solyany V.I., Bibilashvili Yu.K., Dranenko V.V., Izrailevskiy L.B., Levin A.Ya., Morozov A.A. "Characteristics of Corrosion Behavior of Zr-1%Nb WWER Fuel Claddings Within 700-1000°C on Long Term Exposures", *Proc. of IAEA Technical Committee Meet. on "Water Reactor Fuel Behavior and Fission Products Release in Off-Normal and Accident Conditions"*, Vienna, 10-13 November, 1986.

[40] Solyany V.I., Bibilashvili Yu.K., Dranenko V.V., Izrailevskiy L.B., Levin A.Ya., Morozov A.M. "Study of the Corrosion Behavior of Zr-1%Nb Claddings in Steam at High Temperatures", *VANT*, *series "Atomic Material Study"*, issue 2(27), 1988.

[41] Tonkov V.Yu., Kapteltsev A.M., Golikov I.V., Dolgov Yu.N., Perepelkin A.B. "The Impact of Oxidation in Water Steam on Mechanical Properties of Zr-1%Nb Alloy in the Temperature Range 20÷1000°C", VANT, *series "Material Study and New Materials",* issue 4(38), 1990.

[42] Bibilashvili Yu.K., Sokolov N.B., Dranenko V.V., Kulikova K.V., Izrailevskiy L.B., Levin A.Ya., Morozov A.M. "Influence of Accident Conditions due to Loss of Tightness by Primary Circuit on Fuel Claddings", *Proc. of the Ninth Int. Symp. on Zirconium in the Nuclear Industry*, Kobe, Japan, November 5-8, 1990.

[43] Bibilashvili Yu.K., Sokolov N.B., Dranenko V.V., Kulikova K.V., Izrailevskiy L.B., Levin A.Ya., Morozov A.M. "The Impact of Accident Modes with the First Loop Depressurization on the State of VVER-1000 Fuel Elements", *VANT, series "Reactor Material Study"*, issue 2(42), 1991.

[44] Bibilashvili Yu.K., Sokolov N.B., Dranenko V.V., et al. "The Impact of High-Temperature Oxidation and Thermal Shocks on the Deformation up to the Failure of FE Claddings Made of Zirconium-Based Alloys", *VANT*, *series "Material Study and New Materials",* issue 2(42), 1991.

[45] Sokolov N.B., Tonkov V.Yu., Andreeva-Andrievskaya L.N., Salatov A.V. "Experimental Studies for the Justification of the Maximum Design Limit for the Failure of Fuel Rods with Claddings Made of Zr-1%Nb Alloy with Regard to the Allowable Oxidation Depth", *Proc. of the 5th Inter-Branch Conference of Reactor Material Study*, v. 2, part 1, Dimitrovgrad, 1998.

[46] Bibilashvili Yu.K., Sokolov N.B., Andreeva-Andrievskaya L.N., Tonkov V.Yu., Morozov A.M., Smirnov V.P. "Heat Resistance of Oxidized Claddings of the VVER Fuel Rods Made of Zr-1%Nb Alloy on Flooding under Conditions of the Accident with Loss of Coolant", *Proc. of Top Fuel-2001*, Stockholm, May 27-30, 2001.

[47] Bibilashvili Yu.K., Sokolov N.B., Andreeva-Andrievskaya L.N., Tonkov V.Yu., Salatov A.V., Morozov A.M., Smirnov V.P. "Thermomechanical Properties of Zirconium-Based Alloys Oxidized Claddings in LOCA Simulationg Conditions", *Proc. of IAEA Technical Commettee Meet. on "Fuel Behavior under Transient and LOCA conditions"*, Halden, Norway, September 10-14, 2001.

[48] Bibilashvili Yu.K., Sokolov N.B., Andreeva-Andrievskaya L.N., Tonkov V.Yu., Salatov A.V., Morozov A.M., Smirnov V.P. "Thermomechanical Properties of Oxidized Zirconium-Based Alloy Claddings in Loss of the Coolant Accident Conditions", *Proc. of OECD LOCA Topical Meet.*, Cadarache, France, March 22-23, 2001.

[49] Böhmert J. "Embrittlement of Zr-1%Nb at Room Temperature after High-Temperature Oxidation in Steam Atmosphere", *Journal Kerntechnik* 57 No1, 1992.

[50] Böhmert J., Dietrich M., Linek J. "Comparative Studies on High-Temperature Corrosion of Zr-1%Nb and Zircaloy-4", *Nuclear Engineering and Design*, 147 No1, 1993.

[51] Hozer Z., Maroti L., Matus L., Windberg P. "Experiments with VVER Fuels to Confirm Safety Criteria", *Proc. of Top Fuel-2001 Meet.*, Stockholm, May 27-30, 2001.

[52] Hozer Z., Griger A., Matius L., Vasaros L., Horvath M. "Effect of Hydrogen Content on the Embrittlement of ZR Alloys", *Proc. of IAEA Technical Committee Meeting on "Fuel Behavior under Transient and LOCA Conditions"*, Halden, Norway, September 10-14, 2001.

[53] Vrtilkova V., Valach M., Molin L. "Oxiding and Hydrating Properties of Zr-1%Nb Cladding Material in Comparison with Zircaloys", *Proc. of IAEA Technical Committee Meeting on "Influence of Water Chemistry on Fuel Cladding Behavior"*, Rez (Czech Republic), October 4-8, 1993.

[54] Vrtilkova V., Novotny L., Doucha R., Vesely J. “An Approach to the Alternative LOCA Embrittlement Criterion”, *Proc. of SEGFSM Topical Meeting on LOCA Fuel Issues,* Argonne National Laboratory, May 2004 (NEA/CSNI/R(2004)19).

[55] Brachet J., Pelchat J., Hamon D., Maury R., Jaques P., Mardon J. "Mechanical Behavior at Room Temperature and Metallurgical Study of Low-Tin Zry-4 and M5™ (Zr-NbO) Alloys after Oxidation at 1100°C and Quenching", *Proc. of IAEA Technical Committee Meeting on "Fuel Behavior under Transient and LOCA Conditions"*, Halden, Norway, September 10-14, 2001.

3. OXIDATION BEHAVIOR AND EMBRITTLEMENT THRESHOLD OF STANDARD E110 CLADDING: PROGRAM, TEST PROCEDURES, DISCUSSION OF TEST RESULTS

3.1. The program concept and technical requirements to experimental works

Previous investigations of the mechanical behavior of oxidized claddings under the LOCA conditions revealed a series of practical problems. Two of those are related directly to the present investigation:

- a definite separation of such conceptions as the "cladding fragmentation threshold" and "cladding embrittlement threshold" is lacking on analyzing the study results;
- the results of works performed by different researchers are discussed and compared without the analysis of test conditions and regard for peculiar features of procedures employed to determine the output parameters.

As for the first of the problems, the following approach was proposed to specify two criterion conditions of the cladding:

1. The cladding fragmentation threshold characterizes the actual loss of the cladding structural integrity under the impact of a complex combination of loading factors. This threshold can be determined for each of the typical sections of the accident scenario and for each of the post-accident actions only with the help of well-planned integral experiments with fuel rods and simulators of fuel rods.
2. The embrittlement threshold characterizes the conditions under which the cladding ductility is close to zero. In this case, it is of importance that the appropriate threshold value be determined by relatively simple parametric experiments including those using uniaxial mechanical tests.

It is evident that, from the theoretical point of view, the cladding fragmentation threshold should be the major subject of investigation within the context of this program. However, in spite of the fact that almost 30 years after the time when the first licensing criterion for safety was developed, the following basic conclusion about the basis of the criterion has not changed up to now: "There is some lack of certainty as to just what nature of stresses would be encountered during the LOCA" [1]. In turn, the insufficiency of such knowledge leads to the difficulty of justifying requirements on the basis of integral experiments. Therefore, with due respect to the importance of such experiments as a thermal shock, it should be acknowledged that the experimental determination of the embrittlement threshold for claddings -- with the subsequent introduction of coefficients regulating the necessary minimum margin for the residual ductility in oxidized claddings -- was and remains the basic method for the practical safety studies.

Therefore, the further analysis of possible variants for the experiments was restricted to the following list of mechanical tests for oxidized claddings:

- impact tests;
- three-point bending tests;
- tensile tests;
- ring compression tests.

The consideration of these variants showed that:

- impact tests do not allow one to obtain a stress-strain curve in the explicit form and, besides, these tests are not standardized so that one could not directly compare the results obtained for different claddings in different countries;
- three-point bending tests present a very promising type of study; however, the procedure requirements are not quite developed and the comparative data base for these test is practically lacking;

- tensile tests present the most valuable type of mechanical tests; however, tensile tests of claddings with a high level of oxidation require to improve of test techniques and, besides, a comparative data base obtained from these tests is extremely limited;
- ring compression tests present the simplest and accessible type of tests allowing to obtain good statistical data within a limited time. Therefore, this type of tests has a representative data base containing the results of previous investigations of alloys E110, Zry-4, M5, Zirlo.

Taking into account all stated above, the final choice of the method to determine the embrittlement threshold for the E110 cladding was made in favor of ring compression tests. Nevertheless, it should be noted that this type of tests has a series of disadvantages the basic ones of which are as follows:

- the lack of standard requirements imposed on geometrical sizes of tested specimens (specimen length);
- the lack of physically justified rules for the interpretation of test results.

Therefore, special scoping tests were stipulated in the program of these studies. The aim of these tests was to obtain a data base necessary to specify the requirements to the test conditions and to justify the processing procedures for obtained results. It should be noted that the list of procedural issues revealed at the stage of this program development included several problems associated with the oxidation conditions.

The first of these problems may be characterized by the following propositions:

- from the formal point of view, the E110 alloy embrittlement threshold must be determined and compared with the license embrittlement criterion;
- the license embrittlement criterion for the E110 alloy (18%) is based on the employment of the VNIINM conservative correlation for the E110 oxidation kinetic description [2];
- just the same approach is used for Zircaloy-4 alloy (15% in France and 17% in U.S.) but in this case the Baker-Just conservative correlation is often employed [3];
- both conservative correlations were developed according to individual (as applied to each alloy) rules, and the conservatism degree was not necessarily the same. Therefore, a direct comparison of the mechanical behavior of these two alloys (and others such as M5 and Zirlo) with one of the conservative correlations is not meaningful from the physics point of view;
- it is evident that the practical solution of this problem may be provided on moving from the conservative correlations to best-estimated correlations with a simultaneous transformation of the license criteria into the same system of coordinates (i.e., as-measured);
- in this case, the proposed approach allows to solve one more important problem, namely, to obtain a data base characterizing the behavior of claddings fabricated from different alloys in the system of coordinates (ECR vs. time), as it is evident that both these factors are competitively significant in the consideration of accident processes.

However, earlier work demonstrated that different researchers developed a number of different correlations for the E110 alloy oxidation kinetics [4, 5, 6, 7, 8, 9, 10]. Therefore, it was decided to obtain additional data that would allow us to pick the best estimated correlation from those. The initial program stage would thus include the following:

- provide a sufficient quantity of oxidation tests in the research Program necessary to obtain additional data on the E-110 alloy oxidation kinetics;
- perform oxidation within the range of 5-20% ECR.

The final stage of the scoping tests was dedicated to determination of requirements to be imposed on the types of claddings to be tested, on the oxidation conditions and on the parameters of mechanical tests with regard to such potentially significant factors as:

- oxidation type (single-sided or double-sided);
- oxidation temperature;
- heating and cooling rates;

- cladding material (as-received E110, E110K, E635 tubes, as-received E110 cladding (E110A), irradiated commercial E110 cladding);
- temperature of mechanical tests.

To optimize the quantity of tests, it was decided to divide the Program into three relatively independent stages:

1. Scoping tests.
2. Reference tests.
3. Sensitivity studies.

The goals, tasks and results of scoping tests will be discussed in the section 3.2 of the report. Table 3.1 presents the logical principles laid into the basis of the development of reference tests and sensitivity studies as well as the parameters of these tests.

Table 3.1. The list of tasks and technical requirements

Program stage	Major tasks	Technical requirements	Motivation
1. Reference tests	To determine the zero ductility threshold of E110 cladding as a function of the following oxidation parameters: • cladding heating rate • cladding cooling rate • ECR To find the optimal test mode for the sensitivity studies	1.1. Varied parameters: • heating rate: – 0.5 C/s – 25 C/s • cooling rate: – 0.5 C/s – 25 C/s – 200(170–270) C/s – ECR: 1.2. Fixed parameters: • cladding type: as-received E110 cladding tube • coolant (oxidation medium): water steam (0.1 MPa) • oxidation type: double-sided • hold temperature: 1100 C • combination of oxidation modes: – F/F (fast heating (25 C/s) and fast cooling (25 C/s)) – F/Q (fast heating (25 C/s) and quench cooling (200 C/s)) – S/S (slow heating (0.5 C/s) and slow cooling (0.5 C/s)) – F/S (fast heating (25 C/s) and slow cooling (0.5 C/s)) – S/F (slow heating (0.5 C/s) and fast cooling (25 C/s)) • parameters of mechanical tests: – 20 C – 1 mm/min	• Different heating rates allow to determine the sensitivity of embrittlement phenomena to the initial stage of cladding oxidation history (oxidation in the $\alpha-\beta$ temperature range) • Different cooling rates allow to determine the sensitivity of embrittlement phenomena to: – $\beta \rightarrow \alpha'$ phase transient conditions – thermal stresses under cooling conditions • Five combinations of heating and cooling rates (F/F, F/Q, S/S, F/S, S/F) allow to reveal definitely the impact of appropriate parameters on mechanical properties of claddings

Program stage	Major tasks	Technical requirements	Motivation
2. Sensitivity studies 2.1. Tests with Zry-4 cladding	To perform several oxidation and mechanical tests with the Zry-4 cladding and to compare the obtained results with the published Zry-4 data	2.1.1. Varied parameters: • combination of heating and cooling rates: – S/S – F/F • ECR: 11–12 % 2.1.2. Fixed parameters: • cladding type: as-received Zry-4 • coolant: water steam • oxidation type: double-sided • hold temperature: 1100 C • parameters of mechanical tests: – 20 C – 1 mm/min	• Comparison of Zry-4 data obtained in the frame of this work with the Zry-4 data obtained previously allows to verify the whole set of experimental procedures • Comparison of the E110 and Zry-4 data allows to reveal general differences in the physical behavior of these alloys under oxidation conditions • Two combinations of heating and cooling rates allow to reveal the sensitivity of the Zry-4 cladding to oxidation conditions
2.2. Oxidation type	To perform a single-sided oxidation of E110 cladding and to compare single-sided and double-sided test results	2.2.1. Varied parameters: • ECR range: 7–12 % 2.2.2. Fixed parameters: • cladding type: as-received E110 tube • coolant: water steam • oxidation type: single-sided • hold temperature:1100 C • F/F combination of heating and cooling rates • parameters of mechanical tests: – 20 C – 1 mm/min	• A single-sided oxidation characterizes cladding behavior in the undeformed part of the rod (away from balloon) • French data base on the embrittlement threshold of the M5 alloy has been developed for a single-sided oxidation • Comparative data base (single-sided, double-sided oxidized claddings) allows to estimate the dependence of test results on the oxidation type
2.3. Oxidation temperature	To perform a double-sided oxidation of E110 cladding at different hold temperatures and to reveal the sensitivity of the cladding behavior to this parameter	2.3.1. Varied parameters: • hold temperature: – 800, 900, 950, 1000, 1100, 1200 C • ECR: 6–13 % 2.3.2. Fixed parameters: • cladding type: as-received E110 tube • coolant: water steam • oxidation type: double-sided • F/F combination of heating and cooling rates • parameters of mechanical tests: – 20 C – 1 mm/min	• The E110 embrittlement phenomena could be sensitive to the hold temperature in accordance with the previous test data base • Comparative data base obtained for different temperatures allows to estimate this effect

Program stage	Major tasks	Technical requirements	Motivation
2.4. Alloying composition	To perform a double-sided oxidation of as-received E110K, E635 cladding tubes and to determine the sensitivity of cladding behavior to alloying composition	2.4.1. Varied parameters: • cladding material type: – E110K – E635 • ECR: 7–14 % 2.4.2. Fixed parameters: • coolant: water steam • oxidation type: double-sided • F/F combination of heating and cooling rates • hold temperature: 1100 C • parameters of mechanical tests: – 20 C – 1 mm/min	• The E110K alloy has a high concentration of oxygen (approximately the same as the M5 alloy has). Oxygen is considered as an alloying component in case of concentrations like that • The E635 alloy has Fe and Sn as alloying components (similar to those in the Zirlo alloy) • The comparative data base with E110, E110K, E635 test results allows to understand the sensitivity of oxidation behavior of Zr-Nb alloys to the major chemical components of the cladding material
2.5. Temperature of mechanical tests	To perform ring compression tests at 135 C and several ring tensile tests at different temperatures and to determine the sensitivity of embrittlement phenomena to the temperature of mechanical tests	2.5.1. Varied parameters: • temperature of ring compression tests: 20, 135, 200, 300 C • temperature of ring tensile tests: 135, 200, 300 C 2.5.2. Fixed parameters: • E110 oxidized cladding tubes after a double-sided oxidation at 1100 C and F/F combination of heating and cooling rates	• The first safety embrittlement criterion (17 % ECR) was validated at 135 C (the saturation temperature during the reflood) • Possible earlier embrittlement of the E110 alloy may be associated with the generation of hydrides at low temperatures. But it is known that hydrogen solubility in zirconium alloys is a strict function of the temperature • The comparison of mechanical tests performed at different temperatures allows to reveal the sensitivity of the E110 embrittlement behavior to post-LOCA conditions

Program stage	Major tasks	Technical requirements	Motivation
2.6. Type of mechanical tests	To perform several ring tensile tests, several three-point bending tests and to develop the data base characterizing the representativity of the E110 embrittlement threshold determined due to ring compression tests	2.6.1. Varied parameters: • type of mechanical tests: – ring tensile tests; – three-point bending tests 2.6.2. Fixed parameters: • the E110 oxidized cladding after a double-sided oxidation at 1100 C and F/F combination of heating and cooling rates	• The comparative data obtained for three types of mechanical tests (compression, tensile, bending) allow to estimate the representativity of oxidation limits developed on the basis of ring compression tests.
2.7. Fuel burnup	To perform the scoping tests (oxidation and ring compression) with E110 commercial irradiated claddings refabricated from VVER fuel rods and to compare obtained results with the data base on as-received claddings	2.7.1. Varied parameters: • hold temperature: 1000, 1100, 1200 C • combination of heating and cooling rates: S/S, S/F, F/F • ECR: 6–16 % (as-measured) 2.7.2. Fixed parameters: • cladding type: irradiated E110 cladding made from commercial fuel rods with burnup ~50 MWd/kg U • coolant (oxidation medium): water steam • oxidation type: double-sided • parameters of mechanical tests: – 20, 135 C – 1 mm/min	• The preliminary data base obtained in these tests will allow to estimate high burnup fuel effects in the context of embrittlement phenomena of the E110 cladding

3.2. Methodological aspects of oxidation and mechanical tests

3.2.1. Oxidation tests

In accordance with the review results discussed in Chapter 2 oxidation tests have a long historical tradition based on the following approach:

- oxidation is performed under indirect heating of a cladding sample;
- cladding samples are oxidized and the same samples are used in the mechanical tests;
- oxygen weight gain is determined by weighing the sample during the oxidation process or by weighing the sample before and after the test.

However, the analysis performed on preparing this paper has shown that this approach has several disadvantages, the following two of which are the basic ones:

1. Oxidation of the cladding samples of any length is accompanied by the occurrence of end-effects caused by oxygen (hydrogen) absorption at the end-faces of the cladding sample. These end-effects lead to two consequences of importance:

1.1. These parts of the cladding sample are characterized by a higher tendency to the embrittlement caused by: a) a higher ECR and b) additional stresses in the ZrO_2 layer resulting in an early initiation of the breakaway oxidation;

1.2. The ECR (weight gain) of the oxidized cladding sample is overestimated as the area of the cladding end-faces is not taken into account in the ECR (weight gain) calculations.

It is evident that the results of oxidation and mechanical tests are the more sensitive to the end-effects, the less is the length of the cladding samples. This approach is especially unacceptable for E110 claddings as the end-effects intensify the development of the breakaway phenomena.

Besides, the employment of short cladding samples extends the duration and labour-intensiveness of the investigation, on the one hand, and restricts the opportunity to perform other types of tests (except for mechanical ones) with oxidized samples, on the other hand.

2. Determination of the weight gain by measuring the difference in the sample weight before and after oxidation is quite an undesirable procedure for alloys susceptible to such effect as spallation of ZrO_2. This method application for such alloys leads to the underestimation of the actual weight gain.

Basing on this analysis results, on technical requirements presented in Table 3.1, the following major methodical problems have been formulated:

1. To develop the facility and procedure necessary for oxidation of the cladding sample 100 mm long;
2. To develop the experimental procedure independent of end-effects and ZrO_2 spallation and flaking off to determine the ECR (weight gain).

A brief description of this work results is presented in the following sections.

3.2.1.1.Test samples and oxidation apparatus

Fig. 3.1 illustrates the appearance of test samples developed for this program.

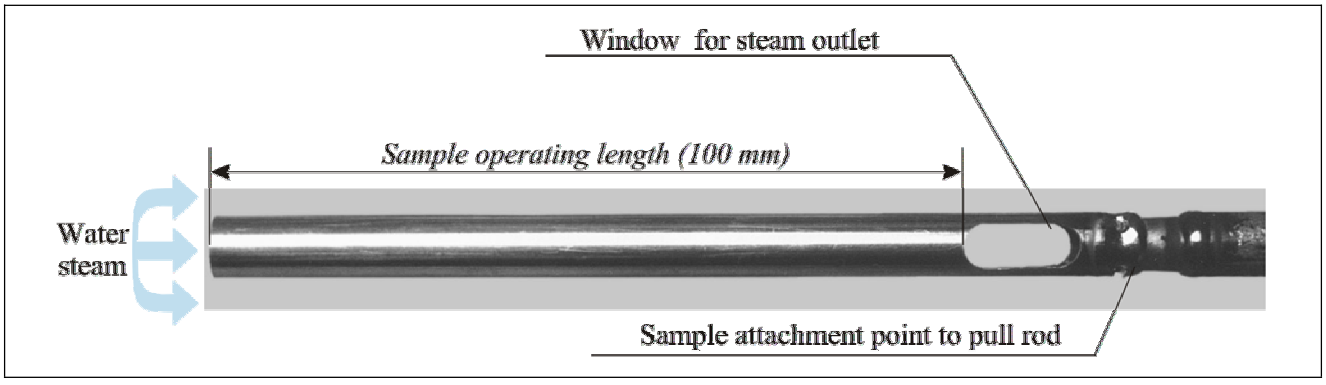

Fig. 3.1. Schematics of the cladding sample

The sample shown in Figure is intended for the double-sided oxidation. The sample for single-sided oxidation had no window for steam outlet and, besides, the sample bottom end was plugged. The sample was oxidized in the facility the basic diagram of which is demonstrated in Fig. 3.2.

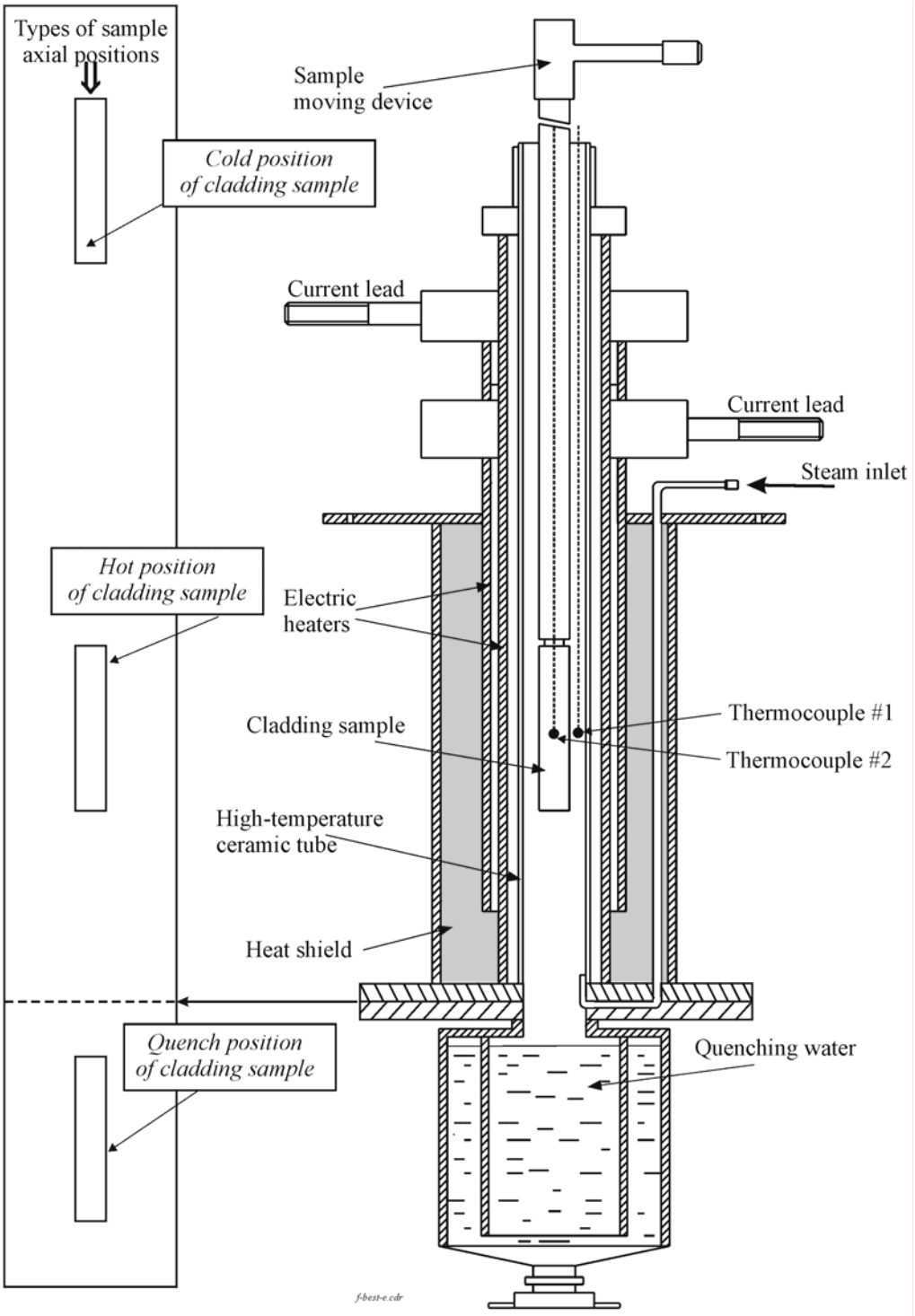

Fig. 3.2. Oxidation test apparatus

Description of the facility and procedures employed for the oxidation of samples are described in more detail in Appendixes A–1, A–2. Parameters of all types of the cladding samples used in this work are presented in Appendix A–3. Results of scoping tests performed to characterize the temperature distribution in the cladding sample are given in Appendix A–4. In accordance with the Program of research, the oxidation facility provided for the following combinations of heating and cooling rates: S/S, S/F, F/S, F/F, F/Q, where S is slow, F is fast, and Q is quench. Fig. 3.3 demonstrates typical examples for the temperature histories for these combinations. p.3.8. It should be noted also, that the preliminary heating of cladding samples to 150 C was performed with the argon flow, and the further heating was performed with the water steam flow.

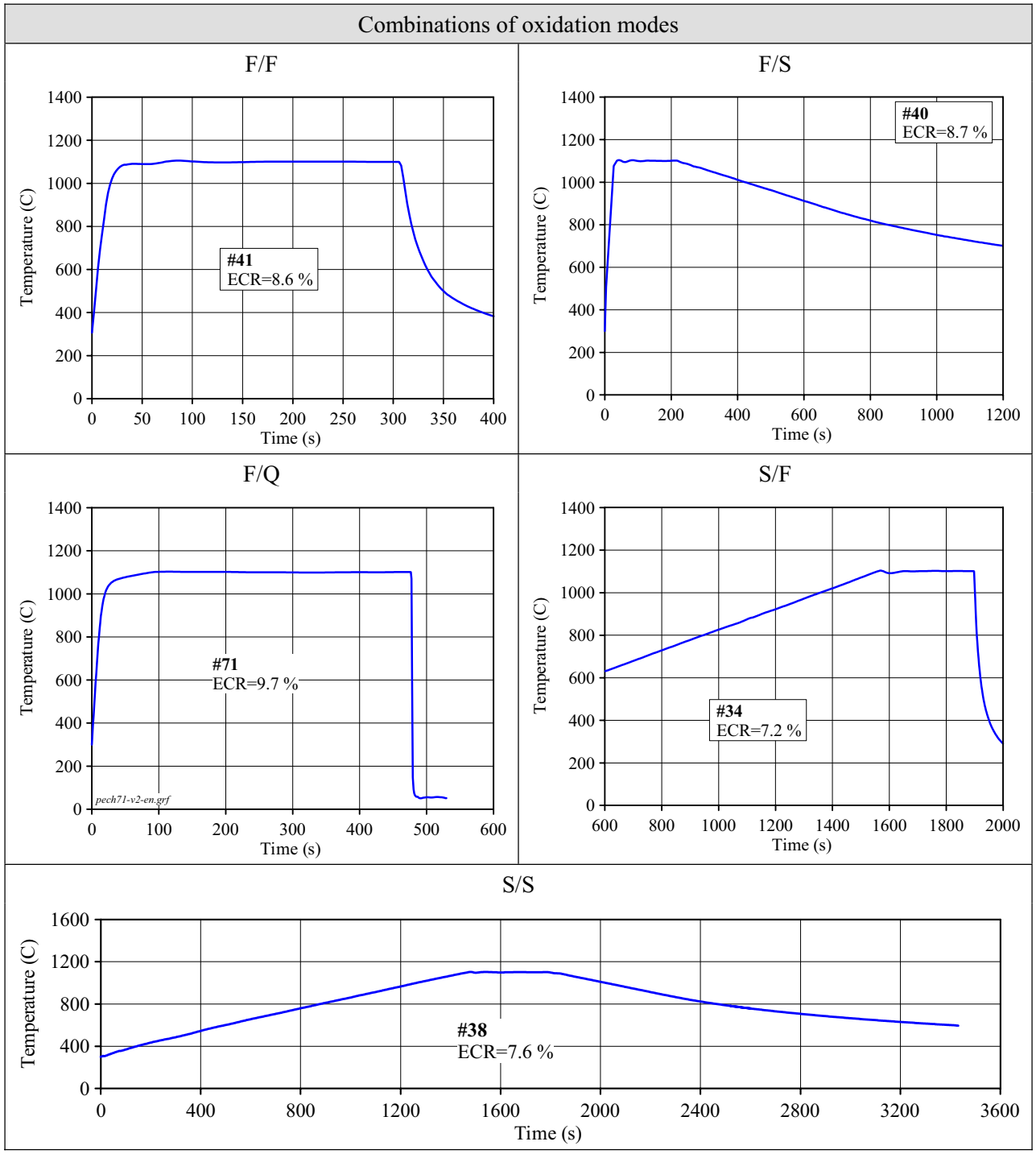

Fig. 3.3. Types of temperature histories for different combinations of heating and cooling rates

Appendix A–5 contains the description of the method for the ECR determination. Major provisions of the method developed in the frame of this work may be characterized by the following way:

$$\Delta W_o = \Delta W_\infty - \Delta W_e,$$

where ΔW_o – the cladding oxygen weight gain obtained during the oxidation test (mg/cm^2);

ΔW_∞ – the oxygen weight gain calculated for the case with the cladding oxidation during the infinite time (full transformation of Zr-1%Nb to ZrO_2 and Nb_2O_5 oxides) (mg/cm^2);

ΔW_e – the oxygen weight gain necessary to oxidize the metallic part of the cladding remaining

after the oxidation test to the stoichiometric oxide.

The concept of this method consists in the fact that a new experimental procedure named the "extra oxidation" is introduced in addition to the oxidation test. This procedure includes the following stages:

- a ring sample (with the measured length) cut out from the oxidized cladding sample of the initial length 100 mm is located into the crucible of the oxidation facility;
- the crucible with the ring sample is weighed;
- the extra oxidation of the ring sample is carried out up to the complete oxidation of a metallic phase and the generation of a stoichiometric oxide;
- the crucible with the extra oxidized ring sample is weighed and oxygen weight gain obtained during the extra oxidation (ΔW_e) is determined.

Thus, the oxygen weight gain during the oxidation test is determined as the difference between the theoretical value of weight gain necessary for the complete oxidation of Zr-1%Nb ring sample (ΔW_∞), and the measured weight gain after the extra oxidation procedure (ΔW_e). The introduction of this procedure for the weight gain determination and employment of a long (100 mm) cladding sample for the oxidation tests allowed to solve the following urgent investigation problems:

- to fabricate several ring samples for mechanical tests from one oxidized sample;
- to perform mechanical tests of ring samples at different temperatures;
- to fabricate special samples from the same oxidized sample for metallographic investigations, fractography research, hydrogen content measurement, scanning electron microscopy examination (SEM), transmission electron microscopy examination (TEM).

Fig. 3.4 presents the major provisions for experimental procedures with cladding samples.

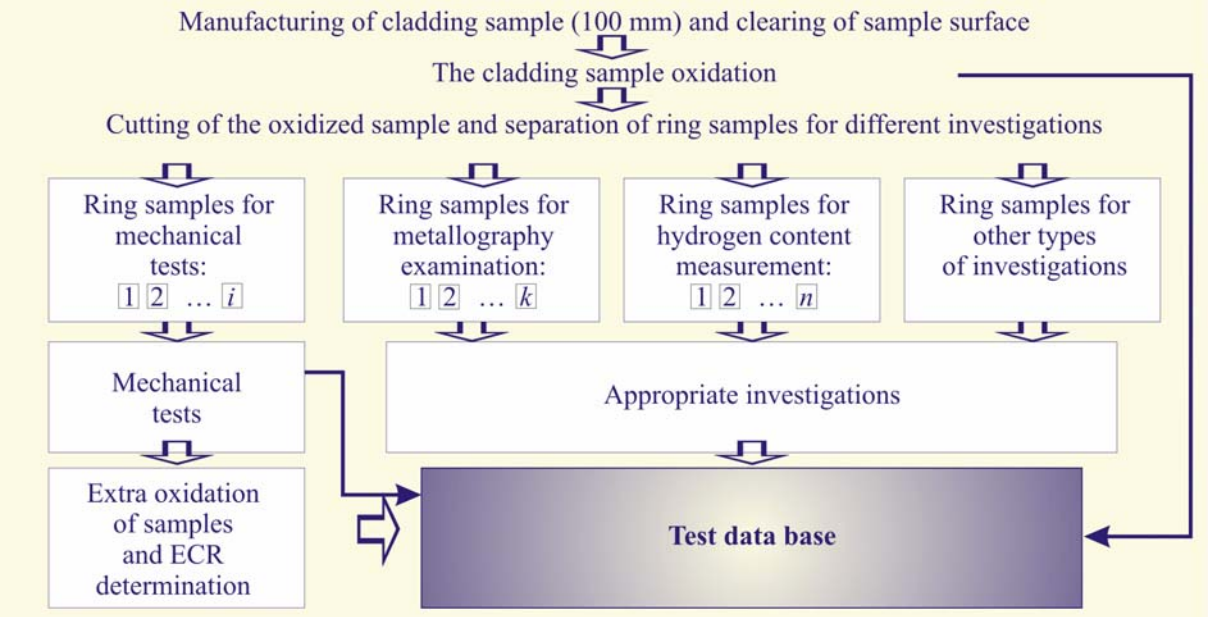

Fig. 3.4. Development of the data base with test results

The procedure developed for mechanical tests is described in the following paragraph. Other special procedures are characterized in Appendix A–6.

3.2.2. Mechanical tests

In accordance with the program, three types of mechanical tests were provided to assess the mechanical behavior of the E110 oxidized cladding:

1. Ring compression tests.
2. Ring tensile tests.
3. Three-point bending tests.

In this case, ring compression tests were considered as the basic type of mechanical tests. And two other types of tests were intended to assess the representativeness of the obtained data base.

3.2.2.1. Ring compression tests

The procedure of ring compression tests may be schematically described in the following way (see Fig. 3.5):

- an oxidized ring sample is located in the test machine;
- a ring sample is compressed at the constant rate of cross-head displacement;
- the load-displacement diagram is noted during the test.

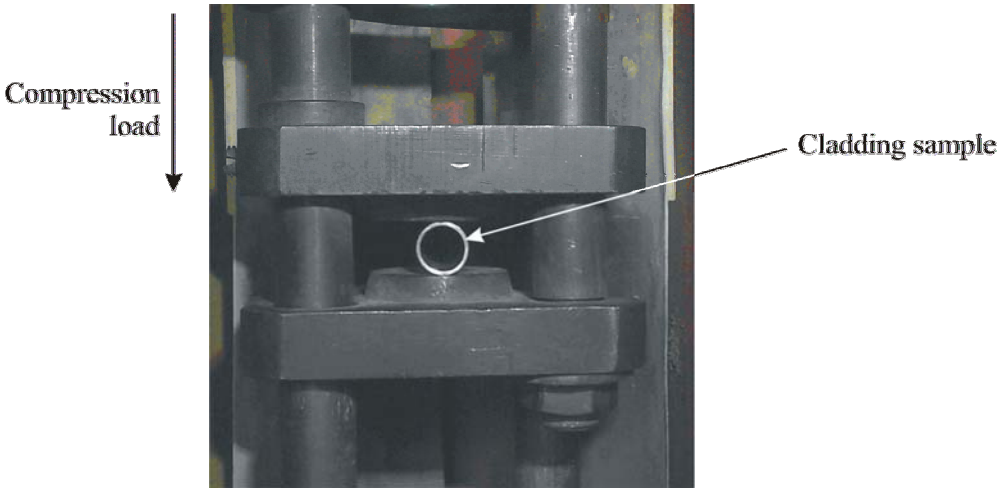

Fig. 3.5. Test machine for ring compression tests of oxidized cladding samples

As it was already mentioned above, this method is not used (as a rule) for the measurement of mechanical properties. However, it allows to determine that the threshold state of oxidized metal at which the cladding failure takes place without macroscopically significant plastic strain. This cladding material may be considered brittle. Accordingly, the ECR of this material is regarded as the cladding embrittlement threshold.

The analysis of previous approaches used to determine the embrittlement threshold of zirconium claddings on the basis of ring compression tests (see Chapter 2) allowed to reveal the following general problems:

- cladding samples of different length (6–30 mm) were used for these tests;
- the standard procedure for the processing of load-displacement diagrams was not developed;
- the cladding embrittlement threshold was estimated by different methods basing on results of ring compression tests;
- the organization of previous data into the summarized data base is not possible for any tested alloys (see the additional information presented in section 3.3.2).

Therefore, thorough development and validation of the procedure for ring compression tests were the most important tasks in this work.

A real load-displacement diagram based on the ring compression test of the E110 oxidized cladding allows to illustrate the above mentioned problems more obviously (see Fig. 3.6)

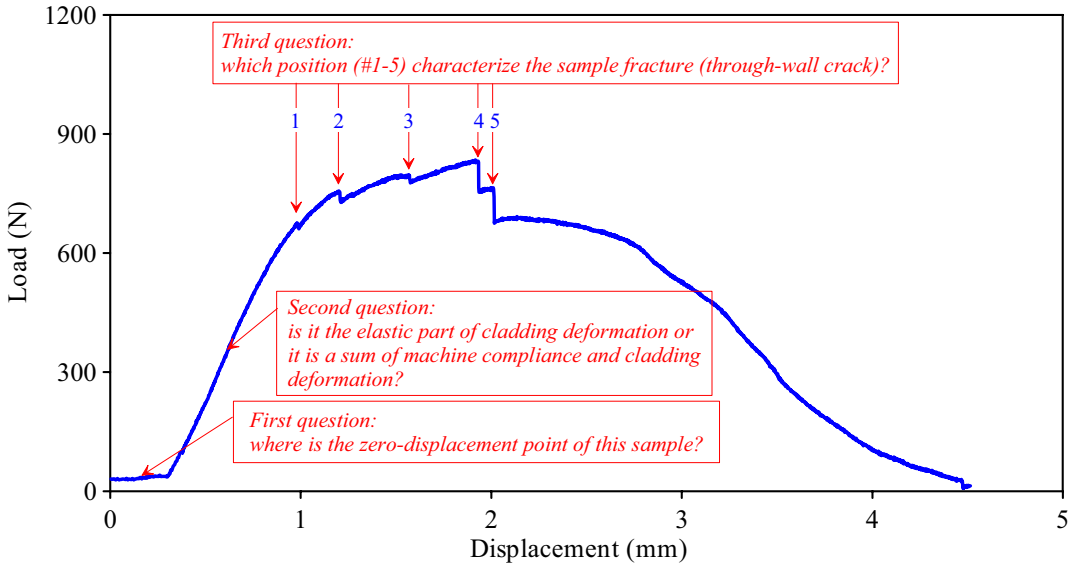

Fig. 3.6. The as-measured load-displacement diagram of the E110 oxidized cladding sample

The list of three questions formulated in Fig. 3.6 should be added with the fourth one: what is the impact of the ring sample length on the parameters of the load-displacement diagram? To find answers to these questions, the program of scoping mechanical tests was worked out the major tasks of which were as follows:

- the determination of an effective elasticity modulus for the ring sample;
- the development of the processing procedure for as-measured load-displacement diagrams;
- the sensitivity studies to validate a standard length of the ring sample;
- the development of a special data base necessary to determine the relationship between the cladding fracture and load-displacement response.

The first step of this work was devoted to the transformation of the as-measured load-grip displacement diagram into the standard form using (for each tested ring sample) the procedure of the zero-displacement point determination in accordance with the approach presented in Fig. 3.7.

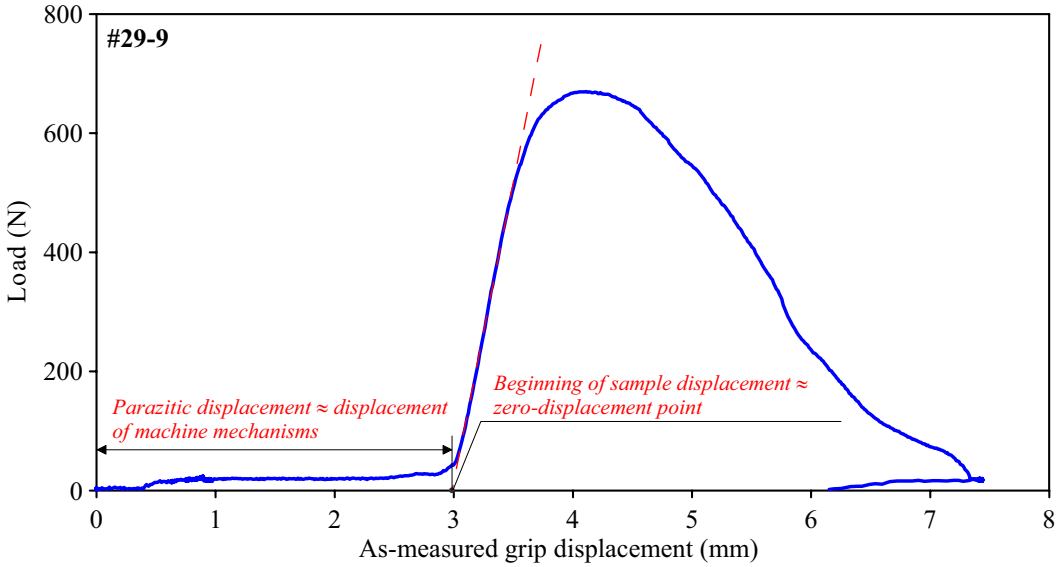

Fig. 3.7. Procedure for the determination of the sample zero-displacement point

After that, special scoping tests were performed to determine the verification data characterizing Young's modulus of the cladding ring sample. It should be noted that the compression diagram consists of two portions:

1. The portion of the sample elastic deformation with the linear relationship between the load and displacement.
2. Nonlinear portion characterizing the plastic component accumulated in the total deformation of sample. The effective modulus of elasticity is employed in the uniaxial mechanical tests to determine the plastic component of a total elongation.

However it is known that the ring sample compression induces not only the compression and tensile stresses but also bending stresses that are distributed along the sample perimeter in the compound way. In this case, it should be pointed out that the investigation of the similar issue performed earlier allowed to develop the procedure of comparison of the effective elastic modulus and the load relief lines [11]. Fig. 3.8 illustrates the results of appropriate scoping compression tests.

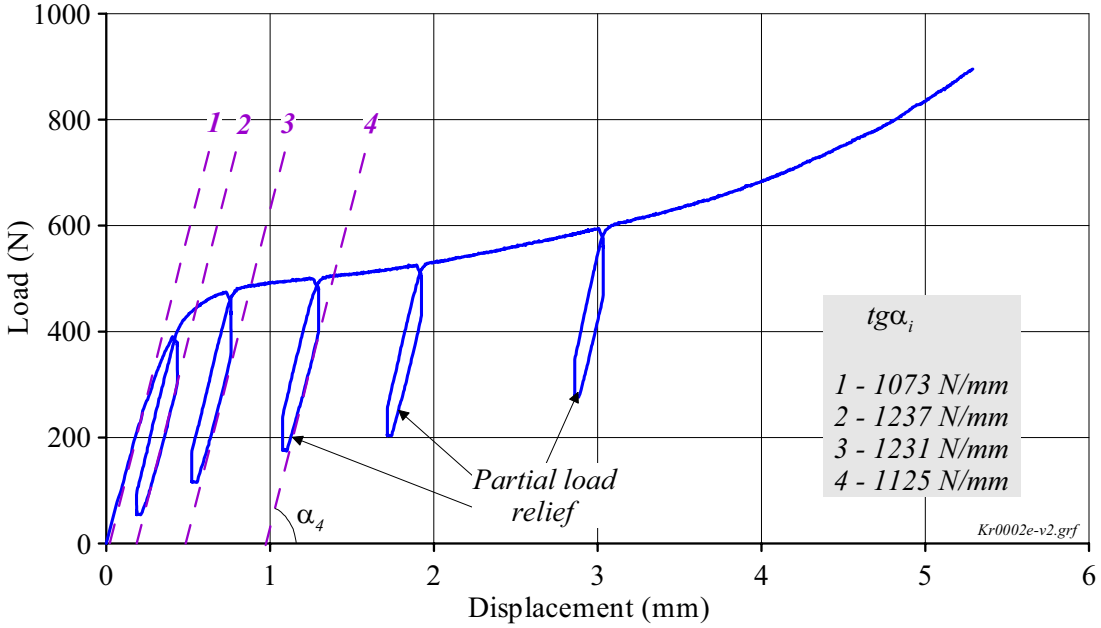

Fig. 3.8. Determination of effective modulus of elasticity basing on the results of scoping compression tests

The procedure of this test included the compression of the ring sample with the load reduction in several points of the diagram (partial load relief). It is known that the process of the load reduction in the elastic deformation area is described by the similar straight line as that describing the sample compression process. The comparative analysis of the obtained data has shown that the linear portion of the load-displacement diagram characterizes the real elastic deformation of the sample ($tg\alpha_1 \approx tg\alpha_{2...i}$). Thus, this part of the diagram can be used to determine the plastic component of the deformation on the diagram processing.

The next step of the procedure development was devoted to the determination of the parameter characterizing the margin of residual ductility in the oxidized cladding. Fig. 3.9 presents the major provisions of the procedure proposed for this work.

In accordance with this procedure, the cladding strain at the compression was assessed by two parameters:

1. Relative displacement at failure (S_f).
2. Plastic component of relative displacement at failure (S_{pl}).

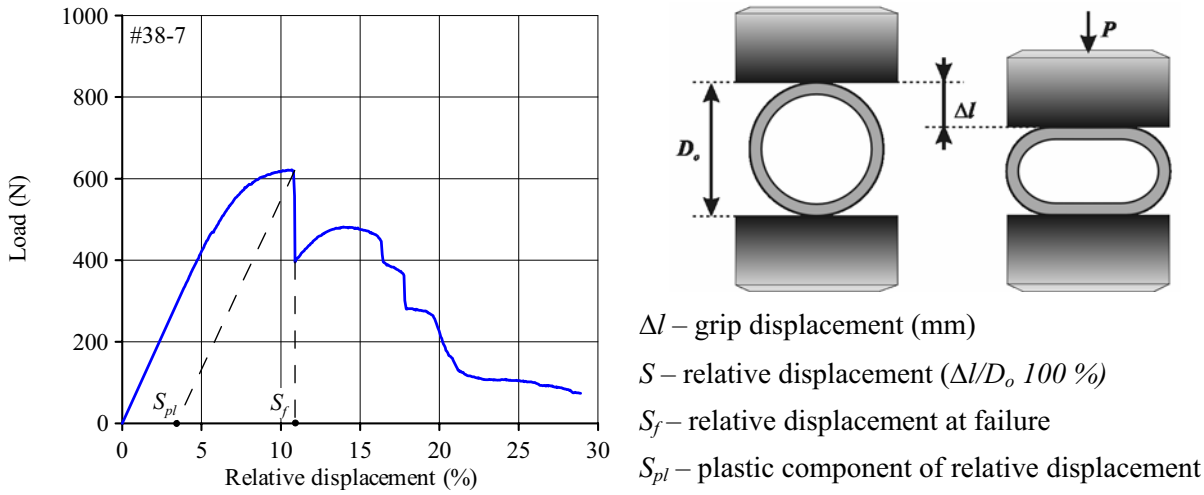

Fig. 3.9. The processing procedure for the load-displacement diagram of the ring compression test of the E110 oxidized cladding

The first of these parameters was used in some of the early ring compression tests [2, 12, 13, 14, 15, 16, 17, 18]. However this approach has several essential weak points:

- the sensitivity of this parameters to the deformation plastic component is reduced as the cladding embrittlement is progressing;
- this parameter does not tend to zero as the cladding approaches the zero-ductility threshold;
- it is impossible to determine the zero-ductility threshold on the basis of the cladding relative displacement as a function of the ECR without an additional relationship connecting these two parameters.

Data presented in Fig. 3.10 illustrate these problems obviously.

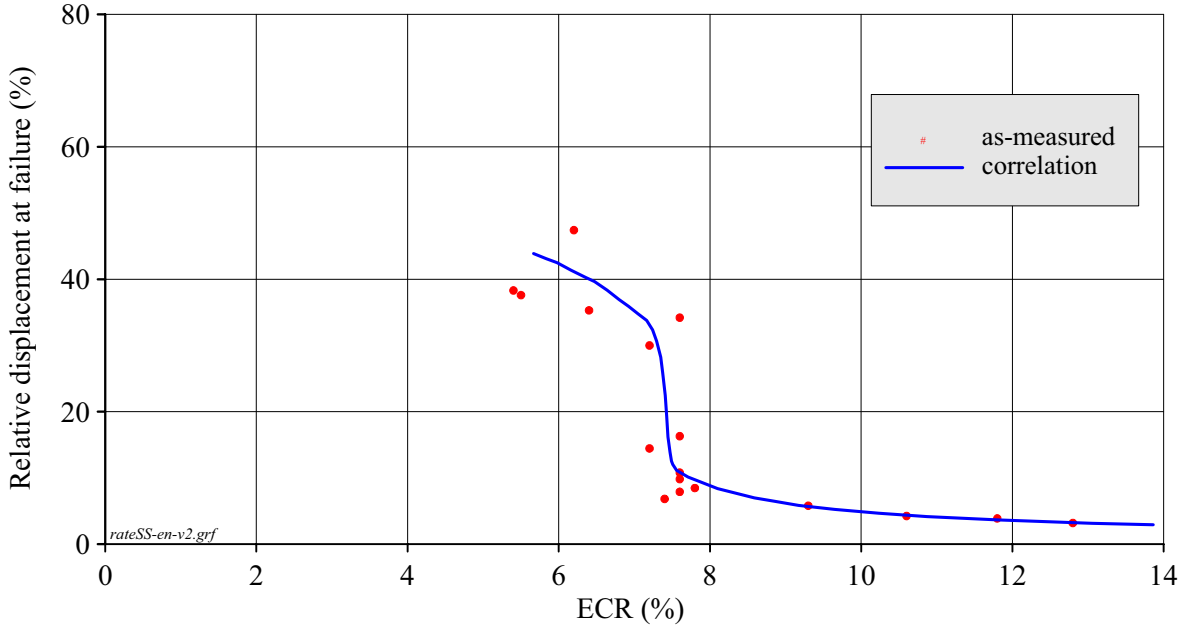

Fig. 3.10. Relative displacement at failure of the E110 cladding after a double-sided oxidation and S/S combination of heating and cooling rates as a function of the ECR

The analysis performed by the report authors to solve these problems has shown that from the physics point of view the macroscopic zero-ductility threshold or, in other words, the macroscopic cladding embrittlement threshold may be defined as such ECR critical value at which the plastic component of the cladding strain at ring compression tests tends to zero. Fig. 3.11 presents the graphic interpretation of this approach for the same data base demonstrated in Fig. 3.10.

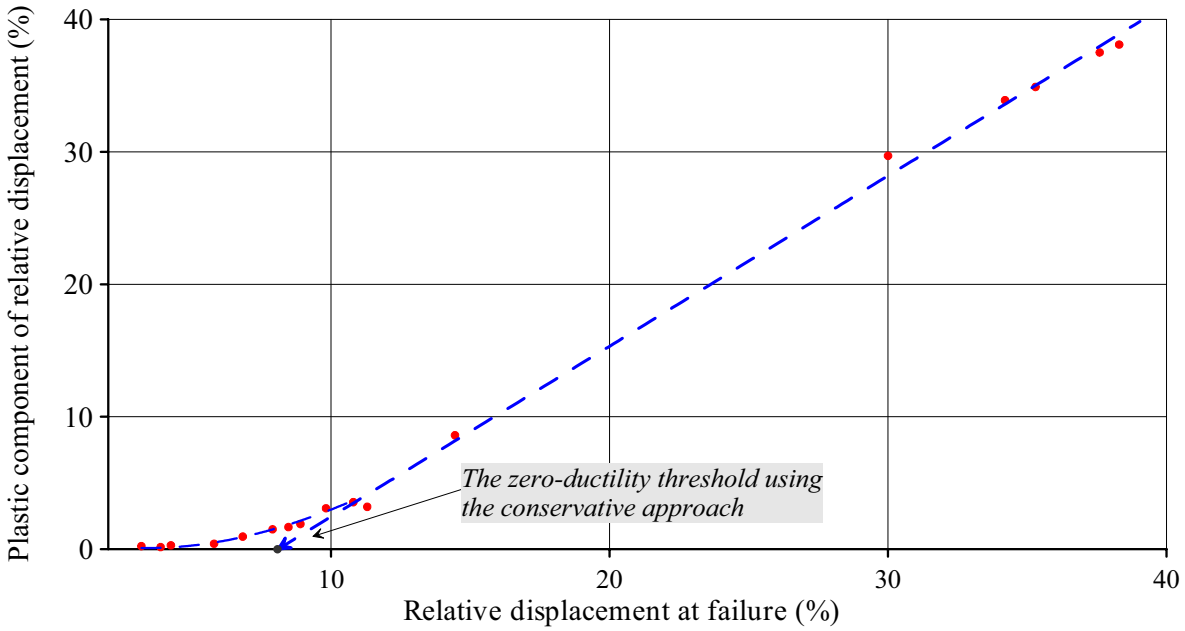

Fig. 3.11. The validation of the procedure for the zero-ductility threshold determination

It should be noted that the term "the plastic component of relative displacement at failure" reflects clearly the physics sense of the appropriate parameter, however, the understanding of this term requires the knowledge of the ring compression test procedure in detail. Therefore, to provide for the understanding of the investigation results by a wide circle of specialists interested in this work, it was decided to replace this term by the term "residual ductility". The term "residual ductility" adequately reproduces the sense of the subject of investigation, on the one hand, and does not require a special study of the procedure for mechanical tests, on the other hand.

The next task of scoping mechanical tests was devoted to the development of the comparative data base for the assessment of sensitivity of the test results to the sample length. The appropriate tests were performed with ring samples the length of which was varied from 8 up to 25 mm. Two oxidized samples 100 mm long were selected for these tests:

- the first sample was characterized by a high margin of residual ductility;
- the second sample was practically brittle.

Fig. 3.12, Fig. 3.13 show the results of these scoping tests.

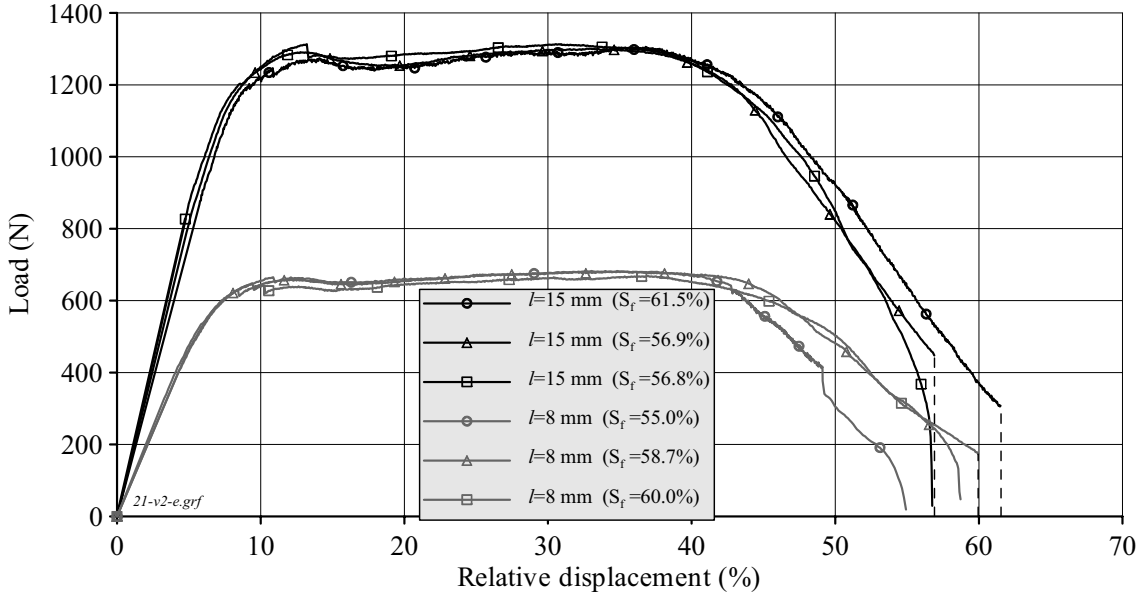

Fig. 3.12. Sensitivity of a relative displacement at failure to the ring sample length for the ductile sample

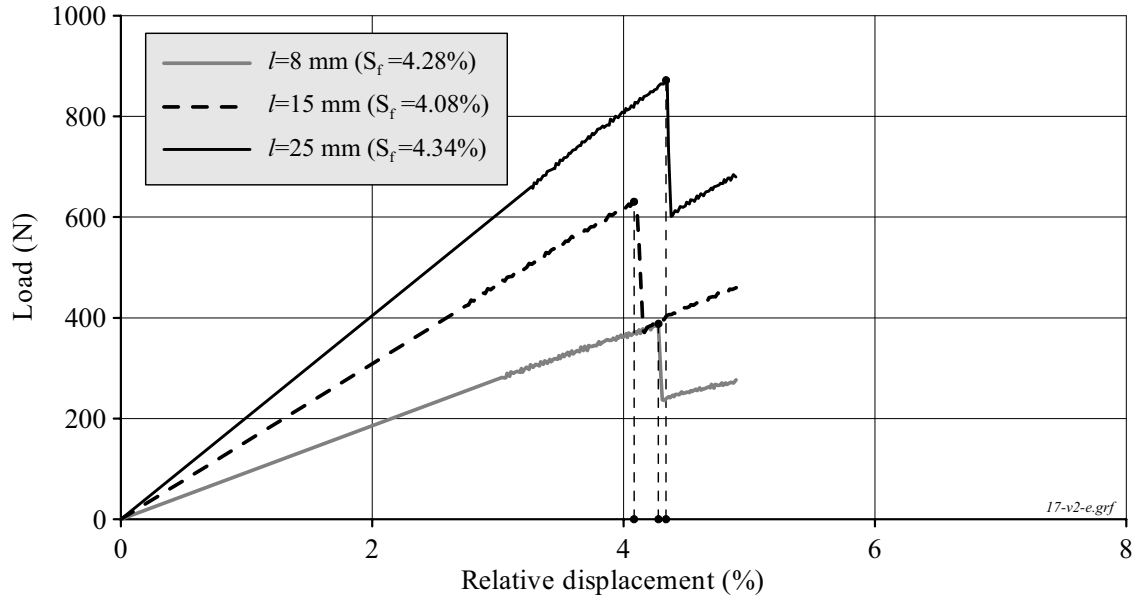

Fig. 3.13. Sensitivity of a relative displacement at failure to the ring sample length for the brittle sample

The analysis of obtained data has allowed to make the following practical conclusion: the relative displacement at failure is independent of the ring sample length. In this case, the increase of the effective modulus of elasticity and maximum load with the sample elongation is quite natural because this effect is explained by a higher stiffness of longer samples. However, it should be pointed out that this conclusion might not be applied to the case when samples of different length were oxidized. As it was already stated, the mechanical behavior of these samples is complicated by the occurrence of end effects (if end parts of oxidized sample were not cut).

The final task of this stage of work was formulated as follows: to develop the experimental data necessary to identify the cladding fracture in load-displacement diagrams obtained from ring compression tests. The appropriate analysis showed that in spite of the evident importance of this issue, the purposeful studies of this subject were performed in neither of the previous programs. The main point of the problem under discussion may be illustrated by the examples presented in Fig. 3.6 and Fig. 3.14.

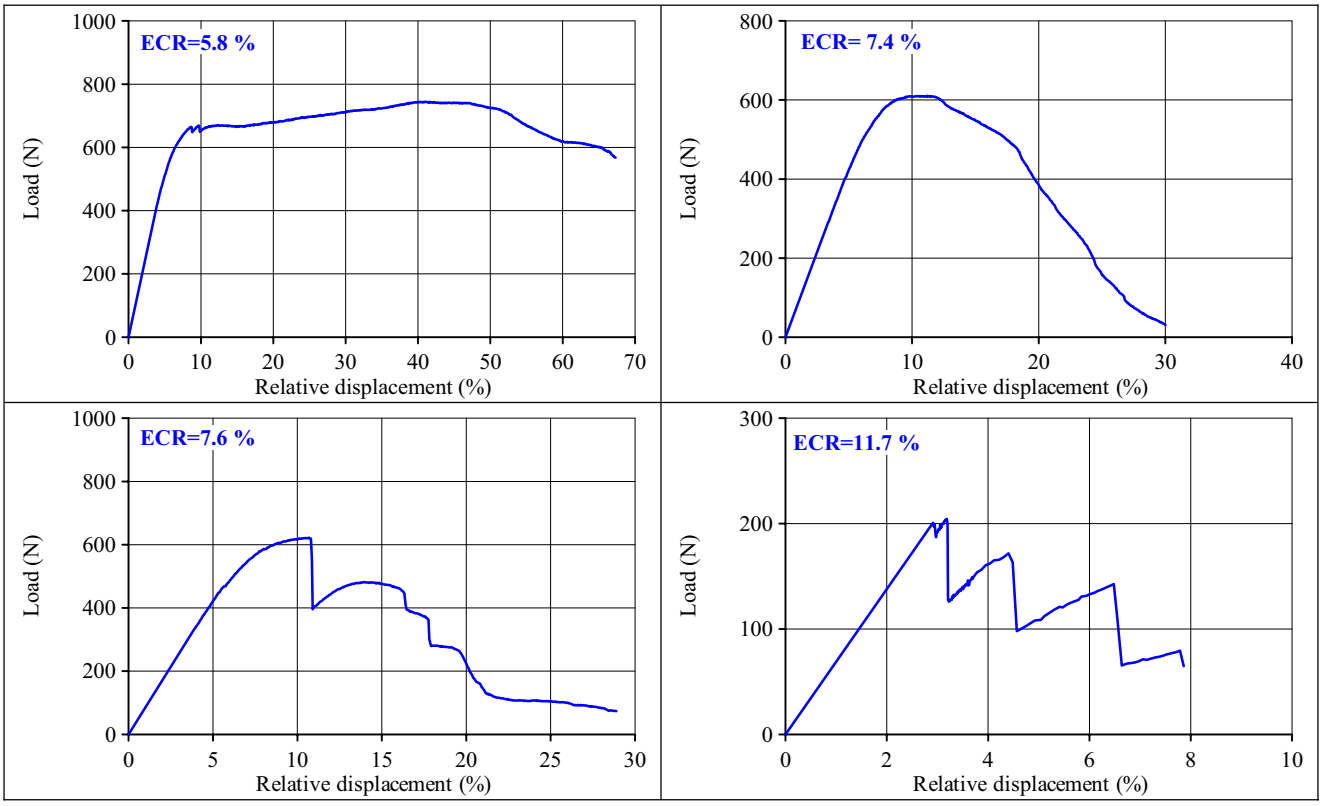

Fig. 3.14. Typical E110 load-displacement diagrams for different oxidation

The obtained results may be divided into two groups:

1. Diagrams with relatively smooth load variation (two upper diagrams in Fig. 3.14).
2. Diagrams with a sharp drop (20% and more) of load with 2–15 % relative displacement (two lower diagrams in Fig. 3.14 and diagram in Fig. 3.6).

Several special tests were performed to interpret sufficiently diagrams of different types. Metallographic cross-sections were prepared from the samples of high residual ductility (a smooth diagram load-displacement). Besides, reference oxidation tests were performed with the ECR two characteristic levels:

3. ECR=5.8 %. The sample with this ECR has a high margin of ductility.
4. ECR=9.9 %. The sample with this ECR is brittle.

Several ring samples were fabricated from each oxidized sample 100 mm long. After that, ring compression tests were performed in accordance with the following outline:

- the ring sample loading up to the occurrence of the first drop of load in the diagram and termination of this sample test;
- the test of the next sample from this batch up to the occurrence of the second drop of load in the diagram and termination of the test;
- and so on.

This approach allowed to visualize the state of the cladding sample in all characteristic points of load-displacement diagrams. Fig. 3.15 demonstrates a typical appearance and cross-section of tested ring samples with a high ductility margin.

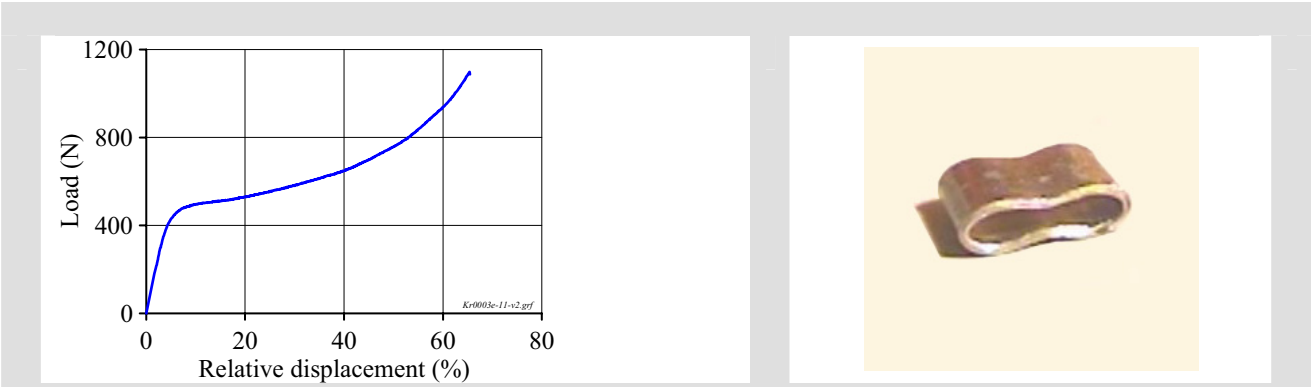

a) unoxidized cladding (appearance of a ring sample after mechanical tests)

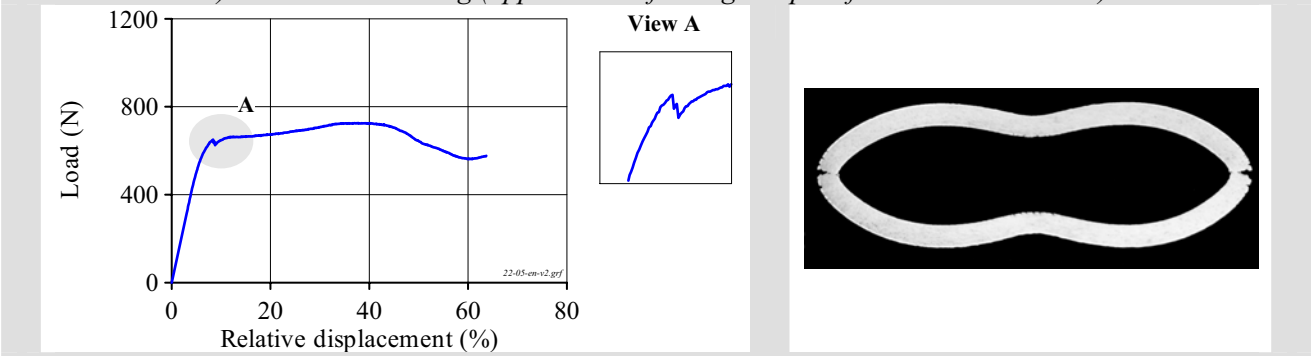

b) oxidized cladding (cross-section of a ring sample after mechanical tests)

Fig. 3.15. Demonstration of the state of ductile claddings after ring compression tests

In accordance with the obtained data, the compression of the unoxidized cladding sample results in its plastic deformation with no indications of failure. The shape of deformed oxidized sample with a high margin of ductility is practically the same as that of the unoxidized sample. However, the comparative analysis of such two phenomena as the drop of load after approximately 40 % displacement and the cross-section view allows to state that two nonthrough sample ruptures appeared in the areas of the maximum tensile stresses. Thus, the low in value and smooth decrease of load indicates the occurrence of a local rupture in the cladding outer layer prior to the β phase. The analysis of the oxidized cladding diagram presented in Fig. 3.15 allows to formulate one more question: what means the local drop of load noted in the diagram on the transfer from the elastic deformation to the plastic deformation (see view A). This question is of sufficient importance because this characteristic area was present in the majority of the load-displacement diagrams.

To answer this question, a series of tests was performed with two rings fabricated from the same sample as the ring shown in Fig. 3.15. Fig. 3.16 presents the results of these tests. The analysis of obtained data shows that the observed load peak is not associated with the cladding failure. This peak indicates the process of formation of microcracks on the cladding surface in the areas of concentrated tensile stresses. The length of these cracks corresponds to ZrO_2 and α-Zr(O) layer thickness. Cross-sections of the ring compressed up to the maximum load (Fig. 3.16b) demonstrate that a growth and some opening of these cracks take place, however, the cladding metal part (the prior β-phase) continues to be deformed plastically.

The next stage of this study was dedicated to the interpretation of load-displacement diagrams having segments with a sharp drop of load. The first type of these diagrams reflects the behavior of oxidized samples with a definite ductility margin (see Fig. 3.6, Fig. 3.14 The lower left diagram). The second type of diagrams characterizes the behavior of a brittle cladding (Fig. 3.14 The lower right diagram). In accordance with this classification, the failure of the following two samples was investigated:

- Zry-4 sample #43;
- E110 sample #25.

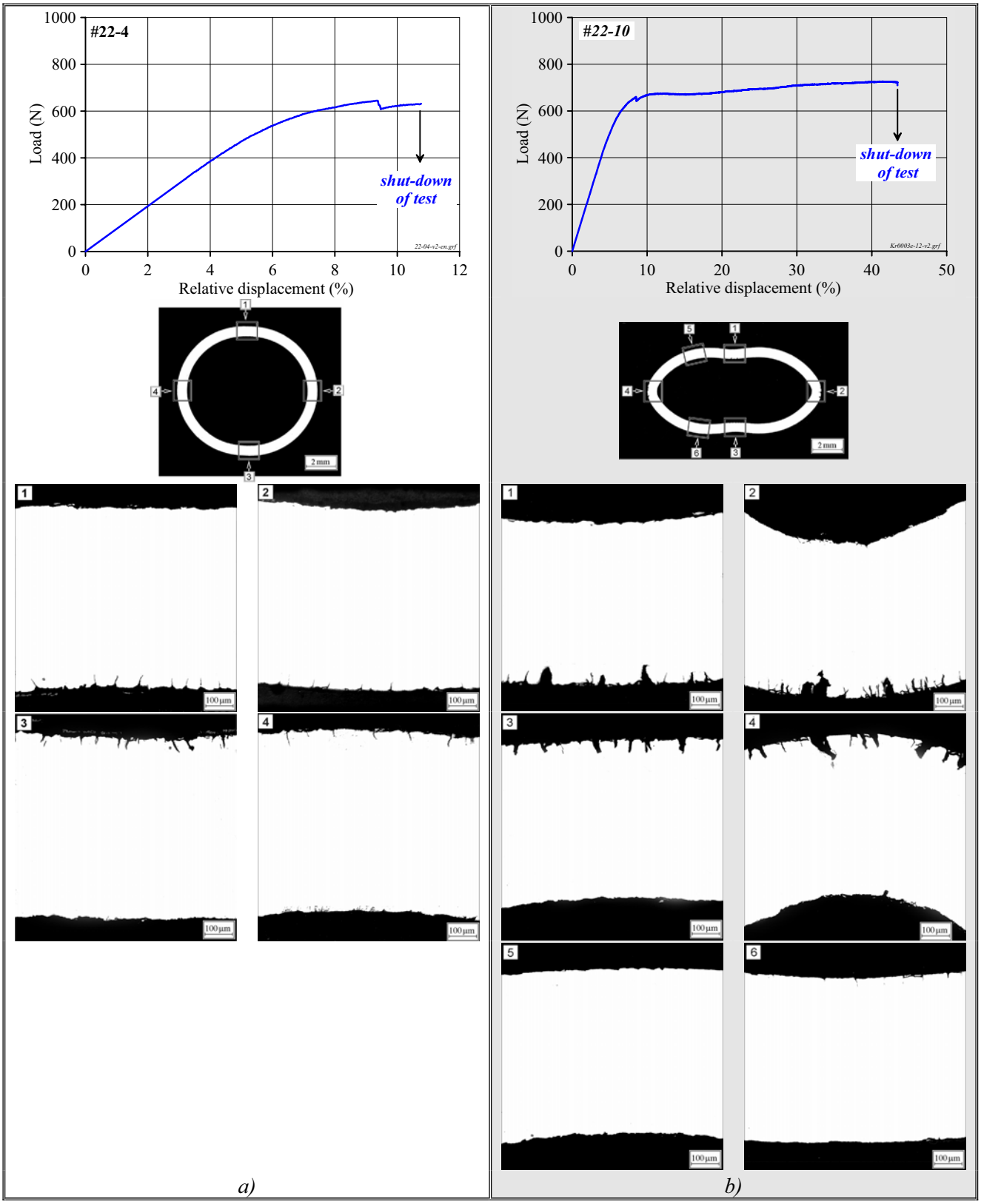

Fig. 3.16. The data base for the interpretation of load-displacement diagrams for oxidized samples with a high ductility margin

The load displacement diagram of Zry-4 samples oxidized up to 11.3 % ECR at S/S combination of heating and cooling rates is shown in Fig. 3.17.

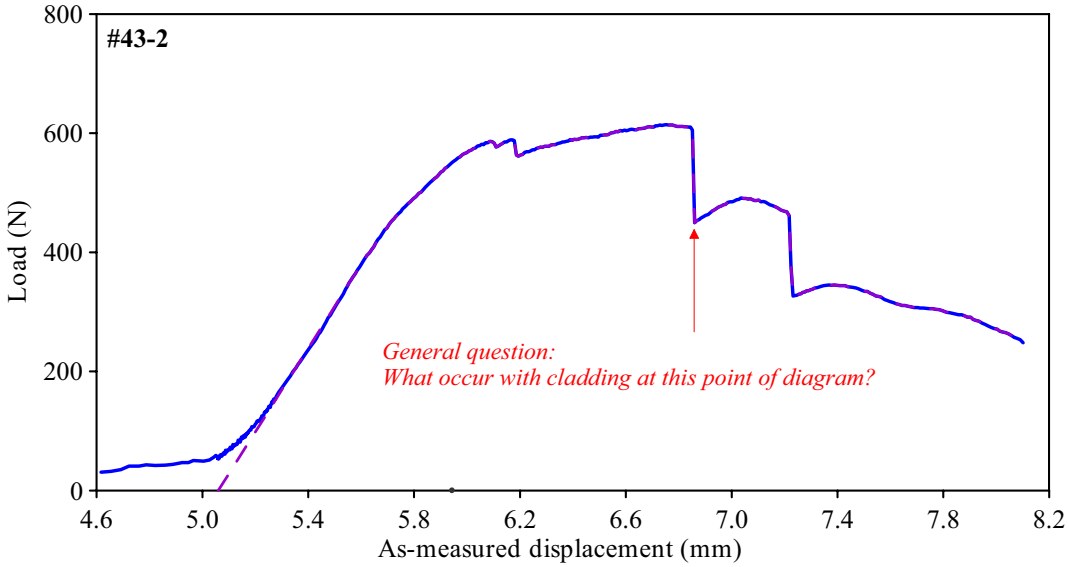

Fig. 3.17. The load-displacement diagram of Zry-4 cladding sample with a partial ductility margin

To get the answer to the question put in Fig. 3.17, additional mechanical tests of two ring samples cut out of the oxidized sample were performed. Fig. 3.18, Fig. 3.19 demonstrate the results of these tests.

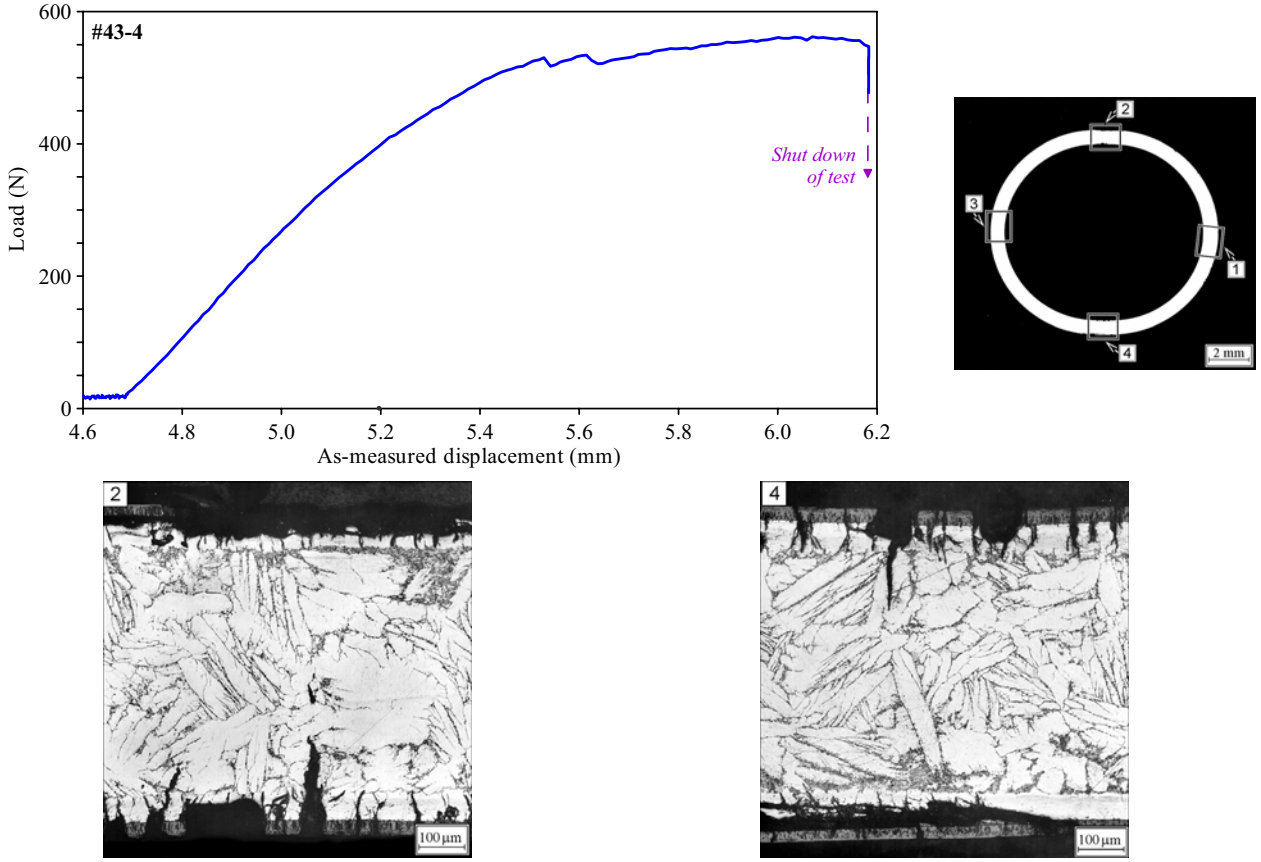

Fig. 3.18. The data base to characterize the mechanical behavior of the cladding sample with a partial residual ductility before the fracture

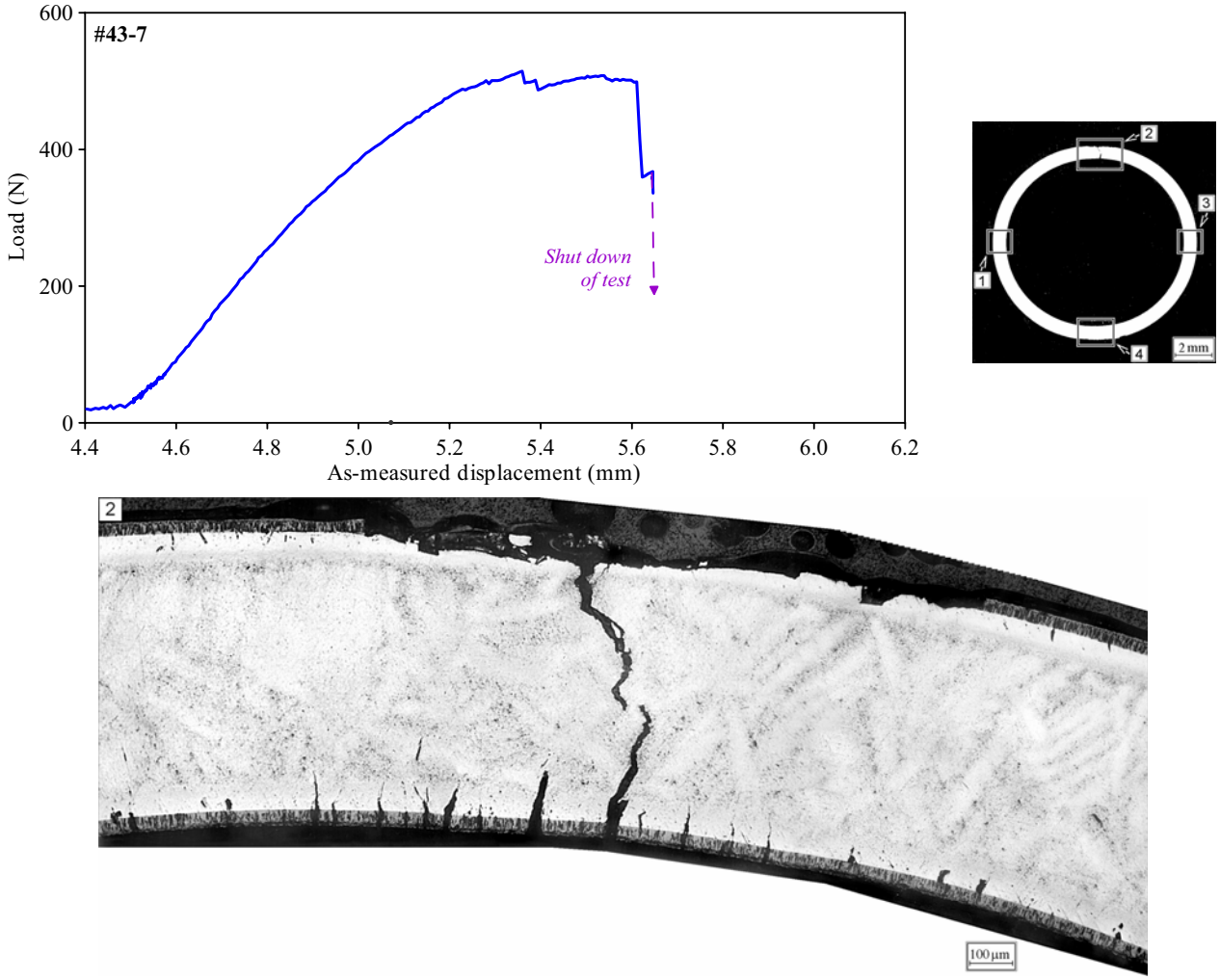

Fig. 3.19. The data base to characterize the mechanical behavior of cladding sample with the partial residual ductility at failure

The compression of the ring sample tested in the first case (Fig. 3.18) was terminated immediately after the sharp load drop was noted. The corresponding sample cross-section made from this ring sample demonstrated that two cracks in prior β-phase were formed on the inside of the sample (that is, on that side which underwent a tensile stress). However, these cracks were not classified as through-wall cracks and, therefore, this test was not accompanied with the cladding failure. The next test was performed with a new ring sample. In this case, the test was terminated at the moment when the load drop not only stopped but the load began to increase again. The analysis of data obtained in this test (see Fig. 3.19) showed that the cladding failure was practically noted. Two cracks formed on the outer and inner sides of the cladding practically joined into the through-wall crack (though, in this cross-section a diminutive bridge of underformed material remained between two cracks).

To supplement the data base necessary to work out the final conclusions on this issue, one more test with the E110 brittle ring sample was performed (see Fig. 3.20).

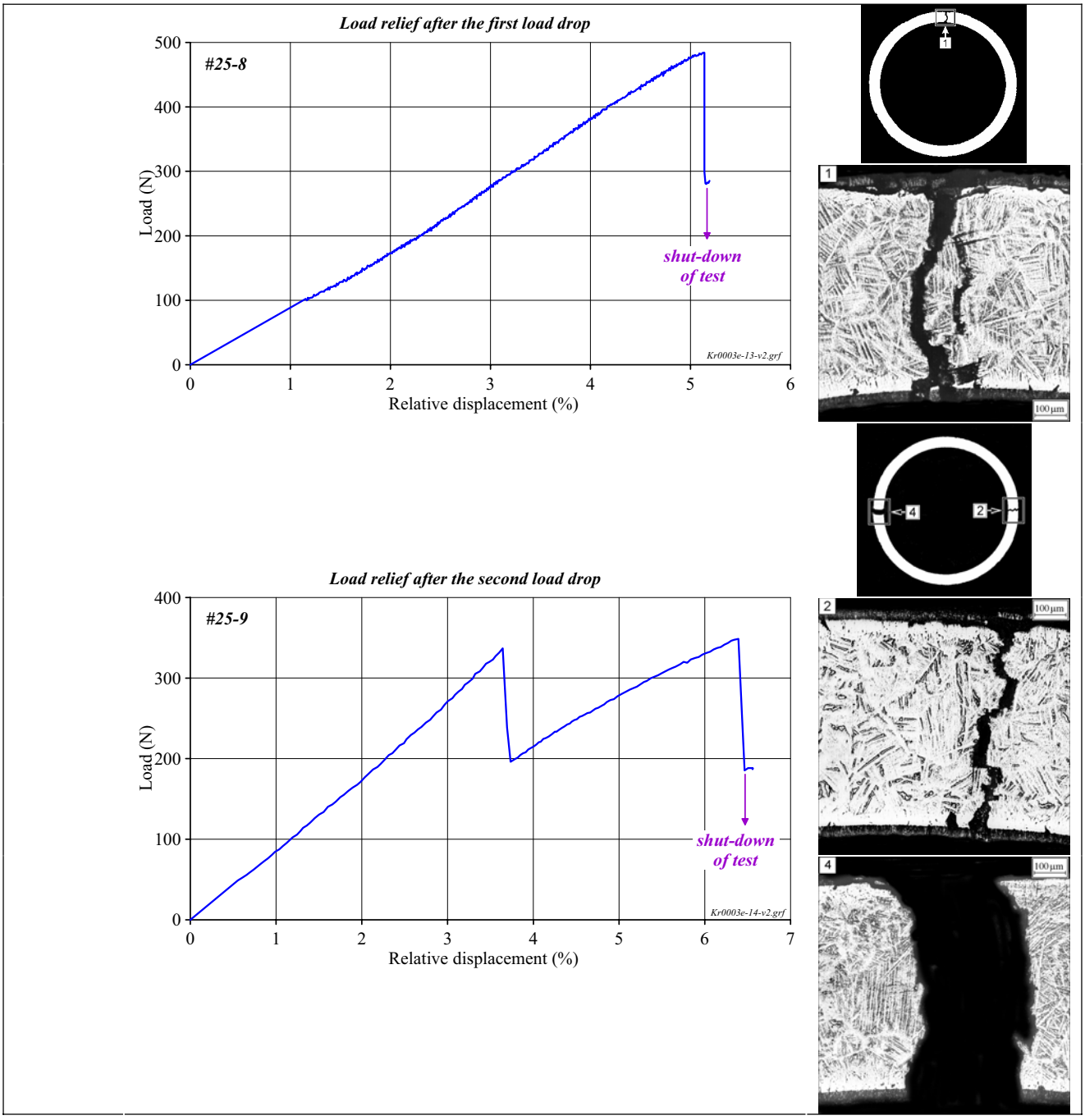

Fig. 3.20. The data base to characterize the mechanical behavior of the brittle ring sample

The analysis of obtained data shows that the first load sharp drop is associated with the formation of the through-wall crack, that is, this point should be qualified as the cladding failure. The second (and the following) load drop indicates the formation of new through-wall cracks in the cladding up to the complete sample fragmentation.

The generalization of all performed investigations allows to make the following conclusions:

- the load displacement diagrams with the monotonic change in the load during the tests (samples with a high residual ductility) are processed using two approaches:

– if the maximum relative displacement is higher than 60 % (see the upper left diagram in Fig. 3.14) it is considered that the sample failure takes place in the point of the sample compression termination (thus, the sample may remain actually unfailed);

– if the maximal relative displacement is less than 60 % (see the right diagram in Fig. 3.14) it is considered that the sample failure takes place at the moment of the load sharp drop.

- the load-displacement diagrams of brittle samples with the low ductility margin (see two lower diagrams in Fig. 3.14) are processed using the following method:

– a local drop of the load (with the value not higher than several tens of newtons) is neglected;

– the moment of the sample failure is determined in the point of the load sharp drop (with the value higher than 100–150 N).

3.2.2.2.Ring tensile tests

Simple ring specimens cut out of the oxidized E110 cladding samples were used for ring tensile tests. Major provisions of these tests were described in [11, 19, 20]. It should be noted that scoping tests necessary to certify the procedure as applied to the oxidized cladding were not provided for in the present research program. Therefore, the obtained results should not be considered as a set of standard mechanical properties for the cladding material. These tests were aimed at the obtainment of a set of experimental data characterizing the tendency towards the cladding ductility reduction as a function of the ECR and at the determination of the zero ductility threshold (the critical ECR). The plastic component of relative displacement (S_{pl}) was determined for each tested specimen in accordance with the procedure presented in Fig. 3.21.

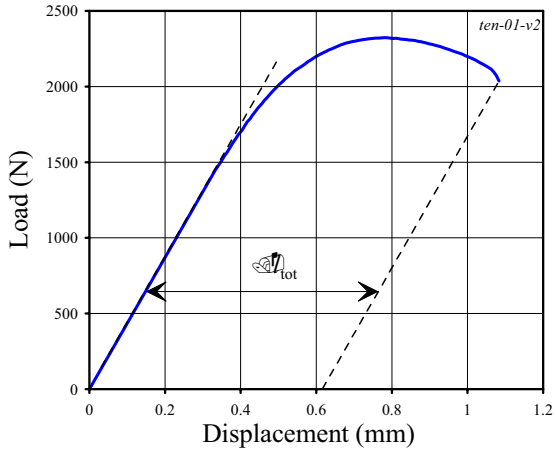

$$S_{pl} = \frac{\Delta l_{tot}}{l_g} 100\ \%,$$

where

S_{pl} – plastic component of relative displacement at failure (%);

Δl_{tot} – total displacement at failure (mm)

l_g – gauge length of a ring specimen (7.85 mm)

Fig. 3.21. Processing of the load-displacement diagram obtained in the ring tensile test of a simple ring sample manufactured from the oxidized E110 cladding tube

3.2.2.3.Three-point bending tests

Three-point bending tests of the oxidized E110 claddings were performed in the universal test machine (1794Y-5) equipped with the device shown in Fig. 3.22.

The oxidized E110 cladding sample 80 mm long was placed on two cylindrical supports of the roller type 5 mm in diameter. The distance between the supports was 70 mm. The third cylindrical roller bearing provided for the impact of the bending load on the cladding sample with the rate of about 1 mm/min. All these tests were performed at 20 C. The load-displacement diagram was recorded during the tests. It should be noted that three-point bending tests of tubular samples were not of the standard type of mechanical tests. Therefore, the experience gained previously in similar tests was specially analyzed [21, 22]. The analysis allowed to formulate the following general requirements imposed on three-point bending tests:

- a roller bearing should be employed as a support and a loading tool to minimize friction during the process of cladding bending;
- the distance between supports must exceed the sample diameter not less than 8–10 times.

Fig. 3.22. Three-point bending test apparatus

The test apparatus illustrated in Fig. 3.22, complies completely with these requirements. Besides that, this approach is in a good agreement with the configuration of similar tests performed with the M5 alloy samples [23].

The major provisions of the result processing procedure for three-point bending tests are shown in Fig. 3.23.

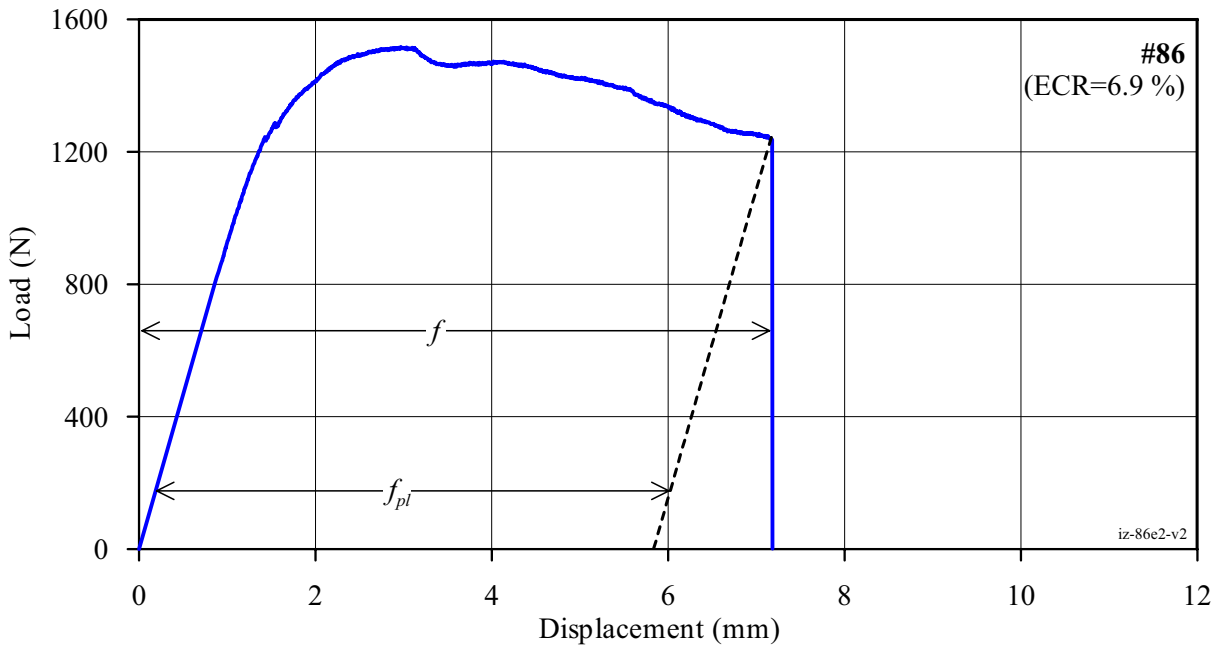

Fig. 3.23. Schematic for the processing of the load-displacement diagram after three-point bending tests

In accordance with the presented scheme, the residual deflection at failure (D_{pl}) as a function of the ECR was used as a result of each three-point bending test.

3.3. Discussion of test results and working out of preliminary conclusions

3.3.1. Reference tests

The goal of reference tests was to determine the dependence of cladding residual ductility on such parameters of the oxidation mode as heating and cooling rates, following which to develop recommendations concerning the oxidation conditions for other stages of the research program. The background of this stage of the work was the following:

- the heating rate defines such processes as the phase transformations ($\alpha \rightarrow \alpha+\beta \rightarrow \beta$) and the diffusion redistribution of alloying and impurity elements in the cladding material, that in its turn predetermines the oxide type (monoclinic, tetragonal) formed on the cladding surface, his protective properties and, as a consequence, H_2 uptake by the cladding material;
- the cooling rate determines specific features of such processes as transition of a high temperature β-phase into low temperature α'-phase as well as the size and distribution of solid hydrides in the prior β-phase of oxidized cladding.

In spite of the fact that the above listed effects were subjected to the attention of many researchers performing similar works, the analysis showed that systematical studies to estimate these effects in the aggregate were not performed. Therefore, the appropriate reference tests were included in this research program in accordance with the following test approach:

- cladding type: as-received E110 tube;
- oxidation type: double-sided;
- isothermal oxidation: 1100 C;
- temperature of mechanical tests: 20 C;
- combination of heating and cooling rates during the oxidation:
  - F/F (fast heating at 25 C/s and fast cooling at 25 C/s);
  - F/Q (fast heating at 25 C/s and quench cooling at 200 C/s);
  - S/S (slow heating at 0.5 C/s and slow cooling at 0.5 C/s);
  - S/F (slow heating at 0.5 C/s and fast cooling at 25 C/s);
  - F/S (fast heating at 25 C/s and slow cooling at 0.5 C/s).

The whole scope of test results obtained due to these tests is presented in Appendixes B, C, D; the organized test results are shown in Fig. 3.24.

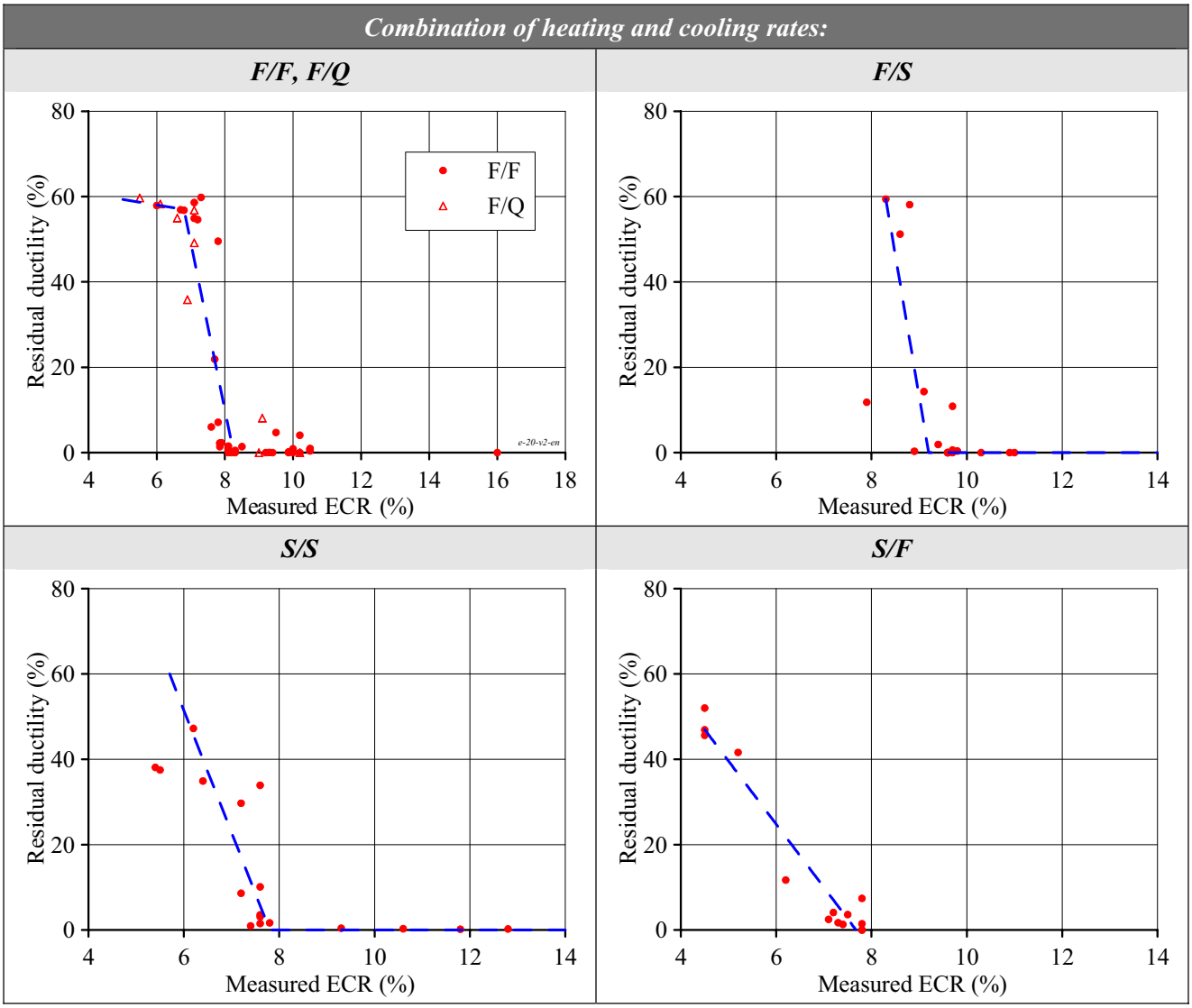

Fig. 3.24. Results of reference tests

The comparative analysis of the mechanical behavior of oxidized E110 claddings after reference tests allowed to reveal the following (see Fig. 3.25):

- the higher the ductility margin in the oxidized cladding, the greater the extent for this margin to be a function of oxidation conditions;
- the less the cladding heating rate and higher the cladding cooling rate, the less degree of oxidation for the proportional decrease of the cladding residual ductility; thus, the decrease of residual ductility down to 40% (approximately 2 times in comparison with the unoxidized cladding) takes place in the following consecution:

– S/F test mode: ECR=5%;

– S/S test mode: ECR=6.3%;

– F/F, F/Q test modes: ECR=7.1%;

– F/S test mode: ECR=8.5%;

- the mechanical behavior of oxidized claddings cooled at 25 C/s and 200 C/s (F and Q) does not differ;
- the closer the cladding is approaching the brittle state, the less its mechanical behavior depends on the studied parameters of the oxidation scenario (see Fig. 3.26) because, apparently, the alloy type is that key factor on which the zero ductility threshold depends.

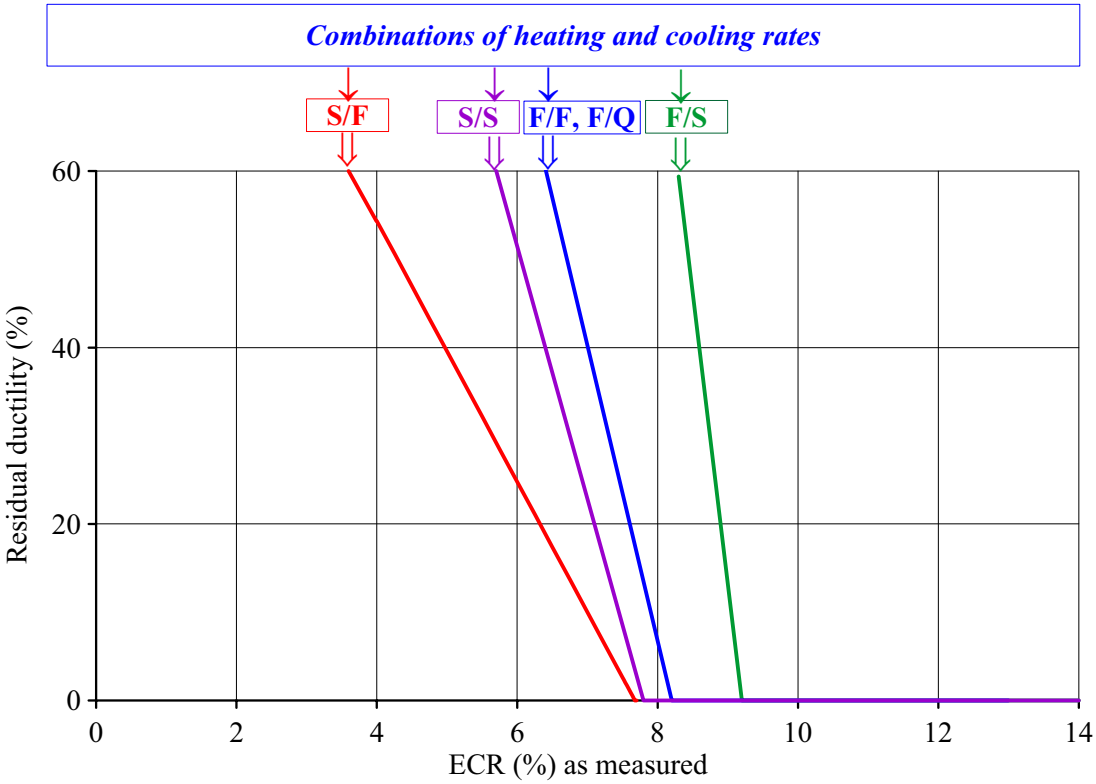

Fig. 3.25. The residual ductility of the E110 cladding vs heating and cooling rates

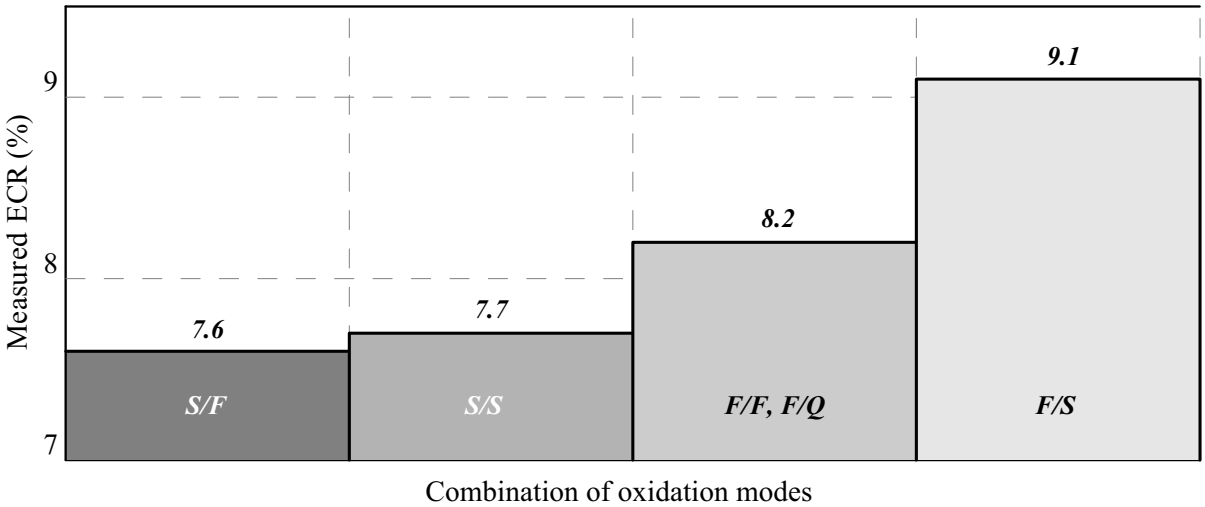

Fig. 3.26. The zero ductility threshold of the E110 cladding vs heating and cooling rates

Thus, the performed reference tests have demonstrated that in spite of the wide range in the variation of heating and cooling rates, the zero ductility thresholds of the oxidized E110 cladding are in the narrow range of ECR (7.9–9.1%). Taking this circumstance into account as well as the fact that slow heating and cooling conditions (used in these tests) are not prototypical for the LOCA analysis and in addition the fact that the difference between the fast cooling and quench cooling was not observed, the following general recommendation was worked out on the basis of reference tests: to perform the oxidation of cladding samples at other stages of the research program at the F/F combination of heating and cooling rates.

3.3.2. The comparative analysis of E110 and Zry-4 oxidation and mechanical behavior

Two cladding samples of Zry-4 alloy were oxidized at 1100 C and F/F, S/S combinations of heating and cooling rates. The oxidation mode with a slow heating and slow cooling was employed to reveal peculiar features in the oxidation of Zry-4 claddings under the most adverse test conditions. The general goals of tests with the Zry-4 cladding were as follows:

- to verify the test procedures and test equipment using the previous test data obtained for the Zry-4 claddings;
- to clarify the major differences in the behavior of the E110 and Zry-4 claddings.

The initial characterization of the Zry-4 cladding and obtained test results are presented in Appendixes A-3, B, G.

3.3.2.1. The verification of test procedures

In spite of the fact that significant efforts have been put into the development and validation of test procedures used for this research, the practical experimental experience shows that the risk of systematical (unaccounted) errors is never too low. Therefore, the only reliable assurance of the fact that these errors are of the acceptable value may be found in the comparison of results obtained in different laboratories employing different experimental apparatus and experimental methods.

The test programs performed in the following countries were selected to compare Zry-4 test results:

- Russia, VNIINM [15];
- Germany, NC Rossendorf [24];
- Hungary, KFKI [25];
- Czech Republic, SCODA-UJP [26];
- France, Framatom [23];
- USA, ANL [27, 28].

The data published for the appropriate tests (table data and numbered graphical output) were used to develop the regression correlations for these six test sets (see Fig. 3.27). The obtained regression correlations are presented in Fig. 3.28.

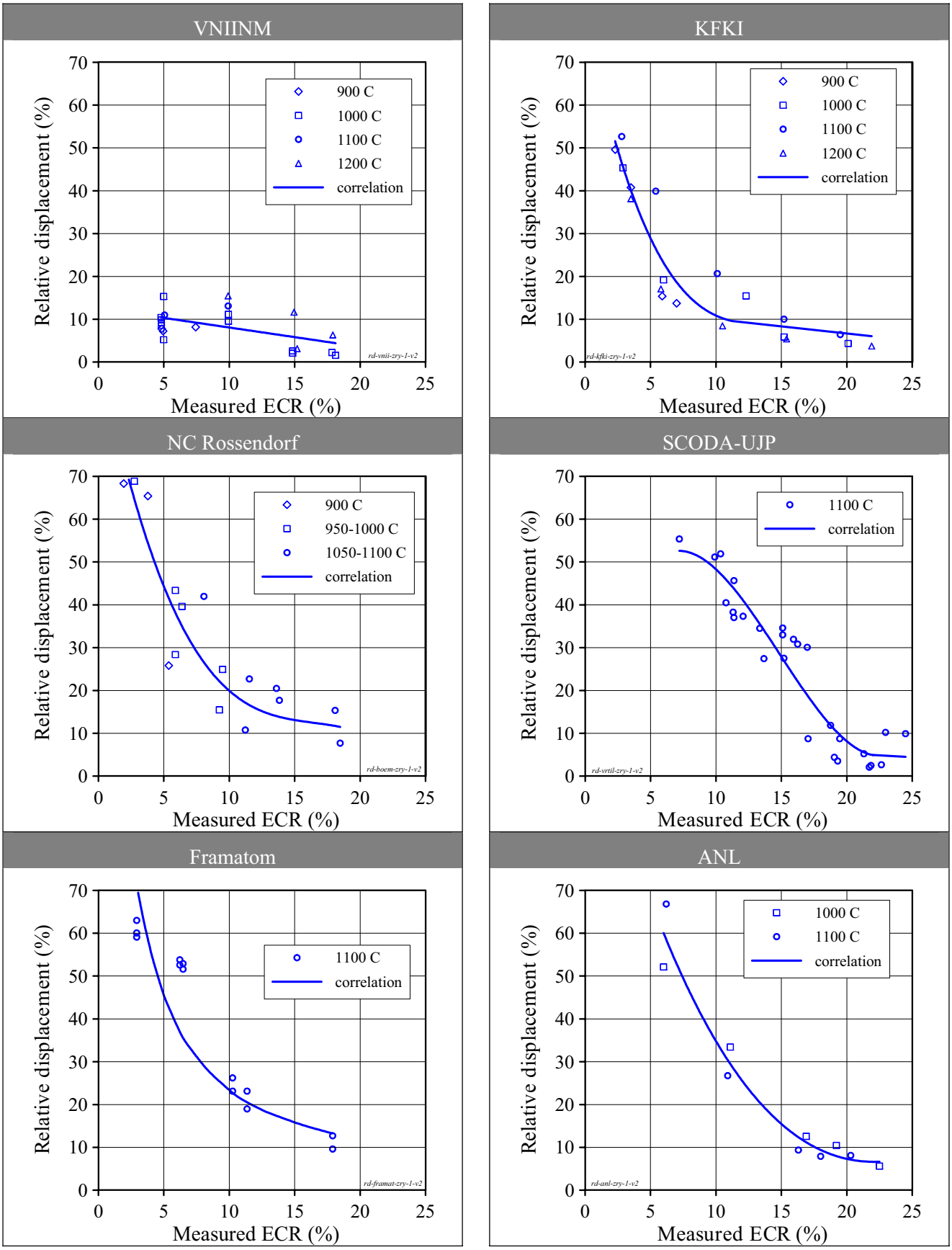

Fig. 3.27. Summary of the ring compression test results performed in different laboratories with the Zry-4 oxidized cladding

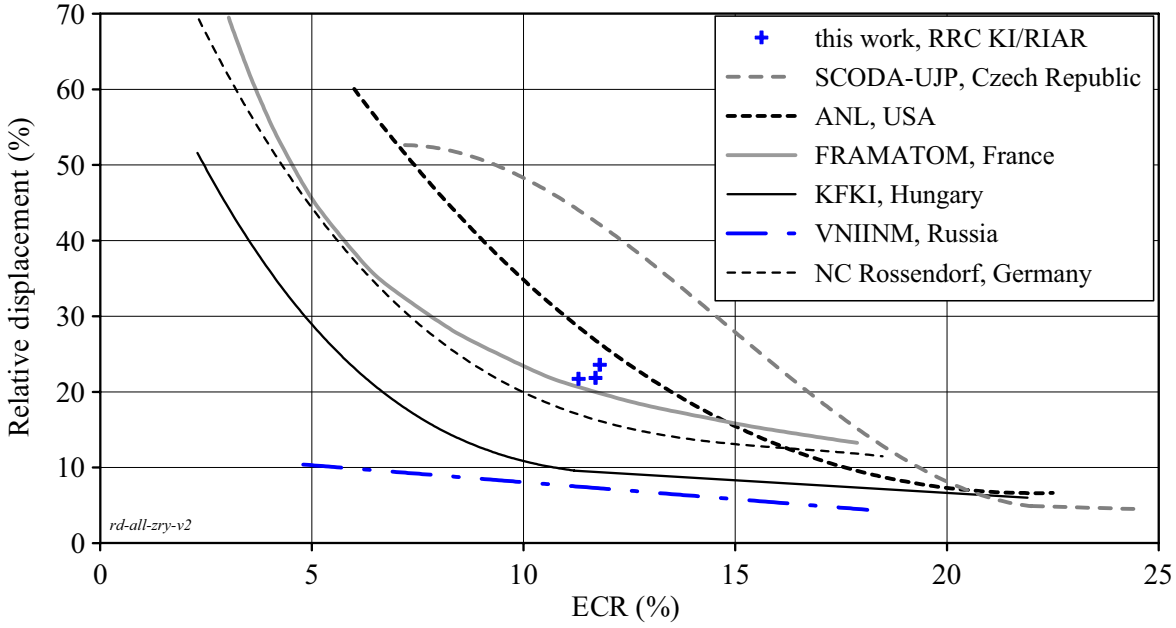

Fig. 3.28. The comparative test data characterizing the ductility of Zry-4 oxidized cladding vs ECR

The comparison of these data with the data obtained by RRC KI/RIAR allows to conclude that:

- the previous VNIINM data [15] must be eliminated from the consideration and, probably, KFKI data [25], also (the motivation to this position will be discussed in the next sections of this Chapter);
- the analysis of the data base confirms the conclusion developed in the section 3.3.1 of this report: "the higher the ductility margin in the oxidized cladding, the greater the extent for this margin to be a function of oxidation conditions". Besides, in this case this margin is a function of the zircaloy type (because the test data base covers more than a twenty-year period, and, accordingly, it cannot be considered that characteristics of tested zircaloy types have been completely identical);
- taking into account the preceding conclusion, different test data in the range 0–10% of the ECR were not compared; as for the presented range of the ECR (10-20%) then everybody can see that the RRC KI/RIAR test data are in the middle of the range for the experimental dispersion of results.

One more proof of the RRC KI/RIAR test data representativity was performed basing of the comparison of data characterizing the Zry-4 oxidation kinetics (see Fig. 3.29).

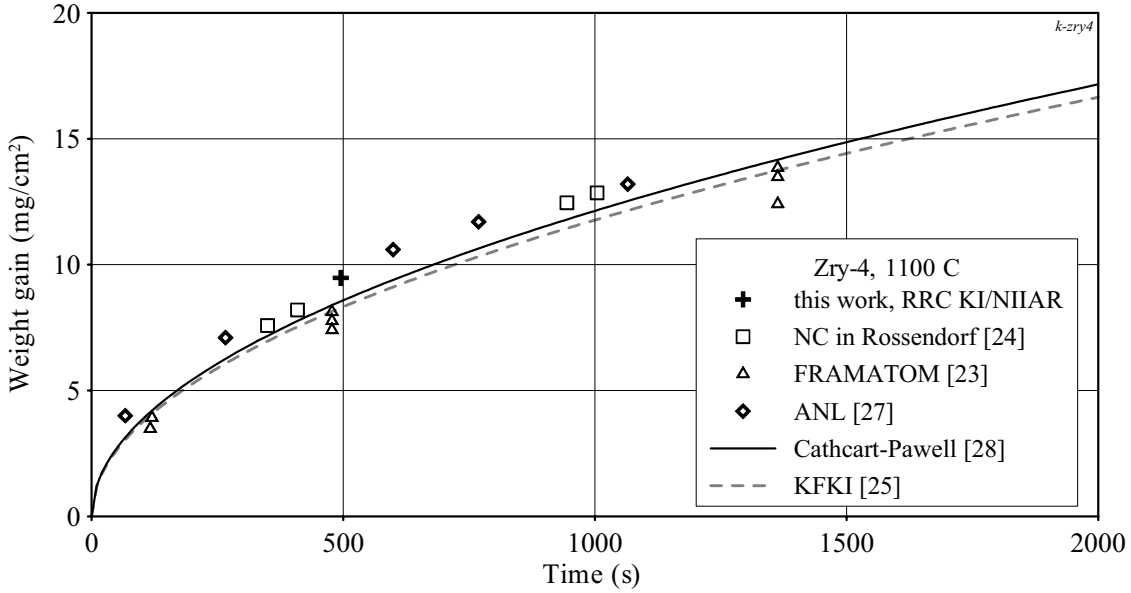

Fig. 3.29. The comparative data obtained in different laboratories to characterize the Zry-4 oxidation kinetics

The analysis of comparative data shows that RRC KI/RIAR data are in a good agreement with the data obtained by other researchers. Consequently, the integral verification the RRC KI/RIAR test approach showed that possible systematical errors connecting with experimental and processing procedures do not exceed reasonable values.

3.3.2.2.The comparison of the E110 and Zry-4 oxidation and mechanical behavior

The comparison of the E110 and Zry-4 residual ductility* as a function of the ECR is presented in Fig. 3.30.

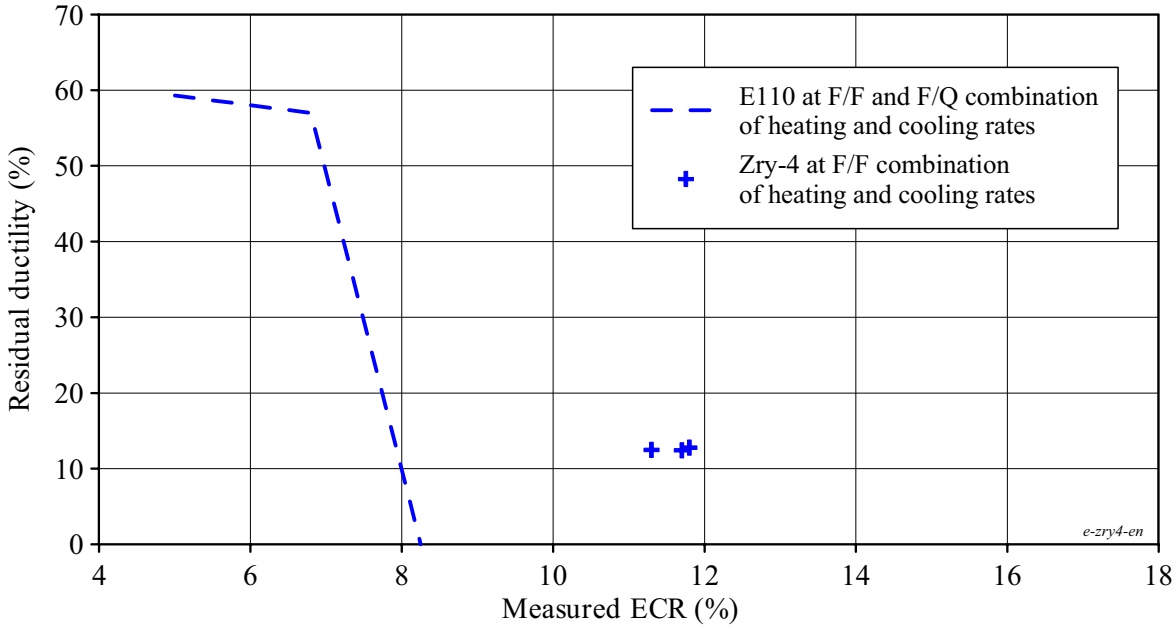

Fig. 3.30. The comparison of E110 and Zry-4 cladding behavior in accordance with RRC KI/RIAR test data

* The characterization of the E110 cladding and test results obtained at 1100 C and F/F, F/Q combinations of heating and cooling rates are presented in Appendixes A–3, B, D

The analysis of these data allowed to state the following:

- the zero ductility threshold of the E110 cladding is 8.3% ECR;
- a sharp decrease of the E110 cladding ductility (from 60% down to 0) occurs in a very narrow range of ECRs (6.7–8.3%) that indicates that some new physical phenomenon takes place in the mechanism of the E110 alloy oxidation;
- in accordance with the data presented in Fig. 3.28 the ductility decrease of the Zry-4 cladding is of a monotonic character, that is, one and the same mechanism accompanies the Zry-4 oxidation in the whole studied range of the ECRs;
- the Zry-4 oxidized cladding has the residual ductility 14.3% (22.4% of the relative displacement) at 11.5% of the ECR.

To clarify the physical phenomena, which are responsible for the revealed differences in the E110 and Zry-4 oxidation behavior, the analysis of data characterizing the appearance of these cladding types was performed first of all (see Fig. 3.31).

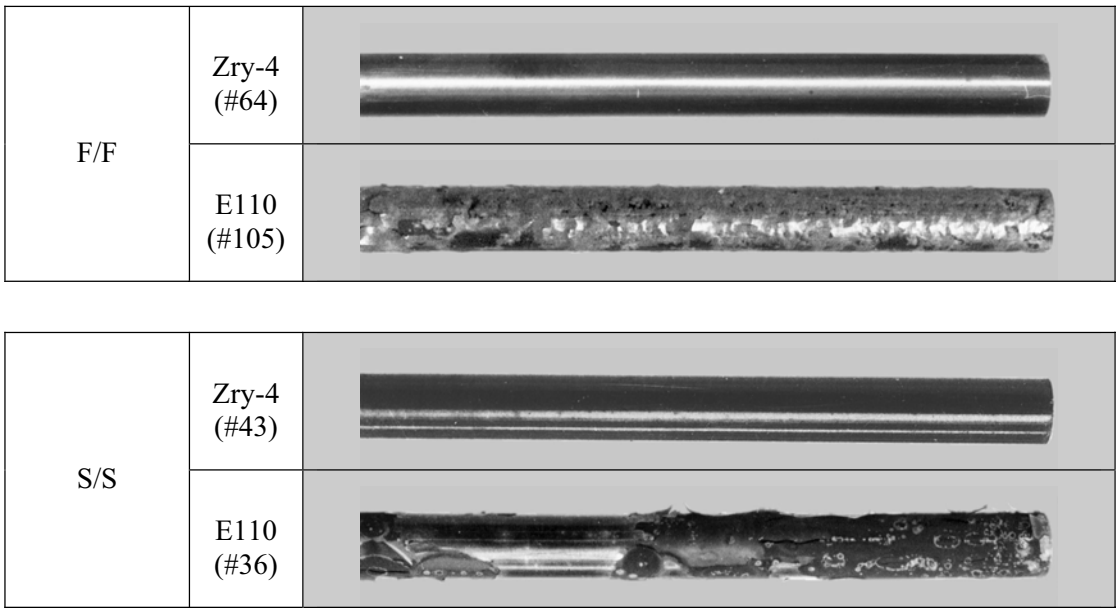

Fig. 3.31. Appearance of the E110 and Zry-4 claddings after the oxidation at 11.3–11.8% ECR and F/F, S/S combinations of heating and cooling rates

These first observations have shown the following:

- the Zry-4 cladding is covered with the lustrous black ZrO_2 oxide in both variants of heating and cooling rates;
- the E110 cladding oxidized at F/F combination of heating and cooling rates has the spalled white oxide on the surface;
- the E110 cladding oxidized at S/S combination of heating and cooling rates has the remains of the lustrous black oxide (outer layer) and very spalled oxide (inner layer).

The noted peculiar features of the oxide state on the E110 cladding surface indicated that the breakaway mechanism of the cladding oxidation took place. In accordance with the data presented in Fig. 3.32, the beginning of this type of oxidation is observed at 6.5% ECR in the form of local white spots on the cladding surface. On the ECR increase, the number of white spots is increased also right up to these white spots joining and producing the outer layer of the spalled oxide.

ECR=6.5%	ECR=7.6%	ECR=7.9%	ECR=14%
#46-9	#65-10	#82-7	#110-4

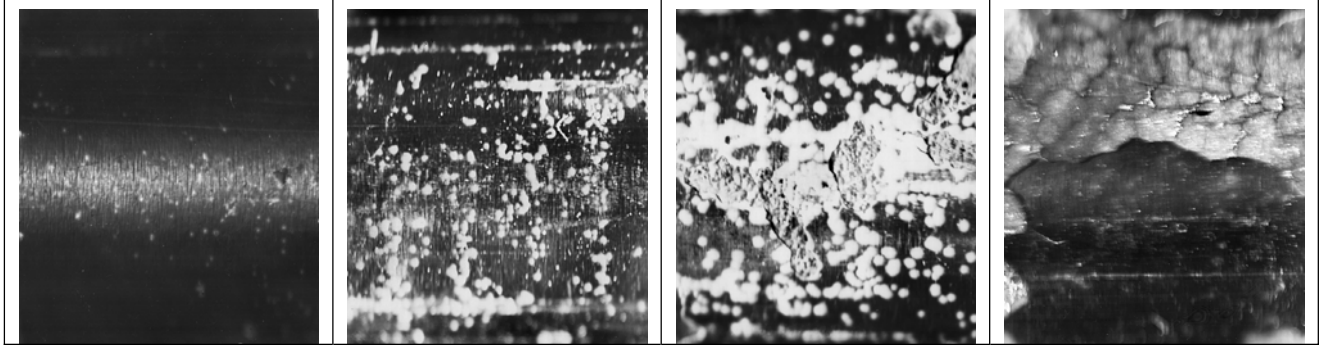

Fig. 3.32. The appearance in detail of the E110 oxidized surface vs the ECR

The additional illustration of this effect presented in Fig. 3.33 shows that two oxide layers are formed on the E110 cladding surface during the oxidation at the ECR higher than 7-8%.

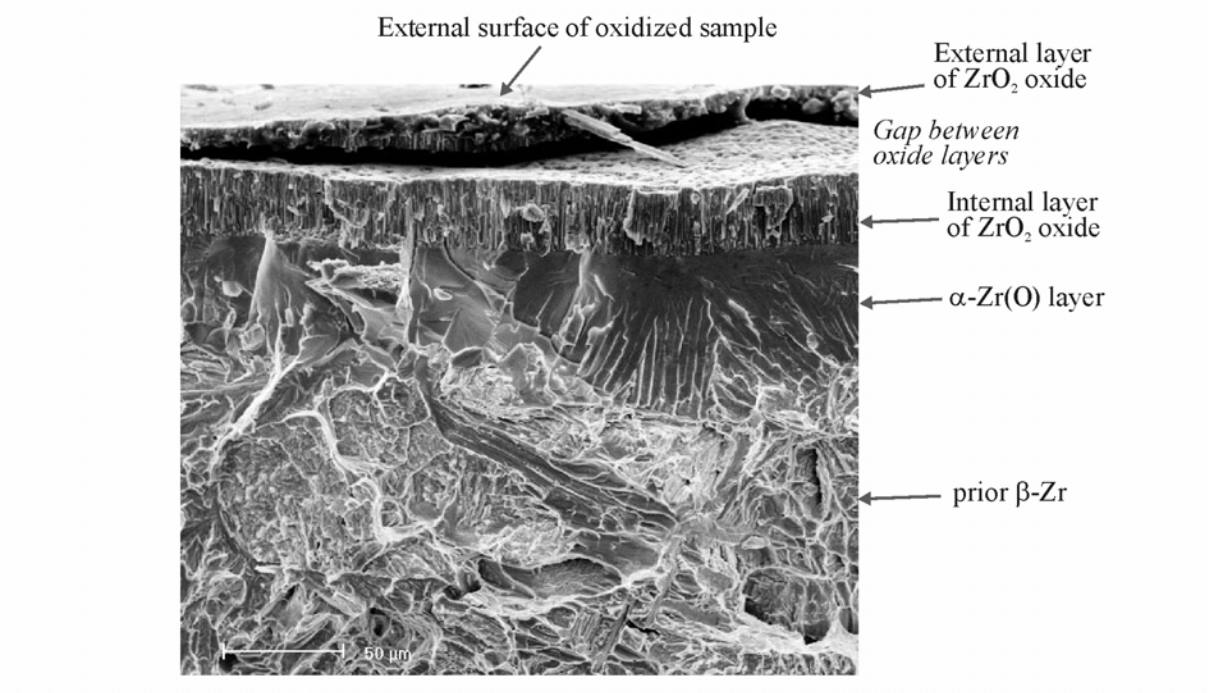

Fig. 3.33. Demonstration of two layers of ZrO_2 oxide on the outer surface of the E110 oxidized standard as-received tube using fractography results

Thus, this stage of the analysis of the E110 specific behavior allowed to determine that the breakaway oxidation occurs in the E110 cladding where breakaway oxidation is not observed in the Zry-4 cladding at 1100 C [13]. Taking into account that the breakaway oxidation may be realized in the form of two different mechanisms (the uniform oxidation and nodular oxidation), additional examinations were performed to study these effects using the metallographic cross-section samples of oxidized claddings (see Appendixes C, D, G).

In parallel with the RRC KI/RIAR studies, several cross-sections of E110 oxidized claddings were prepared in the ANL. The interpretation of the ANL data was made by H.Chung (see Fig. 3.34). In accordance with his position, the nodular type of the breakaway oxidation was observed on the tested E110 cladding samples. The combination of phenomena during the oxidation may be described in the following way [29]:

- "initial development of white nodules;
- coalescence and interconnection of nodules;

- flake-of of gray-white continuous oxide layer".

This point of view was taken as the basis in our previous analysis of this program results [30]. But a more careful analysis of this approach based on the metallographic studies performed by the RRC KI/RIAR has shown that there are some contradictions between this position and the experimental data. To demonstrate the revealed contradictions, the appearances of several oxidized E110 cladding samples are presented in Fig. 3.35.

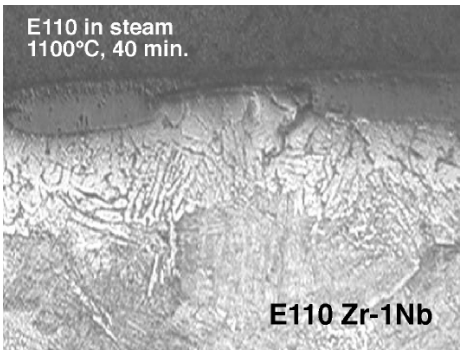

Fig. 3.34. Cross section of the oxide nodule in the E110 cladding

ECR=6.5%	⇒	The microeffects of breakaway oxidation	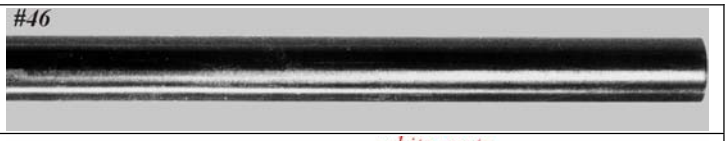
ECR=7.9%	⇒	The macroeffects of breakaway oxidation	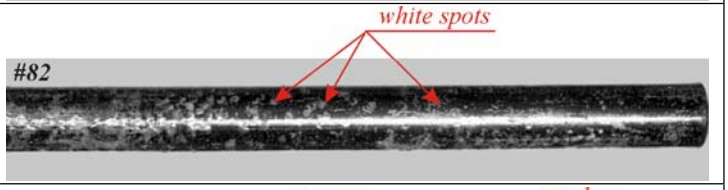
ECR=10.5%	⇒	The heaving of large parts of oxide in the crater form, cracking of oxide	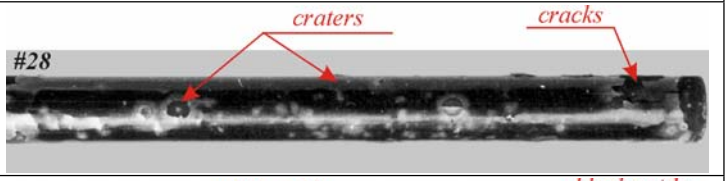
ECR=14%	⇒	The oxidation of previous separated parts into the stoichiometric white oxide	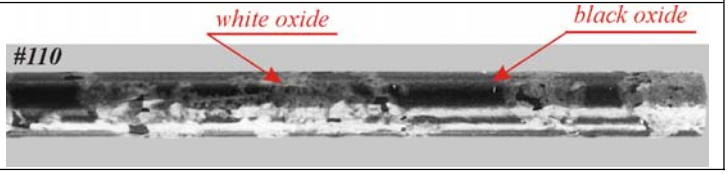

Fig. 3.35. The characterization of the oxidized E110 claddings vs ECR

Thus, if we are based on the concept of the nodular corrosion as the only mechanism determining the E110 cladding behavior as a function of the ECR then it should be expected that the cladding samples will be so much more white the higher is the ECR value. However, analyzing the appearance presented in Fig. 3.35 it can be seen that this thesis is confirmed while turning from the sample #46 to the sample #82 and is not confirmed if to turn from the sample #82 to the sample #28 (as the major part of the sample #28 is covered by the lustrous black oxide having several separate big defects of the crater type, microcracks and the explicit tendency to the whole oxide layer exfoliation from the cladding surface). On the further ECR increase (the sample #110) it may be observed that these sections (separated earlier) of the tetragonal oxide layer located under the stoichiometric oxide are oxidized into the white stoichiometric oxide, while the oxide sections retaining the adhesion with the cladding material remain lustrous and black.

To investigate these processes in more detail, metallographic samples of oxidized cladding were studied. The general tendency of processes, which take place in the E110 cladding as a function of ECR, may be characterized using the data presented in Fig. 3.36.

The consideration of these data confirms that:

- the uniform oxide layer is formed on the E110 cladding surface at the ECR<6.5%;
- at the ECR=8.9% the formation of local parts is observed in which oxide is separated into individual layers due to cracking. In this case, at least the upper layers are of the stoichiometric oxide and are perceived as white spots on the visual inspection.

Thus, the preliminary consideration of the nature of the E110 high temperature oxidation allows to determine that the beginning of the E110 oxidation process is accompanied by the initiation of the breakaway oxidation in small local points of the cladding surface, and this oxidation stage can be characterized as the nodular breakaway oxidation. But the analysis of a number of metallographic samples prepared to observe this process (see Appendixes C, D) has shown that on the ECR increase up to approximately 7% these primary effects remain on the oxide outer surface but are not developed into the depth. Therefore, a typical view of a developed stage for the nodular breakaway oxidation presented for the comparison in Fig. 3.37 is not observed in the tested cladding samples. Moreover, a special set of metallographic samples prepared to reveal the space geometry of oxide layers (see Fig. 3.38) allows to reveal that quite an even boundary separates the α-Zr(O) from the outer and inner oxide layers.

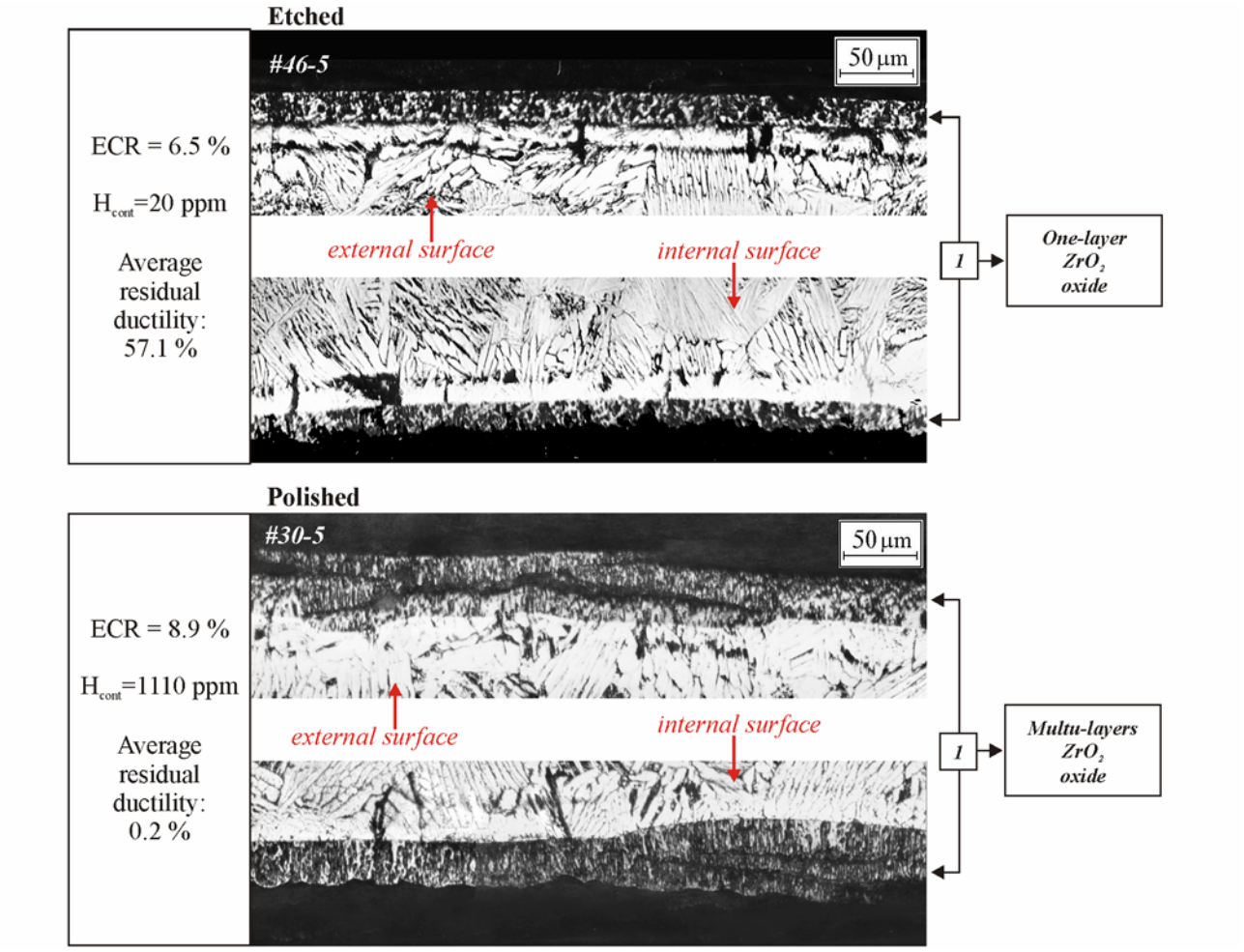

Fig. 3.36. Visualization of ZrO_2 oxide behavior as a function of the ECR after the double-sided oxidation at 1100 C (F/F combination of heating and cooling rates) of E110 standard as-received tubes

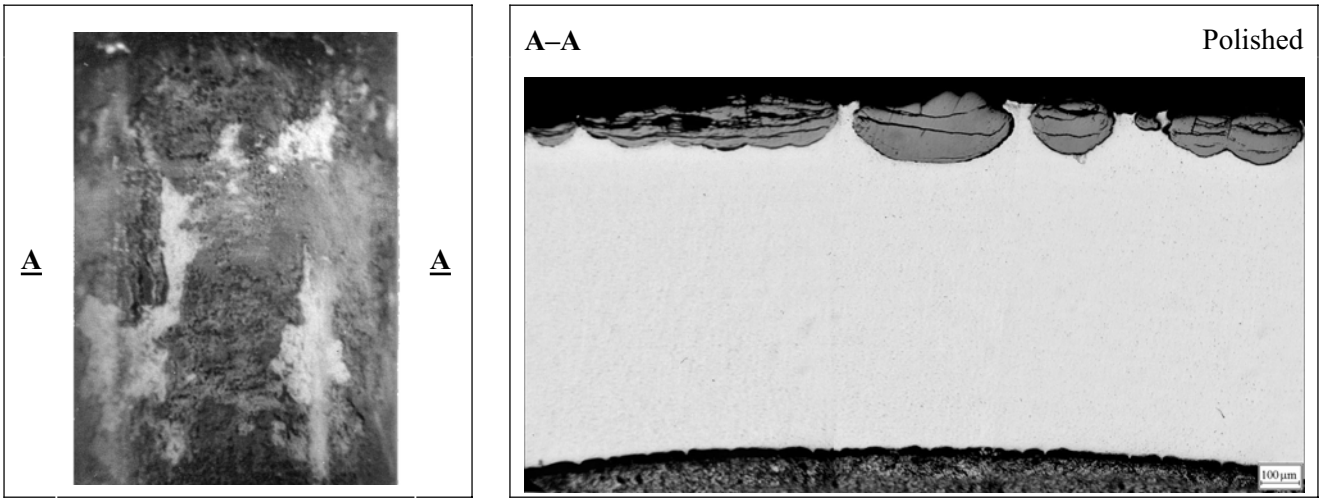

Fig. 3.37. The appearance and microstructure of Zr-Nb oxidized cladding after the operation with the surface boiling (RBMK cladding type)

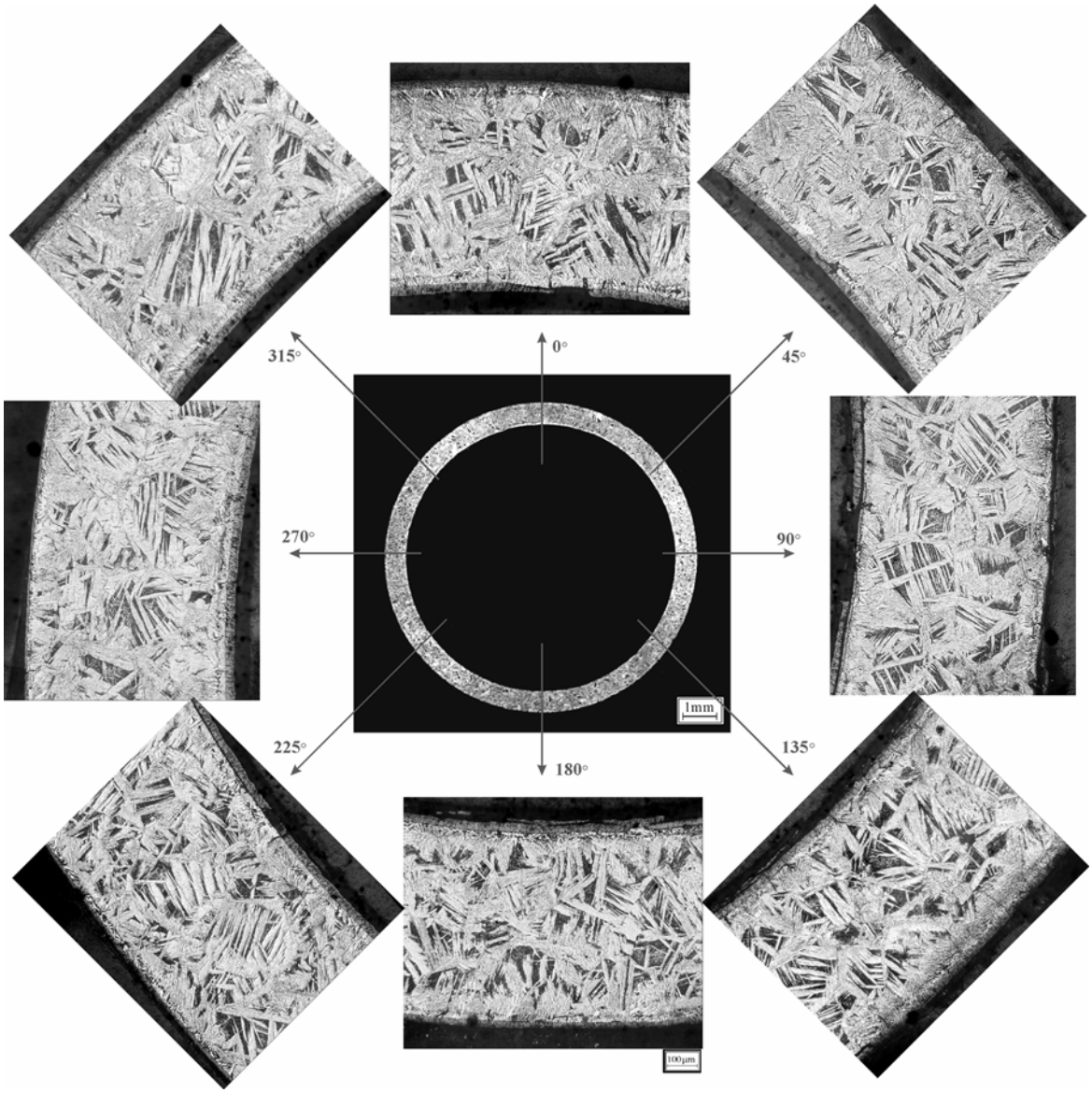

Fig. 3.38. Angular variations of the E110 standard as-received tube microstructure after a double-sided oxidation at 1100 C and 10% ECR (sample #17)

The analysis of the E110 breakaway oxidation nature will be continued in other sections of the report. But to complete the comparison of the E110 and Zry-4 oxidation and mechanical behavior, several other important phenomena are considered in this paragraph:

- oxidation rate;
- the α-Zr(O) thickness;
- oxygen absorption and distribution in the prior β-phase;
- hydriding of prior β-phase.

As for first position of the list, this research confirms that the E110 oxidation rate is somewhat less then that of zircaloy. However, for the objectives of this research it may be considered that the E110 and Zry-4 oxidation kinetics are comparable.

The next important factor influencing the mechanical behavior of the oxidized cladding is the α-Zr(O) phase thickness. A typical feature for the Zry-4 cladding oxidation behavior at high temperatures is the formation of three concentric layers in the oxidized cladding (see Fig. 3.39): ZrO_2, α-Zr(O), prior-β phase.

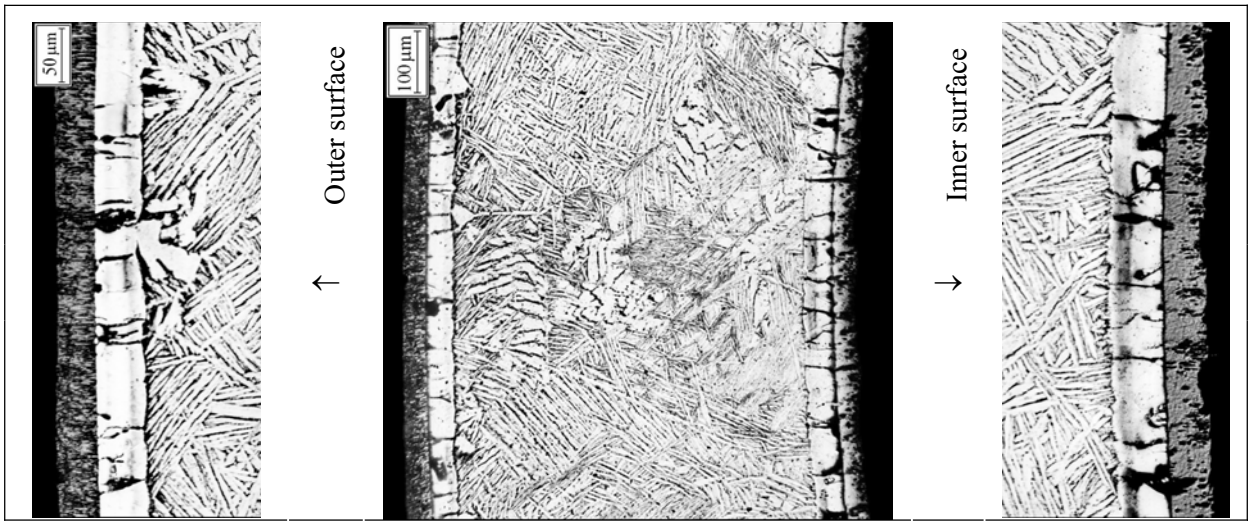

Fig. 3.39. The microstructure of the Zry-4 cladding (sample #64) oxidized at 11.5% ECR at F/F combination of heating and cooling rates

In the Zr-Nb claddings (in contrast to Zry-4), the α-Zr(O) phase (in the form of needles) penetrate deeply into the prior-β phase producing an irregular boundary between these phases. Moreover, as a rule, the boundary line in these phases cannot be legibly determined (see Fig. 3.40).

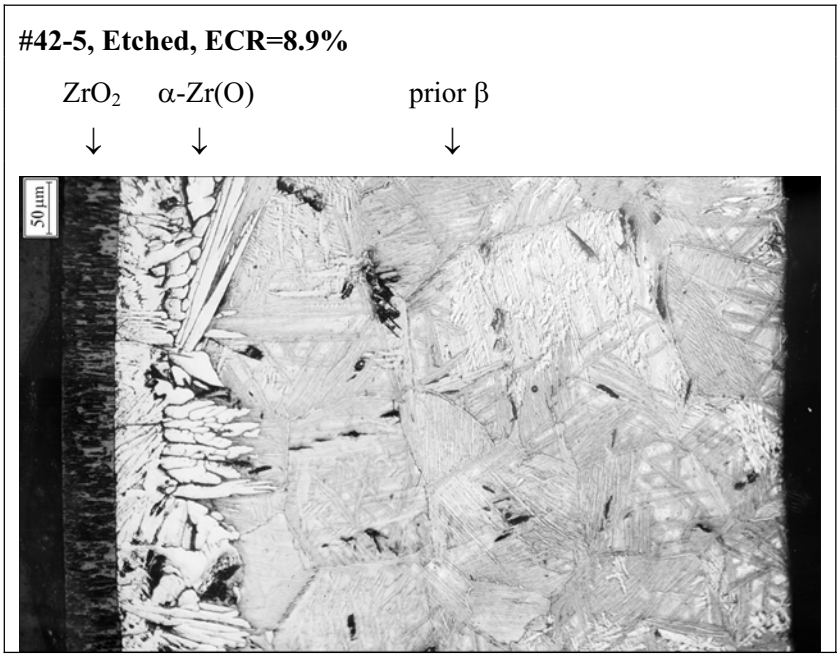

Fig. 3.40. The microstructure of the E110 cladding after a single-sided oxidation at 1100 C

This peculiar feature of the Zr-Nb claddings is supplemented with the fact that the α-Zr(O) layer in the E110 cladding is noticeably thicker then that in the Zry-4 one (see Fig. 3.41).

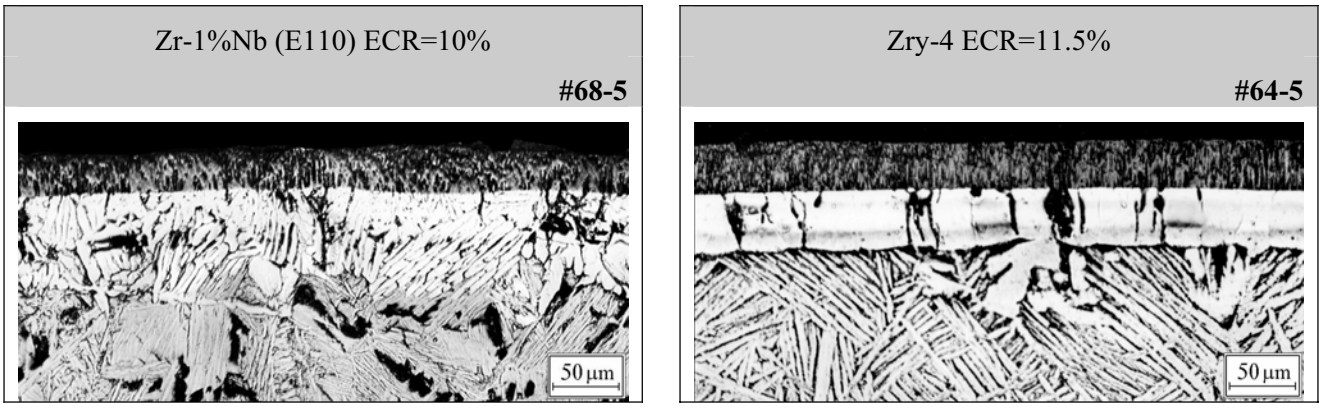

Fig. 3.41. The comparative data characterizing the ZrO_2 and α-Zr(O) thickness

To clarify oxygen absorption by the E110 cladding under oxidation conditions, several special investigations were performed including such methods as:

- the measurement of microhardness across the cladding thickness;
- the measurement of oxygen concentration across the cladding using the Auger spectrometry;
- the determination of oxygen concentration across the cladding using the SEM (scanning electron microscopy) technique.

The comparative data characterizing the microhardness and oxygen distributions in the cladding sample #41 presented in Fig. 3.42 confirm the known thesis that the microhardness distribution corresponds to the oxygen distribution. Besides, both types of test data allow to support the following conclusion formulated earlier [24]: oxygen is uniformly distributed in the prior β-phase of the E110 cladding in contrast to the Zry-4 cladding.

To reveal the character of oxygen distribution in the ZrO_2, α-Zr(O) and prior β-phase of the E110 oxidized cladding, the SEM examinations of the reference cladding sample were performed using the XL 30 ESEM-TMP scanning electron microscope (FEI/Philips Electron Optics) equipped with INCA Energy

300 (Oxford Instruments) EDX (energy dispersion x-ray analyzer). Those allowed to formulate several observations concerning oxygen behavior in the E110 claddings (see Fig. 3.43):

- oxygen concentration in the α-Zr(O) phase of the niobium-bearing cladding is monotonically decreased from the metal-oxide interface down into the depth of α-Zr(O) layer;
- non uniform distribution of oxygen concentration across the ZrO_2 layer has been revealed using the electron probe microanalysis, besides, the secondary electron image of zirconium dioxide has shown that two different types of ZrO_2 are observed on the surface of the reference cladding sample;
- in accordance with the results of investigations performed to interpret similar processes taking place in zircaloy claddings during the base irradiation (see, for illustration [31]), the oxide of this type consists of the outer layer, in which the monoclinic phase (stoichiometric white oxide with the maximum oxygen concentration) of zirconium dioxide prevails, and of the inner layer which represents the tetragonal modification (understoichiometric oxide with lower oxygen concentration).

Appearance of the E110 cladding after the oxidation at 8.2% ECR	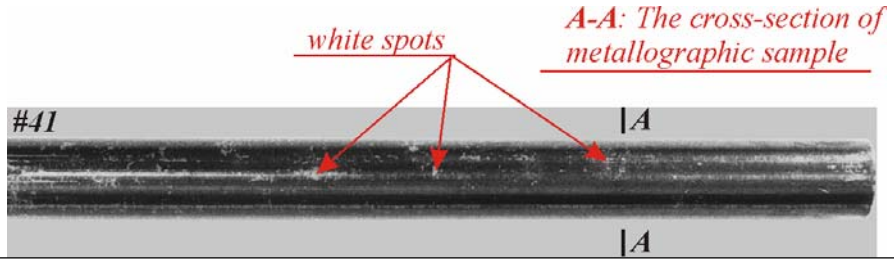
Microstructure of the oxidized cladding (etched)	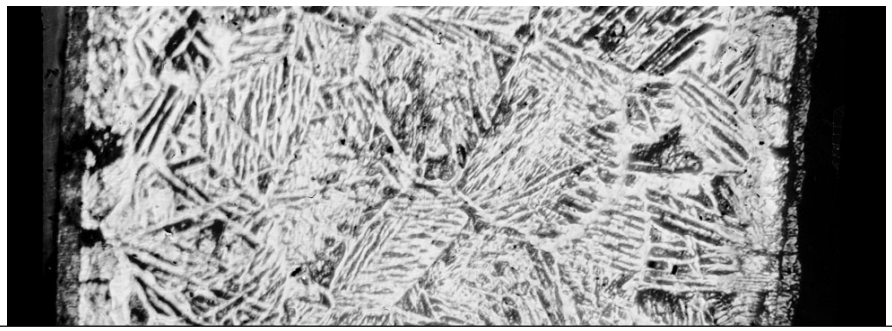
Microhardness across the cladding thickness	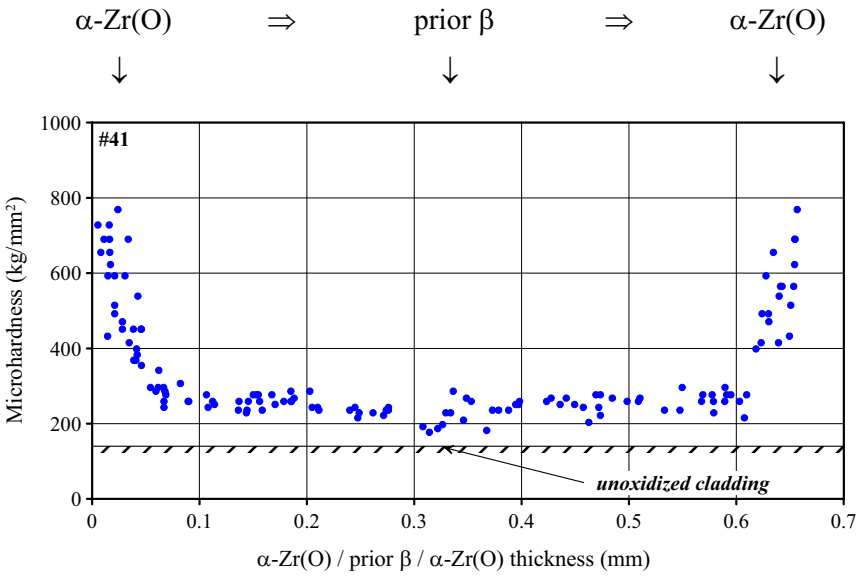
The oxygen distribution across the cladding determined by the Auger analysis	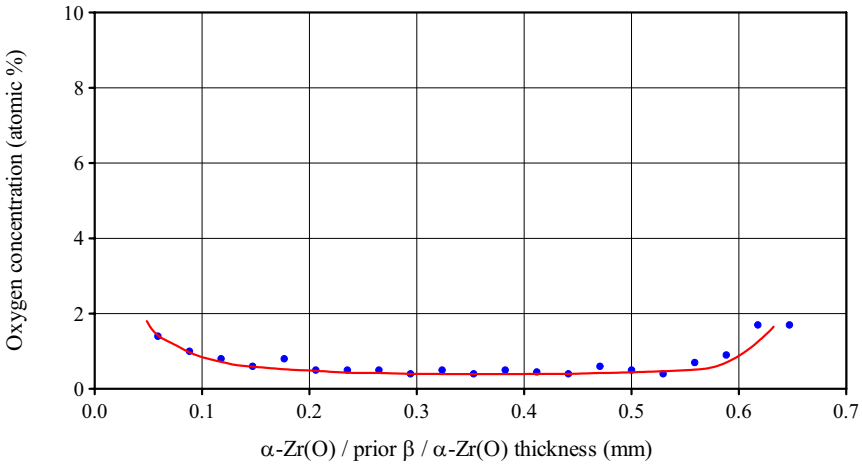

Fig. 3.42. The appearance of microstructure and characterization of oxygen distribution in the E110 cladding after the double-sided oxidation at 1100 C

Secondary electron image of the sample #41-4 with four tracks of oxygen concentration measurements	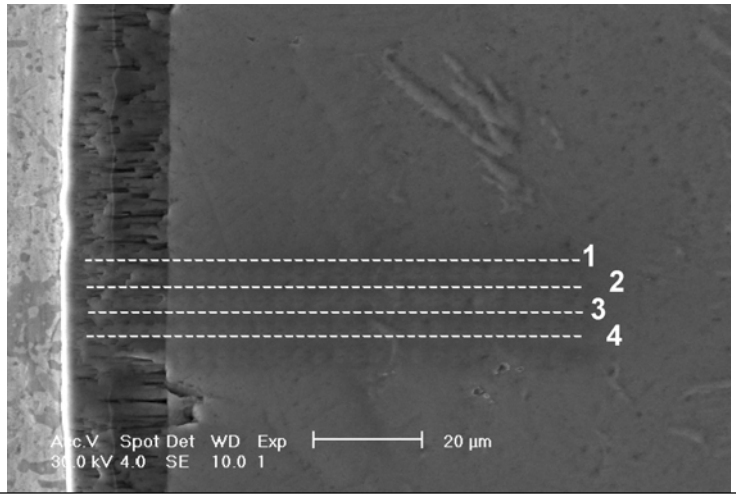
EPMA results (Electron probe x-ray analysis) characterizing the oxygen distribution Comments: 1. Averaged data on four tracks is presented 2. Measurements at the low oxygen concentration in the prior β-phase are more qualitative than quantitative. The systematic error in the measured data was caused by the parasitic oxidation of the sample surface	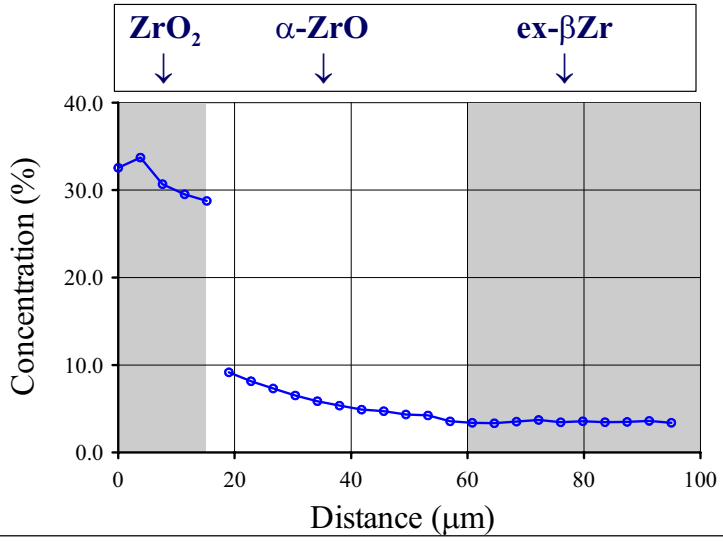
Oxygen EDX dot map	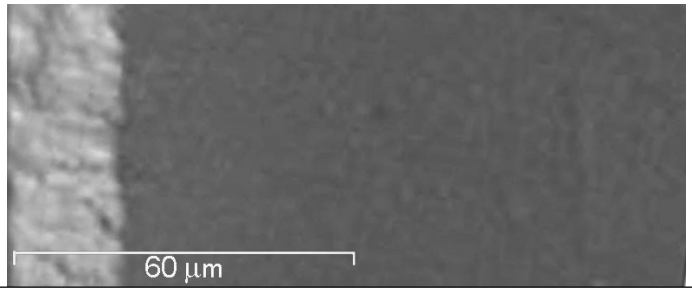

Fig. 3.43. The oxygen distribution in the E110 cladding (1100 C, 8.2% ECR) in accordance with results of SEM examinations

Obtained experimental data prompt to the formulation of the conclusion that general differences in the Zry-4 and the E110 ductility margin as a function of the ECR may be explained by the differences in the oxygen absorption and distribution. However, a more careful analysis shows that this explanation developed on the basis of previous described data contradicts the results presented in Fig. 3.44.

So, two E110 claddings one of which is brittle and another one is ductile have practically the same microhardness (oxygen) distributions across the cladding material. In this connection the question arises: is the oxygen concentration in prior β-phase the only criterion determining the ductility margin of the oxidized cladding?

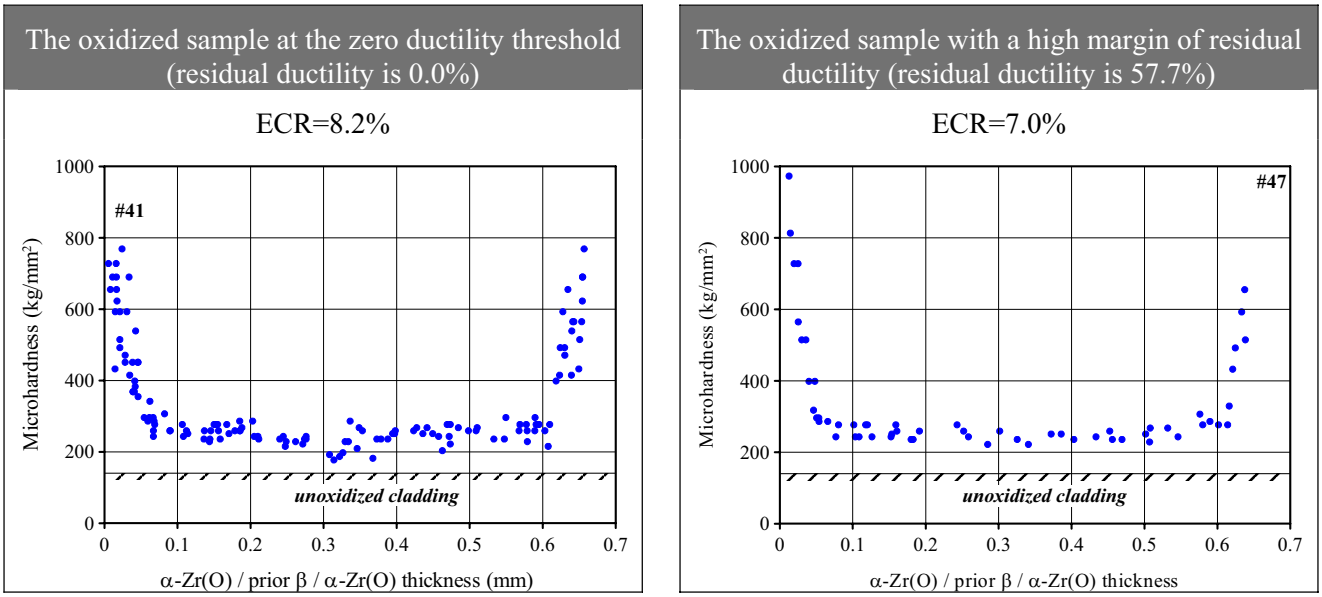

Fig. 3.44. The comparison of microhardness distributions for the brittle and ductile E110 oxidized cladding

The previous classical investigations performed with the Zry-4 claddings have shown that if the breakaway oxidation takes place then two competing processes determine the reduction of ductility margin of the oxidized cladding [13, 32, 33]:

- oxygen absorption by the prior β-phase;
- hydrogen uptake by the prior β-phase.

The significance of the hydrogen effect was later confirmed by the studies performed with the E110 cladding [17, 18, 24, 25, 26, 27]. In accordance with current conception, the effect manifests itself in those cases when the hydrogen concentration in the prior β-phase becomes higher than the hydrogen solubility limit in the zirconium. Taking into account that this limit is a strong function of the temperature, the following physical phenomena occur during the cooling phase with the oxidized cladding absorbing a significant hydrogen portion at the oxidation:

- the formation of solid hydrides at low temperatures;
- the decrease of residual ductility margin caused by hydriding of the prior β-phase.

Obviously, the process of solid hydrides formation is the function of cooling rates (the size of hydrides and, possibly, the orientation of hydrides). These physical phenomena allow to understand the sensitivity of the E110 residual ductility to the cooling rates considered earlier, in spite of the specific response of the E110 cladding on the slow cooling (the improvement of mechanical behavior) which requires the additional analysis.

The quantitative analysis of hydrogen absorption by the E110 claddings will be presented in the next section of the report. But the qualitative consideration of the physical phenomena corresponding to this process is performed in the completion of comparative studies of Zry-4 and E110 claddings.

As it was noted in the comments to Fig. 3.42, the brittle E110 cladding has two different layers of zirconium dioxide:

- white porous monoclinic oxide;
- black protective tetragonal oxide.

The characterization of these two layers of oxide may be also added with the data obtained due to the fracto-graphy observations (the SEM studies of fracture surfaces in the reference cladding sample) presented in Fig. 3.45.

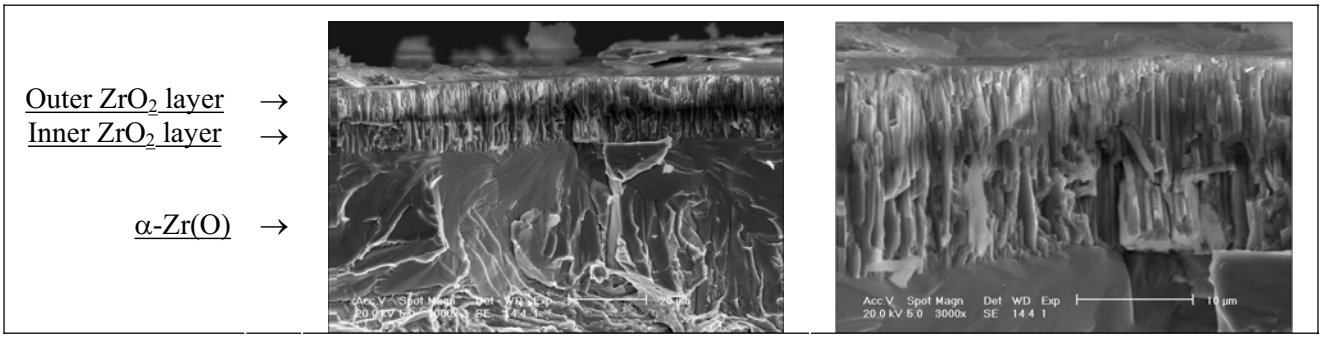

Fig. 3.45. Demonstration of the morphology of ZrO_2 layers in the E110 oxidized cladding (sample #41-4, 1100 C, 8.2% ECR)

To understand a general succession of phenomena that may be responsible for the E110 specific behavior, the following should be preliminary pointed out:

- stabilization of the tetragonal protective oxide layer on the cladding surface is explained, as a rule, by compressive stresses available which are the consequence of the fact that the oxide volume is significantly larger than the initial zirconium volume (in accordance with Pilling-Bedworth ratio) and then the modification of the surface energy balance in the separate ZrO_2 grains;
- besides, the stabilization of the tetragonal phase (slowing-down of the transition of this phase into monoclinic phase) or the improvement of its protective properties is determined also by the behavior of the alloying elements and secondary precipitates in the Zr matrix.

Thus, it is known that the improvement of the corrosion resistance of Zr-Sn alloys was obtained due to the addition of such transition metals as Fe, Cr, Ni at very low concentrations (<0.5%) [31]. A general explanation of this effect is the following: the presence of liquid unoxidized Sn and unoxidized Fe, Cr, Ni precipitates in the zirconium dioxide prevents the hydrogen diffusion and stabilizes the ZrO_2 tetragonal phase. It is also important to point out that tin oxides exist in the tetragonal form only that also leads to the stabilization of tetragonal ZrO_2. As for the niobium-bearing alloys, general considerations on this issue may be formulated in the following way:

- in accordance with results of the diffusion of niobium in the cladding surface layers and its oxidation into Nb_2O_5 may result in destabilization of ZrO_2 layer [29];
- the reason for this destabilization may be associated with the following circumstances:

– if niobium is distributed in ZrO_2 non-uniformly (that is, zirconium dioxide represents a heterogeneous structure containing niobium enriched areas) then, during oxidation of this heterogeneous structure, high volume stresses will occur due to the difference in densities of ZrO_2 and Nb_2O_5, as well as due to stresses caused by the phase transition;

– as it is known, the phase transition takes place practically instantly, therefore, it may be assumed that at that moment when the thickness of the oxide film achieves a definite value the phase transition occurs and the oxide film goes away from the oxide metal interface;

– thus, it becomes evident that all precipitates in the ZrO_2 that are oxidized slowly (such as Sn, Fe) will retain the understoichiometric state of oxide and will correspondingly hinder the sharp phase transition by the stabilization of the tetragonal phase and vice versa.

To clarify the niobium behavior in the E110 alloy at the oxidation, several types of SEM examinations were performed. The results of these examinations are presented in Fig. 3.46.

Secondary electron image of the sample #41-4 with four tracks of niobium concentration measurements	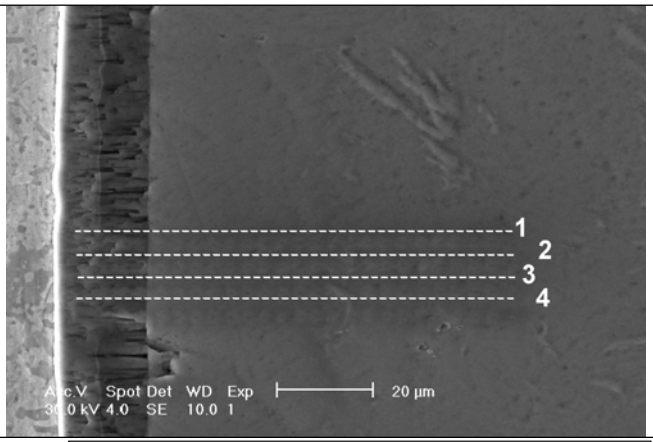
Niobium WDX (wave length dispersive x-ray analysis) dot map	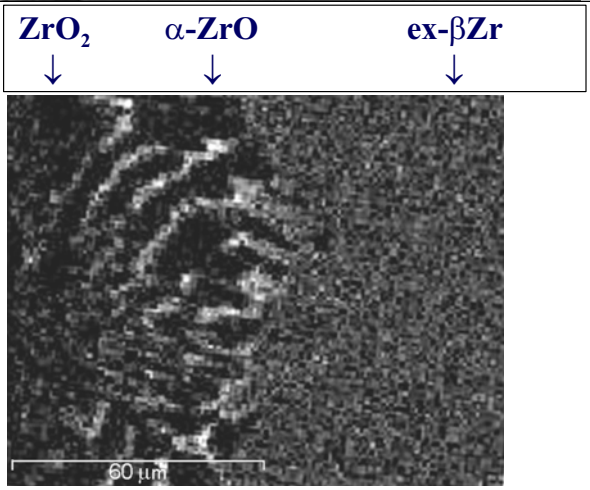

EPMA results characterizing the niobium distribution in accordance with four tracks

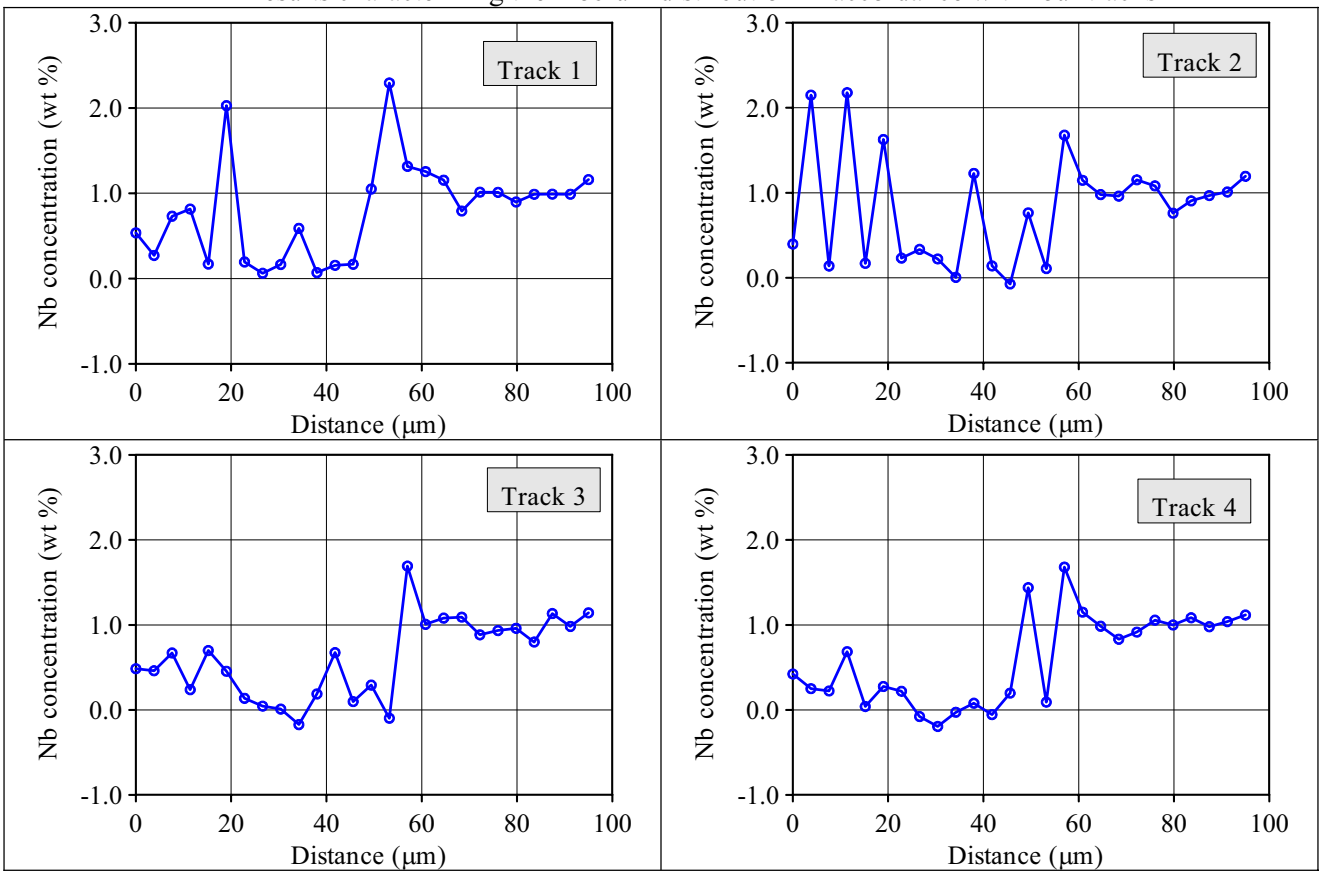

Fig. 3.46. The niobium distribution in the E110 cladding (1100 C, 8.2% ECR) in accordance with results of SEM examinations

The analysis of obtained data has shown that:

- in accordance with the niobium WDX dot map, prolonged niobium enriched areas (white areas) alternate with niobium depleted areas (dark areas) in the α-Zr(O) phase of the E110 cladding;
- the oxidation of α-Zr(O) into ZrO_2 results in the fact that these niobium enriched areas decay into separate niobium enriched points in which niobium concentration is still higher; thus, studied oxide represents heterogeneous ZrO_2 with disseminations of niobium enriched local areas;
- niobium distributions into four tracks obtained due to the EPMA confirm these observations; the irregular niobium distribution in ZrO_2 and α-Zr(O) reflects the niobium concentrations in the niobium enriched areas (up to 2.3%) and in the niobium depleted areas (0%);
- the dot map image and EPMA measurements show that the prior β-phase is characterized by quite a uniform distributions of niobium precipitates (white point on the dot map) in the α'-Zr matrix with the basic concentration in the alloy (1%).

Thus, the experimental data allow to understand the nature of the irregular boundary between α-Zr(O) and prior β-phases in the zirconium niobium alloys. The segregation of niobium with the formation of sequenced in the radial direction areas with different Nb concentration leads to the fact that niobium enriched areas transform into the α-Zr(O) phase at a higher oxygen concentration than the neighboring areas with lower niobium concentration. This effect determines the irregular boundary front between α-Zr(O) and prior β-phases in these alloys.

The performed cycle of studies allowed to return to the consideration of the postponed earlier issue concerning hydrogen absorption by the prior β-phase of the E110 cladding. One of the potential causes that may lead to hydrogen penetration through the oxide-metal boundary has already been named. This cause is the cracking and spallation of oxide due to the tetragonal-monoclinic phase transition in the heterogeneous oxide.

The following specific features of the niobium-bearing cladding discussed above determine other possible causes of hydrogen penetration:

- viens of Nb-rich β-phase in the α-Zr(O) phase represent some sort of channels providing hydrogen diffusion in the prior β-phase matrix;
- hydrogen concentration diffusion is also stimulated by the fact that hydrogen solubility is negligibly low in the α-Zr(O) phase and the surface through which hydrogen diffuses is very large (due to the fact that α-Zr(O) and β-phases have s complicated irregular boundary);
- the preferred radial direction of the α-Zr(O) grain revealed by metallographic examinations also facilitates hydrogen diffusion along grain boundaries into the cladding depth.

Numerical investigations, which were performed earlier with different zirconium alloys, allowed to establish the following principles of hydrogen embrittlement:

- during a high temperature oxidation, hydrogen absorbed by the β-phase is in the solid solution as H_2 solubility in the β-phase is very high under these temperatures;
- during the cooling phase, the precipitation of solid hydrides occurs because hydrogen solubility is a strong function of the temperature, a sharp decrease in hydrogen solubility takes place at the temperature less than 550 C; the solubility limit becomes very low at temperatures less than 100–150 C;
- investigations performed with Zry-4 claddings have shown that the number of hydrides in the prior β-phase is increased up to the hydrogen concentration of 300–400 ppm, at a higher level of hydrogen concentration, the number of hydrides is not increased but the size of these precipitates is enlarged; this effect leads to the initiation of internal stresses and deformation of the cladding matrix;
- the oxidized cladding embrittlement is not a function of hydrogen content only, the embrittlement is a function of hydrogen content, hydrides morphology and hydrides orientation;

- the most negative effect takes place in that case when hydrides form long chains along which a crack may extend.

To find out to what extent the hydrogen embrittlement problem is important for E110 samples tested in this program, two types of investigations were performed:

1. The SEM examinations provided the visualization of hydrides.
2. The hydrogen content was measured in the oxidized cladding samples.

The results of the first of these investigations are presented in Fig. 3.47.

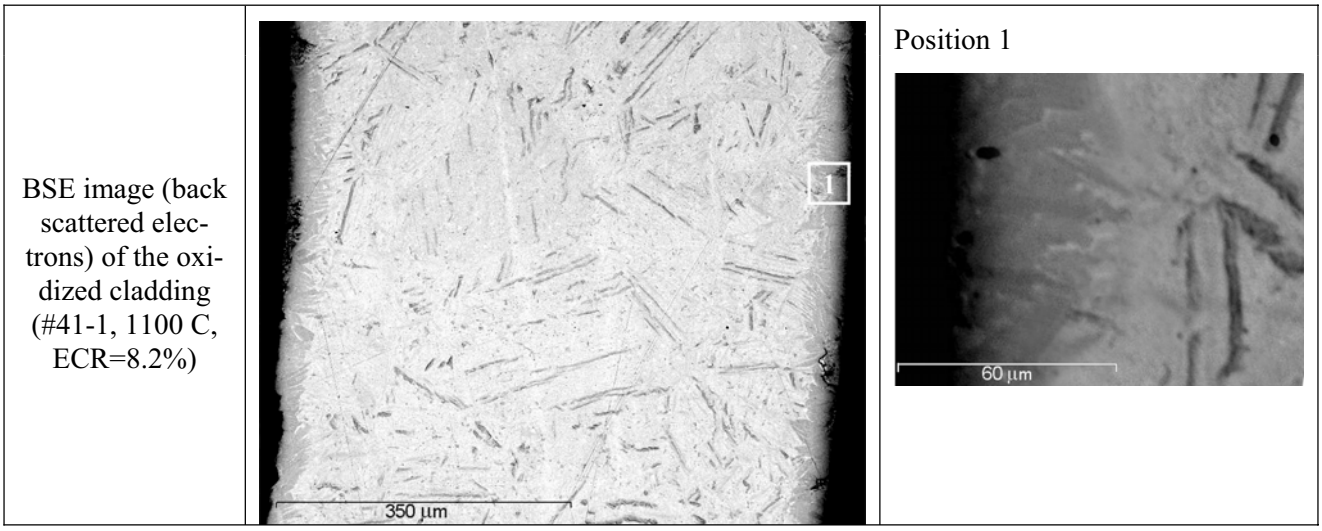

Fig. 3.47. The SEM micrograph of the E110 oxidized cladding

The backscattered electron (BSE) image of the oxidized cladding may be generally interpreted taking into account the following peculiar features of this method:

- the less is the atomic number of a chemical element in the scanning point the darker is the point on the BSE image;
- thus, the areas with high density look as the white ones at the micrograph (white areas), the areas with low density (such as hydrides) look as the black ones.

In accordance with this pattern of the BSE image interpretation, it may be assumed that dark lines scattered about the white field of the Zr prior β-phase represent hydrides (though one cannot also exclude that a part of these lines may indicate the α-Zr(O) phase located along the boundaries of β-Zr grains as this phase density is lower than that of Zr).

To extend the data base necessary for the analysis, the micrographs of one and the same sample obtained due to the optical microscopy are presented in Fig. 3.48:

- the etched structure if the sample allow to see the distribution of α-Zr(O) phase inside the prior β-phase;
- the polished structure of the sample shows the set of solid precipitates in Zr matrix, which could be interpreted as hydides.

Comparison of the BSE image and optical image of polished cladding allow to assume that the prior β-phase of this cladding contains the plate type hydrides. Much of these hydrides are oriented in radial direction and therefore are more critical from viewpoint of the crack propagation during the mechanical loading.

The measurement of the hydrogen contents in the E110 and Zry-4 cladding samples shows that:

- hydrogen content in the E110 sample oxidized at 8.2% ECR was 1130 ppm;
- the hydrogen content in the Zry-4 samples tested at 11.3–11.5% ECR and S/S and F/F combinations of heating and cooling rates was 34–37 ppm.

These measurements confirmed that the embrittlement of Zry-4 cladding is caused by the oxygen absorption in the prior β-phase. The embrittlement of the E110 cladding is provided by the oxygen absorption and hydrogen absorption in the prior β-phase.

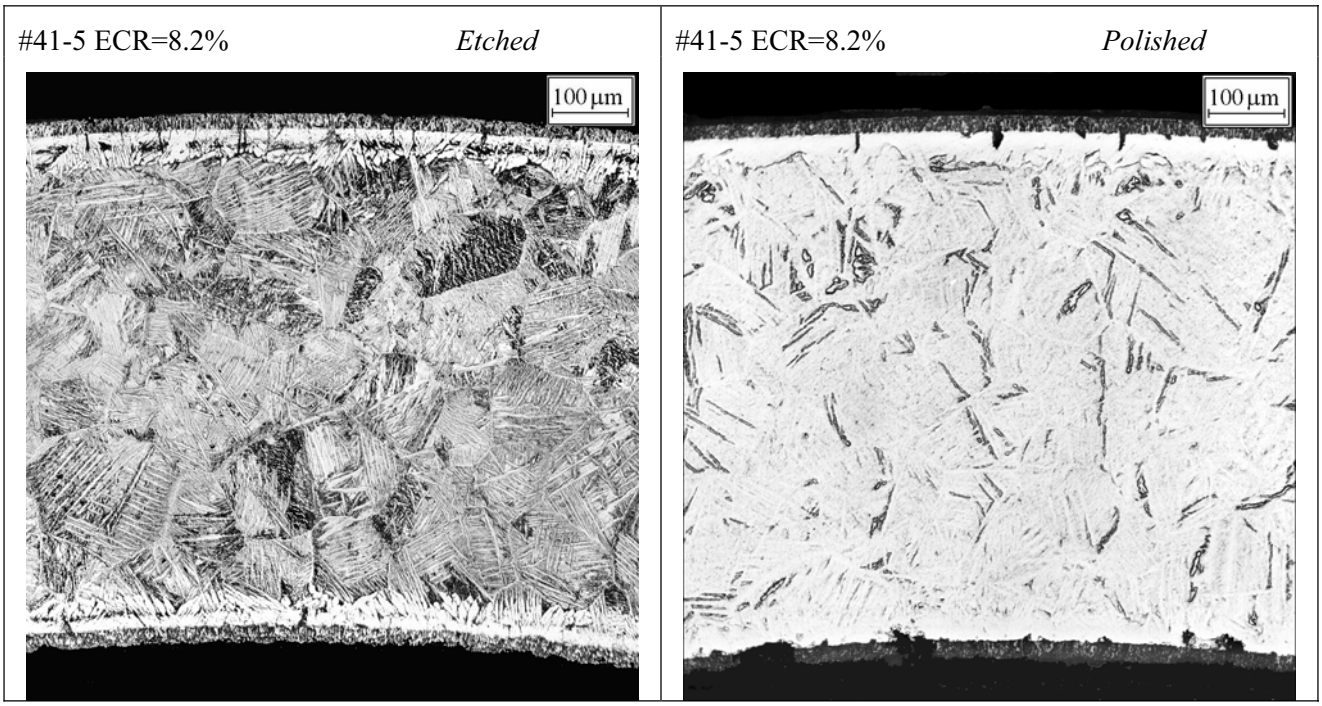

Fig. 3.48. The optical microstructure of the E110 oxidized sample with hydrides in the prior β-phase

3.3.3. Determination of sensitivity of the E110 cladding embrittlement to the oxidation type and the characterization of comparative behavior of E110 and M5 claddings

The previous stages of this research program revealed that the E110 cladding has the inclination to the early breakaway oxidation, and to the increased hydrogen pickup, which facts lead to the zero ductility threshold of the E110 cladding of 8.3% ECR at 1100 C with double-sided oxidation. In this connection, the following natural question was formulated after the analysis of obtained data: do these results characterize the whole family of niobium-bearing claddings or does this effect take place in the E110 cladding only? It is evident, that the comparison of the E110 cladding behavior with the behavior of any other cladding with a close chemical composition might become the best method to find the answer to the formulated question. The appropriate analysis has shown that the M5 cladding [34] is an ideal partner to perform this comparison as both claddings (E110 and M5) are fabricated from the alloys practically similar in the chemical composition: Zr-1%Nb (though it should be noted that they differ in oxygen concentration in the alloy).

However, the consideration of published data characterizing the mechanical behavior of the M5 oxidized cladding showed that the appropriate studies were performed employing a single-sided oxidation [23, 35, 36]. This circumstance became the major incentive to perform sensitivity studies and to develop the comparative data on the E110 cladding behavior as a function of the oxidation type. The results of E110 single-sided tests are presented Appendixes B and E.

The obtained data have shown that (see Fig. 3.49): the pronounced indications of the breakaway oxidation appear in the case of a single-sided oxidation at lower ECR than that on the double-sided oxidation. This fact confirms again the formulated earlier thesis that the tetragonal oxide transition to the monoclinic oxide takes place on some critical oxide thickness. Taking into account that the oxide thickness at the single-sided oxidation is higher than that at double-sided oxidation (with the same ECR), the breakaway oxidation occurs at lower ECR.

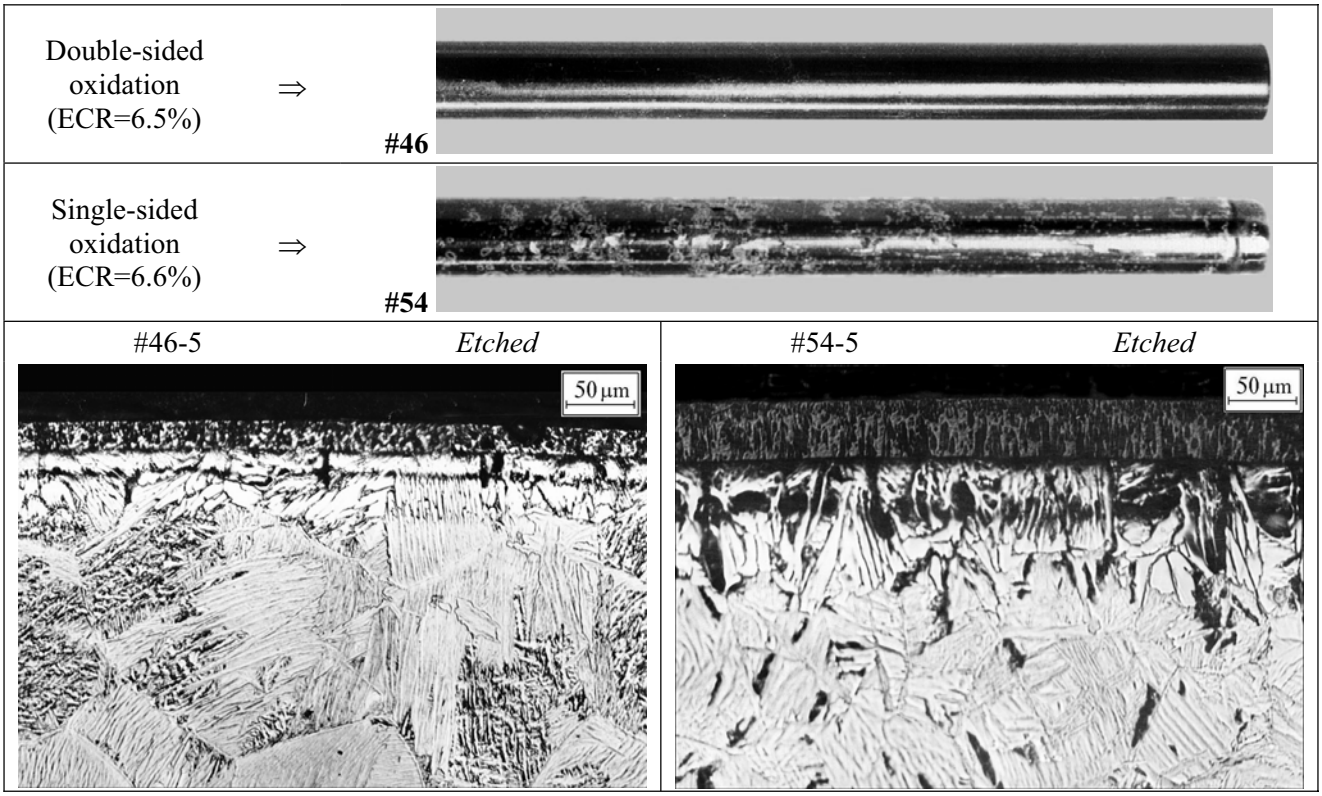

Fig. 3.49. The comparison of the E110 appearance and microstructure after single-sided and double-sided oxidation at 1100 C

The comparison of the E110 oxidized cladding mechanical behavior presented in Fig. 3.50 allows to conclude that the E110 cladding demonstrates the tendency to the increase of the residual ductility margin at the single-sided oxidation (in comparison with the double-sided oxidation) but this difference is not so great.

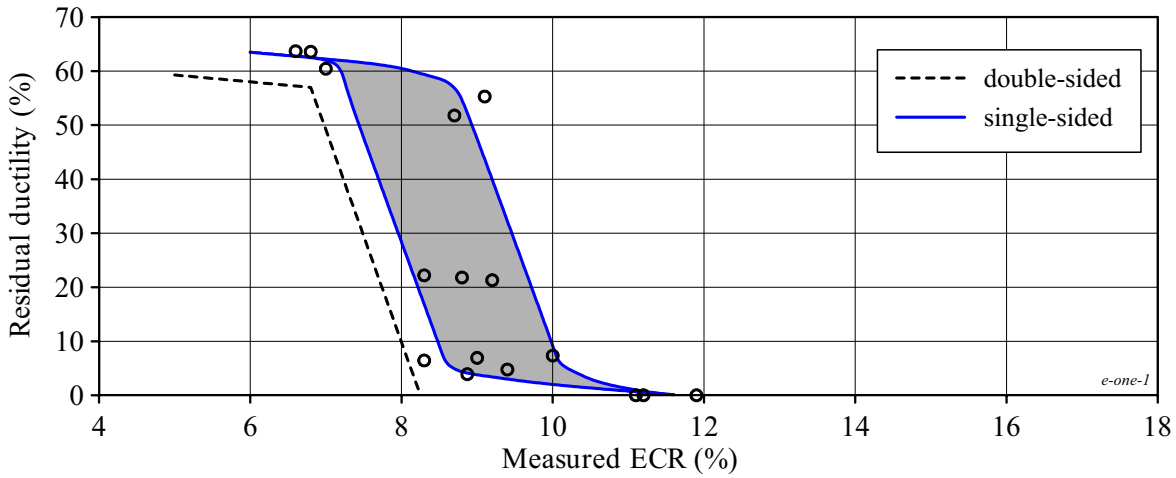

Fig. 3.50. Comparative data characterizing the E110 residual ductility as a function of the oxidation type

The E110 data base obtained due to the tests under the single-sided oxidation conditions allowed to perform a direct comparison of the mechanical behavior of the E110 and M5 claddings on the basis of ring compression tests and three-point bending tests at 20 C. To develop the comparative data, the M5 test results published in Reference 23 were used. Three-point bending test results are compared in this section and the section 3.3.7 of the report. The first set of comparative data organized in Fig. 3.51 allows to formulate several interesting observations listed in Fig. 3.51.

Ring compression tests with the E110 cladding General observations: 1. All tested E110 claddings had approximately the same effective elastic modulus 2. The fracture load at the zero ductility threshold (18.5 mg/cm^2) is corresponds to the "yield" point of load–displacement diagrams of partially ductile E110 samples (9.8–12.3 mg/cm^2)	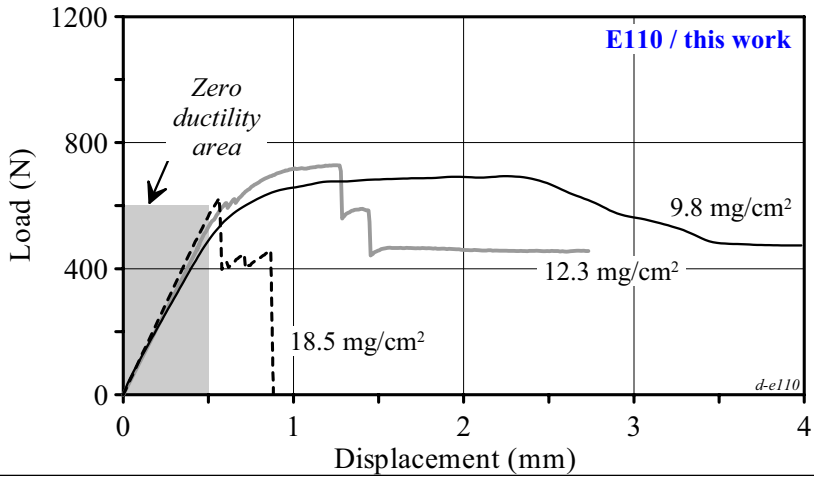
Ring compression tests with the M5 cladding General observations: 1. The claddings oxidized at 8.1–13.6 mg/cm^2) had the same effective elastic modulus 2. The elastic modulus of the sample oxidized at 22.9 mg/cm^2 is lower than that of other samples 3. The maximum load of 22.9 mg/cm^2 sample is lower significantly than the "yield" point	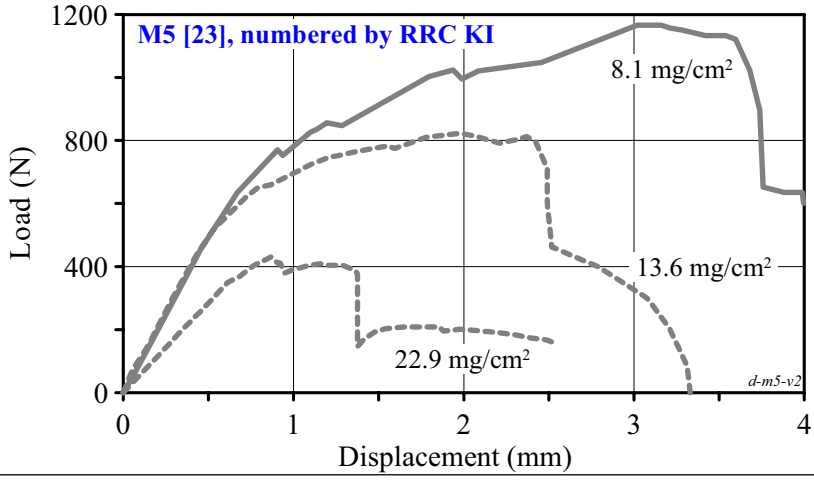
Three-point bending tests with the M5 cladding General observations: 1. All tested samples had approximately the same elastic modulus 2. Taking into account that the fracture load of 22.9 mg/cm^2 sample is significantly lower than the "yield" points of other samples the zero ductility threshold of M5 cladding is located in the range of 13.6–22.9 mg/cm^2	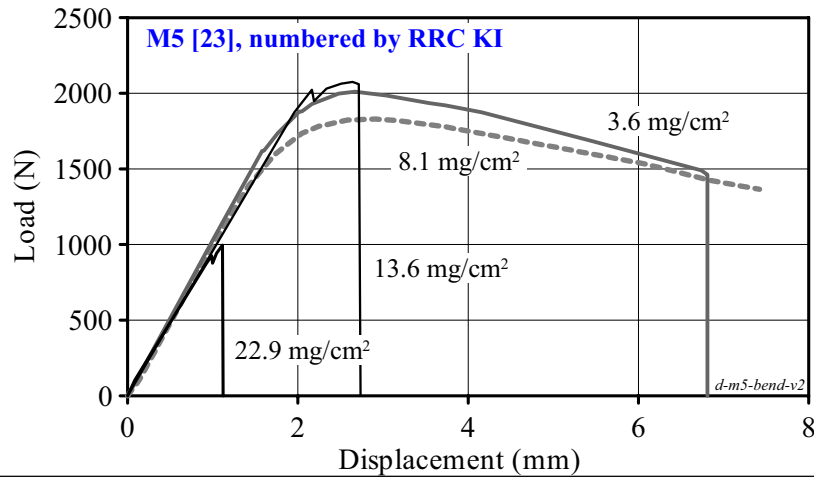

Fig. 3.51. The data base characterizing the mechanical behavior of the E110 and M5 claddings after a single-sided oxidation at 1100 C

The second set of E110 and M5 comparative data presented in Fig. 3.52 allows to make the following conclusions:

- at the low oxidation (8.1–9.8 mg/cm^2) the E110 cladding demonstrates a higher level of residual ductility and lower strength properties than the M5 cladding. Apparently, this may be explained by the effect of different initial oxygen concentration in this two claddings;

- at the middle oxidation (12.3–13.6 mg/cm^2) both claddings demonstrate a very similar behavior at the initial phase of the mechanical loading (the same elastic modulus and the similar level of the maximum load (800 and 720 N for the M5 and E110 claddings respectively) but the M5 cladding has a noticeably higher margin of residual ductility;
- at the high oxidation (18.5–22.9 mg/cm^2) the E110 cladding demonstrates the transition from partially ductile state (14.8 mg/cm^2) to fully brittle state (18.5 mg/cm^2); in this case, taking into account that the maximum load for this sample corresponds to the "yield" point, it may be considered that this sample was tested at the zero ductility threshold; as for the M5 cladding, the load–displacement diagram of the appropriate sample (22.9 mg/cm^2) shows that on the one hand, this sample has the margin of residual ductility (because the yield area is observed) but on the other hand, this sample had the maximum load that was significantly lower than the yield point, the effective elastic modulus of this sample was significantly lower than that of other samples, and, besides three-point bending test showed that this sample was fully brittle; that is why our opinion is that the zero ductility threshold of the M5 cladding is lower than 22.9 mg/cm^2.

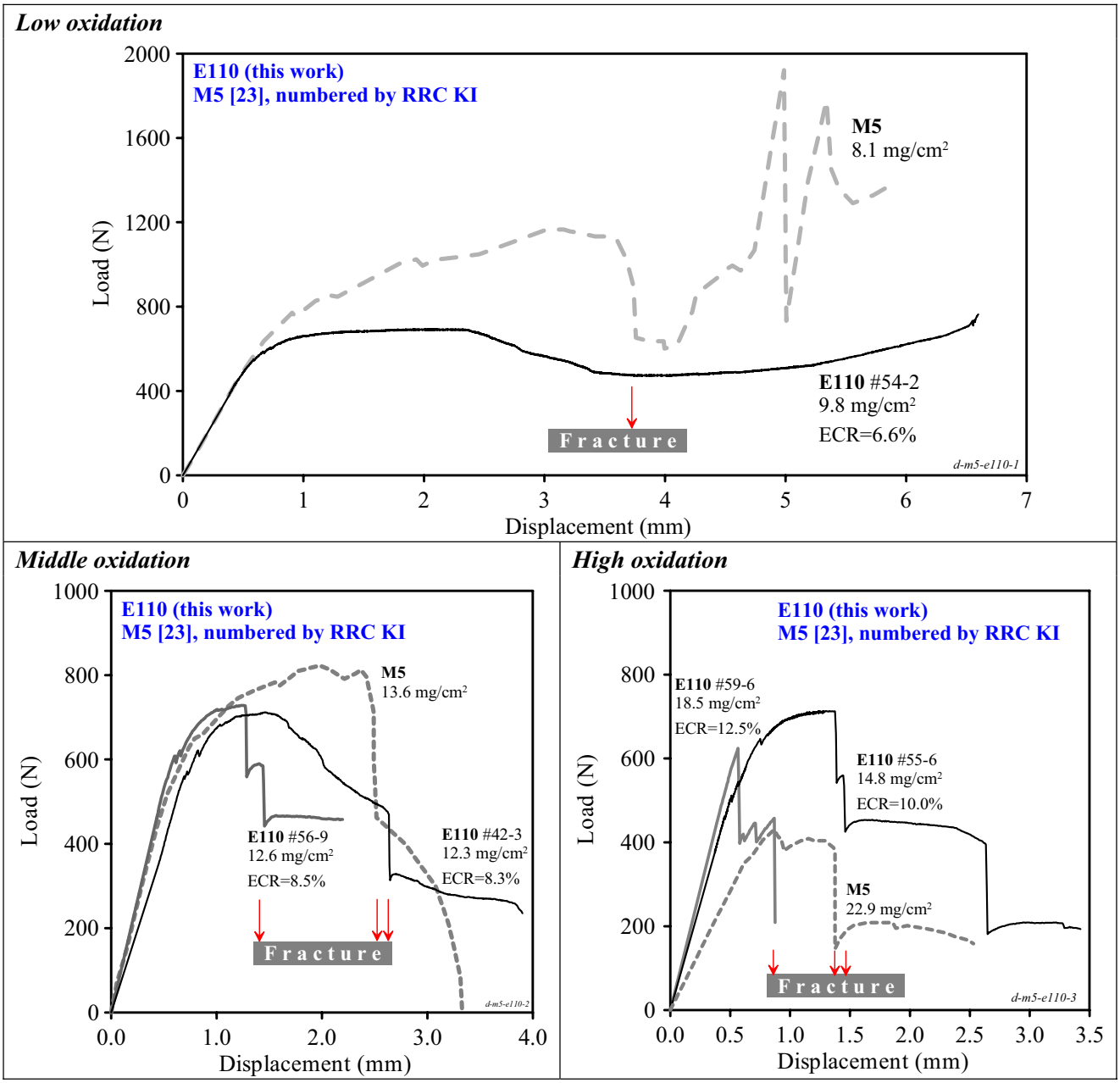

Fig. 3.52. The comparison of the E110 and M5 cladding mechanical behavior after the single-sided oxidation at 1100 C in accordance with the ring compression test results at 20 C

Nevertheless, the comparison of the E110 and M5 cladding mechanical behavior has shown that the M5 cladding has a higher margin of residual ductility at the oxidation level in the weight gain range of 13–20 mg/cm^2. Besides, the following should be pointed out:

- the E110 cladding is embrittled in accordance with the mechanism of the breakaway oxidation;
- the M5 cladding oxidation takes place without any indication of the breakaway oxidation (in accordance with the test data presented in [23], the hydrogen concentration in the oxidized samples was very low and the oxide was lustrous and black).

Thus, the results of this stage of research have shown that there is some cause that determines a specific behavior of the E110 cladding. To determine more accurately the temperature range of this E110 specific behavior, a special subprogram for the oxidation and mechanical tests was developed. The results of this subprogram are analyzed in the next section of the report.

3.3.4. The evaluation of the E110 oxidation and mechanical behavior as a function of oxidation temperature

The results of investigations performed with the E110 cladding on the oxidation at 1100 C have shown that this cladding has the tendency to the breakaway oxidation and the embrittlement caused by the oxygen and hydrogen absorption in the high temperature β-phase. Moreover, tests with the E110 cladding performed at slow heating have demonstrated that the breakaway oxidation effects become still more pronounced. This may be explained by the fact that the initial phase of oxidation took place under the temperatures that were significantly lower than 1100 C. These facts are also confirmed by the results of studies performed by V.Vrtilkova. She has shown that if the E110 cladding is heated up to 1100 C in the inert gas (argon) atmosphere and then is oxidized in water steam, the effect of early breakaway oxidation vanishes [10].

The analysis of these results leads to the conclusion that the most unfavorable test mode for the E110 alloy is the oxidation in the area of the alloy α+β-phase. As for the temperature range at which the E110 cladding has the α-phase, then numerous tests as well as the operation experience demonstrate that the E110 claddings are not susceptible to the breakaway oxidation that is confirmed by the results presented in Fig. 3.53 [37, 38].

Typical appearance of the E110 commercial cladding after irradiation at 60 MW d/kg U and representative parameters of the appropriate claddings: • oxide thickness 10 μm • hydrogen content 50 ppm	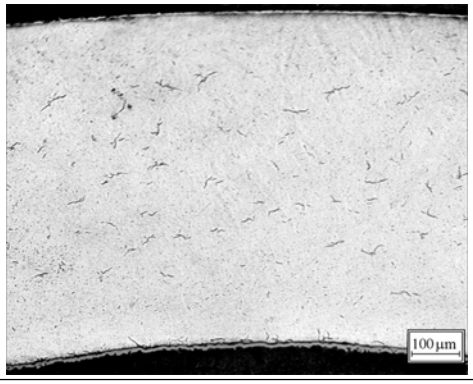
Mechanical properties of the E110 commercial irradiated cladding [19]	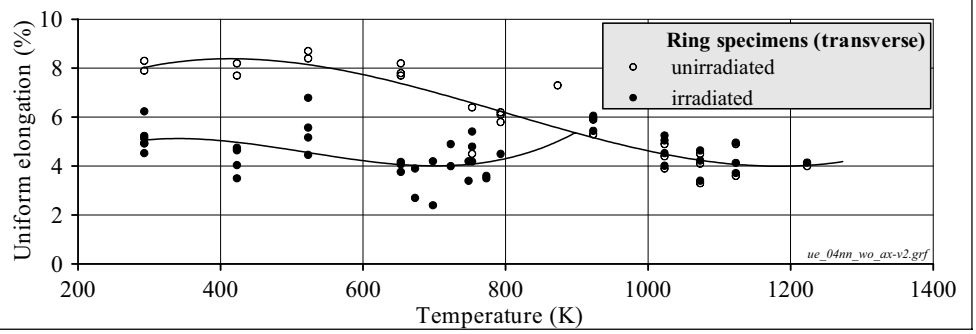

Fig. 3.53. The characterization of the E110 commercial cladding after irradiation and oxidation in the α-phase

To clarify the details for the oxidation and mechanical behavior of the E110 cladding as a function of temperature, special tests were performed in the range of 800–1000 C. Besides, to replenish the data base with the results characterizing the E110 behavior at the maximum temperature typical of the design basis accident area, several tests were performed at 1200 C. The results of these tests are presented in Appendixes B and D of the report.

But before analyzing the results of appropriate tests, it is useful to consider peculiar features of the α to β-phase transformation as applied to Zr-1%Nb alloys. The comparative data characterizing this phenomenon in the E110 and M5 alloys are presented in Fig. 3.54.

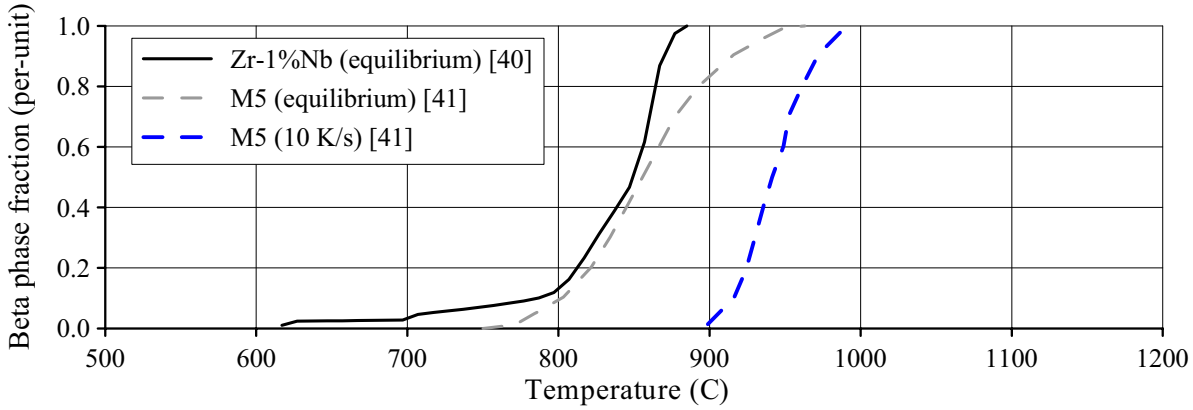

Fig. 3.54. The characterization of the allotropic phase transformation in the E110 and M5 alloys

The analysis of presented data on the M5 alloy shows that the increase of heating rate leads to the displacement of the zirconium α-β phase area towards higher temperatures; with heating rates typical of the fast mode (F) of these tests this effect will be still noticeable. The studies performed in the RIAR during the recent years to understand the behavior of VVER fuel rods with the E110 claddings under RIA conditions showed that in addition to the effects of heating rates as applied to the zirconium matrix the behavior of niobium should be also taken into account. So, the appropriate analysis shows that at the fast heating, the diffusion processes associated with the dissolution of β-Nb precipitates may take place not in full and, consequently, dissolved niobium atoms will localize close to those areas in which β-Nb precipitates are situated. In other words, the areas of niobium oversaturated solid solution may be generated in the zirconium matrix under these conditions. It has been already said before that such niobium-enriched areas may be responsible for the increased hydrogen absorption and other effects being of importance for understanding of the E110 alloy peculiar features.

The analysis of the E110 alloy real behavior in the temperature range 800–1100 C may be started from the consideration of data characterizing the appearance and microstructure of oxidized samples (see Fig. 3.55, Fig. 3.56). The results of this analysis may be formulated in the following way:

- the earliest appearance of the pronounced indications for the breakaway oxidation at the low level of ECRs is noted in the temperature range 900–1000 C;
- at the middle level of ECRs the breakaway oxidation is visually observed under all studied temperatures (800–1100 C), however, the strongest indication of appropriate effects was noted at 900–1000 C;
- at the high level of ECR the most striking demonstration of the breakaway oxidation was noted at the temperature of 950 C, in which connection the microstructure analysis showed that the effect of the oxide foliation was observed on samples tested at 800–950 C, but this effect manifested itself most obviously under the temperatures 900–950 C.

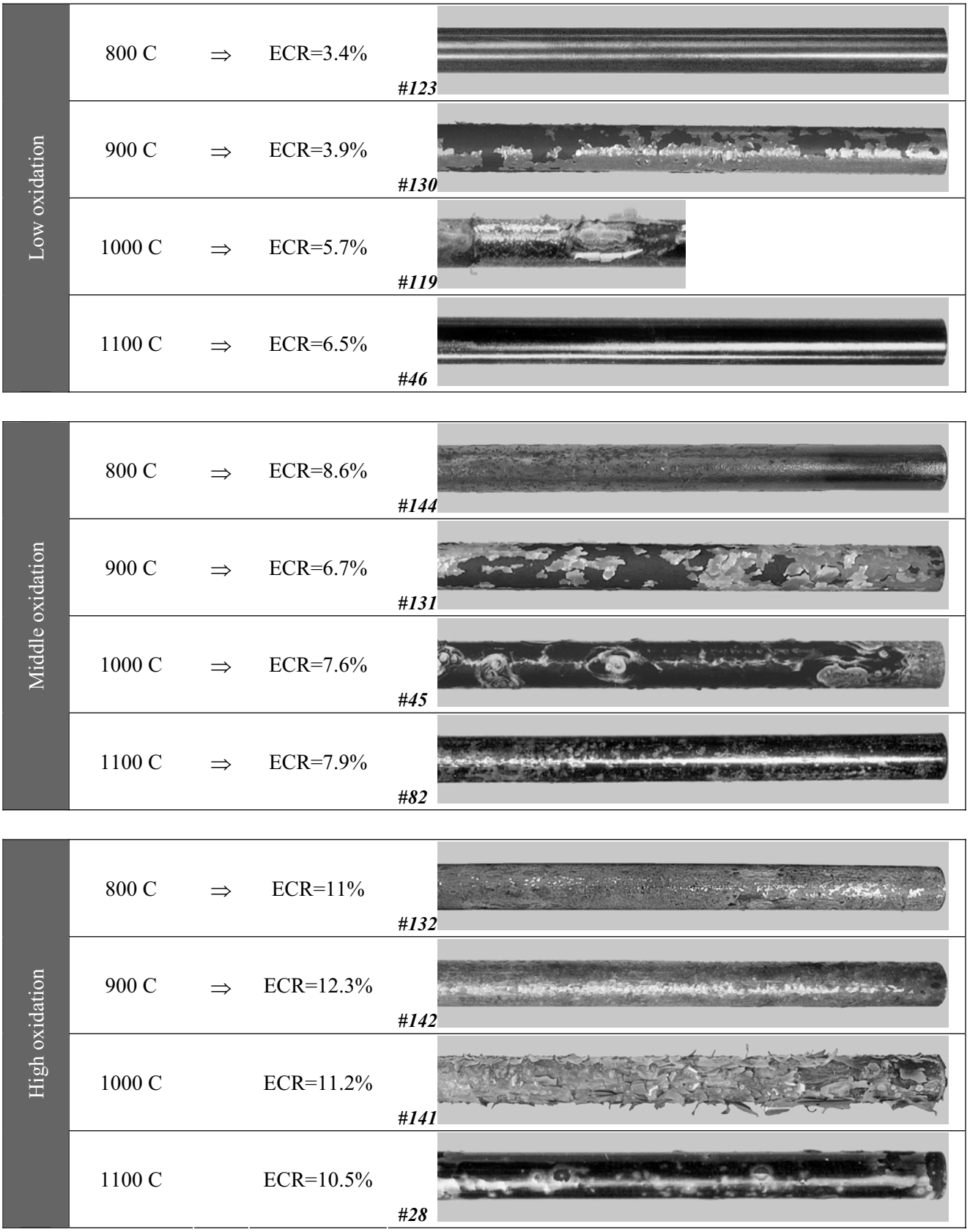

Fig. 3.55. Appearances of the E110 cladding after the double-sided oxidation at 800–1100 C and F/F combination of heating and cooling rates

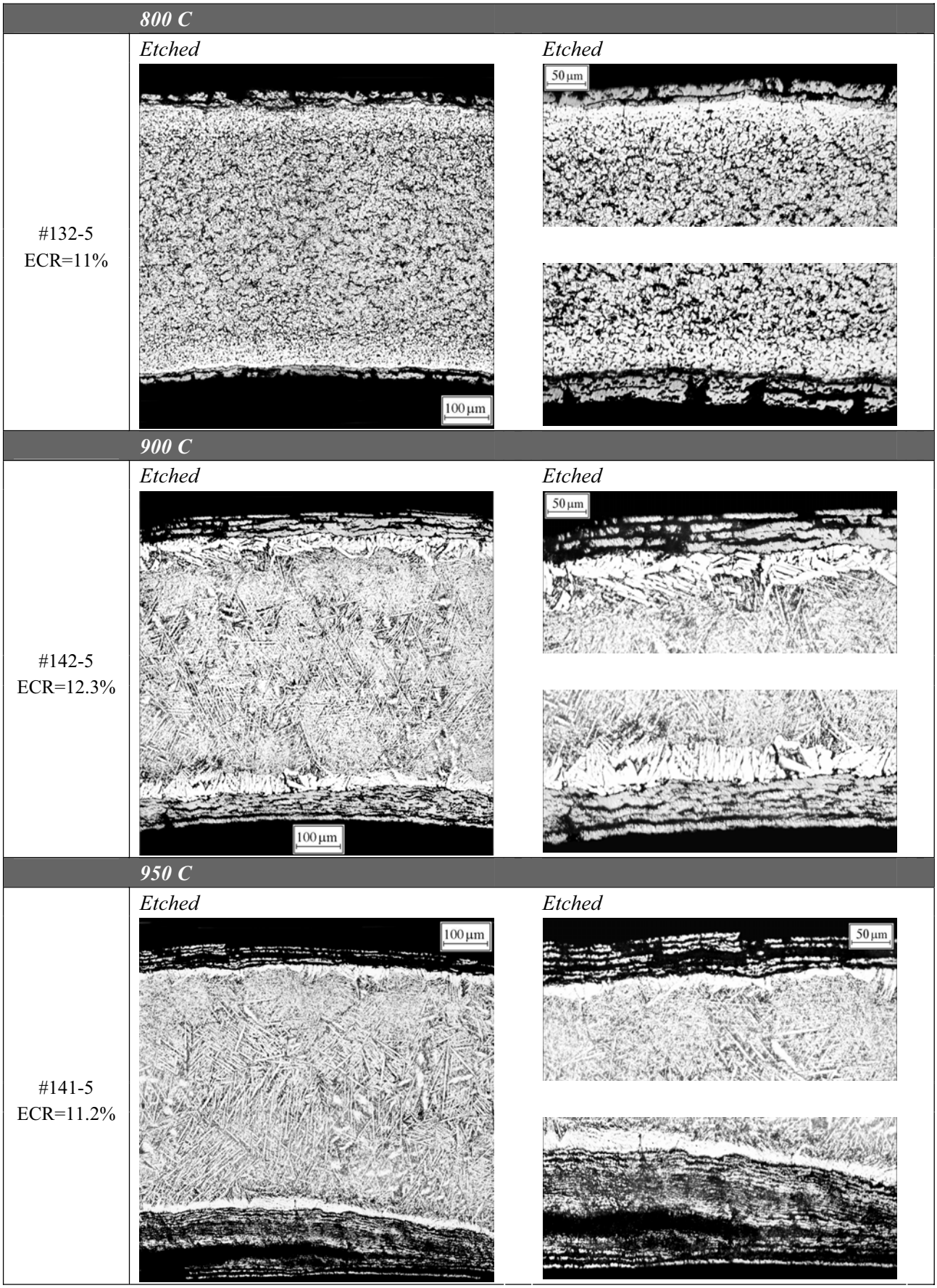

Fig. 3.56. The microstructure of the E110 cladding after a double-sided oxidation at 800–950 C and F/F combination of heating and cooling rates

To understand consequences associated with the availability of stated above effects of the E110 oxidation, the results of mechanical tests were specially organized (see Fig. 3.57).

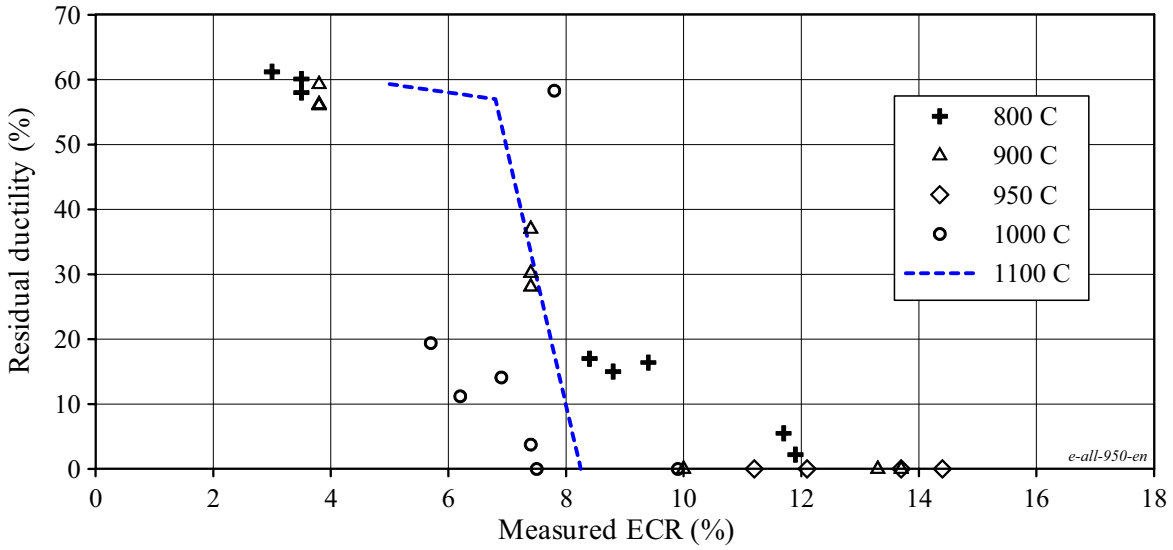

Fig. 3.57. The data base characterizing the residual ductility of the E110 cladding as a function of the ECR and oxidation temperature

In accordance with the data presented in Fig. 3.57, the following additional comments may be made:

- the zero ductility threshold of the E110 claddings oxidized at 800 C is noticeably higher than that in the reference oxidation mode (1100 C);
- the ECR of the E110 claddings oxidized at 900 C is approximately the same as the 1100-degree threshold, but the time threshold is much higher at 900 C than that at 1100 C; it is outside a practical LOCA;
- the zero ductility threshold at 1000 C is possibly a little lower than the 1100-degree threshold.

These observations are in some contradictions with the observations formulated according to the analysis of the cladding appearances and microstructures; but before we go on to the consideration of possible causes for these contradictions, it is useful to add the results of hydrogen concentration measurements in the oxidized claddings to the data base.

The systematic analysis of the data presented in Fig. 3.58 allows to reveal the following regularities in the E110 cladding behavior as a function of the ECR at 1100 C:

- the mechanical behavior of oxidized cladding is characterized with the very high margin of residual ductility in the ECR range approximately up to 7%;
- the cladding hydrogen content is very low in the same range of ECRs;
- the sharp decrease of residual ductility in the ECR range 7–8.3% corresponded with the sharp increase of hydrogen content in the E110 cladding;
- the zero ductility threshold of the E110 cladding is corresponded with the hydrogen concentration of 400 ppm approximately.

Thus, the data base characterizing the hydrogen content in the E110 cladding after the oxidation at 1100 C confirms formulated earlier assumptions concerning the fact that the embrittlement of the E110 cladding is a sum of the oxygen and hydrogen embrittlement. Besides, it should be noted that this critical value of the hydrogen content in the cladding (400 ppm) is in a good correlation with the above mentioned critical value of the hydrogen content, after which the increase of the hydrides volume and internal stresses in the cladding were observed.

Specific features for hydrogen absorption by the E110 cladding as a function of the oxidation temperature may be discussed using the data given in Fig. 3.59.

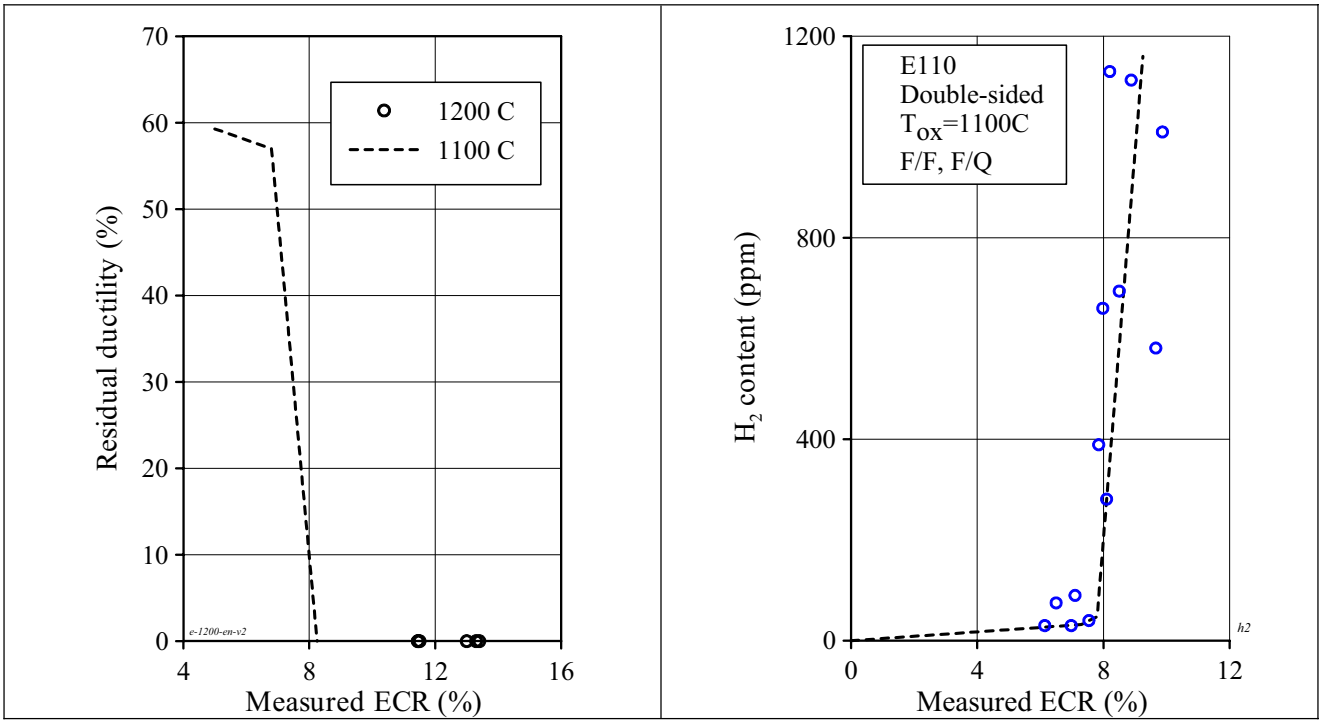

Fig. 3.58. The E110 residual ductility and hydrogen concentration as a function of the ECR after a double-sided oxidation at 1100 C and F/F, F/Q combinations of heating and cooling rates

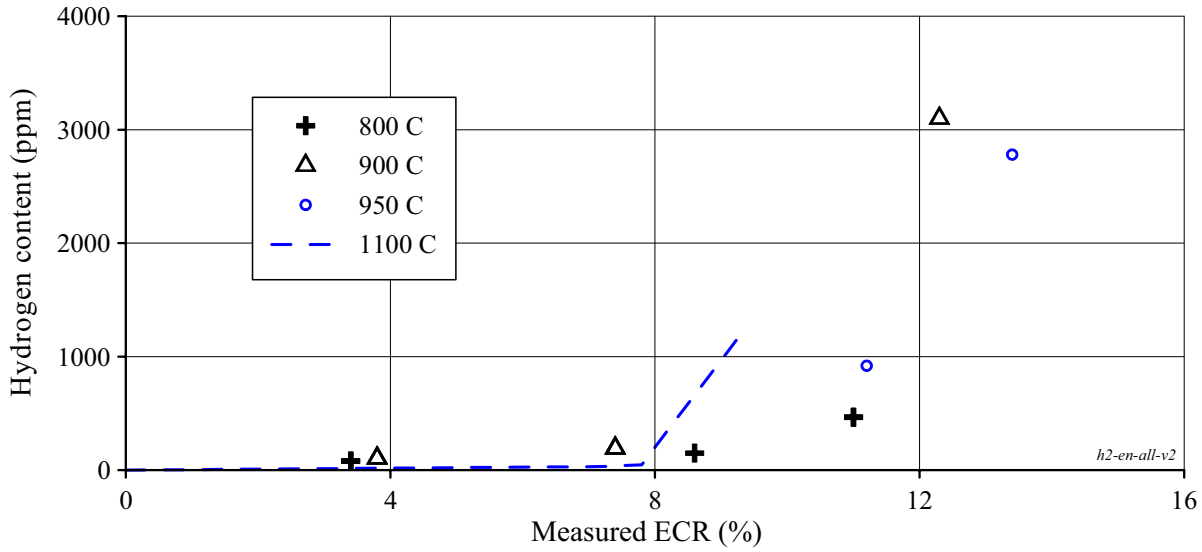

Fig. 3.59. The hydrogen content in the E110 cladding as a function of the ECR and temperature after a double-sided oxidation

A part of obtained data is in a good agreement with the results of mechanical tests presented in Fig. 3.57, so:

- the hydrogen absorption decrease at 800 C leads to the improvement of the E110 mechanical behavior and to the increase of the cladding zero ductility threshold up to the ECR higher than 12% (as-measured);
- the same (approximately) tendency of the hydrogen absorption at 900 C as at 1100 C leads to the same (approximately) mechanical properties of the oxidized cladding.

Unfortunately, it is impossible to continue the appropriate comparison for the second part of experimental data (950 C and 1000 C) in connection with the limited data on the hydrogen content but nevertheless, the

obtained results allow to assume that the transition to the accelerated hydrogen absorption will take place with approximately the same (or a little less) ECR as that for the temperature 1100 C.

As for revealed contradictions, then the following may be referred to those:

- according to the results of visual observations (see Fig. 3.55, Fig. 3.56) the claddings oxidized at 900–1000 C were to demonstrate the worst mechanical properties and, consequently, to show the maximum values for the hydrogen absorption. However, this is not so or not quite so as it can be seen from the above stated analysis;
- according to the data characterizing the allotropic phase transformation in the Zr-1%Nb alloys (see Fig. 3.54) the test results with the E110 cladding oxidized at 800 C may be logically explained by the fact that the β-phase fraction in the E110 cladding at this temperature is very small and, consequently, the general tendency of the cladding behavior corresponds to those of the low temperature oxidation of the E110 alloy in the area of the α-phase existence. All previous investigations have shown that the E110 alloy has the corrosion resistance in the α-phase temperature range;
- but in accordance with the same data (see Fig. 3.54), it is quite difficult to explain by what the oxidation conditions in the temperature range 900–1100 C differ (even if we take into account the effects associated with heating rates) as it is evident that the higher the temperature, the closer the Zr matrix composition approaches the β-phase that must provide the avoidance of the breakaway oxidation.

In connection with the list of revealed contradictions, it is appropriate to note the following:

1. The availability of such contradictions as a rule indicates that the number of key factors taken into account on analyzing is less than it is necessary.
2. The following factors may be referred to the unaccounted ones:

- the behavior of alloying elements (these aspects of the problem will be considered in the section 3.3.5 of the report;
- the behavior of oxygen and α-Zr(O) phase as a function of temperature and the size of Zr-matrix grains as a function of temperature.
- As for the behavior of oxygen α-Zr(O) phase and Zr-matrix as a function of oxidation temperature the appropriate data is organized in Fig. 3.60.

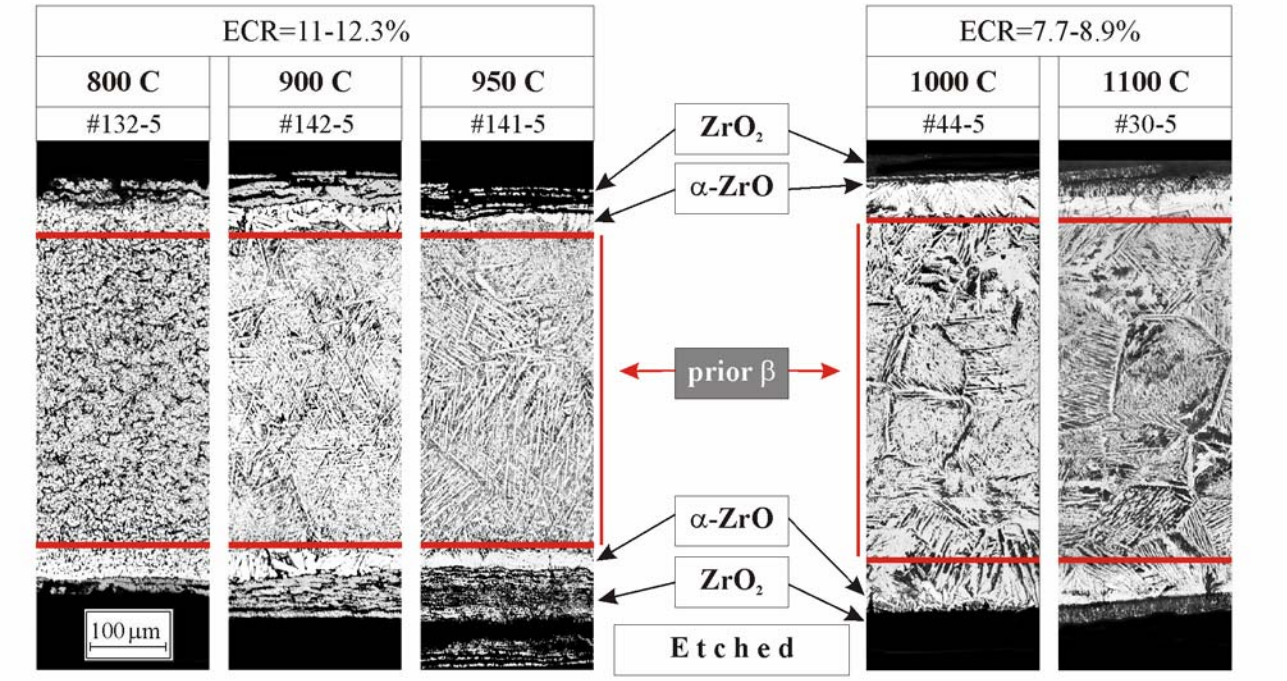

Fig. 3.60. The comparison of the E110 microstructure after a double-sided oxidation at different temperatures

The analysis of these data shown that:

- the thickness of α-Zr(O) phase at 800–950 C is significantly lower than that at 1000–1100 C in spite of difference in the oxidation level: 11–12.3% ECR at 800–950 C and 7.7–8.9% at 1000–1100 C; this effect leads to the fact that the thickness of the prior β-phase is approximately the same for both of the considered sets of data. But it is obvious that the prior β-phase thickness is one of most important factors that determine the residual ductility margin;
- besides, the size of Zr-matrix grain at the lower temperature is a little less than that at 1000–1100 C;
- moreover, the comparison of these two sets of experimental data shows that the tendency to the formation of α-Zr(O) needles that penetrate into the prior β-phase and the tendency to the formation of α-Zr(O) layers along large grains of the prior β-phase are typical only for the temperature range 1000–1100 C.

The revealed features of the E110 behavior at different temperatures allow to understand that multiparametric effects determine the cladding oxidation behavior under these conditions. But the resulting component of the combined effects from many factors may be characterized in the following way:

- the oxidation at 800 C is the upper threshold for a good behavior of the E110 cladding providing the approximate accordance between the experimental zero ductility threshold and the safety criterion;
- the oxidation at 900–1100 C results in the fact that the experimental zero ductility threshold is lower than the safety criterion.

The last position in this cycle of works was concerned with the investigation of peculiar features of the E110 cladding oxidation and embrittlement at the temperature 1200 C. The comparative data base characterizing this item of research is presented in Fig. 3.61.

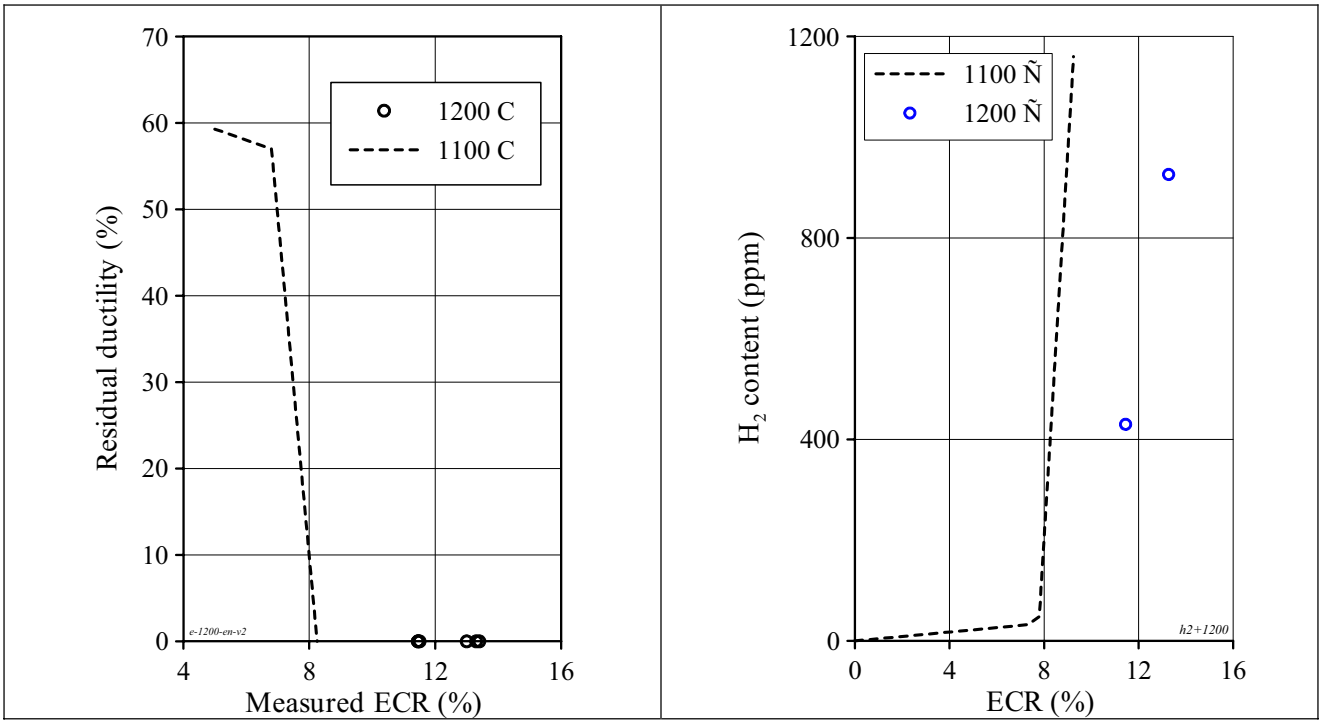

Fig. 3.61. The characterization of the E110 cladding behavior after a double-sided oxidation at 1200 C

The analysis of obtained data leads to the following conclusions:

- the zero ductility threshold of the E110 cladding oxidized at 1200 C is most likely not better than that at 1100 C;
- the tendency to the decrease of hydrogen absorption was observed in accordance with the results of this test. But it is known that the tendency to the increase of the oxygen content in the β-phase characterizes the cladding behavior at this temperature in the comparison with 1100 C.

- the E110 claddings continue to demonstrate the tendency towards the breakaway oxidation under this temperature.

3.3.5. The sensitivity of the behavior of Russian niobium-bearing alloys to the alloying composition

In the previous section of the report it was noted that:

- the oxidation behavior of the Russian Zr-1%Nb cladding (E110) and French Zr-1%Nb cladding (M5) is different;
- the analysis of appropriate effects has shown that the first difference that draws the attention is the following:
  - the initial oxygen concentration in the E110 cladding is 400 ppm (for claddings used in these tests);
  - the nominal oxygen concentration in the M5 cladding is 1350 ppm [35];
- the oxidation behavior of zirconium based claddings is sensitive to the concentration of such elements as Sn and Fe in the alloy.

To verify the sensitivity of the niobium-bearing cladding behavior to these factors, several tests were performed with two following cladding types:

- the E110K cladding: this is the E110 cladding with the increased oxygen concentration (up to 1100 ppm);
- the E635 cladding: this is the niobium-bearing cladding with the following alloying composition: (Zr-1%Nb-1.2%Sn-0.35%Fe [41].

The summary of test results with the E110K cladding is presented in Fig. 3.62.

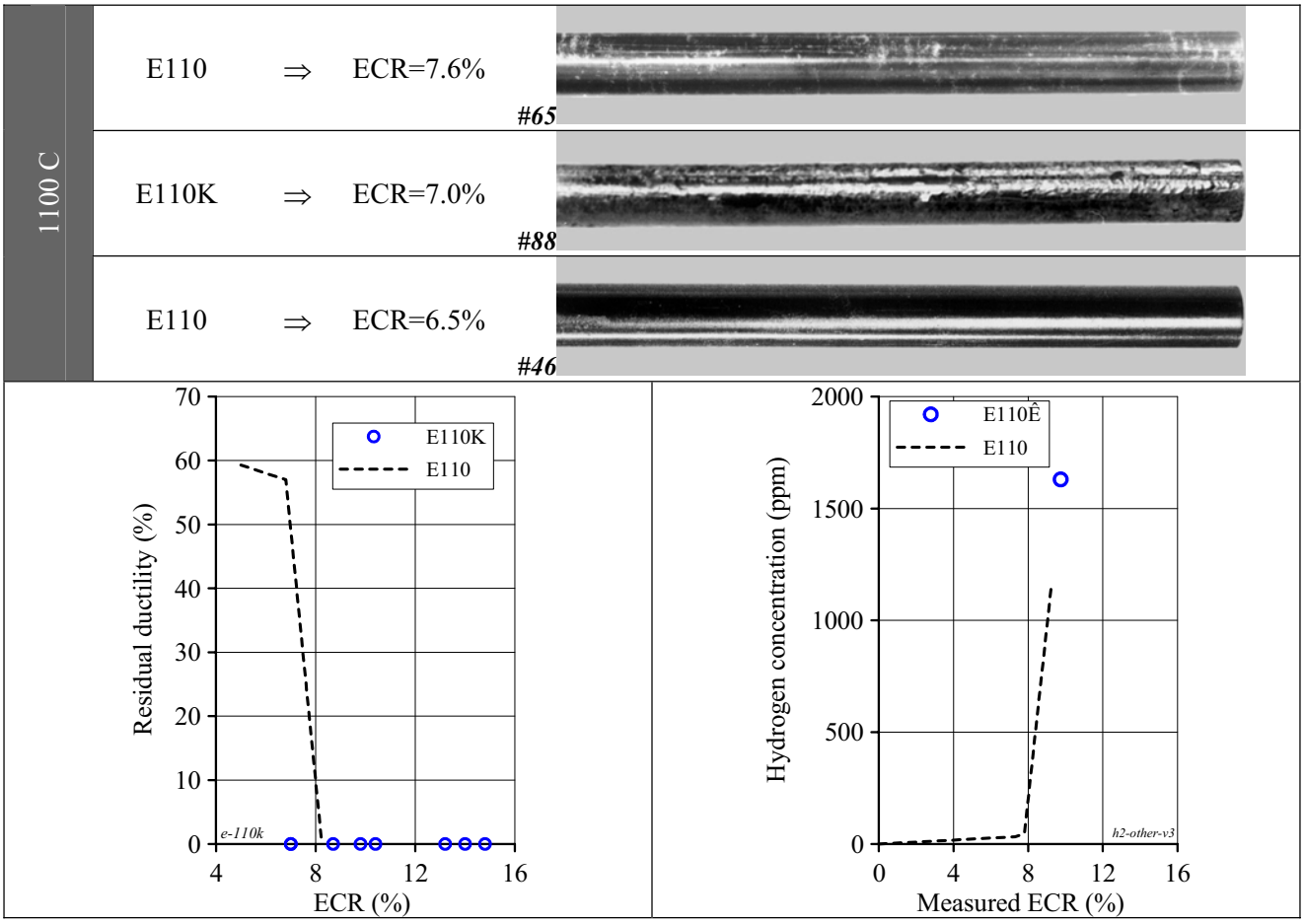

Fig. 3.62. The summary of results characterizing the E110K behavior under oxidation and ring compression test conditions

The analysis of obtained results allows to establish with confidence the following:

- the oxygen concentration increase in the E110 alloy does not lead to the elimination of the effect of of the early breakaway oxidation;
- the zero ductility threshold for the E110K oxidized cladding is not higher than that for the E110 cladding with the standard oxygen concentration. The E110K cladding has the same tendency of the hydrogen absorption by the prior β-phase.

Thus, these results bring to the conclusion that the general difference in the E110 and M5 cladding behavior is not connected with the initial oxygen concentration in the cladding material. The cladding response on the variation of Sn and Fe composition in the cladding material was studied in the experiments with the E635 cladding. The data base characterizing this test direction is presented in Appendixes B and F of the report. The organized results of these tests are shown in Fig. 3.63.

The consideration of test results has led to the following conclusions:

- the oxidation at 1000 C leads to more unfavorable consequences than those occurring at 1100 C, clear indications of the breakaway oxidation are observed on the appearance and microstructure of the cladding oxidized at 1000 C;
- the appearance and microstructure of the E635 cladding oxidized at 1100 C are noticeably better than those of the E110 cladding at 9.3% ECR;
- the hydrogen measurements confirm these observations:

– the hydrogen content in the E635 cladding oxidized up to the 9.3% ECR at 1100 C is significantly less than that in the E110 cladding;

- the hydrogen content in the E635 cladding oxidized at 1000 C even higher than that in the E110 cladding at the 5.3% ECR;
- the results of ring compression tests performed with the E635 cladding oxidized at 1000 C are in a good agreement with the above listed observations. In accordance with these results, all general characteristics for the E635 cladding oxidized at 1000 C are not better than those for the E110 cladding;
- the results of mechanical tests with the E635 cladding oxidized at 1100 C are rather contradictory as some rings have demonstrated the improvement of the mechanical behavior and the increase of residual ductility margin, but many rings have demonstrated the same results as those obtained for the E110 cladding or even worse ones.

The results of this analysis show that apparently, the chemical composition of niobium-bearing alloys is the important factor for the behavior of these alloys under high temperature oxidation conditions. However, tests of the E635 cladding for just another time bring us to the conclusion that there are some other factors unaccounted in the present analysis that influence the oxidation mechanism. The analysis of these will be continued in 4 chapter of the report.

3.3.6. Interrelation between the zero ductility threshold and the temperature of mechanical tests

All test results presented in the previous report sections were obtained in mechanical tests at the temperature 20 C (room temperature). However, it is evident that for safety practical analysis, it is of importance to understand to what extent the zero ductility threshold is sensitive to the temperature at the stage of proceeding from quenching during reflood to post-LOCA cooling. It is known that this stage is characterized by the achievement of the saturation temperature during reflood. This temperature may slightly differ for different reactors, however, by the existing tradition, the value of that is estimated as 135 C.

The preliminary analysis of results from the studies performed earlier allowed to establish the following:

- there are very limited data characterizing the oxygen induced embrittlement in this temperature range (20–135 C);
- quite a number of investigations were performed to study the effect of the hydrogen induced embrittlement.

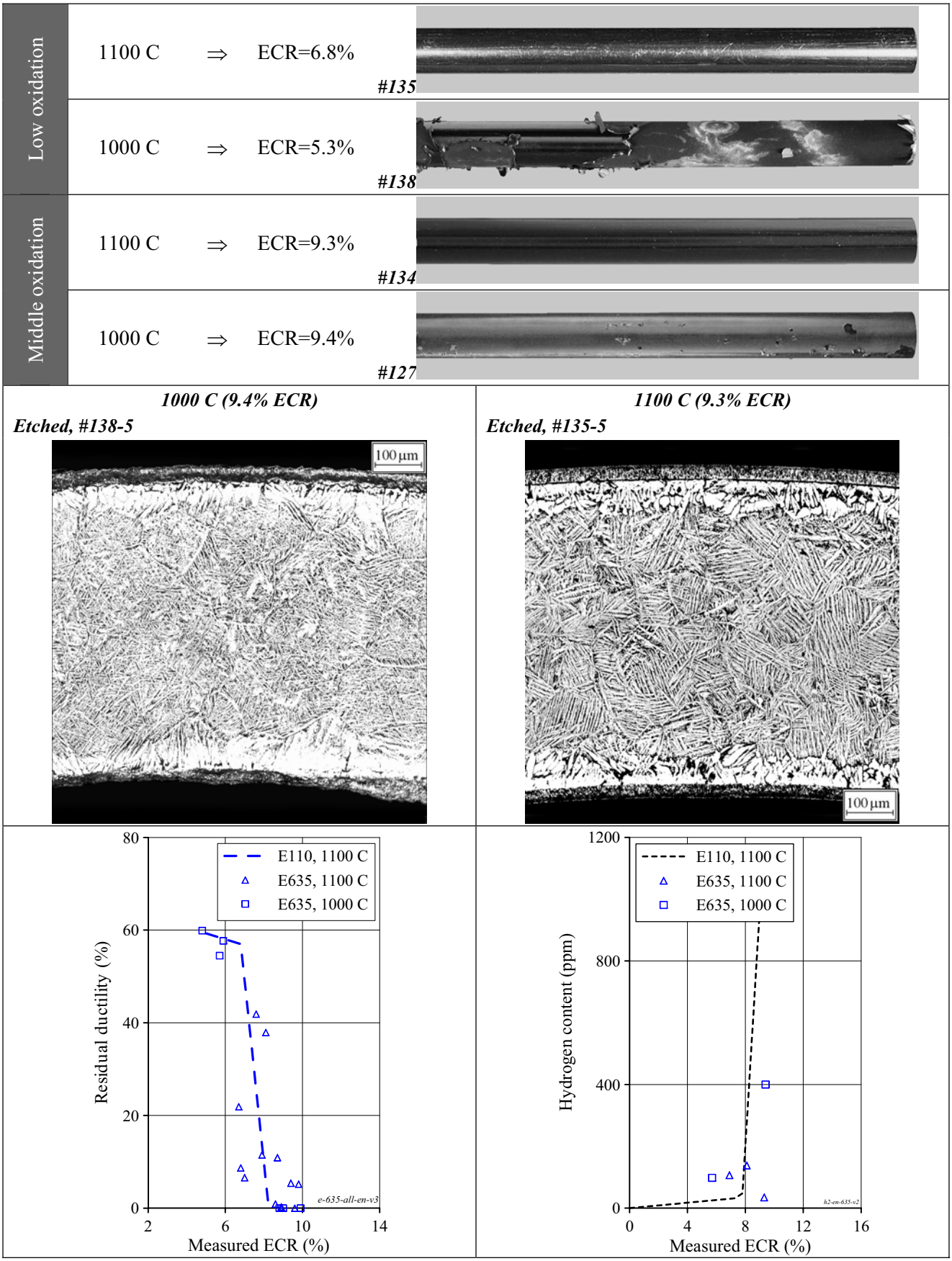

Fig. 3.63. The characterization of the E635 cladding behavior under oxidation and mechanical test conditions

So, as for the oxygen embrittlement, the most part of published data was devoted to the studies of the zirconium cladding mechanical behavior as a function of the initial oxygen concentration in the cladding material. In accordance with Russian data (for Zr-1%Nb) and other data for alloys of the zircaloy type, the elongation of the claddings with oxygen concentration 0.05–0.16% (by weight) in the α-phase is not sensitive to the temperature within the range 20–200 C. The previous Russian investigations performed in the Bochvar Institute (VNIINM, V.Tonkov) have shown that the ductility of the E110 oxidized claddings as a function of temperature of mechanical tests in the range 20–200 C is subjected to the following regularities:

- ZrO_2 and α-Zr(O) ductility is not increased in this temperature range;
- α-phase (prior β-phase) ductility is the function of the temperature especially in the range 100–200 C; however, the researcher associated this effect with the hydrogen behavior in the cladding material.

Unfortunately, this issue (the oxygen induced embrittlement) did not meet with due elucidation even in such a complete monograph which is the monograph of D.L. Douglass [42]. Though, the review made by D.L. Douglass contains the illustration that demonstrates that the samples manufactured from Zr-2.5%Cu alloy and oxidized up to 0.6% of the oxygen content in the zirconium matrix elongate from 2 up to 31% on the temperature increase from 20 up to 200 C.

The previous investigations performed by the authors of this report with unirradiated and irradiated Zr-1%Nb claddings have shown that the cladding elongation is not sensitive to the temperature of mechanical tests (20–200 C) in the presence of irradiation damage effects (50 MWd/kg U), low oxidation (oxide thickness 5 μm) and low hydrogen concentration (30 ppm) [19].

As for the hydrogen embrittlement, the appropriate effects revealed in a number of studies may be characterized in the following way:

- the oxidized cladding fracture resistance is a strong function of precipitated hydrides;
- the cladding ductility margin is a function of hydride concentration, size, orientation and morphology;
- the ductility of hydrides is a function of the temperature in the range from approximately 100 C and higher;
- it was experimentally demonstrated that brittle cracks initiated in the brittle α-Zr(O) layer slow down and are not developed in the prior β-phase while the hydride ductility is increased. In its turn, this effect results in the fact that the cladding elongation is increased also.

Besides, some additional observation of importance should be noted:

- the hydride-related embrittlement of such alloy as the irradiated Zry-4 is a function of a transformed beta microstructure [43];
- the temperature of ductile-brittle transition (DBT) is slowly increased with the hydrogen concentration increase [42];
- for the low hydrogen concentration in the prior β-phase, the transition from the brittle to ductile fracture is very sensitive to the temperature [42];
- the cladding ductility is not sensitive to the hydrogen concentration up to 70 ppm [44];
- the unirradiated cladding ductility at the room temperature is decreased very sharply down to low values with the hydrogen content of about 700 ppm [45];
- the worst ductile behavior was demonstrated at the room temperature in the cladding material with uniformly distributed hydrides [46].

The obvious illustration for some of the listed effects is demonstrated in Fig. 3.64 [47]. In accordance with these data, the cladding samples with lower hydrogen concentration (180 ppm) have demonstrated significantly higher sensitivity to the temperature of mechanical tests in the range 50–150 C than that of the cladding samples with hydrogen concentration of about 700 ppm. At 200 C, the mechanical behavior of both types of samples was quite ductile.

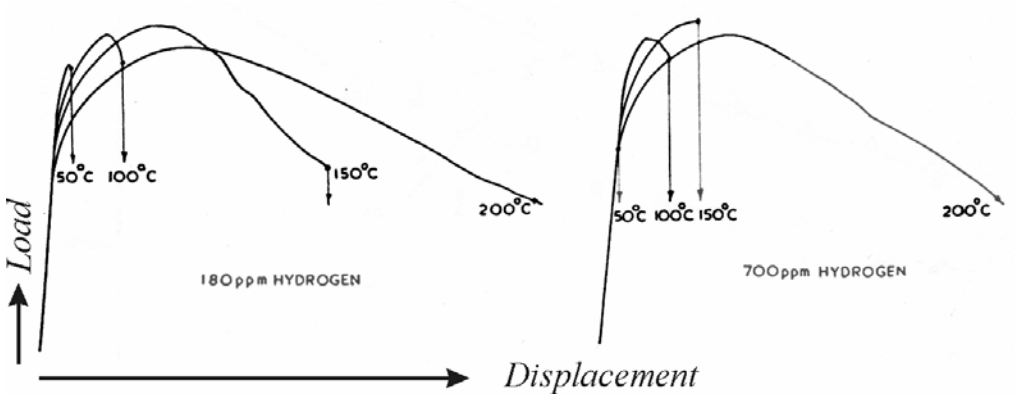

Fig. 3.64. Load-displacement diagrams for two Zry-2 samples hydrided (specially) up to 180 ppm and 700 ppm, respectively, as a function of the temperature mechanical tests of the bending type (reprinted from [47])

To reveal the temperature effects in the E110 oxidized and hydrided cladding after the oxidation tests performed in the frame of this work, the following approach was applied:

- the representative scope of mechanical tests (ring compression tests) was performed at 135 C with the E110 cladding samples oxidized at 800–1200 C and F/F, F/Q combinations of heating and cooling rates;
- several reference ring compression and ring tensile tests were performed with the E110 oxidized cladding samples in the temperature range 20–300 C.

The results of ring tensile reference tests are presented in Fig. 3.65.

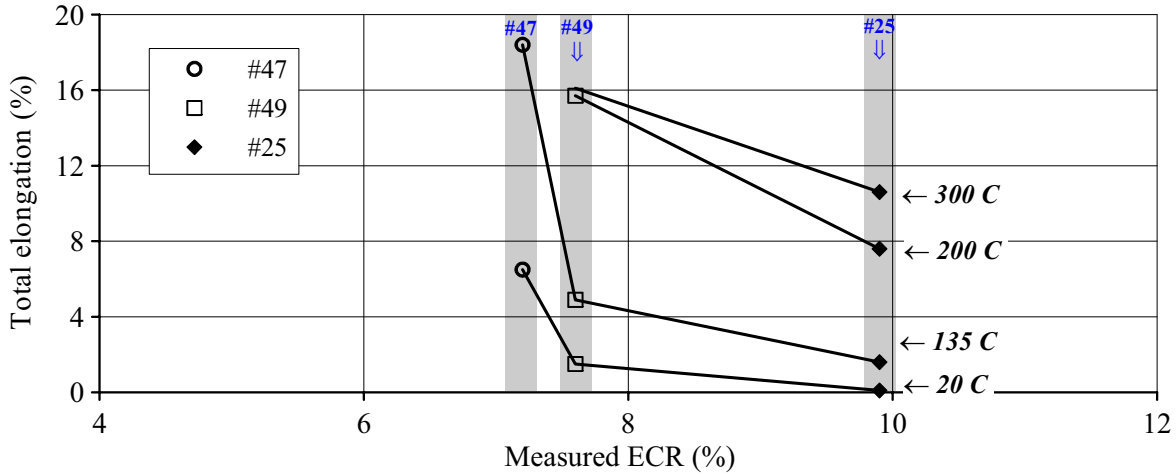

Fig. 3.65. Dependence of the E110 cladding ductility on the ECR (oxidation at 1100 C) and temperature of ring tensile tests

In accordance with these results the following comments can be made:

- the ductile cladding sample (#47, 7% ECR, the residual ductility 55–65% according to ring compression tests, low hydrogen content 30 ppm) demonstrated maximum sensitivity to the temperature of ring tensile tests in the range 20–135 C. The total elongation of this sample increased from 7% at room temperature to 17.5% at 135 C;
- the almost brittle sample (#49, 7.5 % ECR, the residual ductility 1.3–3.6 % according to ring compression tests, critical hydrogen content ~ 500 ppm) demonstrated:

– pronounced sensitivity to the temperature of ring tensile tests in the range 20–135 C. The total elongation increased from 1.5 to 5% respectively;

– very high sensitivity to the tensile test temperature in the range 135–200 C. Total elongation of this quite brittle sample increased from 5 to 16%;

– further increase of tensile test temperature to 300 C did not lead to the increase of ductility;

- the brittle sample with very high hydrogen content in the prior β-phase (#25, 9.9% ECR, hydrogen content 1000 ppm) shown a low sensitivity to the tensile test temperature between 20 and 135 C and high sensitivity in the range 135–300 C, where the total elongation increased from 1.7 to 10.6%.

Before we analyze the above stated comments, it will be useful to supplement this data base with results of the ring compression test performed at 20–300 C. The results are presented in Fig. 3.66.

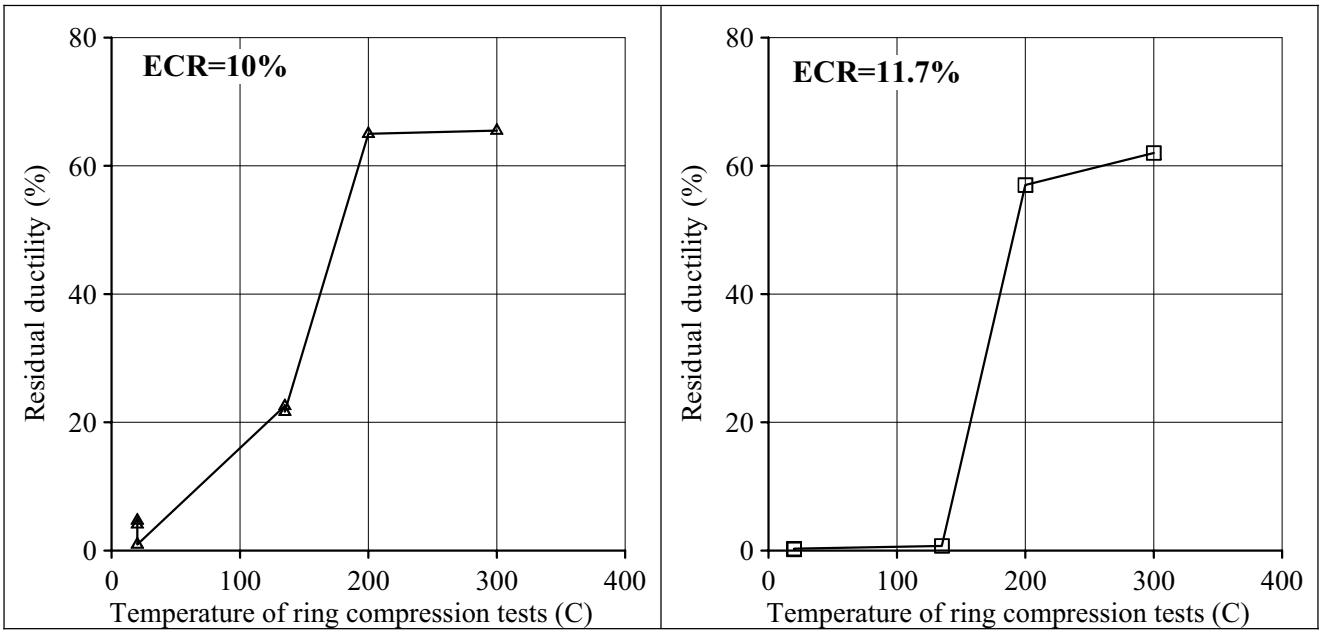

Fig. 3.66. Residual ductility of two E110 samples oxidized at 10 and 11.7% ECR (1100 C) as a function of temperature ring compression tests

The obtained data lead to the following observations:

- the sample (#68), which was oxidized somewhat higher than the zero ductility threshold (10% ECR) up to the hydrogen concentration of about 1000 ppm, has demonstrated definite sensitivity to the temperature of mechanical tests ranging from 20 up to 135 C; the residual ductility of this sample significantly increase in the range 135–200 C. However, we did not manage to reveal the influence of the temperature range 200–300 C over this sample ductility due to the fact that the maximal grip displacement (in these tests corresponded to the residual ductility of about 65%) was already achieved at the 200 C;
- the brittle sample (#36, ECR=11.7%) with a very high concentration of hydrogen (1500 ppm) was insensitive to the temperature of mechanical tests in the range 20–135 C, this sample ductility sharply increased in the temperature range 135–200 C, after that, the additional ductility increase was observed in the temperature range 200–300 C.

If we summarize the results of the preliminary analysis then the following tendencies may be noted:

- the less is the hydrogen concentration, the higher sensitivity to the temperature increase is demonstrated by E110 oxidized samples in the temperature range 20–135 C;
- the influence of the temperature of mechanical tests within the range 20–135 C over ductility of the E110 oxidized samples manifests itself still at the hydrogen concentration 1000 ppm, however, on the further hydrogen concentration increase (up to 1500 ppm), the cladding ductility is insensitive to the temperature within this range;
- the temperature increase up to 200 C leads to the significant increase of the cladding ductility in the whole studied range of the hydrogen concentrations;
- the temperature increase up to 300 C will influence the cladding ductility the more noticeably, the higher it was hydrided at 20 C.

The peculiar features revealed for the mechanical behavior of the E110 oxidized cladding may be clarified still more with the help of the representative data base obtained on the basis of ring compression tests performed at 20 C and 135 C. The first organized data characterize the relationship between the residual ductility of the E110 oxidized cladding and the hydrogen concentration at two temperature levels (see Fig. 3.67).

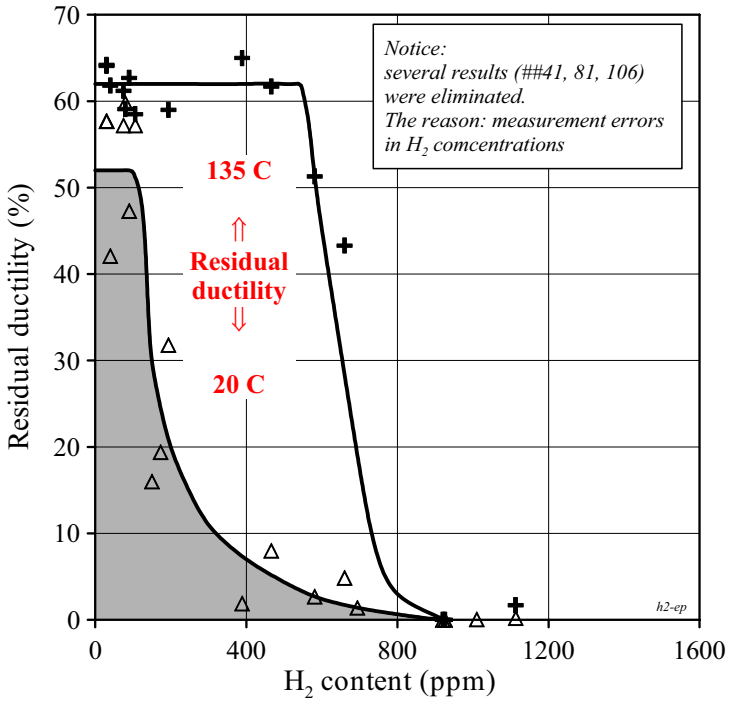

Fig. 3.67. The sensitivity of the E110 residual ductility (800–1200 C, F/f and F/Q) to the hydrogen concentration at 20 and 135 C

These data allow to make the following general conclusions:

- the residual ductility of the E110 oxidized cladding is a function of the hydrogen concentration;
- the E110 cladding has a very high level of residual ductility (higher than 50%) at 20 C within the interval of hydrogen solubility at 20 C (0–100 ppm);
- the residual ductility at 20 C decreases vary sharply in the narrow range of the hydrogen concentration: 100–200 ppm;
- the zero ductility threshold at 20 C is situated between 400–800 ppm of the hydrogen concentration;
- taking into account that the hydrogen solubility limit and ductility of hydrides are increased at 135 C, the E110 cladding samples demonstrate a very high level of residual ductility in the range of the hydrogen concentration 0–500 ppm;
- at 135 C, the decrease of residual ductility takes place very sharply with the hydrogen concentration 500–700 ppm and the zero ductility threshold corresponds to 900 ppm of the hydrogen concentration at this temperature.

The relationship between revealed effects and the oxidation level may be characterized using the second organized data presented in Fig. 3.68. In this case, the increment of residual ductility at 135 C (residual ductility at 135 C minus residual ductility at 20 C) was determined as a function of the ECR.

As it was already mentioned above, the results of ring compression tests do not allow to observe the effect of ductility increase with the temperature increase in mechanical tests for samples with high residual ductility at 20 C because the grip displacement of test machine was specially limited. In this connection, the increment of residual ductility at 135 C was not revealed in the range 0–6.5% (0–100 ppm of the hydrogen concentration). The ECR range of 6.5–8.3% characterizes a sharp decrease of residual ductility at 20 C, the sharp increase of the hydrogen content up to 700 ppm and a fast increase of increment of residual ductility at

135 C up to the maximum value that corresponds to the zero ductility threshold at 20 C (the critical ECR is 8.3%). After that, the increment of residual ductility at 135 C decreases fast down to zero that is associated with the increase of oxygen and hydrogen concentration in the prior β-phase.

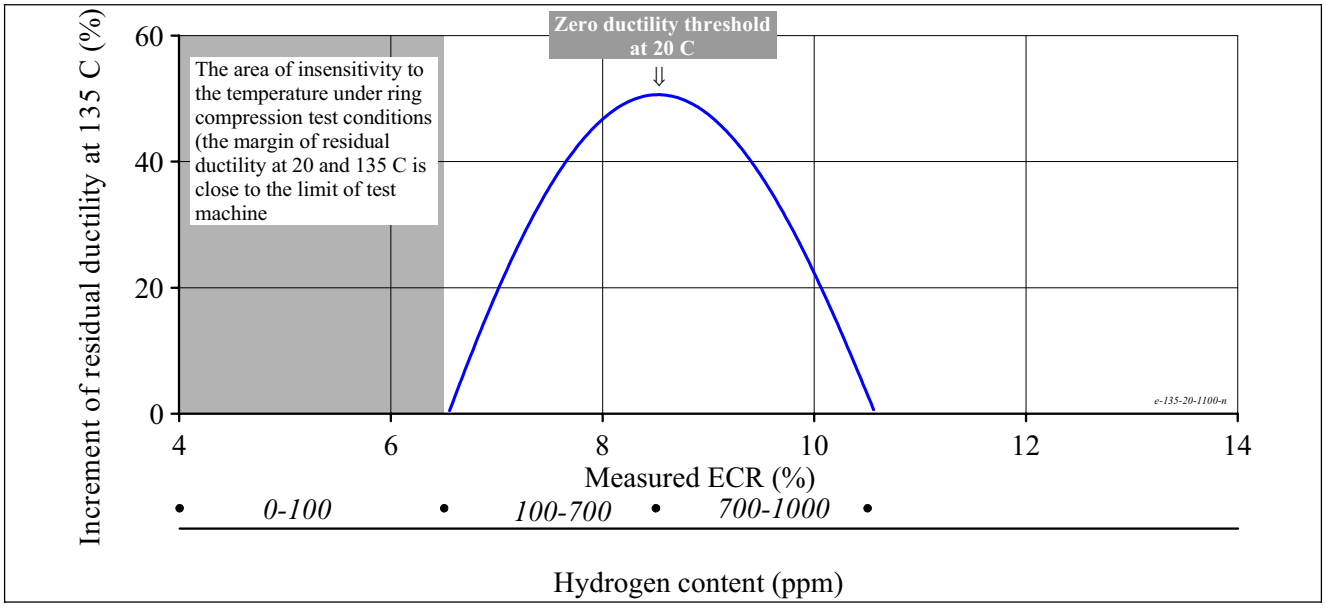

Fig. 3.68. The data characterizing the sensitivity of the E110 residual ductility at 135 C to the ECR (900–1100 C, F/F and F/Q)

Thus, this cycle of investigations allowed:

- to reveal the major effects associated with the hydrides behavior as a function of temperature;
- to reveal the sensitivity of the E110 residual ductility to the temperature.

But the analysis shows that one aspect of this issue remained not quite clear, namely, the consideration of temperature effects, associated not so much with the hydrogen embrittlement as with the oxygen embrittlement. Therefore, the analysis will be continued in chapter 4 of the report.

3.3.7. The analysis of representativity of the zero ductility threshold determined due to ring compression tests

It is obvious that the oxidized claddings of fuel rods will experience complicated multi-dimensional loadings during the real LOCA. Therefore, the problem of representativity of the zero ductility threshold determined using relatively simple ring compression tests is discussed simultaneously with performing studies of this type and during the time of this performance. The cycle of appropriate investigations performed in the frame of this work is the immediate contribution into the solution of this problem.

The approach, developed to obtain the comparative data for this issue analysis included the following items:

- the performance of several tests with other types of mechanical loading for the cladding samples and the comparison of the whole set of obtained results;
- the extension of the test data base involved into the determination of the zero ductility threshold due to the processing of data characterizing the maximum loads at the fracture;
- the comparison of macroscopic and microscopic data to confirm brittle or ductile fracture of oxidized claddings.

The test performed in accordance with the first item of this list included the ring tensile tests and three-point bending tests. The procedures for these tests are described in sections 3.2.2.2, 3.2.2.3 of the report. The comparative data characterizing results of ring tensile and ring compression tests are presented in Fig. 3.69.

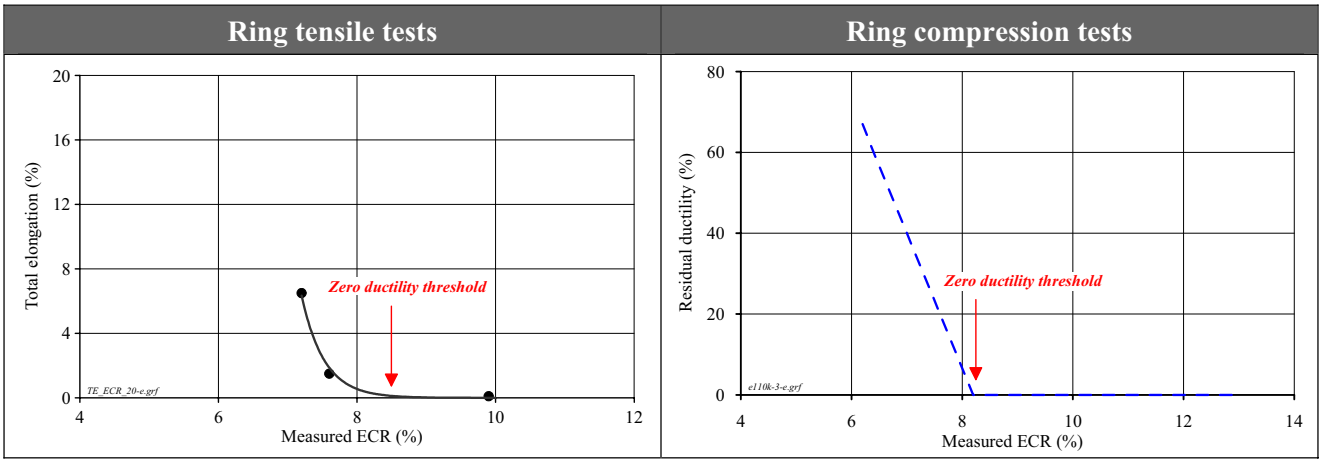

Fig. 3.69. The comparison of zero ductility thresholds determined from the results of ring tensile and ring compression tests (E110, 1100 C)

The obtained data indicate clearly that there is no difference in the zero ductility threshold determined using the ring tensile tests or ring compression tests. The results of three-point bending tests presented in Fig. 3.70 allow to conclude that the zero ductility threshold determined due to this type of tests is higher than that determined using the ring compression tests (11.8% and 8.3% ECR, respectively).

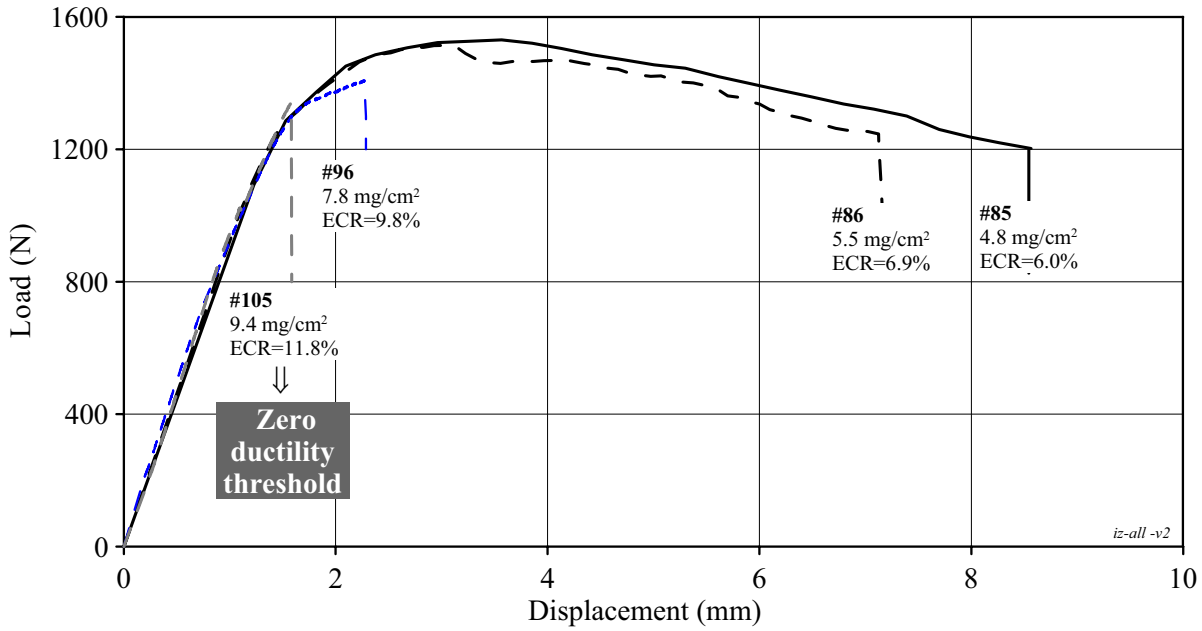

Fig. 3.70. The zero ductility threshold of the E110 cladding determined due to three-point bending tests (1100 C, F/F)

Thus, the comparative data base obtained due to different types of mechanical tests shows that ring compression tests allow to obtain the conservative estimation of the zero ductility threshold. This conclusion made on the basis of macroscopic tests is confirmed by the results of microscopic observations obtained using the fractography examinations. The fragments of two rings were selected for the fractography examinations after the fracture under the ring compression test conditions:

- a brittle ring: 1100 C, 8.2% ECR, double-sided oxidation;
- a ductile ring: 1100 C, 6% ECR, single-sided oxidation.

Two fracture surfaces of the brittle ring fragments were studied in detail (see Fig. 3.71):

- fracture surface characterizing the behavior of sample segment, which experienced the compression stresses on the outer surface and tensile stresses on the inner surface (the first fracture surface);

- fracture surface characterizing the behavior of other part of cladding, which experienced the tensile stresses on outer surface and compression stresses on the inner surface (the second fracture surface).

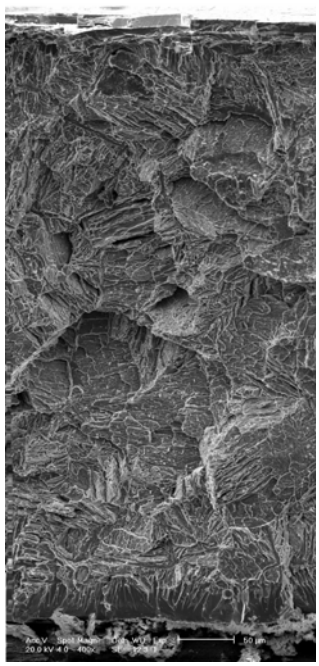

The first fracture surface

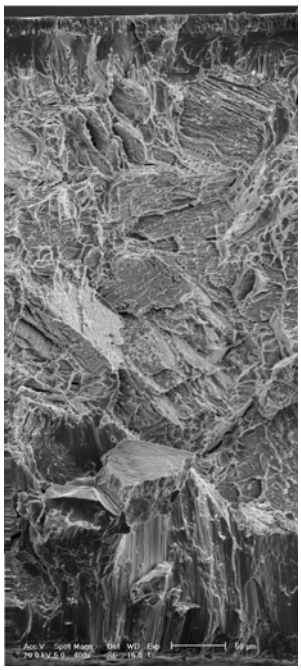

The second fracture surface

Fig. 3.71. SEM micrographs for fracture surfaces of the E110 brittle cladding

The examinations of the first fracture surface performed using the SEM micrographs with a high magnification (see Fig. 3.72) have shown that:

- the oxide layers on the outer and inner cladding surface are of the columnar structure and the oxide thickness is 15 μm (Fig. 3.72a,b);
- a typical pattern for α-Zr(O) surface is of the cleavage type (see Fig. 3.72b);
- the fracture pattern of the prior β-phase layer is quasi-cleavage (Fig. 3.72c), the fracture surface may be characterized as the "terrace" type (Fig. 3.72d), separate small regions of a dimple rupture are observed on the boundary between the α-Zr(O) and prior β-phase layers (Fig. 3.72e); besides, the transition from the quasi-cleavage fracture to the cleavage fracture is revealed in this region.

The structure of the second fracture surface as a whole does not differ from the first fracture surface though, a somewhat higher number of ductile fracture regions was fixed in this sample. Moreover, the fracture surface of the prior β-phase in this sample is characterized by the mixed type of the fracture pattern: the combination of quasi-cleavage facets and the dimples of the ductile fracture (Fig. 3.72f).

The analysis of the fracture surface in the ductile cladding sample confirms that the surface pattern of the prior β-phase is typical for the ductile fracture (see Fig. 3.73). Only separate small regions of the quasi-cleavage fracture type were observed in this sample. Thus, the fractography data have shown that small areas with the residual ductility are present in the material of even brittle samples but on the whole, the reasonable agreement between the microscopic and macroscopic assessments of the zero ductility threshold is observed in the fractography examinations.

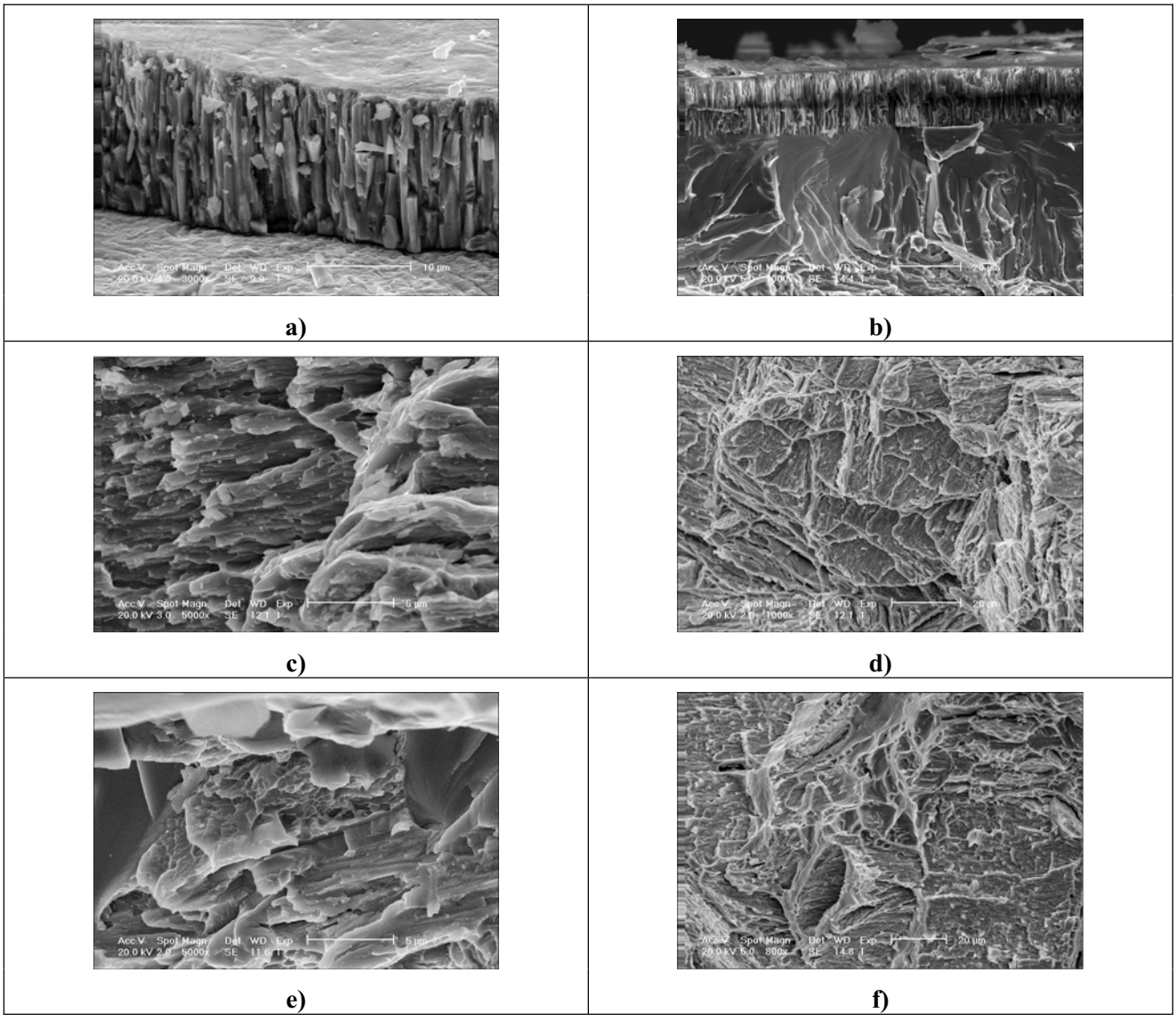

Fig. 3.72. High magnification SEM micrographs of fracture surface regions of the E110 brittle cladding

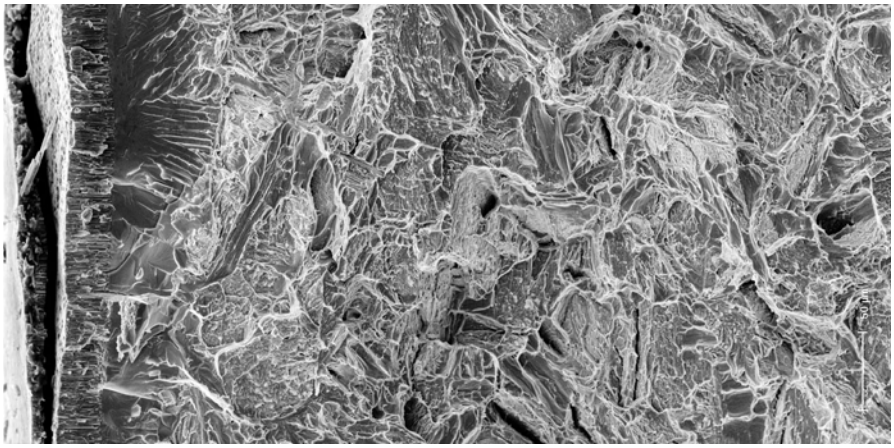

Fig. 3.73. The SEM micrograph for the fracture surface of the E110 ductile sample

It should be noted that the performed cycle of investigations employing ring compression tests for the determination of the zero ductility threshold in the E110 oxidized cladding allowed to reveal some more

issues connected with the representativity of these tests. The following two of those are considered in this report:

- the analysis of correlation between the fracture load and fracture displacement;
- the additional analysis of the sensitivity of the ring compression test results to the test procedures.

The first issue essence my be characterized in the following way: from the practical point of view, the significance of what strain the oxidized cladding has undergone during post-quench actions is not so important as that of what maximum load the cladding can stand before its fragmentation. It may be assumed that this was the reason for the authors of one of the recent papers dedicated to the M5 cladding behavior under the LOCA relevant conditions to present the characterization of the M5 fracture on the basis of the analysis of maximum loads at ring compression tests [46]. The approach of this type was the subject of the analysis performed in the frame of this work also. The organized data to clarify the appropriate issue are presented in Fig. 3.74.

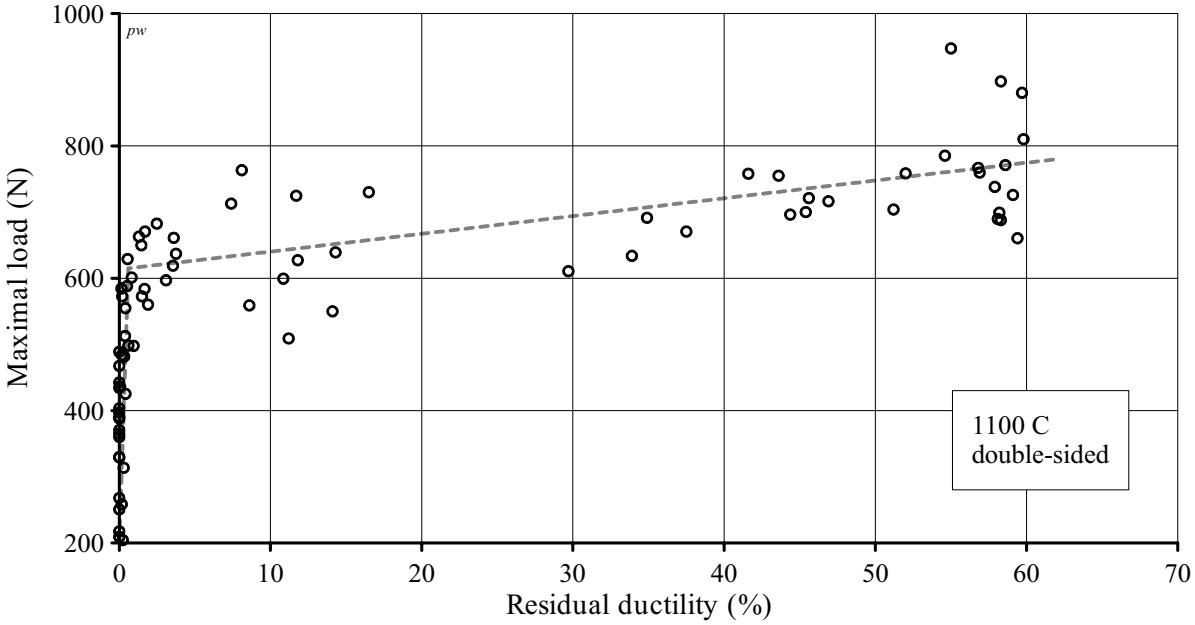

Fig. 3.74. The maximum load on the E110 oxidized sample as a function of residual ductility

The obtained data show the following:

- the decrease in the cladding residual ductility down to several percent affects its capability to withstand the load and indicates low strain hardening of the E110 oxidized cladding;
- there is a clear correlation between the zero ductility threshold and the sharp reduction in the strength properties of the E110 oxidized cladding (thus, the maximum load is decreased 3-fold as the ECR is increased from 8% up to 12%).

In other words, these data confirm that the zero ductility threshold determined as the zero residual ductility margin strongly corresponds to the appropriate critical load. But it should be noted that the employment of the critical load for the evaluation of the zero ductility threshold is not convenient as the critical load is not only the function of the ECR but it is also the function of the cladding sample length. Taking into account that there is no standard sample length for the ring compression tests and that different laboratories use samples with different lengths, in this case, it is impossible to compare the results.

The second issue that will be touched upon in this section of the report concerns just the comparison of the E110 zero ductility thresholds obtained in the ring compression tests performed in different laboratories. The analysis of comparative data base presented in Fig. 3.75 is devoted to the consideration of possible reasons for differences in evaluations of the E110 zero ductility threshold obtained by different laboratories.

The first observations concerning this comparative data base may be formulated in the following way:

- the relative order of the E110 regression correlations for test data obtained at VNIINM [15], KFKI [18, 25], NC Rossendorf [17, 24] and Scoda-UJP [10, 26] corresponds exactly to the order of the Zry-4 regression for these laboratories (see Fig. 3.28); this fact leads to the conclusion that this order is the function of experimental procedures used in each laboratory;
- in contrast to the data characterizing the Zry-4 mechanical behavior, the systematic difference is observed between the RRC KI/RIAR data and all other results;
- the zero ductility threshold of the E110 oxidized cladding is about 4.5–6% ECR in accordance with the VNIINM, KFKI, NC Rossendorf, Scoda-UJP results, while that is about 8.3% ECR in accordance with RRC KI/RIAR results.

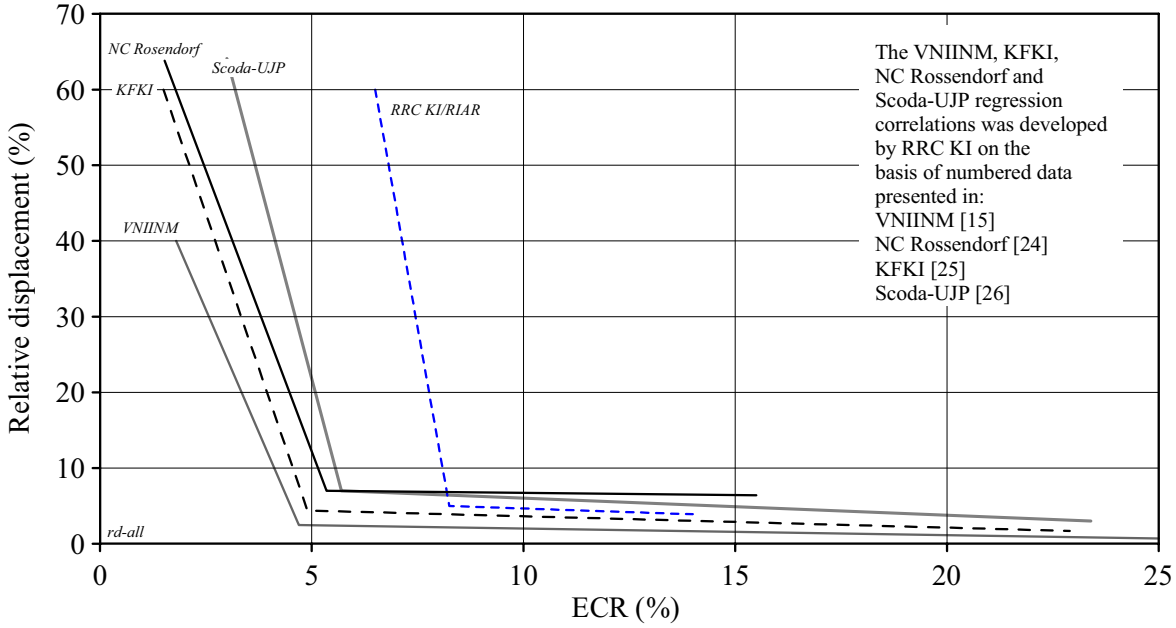

Fig. 3.75. The comparative data characterizing the E110 residual ductility as a function of the ECR obtained on the processing of test data of different laboratories

The special analysis results show that the following effects may be responsible for this difference:

- systematic errors in the procedure of the weight gain determination;
- differences in the E110 cladding material used for the oxidation tests;
- differences in the procedures of the oxidation tests (coolant type (water steam, water steam/argon mixture), heating and cooling rates) and differences in the procedures for the processing of load-displacement diagrams.

As for the procedure of the weight gain determination, the data base presented in Fig. 3.29 may be employed to assess the scale of this effect. These data show that the KFKI data really somewhat underestimate the weight gain in the Zry 4 cladding in comparison to the RRC KI/RIAR and NC Rossendorf data, but this effect is very small; the data presented in Fig. 3.28 allow to assume that the weight gain was very underestimated in the VNIINM tests. Besides, it is known that the Scoda-UJP tests were performed with the E110 claddings manufactured using the previous method of the E110 alloy fabrication, namely, the E110 claddings were fabricated from the iodide zirconium in contrast to iodide/electrolytic Zr used to manufacture the E110 cladding employed in the RRC KI/RIAR tests. The nature of the E110 cladding material used in the VNIINM, NC Rossendorf and KFKI tests is unknown. Besides the steam/argon mixture was used in the some of these tests. The sensitivity of test results to this parameter is not quite understood also.

And, finally, one more important potential cause for revealed differences must be considered. This cause is associated with the procedure for the preparation of the cladding samples for the mechanical tests. So, in section 3.2.2 it was demonstrated that results of the ring compression tests are not the function of the sample length. But this conclusion is referred to the procedure adopted in this study according to which the end parts

of the oxidized cladding were cut off and the mechanical tests with these parts of the cladding were not performed in contrast to the KFKI and VNIINM tests. Besides, the VNIINM tests were performed with very long oxidized samples (30 mm). The end parts of 20 mm samples were apparently removed in the NC Rossendorf tests because in accordance with the description of tests, two ring samples 8 mm and 5 mm long, respectively, were prepared from each of 20 mm oxidized claddings for compression tests and metallography investigations. But in our opinion, the lengths of cut off ends may appear to be not enough to compensate the effects described below. As for the Scoda-UJP tests the 7 mm rings were prepared from 30 mm oxidized samples.

The effects of the end parts of the E110 oxidized cladding may be characterized in the following way:

- the cladding oxidation takes place not only on the sample side surfaces but also on end surfaces of that. This results in the fact that the prior β-phase small cladding sample (for illustration, the sample 6 mm long was used in the KFKI tests) absorbs the oxygen from four sides. It is evident that the residual ductility of such sample will be lower than that of the sample oxidized from two sides only. In this case, this effect will be especially expressed at relatively low ECRs;
- the fact that the similar process taking place at the hydrogen absorption is still of more importance as the E110 alloy embrittlement occurs not so much according to the mechanism of the oxygen embrittlement as to that of the hydrogen embrittlement.

The effect of the hydrogen absorption by the end surface may be qualitatively illustrated by the results presented in Fig. 3.76 (Reprinted from Reference 48, Fig 5b).

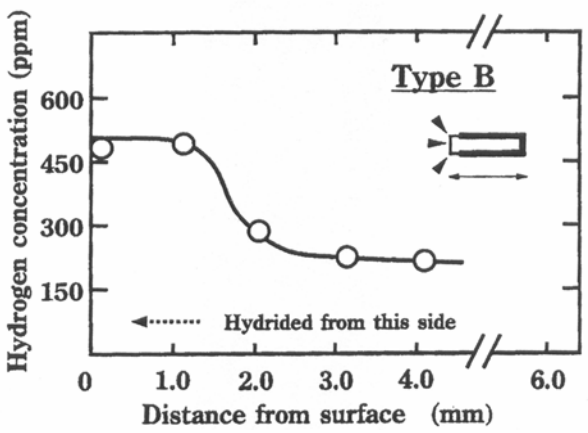

Fig. 3.76. Hydrogen distribution along the width of a special Zry-4 sample

Special investigations performed in JAERI [48] allowed to see that the end effect is strongly expressed on the length of 3 mm under these test conditions. The hydrogen concentration is 2.5 times reduced along the whole length.

Besides, it is necessary to point out once more that the hydrogen absorption by the E110 cladding is the consequence of the breakaway effect. In this case, as it was repeatedly noted earlier, the precise connection is between stresses in the oxide layer and the initiation of this effect. A special analysis performed during this research allowed to establish that the initiation of the breakaway effect takes place at the end parts of the cladding sample as, apparently, this part of the cladding sample represents a special concentrator of stresses occurring on the boundary between the end and side cladding surfaces. This statement is obviously demonstrated by the data presented in Fig. 3.77.

The obtained data obviously indicate that the initiation of the breakaway oxidation and, consequently, the initiation of the cladding hydriding, and then, the cladding embrittlement takes place in the end part of the oxidized cladding noticeably earlier than in the sample basic part.

Taking into account this analysis results, it may be assumed that the difference between the RRC KI/RIAR assessment of the E110 zero ductility threshold and assessments of this threshold performed in other laboratories is explained in the first turn by the fact that the RRC KI/RIAR test data are independent of the end

effects while the results of other investigators are overburdened with the end effect. Though, it is evident that other factors listed in the discussion of this issue additionally contributed into revealed differences.

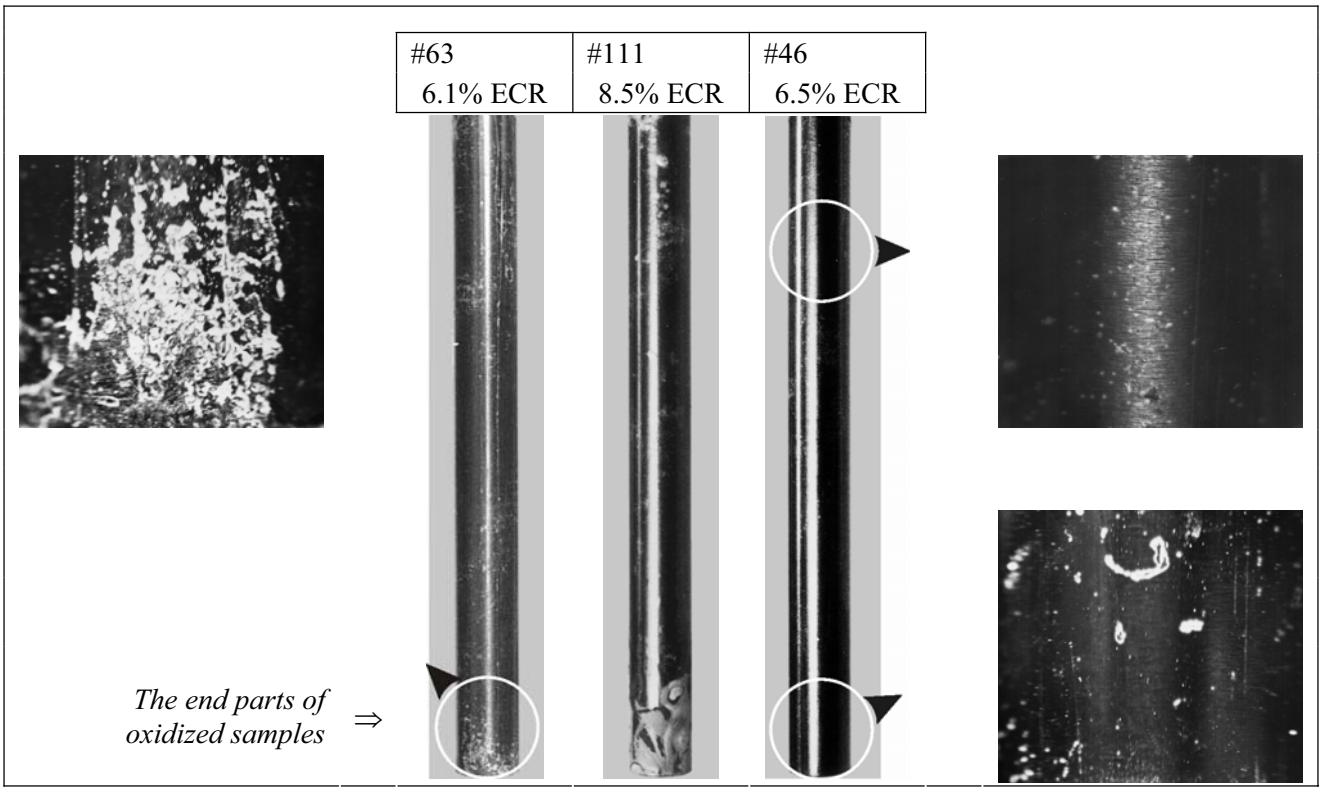

Fig. 3.77. Demonstration of the end effects on the E110 oxidized cladding samples

3.3.8. Consideration of the zero ductility threshold of the E110 cladding as a function of the irradiation effect

It is important to note that this stage of research does not pretend to be completed. The goal of this stage was to obtain the first experimental data characterizing the scale of the irradiation effect as applied to the E110 cladding. To study the appropriate phenomena, eleven irradiated claddings refabricated from the VVER high burnup fuel rods (50 MWd/kg U) were tested. The initial characteristics of irradiated claddings are presented in Appendix A–3. The oxidation and hydrogenation of the E110 irradiated cladding were characterized by the following values before the oxidation tests:

- the outer oxide thickness is 5 μm;
- the inner oxide thickness is 0 μm;
- hydrogen content is 47 ppm.

The results of the irradiated cladding tests are presented in Appendixes B and I of the report. These tests consisted of two stages:

1. Scoping oxidation tests performed at the test modes with S/S (slow/slow) and S/F (slow/fast) combinations of heating/cooling rates.
2. Basic oxidation tests performed at the F/F combination of heating and cooling rates with the variation of temperature in the range 1000–1200 C.

The analysis of the cladding appearance and microstructure after the basic oxidation tests at 1100 C allows to note the following (see Fig. 3.78):

- any indications of the breakaway oxidation are not observed on the outer cladding surface up to 7.0% ECR;
- insignificant indications of the breakaway oxidation occur at the higher ECR, however, these indications are expressed significantly weaker than those for the unirradiated cladding;
- the oxidation behavior of the irradiated cladding differs considerably by the following processes:

– the obviously expressed tendency towards the increase of the oxide thickness on the inner cladding surface in comparison with the outer oxide thickness;

– the obviously expressed tendency towards the formation of the oxide lamination and the tendency towards the oxide spallation starting from 7.7% ECR on the inner cladding surface;

– the more expressed tendency towards the generation of the α-Zr(O) phase along the grain boundaries of the prior β-phase.

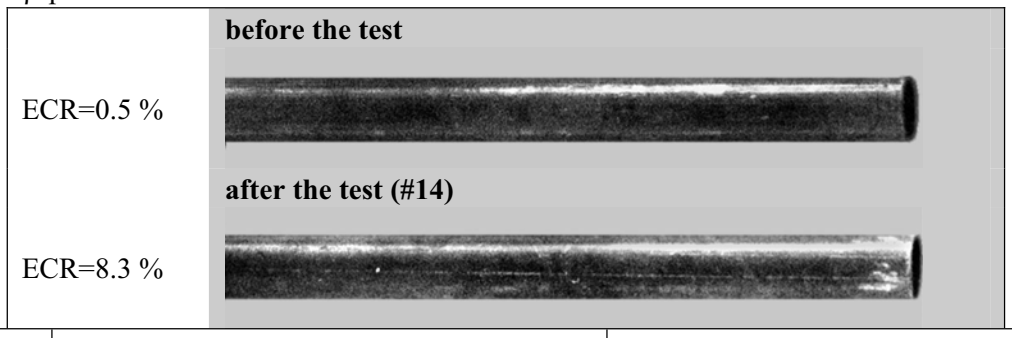

Sample	Outer surface	Inner surface
Before oxidation tests (Polished)	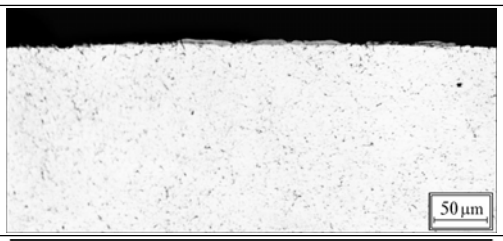	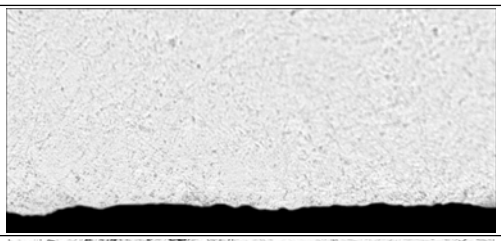
#20-4 ECR=6.3 % (Etched)	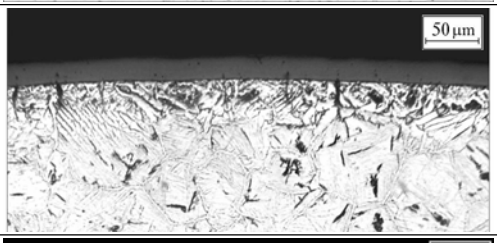	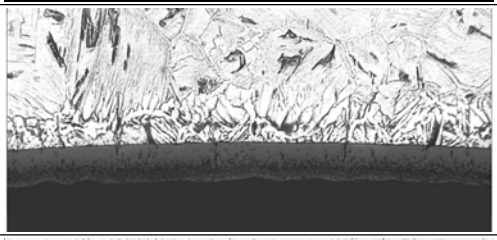
#10-4 ECR=7.7 % (Polished)	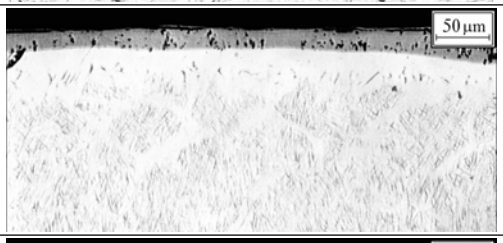	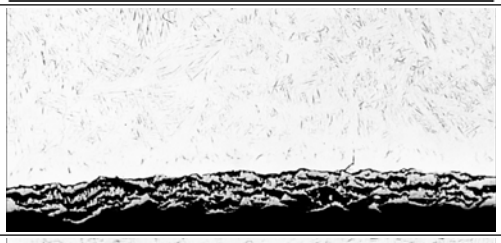
#14-4 ECR=8.3 % (Polished)		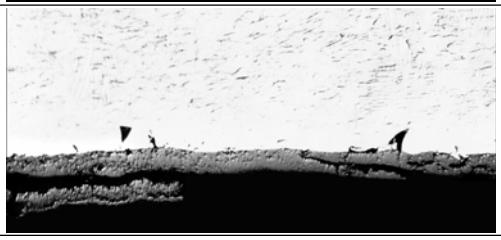

Fig. 3.78. The appearance and microstructure of the E110 irradiated cladding before the tests and after the oxidation tests at 1100 C and F/F combination of heating and cooling rates

It may be assumed that the revealed peculiar features are associated, first, with the presence of fission products on the inner cladding surface and with the participation of some of those in the oxidation reaction and, second, with the change of the cladding microstructure during the base irradiation.

As for the dependence of the oxidation behavior on the test conditions, then the performed studies have shown that:

- the irradiated cladding oxidation under slow transient conditions (S/S combination of heating and cooling rates) leads to the macroscopic effects of the oxide spallation at 10.5% ECR (see Fig. 3.79);
- the oxidation at 1200 C leads to the significant decrease or disappearance of the breakaway effect from the microscopic point of view, nevertheless the microstructure demonstrates the "hydrogen-modified" type (see Fig. 3.79).

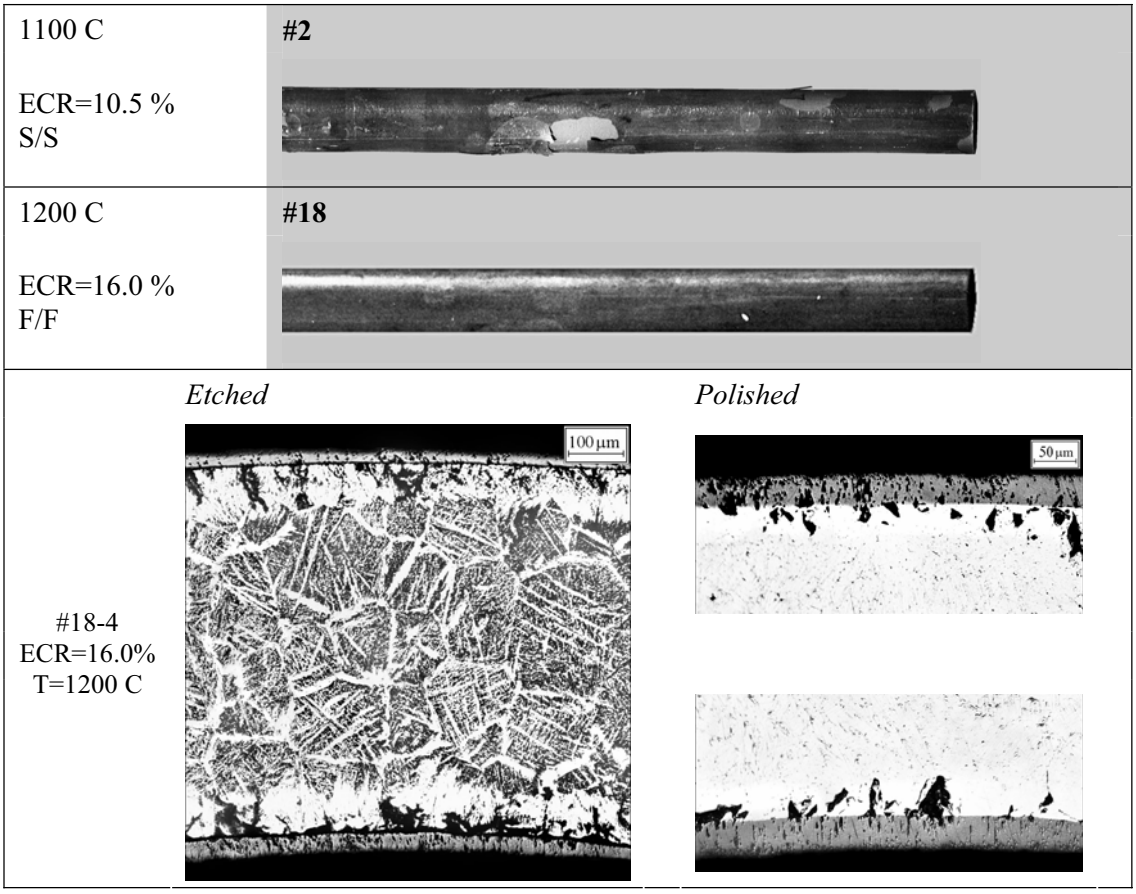

Fig. 3.79. The appearance and microstructure of the E110 oxidized cladding after the slow transient oxidation at 1100 C and standard oxidation at 1200 C

The ring compression tests performed with the E110 oxidized irradiated claddings allows to obtain the results presented in Fig. 3.80. The preliminary analysis of these results shows that a general tendency towards the decrease in the zero ductility threshold (ZDT) is observed in the irradiated claddings. To extend the data base for the more accurate analysis of specific physical processes in these claddings, the following additional investigations were performed:

- the microhardness measurement;
- the hydrogen content measurement.

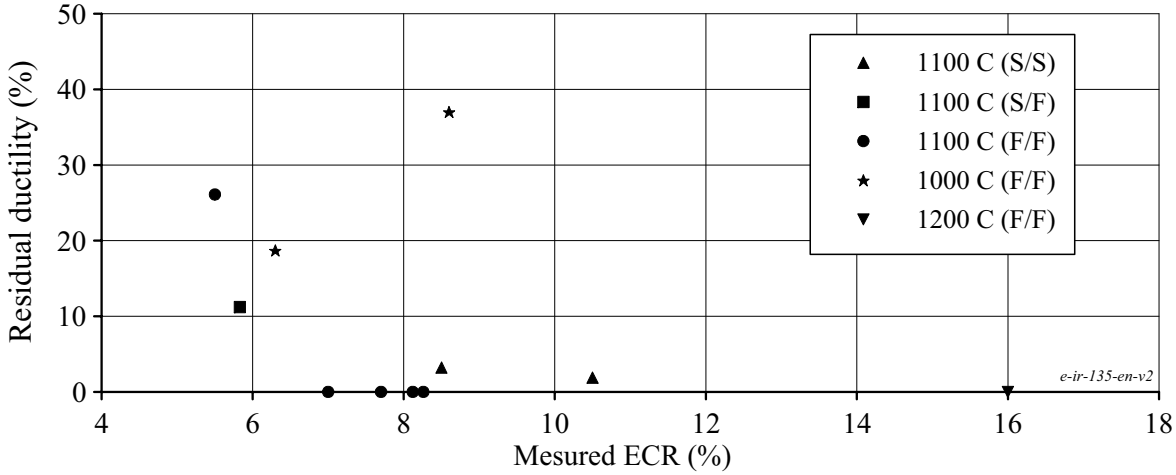

Fig. 3.80. The residual ductility of the E110 irradiated cladding as a function of the ECR

The comparative data presented in Fig. 3.81 to characterize the microhardness of different types of the E110 cladding (unirradiated, irradiated, oxidized and unoxidized) allow to make the following important observations:

- the initial microhardness of the E110 irradiated cladding (before the oxidation) is higher than that of the E110 unirradiated cladding by 60 kg/mm^2;
- the microhardness of the E110 unirradiated oxidized cladding (7.0% ECR) with a high margin of residual ductility (sample #47) is about 250 kg/mm^2 and (as it was demonstrated earlier, see Fig. 3.44) the microhardness of the E110 unirradiated oxidized cladding (ECR=8.2%) at the zero ductility threshold (sample #41) is the same;
- the microhardness of the E110 irradiated oxidized cladding (6.5% ECR) with a significant margin of residual ductility (sample #17) is practically the same as that in the E110 irradiated oxidized cladding (7.7% ECR) close to the ZDT (sample #10); this microhardness is about 300 kg/mm^2;
- the microhardness of the E110 irradiated oxidized cladding increases significantly in the ECR range 7.7–8.3% ECR and after that the microhardness is not practically changed up to 16% ECR.

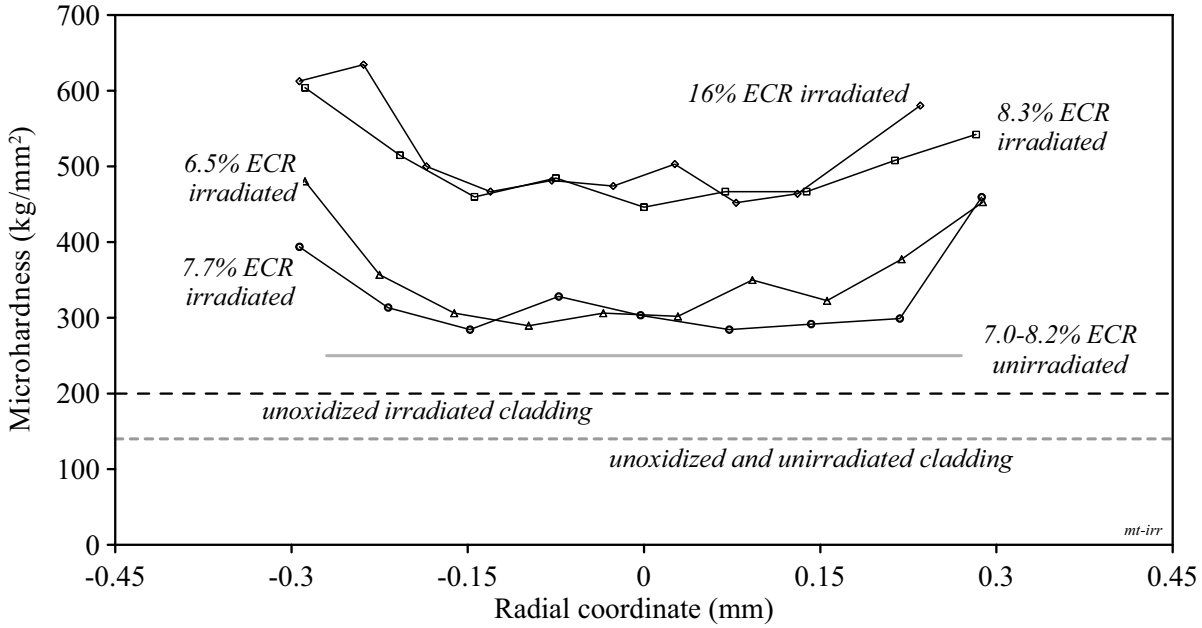

Fig. 3.81. Comparative data characterizing the microhardness of the E110 oxidized irradiated claddings

The analysis of these observations leads to the following conclusions:

- some initial embrittlement effect is observed even in such a “good” irradiated cladding as the E110 cladding;
- the oxygen concentration exceeding the oxygen embrittlement threshold (0.6–0.9% by weight) of the prior β-phase is apparently achieved in the E110 irradiated cladding at the ECR≥8.3%;
- the zero ductility embrittlement threshold of the E110 irradiated oxidized cladding is apparently determined by the same combination of factors that was determined for the E110 unirradiated cladding, namely: by the combined effect of the oxygen and hydrogen embrittlement of the oxidized cladding prior β-phase.

The continuation of this analysis performed using the results of the hydrogen concentration measurements allowed to reveal the following additional peculiar features for the behavior of the E110 irradiated cladding:

- in spite of the fact that the oxide spallation was obviously demonstrated in the oxidation mode under slow transient conditions (S/S combination of heating and cooling rates), all three cladding samples tested at slow heating had a relatively low hydrogen concentration in comparison with the samples tested at fast heating;
- the cladding samples tested under slow heating conditions demonstrated the tendency towards the increase of the zero ductility threshold in comparison with the samples oxidized at fast heating.

Taking into account all above mentioned considerations, two correlations were developed to characterize residual ductility of the E110 irradiated oxidized cladding as a function of the ECR and oxidation modes (see Fig. 3.82).

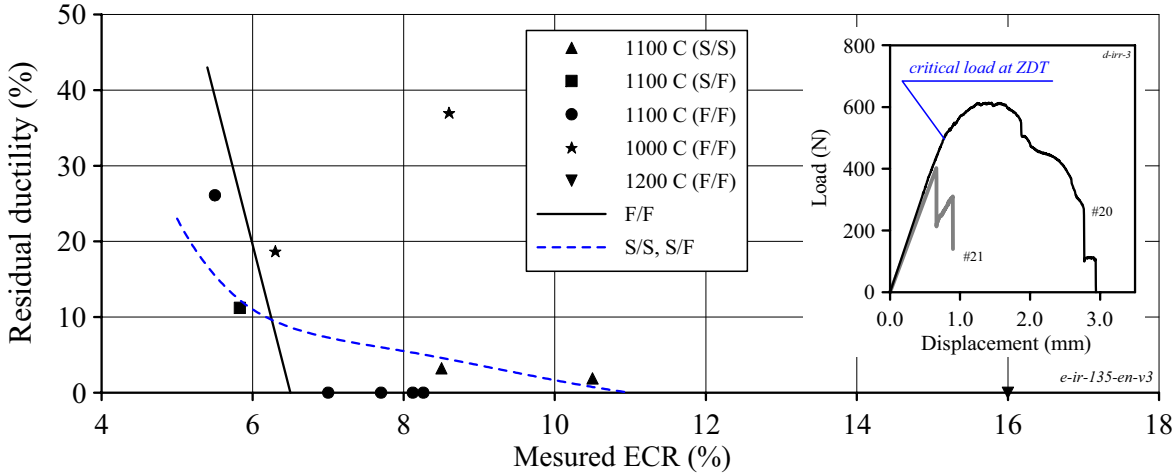

Fig. 3.82. The zero ductility threshold of the E110 irradiated cladding after different oxidation modes

It should be also noted that to minimize a possible error in the assessment of the zero ductility threshold at the F/F oxidation mode, the load-displacement diagrams were additionally analyzed. As it can be observed in the data presented in Fig. 3.82, the cladding sample #21 was tested at the ECR that was somewhat higher than the zero ductility threshold. The quantitative analysis of this discrepancy performed using the analysis of other load-displacement diagrams has shown that the zero ductility threshold for this oxidation mode F/F may be evaluated with a good accuracy as 6.5% ECR.

The organization of the data base characterizing the hydrogen content in the E110 irradiated oxidized cladding as a function of the ECR was performed in accordance with the similar approach (see Fig. 3.83).

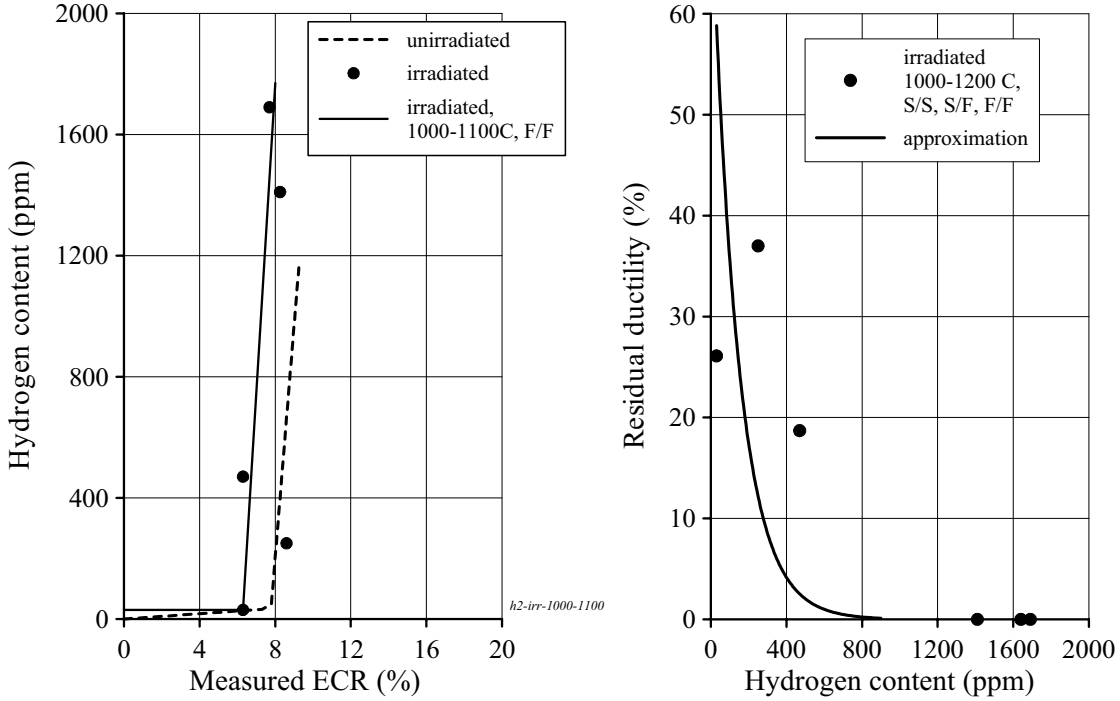

Fig. 3.83. The E110 hydrogen concentration as a function of irradiation and ECR, residual ductility of the E110 irradiated cladding as a function of hydrogen concentration

The regression dependence presented in Fig. 3.83 characterizing the hydrogen content in the E110 irradiated cladding was developed for the F/F oxidation mode in the temperature range 1000–1100 C. The appropriate dependence at the temperature 1200 C will apparently demonstrate a smoother increase of the hydrogen content as a function of the ECR. The comparison of obtained data with results obtained for the E110 unirradiated cladding shows that the hydrogen absorption takes place in the irradiated cladding still more intensively. However, coming back to the results of the analysis performed using the metallographic views, it may be assumed that special processes occurring on the inner cladding surface are responsible for revealed differences.

Additional data presented in Fig. 3.83 to describe the relationship between residual ductility of the E110 irradiated cladding and hydrogen content (developed with regard to all test modes and all temperatures) are in a good agreement with the similar data obtained for unirradiated claddings. Nevertheless, it is impossible to exclude the fact that a definite peculiarity in the behavior of the irradiated cladding during the oxidation may be caused by the changes in its microstructure that took place during the base irradiation. Thus, the SEM investigations performed with the E110 irradiated cladding allowed to reveal the following tendencies:

- the cladding material structure is characterized by the α-Zr phase containing the global β-Nb precipitates;
- the niobium concentration in the matrix is practically equal to zero.

Taking into account the considered earlier oxidation effects associated with niobium, it may be assumed that in this case, the change of the Zr-1%Nb material structure results in some change of its oxidation behavior.

3.3.9. The analysis of the E110 oxidation kinetics

To develop the E110 oxidation kinetics, the parabolic law was used:

$\Delta W^2 = Kt$,

where ΔW – the weight gain (mg/cm^2);

t – time (s);

K – rate constant (mg^2/cm^4 s).

Besides, it was assumed that the rate constant may be described by Arrhenius relation:

$$K = A \exp\left(-\frac{Q}{R\,T}\right),$$

where A – empirical coefficient (mg^2/cm^4 s);

Q – activation energy (J/mol);

R – gas constant (J/mol K);

T – temperature (K).

The processing of test data started from the determination of K using each measured combination of ΔW and t. The averaged value of ΔW obtained in the several ring samples cut off from one 100 mm cladding sample was employed for this goal. These data were used to develop the regression dependence presented in Fig. 3.84. It should be noted that the data obtained at the F/F and F/Q combinations of heating and cooling rates only were used for this procedure.

The obtained correlation is valided for the following oxidation duration as a function of the oxidation temperature:

- 1073 K → 29000 s;
- 1173 K → 4800 s;
- 1223 K → 5000 s;
- 1273 K → 1800 s;
- 1373 K → 1800 s;
- 1473 K → 400 s.

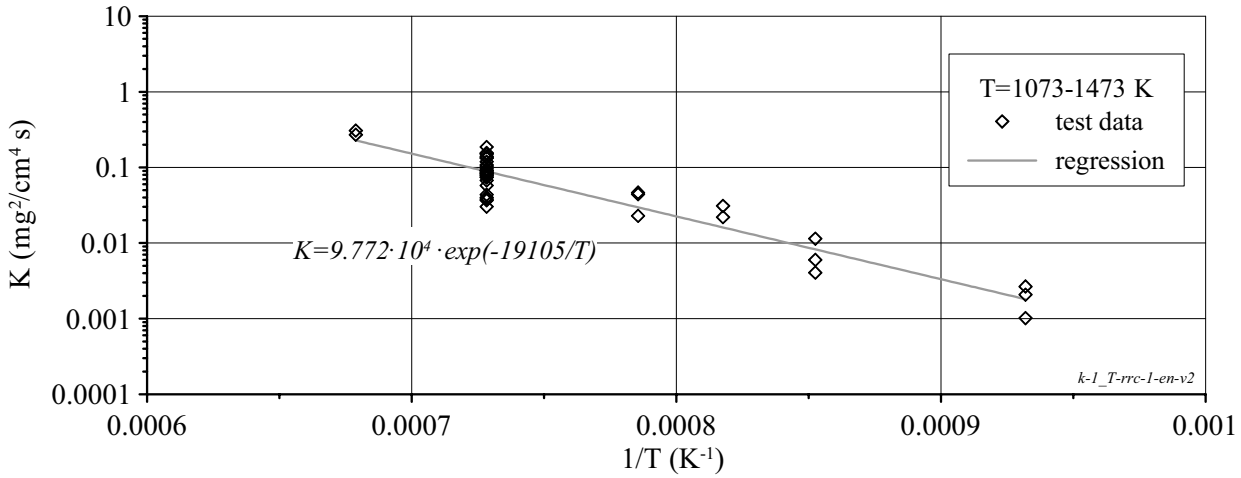

Fig. 3.84. Determination of the rate constant at the oxidation of the E110 unirradiated cladding in the temperature range of 1073–1473 K

The sensitivity of the E110 oxidation kinetics to the irradiation effect may be preliminary estimated using the data presented in Fig. 3.85.

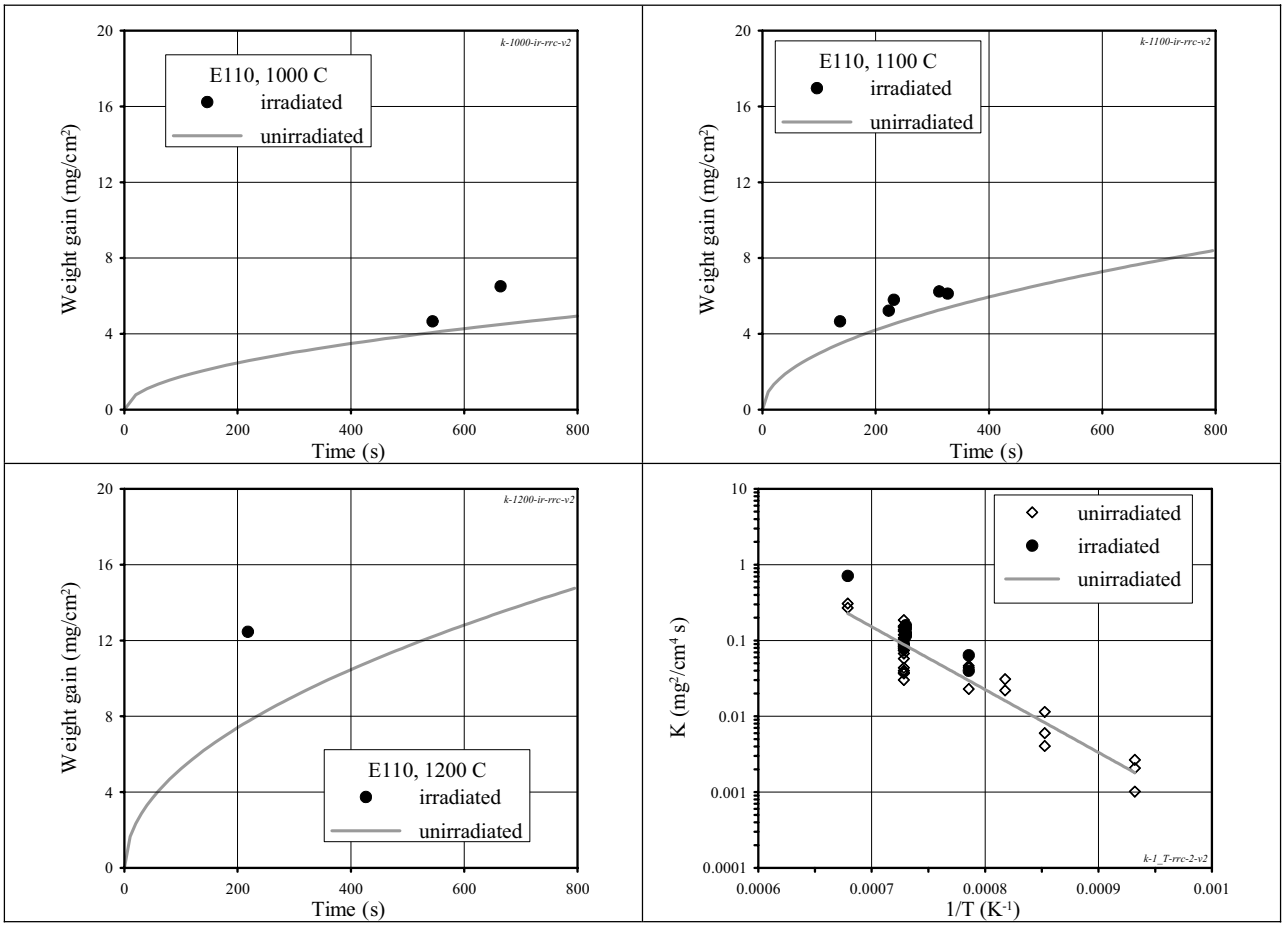

Fig. 3.85. Comparison of the oxidation kinetics for the E110 unirradiated and irradiated claddings

These data show that the oxygen weight gain in the irradiated cladding is somewhat higher than that in the unirradiated cladding, however, taking into account the sparsity of test data available for the E110 irradiated cladding, it seems to be impossible to estimate this effect quantitavely.

The E110 oxidation kinetics was additionally analyzed to clarify the following important issues:

- the assessment of the applicability of the E110 oxidation kinetics (developed basing on the test data with fast heating and fast cooling modes) for the transient oxidation modes such as slow heating and slow cooling (S/S), slow heating and fast cooling (S/F), fast heating and slow cooling (F/S);
- the comparison of the E635, Zry-4, and E110 oxidation kinetics;
- the comparison of the E110 oxidation kinetics developed in different laboratories.

The temperature–time histories of several tests performed at F/S, S/F, S/S combinations of heating and cooling rates were processed using the same procedure of the effective time determination, which was employed for this goal on the processing of F/F and F/Q appropriate data. The major provisions for the procedure are described in Appendix A-6 of the report. The comparative data characterizing the oxidation kinetics at different oxidation modes are presented in Fig. 3.86. In accordance with the obtained data, reasonable correlations are observed between all types of experimental results.

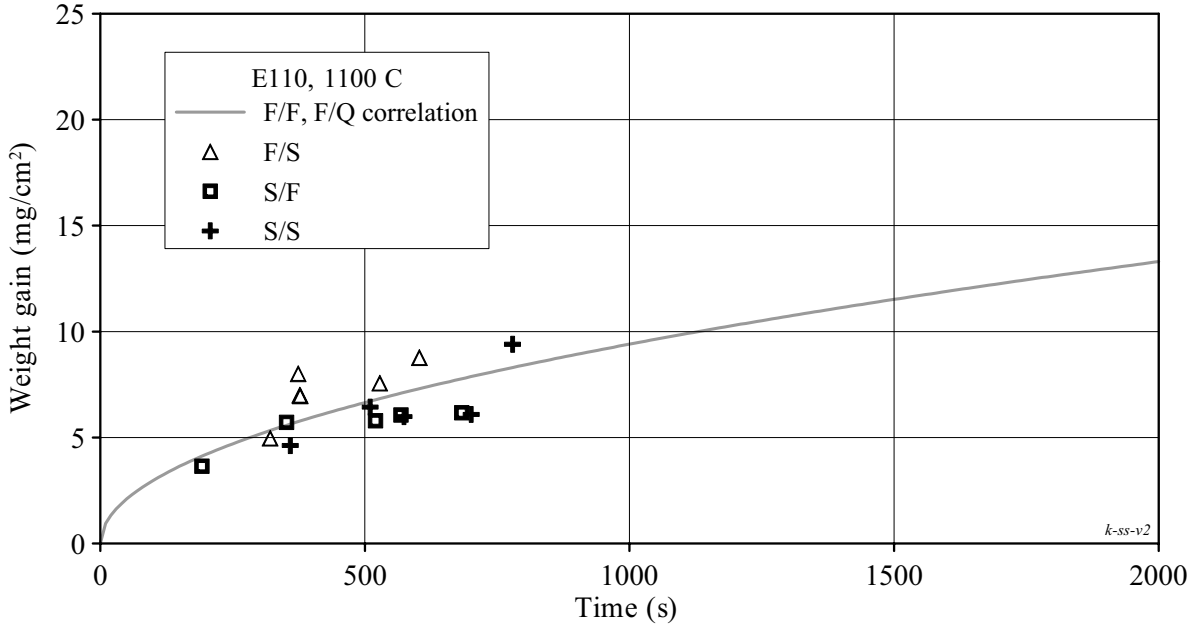

Fig. 3.86. The comparison of data characterizing the transient test modes with the E110 oxidation kinetics

The oxidation kinetics sensitivity of zirconium niobium alloys to the alloying composition was verified using the data presented in Fig. 3.87. The comparison of the E110 and E635 test data shows that the oxidation kinetics of these two alloys are either the similar or very close to each other.

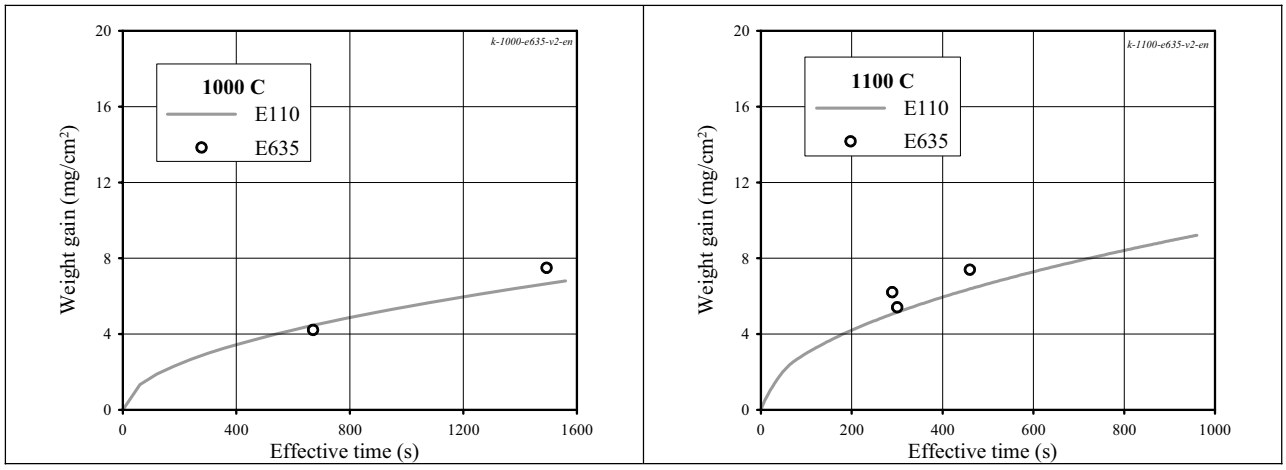

Fig. 3.87. The comparative data on the E110 and E635 oxidation kinetics

The comparison of the E110 and Zry-4 oxidation kinetics confirmed the results obtained by other researchers earlier. The E110 oxidation rate is somewhat less than that for the Zry-4 cladding (see Fig. 3.88).

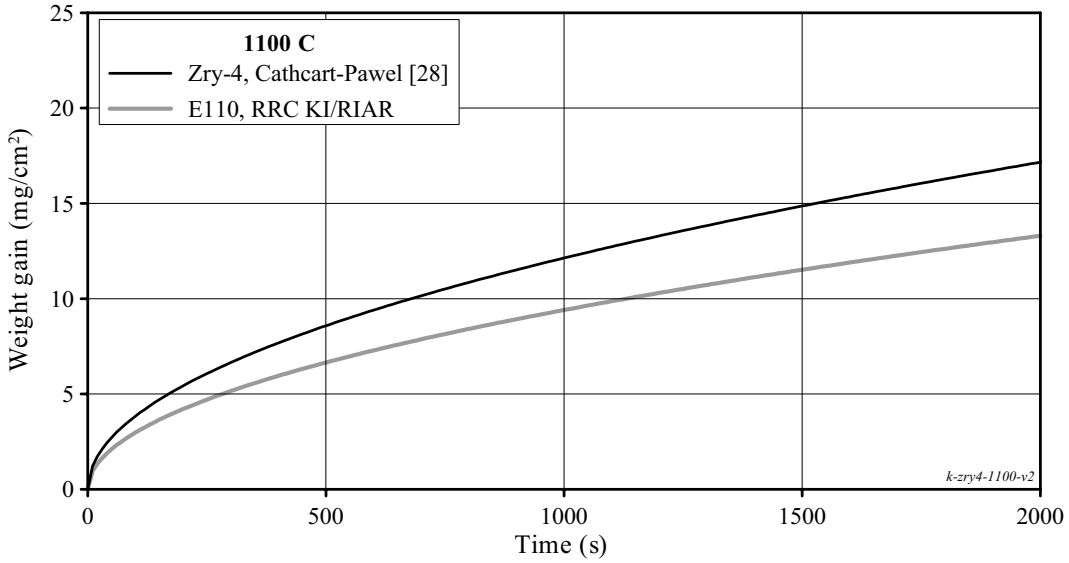

Fig. 3.88. The comparison of the E110 and Zry-4 oxidation kinetics

To estimate the agreement between the E110 oxidation kinetics stated basing on results of this work with the results of other researchers, the appropriate data were compared on the basis of published investigation data obtained in the following organizations:

- KFKI, Hungary [9];
- NFI, Czech republic [26];
- VNIINM, Russia [6];
- NC in Rossendorf, Germany [24].

The comparison of the appropriate results performed at 1100 C allows to conclude that a good agreement is observed between the data of the RRC KI/RIAR (this work), NFI, VNIINM, and NC in Rossendorf (Fig. 3.89). The KFKI data overestimate significantly the E110 oxidation kinetics (may be due to end effects, see section 3.3.7).

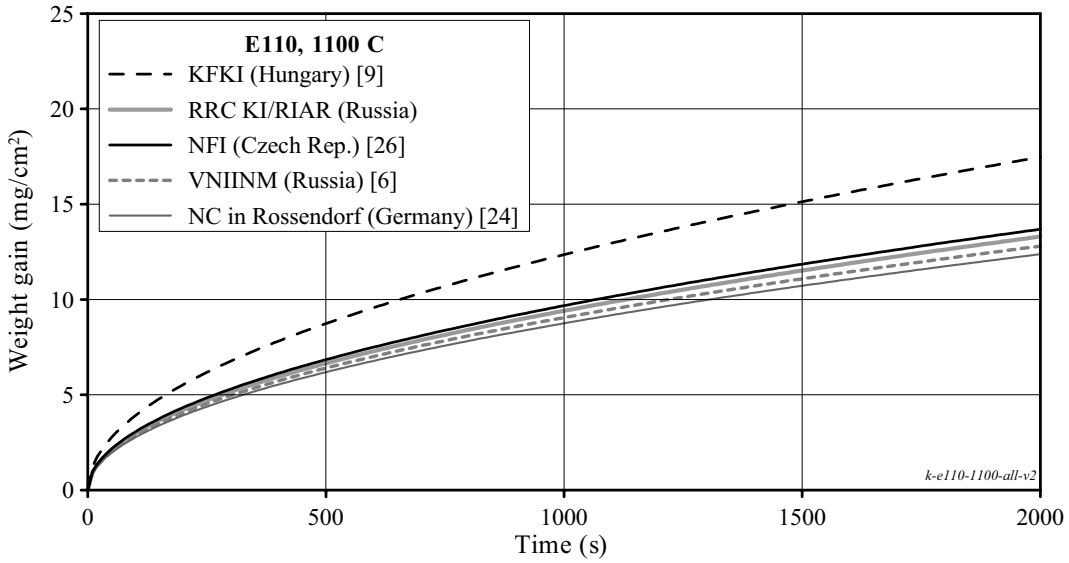

Fig. 3.89. The E110 oxidation kinetics at 1100 C in accordance with the data obtained in different laboratories

REFERENCES FOR SECTION 3

[1] Atomic Energy Commission Rule-Making Hearing, Opinion of the Commission, Docket RM-50-1, 28 December, 1973.

[2] Bibilashvili Yu.K., Sokolov N.B., Andreeva-Andrievskaya L.N., Tonkov V.Yu., Salatov A.V., Morozov A.M., Smirnov V.P. "Thermomechanical Properties of Zirconium-Based Alloys Oxidized Claddings in LOCA Simulationg Conditions", *Proc. of IAEA Technical Commettee Meet. on "Fuel Behavior under Transient and LOCA conditions"*, Halden, Norway, September 10-14, 2001.

[3] Baker L., Just L.C. "Studies of Metal Water Reactions at High Temperatures", Technical report of ANL-6548, 1962.

[4] Solyany V.I., Bibilashvili Yu.K., Dranenko V.V., Izrailevskiy L.B., Levin A.Ya., Morozov A.A. "Characteristics of Corrosion Behavior of Zr-1%Nb WWER Fuel Claddings Within 700-1000°C on Long Term Exposures", *Proc. of IAEA Technical Committee Meet. on "Water Reactor Fuel Behavior and Fission Products Release in Off-Normal and Accident Conditions"*, Vienna, 10-13 November, 1986.

[5] Solyany V.I., Bibilashvili Yu.K., Dranenko V.V., Izrailevskiy L.B., Levin A.Ya., Morozov A.A. "Studies of the corrosion behavior of Zr-1%Nb claddings in steam at high temperatures", VANT, series *" "Materials for Atomic Energy "*, Vol.2(27), 1988, (in Russian).

[6] Bibilashvili Yu.K., Sokolov N.B., Salatov A.V., Andreyeva-Andriyevskaya L.N., Nechayeva O.A., Vlasov F.Yu. "RAPTA-5 Code: Modelling of Behaviour of Fuel Elements of VVER Type in Design Accidents. Verification Calculations", *Proc. of IAEA Technical Committee Meeting on "Behaviour of LWR Core Materials under Accident Conditions", Dimitrovgrad, Russia, on 9-13 October 1995*. IAEA-TECDOC-921, Vienna, 1996.

[7] Bibilashvili Yu.K., Sokolov N.B., Andreyeva-Andriyevskaya L.N., Salatov A.V. "High Temperature Interaction of Fuel Rod Cladding Material (Zr-1%Nb Alloy with Oxygen-Containing Mediums", *Proc. of IAEA Technical Committee Meeting on "Behaviour of LWR Core Materials under Accident Conditions", Dimitrovgrad, Russia, on 9-13 October 1995.*

[8] Böhmert J. "Embrittlement of Zr-1%Nb at Room Temperature after High-Temperature Oxidation in Steam Atmosphere", Kerntechnik ,57 No1, 1992

[9] Gyori Cs. et.al. "Extension of Transuranus code applicability with niobium containing models (EXTRA)". *Proc. of FISA-2003 Conference EU Research in Reactor Safety,* EC Luxembourg, November 2003.

[10] Vrtilkova V., Valach M., Molin L. "Oxiding and Hydrating Properties of Zr-1%Nb Cladding Material in Comparison with Zircaloys", *Proc. of IAEA Technical Committee Meeting on "Influence of Water Chemistry on Fuel Cladding Behavior"*, Rez (Czech Republic), October 4-8, 1993.

[11] Yegorova L., Asmolov V., Abyshov G., Malofeev V., Avvakumov A., Kaplar E., Lioutov K., Shestopalov A., Bortash A., Maiorov L., Mikitiouk K., Polvanov V., Smirnov V., Goryachev A., Prokhorov V., and Vurim A. "Data Base on the Behavior of High Burnup Fuel Rods with Zr-1%Nb Cladding and UO_2 Fuel (VVER Type) under Reactivity Accident Conditions", RRC "Kurchatov Institute" report NSI RRC 2179, Vol.1-3, 1999 (also USNRC report NUREG/IA-0156 and IPSN report IPSN 99/08 - 2).

[12] Hobson D.O. and Rittenhouse P.L. "Embrittlement of Zircaloy Clad Fuel Rods by Steam During LOCA Transient", ORNL-4758, Oak Ridge National Laboratory, 1972.

[13] Chung H.M. and Kassner T.F. "Embrittlement Criteria for Zircaloy Fuel Cladding Applicable to Accident Situations in Light-Water-Reactors", NUREG/CR-1344, January 1980.

[14] Uetsuka H. et.al. "Failure-Bearing Capability of Oxidized Zircaloy-4 Cladding under Simulated Loss-of-Coolant Conditions", J. Nucl. Sci. Tech. 20 (1983).

[15] Bibilashvili Yu.K., Sokolov N.B., Dranenko V.V., Kulikova K.V., Izrailevskiy L.B., Levin A.Ya., Morozov A.M. "Influence of Accident Conditions due to Loss of Tightness by Primary Circuit on Fuel Claddings", *Proc. of the Ninth Int. Symp. on Zirconium in the Nuclear Industry*, Kobe, Japan, November 5-8, 1990.

[16] Bibilashvili Yu.K. et al.,"Influence of Accident Conditions due to Loss of Tightness by Primary Circuit on VVER-1000 Fuel Rod State", VANT, series *"Materials for Atomic Energy"*, Vol.2(42), 1991(rus).

[17] Böhmert J. "Embrittlement of Zr-1%Nb at Room Temperature after High-Temperature Oxidation in Steam Atmosphere", Journal, Kerntechnik 57 No1, 1992.

[18] Hozer Z., Griger A., Matius L., Vasaros L., Horvath M. "Effect of Hydrogen Content on the Embrittlement of ZR Alloys", *Proc. of IAEA Technical Committee Meeting on "Fuel Behavior under Transient and LOCA Conditions"*, Halden, Norway, September 10-14, 2001.

[19] Kaplar E., Yegorova L., Lioutov K., Konobeyev A., Jouravkova N., Smirnov V., Goryachev A., Prokhorov V., Yeremin S., Svyatkin A. "Mechanical Properties of Unirradiated and Irradiated Zr-1%Nb Cladding", RRC "Kurchatov Institute" report NSI RRC 2241, 2001 (also USNRC report NUREG/IA-0199 and IPSN report IPSN 01-16).

[20] Prokhorov V., Makarov O., Smirnov V., Goryachev A., Yegorova L., Kaplar E., and Lioutov K. "Improvement of method to measure tensile properties of Zr-1%Nb alloy cladding with simple ring specimens". *Proceedings of the 6th inter-branch conference on reactor material science*, Dimitrovgrad, Russia, September 11-15, Vol.2, pp. 209-212 (rus).

[21] Bernstein M.L., Zaimovsky V.A. "Mechanical Properties of Metals", Moscow, Metallurgy, 1979, (rus).

[22] Zaimovsky A., Nikulina A., Reshetnikov N. "Zirconium alloys in the Nuclear Industry", Moscow, Energoizdat, 1981 (rus).

[23] Brachet J., Pelchat J., Hamon D., Maury R., Jaques P., Mardon J. "Mechanical Behavior at Room Temperature and Metallurgical Study of Low-Tin Zry-4 and M5™ (Zr-NbO) Alloys after Oxidation at 1100°C and Quenching", *Proc. of IAEA Technical Committee Meeting on "Fuel Behavior under Transient and LOCA Conditions"*, Halden, Norway, September 10-14, 2001.

[24] Böhmert J., Dietrich M., Linek J. "Comparative Studies on High-Temperature Corrosion of Zr-1%Nb and Zircaloy-4", Nuclear Engineering and Design, 147 No1, 1993.

[25] Hozer Z. et. al. "Ring Compression Tests with Oxidised and Hydrided Zr-1%Nb and Zirkaloy –4 Cladding", Hungarian Academy of Sciences, CRIP, Budapest, Report KFKI-2002-01/G.

[26] Vrtilkova V. et. al. "An Approach to the Alternative LOCA Embrittlement Criterion", *Proc. of SEGFSM Topical Meeting on LOCA Fuel Issues,* Argonne National Laboratory, May 2004 (NEA/CSNI/R(2004)19).

[27] Billone M.C., Yan Y. and Burtseva T. "Post-Quench Ductility of Advanced Alloy Cladding", *Nuclear Safety Research Conference (NSRC-2004)*, Washington, DC, October 25-27, 2004.

[28] Cathcart J.V. and Pawel R.E. "Zirconium Metal-Water Oxidation Kinetics: IV. Reaction Rate Studies". ORNL/NUREG-17, 1977.

[29] Chung H.M. "The Effects of Aliovalent Elements on Nodular Oxidation of Zr-based Alloys", *Proceedings of the 2003 Nuclear Safety Research Conference*, Washington DC, October 20-22, 2003, NUREG/CP-0185, 2004.

[30] Yegorova L., Lioutov K., Smirnov V., Goryachev A., Chesanov V. "LOCA Behavior of E110 Alloy", *Proceedings of the 2003 Nuclear Safety Research Conference*, Washington DC, October 20-22, 2003, NUREG/CP-0185, 2004.

[31] Lemaignan C. "Physical Phenomena Concerning Corrosion Under Irradiation of Zr Alloys", *Zirconium in the Nuclear Industry: Thirteenth International Symposium*, ASTM STP 1423, 2002, pp.20-29.

[32] Uetsuka H. et al. "Zircaloy-4 Cladding Embrittlement due to Inner Surface Oxidation under Simulated Loss-of-Coolant Conditions", J. Nucl. Sci. Tech. 18 (1981).

[33] Uetsuka H. et al. "Embrittlement of Zircaloy-4 due to Oxidation in Environment of Stagnant Steam", J. Nucl. Sci. Tech. 19 (1982).

[34] Mardon J.P. et al. "Update on the Development of Advanced Zirconium Alloys for PWR Fuel Rod Claddings", *Proceedings of the International Topical Meeting on Light Water Reactor Fuel Performance,* Portland, Oregon, March 2-6, 1997.

[35] JC. Brachet, L. Portier, V. Maillot, T. Forgeron, JP. Mardon, P. Jacques, A. Lesbros, "Overview of the CEA data on the influence of hydrogen on the metallurgical and thermal-mechanical behavior of Zircaloy-4 and M5™alloys under LOCA conditions", *Nuclear Safety Research Conference (NSRC-2004)*, Washington, DC, October 25-27, 2004.

[36] Mardon J., Frichet A., Bourhis A. "Behavior of M5™ Alloy under Normal and Accident Conditions", *Proc. of Top Fuel-2001 Meet.*, Stockholm, May 27-30, 2001.

[37] Asmolov V., Yegorova L., Lioutov K., Smirnov V., Goryachev A., Chesanov V., Prokhorov V. "Understanding Loca-Related Ductility in E110 Cladding", Proceedings of the 2002 Nuclear Safety Research Conference, Held at Marriott Hotel at Metro Center Washington, DC, October 28-30, 2002, NUREG/CP-0180, pp.109-125.

[38] Yegorova L., Lioutov K., Smirnov V. "Major Findings of E110 Studies under LOCA Conditions", *Proc. of SEGFSM Topical Meeting on LOCA Fuel Issues,* Argonne National Laboratory, May 2004 (NEA/CSNI/R(2004)19).

[39] Pirogov Ye.N., Alimov M.I., Artiuchina L.L. "Creep of H-1 alloy in the range of phase transition" Journal of Soviet Atomic Energy, v.65 (3), p. 293, 1988 (rus).

[40] Forgeron T. et. al, "Experiment and Modeling of Advanced Fuel Rod Cladding Behavior Under LOCA Conditions: Alpha-Beta Phase Transformation Kinetics and EDGAR Methodology", *Zirconium in the Nuclear Industry: Twelfth International Symposium,*. ASTM STP 1354, 2000, pp. 256-278.

[41] Nikulina A. et.al. "Zirconium Alloy E635 as a Material for Fuel Rod Cladding and Other Components of VVER and RBMK Cores", *Zirconium in the Nuclear Industry: Eleventh International Symposium*, ASTM STP-1295, November 1996.

[42] Douglass D.L. "The Metallurgy of Zirconium", International Atomic Energy Agency, 1971.

[43] Garde A.M. "Influence of Cladding Microstructure on Low Enthalpy Failures in RIA Simulation Tests", *Zirconium in the Nuclear Industry: Twelfth International Symposium,* ASTM STP 1354, 2000.

[44] Hache G., Chung H. "The History of LOCA Embrittlement Criteria", Proc. of the 28th Water Reactor Safety Information Meeting, NUREG/CP-0172, 2000.

[45] Bai J., Prioul C., Pelchat J., Barcelo F. "Effects of Hydrides on the Ductile Brittle Transition in Stress–Relieved, Recrystallized and β-Treated Zircaloy", *Proc. of the International Topical Meeting on the LWR Fuel Performance,* Avignon, France, 1991.

[46] Waeckel N., Mardon J.P. "Recent data on M5™Alloy under LOCA Conditions", *Proceedings of the 2003 Nuclear Safety Research Conference*, Washington DC, October 20-22, 2003, NUREG/CP-0185, 2004.

[47] G. Fearnehough and A. Cowan "The effect of hydrogen and strain rate on the "ductile–brittle" behavior of Zircaloy", Journal of Nuclear Materials №22, 1967.

[48] F. Nagase, K. Ishijima, and T. Furuta, "Influence of Locally Concentrated Hydrides on Ductility of Zircaloy-4", *Proc. of the CSNI Specialist Meeting on Transient behaviour of High Burnup Fuel,* Cadarche, France, September 12-14, 1995.

4. OXIDATION BEHAVIOR AND EMBRITTLEMENT THRESHOLD OF THE MODIFIED E110 CLADDING: PROGRAM AND DISCUSSION OF TEST RESULTS

4.1. Major provisions of the test program with a modified E110 cladding

The results of the test program performed with the E110 standard as-received tubes and presented in chapter 1 of the report have shown that:

- the zero ductility threshold of the E110 alloy is lower than that of the Zry-4 alloy;
- the earlier initiation of the breakaway oxidation accompanied by hydrogen absorption in the prior β-phase of the E110 cladding is the major reason for the different mechanical behavior of oxidized claddings fabricated of these two alloys.

The numerous sensitivity studies performed in the frame of this work allowed to establish that variations in oxidation modes may somewhat hasten or delay the initiation of the breakaway oxidation in the E110 alloy, however, any variations in test conditions do not allow to avoid completely this type of oxidation in the ECR range of interest.

Approximately the same conclusion was made basing on the analysis of results of tests performed to check the correlation between some alloying elements (O, Fe, Sn) and the oxidation behavior of niobium-containing claddings.

All these results allowed to report the following general question: is this oxidation behavior typical of the whole family of niobium-bearing alloys or only of the E110 alloy? The comparison of the E110 test results with the published data on the other Zr-1%Nb alloy, namely, the M5 alloy [1, 2], allowed to reveal the following:

- the M5 and Zry-4 claddings are characterized by the similar embrittlement threshold at 1100 C;
- the breakaway oxidation was not observed on the M5 claddings in the tested ECR range.

A careful analysis of the existing situation allowed to assume that the specific behavior of the E110 cladding may be the consequence of two groups of effects connected with the cladding fabrication:

1. Surface effects.
2. Bulk effects.

The surface effects combine such factors as the surface chemistry (surface contaminations) and surface roughness. In their turn, bulk effects may be the manifestation of such factors as the cladding material chemical composition (the composition of impurities) and microstructure effects (the phase composition, grain size, parameters of the secondary precipitates, etc.).

As for the surface effects, it is known that the surface finishing of cladding tubes is the important component for the cladding corrosion resistance. Thus, for illustration, the results of this work confirm the numerous observations concerning the relationship between the initiation of the breakaway oxidation and the localization of the cladding surface scratches (see Fig. 4.1).

To provide the chemical cleaning and chemical polishing of the E110 cladding tube, the standard procedure for the E110 surface finishing is used. This procedure includes the chemical etching and anodizing of the outer surface of the E110 fuel rod. Besides, special studies are performed at present to develop the modified method for the E110 surface finishing. One of the potential variants of new approaches to this problem is the grinding of the cladding outer surface and the jet etching of the cladding inner surface. Taking into account all these considerations, it was decided to perform several special tests the assess the sensitivity of the E110 oxidation behavior to surface effects.

Sample #27 ECR=4.6%	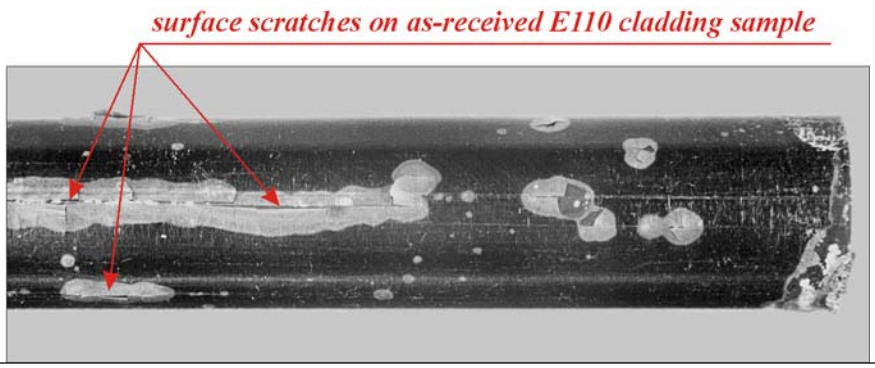

Fig. 4.1. The relationship between surface scratches and localization of the breakaway oxidation areas

The studies of bulk effects associated with the oxidation behavior of niobium-bearing alloys were the subject of numerous investigations performed in Russia and other countries. As for the microstructure effects, the analysis of publications allowed to note the following:

- the corrosion properties of binary zirconium-niobium alloys depend directly on the content and phases of the zirconium and niobium [3];
- the formation of equilibrium α-Zr and β-Nb phases leads to the improvement of corrosion resistance of binary alloys [3];
- the corrosion properties of the E110 alloy depend on the material microstructure; the annealing temperature and duration are the major factors determining the cladding microstructure; the annealing at 580 C during 3 hours (below the monoeutectoid line) leads to the maximum depletion of the α-Zr matrix by the niobium and to the formation of the β-Nb phase that improves the alloy corrosion resistance [4];
- the corrosion behavior of the E110 alloy cladding is shown to be strongly dependent on the material structure (including the grain size), the formation of the completely recrystallized material with a fine grain size determines the best corrosion resistance [5];
- a strong dependence of corrosion properties of binary alloys on heat treatment was revealed; the formation of metastable phases at the annealing temperature higher than the monoeutectoid one leads to the very low corrosion resistance, the annealing in the temperature range of the α-Zr phase presence leads to the formation of the equilibrium structure and high corrosion resistance [6];
- to prevent the degradation in the corrosion resistance, the intermediate and final annealing temperature must not exceed 600 C; in this case, the material of M5 tubes remains in the α-Zr plus β-Nb region under completely recrystallized conditions [7];
- the samples of Zr-xNb binary alloys annealed at 570 C to form β-Nb phase showed a much lower corrosion rate and higher volume fraction of tetragonal ZrO_2 in the oxide than those annealed at 640 C to form β-Zr phase [8];
- basing on the consideration of publications devoted to the corrosion behavior of niobium-bearing alloys, the authors of investigations presented in [9] have declared that the correlation between the oxide characteristics and microstructure or microchemistry, such as β phases, Nb-containing precipitates and soluble Nb in the matrix, is not well understood in Zr-Nb alloys. One of the major results of investigations performed by these researchers could be formulated as following: at high Nb-contents 1.0–5.0 wt%, the corrosion rate was very sensitive to the annealing condition, the transformation of the oxide structure from tetragonal ZrO_2 to monoclinic ZrO_2 and of the oxide microstructure from the columnar to equiaxed structure was accelerated in the samples having β-Zr phase. The corrosion rate of samples annealed at 570 C with the formation of the β-Nb phase was much lower. Moreover, it is assumed that the equilibrium concentration of Nb in the α-matrix would be a more dominant factor to enhance the corrosion resistance that the Nb-containing precipitates.

The above listed results of previous investigations have shown that the corrosion behavior of binary Zr-Nb alloys is very sensitive to the microstructure characteristics that in their turn are determined by the

fabrication procedures and conditions. In this case, the fact cannot be excluded that the annealing condition may be not the only key factor in spite of the fact that recent special studies performed with the M5 alloy have demonstrated that the corrosion resistance is not sensitive to many aspects of the fabrication process [7]. Unfortunately, a direct comparison of manufacturing procedures used on the fabrication of the E110 cladding and M5 cladding to reveal the differences that may be responsible for differences in the corrosion behavior of these two niobium-bearing claddings is not possible because this is confidential commercial information. Therefore, to provide the comparative analysis of possible microstructure effects in these two alloys, it was decided to perform a careful SEM (scanning electron microscopy) and TEM (transmission electron microscopy) examinations of the E110 cladding material and after that to compare the obtained results with the published data characterizing the M5 tube microstructure.

The next position of special investigations performed with the E110 cladding to study of bulk effects was devoted to the studies of the microchemical effects of the cladding material in the context of the E110 oxidation behavior. The analysis of results of previous investigations performed in this line allowed to reveal the following:

- the optimization of Nb concentration in the E110 alloy allowed to minimize the influence of N, Al, C impurities causing the degradation of the corrosion resistance [4];
- the secondary phase particles influence significantly the corrosion behavior of niobium-bearing alloys. Special investigations performed with the cladding samples the surface of which was modified due to the ion alloying have shown that a strong dependence is between the oxide structure and secondary intermetallic participates on the cladding surface. So, the oxide layer has a thickening in this area consisting of metal oxides of the secondary phase participates. The decrease of the participate density at the alloying process leads to the improvement of the oxide contact with the metal matrix [10];
- the corrosion tests have demonstrated that the alloying of the E110 cladding of such elements as Fe, Mo, Sn leads to the decrease in the oxidation rate [11];
- the presence of such elements as Sn, Fe, Cr, Nb improves the corrosion resistance of zirconium [6].

It is evident that the above listed results of previous investigations are remarkable for the fragmentariness and are insufficient to analyze microchemical bulk effects as applied to the corrosion behavior of the E110 alloys. The additional analysis of published data devoted to the relationship between the corrosion behavior of other zirconium alloys and their microchemical compositions has shown that in spite of a great number of investigations performed recently, a clear physical understanding of appropriate phenomena has not been achieved yet. Taking into account this circumstance, the further development of this line of investigations was based on the following considerations:

- if the microchemistry of Zr-Nb alloys is the key factor resulting in differences in the behavior of such two Zr-1%Nb alloys as E110 and M5, then this means that these two alloys have different compositions of impurities in the cladding material. In this case, this conclusion does not concern the differences in the oxygen concentration as this effect has been specially investigated (see chapter 1);
- the analysis of possible reasons for potential differences in the impurity composition and content of these two alloys has shown that two different methods are employed to fabricate the Zr-1%Nb ingot:
  - the sponge Zr is used on the manufacturing of the M5 cladding;
  - the mixture of iodide and electrolytic Zr is used on the manufacturing of the E110 cladding;
- the comparative description of these methods for the preparation of the Zr-1%Nb ingot is given in [12].

It should be noted that the Russian industry is planning in the nearest time to proceed to the employment of sponge Zr to manufacture the E110 cladding taking into account the economic advantage (the fabrication of iodide/electrolytic Zr is significantly more expensive than the fabrication of sponge Zr). In the frame of this work, different types of the E110 claddings were manufactured with the use of sponge Zr. Therefore, it was decided to perform the investigations of microchemistry effects associated with the oxidation behavior of the E110 alloy using several different types of the E110 cladding manufactured on the basis of sponge Zr.

In accordance with the above listed surface and bulk effects, the program of this stage of research was developed. The major provisions of this program are presented in Table 4.1.

Table 4.1. The E110 surface and bulk effects studies: major provisions of experimental program

Program stage	Major tasks	Comments
1. Surface effects investigations 1.1. Tests of the E110 etched and anodized cladding	To perform several oxidation tests with the E110 etched and anodizing cladding and to compare the mechanical behavior of the E110 cladding and E110 as-received tube	The commercial E110 etched and anodizing cladding should be used for these tests
1.2. Tests of the E110 cladding with the modified surface finishing	To perform oxidation tests with two types of surface finishing: 1. Grinding of the cladding outer surface and jet etching of the cladding inner surface 2. Polishing of the cladding outer and inner surfaces	The commercial advanced E110 cladding should be used for the first type of tests. The laboratory procedure for the preparation of special samples with polished outer and inner surfaces of the E110 as-received tubes should be used for the second type of tests
2. Bulk effect investigations: 2.1. Studies of the E110 cladding microstructure	To perform the SEM and TEM examinations of different types of the E110 claddings and to perform the comparative analysis of obtained microstructure characteristics	The samples of the E110 cladding material fabricated with the application of different methods for manufacturing of Zr-1%Nb ingot should be prepared for these examinations
2.2. Studies of dependence of the oxidation and mechanical behavior of the E110 cladding on the chemical composition of Zr-1%Nb	To perform oxidation tests with several types of the E110 and E635 as-received tubes fabricated with the use of sponge Zr-1%Nb. To compare the mechanical behavior of these claddings with the behavior of standard E110 tubes manufactured with the use of iodide/electrolytic Zr	Special cladding samples fabricated in accordance with the standard procedure but with the application of sponge Zr should be used for these tests

All oxidation and mechanical tests performed in the frame of this program were made in accordance with the following technical requirements:

- the oxidation type: the double-sided oxidation with the F/F combination of heating and cooling rates;
- the oxidation temperature: 900–1200 C;
- the characterization of mechanical tests: ring compression tests of 8 mm rings at 20 and 135 C.

4.2. The analysis of experimental results obtained at surface effect studies

As it was noted in section 4.1, three types of cladding samples were used to investigate these effects:

1. Standard E110 etched and anodized cladding (E110A).
2. E110 as-received tube with the modified surface finishing (the outer surface grinding and inner surface jet etching) performed at the tube plant ($E110_m$).
3. E110 as-received tube sample, one half of which remained in the initial state and the second half was polished from the inside and outside in the RIAR laboratory ($E110_{pol}$).

The whole scope of obtained test results is presented in Tables B-1 and B-2 of Appendix B. The appearances of the E110A and $E110_m$ samples before and after oxidation tests are shown in Fig. 4.2.

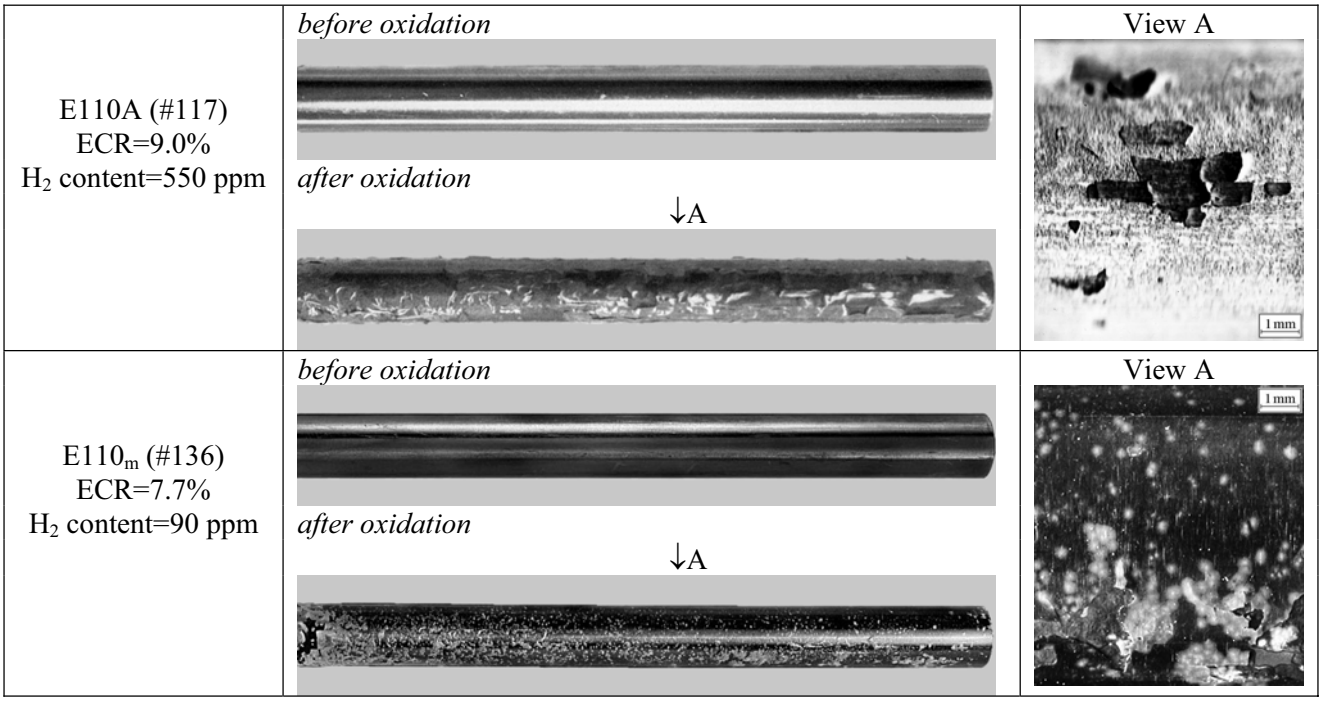

Fig. 4.2. The appearance of the E110 claddings fabricated with the use of two different types of surface finishing before and after oxidation tests at 1100 C

The analysis of these data allows to note the following:

- the standard surface finishing of the E110 cladding does not lead to improvements in comparison with the oxidation behavior of the E110 as-received tubes; the classic breakaway effect accompanied by the hydrogen pickup was observed on the cladding outer surface (see Fig. 4.3 also);
- the modified surface finishing of the E110 tube on the basis of the outer surface grinding and inner surface jet etching does not allow to eliminate the breakaway oxidation. The oxidized cladding appearance and the microstructure of oxides formed on the inner and outer cladding surfaces (see Fig. 4.3) show that the spallation and delamination of ZrO_2 oxide are observed on both surfaces of the cladding. Moreover, the oxide thickness on the etched inner surface is larger than that on the grinded outer surface.

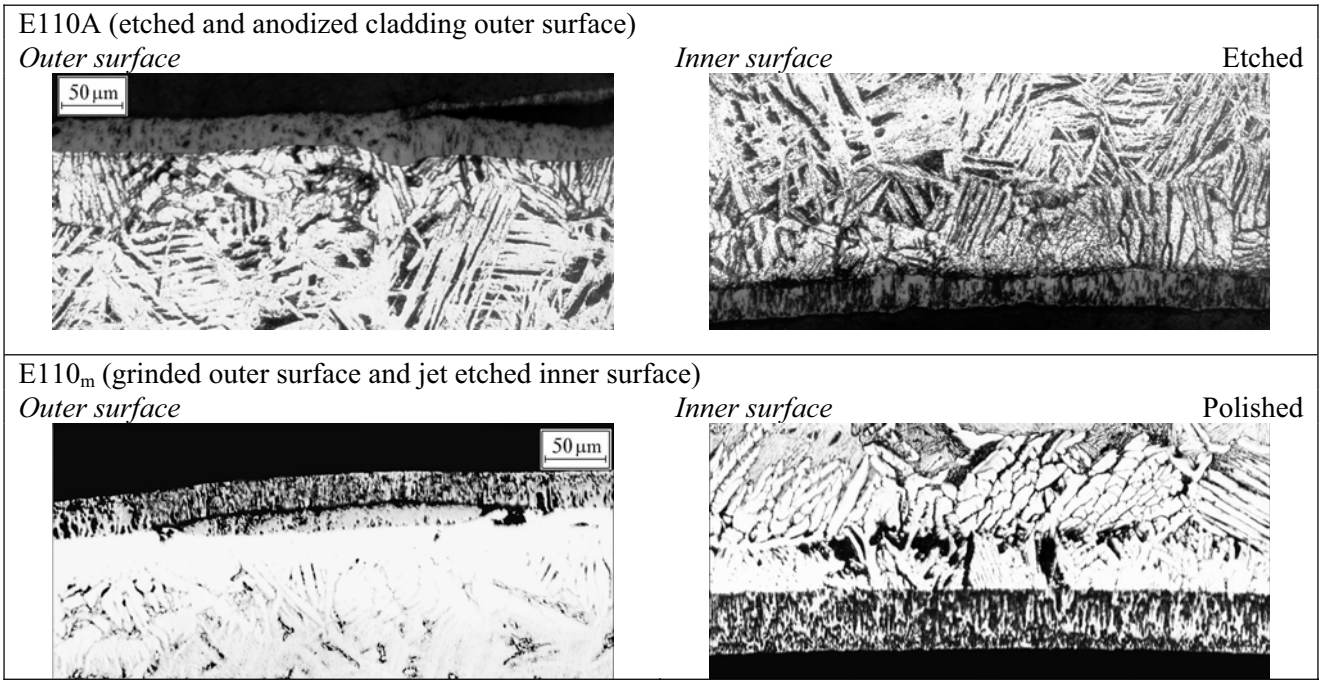

Fig. 4.3. The microstructure of the E110A and $E110_m$ claddings after the oxidation at 1100 C

Obtained observations are in the reasonable agreement with results of ring compression tests performed with the 8 mm samples cut off from 100 mm oxidized samples (see Fig. 4.4). Moreover, numerous special investigations performed in the ANL with the E110 samples which underwent different procedures of the cladding etching and the cladding cleaning after etching have demonstrated that etching is more than undesirable procedure from the point of view of the E110 cladding oxidation behavior [13]. This conclusion is confirmed by the results of previous studies of zirconium alloys [14]. Taking into account a very high sensitivity of the breakaway initiation to the minimum presence of F-contamination on the cladding surface (that was demonstrated many times in previous investigations), it may be assumed that fluorine containing particles remain on the etched cladding surface, though this assumption contradicts the results of the appropriated check procedures that are performed at tube plant. Unfortunately, it was impossible to perform special measurements of fluorine contents on the cladding surface in the frame of this work as those are very difficult from the methodological point of view.

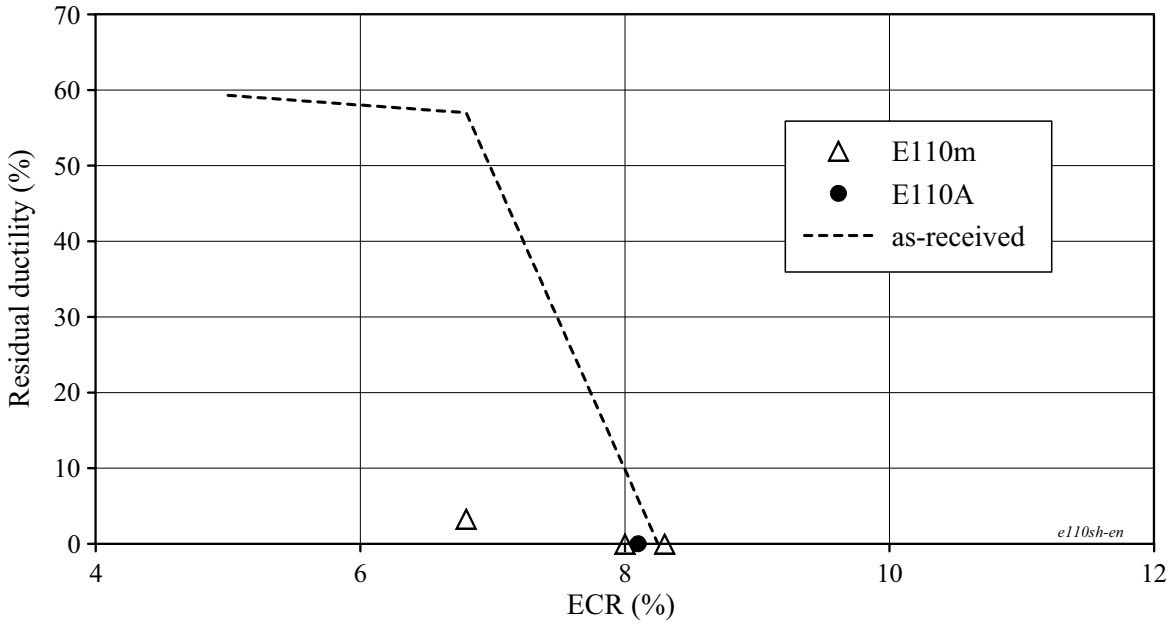

Fig. 4.4. The comparison of residual ductility of the standard E110 as-received tube, E110A and $E110_m$ claddings after the oxidation at 1100 C

The indirect confirmation of this reason for the E110 breakaway initiation was obtained from the results of investigations performed in the ANL. They performed additional polishing of the outer and inner surfaces of the E110A cladding. In this case, the cladding inner diameter was increased after polishing by 100 μm. The oxidation tests at 1100 C and ring compression tests have shown that the margin of residual ductility remains in these claddings up to 16% ECR (as-measured) [13].

The similar tests were performed in the frame of this work also. Polishing of one half of the E110 sample 100 mm long was performed on the inner and outer surfaces of the E110 as-received tube. The second half of this sample remained intact. The surface roughness on the polished part of the cladding sample was about 0.08–0.16 μm that corresponds to the surface roughness of the M5 and Zry-4 claddings (0.1–0.15 μm). Taking into account the effect of the oxidation temperature revealed during the first part of research program, the oxidation tests of these samples were carried out at 1000 and 1100 C. The organized tests are presented in Fig. 4.5. The tabular results of tests are listed in Tables B-1 and B-2 of Appendix B.

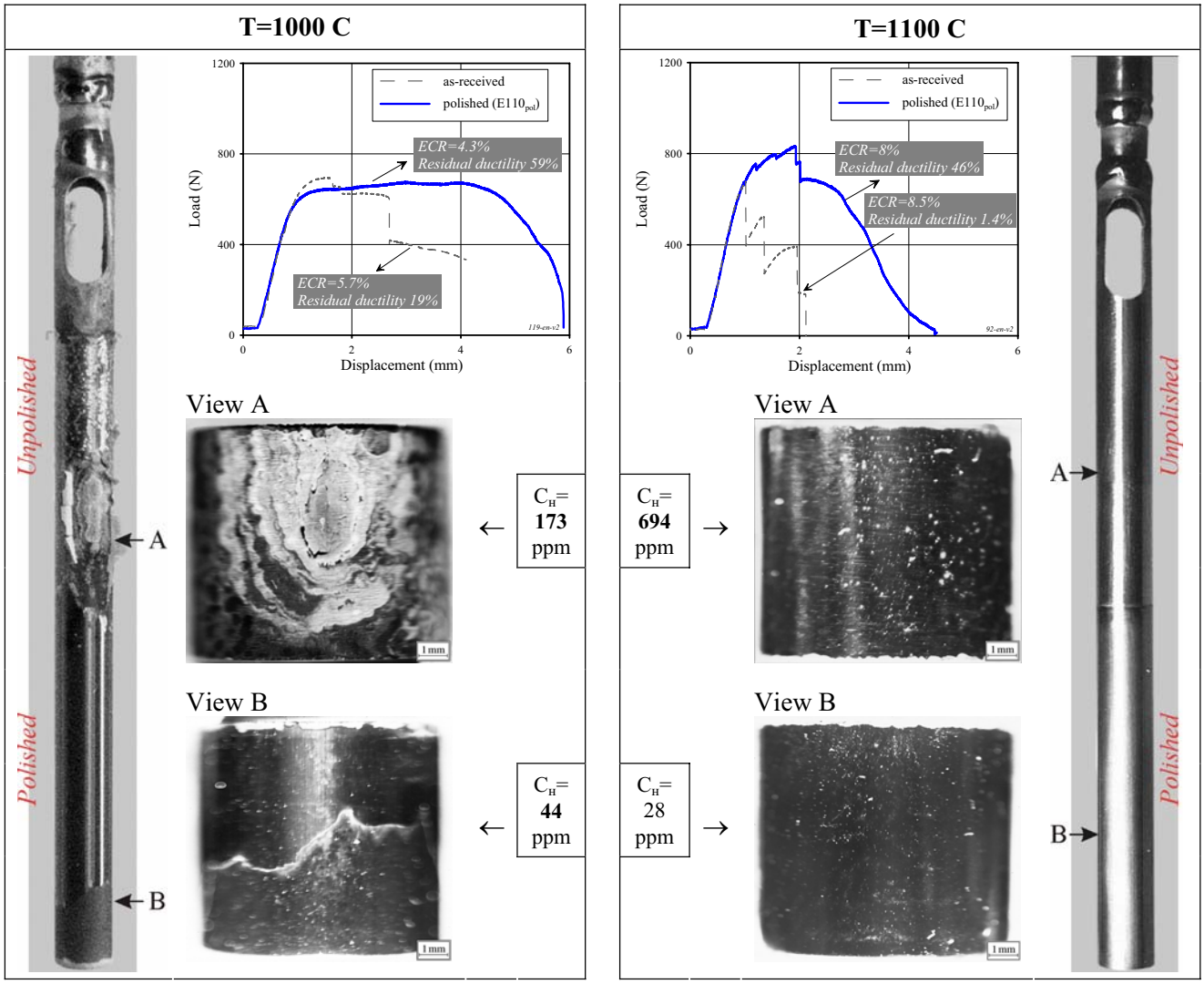

Fig. 4.5. Demonstration of sensitivity of the oxidation and mechanical behavior for the E110 cladding to the cladding surface polishing

The analysis of obtained comparative data allowed to reveal the following important aspects of the E110 oxidation behavior as a function of the cladding surface machining:

- the rate of the E110 cladding unpolished part oxidation is higher than that of the polished region;
- indications of the breakaway oxidation including the hydrogen absorption practically disappear on the polished part of the E110 cladding. This process takes place especially clearly on the oxidation at 1000 C;
- the residual ductility of the E110 cladding polished part is many times increased in comparison with the oxidized cladding unpolished part.

The additional information to characterize the appropriate cladding behavior may be obtained due to the consideration of the oxidized cladding microstructure in the polished and unpolished parts (see Fig. 4.6). As can be observed, the oxide spallation is noted on the outer surface of cladding unpolished part. The contact of oxide with the cladding matrix on the inner side is somewhat better but it is seen that a systematical layer of pores has been already generated on the interface between the oxide and metallic matrix, and, consequently, the oxide layer spallation will take place at the ECR increase. Another case is observed on the oxidized cladding polished part. The uniform oxide layer having a good adhesion with the metallic matrix covers the cladding outer and inner surfaces. This oxide behavior provides the lower oxidation rate and low rate of hydrogen diffusion into the E110 cladding.

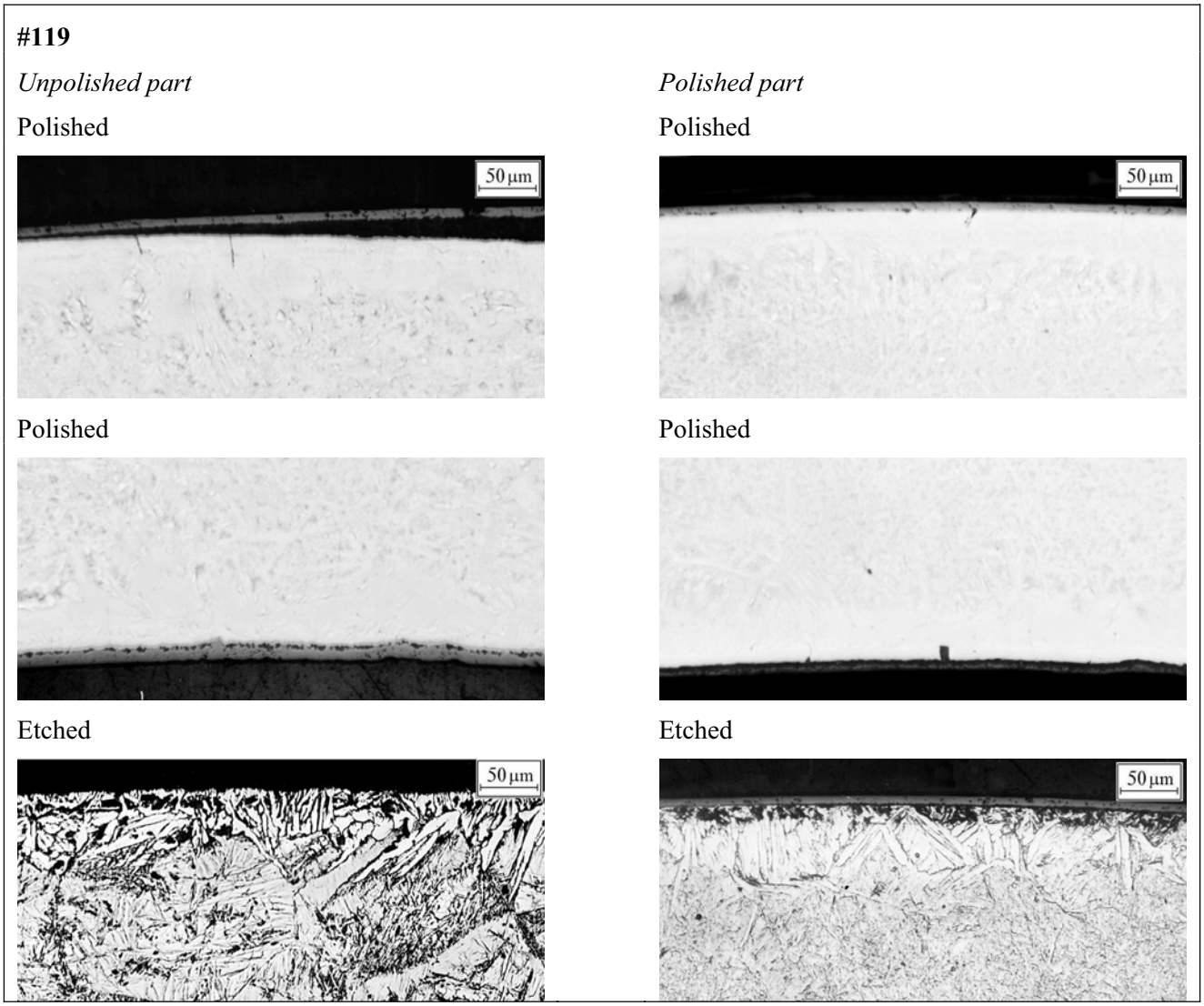

Fig. 4.6. The oxide microstructure on the polished and unpolished parts of the E110 cladding after the oxidation at 1000 C

The same results were obtained from the tests with polished E110 claddings in the ANL [13]. Polishing of the E110 cladding surface allowed to delay greatly the breakaway initiation, that in its turn resulted in the significant improvement of the oxidized cladding mechanical properties.

The results of tests with polished E110 claddings do not allow to formulate the final conclusion concerning the mechanism due to which the E110 cladding oxidation behavior is improved. However, turning back to the consideration of two possible reasons for the surface effect (the surface roughness and surface contamination) and taking into account the obtained test data, the following may be assumed:

- both factors are important for the initiation of the breakaway oxidation;
- but even an ideal surface state from the point of view of the surface roughness does not allow to avoid the breakaway oxidation at the low ECRs in the presence of the surface contaminations that is confirmed by the tests with etched claddings.

Thus, the microchemistry of the cladding surface is apparently the dominant factor influencing the breakaway condition. The further analysis of microchemical effects will be continued in the next section of the report.

4.3. The assessment of relationship between the microchemical composition and oxidation behavior of niobium-bearing alloys

To study these potential effects of the cladding behavior, several types of zirconium niobium claddings were selected for the oxidation and mechanical tests. The specification for the used cladding material is presented in Table 4.2. The additional information characterizing the cladding initial parameters is given in Tables A-1, A-2 of Appendix A.

Table 4.2. The specification for the used cladding material

Notation conventions of cladding types used in this program	Alloying composition	Input components used on the fabrication of the alloy ingot
E110	Zr-1%Nb	Iodide Zr, electrolytic Zr, recycled scrap, Nb
$E110_{G(fr)}$	Zr-1%Nb	French sponge Zr (CEZUS), Nb
$E110_{G(3fr)}$	Zr-1%Nb	French sponge Zr, iodide Zr, recycled scrap, Nb
$E110_{G(3ru)}$	Zr-1%Nb	Russian sponge Zr, iodide Zr, recycled scrap, Nb
$E110_{low\ Hf}$	Zr-1%Nb	Iodide Zr, electrolytic Zr with low Hf content, recycled scrap, Nb
E635	Zr-1%Nb-1.2%Sn-0.35%Fe	Iodide Zr, electrolytic Zr, recycled scrap, Nb, Sn, Fe
$E635_{G(fr)}$	Zr-1%Nb-1.2%Sn-0.35%Fe	French sponge Zr (CEZUS), Nb, Sn, Fe

All types of these claddings were manufactured in accordance with the Russian process for the cladding fabrication. The subprogram of experimental investigations with the cladding material manufactured with the use of sponge Zr and electrolytic Zr with low Hf contents consisted of positions listed in Table 4.3.

Table 4.3. The subprogram major tasks for the test with the sponge cladding material and E110 cladding with low Hf content

Task	Motivation
1. To perform the oxidation tests at 1100 C of the E110 and E635 claddings manufactured with the use of 100% sponge Zr ($E110_{G(fr)}$, $E635_{G(fr)}$) and to perform the ring compression tests of oxidized claddings	To develop the comparative test data on the behavior of iodide/electrolytic E110 and E635 alloys and sponge E110 and E635 alloys
2. To perform the tests with the E110 cladding manufactured by the standard Russian procedure but with low Hf content in the electrolytic Zr ($E110_{low\ Hf}$)	Taking into account that the chemical composition of the standard E110 cladding is characterized by a very high content of Hf (in comparison with the sponge material), to check the dependence of the E110 oxidation behavior on Hf content
3. To perform the oxidation tests at 1100 C of the E110 claddings manufactured from the mixture of iodide, sponge Zr and recycled scrap, after that to estimate the mechanical behavior of oxidized samples ($E110_{G(3ru),\ (3fr)}$)	To clarify the sensitivity of the cladding oxidation behavior to the variation in the microchemical composition of the E110 alloy

Task	Motivation
4. To perform the oxidation tests at 900, 1000, 1200 C with the use of sponge types of the E110 cladding material and to estimate the margin of residual ductility of oxidized samples	To determine the representativity of test results obtained at 1100 C for other temperature regions

The whole scope of test results obtained in the frame of this subprogram is presented in Tables B-1, B-2 of Appendix B and in Appendix H of the report. The major outcomes of the subprogram are discussed in the next paragraphs of this section.

4.3.1. The analysis of the oxidation and mechanical behavior for the $E110_{G(fr)}$ and $E635_{G(fr)}$ claddings fabricated on the basis of 100% French sponge Zr

Two samples from this type of the E110 cladding were oxidized at 1100 C. The appearances of samples after the oxidation tests are presented in Fig. 4.7.

Sample #89: 10.5% ECR 22 ppm of H content	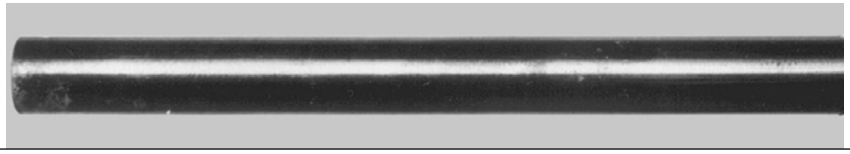
Sample #90 13% ECR 30 ppm of H content	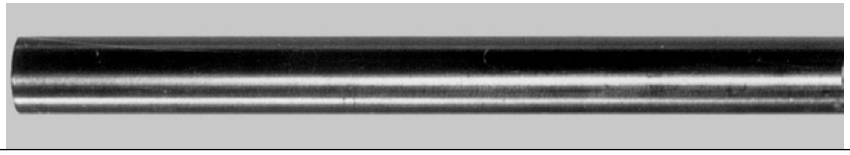

Fig. 4.7. Appearances of $E110_{G(fr)}$ samples after the double-sided oxidation at 1100 C

The appearance of these samples demonstrates that in spite of a high level of measured ECRs (10.5 and 11.0%) the cladding surface is covered with the black bright oxide. This fact indicates that the mechanism of the uniform oxidation was realized on testing of these samples. The results in detail of mechanical tests with this type of the E110 cladding in comparison with the results obtained in the test with the standard E110 cladding allow to note the following (see Fig. 4.8):

- the $E110_{G(fr)}$ oxidized rings have a visible residual plastic deformation after the ring compression tests;
- the load-displacement diagrams of the $E110_{G(fr)}$ oxidized samples demonstrate that a significant part of the sample deformation before the fracture was accompanied by the plastic strain;
- both $E110_{G(fr)}$ oxidized samples are characterized by a very low hydrogen concentration;
- the $E110_{G(fr)}$ oxidized claddings have a significant margin of residual ductility at 13% ECR (as-measured); this margin corresponds to that for the Zry-4 cladding.

This first stage of appropriate investigations has shown that E110 claddings fabricated in accordance with the traditional Russian method of ingot preparation and E110 claddings fabricated in accordance with the western method of ingot preparation have quite a different oxidation behavior.

In the context of investigations presented in this section of the report, the revealed differences may come from the differences in the microchemical composition (impurity content) of the E110 and $E110_{G(fr)}$ cladding materials. To extend the data base for the analysis of these effects, intermediate compositions of cladding materials such as $E110_{G(3fr)}$ and $E110_{G(3ru)}$ were tested.

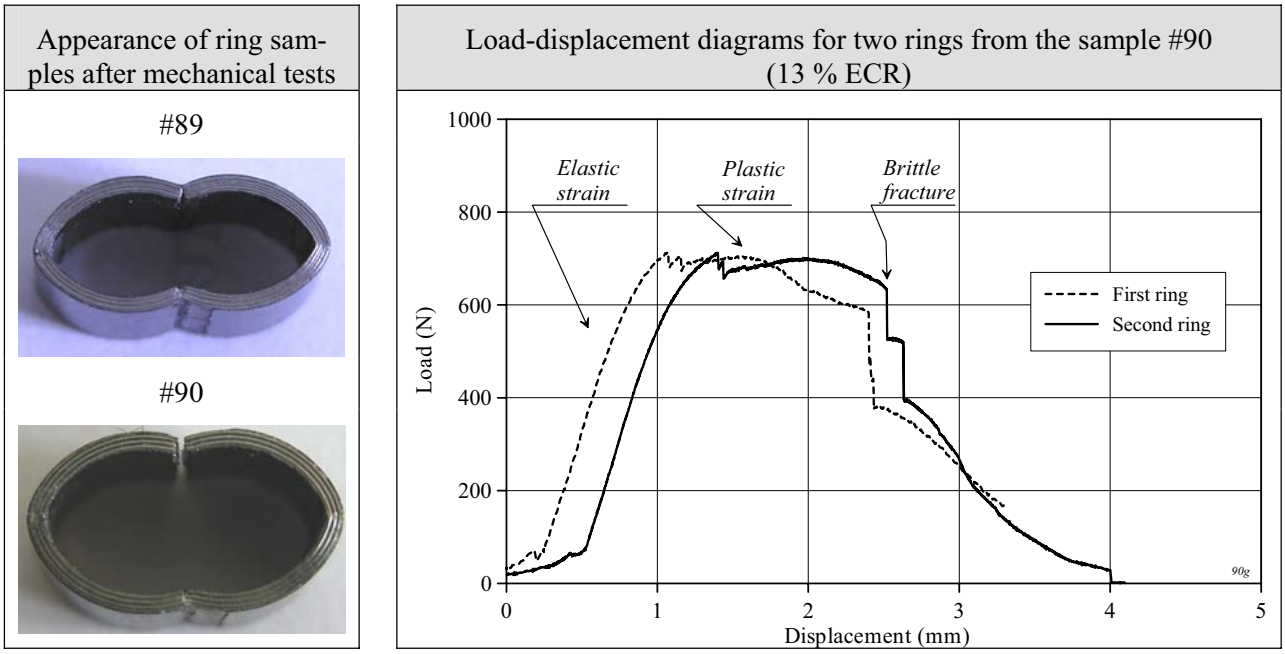

Fig. 4.8. Results of ring compression tests with $E110_{G(fr)}$ oxidized samples

4.3.2. The interpretation of test results with $E110_{G(3fr)}$ and $E110_{G(3ru)}$ claddings

The appearances of these samples after the oxidation test in comparison with the standard E110 cladding and the results of mechanical tests are shown in Fig. 4.9 for an oxidation temperature of 1100 C.

The obtained data showed that all effects revealed in the analysis of the $E110_{G(fr)}$ behavior (a black bright oxide, low hydrogen content, high margin of residual ductility up to 16.7% ECR), were confirmed in the tests of the $E110_{G(3fr)}$ and $E110_{G(3ru)}$ claddings. This observation indicates that in spite of the fact that $E110_{G93fr)}$ and $E110_{G(3ru)}$ claddings contain only 70% of sponge Zr-1%Nb this turned out to be enough to improve considerably the oxidation behavior of the E110 cladding.

The additional confirmation of this conclusion can be obtained due to the comparative analysis of the cladding microstructures presented in Fig. 4.10. As can be seen from this data, the prior β-phase of the cladding samples manufactured from the iodide/electrolytic alloy and oxidized to the 10.0% ECR (#65) was so embrittled that local areas of the prior β-phase flaked off on polishing of the metallographic sample (black areas on the sample surface). Besides, this sample has no clearly marked boundary between the α-Zr(O) and prior β-phases. In contrast to this cladding, the cladding manufactured on the basis of sponge Zr (#89) is characterized by a clear boundary line between α-Zr(O) and prior β-phases and the structure of the prior β-phase without visible indications of α-Zr(O) phase and solid hydrides.

As a whole, these differences indicate that the diffusion processes in these two types of the E110 cladding determining the diffusion of alloying elements (including such minor alloying elements as impurities), proceeded in these cladding in different ways. It may be assumed that these differences represent the key factor predetermining the differences in the oxygen and hydrogen pick up and the distribution in the E110 standard and E110 sponge claddings. At this stage of the preliminary analysis of revealed effects the so-called “hafnium issue” arose.

The basis for the hafnium issue lies in the fact that hafnium concentration in the E110 standard alloy (up to 500 ppm) and hafnium concentration in the E110 alloy fabricated with the use of sponge (<100 ppm) differ greatly. Therefore, in spite of the fact that the difference in the Hf concentration cannot cause the general difference in the oxidation behavior of these cladding from the physical point of view, it was decided to perform special investigations to study this effect.

E110 (standard)	#96 9.8% ECR	
$E110_{G(3ru)}$	#95 11.6% ECR (4 ppm of H content)	
$E110_{G(3fr)}$	#99 11.5% ECR (13 ppm of H content_	
$E110_{G(3ru)}$	#97 16.7% ECR (17 ppm of H content)	

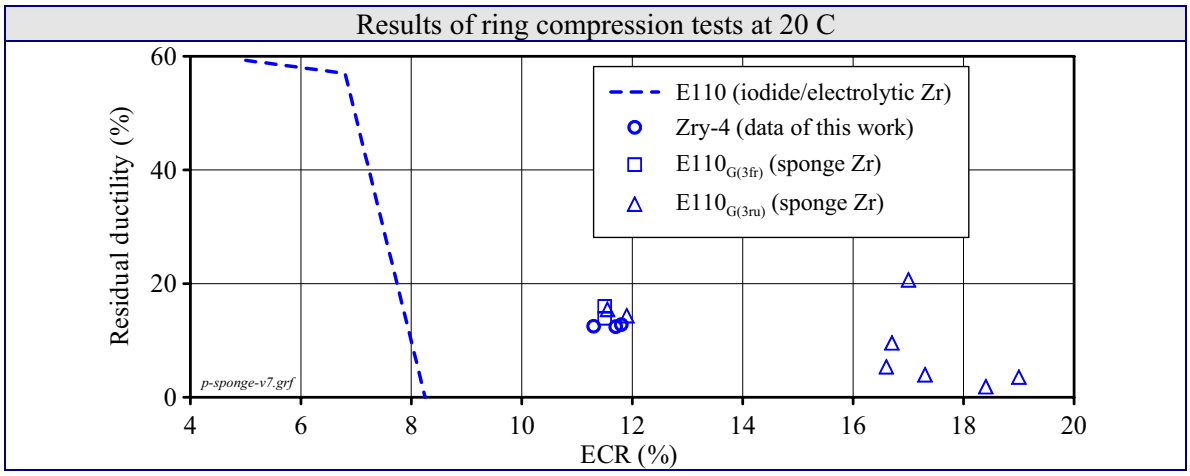

Fig. 4.9. Comparative data base characterizing the $E110_{G(3fr)}$ and $E110_{G(3ru)}$ oxidation/mechanical behavior

Iodide/electrolytic E110	**Sponge E110**
Etched	Etched
#68-5 ECR=10.0% (E110)	**#89-4** ECR=10.5% ($E110_{G(fr)}$)

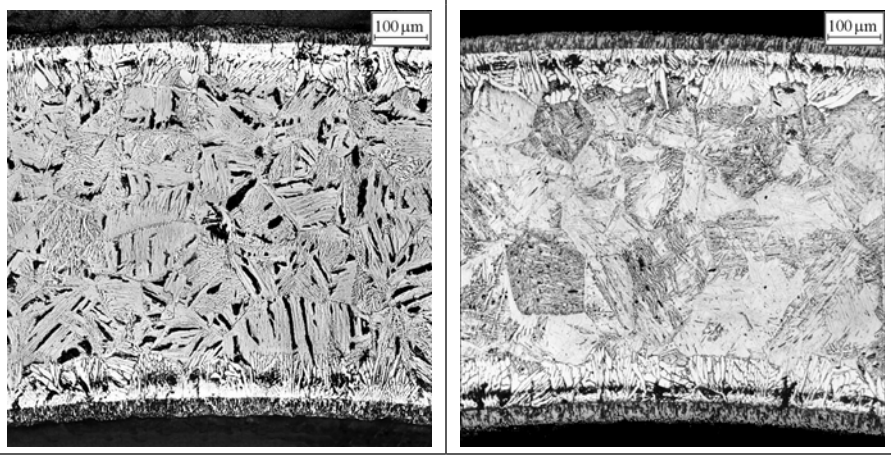

Fig. 4.10. The comparison of microstructures for iodide/electrolytic and sponge E110 claddings after the oxidation at 1100 C

Two cladding samples manufactured with the employment of electrolytic Zr with low Hf content (90 ppm) were used for this goal. The results of tests performed with these samples are presented in Fig. 4.11, in Tables B-1, B-2 of Appendix B and Fig. H-15 of Appendix H.

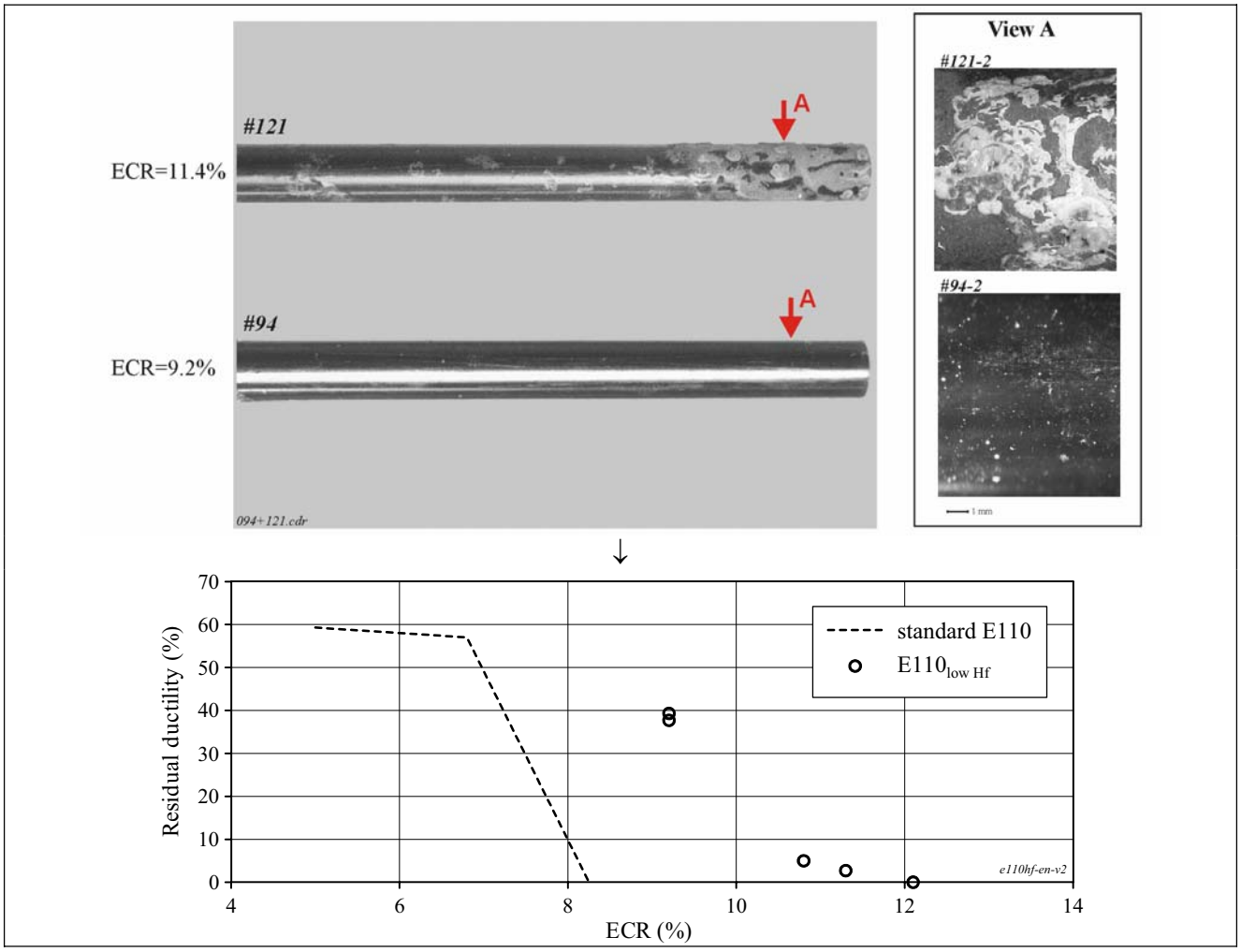

Fig. 4.11. The appearance of the $E110_{low\ Hf}$ cladding after the oxidation at 1100 C and results of mechanical tests

The analysis of obtained data allows to state the following:

- the decrease of Hf content in the Zr-1%Nb alloy improves the oxidation behavior of the E110 cladding; so, the first indications of the breakaway oxidation were fixed at 9.2% ECR;
- the $E110_{low\ Hf}$ sample oxidized up to 9.2% ECR has a significant margin of residual ductility and low hydrogen content (17 ppm);
- the zero ductility threshold of the $E110_{low\ Hf}$ cladding is increased up to 12% ECR but the breakaway oxidation was observed in the ECR range 9-12% and the embrittlement of the E110 cladding was caused by oxygen and hydrogen pickup (the hydrogen concentration was about 430 ppm) at 11-12% ECR.

Therefore, it can be assumed that the process of electrolytic Zr cleaning of hafnium was associated with a change in the level of other chemical impurities. In this case, this change led to some improvement of the E110 oxidation behavior but not so radically as it took place for sponge types of the E110 cladding. Therefore, further investigations were continued with the $E110_{G(fr)}$ and $E110_{G(3ru)}$ claddings to adjust the sensitivity of the oxidation behavior of these claddings to the oxidation temperature.

4.3.3. The sensitivity of the oxidation behavior of the sponge E110 cladding to the oxidation temperature

The temperature range 900–1200 C was studied in these investigations. Taking into account the results of tests with the traditional E110 cladding that showed that the oxidation behavior of the E110 alloy at 1000 C

was somewhat worse than at 1100 C, the first stage of temperature dependent tests was performed at 1000 C. These tests allowed to reveal the unexpected effect associated with a sharp decrease in the oxidation rate of the sponge type cladding at 1000 C. The scale of this effect can be characterized using the following experimental data:

- it takes 865 seconds to oxidize the standard E110 cladding up to 7.7% ECR;
- it takes 2519 seconds to oxidize the sponge type of the E110 cladding up to 6.9%;
- and it takes 5028 seconds to oxidize the sponge type of the E110 cladding up to 8.9% ECR.

The oxidation kinetics of different types for the E110 cladding will be considered in detail in the next paragraphs of the report.

As for this paragraph, the following notice concerning the oxidation rate problem should be made: a very low oxidation rate of sponge E110 cladding at 1000 C led to the fact that the time limit for the steam generator used in this test series (approximately 5000 s) was exhausted at the ECR of about 8.5–8.9%. Thus, this ECR range was the maximum one in the oxidation tests at 1000 C. The results of tests at 1000 C are presented in Fig. 4.12.

Cladding characterization		Oxidation duration	Cladding appearance
E110 (tradi-tional)	ECR=7.7%	t_{ef}=865 s	#44
$E110_{G(fr)}$	ECR=6.5% (28 ppm of H content)	t_{ef}=2016 s	#91
$E110_{G(3ru)}$	ECR=6.9% (16 ppm of H content)	t_{ef}=2519 s	#98
$E110_{G(3ru)}$	ECR=8.9% (11 ppm of H content)	t_{ef}=5028 s	#101
$E110_{G(fr)}$	ECR=8.5% (12 ppm of H content)	t_{ef}=5013 s	#93

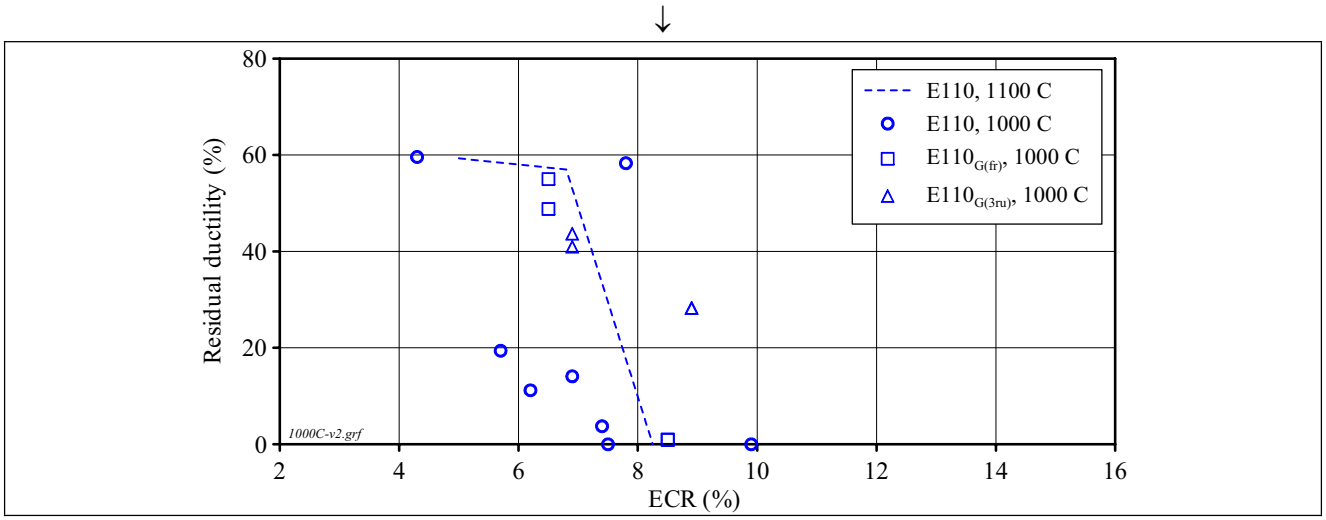

Fig. 4.12. The appearance and mechanical properties of different E110 claddings after the oxidation at 1000 C

The obtained data allow to formulate the following important observations:

- after the oxidation during 800 s at 1000 C, the E110 cladding manufactured in accordance with the traditional method of Zr-1%Nb ingot preparation has typical indications of the breakaway oxidation;
- the E110 standard cladding achieves the zero ductility threshold after the oxidation during somewhat longer than 800 s at this temperature;
- the sponge types of the E110 cladding oxidized at 1000 C during 2500 s have a significant margin of residual ductility, low hydrogen concentration in the prior β-phase, and the uniform corrosion type of oxidation;
- the first demonstration of the breakaway oxidation of the sponge E110 claddings appears after 5000 s of oxidation, hydrogen content in the cladding remains still low but the zero ductility threshold is achieved due to the decrease in the prior β-phase thickness and the increase of oxygen concentration in the cladding matrix.

Besides, the obtained data allow to formulate one new problem: for oxidation at 1000 C, the critical measured ECRs corresponded with the zero ductility thresholds of standard and sponge ECR claddings are similar to both types of the cladding but the oxidation duration differs approximately six times. In the context of this problem, the following question could be formulated: is the measured (calculated) ECR a unequivocal criterion characterizing the zero ductility conditions? The additional consideration of this issue will be continued in one of next paragraphs of the report. To investigate the sponge E110 cladding behavior at temperatures lower than 1000 C, one reference test was performed at 900 C (with modified steam generator). The results of this test are shown in Fig. 4.13.

Cladding characterization		Oxidation duration	Cladding appearance
E110 (standard)	ECR=6.7%	t_{ef}=4804 s	#131 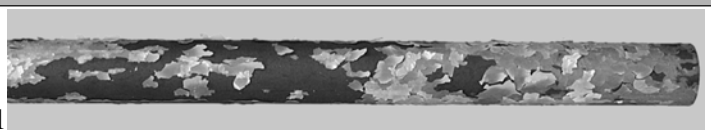
$E110_{G(3ru)}$	ECR=7.5%	t_{ef}=14400 s	#137 

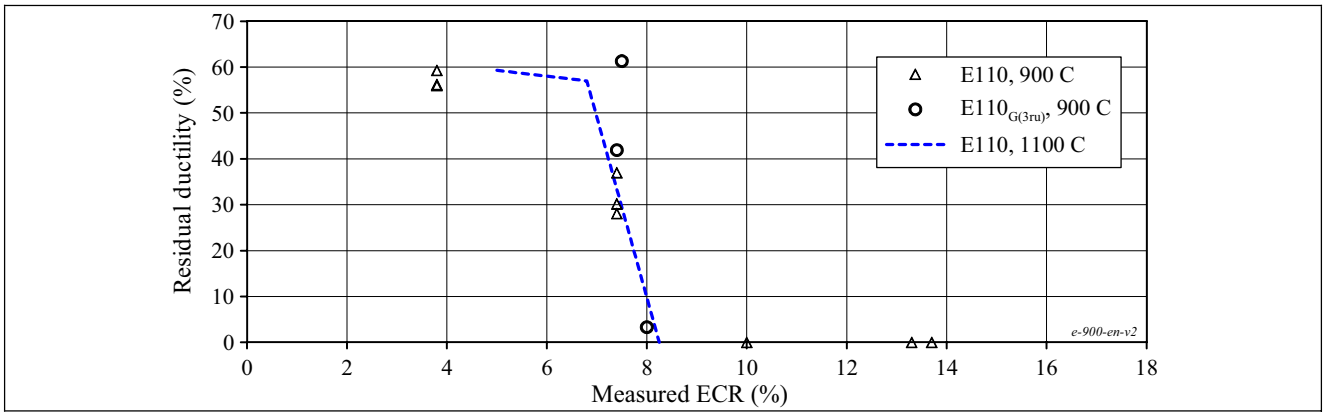

Fig. 4.13. The comparative test data characterizing the E110 and $E110_{G(3ru)}$ behavior after the oxidation at 900 C

The present data allow to observe that general tendencies revealed for two types of the E110 cladding at 1000 C are retained at 900 C also:

- the embrittlement of the $E110_{G(3ru)}$ cladding is not the consequence of the breakaway oxidation in contrast to the standard E110 cladding;
- much more time is needed to achieve approximately the same ECR in the sponge E110 cladding and the same margin of residual ductility as those in the standard E110 cladding (14400 s and 4800 s respectively);
- the critical measured ECR characterizing the zero ductility threshold of sponge type in the E110 cladding ($E110_{G(3ru)}$) at 900 C is approximately the same as that for the sponge E110 at 1000 C and the standard E110 at 1100 C (8.3% ECR) but the causes for embrittlement are different. The embrittlement of sponge E110 is caused by the oxygen induced mechanism but the embrittlement behavior of the standard E110 is determined by the combination of oxygen and hydrogen effects.

The last position of temperature dependent investigations with the sponge E110 cladding was devoted to the tests at 1200 C. The results of these tests are shown in Fig. 4.14.

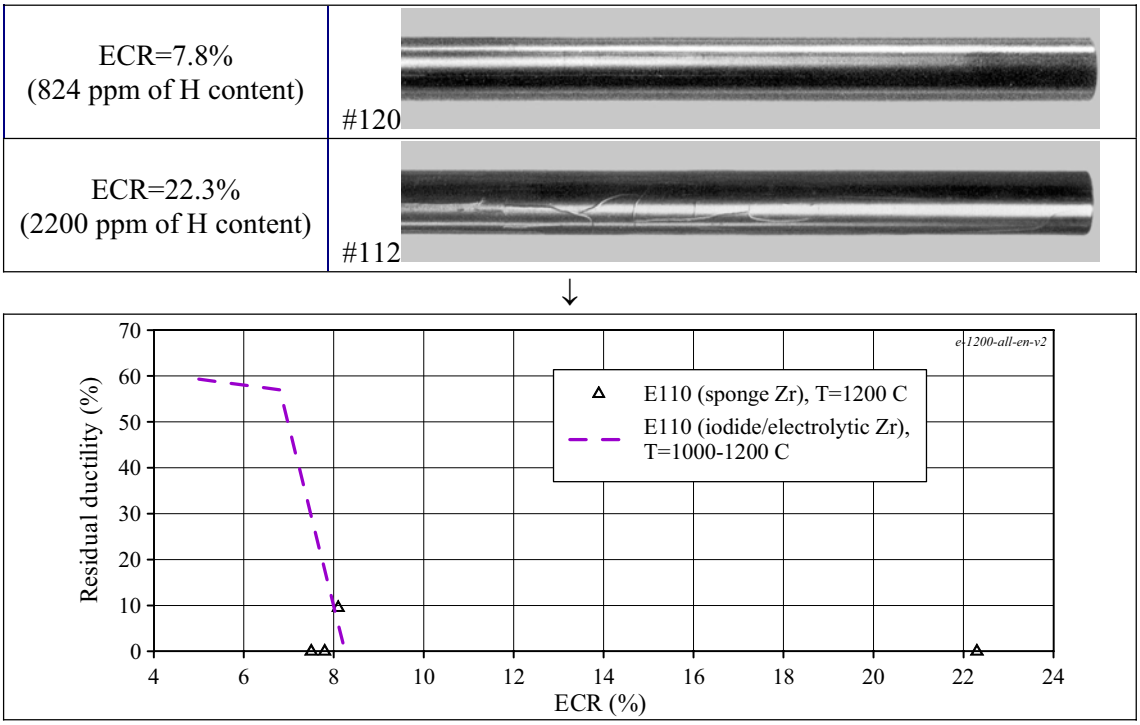

Fig. 4.14. The characterization of appearance and RT mechanical properties of the $E110_{G(3ru)}$ cladding after the oxidation at 1200 C

The major conclusion from these test is the following: for oxidation at 1200 C, and in spite of the presence of black bright oxide on the tested cladding, the zero ductility of sponge E110 cladding of the $E110_{G(3ru)}$ type was approximately the same as that for the standard E110 cladding. The oxidation of the $E110_{G(3ru)}$ cladding corresponded to the significant hydrogen absorption.

Thus, the results of these tests have demonstrated that the oxidation behavior of the $E110_{G(3ru)}$ cladding deteriorated sharply at 1200 C. In this problem, it is interesting to note that ring compression tests performed at 20 C in the ANL with Zry-4, Zirlo, M5 samples oxidized at 1200 C have shown that the residual ductility of these claddings "decreased rather abruptly from 5 to 10% ECR" [13]. These data confirm that the oxygen diffusion processes in zirconium claddings are considerably changed on proceeding from 1100 C up to 1200 C. However, the nature of these processes is not quite understood now. Besides, in spite of the similarity in the $E110_{G(3ru)}$ behavior and Zry-4, M5, Zirlo one at 1200 C, a significant difference has been revealed also. These differences are associated with the hydrogen content in the oxidized cladding. The embrittled Zry-4, Zirlo cladding have a low hydrogen content and (on our opinion) due to this reason these claddings have demonstrated the remarkable improvement in the cladding ductility at the temperature increase in mechanical tests up to 135 C. The embrittled $E110_{G(3ru)}$ cladding has a high hydrogen content and the temperature increase in mechanical tests up to 135 C has not led to the increase in residual ductility. In this connection, it is reasonable to assume that the revealed difference in the behavior of these claddings is associated with the fact that $E110_{G(3ru)}$ is not 100% sponge material.

4.3.4. The analysis of results obtained in the test with the E635 cladding fabricated using sponge Zr

The $E635_{G(fr)}$ cladding fabricated on the basis of 100% French sponge Zr was the last type of niobium-bearing claddings manufactured with the use of sponge Zr and tested in the frame of this work. These several tests were performed to extend the test data base developed to determine the sensitivity of the cladding oxidation behavior to the alloy chemical composition. The major results of tests with the $E635_{G(fr)}$ cladding oxidized at 1100 C are presented in Fig. 4.15.

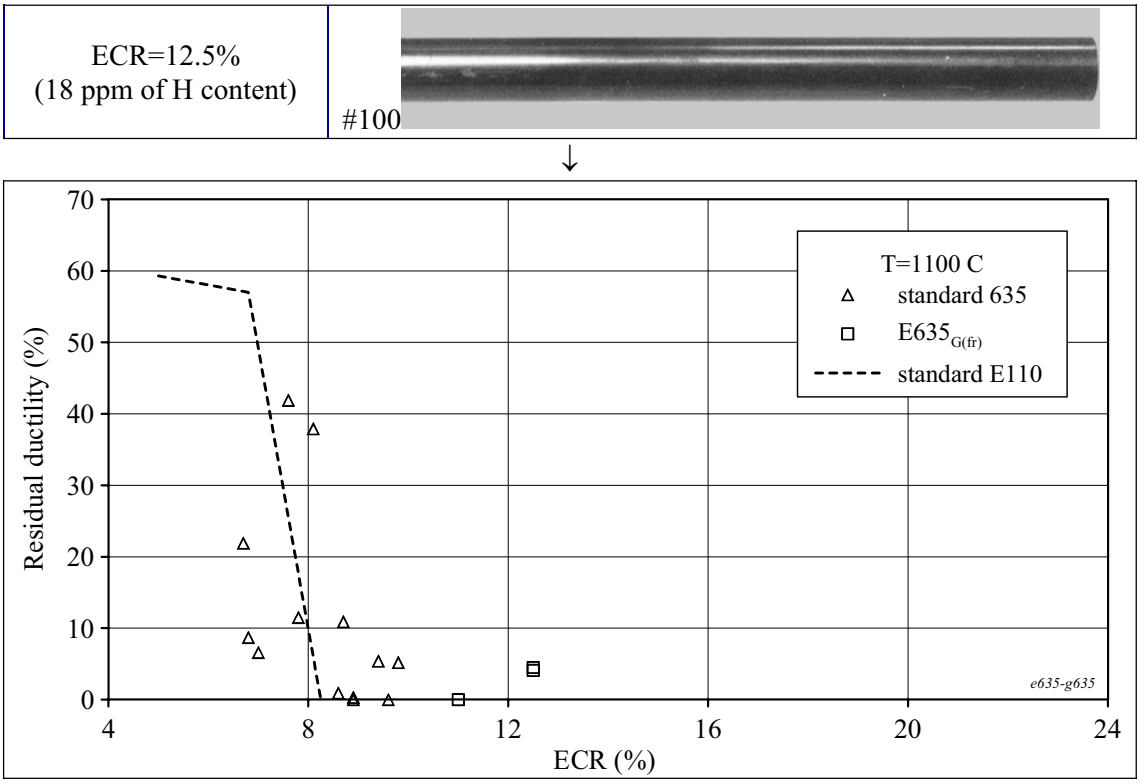

Fig. 4.15. The appearance of the $E635_{G(fr)}$ cladding after the oxidation test at 1100 C and comparative E635 (standard), E110 (standard), $E635_{G(fr)}$ results of ring compression tests

The obtained data allow to note the following:

- In spite of the fact that the $E635_{G(fr)}$ oxidized cladding is characterized by a low hydrogen content in the prior β-phase up to 12.5% ECR, the first visible indications of the breakaway oxidation were observed on the cladding surface at 11% ECR;
- in contrast to sponge types of the E110 cladding, the general difference in zero ductility thresholds of the standard E635 and sponge E635 was not revealed.

4.3.5. The comparative consideration of a microchemical composition of different types of the E110 alloy

Results of tests performed with the sponge E110 cladding have demonstrated a significant improvement in the E110 corrosion resistance. To explain this phenomenon, the microchemical aspects of difference between the iodide/electrolytic E110 and sponge E110 alloys were considered. The first step in these investigations was connected with the analysis of results of previous investigations performed in this line. H.Chung developed a very interesting model for aliovalent elements specially for the interpretation of the revealed difference in the E110 and M5 alloy behavior [12]. This model is based on Wagner electrochemical theory of oxygen ions passing through oxide to the oxide/metal interface with regard to the presence of impurity and secondary phase precipitates in the cladding material [15]. The employment of this theory performed by H. Chung using the aliovalent element model in our case allowed to develop the following conception of the oxide behavior at the high temperature oxidation (>800 C) of niobium-bearing alloys:

- the impurity and alloying element should be subdivided into overvalent elements and undervalent elements in relation to the tetragonal zirconium;
- the presence of overvalent elements leads to the decrease of O^- vacancies and to the increase of the stoichiometric degree of oxide (a low fraction of the protective tetragonal oxide);
- undervalent elements provide:

- a high density of oxygen ions vacancies;
- the tendency towards the retention of under-stoichiometric oxide with a high fraction of tetragonal protective oxide;

- such binary alloys as the E110 and M5 contain a definite quantity of undervalent beneficial impurities: Ca, Al, Mg, Fe, Ni and a definite quantity of one overvalent alloying element Nb.

The comparative analysis of the M5 and standard E110 fabrication processes including the surface finishing performed by H. Chung led him to the following conclusions:

- both alloys have the same content of deleterious overvalent niobium;
- the M5 alloy is enriched with such beneficial elements as Ca, Al, Mg, Fe, Y during the fabrication process;
- the standard E110 alloy is enriched with such specific deleterious impurity as F during the fabrication process (electrolytic Zr production);
- the general difference in the oxidation behavior of the standard E110 and M5 alloys is caused by the differences in the above listed beneficial and deleterious impurities.

In the context of these conclusions, it should be specially noted that:

- the use of fluoride compounds during the electrolytic E110 fabrication was always the object of a special attention and control of F content during the E110 manufacturing process;
- the results obtained by V. Vrtilkova after the oxidation tests with the E110 alloy were used by H. Chung on the validation of his position in this issue [16]. However, it should be pointed out that V. Vrtilkova used the E110 tubes manufactured from iodide Zr only because only this method of the E110 fabrication was employed in Russia before 1985. But it is known that the iodide Zr contains much less impurities than electrolytic and sponge Zr;
- besides, Wagner theory could be used for the impurity elements having a significant solubility in ZrO_2 (Ca, Mg, Al, Y), but it is known that such elements as Fe, Nb, Sn are practically insoluble in ZrO_2 and these elements are present in the oxide on the crystalline grains as independent phases.

Russian investigations performed on developing the E110 alloy have shown that the most deleterious impurities in the zirconium alloys are the following: C, N, F, Cl, Si. Besides, such elements as Ti, Al, Mo, Ta, V negatively influence the corrosion resistance, the beneficial influence was revealed for Fe and Cr. The influence of major alloying elements such as Nb and Sn is not univocal. The corrosion resistance of zirconium alloys with the Nb and Sn alloying elements is the function of the content of these elements in alloys. The investigations in detail of the corrosion resistance sensitivity of Zr-Nb-based alloys and Zr-Sn-based alloys to the alloying element content performed recently confirmed this statement [9, 17]. The recent reassessment of results of autoclave corrosion tests (500 C was the maximum temperature) with the M5 cladding has shown that C (with the content >100 ppm), Al (with the content 20–150 ppm), N, Sn (with the content >100 ppm), Si (with the content >80 ppm) have a detrimental influence over the M5 corrosion behavior [7, 18]. In addition to that:

- the beneficial influence of Fe, Cr and Fe/Cr ratio over the corrosion resistance of Zr-Sn alloys was revealed [19, 20, 21, 22];
- the acceleration in the corrosion process was observed as a function of such impurities as Al, Ti, Mn, Pt, Ni, Cu in the Zr-2.5%Nb alloy [23];
- the optimal corrosion resistance was obtained for C and Fe impurities in the Zr-2.5%Nb alloy. It was revealed that the optimal content of these elements is about 30 ppm C and 1100 ppm Fe [23].

In conclusion of this overview of previous investigations, the following information concerning such elements as Nb, O, Hf may be added:

- Russian investigations on the oxygen content in the Zr-Nb alloy of 400–1000 ppm and French investigations on the oxygen content in the Zr-Nb alloy of 900–1800 ppm [18] have shown that the oxygen concentration has the negligible influence over the corrosion resistance of niobium-bearing alloys;
- the same investigation and results of investigations published in [9] allow to consider that the corrosion behavior of niobium-bearing alloys is not sensitive to the variations of Nb content in the alloy in the range 0.9–1.1 wt%;
- the role of hafnium is not completely clarified now but this element is usually considered as neutral.

Unfortunately, the comparative analysis in detail of this research results with results of previous investigations devoted to the relationship between the microchemical composition of niobium-bearing alloys and the corrosion behavior of these alloys allow to formulate the only following general conclusions:

1. The high corrosion resistance of Zr-Nb alloy under operating conditions (a low temperature range) is the necessary requirement for this type of zirconium cladding but this requirement fulfillment does not guarantee that the alloy will demonstrate a high corrosion resistance under LOCA relevant conditions (a high temperature range) also.
2. In spite of the numerous investigations performed in this line, the nature of the relationship between the corrosion resistance and chemical composition of the alloy is not quite understood yet.

Taking into account these conclusions, the plan for comparative studies of the chemical composition of the iodide/electrolytic E110 and sponge E110 was developed on the basis of the following major provisions: the measurement results of the standard E110 alloy chemical composition (used for our oxidation tests) and measurement results of sponge types of the E110 alloy chemical composition (tested during this program) must be compared. Reasonable differences in the content of chemical elements should be revealed and analyzed.

At the first stage of this plan, a typical content of the E110 alloy presented in Table 4.4 was compared with a real content of chemical elements in each batch of tested E110 alloy. This comparison showed that the typical composition of the E110 alloy was representative for the tested E110 material except for Fe content. Real Fe content in the E110 alloy used for this program was 86 ppm.

Table 4.4. Chemical composition of the E110 alloy (standard) [5]

Typical content (ppm)	Chemical element												
	Al*	B	Be	C	Ca	Cd	Cl	Cr	Cu	F	Fe	H	Hf
	<30	<0.4	<30	<40-70	<100	<0.3	<7	<30	<10	<30	140	4–7	300-400
	K	Li	Mn	Mo	N	Ni	O	Pb	Si	Sn	Ti	Nb	
	<30	<2	<3	<30	<30-40	<30-39	500-700	<50	46-90	<100	<30	0.95-1.1 wt%	

** Concentrations marked as <30,… reflect that fact that the real concentration of elements was not measured, because it was less than the low threshold of the detector (procedure) sensitivity*

At the second stage of the research, chemical compositions of the $E110_{G(fr)}$, $E110_{G(3fr)}$, $E110_{G(3ru)}$ alloys were compared with the standard E110 composition. The comparative analysis of the appropriate data allowed to establish the reasonable difference in the impurity contents for Fe and Hf only. Nevertheless, other several beneficial and deleterious elements were added into the comparative results presented in Fig. 4.16. It should be noted that in spite of the fact that Hf influence over the corrosion resistance is not understood, we attributed this element to deleterious impurities taking into account:

- results of tests with the $E110_{low\ Hf}$ cladding;
- the fact that Hf stabilizes the monoclinic oxide at higher temperatures.

By the way, the comparative analysis of the $E110_{low\ Hf}$ and standard E110 cladding chemical compositions showed that the impurity contents in these materials were the same except for Hf content.

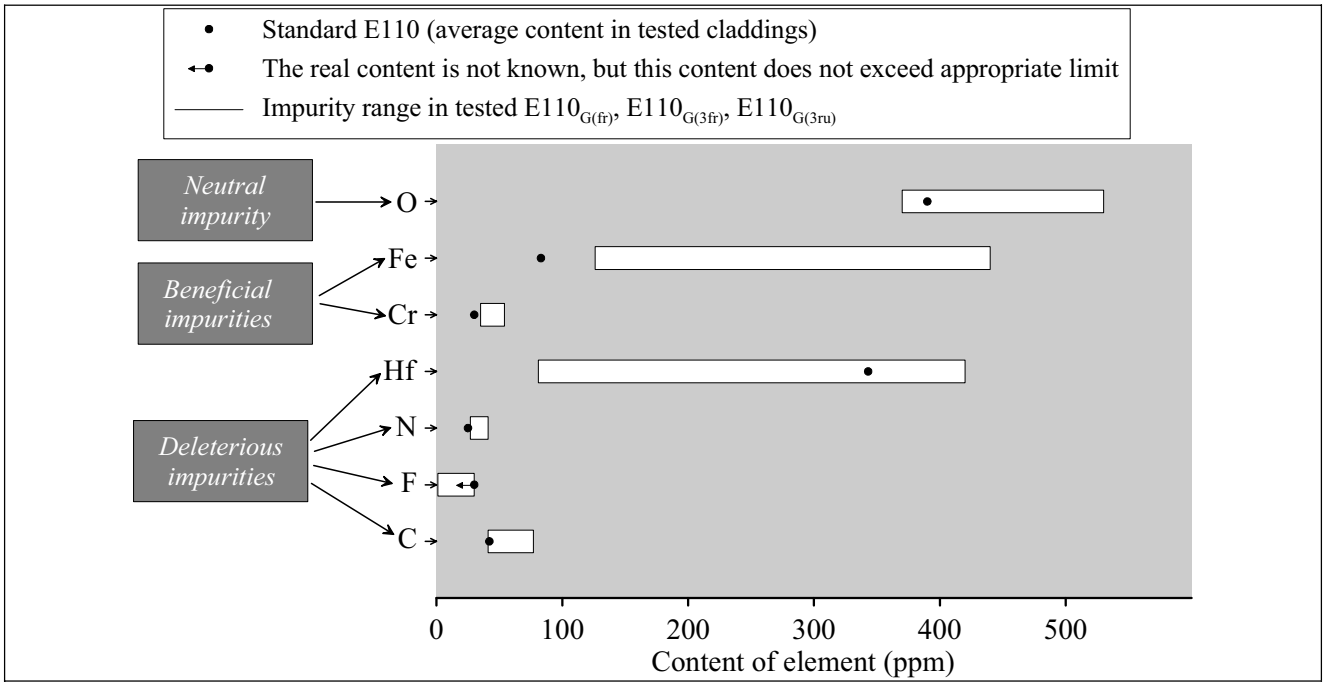

Fig. 4.16. Comparison of some data on the impurity content in the standard E110 and $E110_{G(fr)}$, $E110_{G(3fr)}$, $E110_{G(3ru)}$ at the beginning of the cladding fabrication

Thus, the obtained data showed that one significant difference in the standard E110 and sponge E110 chemical composition was observed: Fe content in the sponge E110 is higher than that in the standard E110. But the beneficial effect of iron on the corrosion behavior of zirconium alloys is known for a long time. Therefore, the majority of alloys including such Russian alloy as E635 have a high or quite high Fe content (see Table 4.5). In this case, such alloys as Zircalys, Zirlo and E635 employ iron as the alloying element.

Table 4.5. Composition of zirconium alloys used in reactor fuel design [24]

Element	Zircaloy–4	ZIRLO	E635	M5	E110
Nb (wt%)	–	0.9–1.3	0.95–1.05	0.8–1.2	0.95–1.05
Sn (wt%)	1.2–1.7	0.9–1.2	1.2–1.3	–	–
Fe (wt%)	0.18–0.24	0.1	0.34–0.40	0.015–0.06	0.006–0.012
Cr (wt%)	0.07–0.13	–	–	–	–
Zr	Balance	Balance	Balance	Balance	Balance

The results obtained during this research confirm the important role of iron in the cladding oxidation behavior. This thesis is based on the fact that sponge types of the E110 cladding with the higher content of iron demonstrate the better corrosion behavior than the standard E110 alloy with low Fe content as well as on the fact that the results of oxidation tests of the E635 cladding (iodide/electrolytic) with a very high content of iron have shown that the oxidation behavior of the standard E635 cladding is somewhat better than that of the standard E110 cladding. Though, in this case the absence of a general difference in the oxidation behavior of the standard E635 and sponge E635 impels to involve additional test data to continue the analysis of this and other issues connected with the chemical composition of Zr-Nb alloys. The interesting scope of investigations was recently performed in the VNIINM (Russia) [25].

Seven types of niobium-bearing claddings (iodide/electrolytic) were oxidized at 1100 C and mechanically tested. These seven types of the cladding are characterized by the following range of chemical composition variations:

- Nb → 0.9–11 wt%;

- Fe → 80–1400 ppm;
- C → 45–200 ppm;
- Hf → 100–430 ppm;
- Cr → 30–60 ppm;
- O → 350–1300 ppm.

The analysis shows that these claddings have demonstrated quite different oxidation and mechanical behavior. These types of this behavior and appropriate contents of chemical elements in the cladding material are characterized in Table 4.6.

Table 4.6. The organized results of oxidation and mechanical tests with seven types of the standard E110 and modified E110 (the data of [25])

Test parameters	Corrosion resistance at 10% ECR		
	Best	Intermediate	Worst
The cladding sample number	##2, 3, 4	##5, 6	##1, 7
The corrosion type	Uniform (lustrous black protective oxide)	Beginning of the nodular oxidation (white spots on the cladding surface)	Typical breakaway oxidation. The spallation of white oxide
Hydrogen content (ppm)	60–200	200–400	400–600
Mechanical properties	Maximum residual ductility and fracture energy	Very low residual ductility and fracture energy	Very low residual ductility and fracture energy
The impurity content (ppm):			
Fe	130–450	80–1400	100–140
O	350–600	890–1300	350–500
C	<45–65	70–200	60–80
Hf	100–430	360–370	100–360
Cr	<30–60	<30	<30

The consideration of the data presented in Table 4.6 shows that:

- the cladding with the iron content of about 130–450 ppm having relatively low C content and low Hf content (~100 ppm) have demonstrated the best corrosion resistance;
- the intermediate corrosion resistance was observed at very low and very high Fe content (80 and 1400 ppm) and high Hf content, in this case, the direct sensitivity to the C content in the range of 70–200 ppm was not revealed;
- the relationship between the worst corrosion resistance and the concentration of chemical elements listed in Table 4.6 is not quite understood.

The analysis of these results performed by the VNIINM researchers led them to the assumption that the oxidation behavior of the E110 alloy is not so much the function of Fe, C, … concentration as the function of the quantity of impurities in the alloy. Special measurements performed for this goal showed the following [25]:

- the sum of Ni, Al, Si, Ca, K, F, Cl, Na, Mg impurities in the E110 cladding, having the intermediate and worst corrosion behavior was about 110–135 ppm;

- the appropriate sum in the E110 claddings that demonstrated the best corrosion behavior was about 25–45 ppm, in this case, the corrosion resistance decreased as impurity contents increased from 25 up to 45 ppm.

Unfortunately, it was impossible to perform the comparison of this type for impurity contents in the standard E110 and sponge E110 on the basis of data presented in Table 4.4 and in the Fig. 4.16. The thing is that the methods used to measure the concentration of very many impurities allowed to guarantee that the concentration of some impurity was not higher than the value presented in Table and Figure (<30, <40, …). However, these methods did not allow to measure the real impurity concentration in the alloy. It was also impossible to estimate the impurity contents in the M5 alloy because these data were not published. But some additional data useful for the analysis of this issue could be taken into account from the consideration of impurity contents in Zirlo presented in Table 4.7.

Table 4.7. Chemical composition of the Zirlo cladding tube [26]

Element content (ppm)	Chemical element																
	Al	C	Cr	Cu	Hf	Fe	Mg	Mo	Ni	Nb	N	O	Si	Sn	Ti	W	Zr
	120	20	10	20	<40	1000	<10	<10	<10	1.23 wt%	50	1450	130	1.08 wt%	19	<40	Balance

A special comment must be done before the analysis of these data:

- chemical compositions of the E110 alloy presented in Table 4.4, Table 4.6 characterize the ingot compositions;
- the E110 chemical compositions presented in Fig. 4.16 characterize the beginning of the cladding fabrication processes;
- special measurements of the E110 overall impurity contents were performed in the unoxidized E110 tubes;
- the Zirlo composition presented in Table 4.7 was measured using the Zirlo tubing.

Thus, the cladding tubes were used in both cases for the measurement of the sum of the E110 impurity content and Zirlo impurity content. The comparison of appropriate data showed that the hypothesis proposed in [25] to explain the E110 oxidation behavior on the basis of the sum of impurity contents was not confirmed as applied to the Zirlo claddings. So, the sum of two impurities only (Al and Si) is 250 ppm in the Zirlo cladding. But the oxidation behavior of the Zirlo cladding is characterized by the uniform corrosion and low hydrogen concentration in accordance with the data obtained in the ANL. Though, on the other hand, some data characterizing the content of impurities in the M5 alloy is in a good agreement with the assumption about the fact that the optimization of the content of beneficial impurities does not allow to achieve a high corrosion resistance at a high overall concentration of other impurities in the alloy. So, these some data characterizing the M5 alloy are the following [7, 18]:

- the sum of Ca, Mg, Sn, S contents in the alloy is less than 1 ppm;
- the sum of Si, Zn, Al contents in the alloy is less than a few ppm;
- the C content is 25–120 ppm.

Besides, these data characterizing the chemical composition of the M5 alloy allow to return to the discussion of the fact that the electrochemical theory of the cladding oxidation and the model of aliovalent elements (developed on the basis of this theory) must be added with models taking into account other competing processes in the niobium-bearing claddings under high temperature oxidation conditions.

If the experimental and analytical data presented in this paragraph are generalized then the following conclusions may be made:

- the cladding high temperature oxidation behavior has a series of peculiar features associated with the phase compositions and temperature dependent characteristics of the solubility and diffusion of alloying and impurity elements in the oxide and metallic matrix. Therefore, the studies of these processes should be performed under high temperature conditions. A direct transfer of results for low temperature corrosion tests to the high temperature corrosion behavior may result in grand errors;
- the impurity composition is one of the key factors determining the oxidation behavior of Zr-Nb alloys at high temperature conditions;
- there is a serious reason to change the current approach from the classification of impurities by the beneficial and deleterious ones to the following approach:

– minor alloying elements (this term was proposed in [23]), these are impurities allowing to provide the uniform mechanism of oxidation and to minimize the hydrogen content in the oxidized cladding; the requirements for the content of these elements must be developed;

– deleterious impurities for which the requirements must be stipulated for their individual content in the alloy or the requirements for their total content in the alloy;

– neutral impurities; the concentration of these impurities in the alloys in the current limits do not affect the oxidation mechanism and oxidation rate.

As for the E110 alloy, the list of impurities in accordance with this new classification cannot be determined basing on the results of this research. But it seems that iron is the first candidate for the incorporation into the set of the E110 minor alloying elements.

4.4. The comparative analysis of the E110 material microstructure

As it was reported at the beginning of this section, the bulk effects (in the context of the cladding oxidation behavior) are considered on the basis of two independent experimental data bases:

1. The data base characterizing the dependence of the cladding oxidation behavior in a function of the cladding material chemical composition.
2. The data base characterizing the dependence of the oxidation phenomena in a function of the cladding microstructure.

In our case, the microstructure investigations with samples from different types of the E110 cladding were especially urgent because of the fact that the analysis of results obtained in microchemical investigations presented in the previous paragraph did not allow to develop the unequivocal explanation of the E110 specific behavior.

The program for special TEM examinations was worked out to determine the following comparative data characterizing the microstructure of tested claddings:

- phase conditions and phase compositions;
- the grain size in the cladding matrix;
- the characterization of the secondary phase precipitates including: the chemical composition, size, density, the character of precipitates' distribution.

The following as-received tube samples were used for this research:

- standard E110;
- $E110_{G(fr)}$;
- $E110_{\text{low Hf}}$.

The basic examinations were performed in the RIAR using the transmission electron microscope JEM-2000 FX II at the acceleration voltage 120 kV.

Taking into account that results of numerous investigations performed recently with different claddings showed a strong dependence of the corrosion resistance on parameters of intermetallic precipitates in the alloy, the examinations in detail of precipitates were carried out using thin foils and carbon replicas.

The comparative data characterizing TEM images of different E110 claddings are presented in Fig. 4.17 together with the M5 TEM image reprinted from [27]. The analysis of visual observations obtained after studies of this information has shown that:

- all presented cladding samples have the equiaxed α–Zr grains and globular secondary phase particles (SPP) uniformly distributed in the α–Zr matrix (see also Fig. 4.18);
- the microstructure of all cladding samples is completely recrystallized.

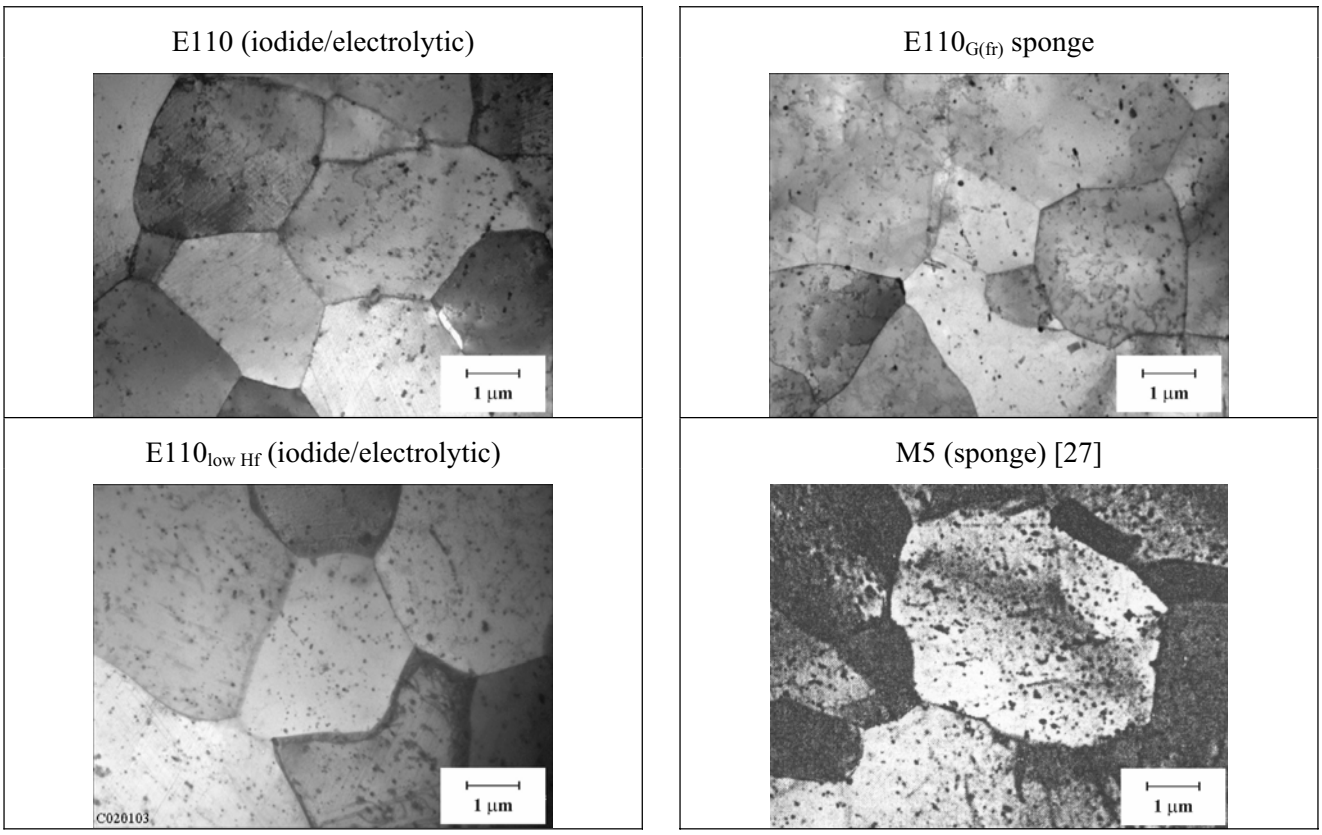

Fig. 4.17. Low magnification of TEM micrographs for E110, $E110_{G(fr)}$, $E110_{low\ Hf}$ claddings and the M5 cladding [reprinted from 27]

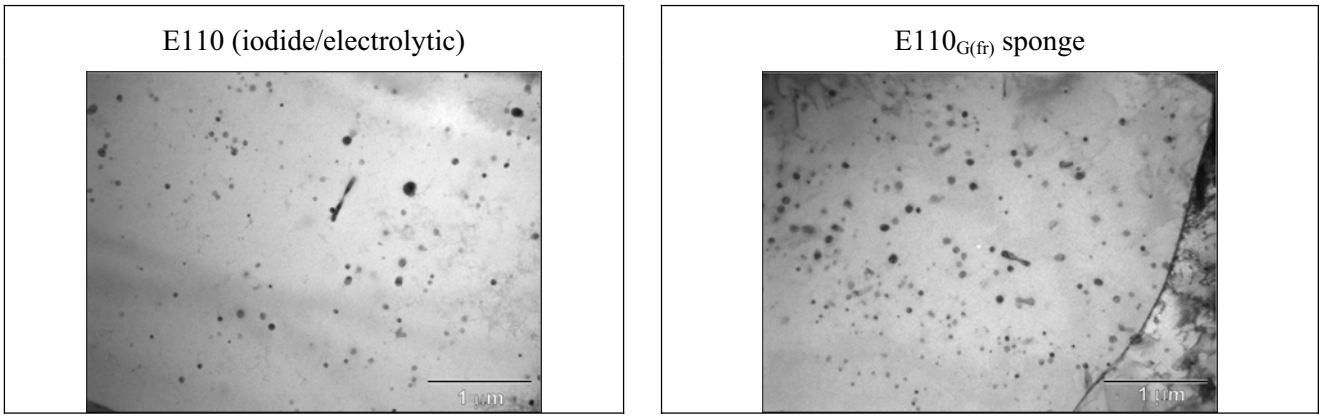

Fig. 4.18. The characterization of the SPP distribution in the α–Zr grains of the E110 and $E110_{G(fr)}$ claddings

The next stage of examinations was devoted to the determination of the α–Zr matrix chemical composition, the grain boundary and SPPs. The energy dispersion X-ray analysis (EDX) was employed for these quantitative measurements. Besides, the SPP sizes and SPP density were measured also.

The measured chemical compositions of the α–Zr matrix and β-Nb precipitates in different E110 claddings are presented in Table 4.8.

Table 4.8. Zr, Nb content in the matrix, grain boundary and β-Nb precipitates

Element	Concentration (wt%)								
	Matrix			Grain boundary			β-Nb		
	E110	$E110_{low\ Hf}$	$E110_{G(fr)}$	E110	$E110_{low\ Hf}$	$E110_{G(fr)}$	E110	$E110_{low\ Hf}$	$E110_{G(fr)}$
Zr	$99.59^{\pm0.97}$	$99.34^{\pm1.03}$	$99.51^{\pm1.17}$	$99.54^{\pm1.11}$	$99.62^{\pm0.92}$	$99.54^{\pm1.14}$	$11.03^{\pm1.17}$	$9.66^{\pm0.48}$	$11.49^{\pm0.65}$
Nb	$0.41^{\pm0.26}$	$0.66^{\pm0.28}$	$0.49^{\pm0.31}$	$0.46^{\pm0.29}$	$0.38^{\pm0.26}$	$0.46^{\pm0.32}$	$88.97^{\pm2.68}$	$90.34^{\pm1.19}$	$88.51^{\pm1.56}$

The analysis of obtained data showed that no significant differences regarding Zr and Nb content in the microstructure components of E110, $E110_{G(fr)}$, $E110_{low\ Hf}$ claddings were revealed. It is known that the best corrosion resistance is observed in the cladding material with fine α–Zr grains and fine β-Nb precipitates distributed uniformly. Therefore, the next task of TEM examinations was focused on measurements of SPP size distributions and on the determination of the average size for α–Zr grains and intermetallic precipitates.

The results of appropriate measurements allowed to reveal the following:

- the α–Zr average grain size in the tested cladding materials was very similar (2.8–3.2 μm);
- the average size of secondary precipitates was similar also (43–48 nm), SPP size distributions in the E110, $E110_{G(fr)}$, $E110_{low\ Hf}$ samples are presented in Fig. 4.19;
- the SPP density was about 1.8×10^{20} m^{-3}.

To improve the representativity of TEM data obtained in the RIAR with the use of a very limited number of samples, the independent TEM investigations were performed in another Russian scientific institute (Institute of Reactor Materials) also. The results of these examinations are in a good agreement with the RIAR data except for the SPP average size in the E110 cladding which was determined as 60 nm. The SPP average size in $E110_{low\ Hf}$ and $E110_{G(fr)}$ claddings were estimated as 55 and 41 nm, respectively.

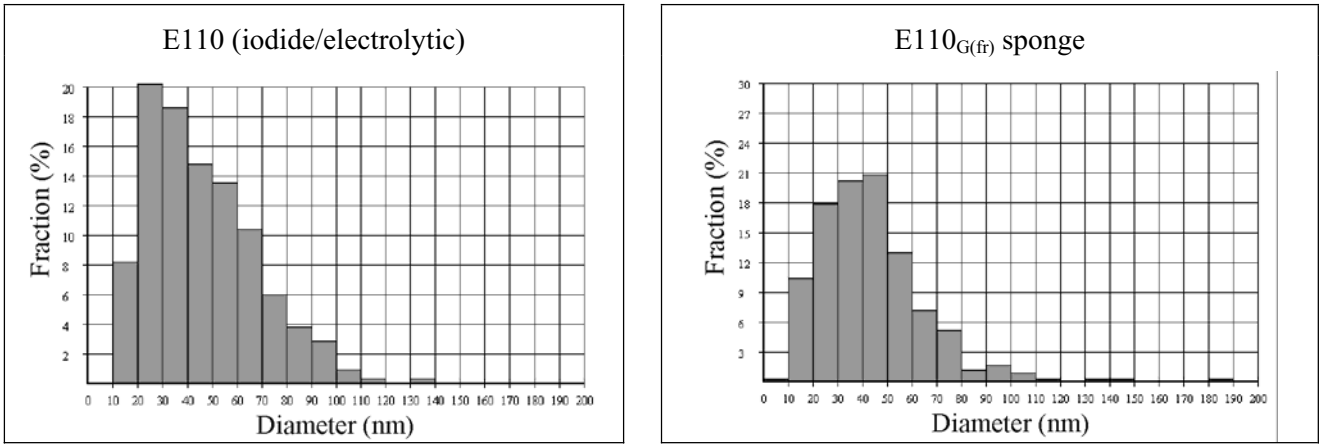

Fig. 4.19. The SPP distribution in the E110 and $E110_{G(fr)}$ claddings

The analysis of TEM micrographs and TEM SPP distributions allowed to reveal the following general differences in the E110 ($E110_{low\ Hf}$) and $E110_{G(fr)}$ cladding microstructures:

- the E110 cladding contained only one type of secondary precipitates, this is a beta-phase particle enriched with niobium (86–91%);

- the $E110_{G(fr)}$ cladding contained (in addition to β-Nb precipitates) the intermetallic phase of the $Zr(Nb,Fe)_2$ type (see Fig. 4.20) with the average size 180 nm.

To compare the obtained TEM results, the organized data base with parameters of iodide/electrolytic and sponge E110 was developed and presented in Table 4.9. Taking into account the limited number of TEM examinations performed in the frame of this work, the E110 data were added with the results of VNIINM investigations [25]. Besides, the published data on the M5 cladding [7] were incorporated in this Table also.

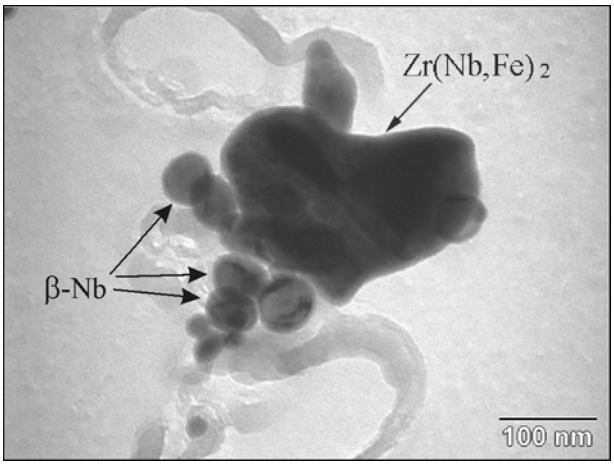

Fig. 4.20. High magnification of the SPP TEM micrograph in the $E110_{G(fr)}$ cladding

Table 4.9. The comparative data characterizing the microstructure of E110, $E110_{G(fr)}$ claddings and the M5 cladding [7]*

List of parameters	Cladding type		
	E110 (iodide/electrolytic)	$E110_{G(fr)}$ (sponge)	M5 (sponge)
1. Intermediate and final annealing temperature (C)	580	580	580
2. The phase state due to the thermal treatment	The fully recrystallized microstructure (αZr+βNb)	The fully recrystallized microstructure (αZr+βNb)	The fully recrystallized microstructure (αZr+βNb)
3. The type of α-Zr grain	Equiaxed	Equiaxed	Equiaxed
4. The average size of α-Zr grain (μm)	• 2.8 (this work) • 4–4.5 [25]	3.2	3–5
5. The characteristics of β-Nb precipitates: • the geometrical form	Globular	Globular	Globular
• the average size (nm)	45–60 (this work) 50 [25]	41–43	45
• the distribution density (cm^{-3})	$1.84 \cdot 10^{14}$	$1.8 \cdot 10^{14}$	$1.5 \cdot 10^{14}$
6. The intermetallic precipitates:			

* The all data characterizing the M5 cladding was taken from [7]

List of parameters	Cladding type		
	E110 (iodide/electrolytic)	$E110_{G(fr)}$ (sponge)	M5 (sponge)
• the type	–**	$Zr(Nb,Fe)_2$	$Zr(Nb,Fe,Cr)_2$
• the size (nm)	–	180	100–200

The analysis of comparative data allows to conclude the following:

- the most of the key parameters characterizing the cladding microstructure are practically the same in the E110 ($E110_{low\ Hf}$), $E110_{G(fr)}$ and M5 claddings;
- the major and the only revealed distinction between the E110 and $E110_{low\ Hf}$ claddings and the $E110_{G(fr)}$ and M5 claddings regards to the absence of iron-based precipitates in the cladding material. Some distinction between the chemical composition of intermetallic SPPs in the $E110_{G(fr)}$ and the M5 alloy ($Zr(Nb,Fe)_2$ and $Zr(Nb,Fe,Cr)_2$, respectively) may be associated with an insufficient scope of appropriate measurements performed in the $E110_{G(fr)}$ samples.

The revealed differences in the presence and absence of iron-based precipitates are in the complete agreement with the results of microchemical investigations presented in the previous paragraph and with the data characterizing the iron solubility limit in zirconium claddings. This limit is about 100 ppm. Taking into account that iron content in the E110 alloy is about 90 ppm, it is fully dissolved in the zirconium matrix. Iron concentration in the sponge types of the E110 cladding is in range 130–430 ppm. Therefore, one part of iron is dissolved in the matrix and the second part is presented as the intermetallic precipitates. As it was mentioned in the previous sections of the report, the most of the appropriate investigations have demonstrated a high importance of intermetallic precipitates in the oxidation behavior of zirconium cladding. Moreover, it was revealed that the iron-based precipitates improve significantly the corrosion resistance and reduce H uptake.

But the analysis of this research data and data obtained in the VNIINM [25] allows to assume that there is an optimal content of iron in the alloy with which the best corrosion behavior is observed. Lower and higher Fe concentrations deteriorate the corrosion resistance.

The following general conclusions may be made on the basis of the whole scope of obtained results:

- the differences in the oxidation behavior of the standard E110 and sponge-based E110 claddings are not a function of the cladding fabrication;
- the differences in microchemical compositions of impurities are probably the major factor for the different oxidation behavior of these types of the E110 claddings;
- more careful measurements of the chemical composition of impurities especially such as C, N, F and other nonmetallic deleterious impurities must be performed in the future to adjust these phenomena;
- additional investigations must be performed also to adjust Hf and Cr influence;
- special experimental investigations with the E110 cladding containing different Fe contents may also be useful for the determination of the optimal Fe concentration.

4.5. The oxidation kinetics of the sponge type E110 cladding

The oxidation tests with the E110 claddings manufactured on the basis of sponge Zr showed that the oxidation kinetics for the standard iodide/electrolytic and sponge E110 cladding was similar, though some tendency towards the increase of oxidation rate was observed for the sponge type E110 cladding in the temperature range 1100–1200 C (see Fig. 4.21). These results are in the good agreement with the published data characterizing the oxidation kinetics of the M5 cladding [18].

** The iron-based intermetallic precipitates was not observed in the E110 cladding

Unexpected results on the oxidation kinetics of the sponge E110 were obtained in the temperature range 900–1000 C. In accordance with experimental results presented in Fig. 4.22, the oxidation rate of the sponge E110 was much less than that of the standard E110. The comparison of the sponge E110 behavior with the M5 behavior demonstrated the same effect for this alloy also.

The processing of data base characterizing the oxidation kinetics of the $E110_{G(fr)}$, $E110_{G(3fr)}$, $E110_{G(3ru)}$ claddings allowed to develop the approximation for the oxidation rate of the sponge type E110 claddings as a function of the reciprocal oxidation temperature. The comparative data on the oxidation rate of two types of the E110 cladding are presented in Fig. 4.23.

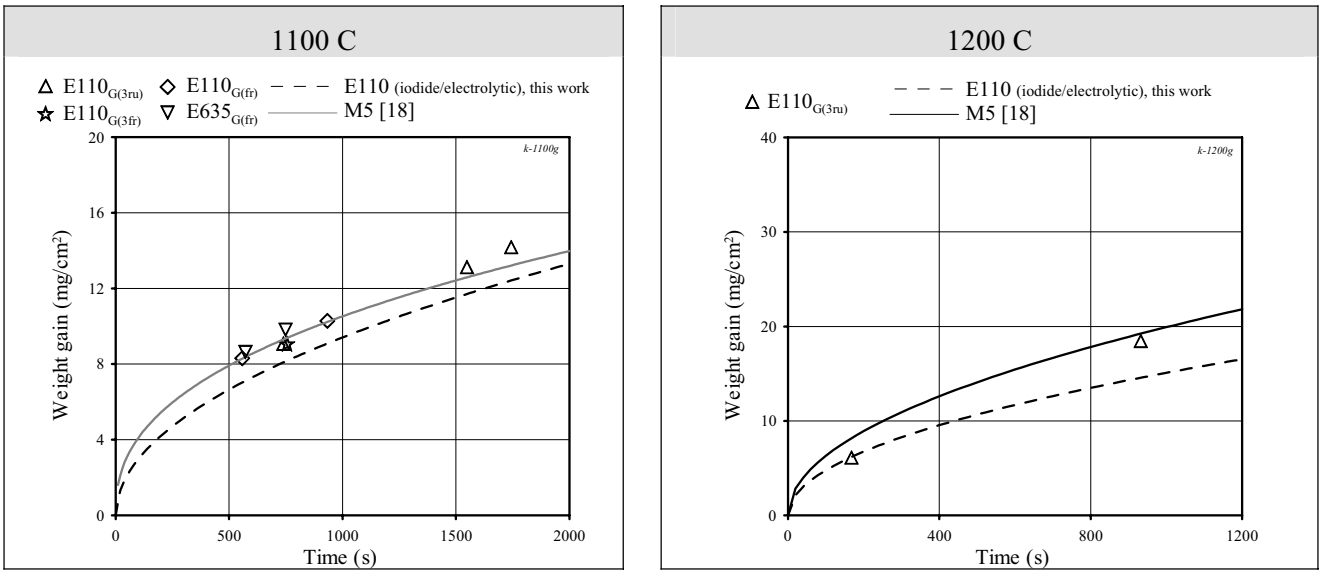

Fig. 4.21. The oxidation kinetics of different types of Zr-1%Nb claddings at 1100 and 1200 C

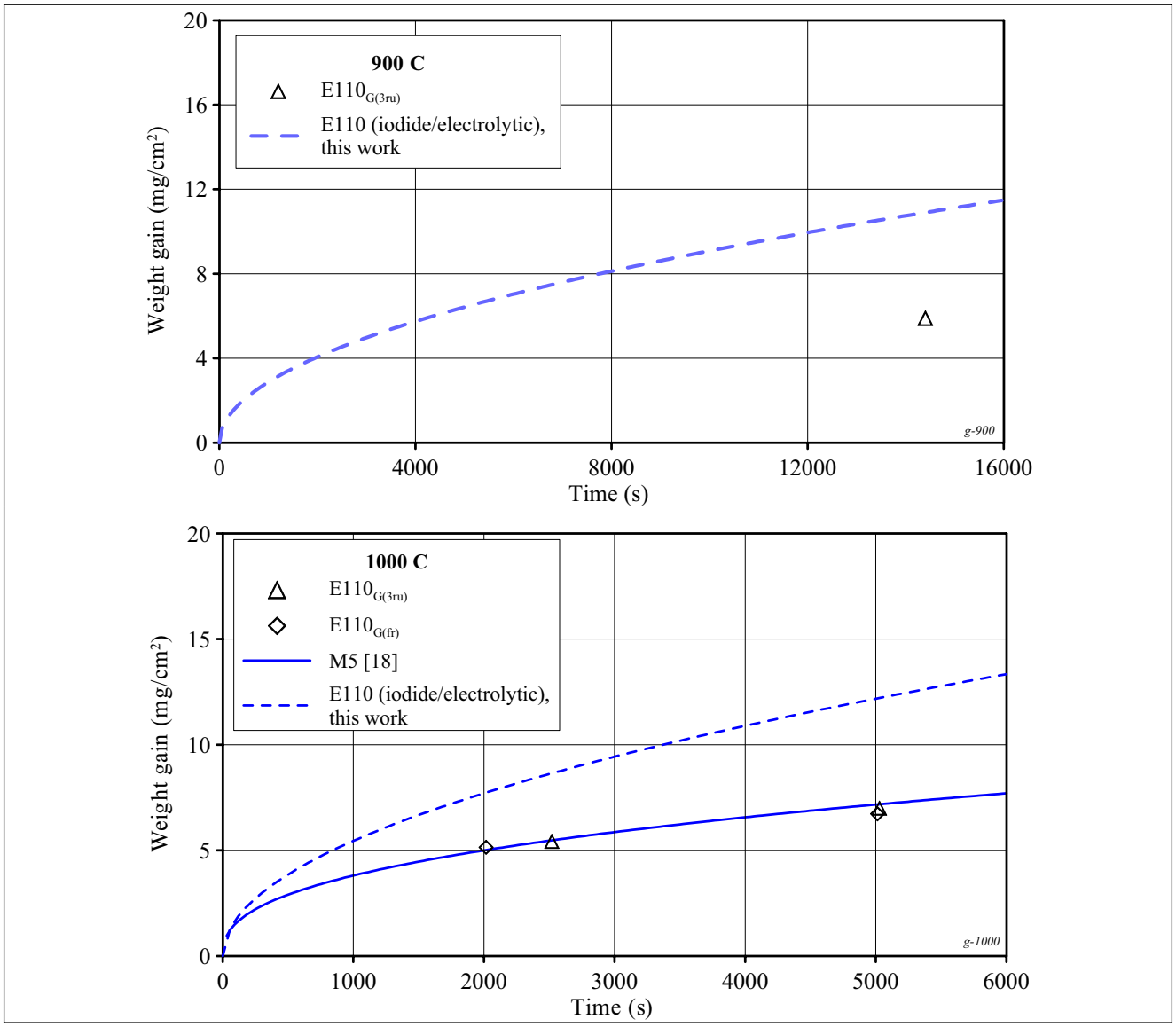

Fig. 4.22. The oxidation kinetics of different types of Zr-1%Nb claddings at 900 and 1000 C

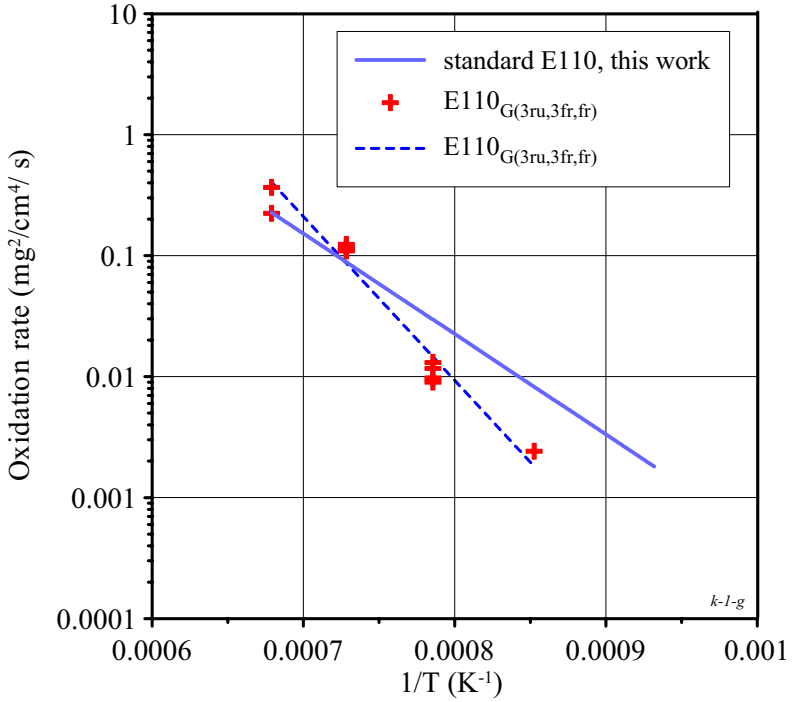

Fig. 4.23. The characterization of the oxidation rate for the standard E110 (iodide/electrolytic) and E110 claddings manufactured with the use of sponge Zr in the temperature range 900–1200 C

This effect was adjusted basing on the analysis of the following microstructural characteristics of the oxidized cladding:

- the comparison of ZrO_2 and α-Zr(O) thicknesses formed in the iodide/electrolytic and sponge E110 during the oxidation at 1000 C (Fig. 4.24);
- the comparison of ZrO_2 and α-Zr(O) thicknesses formed in the sponge type E110 cladding during the oxidation at 1000 and 1100 C (Fig. 4.25).

The procedure of these studies was complicated by the fact that metallographic samples prepared from the standard E110 claddings oxidized at 1000 C are characterized by a partial or complete loss of ZrO_2 layer. The oxide flake off occurred during the oxidation post-oxidation manipulations (including cutting of the oxidized cladding on preparing the metallographic sample). Nevertheless, the consideration of appropriate metallographic samples allowed to select the fragment of the polished sample with the representative thickness of ZrO_2 and the fragment of the etched sample for the estimation of α-Zr(O) thickness (see Fig. 4.24).

The analysis of this data allowed to reveal a general difference in two main competing processes, which define the oxygen uptake by the zirconium cladding: oxygen uptake during the oxidation of a relatively narrow surface layer still to ZrO_2 and the oxygen uptake due to the oxygen transport into the cladding depth with the formation of α-Zr(O) layer. The comparative data presented in Fig. 4.24 show that ZrO_2 is thicker and α-Zr(O) is thinner in the iodide/electrolytic E110 than those in the sponge E110 at approximately the same weight gain. The similar case is observed at the comparison of the sponge E110 oxidized at 1100 C with the sponge E110 oxidized at 1000 C (see Fig. 4.25).

It is obvious that this specific behavior of the sponge type zirconium-niobium binary alloys in the temperature range 900–1000 C is a function of the behavior of minor alloying elements (impurity elements) in this temperature range. The clarification of the physical nature in these processes is the task for future investigations.

Moreover, the extension of experimental data base, which will be obtained due to future investigations will allow to develop the practical approach to the assessment of the safety criteria for this temperature range because two opposite effects must be taken into account:

1. Decrease of the oxidation rate.

2. Increase of the brittle α-Zr(O) layer thickness and, consequently, the reduction of the ductile prior β-layer after comparing as a function of time (taking into account the phenomena associated with p.1).

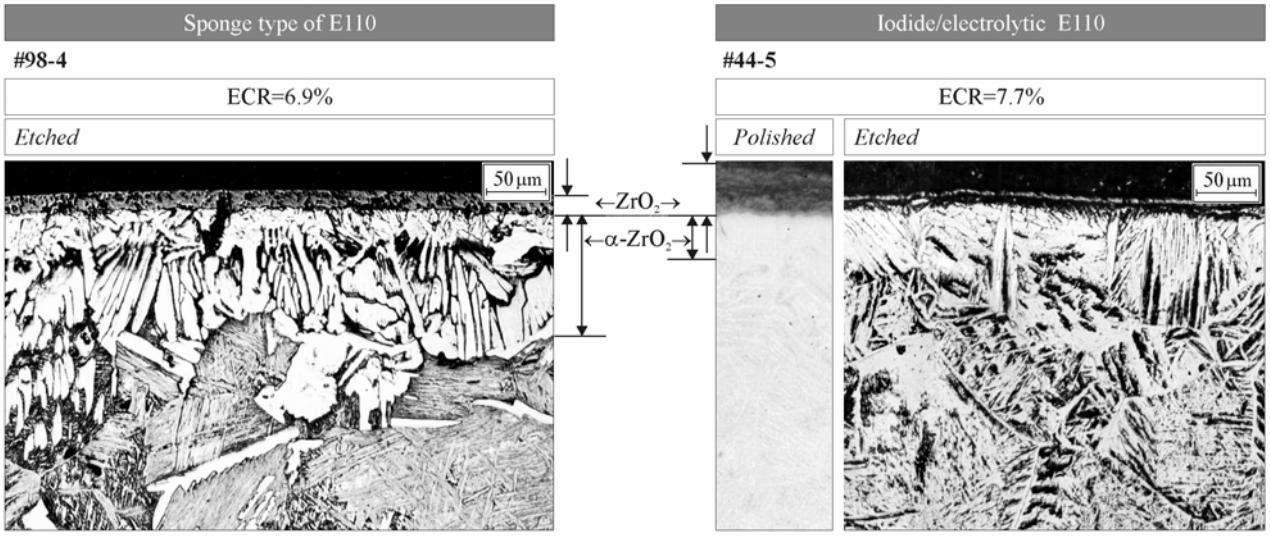

Fig. 4.24. The difference in the thicknesses of ZrO_2 and α-Zr(O) layers in the E110 cladding of sponge and iodide/electrolytic types at the oxidation at 1000 C

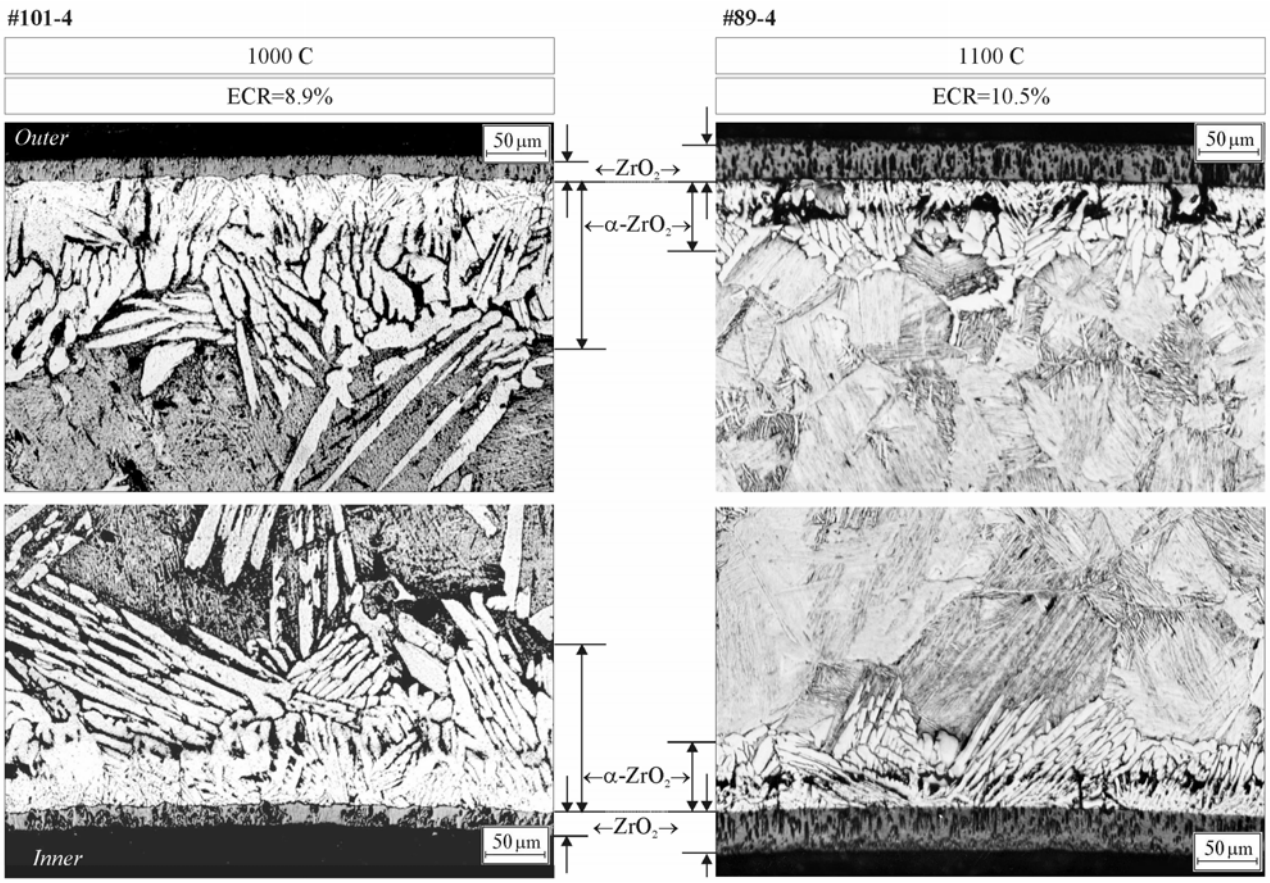

Fig. 4.25. The difference in the formation of oxide and α-Zr(O) layers in the E110 cladding of sponge type at 1000 and 1100 C

The preliminary recommendations concerning this issue will be presented in the Summary of the report.

REFERENCES FOR SECTION 4

[1] Brachet J., Pelchat J., Hamon D., Maury R., Jaques P., Mardon J. "Mechanical Behavior at Room Temperature and Metallurgical Study of Low-Tin Zry-4 and M5™ (Zr-NbO) Alloys after Oxidation at 1100°C and Quenching", *Proc. of IAEA Technical Committee Meeting on "Fuel Behavior under Transient and LOCA Conditions"*, Halden, Norway, September 10-14, 2001.

[2] Mardon J., Frichet A., LeBourhis A. "Behavior of M5™ Alloy under Normal and Accident Conditions", *Proc. of Top Fuel-2001 Meet.*, Stockholm, May 27-30, 2001.

[3] Ageenkova L., Braslavsky G., Kishenevsky V., Nikulina A., Tararaeva E., Shebalov P., Zaimovsky A "Structural and Phase Transformation in Zr-Nb Binary Alloys and their Relation to Properties", *Proc. of Conference on Reactor Physical Metallurgy,* v.6, 29.5–1.6 1978, Alushta, Russia (rus).

[4] Zaimovsky A., Nikulina A., Reshetnikov N. "Zirconium alloys in the Nuclear Industry", Moscow, Energoizdat, 1981 (rus).

[5] Shebaldov P., Peregud M., Nikulina A., Bibilashvili Yu., Lositski A., Kuz'menko N., Belov V., Novoselov A. "E110 Alloy Cladding Tube Properties and their Interrection with Alloy Structure Phase Conditions and Impurity Content", *Proc. of Zirconium in the Nuclear Industry: Twelfth International Symposium,* ASTM STP 1354 (p. 545), 2000.

[6] Reshetnikov F., Bibilashvili Yu., Golovnin I. "The Development, Manufacture and Operation of Fuel Rods of Nuclear Power Reactors", Moscow, Energoatomizdat (rus), 1995.

[7] Mardon J., Charquet D., Senevat J. "Influence of Composition and Fabrication Process on Out-of-Pile and In-Pile Properties of M5 alloy", *Proc. of Zirconium in the Nuclear Industry: Twelfth International Symposium,* ASTM STP 1354 (p. 505), 2000.

[8] Jeong Y., Kim H., Kim T., Jung Y. "Effect of Nb-concentration, Precipitate, and Beta Phase on Corrosion and Oxide Characteristics of Zr-xNb Binary Alloys", *Zirconium in the Nuclear Industry: Thirteenth International Symposium* (poster paper).

[9] Jeong Y., Kim H., Kim T. "Effect of β-phase, Precipitate, and Nb-concentration in Matrix on Corrosion and Oxide Characteristics of Zr-xNb Alloys", *Journal of Nuclear Materials*, v.317, 2003.

[10] Kalin B. "The Investigation of Structure of Zirconium Alloys at the Alloy Modifications with the Use of Power and Radiation Attacks", *Proc. of Nuclear Power on the Threshold of the XXI Century Conference,* 8–10 June 2000, Electrostal, Russia (rus).

[11] Kalin B., Osipov V., Volkov N, Gurovich B., Atalikova I., Menaykin S. "The oxide morphology in the zirconium alloys after its modification by the ion alloying technic", *Proc. of the 5th Conference on the Reactor Physical Metallurgy,* Dimitrovgrad, Russia, 8–12 September 1997.

[12] Chung H.M. "The Effects of Aliovalent Elements on Nodular Oxidation of Zr-based Alloys", *Proc. of the 2003 Nuclear Safety Research Conference*, Washington DC, October 20-22, 2003, NUREG/CP-0185, 2004.

[13] M. Billone, Y. Yan and T. Burtseva. "Post-Quench Ductility of Advance Alloy Cladding", *NSRC Conference,* Washington DC, USA, October 20–22, 2004.

[14] Lunde L., Videm K. "Effect of Material and Environmental Variables on Localized Corrosion of zirconium Alloys", *Proc. of Zirconium in the Nuclear Industry Conference,* ASTM STP 681, 1979.

[15] Wagner C., Naturwissenschaften, 31(1943), 265.

[16] Vrtilkova V., Valach M., Molin L. "Oxiding and Hydrating Properties of Zr-1%Nb Cladding Material in Comparison with Zircaloys", *Proc. of IAEA Technical Committee Meeting on "Influence of Water Chemistry on Fuel Cladding Behavior"*, Rez (Czech Republic), October 4-8, 1993.

[17] Takeda K., Anada H. "Mechanism of Corrosion Rate Degradation Due to Tin", *Proc. of Twelfth International Symposium "Zirconium in the Nuclear Industry",* ASTM STM 1354 (p. 592), 2000.

[18] Mardon J.P., Waeckel N. "Behavior of M5™ Alloy under LOCA Conditions", *Proc. of Top Fuel-2003 meetings "Nuclear Fuel for Today and Tomorrow Experience and Outlook",* March 16-19, 2003, Wurzburg, Germany.

[19] Charquet D. “Microstructure and Properties of Zirconium Alloys in the Absence of Irradiation”, *Proc. of Twelfth International Symposium: Zirconium in the Nuclear Industry,* ASTM STP 1354.

[20] Kakiuch K., Itagaki, Furuya T., Miyazaki A., Ishii Y., Suzuki S., Yamawaki M. “Effect of Iron for Hydrogen Absorption Properties of Zirconium Alloys”, *Proc. of Top Fuel-2003 Meeting “Nuclear Fuel for Today and Tomorrow Experience and Outlook”,* March 16–19, 2003, Wurzburg, Germany.

[21] Murai T., Isobe T., Takizawa Y., Mae Y. “Fundamental Study on the Corrosion Mechanism of Zr-0.2Fe, Zr-0.2Cr, and Zr-0.1Fe-0.1Cr Alloys”, *Proc. of Twelfth International Symposium: Zirconium in the Nuclear Industry,* ASTM STP 1354.

[22] Warr B.D., Perovic V., Lin Y.P., Wallace A.C. “Role of Microchemistry and Microstructure on Variability in Corrosion and Deuterium Uptake of Zr-2.5Nb Pressure Tube Material”, *Proc. of Zirconium in the Nuclear Industry: Thirteenth International Symposium,* ASTM STP 1423.

[23] Ploc R.A. “The Effect of Minor Alloying Elements on Oxidation and Hydrogen Pickup in Zr-2.5Nb”, *Proc. of Zirconium in the Nuclear Industry: Thirteenth International Symposium,* ASTM STP 1423.

[24] Meyer R. “NRC Activities Related to High Burnup New Cladding Types, and Mixed-Oxide Fuel”, *Proc. of an International Topical Meeting on Light-Water-Reactor-Fuel-Performance,* April 10-13, 2000, Park City, Utah, USA, (v.1).

[25] Nikulina A.V., Andreeva-Andrievskaya L.N., Shishov V.N., Pimenov Yu.V. “Influence of Chemical Composition of Nb Containing Zr Alloy Cladding Tubes on Embrittlement under Conditions Simulating Design Basis LOCA”, *Fourteenth International Symposium on Zirconium in the Nuclear Industry,* June 13-17, 2004.

[26] Motta A., Ervin K., Delaire O., Birtcher R. Chu Y., Maser J., Mancini D., Lai B. “Synchrotron Radiation Study of Second-Phase Particles and Alloying Elements in Zirconium Alloys”, *Proc. of Zirconium in the Nuclear Industry: Thirteenth International Symposium,* ASTM STP 1423.

[27] D.Gilbon et.al. "Irradiation Creep and Growth Behavior, and Microstructural Evolution of Advanced Zr-Base Alloys", *Proc. of Zirconium in the Nuclear Industry: Twelfth International Symposium,* ASTM-STP 1354.

5. SUMMARY

During 2001–2004, research was performed to develop test data on the embrittlement of niobium-bearing cladding of the VVER type under LOCA relevant conditions. The program variability is shown in Fig. 5.1.

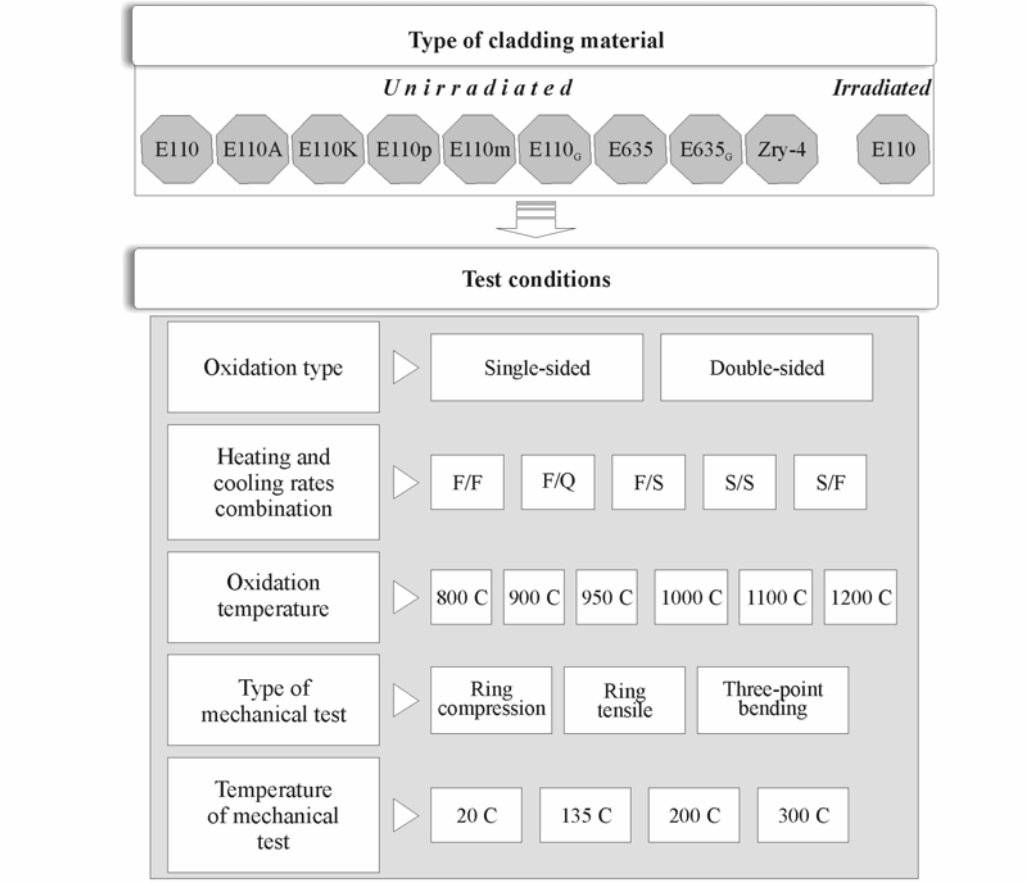

Fig. 5.1. Outline of the research program

The results of previous investigations suggested the following list of tasks for the program first part:

- procedure development and validation to determine the zero ductility threshold;
- determination of the zero ductility threshold sensitivity to transient conditions of the LOCA scenario (variations of heating and cooling rates during the oxidation);
- development of the experimental data base characterizing the oxidation kinetics in the temperature range 800–1200 C and zero ductility threshold of Zr-1%Nb cladding of the VVER type (the E110 alloy);
- comparative analysis of the oxidation and mechanical behavior of Zircaloy-4, E110 (Zr-1%Nb) and other niobium-bearing claddings.

5.1. Major findings of the program first part

5.1.1. Methodological aspects of mechanical tests

Consideration of the safety problem associated with the prevention of a fuel rod fragmentation caused by the embrittlement of a fuel rod cladding during the high temperature oxidation under LOCA conditions has shown that two general approaches could be used to estimate the appropriate phenomena:

1. An approach based on the determination of the oxidized cladding fragmentation threshold.
2. An approach based on the determination of the cladding material embrittlement threshold.

From the formal point of view, the approach based on the determination of the cladding fragmentation threshold is preferable because the loss of resistance to the combination of accident loads is directly estimated in this case. Impact tests and thermal-shock tests are typical examples of this approach practical implementation. However, to use results of these tests for the safety analysis, the representativity of test conditions should be demonstrated in comparison with the combination of loads under real accident conditions. But it is known that real loads on the embrittled cladding during the accident cannot be estimated at present with sufficient accuracy. Besides, the whole previous experience shows that the cladding fragmentation threshold cannot be less than the cladding embrittlement threshold. Moreover, taking into account that embrittlement threshold is the basic material property this threshold depends only weakly on the type of mechanical tests. Therefore, the conservative approach was used to estimate the Zr-1%Nb (E110) embrittlement condition.

Special scoping tests were performed to develop a comparative data base characterizing the E110 zero ductility threshold using the following types of mechanical tests:

- ring tensile;
- ring compression;
- three-point bending.

In accordance with the obtained data, the ring tensile and ring compression tests led to the same zero ductility threshold of the oxidized cladding. Three-point bending tests overestimated this threshold in comparison with ring compression and ring tensile tests.

Taking into account these results and the fact that ring compression tests were used for the validation of the current safety criteria for the zircaloy cladding, this type of mechanical tests was chosen for the research. Some characterization of the oxidized cladding behavior under these test conditions are presented in Fig. 5.2.

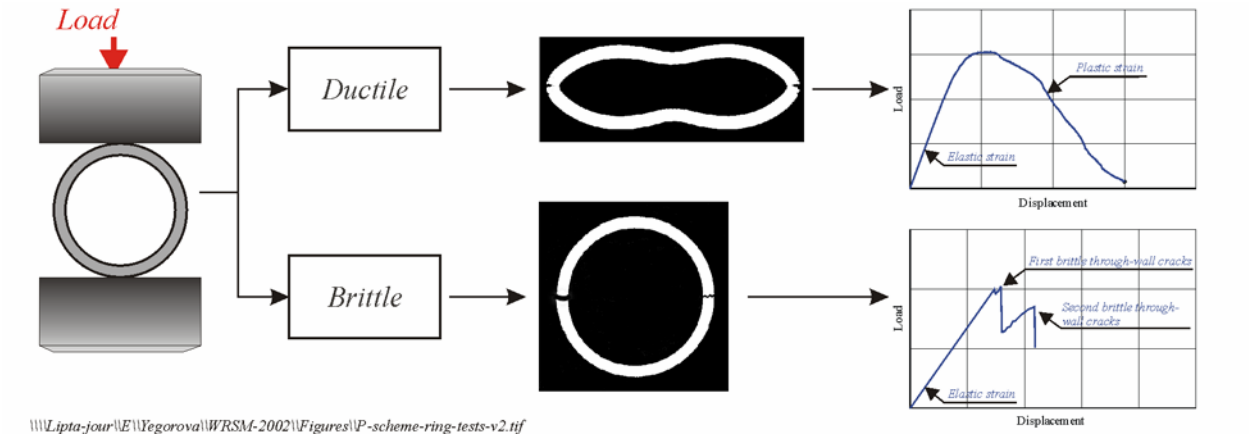

Fig. 5.2. The schematics of ring compression tests

The additional analysis has shown that in spite of the fact that ring compression tests have the thirty year history many issues concerning the procedure of these tests still remain to be solved. Thus, the previous popular approach to the processing of ring compression test results based on the determination of relative displacement at failure (the sum of "elastic" and "plastic" displacement divided by the cladding outer diameter) did not allow to estimate the zero ductility threshold in the explicit form (see Fig. 5.3). Besides, the length of ring samples varied in the range 6–30 mm and the procedure for the fracture determination on the basis of load-displacement diagrams was not validated.

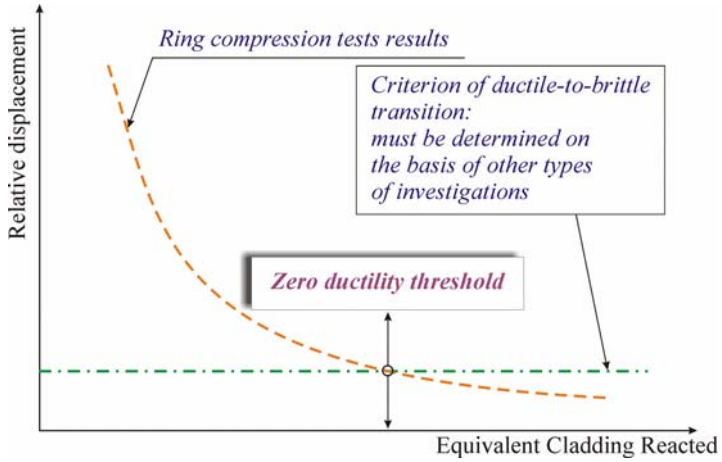

Fig. 5.3. The schematic of previous approach to the determination of zero ductility threshold

Using results of a special experimental subprogram the following outcomes were obtained:

- an approach to the determination of the zero ductility threshold on the basis of processing of load-displacement diagrams has been selected;
- major provisions of this approach are based on the direct connection between the ductility margin and plastic strain value. To estimate the plastic strain, the parameter named the residual ductility at failure has been defined (see Fig. 5.4). When the residual ductility at failure tends to zero the ductile-to-brittle transition (zero ductility threshold) occurs in the oxidized cladding;
- it is obvious that the selected method allows to obtain the macroscopic estimation of the zero ductility threshold only. But the fractography examinations performed with several samples confirm that the macroscopic and microscopic experimental data are in a good agreement;
- to determine the fracture condition (the first through-wall crack) at the processing of load-displacement diagrams, a special reference data base has been developed;
- the ring compression tests performed with rings of different length have shown that the residual ductility at failure does not depend on ring length in the range 8–25 mm for specially prepared ring samples. This special preparation consists in the elimination of the oxidized sample end parts (5 mm approximately) before the ring compression test. In other case the zero ductility threshold may be underestimated significantly.

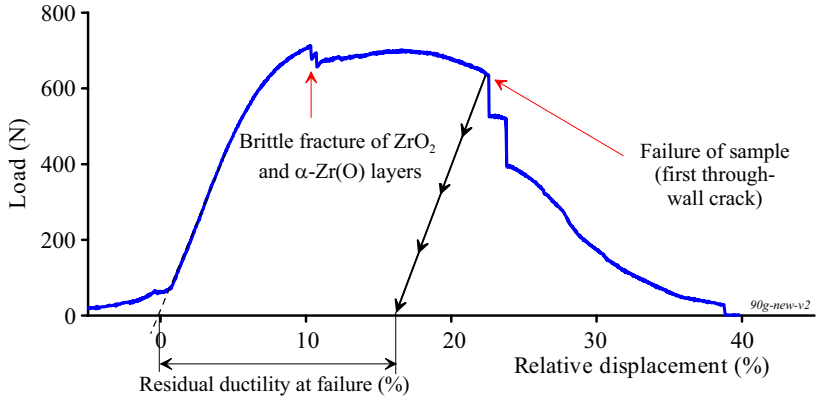

Fig. 5.4. The interpretation of ring compression test results on the basis of the load-displacement diagram

5.1.2. Methodological aspects of oxidation tests

A special scope of analytical and experimental work was performed to validate the following parameters of the oxidation facility:

- the uniformity of the temperature distribution along the long cladding sample (100 mm);
- the representativity of the cladding temperature measurements;
- the absence of steam starvation conditions around the cladding sample.

Taking into account the likely spallation and loss of zirconium dioxide on the oxidation of the E110 cladding a special method for the weight gain measurement was developed, verified and implemented.

To determine the zero ductility threshold sensitivity to such parameters of the oxidation scenario as heating and cooling rates, special scoping tests were performed. The major parameters of these tests are shown in Fig. 5.5.

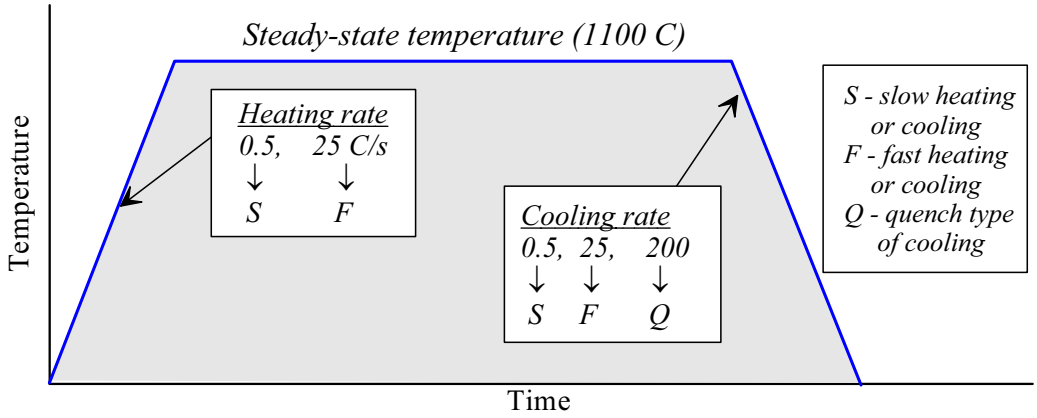

Fig. 5.5. The variability of oxidation tests with different heating and cooling rates

Numerous oxidation tests were performed with five combinations of heating and cooling rates: S(0.5 C/s)/F(25 C/s), S(0.5 C/s)/S(0.5 C/s), F(25 C/s)/S(0.5 C/s), F(25 C/s)/F(25 C/s), F(25 C/s)/ Q(200 C/s) where S means slow, F means fast, and Q means quench. Test results have shown that:

- the specific features of the E110 oxidation behavior are present at any combination of heating and cooling rates;
- the most pronounced negative phenomena accompanying the E110 high temperature oxidation are observed at slow heating rate (0.5 C/s).

Nevertheless, the comparative analysis of zero ductility thresholds obtained for these five combinations of heating and cooling rates allowed to make the following important conclusions:

- the zero ductility threshold has a low sensitivity to the combination of heating and cooling rates;
- the zero ductility threshold of the oxidized cladding at cooling with 25 C/s (F) and 200 C/s (Q) is practically the same.

These test results allowed to perform all subsequent investigations using the F/F (25 C/s/25 C/s) combination of heating and cooling rates.

In the frame of this research program, almost all oxidation tests were performed under double-sided oxidation conditions. But to widen the data base for the comparative analysis, a special subprogram was carried out under single-sided oxidation conditions. The obtained results have shown that the zero ductility threshold of the E110 is increased from about 8% ECR for double-sided oxidation to about 11% for single-sided oxidation.

The general verification of experimental procedures developed for this program was the final stage of methodological work. The verification was performed in reference tests with Zry-4 cladding. After that, the obtained results were compared with the numerous published data on this alloy. Results of this comparison

have shown that the set of experimental procedures developed to determine the zero ductility threshold of Zr-1%Nb (E110) cladding do not introduce large systematic errors.

5.1.3. The embrittlement behavior of Zr-1%Nb (E110) cladding

This stage of the research program was performed with the use of commercial as-received E110 cladding tubes. The double-sided oxidation tests were carried out with these tubes in the temperature range 800–1200 C at F/F (25 C/s/25 C/s) and F/Q (25 C/s/200 C/s) combinations of heating and cooling rates. The embrittlement characteristics of oxidized claddings were determined using the ring compression tests at 20 C. For reference, mechanical tests were also performed at 135, 200, 300 C. This data base was supplemented with results of reference tests with the Zry-4 cladding, which was oxidized at 1100 C and tested at 20 and 135 C.

The visual observations of oxidized E110 claddings have shown that this material is characterized by the initiation of the breakaway oxidation and earlier embrittlement in comparison with the Zry-4 cladding. So, some experimental data obtained at 1100 C and presented in Fig. 5.6 allow to make the following general conclusions (all ECR values are as measured):

- the uniform oxidation mode characterizes the E110 oxidation at low ECR (0–6.5% in this case). This oxidation mode leads to the formation of a black protective oxide on the cladding surface;
- the breakaway oxidation mode occurs with the increase of the ECR up to 10.5% (in presented case). This oxidation mode is accompanied by oxide spallation;
- the reference Zry-4 cladding surface oxidized at 11.3% ECR is covered with the black lustrous oxide. This fact confirms that the breakaway oxidation condition was not achieved in the Zry-4 cladding material.

Cladding material	As-measured ECR (%)	Appearance of 100 mm oxidized samples
E110	6.5	
	10.5	
Zry-4	11.3	

Fig. 5.6. The appearance of the E110 and Zry-4 claddings (1100 C) as a function of the ECR

The reassessment of previous investigations allow to establish that the cladding embrittlement after the breakaway oxidation is a sum of two processes:

1. The oxygen induced embrittlement caused by the formation of ZrO_2 and α-Zr(O) brittle layers, the decrease of the prior β-phase thickness and the increase of oxygen concentration in the prior β-phase.
2. The hydrogen induced embrittlement caused by the hydrogen absorption in the prior β-phase and hydriding of the cladding material.

Taking into account these considerations, the data base characterizing the residual ductility of the oxidized E110 cladding as a function of the ECR was supplemented with the numerous measurements of hydrogen concentration in the oxidized claddings (see Fig. 5.7).

The major outcomes of results obtained at 1100 C are the following:

- the E110 oxidized cladding has a very high ductility margin and low hydrogen content in the cladding material at the ECR up to 7.0%;

- a sharp decrease of the E110 ductility occurs in the range of 7–8% ECR. This process corresponds to a sharp increase of hydrogen content in the prior β-phase of the E110 oxidized cladding;
- the E110 zero ductility threshold is achieved at 8.3% ECR (as-measured) with 300–400 ppm of hydrogen content;
- the Zry-4 reference cladding has demonstrated sufficient margin of residual ductility and very low hydrogen content at 11.3% ECR.

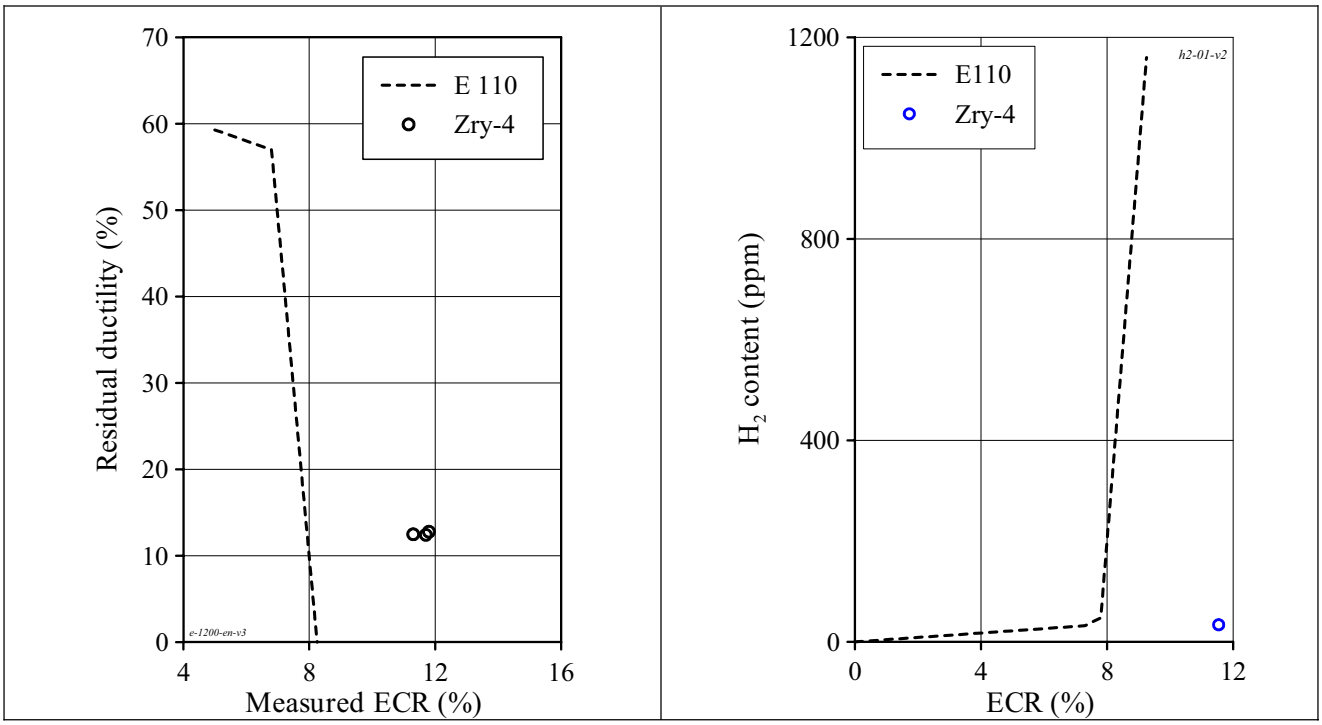

Fig. 5.7. The E110 residual ductility and hydrogen concentration as a function of the ECR after the double-sided oxidation at 1100 C and F/F, F/Q combinations of heating and cooling rates

To understand and to interpret the obtained results, special post-test examinations of metallographic samples were performed on the basis of the optical microscopy, SEM investigations, Auger spectroscopy, fractography, and microhardness measurements. The analysis of these results with the support of data obtained during previous investigations allowed to make the following important observations and comments:

- the cracking and spallation of the ZrO_2 layer observed on the E110 cladding at the ECR higher than 7% provide hydrogen penetration into the oxide metal interface;
- the cracking and spallation of the ZrO_2 layer is the result of transition from the understoichiometric protective tetragonal oxide to the stoichiometric porous monoclinic oxide;
- this tetragonal-monoclinic phase transition is a function of temperature and volume stresses;
- the stabilization of the protective tetragonal oxide prevents the hydrogen penetration into the cladding material;
- most impurities in ZrO_2 that oxidize slower than Zr will stabilize the tetragonal oxide. It appears that a minor concentration of such elements as Sn, Fe, Cr in the zirconium dioxide allows to achieve this effect. This observation is in a good agreement with the Zry-4 alloying composition and oxidation behavior;
- but the presence of some other precipitates leads to the formation of heterogeneous ZrO_2 characterized by high volume stresses and the tendency towards early tetragonal-monoclinic transformation. It is obvious that ZrO_2 on the E110 cladding surface contains this type of precipitates.

The analysis of the wavelength dispersive x-ray (WDX) dot maps and electron probe microanalyzer (EPMA) results obtained in the frame of this work has shown that the redistribution of niobium in the α-Zr(O) layer is observed in the Zr-1%Nb oxidized cladding. This process is characterized by the formation of radially oriented Nb-enriched and Nb-depleted areas. This phenomenon may facilitate the development of the heterogeneous oxide ($ZrO_2(Nb_2O_5)$) with the tendency towards spallation. Besides, taking into account that niobium stabilizes the β-Zr phase, the transformation of niobium enriched areas into the α-Zr(O) phase occurs at a higher oxygen concentration than in the areas with the lower niobium concentration. This effect is responsible for the irregular boundary front between α-Zr(O) and prior β-phase in these alloys.

In spite of the fact that the E110 oxidation rate is somewhat less than that in the Zry-4, the E110 α-Zr(O) thickness is larger due to the difference in the allotropic transition temperature of the α-Zr(O) phase in the E110 alloy produced at the higher oxygen concentration in the β-phase. This fact and the irregular α-Zr(O)/β-phase boundary lead to the reduction in the effective prior β-phase thickness and to the increase of oxygen concentration in the prior β-phase. The tendency towards the uniform oxygen distribution across the prior β-phase does not improve the ductility margin also. But the analysis of the microhardness measurements has shown that the revealed differences in the embrittlement behavior of the E110 and Zry-4 claddings cannot be explained by the differences in the oxygen concentration in the β-phase because the E110 cladding with the high ductility margin and E110 cladding on the zero ductility threshold are characterized by similar microhardness values. This result confirms that the hydrogen absorption by the E110 cladding is the key factor determining the E110 embrittlement behavior. The hydrogen diffuses in the prior β-phase along radially oriented α-Zr(O) grains, the Nb-enriched β-phase lines in the α-Zr(O) are the channels for the hydrogen penetration also. Taking into account that the hydrogen solubility in the zirconium matrix is very sensitive to the temperature and, besides, the ductility of solid hydrides is strongly dependent on temperature, the mechanical behavior of the E110 oxidized cladding was compared at 20 C and 135 C (the coolant saturation temperature at the end of the LOCA reflood mode). The obtained results have shown that:

- in the case when the whole absorbed hydrogen inside the zirconium matrix is in solid solution at 20 C (<100 ppm), the E110 has very high ductility at 20 C. Therefore the increase of ductility margin does not occur in the range 20–135 C;
- the critical value of hydrogen content associated with the E110 zero ductility threshold is increased from 400 ppm at 20 C up to 900 ppm at 135 C. This effect is most likely associated with the increase of hydride ductility;
- the embrittled sample with hydrogen content higher than 1000 ppm is insensitive to the temperature in this range.

Several ring compression and ring tensile tests performed at the temperature 200–300 C have shown that the cladding ductility is sharply increased in the temperature range 20–200 C with any hydrogen content (1500 ppm is the maximum value). The temperature increase up to 300 C does not change the ductility margin in general.

Therefore, the results of these investigations allowed to conclude that:

- the Zry-4 embrittlement is caused by the oxygen absorption in the prior β-phase and by the reduction in prior β-phase thickness;
- the E110 embrittlement is a function of two processes: oxygen embrittlement and hydrogen embrittlement accompanied by the reduction in the prior β-phase thickness.

To estimate the representativity of obtained results for other oxidation temperatures, the additional oxidation tests were performed in the range 800–1200 C. This stage of investigations has shown that:

- the most pronounced effects of the breakaway oxidation were observed at the temperatures 950–1000 C (see Fig. 5.8). The zero ductility threshold in this temperature range is a little lower than that at 1100 C (7.5% ECR at 1000 C);
- in spite of the presence of breakaway effects at the temperature 800 C, the zero ductility threshold is increased at that temperature to more than 12% ECR. This conclusion is confirmed by the low hydrogen content in the oxidized cladding. The critical hydrogen concentration (about 400 ppm) is achieved at

about 12% ECR. A detailed analysis of appropriate physical processes is a task for the future research but preliminary it should be noted that this improved behavior of the E110 cladding can be associated with the two phase compositions of the zirconium matrix (α and β-phases, in this case, the concentration of β-phase is relatively low at this temperature), a very low thickness of α-Zr(O) at this temperature, and some other phenomena considered in the report;

- as for the temperature 1200 C, the zero ductility threshold of the E110 cladding is most likely not better than that at 1100 C in spite of the tendency towards the decrease of hydrogen absorption rate.

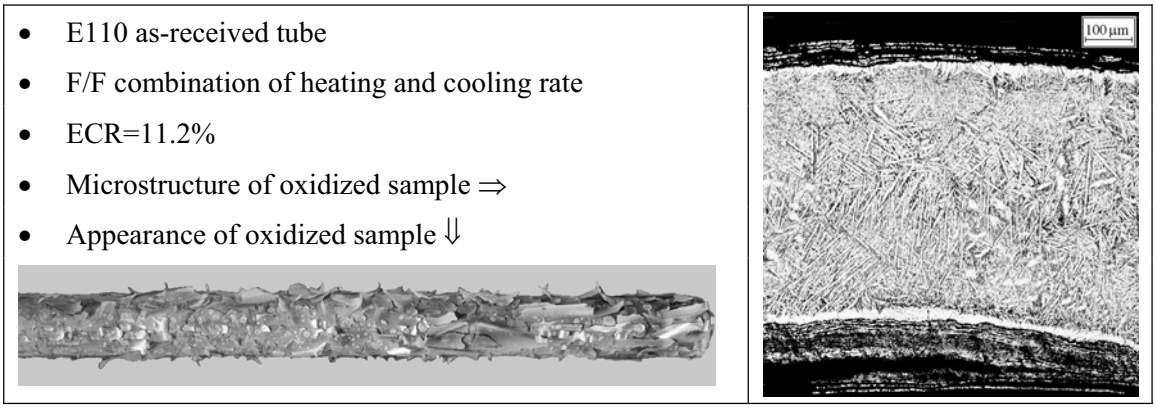

Fig. 5.8. Demonstration of the E110 breakaway oxidation effects at 950 C

To determine the sensitivity of the embrittlement behavior of niobium-bearing claddings to such alloying components as Sn and Fe, special investigations were performed with the E635 cladding (Zr-1%Nb-1.2%Sn-0.35%Fe). The analysis of obtained results showed that the visual appearance of E635 oxidized claddings was better than that of E110 claddings but in spite of this fact, the zero ductility threshold for these cladding materials was practically the same.

The last line of experimental investigations performed with the as-received E110 cladding tube was connected with the determination of the sensitivity of oxidation and mechanical behavior to the initial oxygen concentration in niobium-bearing alloys. The motivation to perform these studied was associated with the absence of a precise position on this issue in the current scientific publications and with the fact that the initial oxygen concentration in the tested E110 cladding was very low (~0.05%) in comparison with other alloys (including other niobium-bearing alloys). To develop the comparative data base, E110K as-received cladding tubes were tested. The initial oxygen concentration in this modification of the E110 alloy was about 0.11% by weight. The obtained test results allowed to establish that:

- the increase of oxygen concentration in the E110 alloy does not lead to suppression of the breakaway oxidation effect;
- the zero ductility threshold of the E110K cladding is not higher than that of the standard E110 cladding.

5.1.4. The embrittlement behavior of Zr-1%Nb (E110) cladding as a function of irradiation effects

Taking into account that the validation of high burnup fuel behavior under LOCA conditions is one of the urgent research problems, the preliminary stage of this type of investigations was performed in the frame of this work.

The irradiated E110 claddings refabricated from VVER high burnup fuel rods with burnup of about 50 MW d/kg U had the following characteristics before the oxidation tests:

- ZrO_2 thickness on the outer cladding surface was 5 μm;
- ZrO_2 thickness on the inner cladding surface was 0 μm;
- hydrogen content in the cladding material was 47 ppm.

The analysis of the appearance and metallographic examinations of the irradiated cladding oxidized in the temperature range 1000–1200 C at the F/F combination of heating and cooling rates allowed to reveal the following (see Fig. 5.9):

- the outer surface of oxidized irradiated claddings are covered with the black uniform oxide without the spallation effects up to 16% ECR based on the results of visual examinations;
- as for the inner surface, the tendency towards oxide spallation was noted at the 7.7% ECR and higher.

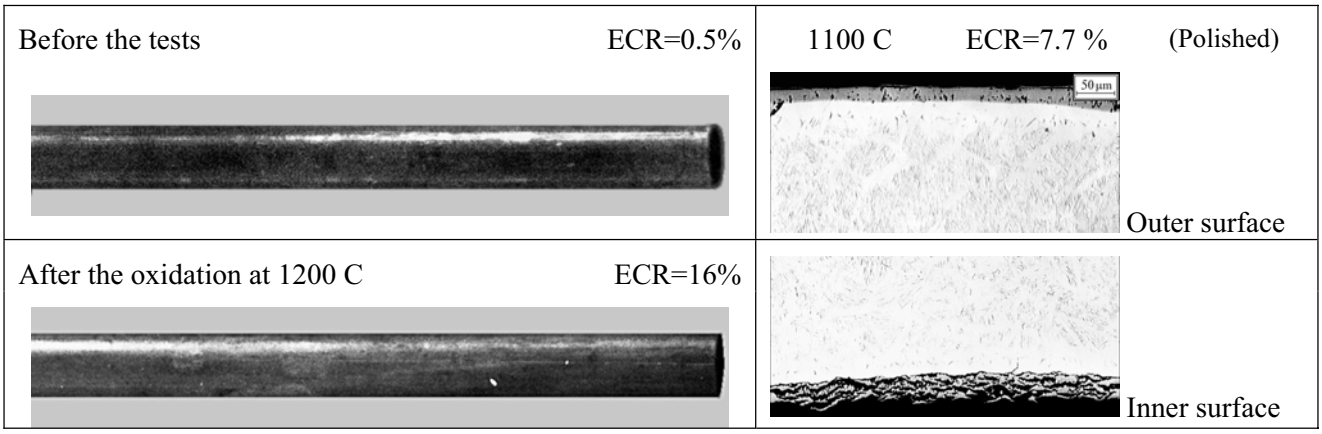

Fig. 5.9. The appearance and microstructure of the E110 irradiated claddings as a function of the ECR

The obtained data are in a good agreement with other Russian investigations performed in the MIR research reactor under LOCA conditions. The following general observations may be made on the basis of the whole scope of experimental data:

- the irradiation inhibits the breakaway oxidation tendency on the outer surface of the E110 cladding;
- the tendency towards oxide spallation is supplemented with the tendency towards an increase in oxidation rate (the oxide thickness increase) on the cladding inner surface. In accordance with these data, it may be assumed that the contamination of the cladding inner surface by fission products is responsible for these effects.

The consideration of the data base characterizing the residual ductility microhardness and hydrogen content in the oxidized irradiated cladding as a function of the ECR has shown that:

- in accordance with the postulated relationship between the oxygen concentration in the prior β-phase, microhardness, and the oxygen induced zero ductility threshold, this threshold corresponds to 8.3% ECR;
- the combination of the oxygen induced and hydrogen induced embrittlement of the E110 irradiated cladding leads to the reduction of the zero ductility threshold down to 6.5% ECR at the F/F combination of heating and cooling rates.

5.1.5. The oxidation kinetics and embrittlement behavior of the E110 cladding according to results of previous investigations in different laboratories

Earlier oxidation and ring compression tests with the E110 unirradiated cladding were performed in the following institutes:

- VNIINM, Russia [1];
- KFKI, Hungary [2, 3];
- NFI, Czech republic [4, 5];
- NC in Rossendorf, Germany [6, 7].

It should be noted that the comparative analysis of VNIINM test results was performed on the basis of data obtained at the end of 1980s of the past century. The recent VNIINM tests were not used because open VNIINM publications devoted to these issues did not contain the information in detail concerning test modes and test parameters.

The comparison of the E110 oxidation kinetics estimated according to the results of this work with oxidation kinetics obtained earlier has shown that the discrepancy between the RRC KI/RIAR, VNIINM, NFI, NC in Rossendorf results is low in the studied range of weight gains and temperatures (see Fig. 5.10). The KFKI data overestimates noticeably the E110 oxidation kinetics.

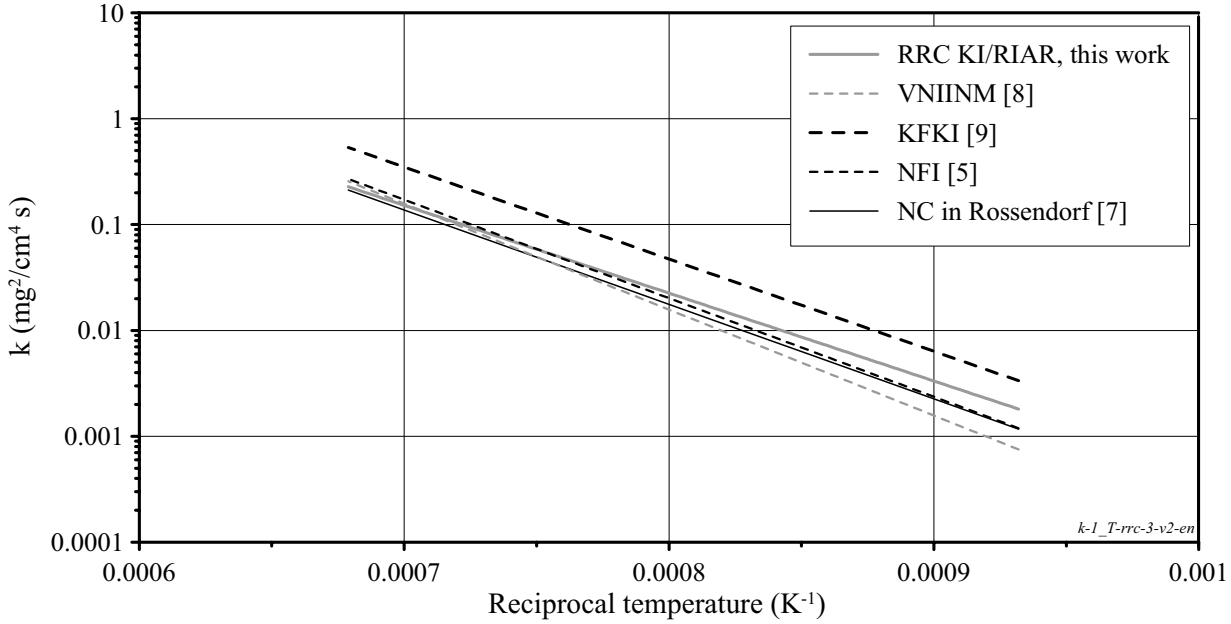

Fig. 5.10 The comparison of the E110 oxidation kinetics (1073–1473 K) in accordance with the data of different investigations

The comparison of the E110 and Zry-4 oxidation kinetics presented in Fig. 5.11 for the as-measured data and for the as-calculated data (with the use of Zry-4 conservative kinetics based on the Baker–Just correlation and E110 conservative kinetics developed in the VNIINM) allows to note the following:

- practically the same conservative kinetics is used for the safety analysis of the E110 and Zry-4 claddings;
- the as-measured E110 oxidation kinetics is noticeably less than that for the Zry-4 cladding.

The difference in the postulated safety criteria characterizes the E110 and Zry-4 fragmentation thresholds (18% and 17% respectively) and the difference in the E110 and Zry-4 oxidation kinetics leads to the following estimations of the as-measured oxidation corresponding to safety criteria at 1100 C:

- 11.5% ECR for E110;
- 13.5% ECR for Zry-4.

The preliminary data characterizing the oxidation kinetics of the E110 irradiated cladding showed that the oxidation rate of irradiated claddings was somewhat higher than that of unirradiated claddings at all oxidation temperatures (1000–1200 C). But taking into account the limited number of these tests, the investigations in this line should be continued in the future.

The analysis of comparative data characterizing the embrittlement behavior of the E110 unirradiated claddings allowed to note that all investigators revealed the tendency towards the breakaway oxidation of the E110 cladding accompanied by the hydrogen absorption and a sharp reduction in the residual ductility margin after the initiation of oxide spallation.

The consideration of the whole scope of the E110 test data obtained in the first part of this research led to the decision concerning the development of the program second stage to be devoted to the analysis of reasons for the E110 specific behavior in comparison with other niobium-bearing alloys.

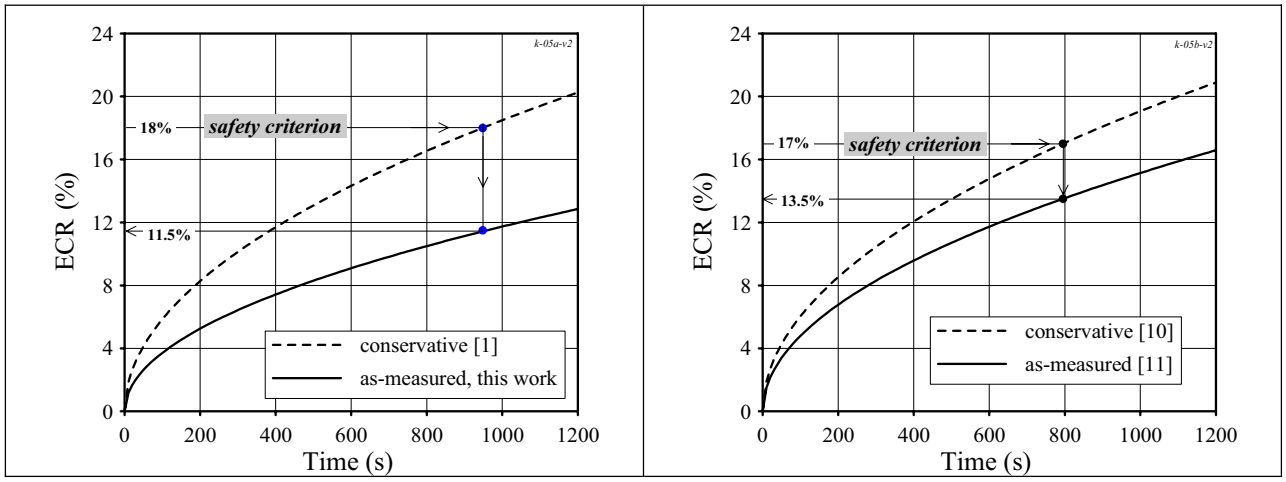

Fig. 5.11. The comparison of the E110 (on left) and Zry-4 (on right) conservative and as-measured kinetics at 1100 C

5.2. Major findings of the program second part

5.2.1. The concept of special investigations

The following general questions were formulated on the basis of the revealed general difference in the oxidation and embrittlement behavior of Zr-1%Nb (E110) and Zry-4 claddings:

> Is the earlier breakaway initiation and the embrittlement caused by combined effects of oxygen and hydrogen uptake typical of the whole family of niobium-bearing alloys or does this phenomenon characterize the E110 alloy only?

The beginning of investigations to provide the answer to this question was devoted to the comparison of Zr-1%Nb (E110) embrittlement behavior with the behavior of other Zr-1%Nb claddings manufactured from the M5 alloy [12]. Published data with experimental results on the M5 cladding available by that time were used for this goal [13, 14]. The analysis of these M5 test results has shown that:

- the zero ductility threshold of the M5 cladding is higher than that of the E110 cladding;
- the breakaway oxidation is not observed in the investigated range of parameters;
- the M5 embrittlement is not accompanied by hydrogen uptake.

The analysis of possible reasons for the revealed difference between E110 and Zry-4 or M5 cladding behavior allowed to select the following phenomena for special studies:

- surface effects;
- bulk effects associated with the chemical composition of impurities in the cladding material;
- bulk effects associated with the cladding microstructure.

This part of the research program was closely coordinated with another experimental program being conducted at ANL at approximately the same time [15, 16]. The oxidation and mechanical tests were performed with M5, Zirlo, E110, and Zry-4 claddings in that program. The results of both programs allowed an extension of the comparative data base for observations and conclusions.

5.2.2. Surface effect studies

These studies were based on the following considerations:

- the corrosion resistance is a function of the cladding surface finish because the corrosion behavior depends on the surface chemistry (contaminations) and surface roughness;
- the sensitivity of the E110 cladding material to these phenomena should be estimated.

The urgency of this issue was determined by the fact that as-received E110 tubes used in the first part of the program were not subjected to surface finishing. The current E110 surface finishing procedure consisted of the final etching and anodizing of the cladding outer surface. To determine the sensitivity of the cladding embrittlement behavior to this procedure, the oxidation and mechanical tests with the etched and anodized E110A cladding were performed. The results of tests have shown that this surface finishing procedure does not allow to eliminate the earlier breakaway oxidation and to improve the embrittlement behavior of the E110 cladding.

Besides, one of the advanced methods for the surface finishing with the use of the outer surface grinding and inner surface jet etching was investigated also. But the conclusion was the same. Moreover, the tendency towards an increase in oxide thickness was revealed on the cladding inner etched surface. These results were in a good agreement with the ANL test data obtained with the E110 as-received tubes subjected to the special etching. The ANL tests showed that any etching led to the degradation of the cladding embrittlement behavior.

To eliminate the chemical contamination of the cladding surface caused by etching, special polished E110 samples were used for the next stage of the surface effect studies. The results of tests with this type of the cladding samples allowed to reveal the following (see Fig. 5.12):

- the visual indicators of the breakaway oxidation practically disappeared from polished parts of oxidized samples. The most pronounced effect was noted at 1000 C;
- the polished and unpolished parts of the oxidized cladding were characterized with quite a different hydrogen uptake;
- the residual ductility increased very significantly on the polished part of the oxidized cladding.

The same results have been obtained in similar investigations performed at ANL [15, 16].

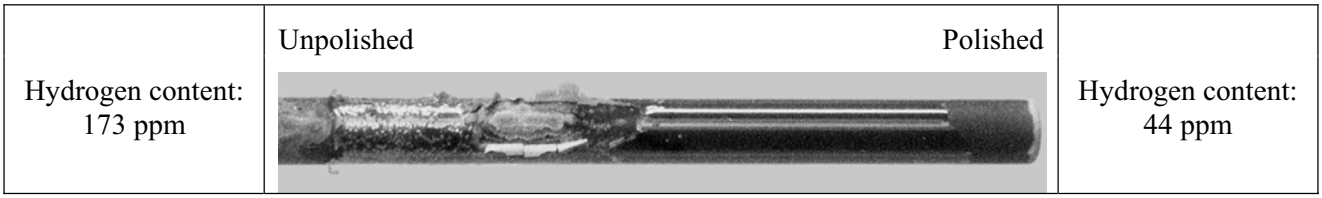

Fig. 5.12. The appearance of the E110 polished and unpolished parts after the oxidation at 1000 C

Thus, the surface polishing allows to improve the oxidation and embrittlement behavior of the niobium-bearing cladding of the E110 type.

5.2.3. Bulk chemistry studies

Several investigations performed during last years have demonstrated that the oxidation behavior of niobium-bearing alloys is very sensitive not only to alloying components but also to the impurity composition. The analysis of the E110 problems in this context has shown that different methods are used to produce zirconium alloys for PWR and VVER claddings. In accordance with these methods, the sponge Zr is used to produce such alloys as Zry-4, M5, Zirlo and the mixture of iodide and electrolytic Zr is used for the fabrication of the E110 alloy.

It is obvious that the difference in the alloy production leads to the difference in the impurity compositions. This fact was accepted for the basis while developing a special subprogram devoted to the oxidation and ring compression tests with modified types of the E110 claddings ($E110_G$).

These modified types of the E110 claddings are the pilot samples produced by the Russian industry in accordance with the program of the sponge Zr introduction in the production of VVER claddings. The oxidation tests performed at 1100 C with different variants of the E110 sponge type claddings have demonstrated prac-

tically the same result. Macroscopic effects of the breakaway oxidation mode disappeared in the as-measured ECR range 10.5–18% (see Fig. 5.13).

Iodide/ electrolytic E110	ECR=16%	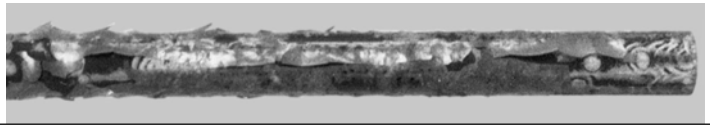
Sponge E110	ECR=18%	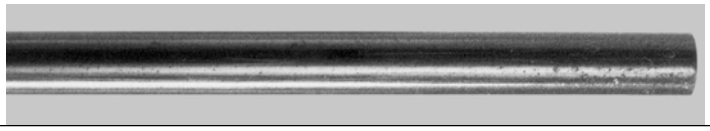

Fig. 5.13. The comparison of the iodide/electrolytic and sponge E110 cladding oxidation behavior at 1100 C

For oxidation at 1100 C, ring compression tests with oxidized claddings confirmed that the zero ductility threshold of the sponge E110 increased up to 19% ECR (as-measured) due to the low hydrogen uptake. The preliminary comparison of the embrittlement behavior of the sponge E110 and other alloys oxidized at 1100 C with the ANL published data on Zry-4, Zirlo, M5 test results [16] showed approximately the same zero ductility threshold.

Nevertheless, some difference was revealed in the hydrogen uptake for these claddings at 1100 C. Thus, Zry-4, Zirlo and M5 were characterized by the hydrogen content of 17–22 ppm at 19.1–21.1% ECR [16]. The E110 cladding kept the same hydrogen content (17 ppm) up to 16.7% ECR. But at 18% ECR, the hydrogen content increased up to 102 ppm. To determine the sensitivity of the sponge E110 to the oxidation temperature, special investigations were performed in the range 900–1200 C. These tests allowed to reveal several new phenomena.

For oxidation at 900 – 1000 C, major new phenomena were revealed and are associated with a sharp reduction of the sponge E110 oxidation rate in comparison with that of the iodide/electrolytic E110 (see Fig. 5.14), although at 1100 - 1200 C the oxidation kinetics of the sponge E110 and iodide/electrolytic E110 were similar with some tendency towards an increase of the oxidation rate in the sponge E110 claddings. The comparison of the sponge E110 with the other sponge type of Zr-1%Nb cladding (M5 alloy) performed with the use of French data [17] showed that oxidation kinetics of these alloys were the same at both temperatures.

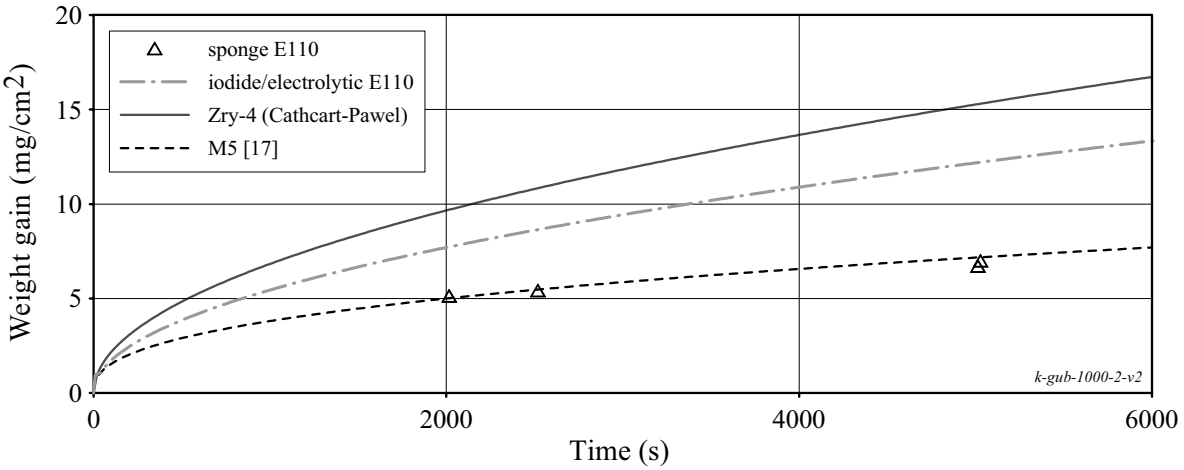

Fig. 5.14. The comparison of the Zry-4, sponge E110, iodide/electrolytic E110, M5 oxidation kinetics at 1000 C

The comparison of obtained data with the Zry-4 oxidation kinetics is presented as a function of temperature in Fig. 5.15.

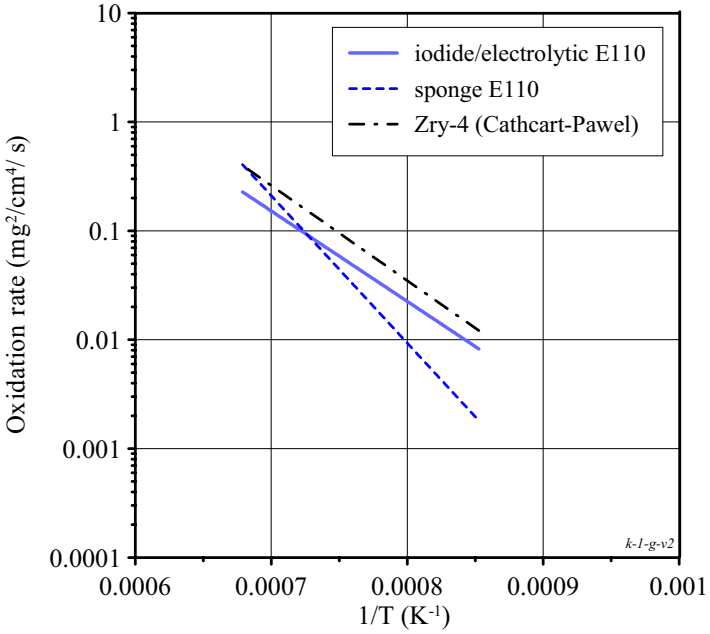

Fig. 5.15. The comparison of the Zry-4, sponge E110, iodide/electrolytic E110 oxidation rates in the temperature range of 900 - 1200 C

The data base obtained at 900 C and 1000 C to characterize the embrittlement behavior of the sponge E110 is not sufficient for the determination of the zero ductility threshold. Nevertheless, the analysis of test results allowed to make the following important conclusions:

- the ductility reduction as a function of ECR is caused by the oxygen induced mechanism at the low hydrogen uptake;
- the critical ECR associated with the zero ductility threshold at 900 C and 1000 C will be significantly lower than that at 1100 C, although the critical time will be significantly higher;
- a possible explanation of this phenomenon can be associated with the formation at 1000 C of a thicker α-Zr(O) layer in comparison with the α-Zr(O) layer formed at 1100 C or in comparison with the α-Zr(O) layer in the iodide/electrolytic E110 formed at 1000 C. This effect leads to the reduction of the effective thickness in the prior β-phase layer and to the increase of oxygen content in the metallic matrix;
- besides, the first indications of the breakaway oxidations (white spots on the cladding) appear at the ECR≥8.5%, but this corresponds to a very long time.

It should be noted in the context of the revealed features that similar tendencies were noted in other Zr-1%Nb cladding alloys. Thus, a sharp reduction of M5 ductility was observed in the ECR range 11–12% (as-measured) in the ANL test data [15, 16]. Moreover, in accordance with results of French investigations, the breakaway phenomena accompanied by high hydrogen and nitrogen pickup were noted at 1000 C under the following conditions: the oxidation time was much higher than 1800 s but less than 135000 s [18]. It is of interest that the ANL data showed that Zirlo cladding did not demonstrate the tendency towards the earlier ductility reduction at 1000 C and it did not demonstrate a tendency of a sharp reduction in oxidation rate [15].

The next important data characterizing the sponge E110 behavior were obtained at the oxidation temperature 1200 C. The overview of appropriate results is as follows:

- in spite of the fact that visual indications of the breakaway oxidation were not observed up to the 23.3% ECR, a significant hydrogen uptake was revealed already at 8% ECR;
- the zero ductility threshold of the sponge E110 did not exceed the 8% ECR at 1200 C.

The comparison of these data with the ANL data [15, 16] characterizing the Zry-4, M5, Zirlo embrittlement behavior after the oxidation at 1200 C showed that:

- all tested alloys showed a tendency towards the reduction of the zero ductility threshold at this temperature. The Zry-4, Zirlo, M5 ductility reduction down to 5% (the residual ductility or offset hoop strain) occurred in the measured ECR range 8.2–10% ECR;
- but the Zry-4, Zirlo, M5 embrittlement was not accompanied by high hydrogen uptake. The hydrogen content in these claddings remained at the level ranging from 17–19 ppm up to 18.8–22.3% ECR.

The consideration of iodide/electrolytic and sponge E110 comparative data allows to assume that revealed general differences in the behavior of these cladding materials are a function of differences in the microchemical composition of these two modifications of the E110 alloy. To clarify the background of the problem, the results of previous investigations devoted to the relationship between the corrosion resistance of zirconium-based claddings and microchemical composition of the cladding alloy were reassessed. The major outcomes of this work were the following:

- the stabilization of zirconium dioxide tetragonal form led to the improvement of the cladding corrosion resistance;
- in this context, all impurities can be subdivided into the beneficial and deleterious impurities;
- in accordance with the physical theories and empirical data, the beneficial and deleterious impurities consisted of the following elements:

– beneficial impurities: Fe, Cr, Ca, Mg, Y…

– deleterious impurities: C, N, F, Cl, Si, Ti, Ta, V, Mn, Pt, Cu…

- there are contradictory points of view regarding such elements as Al, Ni, Mo. As for oxygen, the majority of investigators consider that this element is neutral with respect to corrosion resistance;
- the corrosion behavior was very sensitive to the concentration of such alloying elements as Nb and Sn. Moreover, each type of alloy had the optimal concentration of the alloying element at which the best corrosion resistance was provided;
- the main potential differences between the microchemical compositions of the iodide/electrolytic and sponge E110 alloy may be associated with the following:

– the method of the electrolytic E110 production led to the risk of the alloy enrichment with such deleterious impurity as fluoride. Besides, the electrolytic E110 had a very high Hf content, the role of which was not quite understood with respect to the cladding corrosion behavior. The iodide Zr component of the alloy may be considered as neutral because this component had a very low content of both beneficial and deleterious impurities;

– the method of the sponge E110 production facilitated the alloy enrichment with such beneficial impurities as Ca, Mg, Fe, Y.

Taking into account the results of this analysis, chemical compositions of iodide/electrolytic and sponge E110 alloys were compared. The comparison showed that reasonable differences in the impurity contents were revealed for two elements only:

- Fe: 86 ppm in the iodide/electrolytic E110 and 120–140 ppm in the sponge E110;
- Hf: 350 ppm in the iodide/electrolytic E110 and 90–420 ppm in the different modifications of the sponge E110.

It should be noted that it was impossible to compare directly the contents of many impurities of a low content in the alloy due to very low concentrations: the content was less than 10 ppm, 30 ppm, etc.

To determine the sensitivity of the E110 oxidation behavior, special tests were performed using the iodide/electrolytic E110 cladding with a low hafnium content ($E110_{low\ Hf}$, 90 ppm). These tests showed that the corrosion resistance was a function of hafnium content in the studied range of Hf variation (350 ppm in the iodide/electrolytic E110 and 90 ppm in the $E110_{low\ Hf}$).

The $E110_{low\ Hf}$ cladding was characterized by the increase of the zero ductility margin from 8.3% ECR (standard E110) up to 12% ECR due to the significant delay in the breakaway initiation as a function of ECR. However, the fact cannot be ruled out that in this case the process of the E110 alloy purification from

hafnium might be accompanied by the change in the content of any other impurity because some modifications of the sponge E110 tested in the frame of this work constituted the mixture of sponge Zr, iodide Zr and recycled scrap with a high hafnium content but the corrosion resistance of these modifications was very high.

The next position of special investigations was associated with the determination of the sensitivity of the oxidation behavior of niobium-bearing alloys to the iron content:

- the oxidation and mechanical tests of the E635 cladding with a very high iron content in the cladding material (0.34–0.4% by weight) showed that the oxidation behavior and embrittlement threshold of iodide/electrolytic E635 was somewhat better than that for the iodide/electrolytic E110 but the sponge variant of E635 had practically the same embrittlement characteristics as iodide/electrolytic E635. And both versions of the E635 alloy had lower zero ductility thresholds (at 1100 C) than the sponge E110;
- the analysis of special investigations performed by the VNIINM [19] with the variation of iron content in the range 80–1400 ppm and the variation of such elements as O, C, Hf, Cr showed that:
  - in spite of the fact that the oxidation and mechanical response of seven types of the oxidized cladding (10% ECR) differentiated from the best (lustrous black oxide, low hydrogen content, reasonable margin of residual ductility) to the worst (breakaway effects, oxide spallation, high hydrogen content, low residual ductility), a direct association between the appropriate response and combinations of the chemical composition limited with such elements as Nb, Fe, C, Hf, Cr, O was not managed to be revealed. This fact undoubtedly indicated that the influence of other varied elements or some other parameters was not taken into account;
  - nevertheless, it should be noted that the best corrosion behavior of the tested cladding was obtained with an iron content of about 130–450 ppm and low hafnium content (~100 ppm) and a low carbon content. Very low (80 ppm) and very high (1400 ppm) iron contents were associated with the intermediate corrosion behavior but were also associated with very high carbon content (up to 200 ppm) in several samples.

Finally, the following general recommendations concerning the relationship between the microchemical composition and embrittlement behavior of niobium-bearing alloys can be given:

- the characterization of types of niobium-bearing alloys based on the current list of alloying elements should be reassessed;
- the status of some impurity elements must be changed and the definition of minor alloying elements should be added to the characterization of the cladding alloy;
- special investigations to determine the deleterious, beneficial and neutral impurities in the niobium-bearing alloys should be performed additionally.

5.2.4. Bulk microstructure studies

The last position of this stage of the research program was connected with the comparison of the microstructure parameters of different types of E110 cladding. To develop the data base for the comparison, TEM examinations of iodide/electrolytic E110 and sponge E110 cladding materials were performed.

In accordance with the results of analytical studies, the following comparative data were measured:

- phase conditions and phase composition;
- the grain size of zirconium in the cladding matrix;
- the parameters of the secondary phase precipitates being of importance for the corrosion resistance: the chemical composition, size, density, uniformity of distribution.

The choice of these comparative data was based on the results of inside and outside Russian investigations devoted the determination of the relationship between the corrosion behavior and cladding microstructure.

The results of TEM investigations showed that:

- iodide/electrolytic E110 and sponge E110 had a completely recrystallized microstructure (α+β-Nb);
- the average size of α-Zr grain in the matrix was similar for both types of E110 claddings (2.8 μm for iodide/electrolytic E110 and 3.2 μm for the sponge E110);
- the globular type of β-Nb precipitates uniformly distributed in the α-Zr matrix characterized both E110 modifications;
- the average size of the secondary β-Nb precipitates was practically the same in the iodide/electrolytic and sponge E110 (41–60 μm);
- the iodide/electrolytic E110 did not contain the intermetallic precipitates; the sponge E110 had the intermetallic precipitates of the $Zr(Nb,Fe)_2$ type, and the size of these precipitates was about 180 μm.

The comparative analysis of the iodide/electrolytic E110 and sponge E110 microstructures with the French published data on the M5 microstructure allowed to conclude the following:

- iodide/electrolytic E110 ($E110_{low\ Hf}$), sponge E110 and M5 had practically the same parameters for the microstructure;
- the only distinction between the microstructure of iodide/electrolytic E110 and sponge types of Zr-1%Nb cladding (sponge E110, M5) was that the sponge Zr-1%Nb types of alloy had the iron-based precipitates in addition to the β-Nb precipitates.

5.2.5. Final Remarks

Taking into account the results of investigations devoted to the microstructure, microchemical and surface effects, the following general conclusions can be made:

- the current type of the E110 (Zr-1%Nb) cladding (standard iodide/electrolytic) has quite an optimal microstructure. The specific oxidation behavior of this cladding at high temperatures is not a function of the cladding microstructure;
- the performed research allowed to establish that the oxidation behavior and ductility margin of the E110 oxidized cladding are very sensitive to the cladding microchemical composition and surface finishing;
- the use of the sponge type of zirconium for the fabrication of cladding tubes provides a significant reduction of the cladding oxidation rate, especially in the temperature range of 900 – 1000 C, and an increase in the zero ductility threshold;
- additional improvement of the oxidation behavior and a significant increase of the residual ductility margin in the E110 oxidized cladding can be achieved by polishing of the outer and inner cladding surfaces.

REFERENCES FOR SECTION 5

[1] Bibilashvili Yu.K., Sokolov N.B., Dranenko V.V., Kulikova K.V., Izrailevskiy L.B., Levin A.Ya., Morozov A.M. "Influence of Accident Conditions due to Loss of Tightness by Primary Circuit on Fuel Claddings", *Proc. of the Ninth Int. Symp. on Zirconium in the Nuclear Industry*, Kobe, Japan, November 5-8, 1990 (ASTM STP-1132, 1991).

[2] Hozer Z., Griger A., Matius L., Vasaros L., Horvath M. "Effect of Hydrogen Content on the Embrittlement of ZR Alloys", *Proc. of IAEA Technical Committee Meeting on "Fuel Behavior under Transient and LOCA Conditions"*, Halden, Norway, September 10-14, 2001.

[3] Hozer Z., Matus L., Horvath M., Vasaros L., Griger A., Maroti L. "Ring Compression Tests with Oxidized and Hydrided Zr-1%Nb and Zirkaloy–4 Cladding", Hungarian Academy of Sciences, CRIP, Budapest, Report KFKI-2002-01/G.

[4] Vrtilkova V., Valach M., Molin L. "Oxiding and Hydrating Properties of Zr-1%Nb Cladding Material in Comparison with Zircaloys", *Proc. of IAEA Technical Committee Meeting on "Influence of Water Chemistry on Fuel Cladding Behavior"*, Rez (Czech Republic), October 4-8, 1993.

[5] Vrtilkova V., Novotny L., Doucha R., Vesely J. "An Approach to the Alternative LOCA Embrittlement Criterion", *Proc. of SEGFSM Topical Meeting on LOCA Fuel Issues,* Argonne National Laboratory, May 2004 (NEA/CSNI/R(2004)19).

[6] Böhmert J. "Embrittlement of Zr-1%Nb at Room Temperature after High-Temperature Oxidation in Steam Atmosphere", Journal, Kerntechnik 57 No1, 1992.

[7] Böhmert J., Dietrich M., Linek J. "Comparative Studies on High-Temperature Corrosion of Zr-1%Nb and Zircaloy-4", Nuclear Engineering and Design, 147 No1, 1993.

[8] Bibilashvili Yu.K., Sokolov N.B., Salatov A.V., Andreyeva-Andriyevskaya L.N., Nechayeva O.A., Vlasov F.Yu. "RAPTA-5 Code: Modelling of Behaviour of Fuel Elements of VVER Type in Design Accidents. Verification Calculations", *Proc. of IAEA Technical Committee Meeting on "Behavior of LWR Core Materials under Accident Conditions", Dimitrovgrad, Russia, on 9-13 October 1995*. IAEA-TECDOC-921, Vienna, 1996.

[9] Gyori Cs. et.al. "Extension of Transuranus code applicability with niobium containing models (EXTRA)". *Proc. of FISA-2003 Conference EU Research in Reactor Safety,* EC Luxembourg, November 2003.

[10] Baker L., Just L.C. "Studies of Metal Water Reactions at High Temperatures", Technical report of ANL-6548, 1962.

[11] Cathcart J.V. and Pawel R.E. "Zirconium Metal-Water Oxidation Kinetics: IV Reaction Rate Studies", ORNL/NUREG-17, 1977.

[12] Mardon J.P., Garner G., Beslu P., Charquet D., Senevat J. "Update on the Development of Advanced Zirconium Alloys for PWR Fuel Rod Claddings", *Proceedings of the International Topical Meeting on Light Water Reactor Fuel Performance,* Portland, Oregon, March 2-6, 1997.

[13]Brachet J., Pelchat J., Hamon D., Maury R., Jaques P., Mardon J. "Mechanical Behavior at Room Temperature and Metallurgical Study of Low-Tin Zry-4 and M5™ (Zr-NbO) Alloys after Oxidation at 1100°C and Quenching", *Proc. of IAEA Technical Committee Meeting on "Fuel Behavior under Transient and LOCA Conditions"*, Halden, Norway, September 10-14, 2001.

[14] Mardon J., Frichet A., Bourhis A. "Behavior of M5™ Alloy under Normal and Accident Conditions", *Proc. of Top Fuel-2001 Meet.*, Stockholm, May 27-30, 2001.

[15] Billone M.C., Yan Y. and Burtseva T. "Post-Quench Ductility of Zircaloy, E110, ZIRLO and M5", *Proc. of SEGFSM Topical Meeting on LOCA Fuel Issues,* Argonne National Laboratory, May 2004 (NEA/CSNI/R(2004)19).

[16] Billone M.C., Yan Y. and Burtseva T. "Post-Quench Ductility of Advance Alloy Cladding", *2004 Nuclear Safety Research Conference,* Washington DC, October 2004.

[17] Mardon J.P., Waeckel N. "Behavior of M5^{TM} Alloy under LOCA Conditions", *Proc. of Top Fuel-2003 meetings "Nuclear Fuel for Today and Tomorrow Experience and Outlook",* March 16-19, 2003, Wurzburg, Germany.

[18] Waeckel N., Mardon J.P. "Recent data on M5™Alloy under LOCA Conditions", *Proceedings of the 2003 Nuclear Safety Research Conference*, Washington DC, October 20-22, 2003, NUREG/CP-0185, 2004.

[19] Nikulina A.V., Andreeva-Andrievskaya L.N., Shishov V.N., Pimenov Yu.V. "Influence of Chemical Composition of Nb Containing Zr Alloy Cladding Tubes on Embrittlement under Conditions Simulating Design Basis LOCA", *Fourteenth International Symposium on Zirconium in the Nuclear Industry,* ASTM STP.

APPENDIX A

Description of Test Apparatus and Test Procedures

A-1. Description of oxidation test apparatus

The scheme of oxidation apparatus is presented in Fig. 3.2 (see section 3). The oxidation facility consists of the following basic elements:

- electric furnace;
- device for the movement of E110 sample in the several given positions (cold position, hot position, quench position);
- steam generator;
- system to supply the argon to the oxidation facility;
- measurement apparatus (measurement of temperature inside and outside of E110 sample, temperature of water in the steam generator);
- tank with the water in the low part of facility.

The electric furnace provided the radiant heating and cooling of cladding sample with the different temperature rates (see the more detail information in Appendix A-2). The steam generator provided the generation of water steam with the following parameters:

- temperature: 150 C;
- mass flow rate: 0.01–0.04 g/s (mass flow rate is a function of electric power);
- atmospheric pressure.

The system to supply the argon to the oxidation facility was used at the beginning of each test mode. This system devoted the cleaning of gas atmosphere inside the test facility from air. The temperature limit was used to change the type of coolant. The Ar flow was stopped at the temperature about of 300 C and after that the heating was continued with the water steam.

The important details of temperature measurements are described in Appendix A-4. The tank with water in the low part of facility devoted the opportunity to perform cooling of cladding sample under quench conditions.

A-2. Description of oxidation procedures

The five combinations of heating and cooling rates were used for this experimental program (see Fig. 3.3 in section 3):

1. Slow heating and slow cooling (S/S).
2. Slow heating and fast cooling (S/F).
3. Fast heating and slow cooling (F/S).
4. Fast heating and fast cooling (F/F).
5. Fast heating and quench cooling (F/Q).

The characterization of major types of test modes is described below.

Slow heating (Fig. A-1):

- the cladding sample was installed in the hot position (see Fig. 3.2 of section 3);
- the air atmosphere in the electric furnace was replaced on the argon atmosphere;
- the electric furnace was switched on and the cladding sample was heated to 150 C with the temperature rate 0.5 C/s;
- the argon atmosphere was replaced on the water steam atmosphere and the heating of cladding sample was continued with the rate 0.5 C/s to the hold temperature.

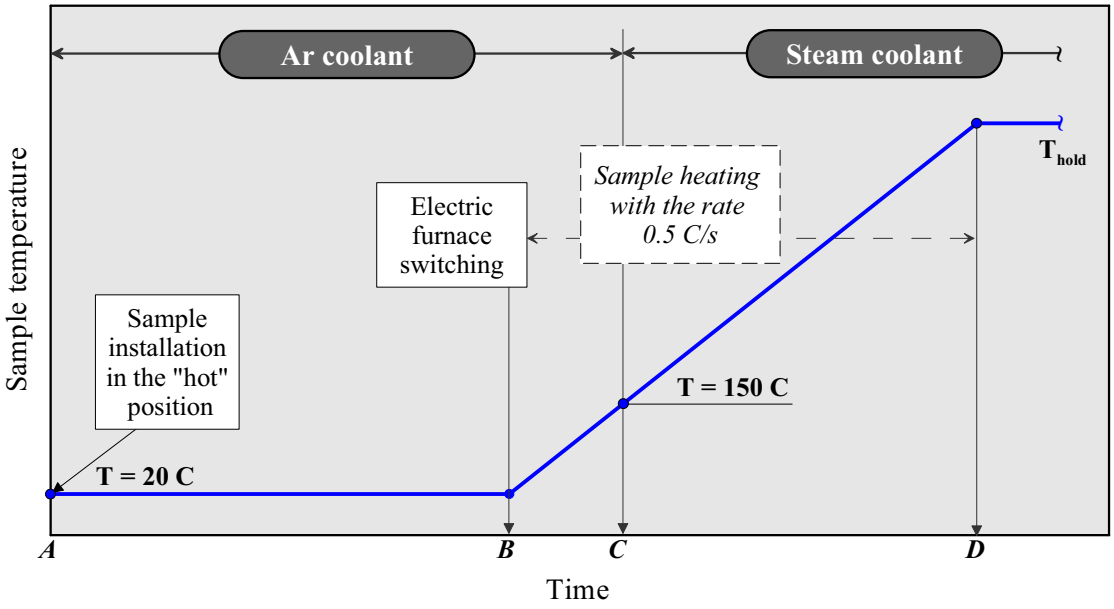

Fig. A-1. Oxidation mode with the “slow” heating: sequence diagram

Fast heating (Fig. A-2):

- the cladding sample was installed in the cold position (see Fig. 3.2 of section 3);
- the air atmosphere in the electric furnace was replaced on the argon atmosphere;
- the electric furnace was switched on and the gas medium inside the electric furnace (in the hot position) was heated to 150 C after that the argon atmosphere was replaced on the water steam and the heating of the furnace was continued during 600 seconds to the hold temperature (in accordance with the thermocouple #2 data (see Fig. 3.2 of section 3)), the temperature of cladding sample, which was located in the cold position was not above 150 C at the end of this stage;
- the cladding sample was moved in the hot position the such a way to provide the heating rate 25 C/s in the temperature range 150–800 C.

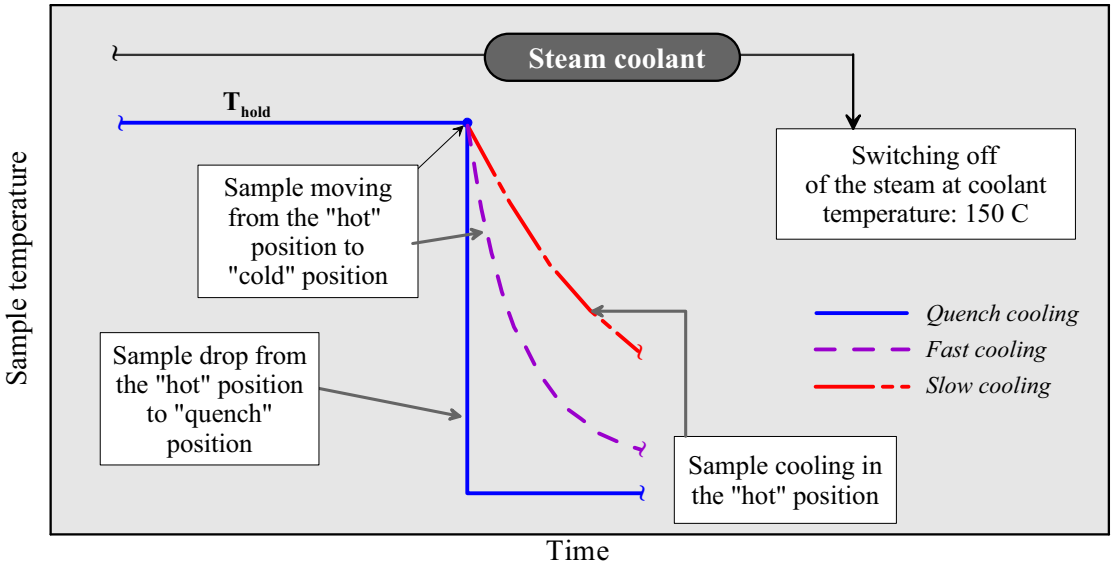

Fig. A-2. Oxidation modes with “slow”, “fast”, “quench” cooling: sequence diagram

Different types of cooling (Fig. A-3):

- As the slow cooling the cladding sample was cooled in the hot position with the temperature rate 0.5 C/s to 150 C, after that the steam atmosphere was replaced on the argon atmosphere and the cooling of cladding sample was continued with the same cooling rate.
- At the fast cooling the cladding sample was moved from the hot position to the cold position the such a way that the cooling rate at initial phase of this process was 25 C/s. The replacement of steam coolant to the argon coolant was made at the temperature of cladding sample 150 C.
- At the quench cooling the cladding sample was moved from the hot position to the quench position (to the cold water) with cooling rates about of 200 C/s.

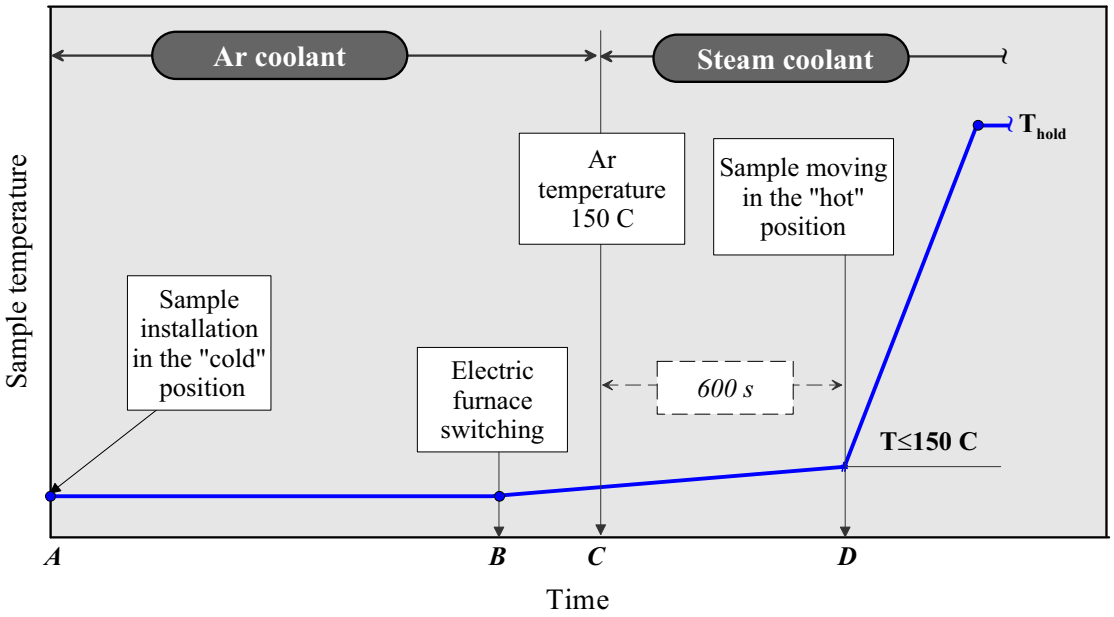

Fig. A-3. Oxidation mode with the "fast" heating: sequence diagram

A-3. The characterization of cladding samples

Table A-1. The list of tested cladding materials

Abbreviation	Alloying composition	Additional comments
E110	Zr-1%Nb	as-received E110 cladding tube manufactured from the iodide Zr, electrolytic Zr, and recycled scrap (the oxygen concentration ~0.04 % by weight)
E110A	Zr-1%Nb	as-received E110 cladding after the etching and anodizing of as-received E110 cladding tube
E110K	Zr-1%Nb	as-received E110 cladding tube manufactured from the iodide Zr, electrolytic Zr, and recycled scrap with the high content of oxygen concentration (0.11 % by weight)
$E110_{low\ Hf}$	Zr-1%Nb	as-received E110 cladding tube manufactured from the iodide Zr, electrolytic Zr, and recycled scrap with the low content of Hf (90 ppm). The standard content of Hf is about of 350 ppm
E635	Zr-1%Nb-1.2%Sn-0.35%Fe	as-received E635 cladding tube manufactured from the iodide Zr, electrolytic Zr, and recycled scrap
Zry-4	Zr-1.4%Sn	the cladding tube manufactured by Framatom ANP GmbH on January 1989

Abbreviation	Alloying composition	Additional comments
$E110_{irr}$	Zr-1%Nb	the irradiated E110 cladding refabricated from the commercial VVER-1000 fuel elements irradiated to 50–53 MWd/kg U
$E110_{G(fr)}$	Zr-1%Nb	as-received E110 cladding tube manufactured from French sponge Zr by the Russian process
$E110_{G(3fr)}$	Zr-1%Nb	as-received E110 cladding tube manufactured from 70% French sponge Zr, 30% iodide Zr and recycled scrap by the Russian process
$E110_{G(3ru)}$	Zr-1%Nb	as-received E110 cladding tube manufactured from 70% Russian sponge Zr, 30% iodide Zr and recycled scrap
$E635_{G(fr)}$	Zr-1%Nb-1.2%Sn-0.35%Fe	as-received E635 cladding tube manufactured from French sponge Zr by the Russian process

Table A-2. The geometry of unirradiated cladding materials

Parameter (mm)	Cladding material									
	E110	E110A	E110K	$E110_{low\ Hf}$	E635	Zry-4	$E110_{G(fr)}$	$E110_{G(3fr)}$	$E110_{G(3ru)}$	$E635_{G(fr)}$
Outer diameter	9.145 – 9.148	9.130	9.170	9.100	9.142	10.750	9.140	9.141	9.130	9.140
Inner diameter	7.73	7.73	7.72	7.73	7.78	9.35	7.74	7.74	7.73	7.74
Cladding thickness	0.708 – 0.709	0.700	0.725	0.685	0.681	0.700	0.700	0.700	0.700	0.700

Table A-3. Initial characteristics of irradiated cladding material

Characteristic	Unit	Value
The type of fuel assembly	–	VVER-1000 (the first unit of Zaporozhie Nuclear Power Plant)
Fuel assembly number	–	E0325
Fuel elements number	–	#156, #273
Axial coordinates of fuel element section used for the refabrication of irradiated cladding	mm	• Fuel element #156: 1640–2890 • Fuel element #273: 1800–2240
Fuel burnup as a function of axial coordinate	–	see Fig. A-4
Outer diameter of fuel element cladding as a function of axial coordinate	–	see Fig. A-5
Average fuel burnup in the section of fuel element	MWd/kg U	• Fuel element #156: 52.0 • Fuel element #273: 49.5
Average outer cladding diameter in the section of fuel element	mm	• Fuel element #156: 9.03 • Fuel element #273: 9.04
Average cladding thickness in the section of fuel element	mm	• Fuel element #156: 0.68 • Fuel element #273: 0.69
Microstructure of irradiated cladding	–	see Fig. A-6

Characteristic	Unit	Value
Average ZrO_2 thickness on the outer surface of irradiated cladding	μm	• Fuel elements ##156, 273: 5
Average ZrO_2 thickness on the inner surface of irradiated cladding	μm	• Fuel elements ##156, 273: 0
Hydrogen content in the irradiated cladding	% by weight	• Fuel elements ##156, 273: 0.0047

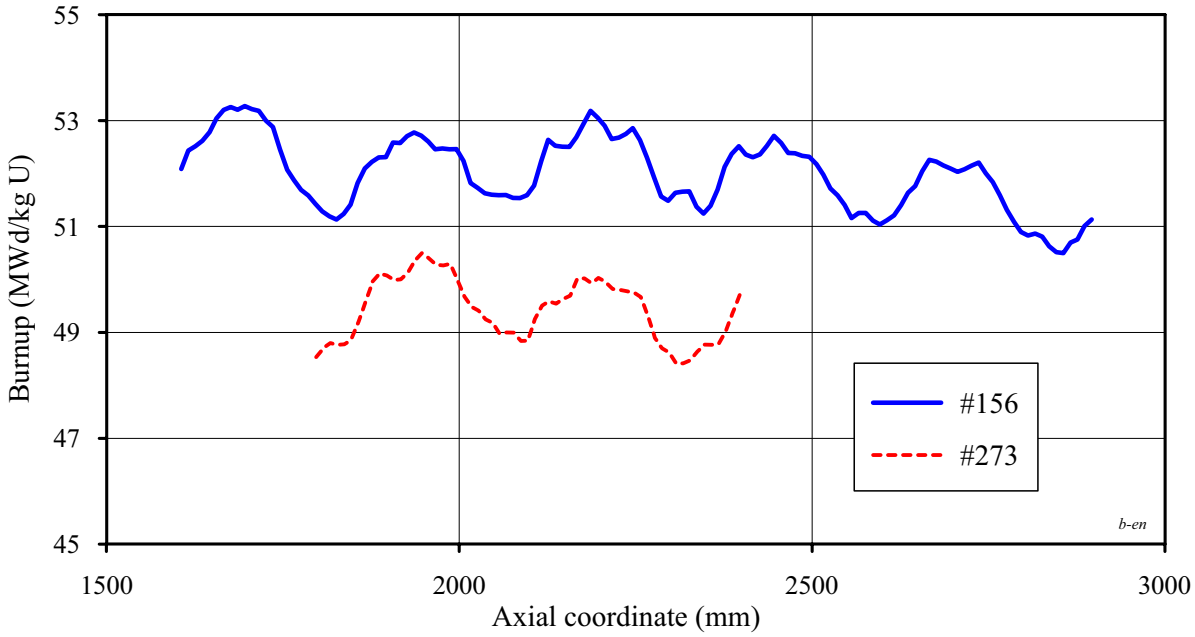

Fig. A-4. Axial burnup distribution for fuel element #156 and #273 (experimental data)

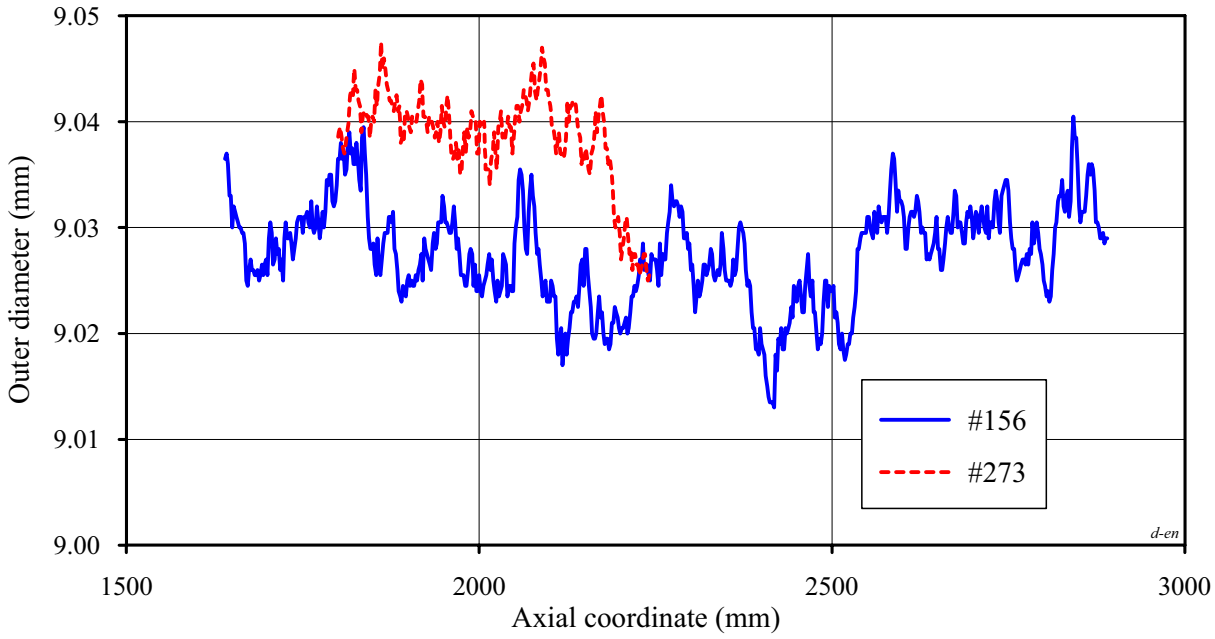

Fig. A-5. Profilometry of cladding outer diameter as a function of axial coordinate

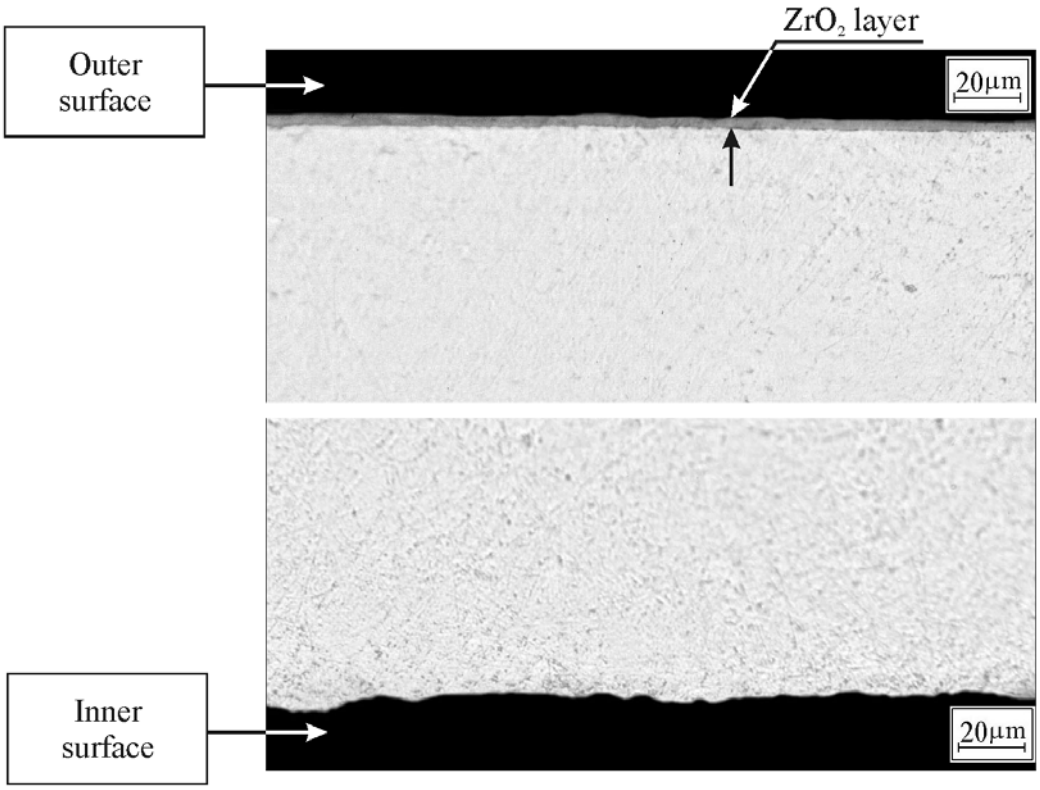

Fig. A-6. The microstructure of irradiated E110 cladding before the oxidation tests

A-4. Scoping tests performed to verify the experimental procedure of cladding temperature measurements

The following scoping tests were developed and performed to validate and verify the procedure of temperature measurements at the oxidation of cladding samples:

- scoping tests to reveal the axial temperature distribution inside the electric furnace;
- scoping tests to reveal the temperature distribution as a function of cladding sample length;
- scoping tests to obtain the comparative data characterizing two different methods of determination of cladding sample temperature:
  - the method on the basis of thermocouple, which was welded on the cladding surface;
  - the method on the basis of thermocouple, which was installed in the gas volume inside the cladding sample.

The major results of these scoping tests are presented below.

The data base characterizing the axial temperature distribution inside the electric furnace

The procedure of this test consisted of the following options:

- the electric furnace was heated to 1100 C (at the middle of furnace);
- the thermocouple (which was installed along the axis of electric furnace) was moved the step by step from the position #1 to the #15 (Fig. A-7);
- the processing of measured data allowed to obtain the axial temperature profile inside electric furnace;
- these data were used to determine the “cold” and “hot” positions of cladding sample (see Fig. 3.2, section 3).

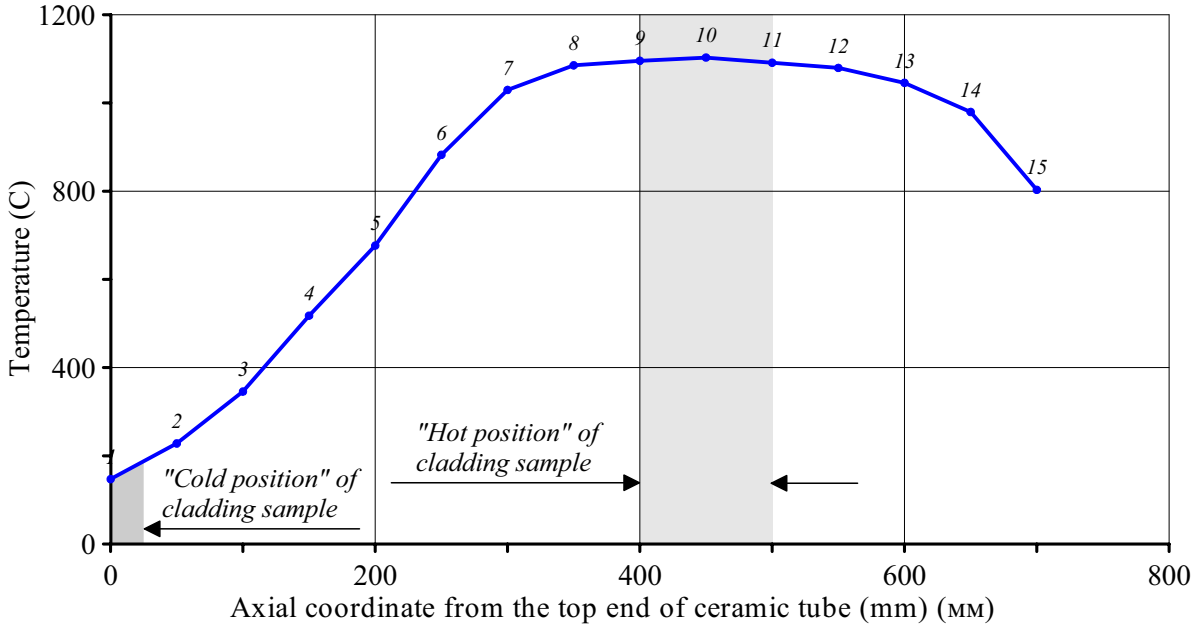

Fig. A-7. The axial temperature distribution inside the electric furnace

The measurement of axial temperature distribution along the cladding sample length

These measurements were performed using the following procedure:

- seven thermocouples were installed sequentially on the length of "hot" position (Fig. A-8);
- the electric furnace was heated to 1100 C (at the "hot" position);
- the processing of temperature measurements allow to reveal that the temperature nonuniformity is not more than 6 C.

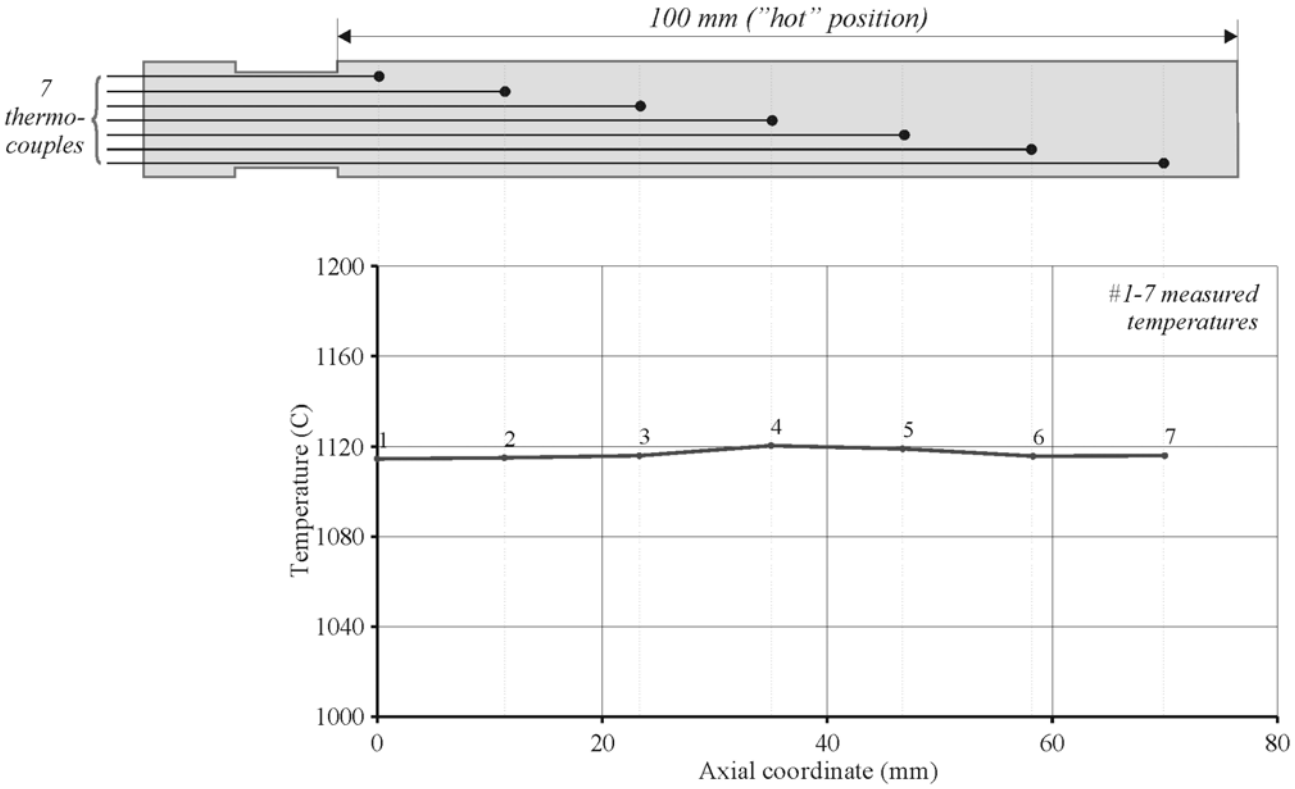

Fig. A-8. The axial temperature profile at the "hot" position

The development of comparative data to characterize two possible methods of measurement of cladding sample temperature

The following experimental procedure was used to obtain the appropriate data:

- the one thermocouple was welded on the outer surface of cladding sample;
- the second thermocouple was installed inside cladding sample along the sample axis;
- axial coordinates of both thermocouples were the same;
- the cladding sample with thermocouples was installed in the "cold" position (see Fig. 3.2., section 3);
- the electric furnace was heated to 1100 C;
- the cladding sample was removed from the "cold" position to the "hot" position, after that the cladding sample was oxidized at the hold temperature (1100 C) during approximately 400 seconds and finally the cladding sample was removed from the "hot" position to the cold position. Such a way, the oxidation of cladding sample at the F/F combinations of heating and cooling rates was performed.

The results of these comparative temperature measurements are presented in Fig. A-9.

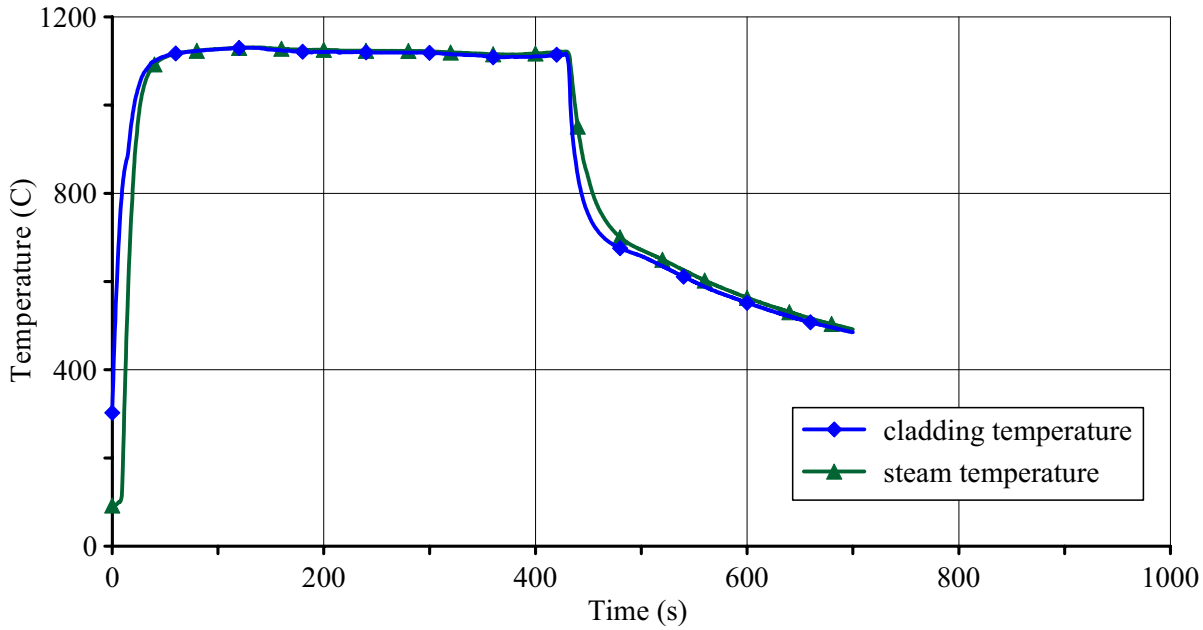

Fig. A-9. The cladding and steam temperatures under oxidation conditions with F/F combinations of heating and cooling rates

The analysis of obtained data allowed to make the following conclusions:

- the differences in the both temperature measurements at the stationary mode do not exceed the instrumental error of thermocouples;
- the thermocouple measuring the steam temperature under estimates the real cladding temperature at the heating mode, this thermocouple overestimates the cladding temperature at the beginning of cooling mode;
- the appropriate calculations shown that the systematic error of determination of effective time of oxidation (caused by above mentioned transient effects under heating and cooling conditions) is very insignificant;
- taking into account obtained comparative data it was decided to use the thermocouple placed inside the cladding sample for the temperature measurement at the oxidation tests.

A-5. The ECR measurement

By definition, the equivalent cladding reacted (ECR) is a total thickness of zirconium layer that reacts with steam assuming that all absorbed oxygen were converted to a stoichiometric zirconia layer, divided by the initial thickness of the cladding. Besides it can be shown that the ECR is the ratio between the oxygen weight, which was absorbed by the cladding during the oxidation test to the oxygen weight, which could be absorbed by the cladding at the full (100 %) oxidation.

To determine the experimental ECR, two alternative methods are used as a rule:

- the measurement of oxygen weight gain using the determination of the cladding sample weight before and after the oxidation test;
- the metallographic method which is based on the thickness measurement of the ZrO_2 and α–Zr(O) layers.

However, the following specific features of the Zr-1%Nb (E110) cladding material hamper the use of these methods:

- the spallation and falling of oxide caused by the breakaway oxidation;
- the nonuniform boundary between the α–Zr(O) layer and prior-β phase (that does not allow to measure the macroscopic value of the α–Zr(O) layer using limited numbers of metallographic samples);
- the inexact knowledge of the radial distribution of oxygen concentration in the α–Zr(O) and prior-β phase layers.

Taking into account the above stated issues a special method of the ECR measurement was developed for this work. The general idea of this method is based on the following consideration:

- the weight gain of the E110 sample obtained during the oxidation test is determined as the difference between the weight gain of this sample oxidized up to 100% zirconium/niobium oxide (this value can be calculated with a high accuracy) and the weight gain of this sample at the additional full oxidation of the E110 sample metallic part (remained after the test oxidation).

In accordance with this approach, the following additional procedures were performed for the tested ring oxidized E110 sample:

- the weight of the oxidized sample (as a rule, the weight of the ring oxidized sample fragments after the ring compression tests) was measured;
- the oxidized sample (or the sample fragments) was additionally oxidized at 1100 C in air atmosphere during 4 hours;
- the weight of the completely oxidized (100 % oxide) sample was measured.

This procedure (the extra oxidation of the E110 ring samples) is explained in detail in Table A-4.

Table A-4. The major provisions of the ECR determination procedure

Stage of procedure	Comments
1. The weight gain of the E110 cladding sample after the oxidation test (Δm_o): $\Delta m_o = \Delta M_{100} - \Delta m_c$ where ΔM_{100} – the weight gain of the cladding sample at the complete 100 % oxidation (g); Δm_c – the weight gain of the cladding sample, obtained during the extra oxidation procedure (g)	
2. The weight gain of the E110 cladding sample at the complete oxidation in air atmosphere can be determined using the following equation: $\Delta M_{100} = M\left(0.99\frac{2\,A_O}{A_{Zr}} + 0.01\frac{5\,A_O}{2\,A_{Nb}}\right) = 0.3516\,M$ where A_O =16 (oxygen atomic mass);	The following assumptions were used: • Zr concentration in the E110 alloy is 0.99 (by weight); • the stoichiometric ZrO_2 and Nb_2O_5 are formed at the complete oxidation of the E110 alloy in the air

Stage of procedure	Comments
A_{Zr} =91.22 (zirconium atomic mass); A_{Nb} =92.91 (niobium atomic mass); M = the weight of the unoxidized ring sample (g)	
3. Thus, the ECR (%) can be calculated using the following equation: $ECR = \frac{\Delta m_o}{\Delta M_{100}} \cdot 100\ \% = 1 - \frac{\Delta m_c}{0.3516\ M}$ Special scoping tests have been performed to estimate the calculation accuracy on determining the ΔM_{100} parameter. Results of these tests have shown that the range of relative differences between the calculated and measured ΔM_{100} is 0.01–0.12 %	It should be noted that the weight gain of the E110 cladding sample after the oxidation test (Δm_0) is not contained in the ECR equation. Therefore, the ECR measurement error is not the function of oxide weight and, consequently, the spallation and falling of the ZrO_2 oxide during the oxidation and handling (procedures after the test) are not important for the accuracy of the ECR measurement. This accuracy is determined by the accuracy of the sample weight measurements (the unoxidized sample and the sample before and after the extra oxidation) and by the accuracy of several other measurements described below
4. The unoxidized ring sample weight (M) can be determined using the following considerations: $M = m_l \cdot L$ where m_l – the weight of the unoxidized cladding sample 1 cm long (g/cm); L – the unoxidized ring sample length (cm)	Special scoping tests performed with nine cladding samples have shown that the m_l average value is 0.01218 g/cm. The mean square error of this parameter is very small (0.0001)
5. The unoxidized ring sample length (L) is determined by $L = L_o \frac{l}{l_o}$ where L_o – the measured length of the oxidized ring sample (cm); l – the measured length of the unoxidized (100 mm) sample; l_o – the measured length of the oxidized (100 mm) sample	The set of measurements allowed to reveal that the length (100 mm) of the E110 sample is extended by 0.5–1 % during the oxidation
6. The weight gain of the cladding sample obtained during the extra oxidation (Δm_c) can be expressed by $\Delta m_c = m_c - m_s$ where m_s – the sample mass before the extra oxidation (g); m_c – the sample mass after the extra oxidation (g)	
7. The sample mass before the extra oxidation (m_s) will be $m_s = m_{O+Me} + m_H$ where m_{O+Me} – the mass of the sample metallic part and that of absorbed oxygen (g); m_H – the mass of absorbed hydrogen (g)	It should be taken into account that the increase in the E110 sample mass is the result of two processes: • oxygen absorption; • hydrogen absorption
8. Thus, the ECR expression is $ECR = \left(1 - \frac{\Delta m_C}{0.3516\ M} - \frac{m_H}{0.3516\ M}\right) \cdot 100\ \%$	
9. The absorbed hydrogen mass (m_H) can be determined by $m_H = C_H \cdot 10^{-6}\ m_s$	

Stage of procedure	Comments
where C_H – the measured hydrogen concentration in the ring sample (per-unit: ppm)	
10. Taking into account that the ratio of m_s to M is close to 1, the hydrogen correction factor ($\Delta ECR_H = (m_H/0.3516)100$ %) can be presented with the reasonable accuracy by $\Delta ECR_H = \frac{C_H \cdot 10^{-4}}{0.3516}$	C_H (ppm) $10^{-4} = C_H$ (% by weight)
11. Finally, the equation for the ECR determination has the following form: $ECR = 100\%\left(1 - \frac{\Delta m_C \; l_O}{0.3516 \; m_l \; L_O \; l}\right) - \frac{C_H \cdot 10^{-4}}{0.3516}$	
12. The ECR measurement error was estimated using the following experimental data characterizing the errors of individual measurements: • the absolute error of m_c measurement: 0.0002 g • the absolute error of l measurement: 0.01 cm • the absolute error of l_o measurement: 0.01 cm • the relative error of m_l measurement: 1.6 % • the maximum relative error of Δm_C determination: – 2.3 % at the 5 % ECR – 1.2 % at the 10 % ECR • The relative error of L_O measurement (using five azimutally distributed measurements): 0.8 %	
• The relative error of l/l_O determination: 1 % The relative error of ECR measurement is • 3.1 % at the ECR=5 • 2.4 % at the ECR=10 %	
13. The expression to determine the specific weight gain $\Delta m_{O(SP)}$ was formulated on the basis of the ECR data: $\Delta m_{O(SP)} = \frac{0.3516 \; m_l \; l \, 10^3}{\pi (d_O + d_i) \; l_O \; 100\%} ECR$ at the double-sided oxidation $\Delta m_{O(SP)} = \frac{0.3516 \; m_l \; l \, 10^3}{\pi \; d_O \; l_O \; 100\%} ECR$ at the single-sided oxidation where $\Delta m_{O(SP)}$ – the specific weight gain (mg/cm^2); d_O – the outer cladding diameter (cm); d_i – the inner cladding diameter (cm)	The following equation was used to determine the specific weight gain: $\Delta m_{O(SP)} = \frac{\Delta m_O}{S}$ where: S – the sample surface area
14. Several modifications were developed to determine the ECR in the irradiated claddings: • the weight of the irradiated cladding 1 cm long before the oxidation (m_l) was determined • the initial ECR of irradiated claddings (the ECR developed during the irradiation) was determined (ECR_i = 0.5 %)	a) Several scoping tests were performed with the irradiated cladding samples to measure the parameter m_l in accordance with the approach presented in the item 4. b) The following expression was used to determine the ECR_i:

Stage of procedure	Comments
	$ECR_i = \frac{\delta_{ZrO_2}}{1.56\ \delta_{cl}} 100\%$
	where δ_{ZrO2} – ZrO_2 layer thickness on the outer and inner cladding surfaces before the oxidation (5 μm)
	δ_{cl} – the irradiated cladding thickness (685 μm)
	1.56 – Pilling-Bedworth coefficient
15. The final equation for the ECR in the irradiated cladding is $ECR = 100\%\left(1 - \frac{\Delta m_C\ l_O}{0.3516\ m_l\ L_O\ l}\right) - \frac{C_H 10^{-4}}{0.3516} + 0.5\%$	

A-6. Determination of the oxidation equivalent time

It is known that to estimate the oxidation kinetics of the cladding, the experimental data characterizing the specific weight gain dependence on the oxidation time at the given temperature are required. But the real experimental oxidation history of the tested cladding sample consists of three test modes (Fig. A-10):

1. The transient mode (the oxidation temperature transient) on the sample heating.
2. The steady state mode (the oxidation temperature is approximately constant).
3. The transient mode on the sample cooling.

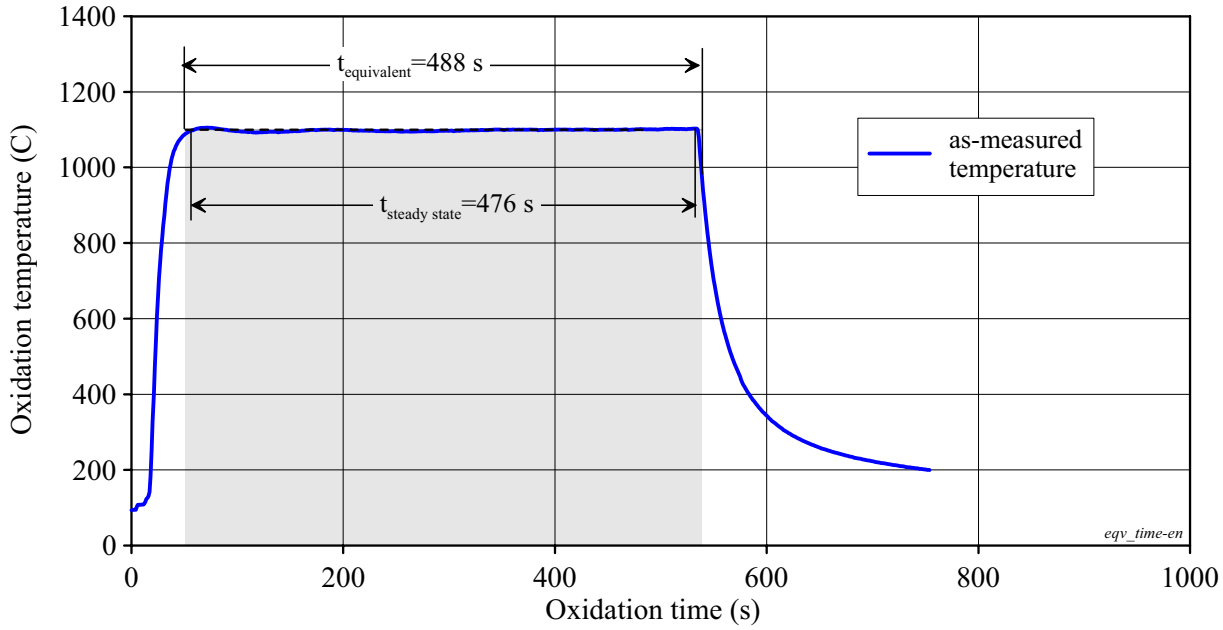

Fig. A-10. The oxidation history of the E110 as-received tube at 1100 C and F/F combination of heating and cooling rates

To transform the transient oxidation conditions into the oxidation kinetics (T=const), the equivalent time (t_{eq}) is used:

$$t_{eq} = \frac{\int_0^{t_{ox}} \exp\left(-\frac{Q}{R\,T(t)}\right) dt}{\exp\left(-\frac{Q}{R\,T_{eq}}\right)},$$

where: t_{ox} – time for the complete oxidation (s);

Q – the activation energy (cal/mole);

R – the gas constant (1.987 cal/mole K);

T(t) – the oxidation temperature as a function of time (K);

T_{eq} – the assigned steady temperature (K).

In accordance with the published data [1, 2, 3], the following value for the activation energy was used:

Q=39940 cal/mole.

The appropriate estimates have shown that the relative error of the equivalent time on using other values for the activation energy do not exceed 0.3 %.

References

[1] Cathcart J.V., Pawel R.E. at. al. "Zirconium Metal-Water Oxidation Kinetics: IV. Reaction Rate Studies". ORNL/NUREG-17, 1977.

[2] Bibilashvili Yu.K., Sokolov N.B., Salatov A.V., Andreyeva-Andriyevskaya L.N., Nechayeva O.A., Vlasov F.Yu. "RAPTA-5 Code: Modelling of Behaviour of Fuel Elements of VVER Type in Design Accidents. Verification Calculations", *Proc. of IAEA Technical Committee Meeting on "Behaviour of LWR Core Materials under Accident Conditions", Dimitrovgrad, Russia, on 9-13 October 1995*. IAEA-TECDOC-921, Vienna, 1996.

[3] Bohmert J., Dietrich M., Linek J. "Comparative Studies on High-Temperature Corrosion of Zr-1%Nb and Zircaloy-4", Nuclear Engineering and Design, 147 No1, 1993.

APPENDIX B

Tables with Results of Oxidation and Mechanical Tests: E110, E110A, E110K, E110pol, E635, $E110_{G(fr)}$, $E110_{G(3ru)}$, $E110_{G(3fr)}$, $E110_{low\ Hf}$, $E635_{G(fr)}$, Zry-4 as-Received Tubes and E110 Commercial Irradiated Claddings

Table B-1. A summary list of tested unirradiated tube samples. Characterization of test conditions and major test results

Material	Oxidation type	Heating/ Cooling comb.	Steady temp. (C)	Sample number	Equiv. Time (s)	Measured ECR (%)	Weight gain (mg/cm^2)	Residual ductility (%)	Relative displacement (%)	H cont. (ppm)
E110	double-sided	F/F	800	123	7205	3.4	2.7	59.8	65.3	80
				132	28814	10.7	8.5	8.0	15.6	466
				144	21850	8.6	6.7	16.0	23.0	150
			900	130	2407	3.9	3.1	57.2	58.2	106
				131	4804	6.7	5.4	31.8	32.1	194
				142	8120	12.3	9.6	0.0	2.7	3010
			950	140	5012	13.4	10.5	0.0	3.2	2780
				141	2490	11.2	8.8	0.0	2.9	920
			1000	44	865	7.7	6.2	8.4	13.0	
				45	798	7.6	6.1	20.7	24.4	
				119	871	5.7	4.5	19.4	26.4	173
			1100	28	529	10.5	8.4	0.6	6.9	
				30	426	8.9	7.1	0.2	5.1	1110
				41	284	8.2	6.6	0.0	4.5	1130
				46	194	6.5	5.2	57.2	57.7	75
				47	209	7.0	5.6	57.7	58.3	30
				62	445	8.0	6.4	4.9	11.9	660
				65	488	7.5	6.0	42.1	44.3	40
				68	605	10.0	7.9	3.3	10.0	
				81	496	8.1	6.5	1.5	8.5	280
				82	499	7.9	6.3	1.9	6.9	390
				83	341	10.0	8.0	0.5	5.5	
				85	307	6.0	4.8	- *	- *	
				86	336	6.9	5.5	- *	- *	
				92	555	8.5	6.8	1.4	7.2	690
				96	762	9.8	7.8	- *	- *	
				104	1814	16.1	12.8	0.0	4.8	
				105	818	11.8	9.4	- *	- *	
				110	1714	13.7	10.7	0.0	4.4	
				111	770	8.5	6.7	8.4	14.2	
			1120	25	403	9.9	7.9	0.1	4.7	1010
			1200	102	364	13.3	10.6	0.0	4.5	926
				106	308	11.5	9.1	0.0	4.4	430
		F/Q	1100	63	250	6.1	4.9	57.7	58.2	30
				66	375	7.1	5.7	47.3	49.3	90
				71	445	9.7	7.7	2.7	9.4	580
		F/S	1100	17	- **	10.0	8.0	0.0	4.2	730
				19	-	14.2	11.3	0.0	4.5	
				35	-	11.0	8.8	0.0	3.1	1150
				37	-	9.4	7.6	14.1	19.2	
				40	-	8.7	7.0	6.1	10.8	
				48	-	8.7	7.0	56.2	56.4	
				52	-	6.2	5.0	57.0	54.8	180
		S/F	1100	27	-	4.6	3.6	40.3	42.3	150
				32	-	7.1	5.7	24.4	28.0	
				34	-	7.2	5.8	2.1	8.5	
				49	-	7.6	6.1	4.1	11.2	
				51	-	7.7	6.2	0.5	5.6	

Material	Oxidation type	Heating/ Cooling comb.	Steady temp. (C)	Sample number	Equiv. Time (s)	Measured ECR (%)	Weight gain (mg/cm^2)	Residual ductility (%)	Relative displacement (%)	H cont. (ppm)
E110	double-sided	S/S	1100	29	-	5.8	4.6	45.2	39.7	320
				31	-	8.0	6.4	21.3	23.3	
				33	-	7.5	6.0	3.8	10.0	530
				36	-	11.7	9.4	0.2	3.8	1460
				38	-	7.6	6.1	4.6	9.5	360
	single-sided	F/F	1100	42	1374	8.9	13.1	24.4	32.9	540
				54	936	6.6	9.8	62.6	70.4	650
				55	1457	9.5	14.4	21.3	28.3	300
				56	1245	8.6	12.7	11.7	19.2	360
				76	1821	11.2	16.5	0.0	3.3	
E110A	double-sided	F/F	1100	117	675	9.0	7.1	0.0	5.1	554
E110K	double-sided	F/F	1100	58	488	14.0	11.4	0.0	3.1	
				67	480	9.7	7.9	0.0	3.1	1630
				88	559	7.0	5.7	0.0	2.7	
$E110_{low\ Hf}$	double-sided	F/F	1100	94	672	9.2	7.1	38.0	41.6	17
				121	1289	11.4	8.8	2.6	9.0	426
E110pol	double-sided	F/F	1000	119	871	4.3	3.4	59.6	60.0	44
			1100	92	555	8.0	6.4	46.3	52.0	28
E635	double-sided	F/F	1000	127	670	5.3	4.2	57.4	57.6	98
				138	1493	9.4	7.5	0.0	5.5	400
			1100	60	-	8.8	7.0	0.4	6.3	
				61	-	9.6	7.6	0.0	4.8	
				126	289	7.8	6.2	30.4	32.6	138
				134	300	6.9	5.5	12.4	18.7	107
				135	460	9.3	7.4	7.2	13.8	35
$E110_{G(3fr)}$	double-sided	F/F	1100	99	755	11.5	9.1	15.0	23.6	13
$E110_{G(3ru)}$	double-sided	F/F	900	137	14400	7.5	5.9	35.5	38.3	66
			1000	98	2519	6.9	5.4	42.4	46.0	16
				101	5028	8.9	7.0	28.3	31.1	11
			1100	95	739	11.6	9.1	15.0	22.5	4
				97	1548	16.7	13.1	11.4	17.3	17
				109	1743	18.0	14.2	3.6	9.2	101
			1200	112	932	23.5	18.5	0.0	4.9	2200
				120	168	7.8	6.1	3.2	8.0	824
$E110_{G(fr)}$	double-sided	F/F	1100	89	558	10.5	8.3	11.7	18.7	15
				90	933	13.0	10.3	17.1	22.8	48
			1000	91	2016	6.5	5.1	51.9	54.3	17
				93	5013	8.5	6.7	0.9	6.6	12
$E635_{G(fr)}$	double-sided	F/F	1100	100	749	12.5	9.8	4.3	11.0	18
				108	572	11.0	8.6	0.0	2.5	
Zry-4	double-sided	F/F	1100	64	495	11.5	9.5	14.3	22.4	34
		S/S	1100	43	-	11.3	9.3	4.8	12.7	37
$E110_m$	double-sided	F/F	1100	136	604	7.7	6.1	1.1	8.9	90

* - Tube sample was used for the three-point bending test

** - Equivalent time calculation procedure was not developed for slow heating and slow cooling test modes

F/F, F/Q, F/S, S/F, S/S characterize the heating/cooling combinations of the oxidation mode

(F - fast, Q - quench, S - slow)

ECR, weight gain, residual ductility, relative displacement are average values obtained due to the procedure of processing of individual measurements these parameters on several rings cutted from the tube sample (see Table B-2)

Table B-2. A summary data base on results of oxidation and mechanical tests with unirradiated cladding samples[1]

Tube sample number	Material, Oxid. Type	Steady temp. (C) Heat/Cool. Comb.	Average ECR (%)	Ring sample number	As-measu-red ECR (%)	H cont. (ppm)	Temp. of mech. Tests (C)	Relative disp.[2] (%)	Resid. Duct.[3] (%)	Other investigations[4]
17	E110 double-sided	1100 F/S	10.0	2_{15}*	10.3		20	4.1	0.0	
				4			20	4.3	0.0	
				5						MG
				6_{25}*	9.7		20	4.3	0.0	
				8		730				H2
19	E110 double-sided	1100 F/S	14.2	2_{15}	13.9		20	3.9	0.0	
				4			20	5.6	0.0	
				6_{20}*			20	3.7	0.0	
				7						MG, HV
				8_{25}*	14.4		20	4.8	0.0	
25	E110 double-sided	1120 F/F	9.9	2						MG, HV
				3						MG
				4	9.4		20	4.5	0.0	
				5			20	4.4	0.0	
				6	10.0		20	6.0	0.2	
				7	10.2		20	3.9	0.0	
				8			20	4.7	0.2	
				9		1010				H2
				10			135,200,300			MTt
27	E110 double-sided	1100 S/F	4.6	1		199				H2
				2			20	48.1	45.6	
				3			135	63.0	54.1	
				4	4.5		20	47.4	46.9	
				5						MG
				6	4.6		20	21.7	16.5	
				8		90				H2
				9						MG
				10			20	52.1	52.0	
				11		162				H2
28	E110 double-sided	1100 F/F	10.5	5	10.5		20	6.5	0.4	
				6			135	15.0	6.2	
				7			20	7.2	0.8	
29	E110 double-sided	1100 S/S	5.8	2	5.4		20	38.3	38.1	
				3						MG
				4		319				H2
				5	5.5		20	37.6	37.5	
				6			135	63.5	60.4	
				7			135	64.5	60.5	
				8	6.4		20	35.3	34.9	
				9			20	47.4	47.2	
30	E110 double-sided	1100 F/F	8.9	2	9.2		20	4.0	0.0	
				3		1113				H2
				4			135	9.4	1.8	
				5						MG
				6			135	9.0	1.7	
				7	9.2					
				8	8.3		20	6.7	0.5	
				9	8.4					
				10	9.3		20	4.5	0.0	

Tube sample number	Material, Oxid. Type	Steady temp. (C) Heat/Cool. Comb.	Average ECR (%)	Ring sample number	As-measu-red ECR (%)	H cont. (ppm)	Temp. of mech. Tests (C)	Relative disp.[2] (%)	Resid. Duct.[3] (%)	Other investigations[4]
31	E110 double-sided	1100 S/S	8.0	2	9.3		20	5.8	0.4	
				6						MG
				8	7.6		20	34.2	33.9	
				9	7.2		20	30.0	29.7	
32	E110 double-sided	1100 S/F	7.1	2	6.6		20	7.6	0.6	
				5			20	18.7	11.7	
				6						MG
				8	7.6		20	43.7	43.6	
				9	7.2		20	41.8	41.6	
33	E110 double-sided	1100 S/S	7.5	2	7.2		20	14.5	8.6	
				4			135	63.2	60.7	
				5		870				H2
				6						MG
				7		213				H2
				8	7.4		20	6.8	1.0	
				9	7.8		20	8.5	1.7	
34	E110 double-sided	1100 S/F	7.2	2	7.3		20	8.7	1.7	
				4	7.2			12.7	4.1	
				5						MG
				8	7.1		20	9.8	2.5	
				9	7.3		20	6.9	0.1	
35	E110 double-sided	1100 F/S	11.0	2	10.9		20	3.7	0.0	
				3			135	4.7	0.0	
				4		1150				H2
				5						MG
				8	11.0		20	3.1	0.0	
				10			20	2.6	0.0	
36	E110 double-sided	1100 S/S	11.7	2	12.8		20	3.2	0.2	
				4		1457				H2
				5						MG
				6	11.8		20	3.9	0.2	
				7			135	6.6	0.7	
				8			200	57.4	57.0	
				9			300	62.3	62.0	
				10	10.6		20	4.3	0.3	
37	E110 double-sided	1100 F/S	9.4	1						MG
				2	8.9		20	44.7	44.4	
				4	9.1		20	20.2	14.3	
				5			135	64.3	60.3	
				7	9.7		20	17.1	10.9	
				9	9.7		20	7.2	0.6	
				10	9.8		20	6.6	0.4	
				11						MG
38	E110 double-sided	1100 S/S	7.6	2			20	7.9	1.5	
				3			135	60.9	60.3	
				4		315				H2
				5						MG
				7	7.6		20	10.8	3.6	
				8			135	59.5	58.4	
				9		400	20			H2, Fr
				10			20	9.8	3.1	

Tube sample number	Material, Oxid. Type	Steady temp. (C) Heat/Cool. Comb.	Average ECR (%)	Ring sample number	As-measu-red ECR (%)	H cont. (ppm)	Temp. of mech. Tests (C)	Relative disp.[2] (%)	Resid. Duct.[3] (%)	Other investigations[4]
40	E110 double-sided	1100 F/S	8.7	2	7.9		20	17.5	11.8	
				5						MG
				6	9.4		20	8.5	1.9	
				8			135	17.7	10.5	
				10	8.9		20	6.4	0.3	
41	E110 double-sided	1100 F/F	8.2	3			135	67.5	60.1	
				4			20	6.5	0.0	Fr,HV,SEM
				5						MG
				6	8.1		20	4.0	0.0	
				8		1130				H2
				10	8.3		20	4.9	0.0	
42	E110 single-sided	1100 F/F	8.9	1		519				H2
				2			20	14.6	3.9	
				3	8.3		20	28.8	22.2	
				4	9.1		20	61.8	55.3	
				5						MG
				6	9.2		20	26.2	21.3	
				7		555				H2
43	Zry-4 double-sided	1100 S/S	11.3	1		37				H2
				2	9.9		20	16.5	8.6	
				3						MG
				4						MG
				5						MG
				6	11.4		20	12.4	4.6	
				7						MG
				8			135	18.7	11.4	
				10	12.7		20	7.9	1.1	
				11		271				H2
44	E110 double-sided	1000 F/F	7.7	2	9.9		20	3.8	0.0	
				5						MG
				6	6.9		20	19.6	14.1	
				10	6.2		20	15.7	11.2	
45	E110 double-sided	1000 F/F	7.6	2	7.5		20	3.8	0.0	
				5						MG
				6	7.8		20	58.9	58.3	
				10	7.4		20	10.4	3.8	
46	E110 double-sided	1100 F/F	6.5	2	6.0		20	58.9	57.9	
				3		129				H2
				4		20				H2
				5						MG
				6	6.8		20	57.2	56.8	
				7	6.5		135	71.6	61.2	
				10	6.7		20	57.1	56.9	
47	E110 double-sided	1100 F/F	7.0	2	7.1		20	58.9	58.6	
				4			135	72.4	64.2	
				5						MG
				6	7.3		20	60.2	59.8	
				7		30				H2
				8			20, 135			MTt
				9	6.3					
				10	7.2		20	55.9	54.6	

Tube sample number	Material, Oxid. Type	Steady temp. (C) Heat/Cool. Comb.	Average ECR (%)	Ring sample number	As-measu-red ECR (%)	H cont. (ppm)	Temp. of mech. Tests (C)	Relative disp.[2] (%)	Resid. Duct.[3] (%)	Other investigations[4]
48	E110 double-sided	1100 F/S	8.7	2	8.6		20	51.4	51.2	
				5						MG
				6	8.8		20	58.4	58.1	
				7	9.1		135	69.7	62.6	
				10	8.3		20	59.8	59.4	
49	E110 double-sided	1100 S/F	7.6	2	7.5		20	10.3	3.6	
				5						MG
				6	7.8		20	14.3	7.4	
				7			20, 135			MTt
				8			200, 300			MTt
				10	7.4		20	8.9	1.3	
51	E110 double-sided	1100 S/F	7.7	2			20	8.8	1.5	
				5						MG
				6	7.8		20	5.2	0.0	
				7	7.6		135	10.9	2.5	
				10			20	2.7	0.0	
52	E110 double-sided	1100 F/S	6.2	2			20	46.3	45.4	
				4		180				H2
				5						MG
				6	6.6		20	58.6	58.2	
				7	6.5		135	72.5	63.9	
				10	5.5		20	59.4	59.1	
54	E110 single-sided	1100 F/F	6.6	2	6.6		20	72.1	63.7	
				3	6.0		135	73.7	63.2	
				4		650				H2
				5						MG
				6	7.0		20	67.5	60.5	
				7	6.8		135	64.9	53.9	
				10	6.8		20	71.8	63.6	
55	E110 single-sided	1100 F/F	9.5	2	8.7		20	57.6	51.8	
				3	9.6		135	67.5	55.0	
				4		300				H2
				6	10.0		20	15.0	7.3	
				7	10.0		135	72.5	61.9	
				9	9.4		20	12.3	4.8	
56	E110 single-sided	1100 F/F	8.6	2	8.8		20	28.5	21.8	
				3	8.3		135	63.1	52.4	
				4		360				H2
				6	9.0		20	15.1	6.9	
				7	8.5		135	73.8	61.3	
				9	8.3		20	13.9	6.4	
58	E110K double-sided	1100 F/F	14.0	2	14.8		20	3.4	0.0	
				6			20	3.2	0.0	
				9	13.2		20	2.8	0.0	
60	E635 double-sided	1100 F/F	8.8	2	8.9		20	6.2	0.3	
				5						MG
				6	8.6		20	7.4	0.9	
				9	8.9		20	5.2	0.0	
61	E635 double-sided	1100 F/F	9.6	2	9.6		20	4.8	0.0	

Tube sample number	Material, Oxid. Type	Steady temp. (C) Heat/Cool. Comb.	Average ECR (%)	Ring sample number	As-measured ECR (%)	H cont. (ppm)	Temp. of mech. Tests (C)	Relative disp.[2] (%)	Resid. Duct.[3] (%)	Other investigations[4]
62	E110 double-sided	1100 F/F	8.0	2	7.6		20	13.7	6.0	
				3	8.1		135	62.8	61.8	
				4		660				H2
				6	7.8		20	13.9	7.1	
				8	8.3		135	31.9	24.9	
				9	8.1		20	8.0	1.5	
63	E110 double-sided	1100 F/Q	6.1	2	5.5		20	60.6	59.7	
				3	5.8		135	75.5	65.4	
				4		30				H2
				6	6.1		20	58.9	58.3	
				8	6.7		135	74.3	62.8	
				9	6.6		20	55.2	55.0	
64	Zry-4 double-sided	1100 F/F	11.5	2	11.3		20	21.7	12.5	
				3	11.4		135	26.5	17.0	
				4		34				H2
				5						MG
				6	11.7		20	21.9	12.4	
				8	11.5		135	28.2	18.8	
				9	11.8		20	23.6	12.8	
65	E110 double-sided	1100 F/F	7.5	2	7.1		20	55.1	54.9	
				3	7.7		135	62.5	59.2	
				4		40				H2
				5						MG
				6	7.8		20	49.8	49.5	
				8	7.4		135	72.0	64.5	
				9	7.7		20	28.0	21.9	
66	E110 double-sided	1100 F/Q	7.1	2	6.9		20	41.2	35.9	
				3	7.0		135	67.7	63.0	
				4		90				H2
				5						MG
				6	7.1		20	57.2	56.8	
				8	7.4		135	71.1	62.4	
				9	7.1		20	49.4	49.2	
67	E110K double-sided	1100 F/F	9.7	2	9.8		20	3.3	0.0	
				3	9.3		135	3.8	0.0	
				4		1630				H2
				5						MG
				6	8.7		20	3.1	0.0	
				8	10.5		135	3.9	0.0	
				9	10.4		20	2.9	0.0	
68	E110 double-sided	1100 F/F	10.0	2	9.5		20	12.4	4.7	
				3	9.6		135	30.4	22.6	
				4			200	76.3	65.0	
				5						MG
				6	10.2		20	10.7	4.1	
				7			300	76.5	65.5	
				8	10.0		135	29.1	21.7	
				9	10.5		20	6.9	1.0	

Tube sample number	Material, Oxid. Type	Steady temp. (C) Heat/Cool. Comb.	Average ECR (%)	Ring sample number	As-measured ECR (%)	H cont. (ppm)	Temp. of mech. Tests (C)	Relative disp.[2] (%)	Resid. Duct.[3] (%)	Other investigations[4]
71	E110 double-sided	1100 F/Q	9.7	2	9.1		20	17.4	8.1	
				3	9.9		135	55.7	53.0	
				6	9.0		20	4.1	0.0	
				7		581				H2
				8	10.1		135	52.1	49.6	
				9	10.2		20	6.7	0.0	
76	E110 single-sided	1100 F/F	11.2	2	11.9		20	3.2	0.0	
				3	11.8		135	5.6	0.7	
				6	11.1		20	3.4	0.0	
				8	10.0		135	12.2	2.1	
				9			20	3.3	0.0	
81	E110 double-sided	1100 F/F	8.1	1						
				2	7.9		20	9.4	2.3	
				3	8.3		135	25.1	19.1	
				4		140				H2
				5						MG
				6			20	7.5	0.8	
				9			20	8.5	1.4	
				10		422				H2
82	E110 double-sided	1100 F/F	7.9	2			20	7.1	2.2	
				3	7.7		135	65.0	64.2	
				4		170				H2
				5						MG
				6			20	7.3	2.2	
				8	8.0		135	66.1	65.8	
				9			20	6.2	1.4	
				10		607				H2
83	E110 double-sided	1100 F/F	10.0	1	10.0		20	7.0	0.9	
				3			20	4.0	0.0	
85	E110 double-sided	1100 F/F	6.0				20			3B
86	E110 double-sided	1100 F/F	6.9				20			3B
88	E110K double-sided	1100 F/F		3	7.0		20	2.7	0.0	
				4			20	2.6	0.0	
89	$E110_{G(fr)}$ double-sided	1100 F/F	10.5	3			135	59.8	56.5	
				4						MG
				5			20	21.2	12.4	
				6	10.5		20	16.2	10.9	
				7		7				H2
				8		22				H2
90	$E110_{G(fr)}$ double-sided	1100 F/F	13.0	3			135	60.1	59.6	
				4						MG
				5			20	24.3	18.2	
				6	13.0		20	21.4	16.0	
				7		30				H2
				8		107				H2
				10		6				H2

Tube sample number	Material, Oxid. Type	Steady temp. (C) Heat/Cool. Comb.	Average ECR (%)	Ring sample number	As-measured ECR (%)	H cont. (ppm)	Temp. of mech. Tests (C)	Relative disp.[2] (%)	Resid. Duct.[3] (%)	Other investigations[4]
91	$E110_{G(fr)}$ double-sided	1000 F/F	6.5	3			135	60.8	59.7	
				4						MG
				5	6.5		20	49.2	48.8	
				6			20	59.4	55.0	
				7		5				H2
				8		28				H2
92	E110pol double-sided	1100 F/F	8.0	2						MG
				3		28				H2
				4			20	52.0	46.3	
	E110 double-sided	1100 F/F	8.5	7			20	7.2	1.4	
				8		694				H2
				9	8.5					MG
93	$E110_{G(fr)}$ double-sided	1000 F/F	8.5	3			135	58.4	53.8	
				4						MG
				5	8.5		20	6.3	0.9	
				6			20	6.8	1.0	
				7		12				H2
94	$E110_{lowHf}$ double-sided	1100 F/F	9.2	3			135	60.2	58.5	
				4						MG
				5	9.2		20	45.2	39.3	
				6			20	37.9	37.7	
				7		17				H2
95	$E110_{G(3ru)}$ double-sided	1100 F/F	11.6	1	11.2					
				3			135	59.1	57.4	
				4						MG
				5			20	22.6	15.5	
				6	11.9		20	22.3	14.4	
				7						MG
				8		4				H2
96	E110 double-sided	1100 F/F	9.8				20			3B
97	$E110_{G(3ru)}$ double-sided	1100 F/F	16.7	1	15.8		20			
				3			135	53.8	50.4	
				4						MG
				5			20	16.9	9.6	
				6	17.0		20	25.9	20.7	
				7	17.3		20	9.2	4.0	
				8		17				SEM, H2
				10						MG
98	$E110_{G(3ru)}$ double-sided	1000 F/F	6.9	3			135	60.1	59.0	
				4						MG
				5			20	44.0	43.7	
				6	6.9		20	47.0	41.0	
				7		16				H2
99	$E110_{G(3fr)}$ double-sided	1100 F/F	11.5	3			135		57.1	
				4						MG
				5			20	23.8	16.0	
				6	11.5		20	23.4	13.9	
				7		13				H2

Tube sample number	Material, Oxid. Type	Steady temp. (C) Heat/Cool. Comb.	Average ECR (%)	Ring sample number	As-measured ECR (%)	H cont. (ppm)	Temp. of mech. Tests (C)	Relative disp.[2] (%)	Resid. Duct.[3] (%)	Other investigations[4]
100	$E635_{G(fr)}$ double-sided	1100 F/F	12.5	3			135	60.7	59.5	
				4						MG
				5			20	12.1	4.1	
				6	12.5		20	9.9	4.5	
				7		18				H2
101	$E110_{G(3ru)}$ double-sided	1000 F/F	8.9	3			135	55.0	50.4	
				4						MG
				5			20	28.3	28.3	
				6	8.9		20	33.8	28.3	
				7		11				H2
102	E110 double-sided	1200 F/F	13.3	2	13.0		20	4.6	0.0	
				3	13.5		135			
				4						MG
				6	13.3		20	4.5	0.0	
				7		926				H2
				8			135			
				9			20	4.5	0.0	
104	E110 double-sided	1100 F/F	16.1	5						MG
				6	16.0		20	4.8	0.0	
				7	16.0					
				8	16.2		135	4.2	0.0	
105	E110 double-sided	1100 F/F	11.8				20			3B
106	E110 double-sided	1200 F/F	11.5	2			20	4.4	0.0	
				3	11.4		135	7.7	0.9	
				4						MG
				6	11.5		20	4.4	0.0	
				7		430				H2
				8			135	8.9	1.2	
				9			20	4.3	0.0	
108	$E635_{G(fr)}$ double-sided	1100 F/F	11.0	3			135	25.1	19.6	
				4						MG
				6			20	2.5	0.0	
				8			135	5.4	0.0	
109	$E110_{G(3ru)}$ double-sided	1100 F/F	18.0	2	16.6		20	10.6	5.4	
				3	17.2		135	44.7	44.3	
				5						MG
				6	18.4		20	8.0	1.9	
				8	19.0		135	29.3	29.0	
				9	19.0		20	9.0	3.6	
				10		101				H2
110	E110 double-sided	1100 F/F	13.7	2	13.5		20	3.8	0.0	
				3	13.5		135	19.2	12.4	
				5						MG
				6	14.0		20	3.9	0.0	
				8	13.8		135	8.9	2.5	
				9	13.8		20	5.6	0.0	
				10		509	20	5.6	0.0	H2

Tube sample number	Material, Oxid. Type	Steady temp. (C) Heat/Cool. Comb.	Average ECR (%)	Ring sample number	As-measured ECR (%)	H cont. (ppm)	Temp. of mech. Tests (C)	Relative disp.[2] (%)	Resid. Duct.[3] (%)	Other investigations[4]
111	E110	1100	8.5	2	7.9		20	4.4	0.0	
	double-sided	F/F		3			135	59.3	58.5	
				5						MG
				6	8.3		20	19.1	12.3	
				8	8.8		135	59.5	57.8	
				9	9.0		20	19.2	13.0	
112	$E110_{G(3ru)}$	1200	23.5	2						MG
	double-sided	F/F		3	22.3		20	4.9	0.0	
				5	24.7		135	3.2	0.0	
				6		2200				H2
117	E110A	1100	9.0	3	9.3		135	11.8	4.7	
	double-sided	F/F		5						MG
				6	8.1		20	5.1	0.0	
				8	9.5		135	11.3	4.2	
				10		554				H2
119	E110pol	1000	4.3	2						MG
	double-sided	F/F		3	4.3		20	60.0	59.6	
				5		44				H2
	E110	1000	5.7	8	5.7		20	26.4	19.4	
	double-sided	F/F		9		173				H2
				10						MG
120	$E110_{G(3ru)}$	1200	7.8	2	8.1		20	18.3	9.5	
	double-sided	F/F		3			135	2.2	0.0	
				4		824				H2
				5						MG
				6	7.5		20	2.3	0.0	
				8			135	27.3	20.5	
				9			20	3.5	0.0	
121	$E110_{lowHf}$	1100	11.4	2	12.1		20	4.5	0.0	
	double-sided	F/F		4						MG
				6	10.8		20	12.0	5.0	
				9	11.3		20	10.4	2.7	
				10		426				H2
123	E110	800	3.4	2	3.0		20	67.7	61.2	
	double-sided	F/F		3	3.0		135	67.4	61.3	
				5						MG
				6	3.5		20	63.8	58.0	
				7		80				H2
				8	3.8		135	63.9	56.9	
				9	3.5		20	64.5	60.1	
126	E635	1100	7.8	2	7.6		20	42.1	41.9	
	double-sided	F/F		3	7.6		135	62.4	62.0	
				5						MG
				6	8.1		20	38.3	37.9	
				7		138				H2
				8	7.9		135	56.9	56.3	
				9			20	17.5	11.5	

Tube sample number	Material, Oxid. Type	Steady temp. (C) Heat/Cool. Comb.	Average ECR (%)	Ring sample number	As-measured ECR (%)	H cont. (ppm)	Temp. of mech. Tests (C)	Relative disp.[2] (%)	Resid. Duct.[3] (%)	Other investigations[4]
127	E635 double-sided	1000 F/F	5.3	2	4.8		20	60.1	59.9	
				3	4.8		135	70.0	65.5	
				5						MG
				6	5.7		20	54.7	54.5	
				7		98				H2
				8	5.9		135	63.5	61.2	
				9			20	58.0	57.7	
130	E110 double-sided	900 F/F	3.8	2			20	57.3	56.0	
				3	3.7		135	64.0	56.8	
				5						MG
				6	3.8		20	60.4	59.3	
				7		106				H2
				8			135	64.9	60.1	
				9			20	56.8	56.2	
131	E110 double-sided	900 F/F	7.4	2			20	30.6	30.2	
				3			135	63.4	61.2	
				5						MG
				6	7.4		20	28.4	28.1	
				7		194				H2
				8			135	59.0	56.8	
				9			20	37.2	37.0	
132	E110 double-sided	800 F/F	11.0	2	9.4		20	23.6	16.4	
				3	9.7		135	70.4	64.4	
				5						MG
				6	11.7		20	12.3	5.5	
				7		466				H2
				8	12.2		135	67.7	59.0	
				9	11.9		20	10.9	2.2	
134	E635 double-sided	1100 F/F	6.9	2	6.8		20	14.5	8.7	
				4						MG
				6	7.0		20	15.5	6.6	
				7		107				H2
				9	6.7		20	26.2	21.9	
135	E635 double-sided	1100 F/F	9.3	2	8.7		20	16.3	10.9	
				3			135	53.6	52.5	
				5						MG
				6	9.4		20	13.1	5.4	
				7		35				H2
				8			135	53.5	52.1	
				9	9.8		20	12.0	5.2	
136	E110m double-sided	1100 F/F	7.7	2	6.8		20	10.9	3.3	
				3			135	61.9	58.4	
				5						MG
				6	8.0		20	7.7	0.0	
				7		90				H2
				8			135	59.0	56.8	
				9	8.3		20	8.1	0.0	

Tube sample number	Material, Oxid. Type	Steady temp. (C) Heat/Cool. Comb.	Average ECR (%)	Ring sample number	As-measured ECR (%)	H cont. (ppm)	Temp. of mech. Tests (C)	Relative disp.[2] (%)	Resid. Duct.[3] (%)	Other investigations[4]
137	$E110_{G(3ru)}$ double-sided	900 F/F	7.5	2			20	63.0	61.3	
				3	6.6		135	61.2	59.8	
				5						MG
				6	7.4		20	42.6	41.9	
				7		66				H2
				8	7.9		135	60.1	59.0	
				9	8.0		20	9.3	3.3	
138	E635 double-sided	1000 F/F	9.4	2	8.8		20	6.9	0.0	
				3	8.7		135	12.0	3.2	
				5						MG
				6	9.9		20	3.7	0.0	
				7		400				H2
				8	10.5		135	20.8	13.1	
				9	9.0		20	6.0	0.0	
140	E110 double-sided	950 F/F	13.4	2	13.7		20	2.9	0.0	
				3			135	5.9	0.0	
				5						MG
				6	12.1		20	3.5	0.0	
				7		2780				H2
				8			135	6.4	0.0	
				9	14.4		20	3.2	0.0	
141	E110 double-sided	950 F/F	11.2	2	11.2		20	3.5	0.0	
				3			135	7.7	0.0	
				5						MG
				6			20	3.1	0.0	
				7		920				H2
				8			135	5.3	0.0	
				9			20	2.2	0.0	
142	E110 double-sided	900 F/F	12.3	2	10.0		20	3.3	0.0	
				3			135	4.2	0.0	
				5						MG
				6	13.3		20	2.5	0.0	
				7		3100				H2
				8			135	4.0	0.0	
				9	13.7		20	2.2	0.0	
144	E110 double-sided	800 F/F	8.6	5						MG
				6	8.4		20	21.0	15.0	
				7		150				H2
				8	8.8		20	25.0	17.0	

[1] Ring tensile tests and three point bending tests are indicated in "Other investigations" column, all other mechanical tests are ring compression tests

[2] Relative displacement at failure

[3] Residual ductility at failure

[4] Abbreviations:

MG metallographic cross-section
HV microhardness measurements
MTt ring tensile mechanical tests
3B three point bending tests
Fr fractography investigation
SEM scanning electron microscope examinations

Table B-3. A summary list of tested irradiated commercial claddings. Characterization of test conditions and major test results

Material	Oxidation type	Heating/ Cooling comb.	Steady temp. (C)	Sample number	Equiv. Time (s)	Measured ECR[1] (%)	Weight gain[2] (mg/cm^2)	Residual ductility (%)	Relative displacement (%)	H cont.[3] (ppm)
E110	double-sided	F/F	1000	16	544	6.3	4.7	18.7	26.7	470
				17	664	8.6	6.5	37.0	39.6	250
			1100	10	232	7.7	5.8	0.0	8.4	1690
				14	312	8.3	6.2	0.0	8.3	1410
				15	327	8.1	6.1	0.0	6.6	-
				20	137	6.3	4.7	26.1	30.4	30
				21	223	7.0	5.2	0.0	6.3	-
			1200	18	218	16.0	12.5	0.0	3.4	-
		S/F	1100	3	-*	5.8	4.3	11.2	20.4	170
		S/S	1100	1	-*	8.5	6.4	3.2	11.3	280
				2	-*	10.5	8.0	1.9	8.9	270

* - Equivalent time calculation procedure was not developed for slow heating and slow cooling test modes

F/F, F/Q, F/S, S/F, S/S characterize the heating/cooling combinations of the oxidation mode

(F - fast, Q - quench, S - slow)

[1] A sum of the ECR before the oxidation (0.5 %) and the ECR during the oxidation

[2] A sum of the weight gain before the oxidation (0.4 mg/cm^2) and the weight gain during the oxidation

[3] A sum of the H content before the oxidation (47 ppm) and the H content during the oxidation

Table B-4. A summary data base on results of oxidation and mechanical tests (ring compression tests) with irradiated commercial cladding samples

Tube sample number	Material, Oxid. Type	Steady temp. (C) Heat/Cool. Comb.	Ring sample number	As-measu-red ECR (%)	H cont. (ppm)	Temp. of mech. Tests (C)	Relative disp.[1] (%)	Resid. Duct.[2] (%)	Other investigations[3]
1	E110 double-sided	1100 S/S	1			20	11.3	3.2	
			2			135	30.5	25.1	
			3		280				H2
			4						MG
			5	8.5					
2	E110 double-sided	1100 S/S	1			20	8.9	1.9	
			2			135	17.5	10.9	
			3		270				H2
			4						MG
			5	10.5					
3	E110 double-sided	1100 S/F	1			20	20.4	11.2	
			2			135	67.6	58.6	
			3		170				H2
			4						MG
			5	5.8					
10	E110 double-sided	1100 F/F	1			20	8.4	0.0	
			2			135	14.0	2.0	
			3		1690				H2
			4						MG, HV
			5	7.7					

Tube sample number	Material, Oxid. Type	Steady temp. (C) Heat/Cool. Comb.	Ring sample number	As-measured ECR (%)	H cont. (ppm)	Temp. of mech. Tests (C)	Relative disp.[1] (%)	Resid. Duct.[2] (%)	Other investigations[3]
14	E110 double-sided	1100 F/F	1			20	8.3	0.0	
			2			135	75.8	68.7	
			3		1410				H2
			4						MG, HV
			5	8.3					
15	E110 double-sided	1100 F/F	1			20	6.6	0.0	
			2			135	72.5	63.0	
			3						
			4						MG, HV
			5	8.1					
16	E110 double-sided	1000 F/F	1			20	26.7	18.7	
			2			135	48.0	36.0	
			3		470				H2
			4						MG, HV
			5	6.3					
17	E110 double-sided	1000 F/F	1			20	39.6	37.0	
			3		250				H2
			4						MG, HV
			5	8.6					
18	E110 double-sided	1200 F/F	1			20	3.4	0.0	
			2			135	11.3	1.2	
			3						
			4						MG, HV
			5	16.0					
20	E110 double-sided	1100 F/F	1			20	30.4	26.1	
			3		30				H2
			4						MG
			5	6.3					
21	E110 double-sided	1100 F/F	1			20	6.3	0.0	
			4						MG
			5	7.0					

[1)] Relative displacement at failure

[2)] Residual ductility at failure

[3)] Abbreviations:

MG - metallographic cross-section

H2 - hydrogen content measurements

HV - microhardness measurements

Notice. The numeration of the rings begins from the bottom of the tube based on its location in the furnace. As a rule, parts of approximately 7 mm long were cut from top and bottom of oxidized tube and rejected to avoid end effects. After that the 8 mm rings were cut and numbered from bottom. The photos of tubes in the report and in the appendices (the photos represent entire uncut tubes) are shown such that the numeration increases from the right to the left.

APPENDIX C

Temperature Histories, Appearances and Microstructures of E110 Standard As-received Tubes after a Double-sided Oxidation at 1100 C and S/S, S/F, F/S Combinations of Heating and Cooling Rates

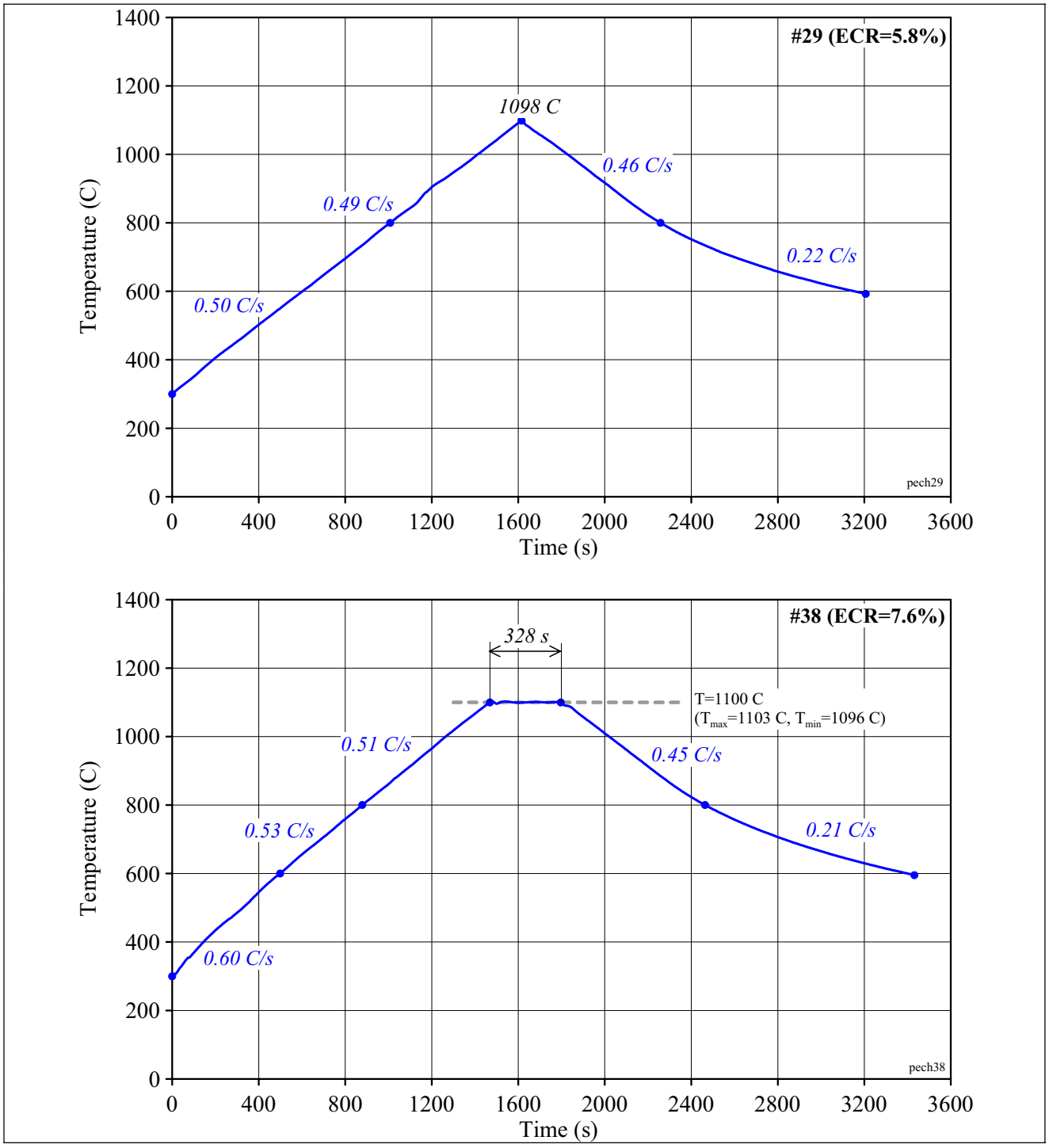

Fig. C-1. Typical temperature histories for cladding samples oxidized at S/S combination of heating and cooling rate

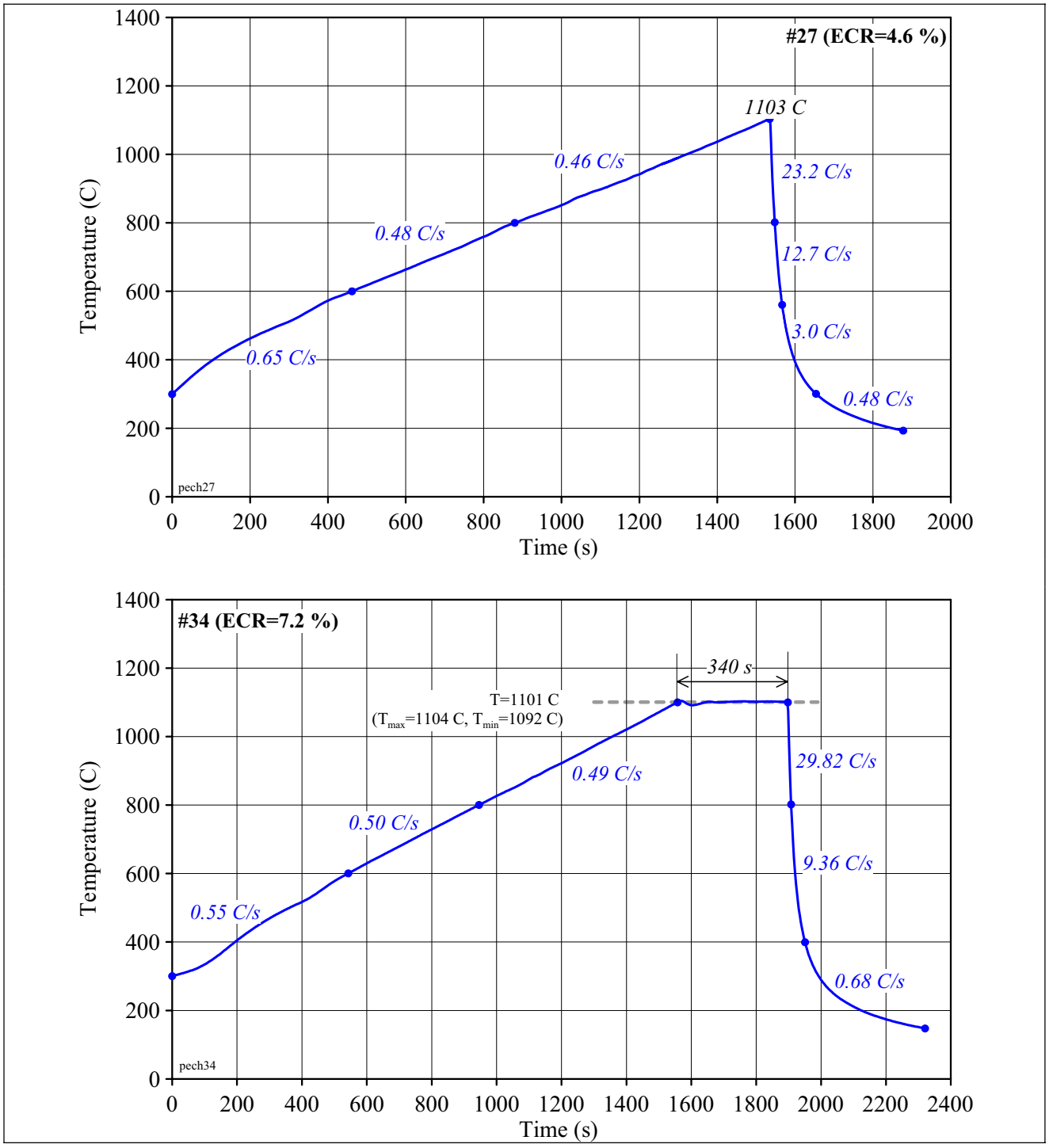

Fig. C-2. Typical temperature histories for cladding samples oxidized at S/F combination of heating and cooling rate

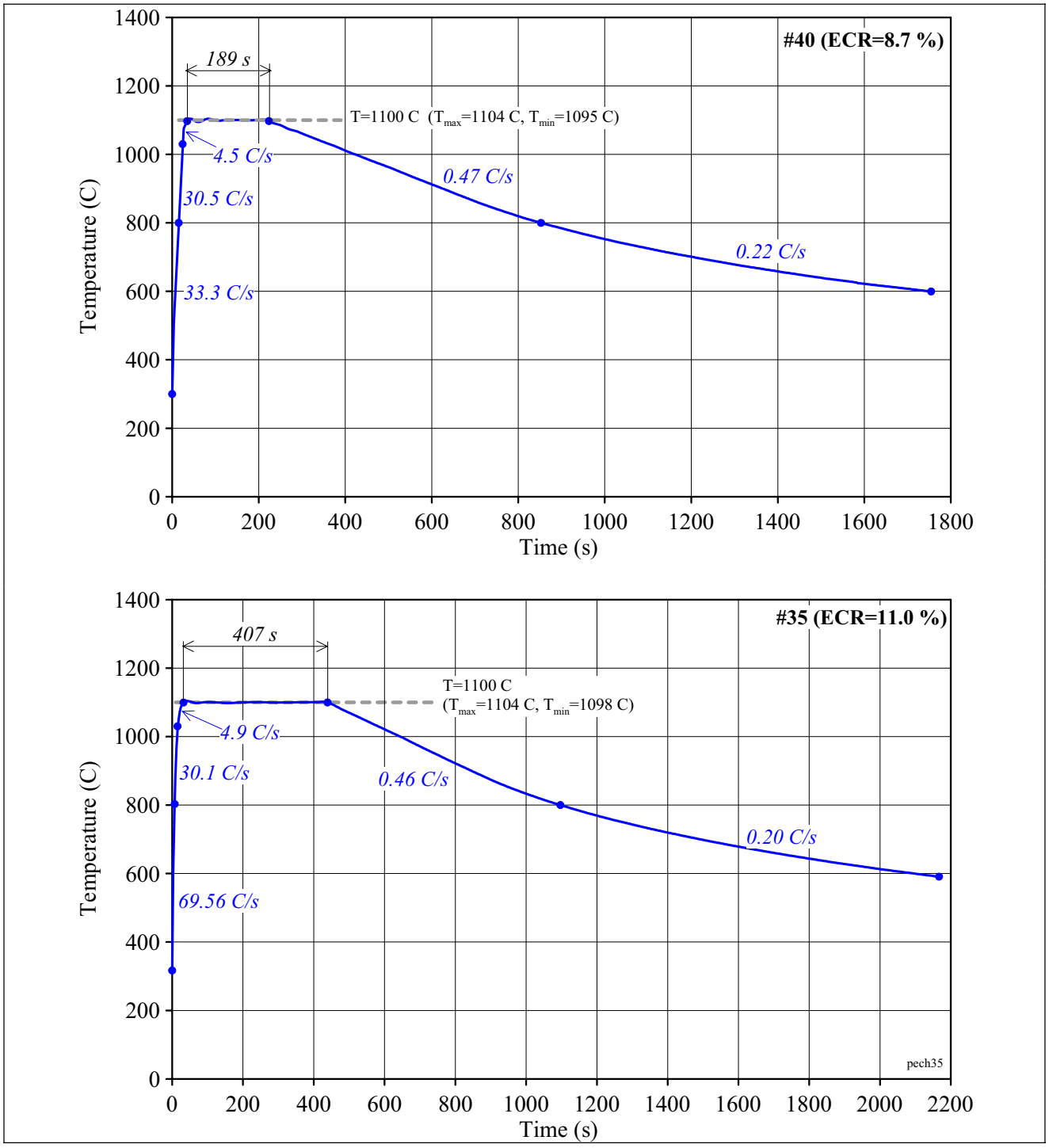

Fig. C-3. Typical temperature histories for cladding samples oxidized at F/S combination of heating and cooling rate

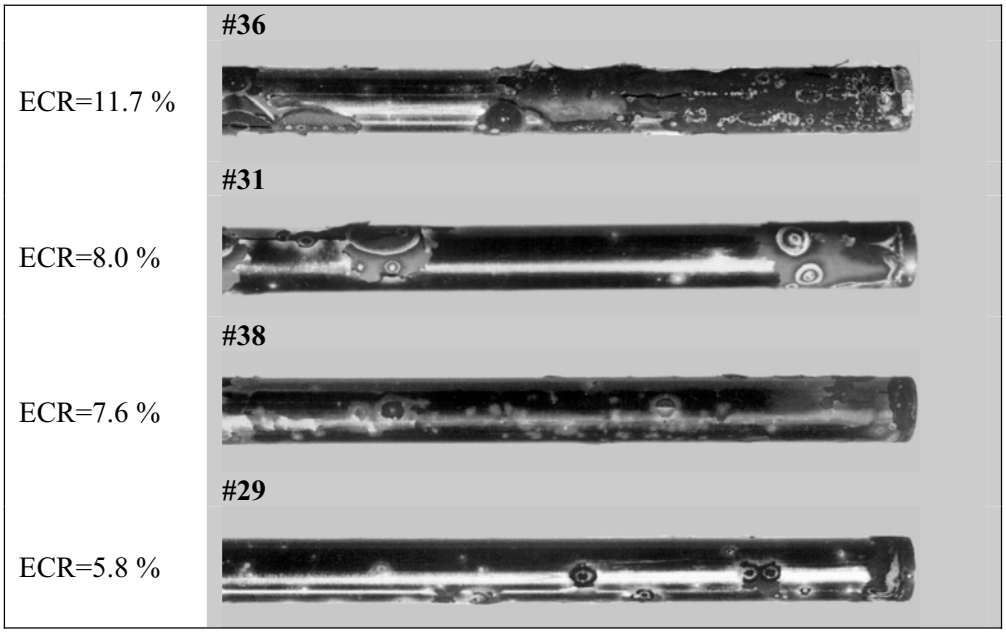

Fig. C-4. Appearance of E110 standard as-received samples as a function of the ECR after a double-sided oxidation at 1100 C and S/S combination of heating and cooling rates

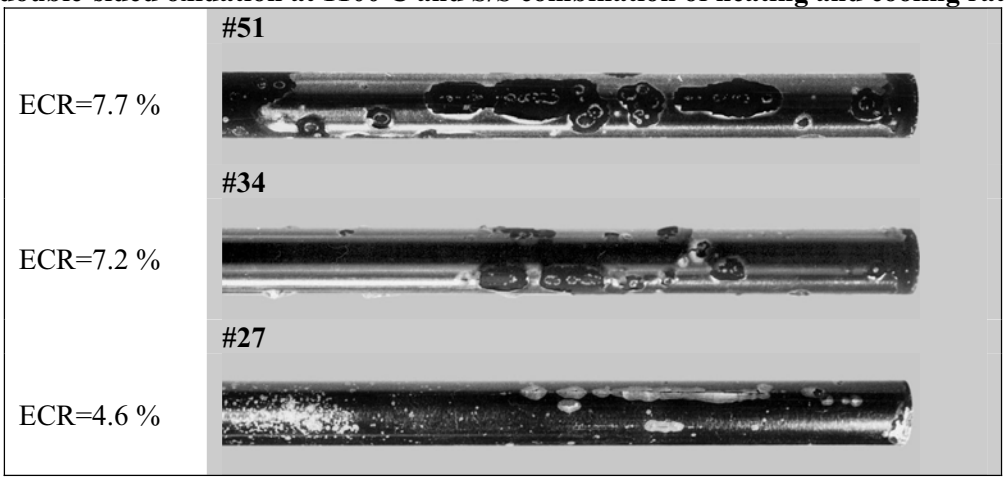

Fig. C-5. Appearance of E110 standard as-received tubes as a function of the ECR after a double-sided oxidation at 1100 C and S/F combination of heating and cooling rates

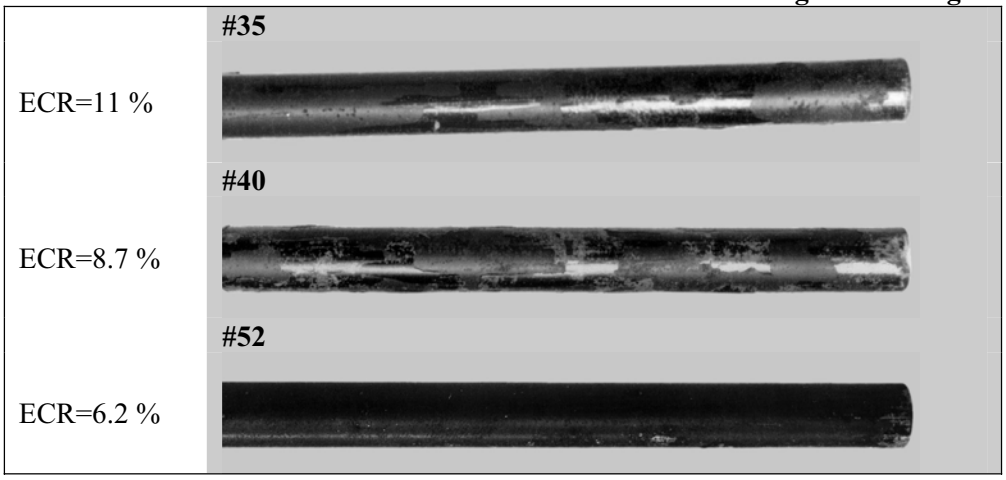

Fig. C-6. Appearance of E110 standard as-received tubes as a function of the ECR after a double-sided oxidation at 1100 C and F/S combination of heating and cooling rates

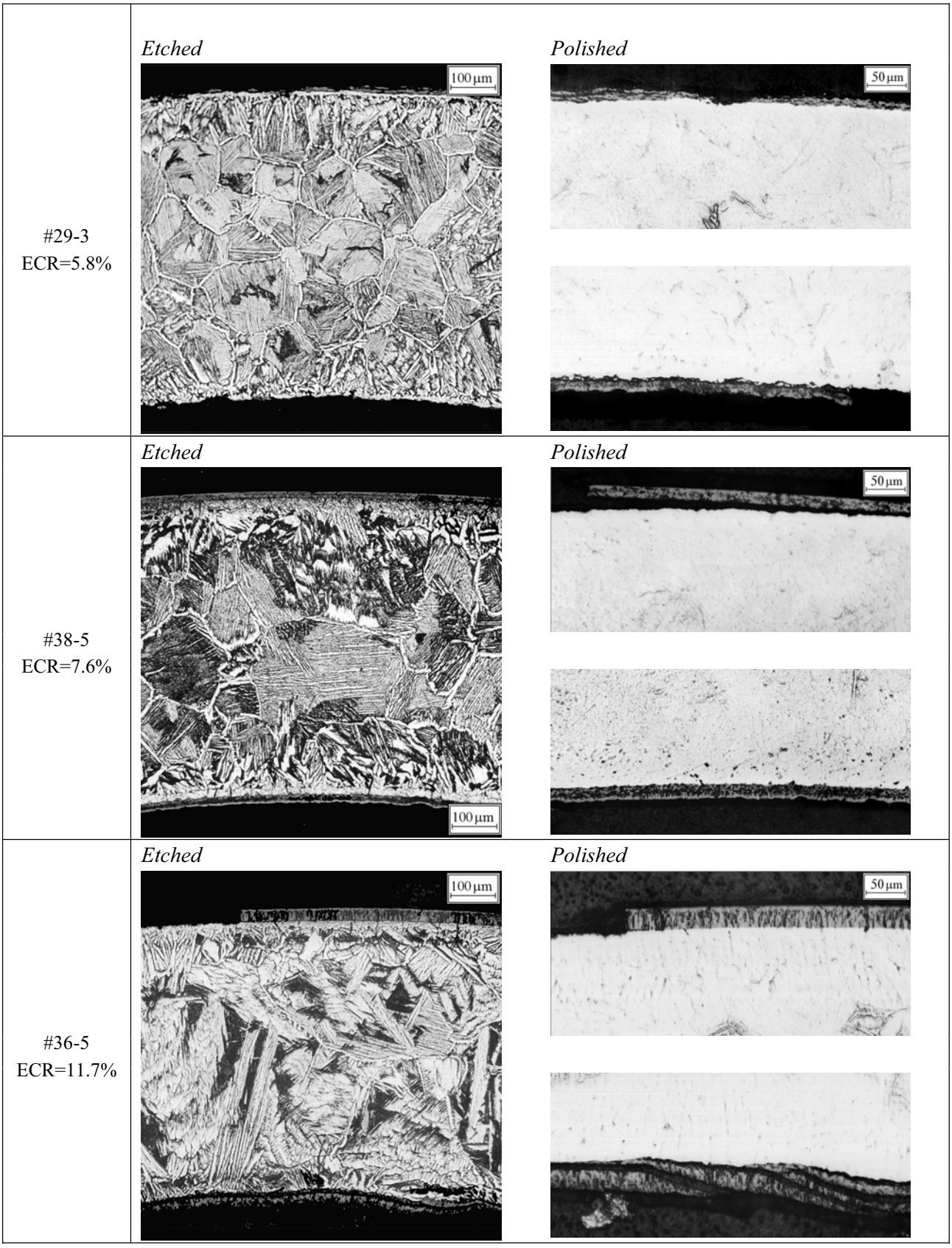

Fig. C-7. Microstructure of E110 standard as-received tubes after a double-sided oxidation at 1100°C and S/S combination of heating and cooling rates

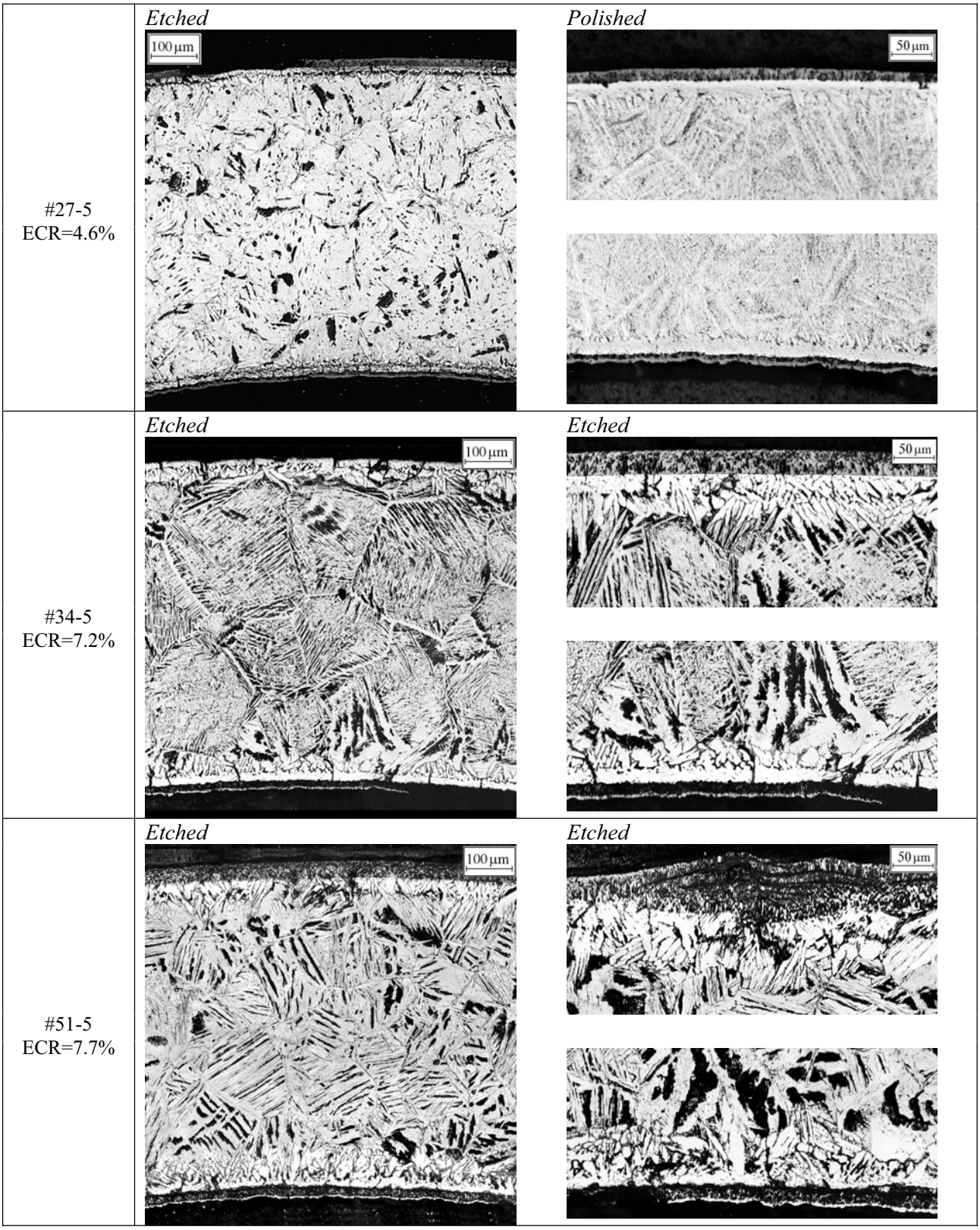

Fig. C-8. Microstructure of E110 standard as-received tubes after a double-sided oxidation at 1100°C and S/F combination of heating and cooling rates

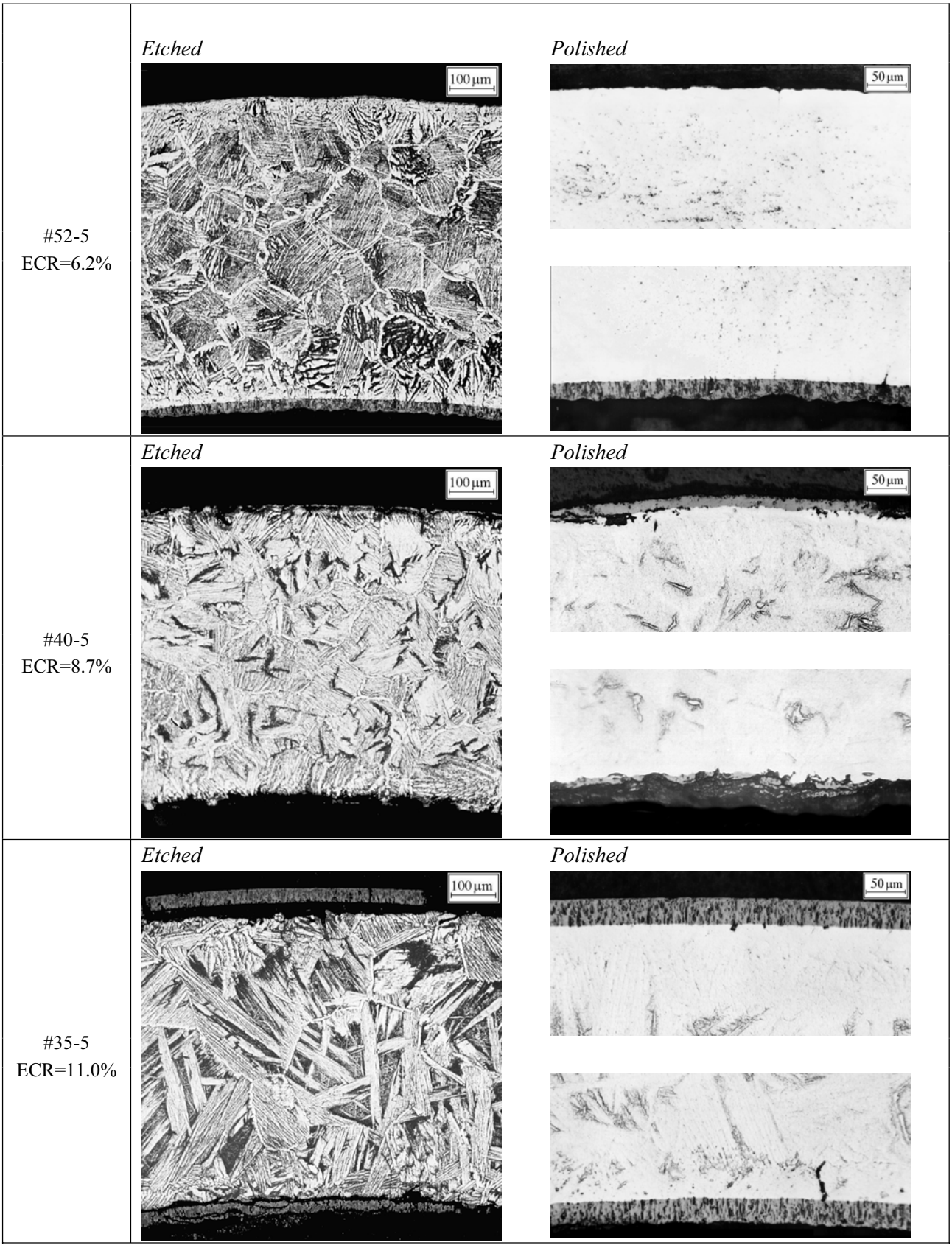

Fig. C-9. Microstructure of E110 standard as-received tubes after a double-sided oxidation at 1100°C and F/S combination of heating and cooling rates

APPENDIX D

Temperature Histories, Appearances and Microstructures of E110 Standard As-received Tubes after a Double-sided Oxidation at 800, 900, 950, 1000, 1100, 1200 C and F/F (F/Q) Combinations of Heating and Cooling Rates

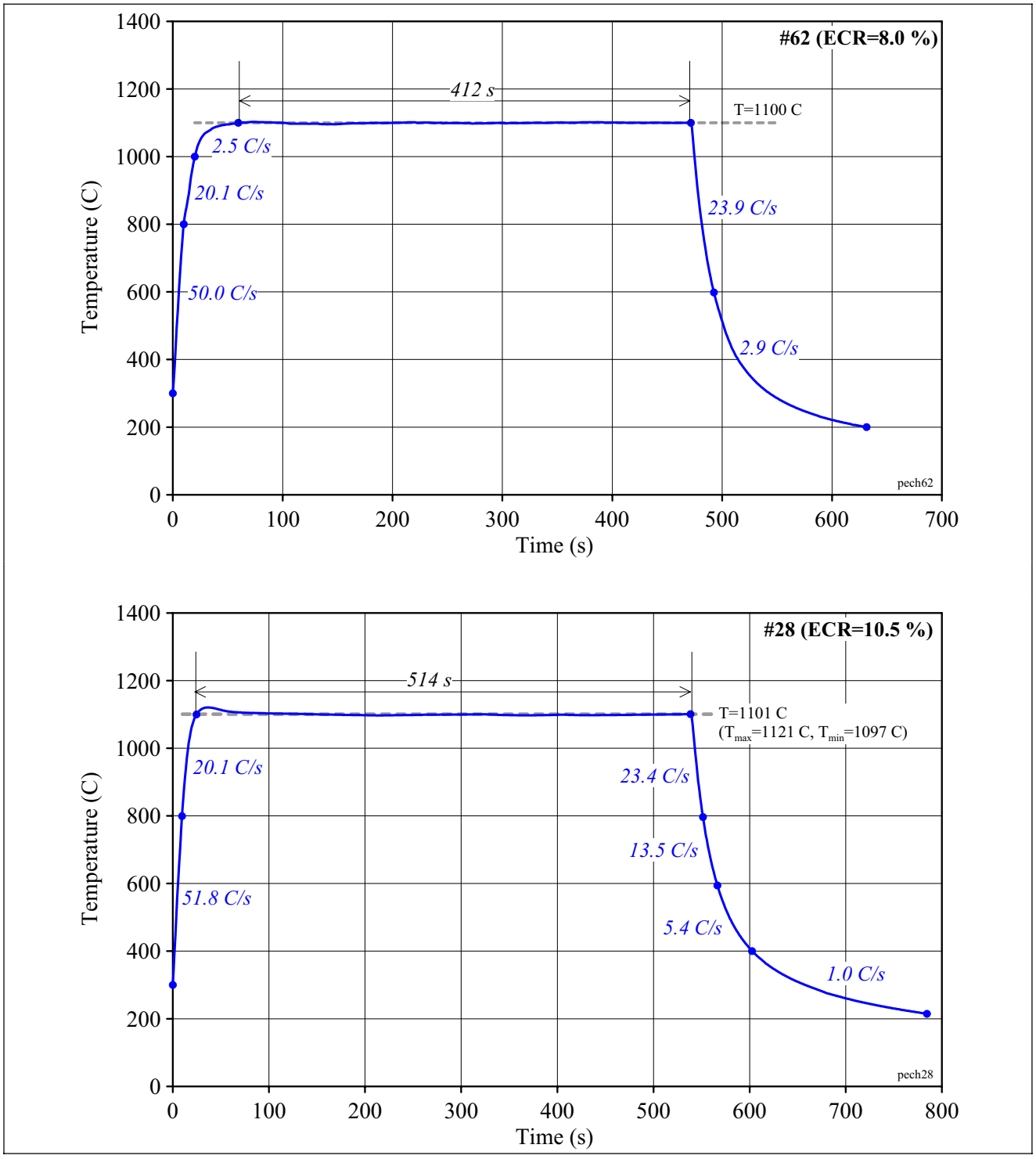

Fig. D-1. Typical temperature histories for cladding samples oxidized at F/F combination of heating and cooling rate

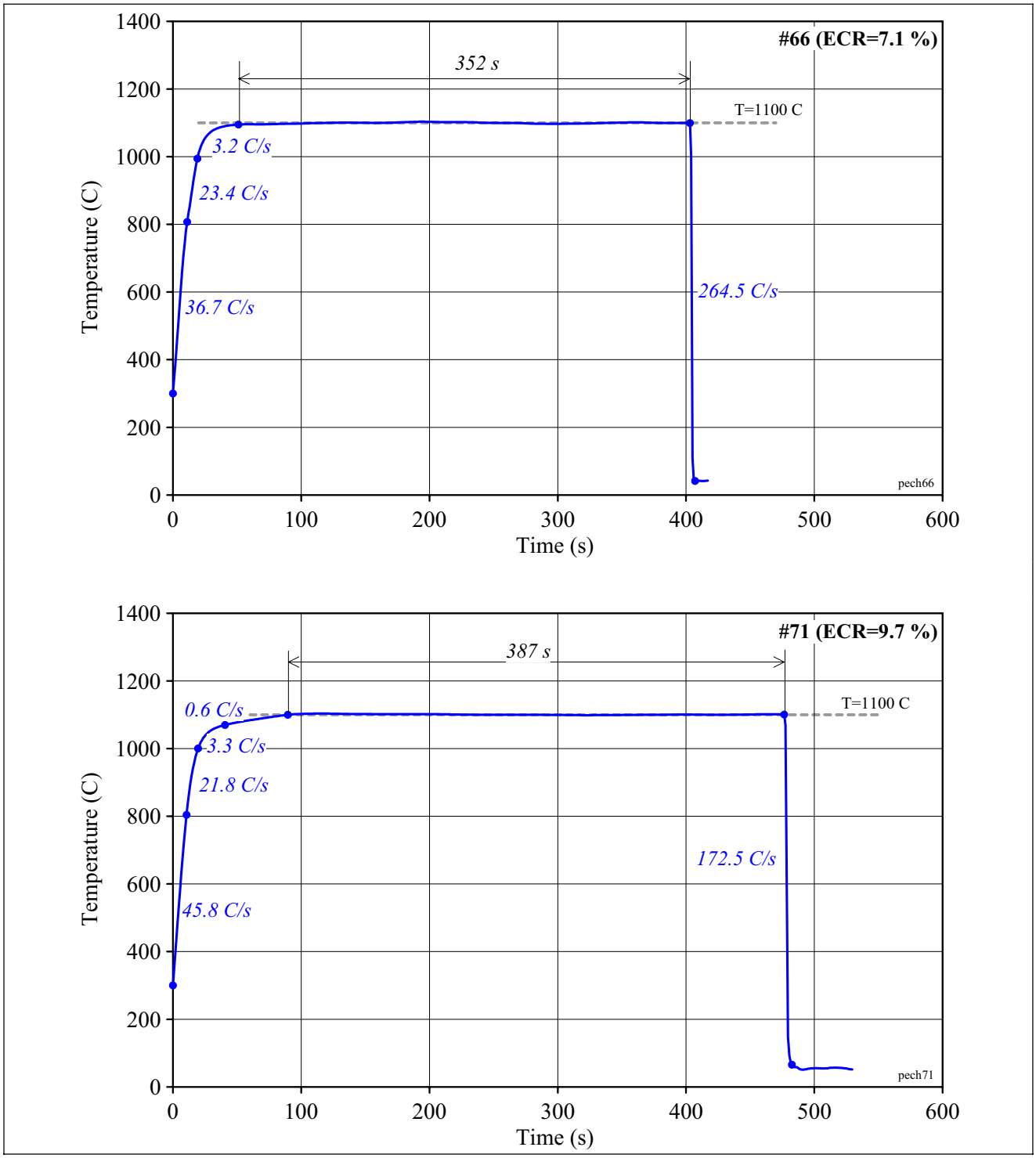

Fig. D-2. Typical temperature histories for cladding samples oxidized at F/Q combination of heating and cooling rate

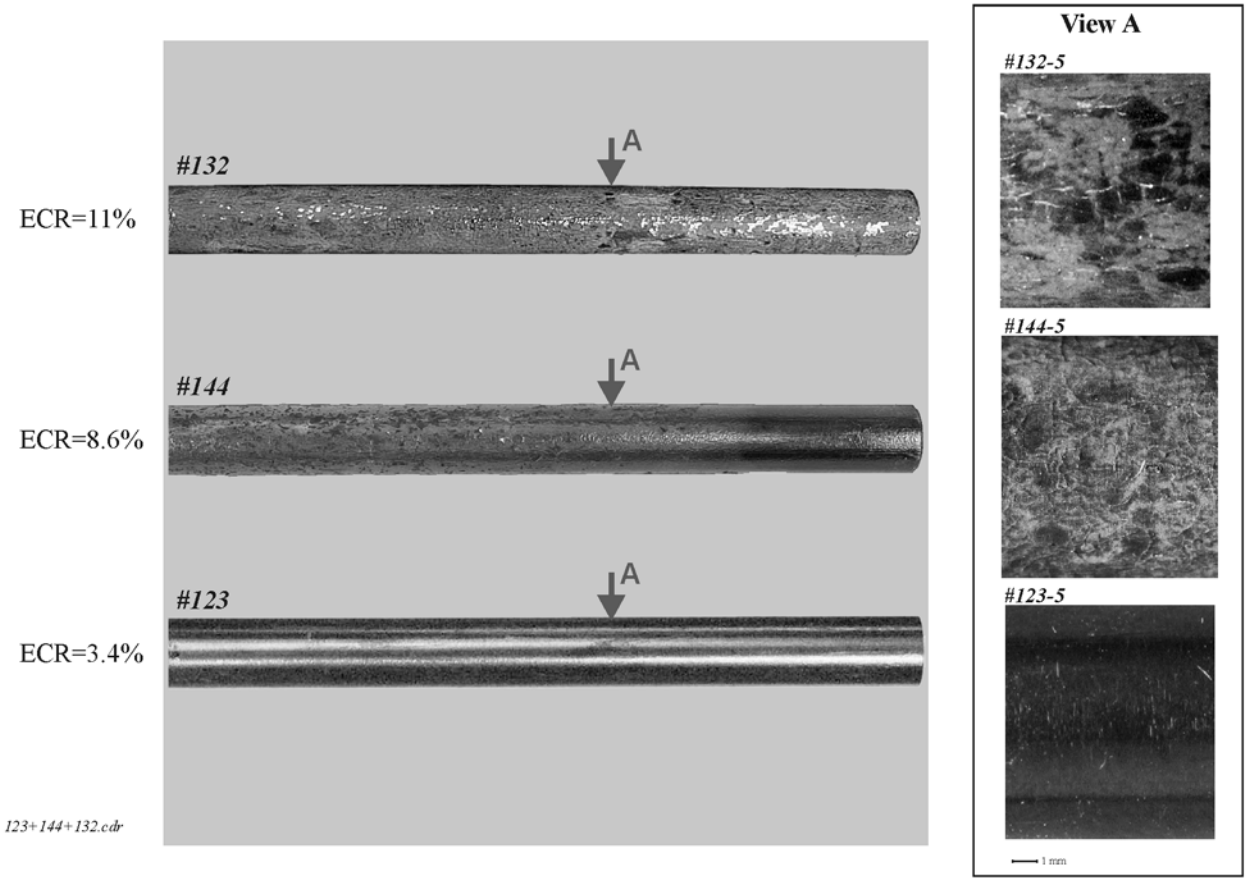

Fig. D-3. Appearance of E110 standard as-received tubes as a function of the ECR after a double-sided oxidation at 800 C and F/F combination of heating and cooling rates

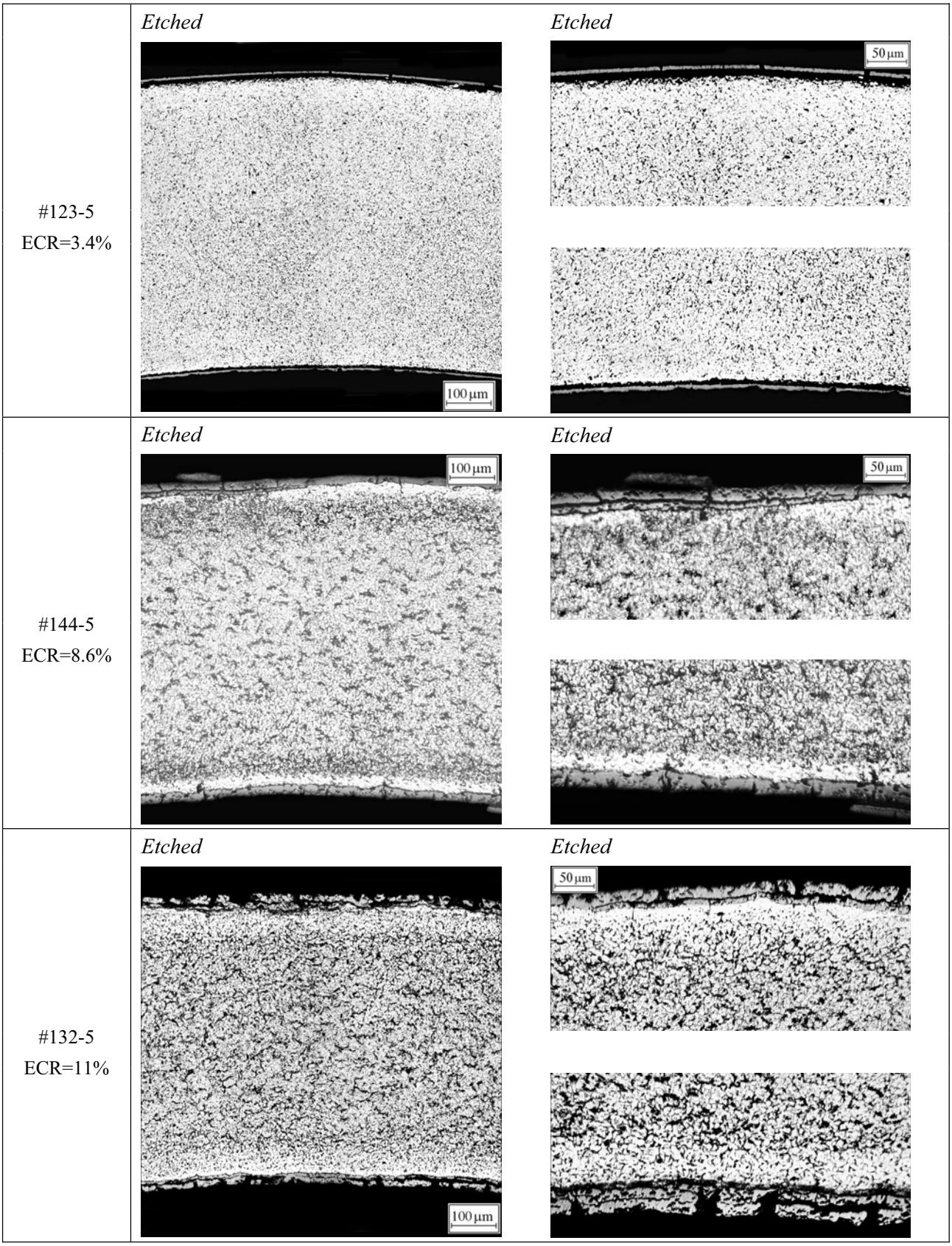

Fig. D-4. Microstructure of E110 standard as-received tubes after a double-sided oxidation at 800°C and F/F combination of heating and cooling rates

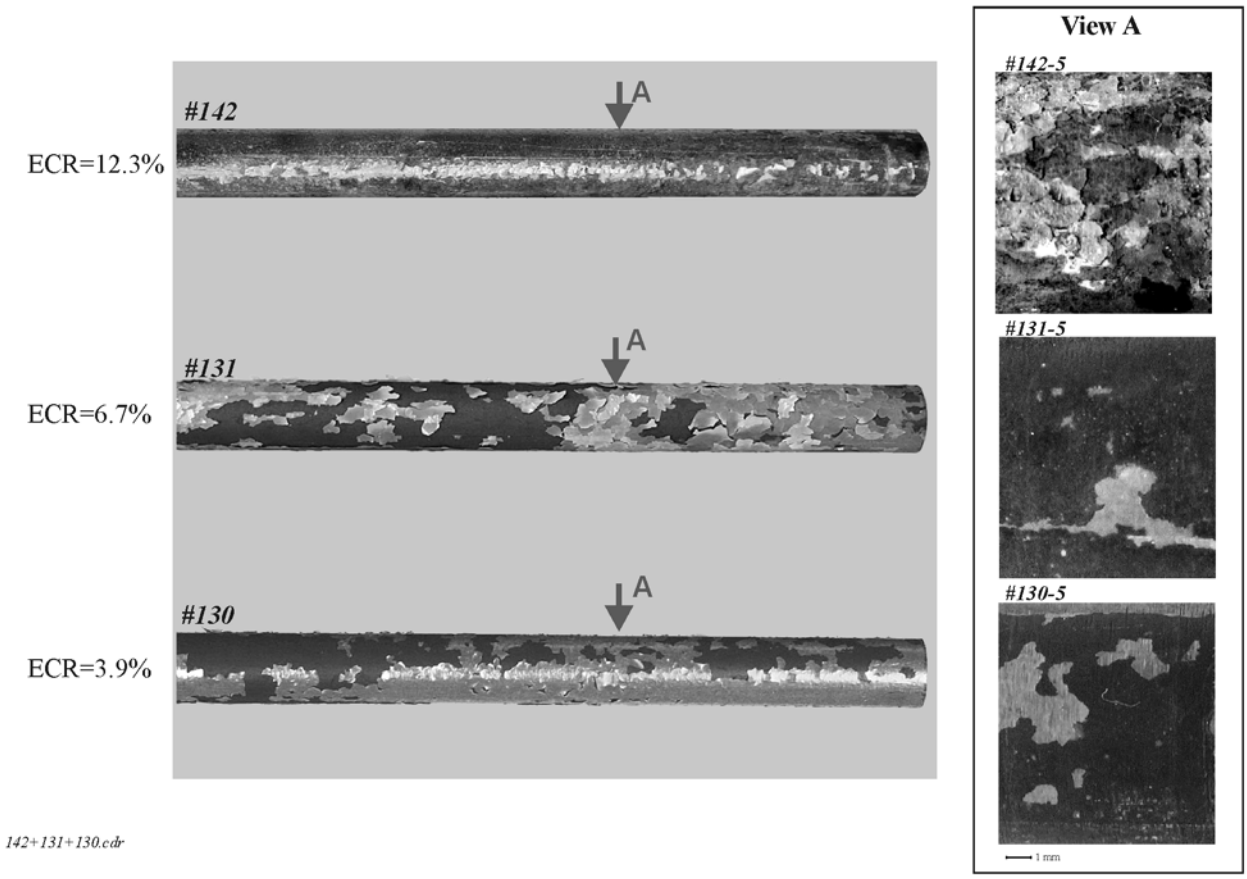

Fig. D-5. Appearance of E110 standard as-received tubes as a function of the ECR after a double-sided oxidation at 900 C and F/F combination of heating and cooling rates

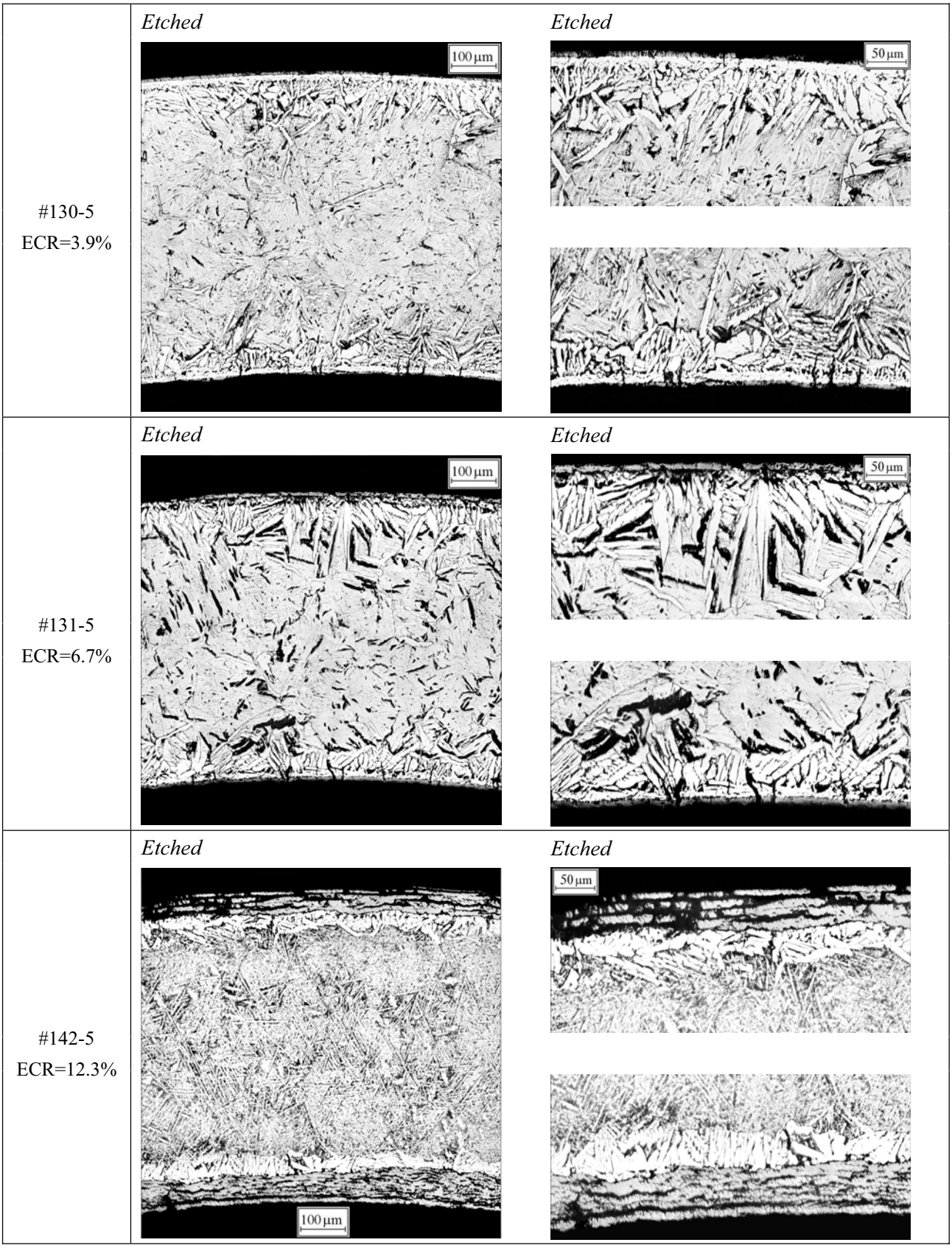

Fig. D-6. Microstructure of E110 standard as-received tubes after a double-sided oxidation at 900°C and F/F combination of heating and cooling rates

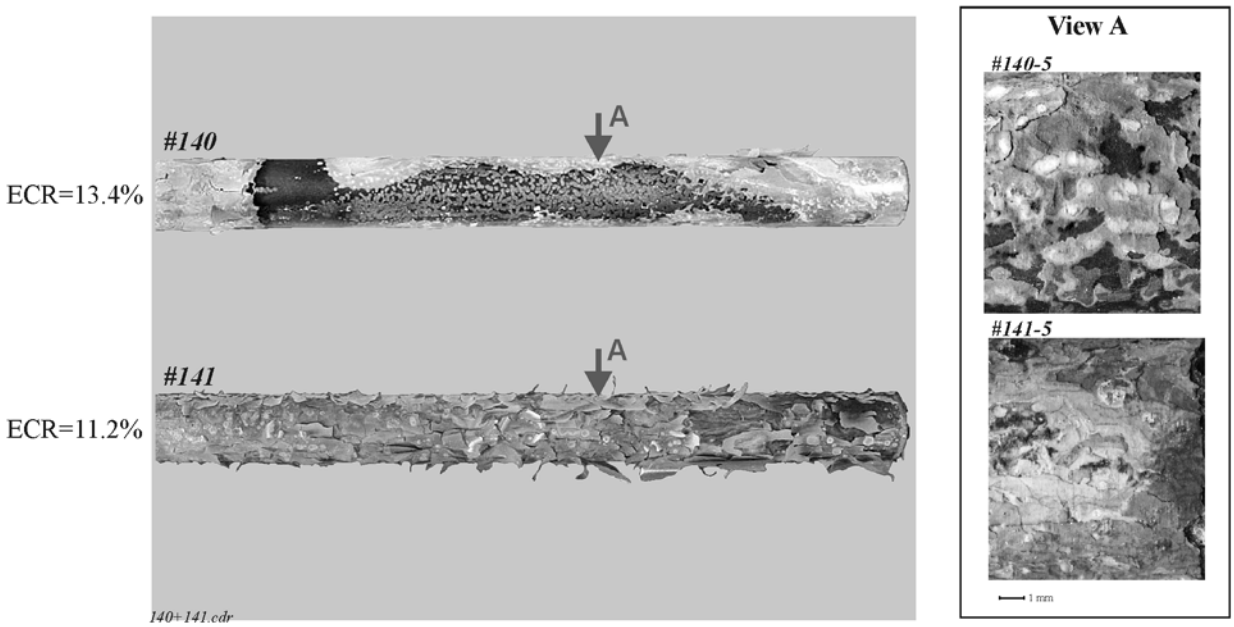

Fig. D-7. Appearance of E110 standard as-received tubes as a function of the ECR after a double-sided oxidation at 950 C and F/F combination of heating and cooling rates

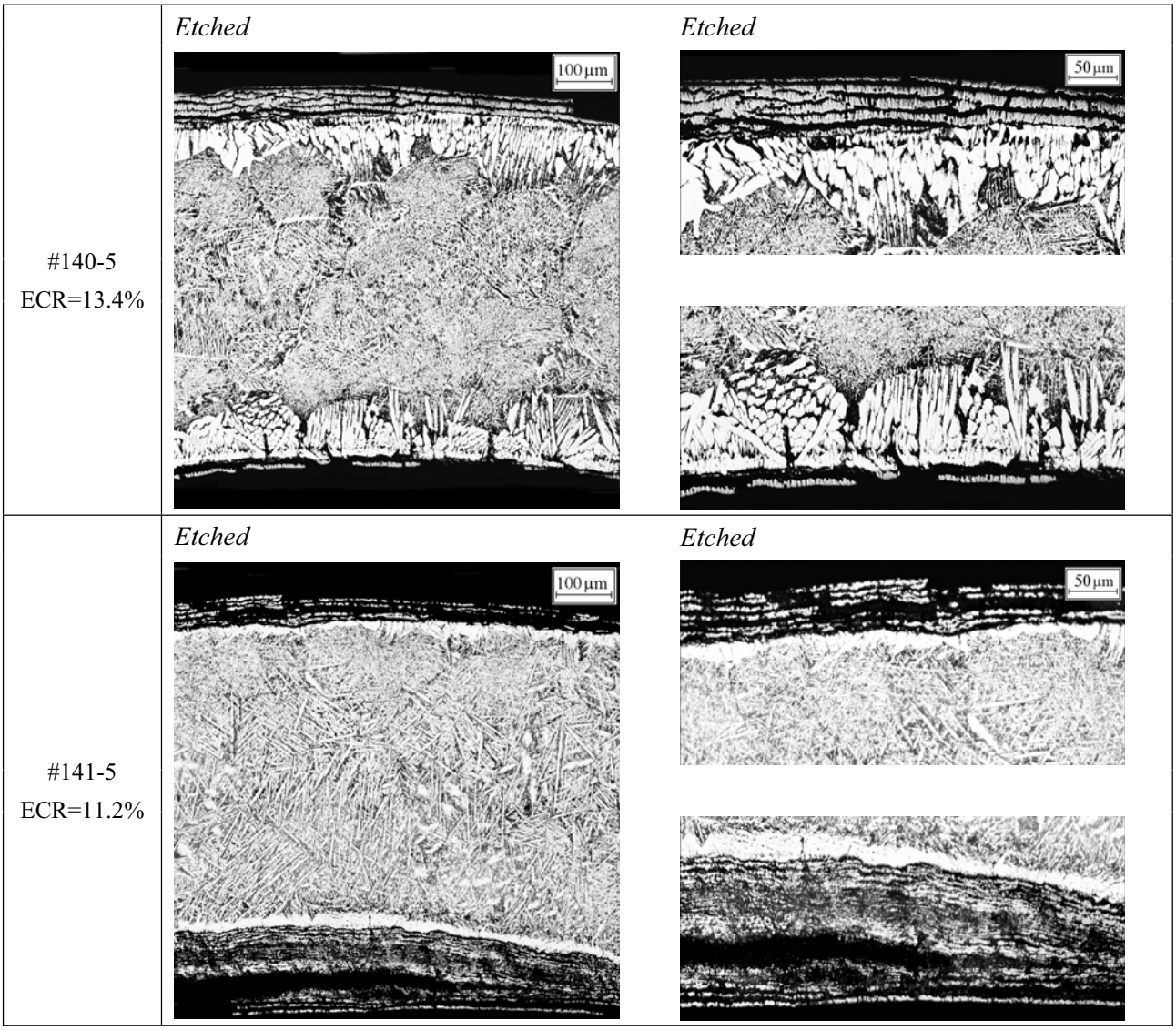

Fig. D-8. Microstructure of E110 standard as-received tubes after a double-sided oxidation at 950°C and F/F combination of heating and cooling rates

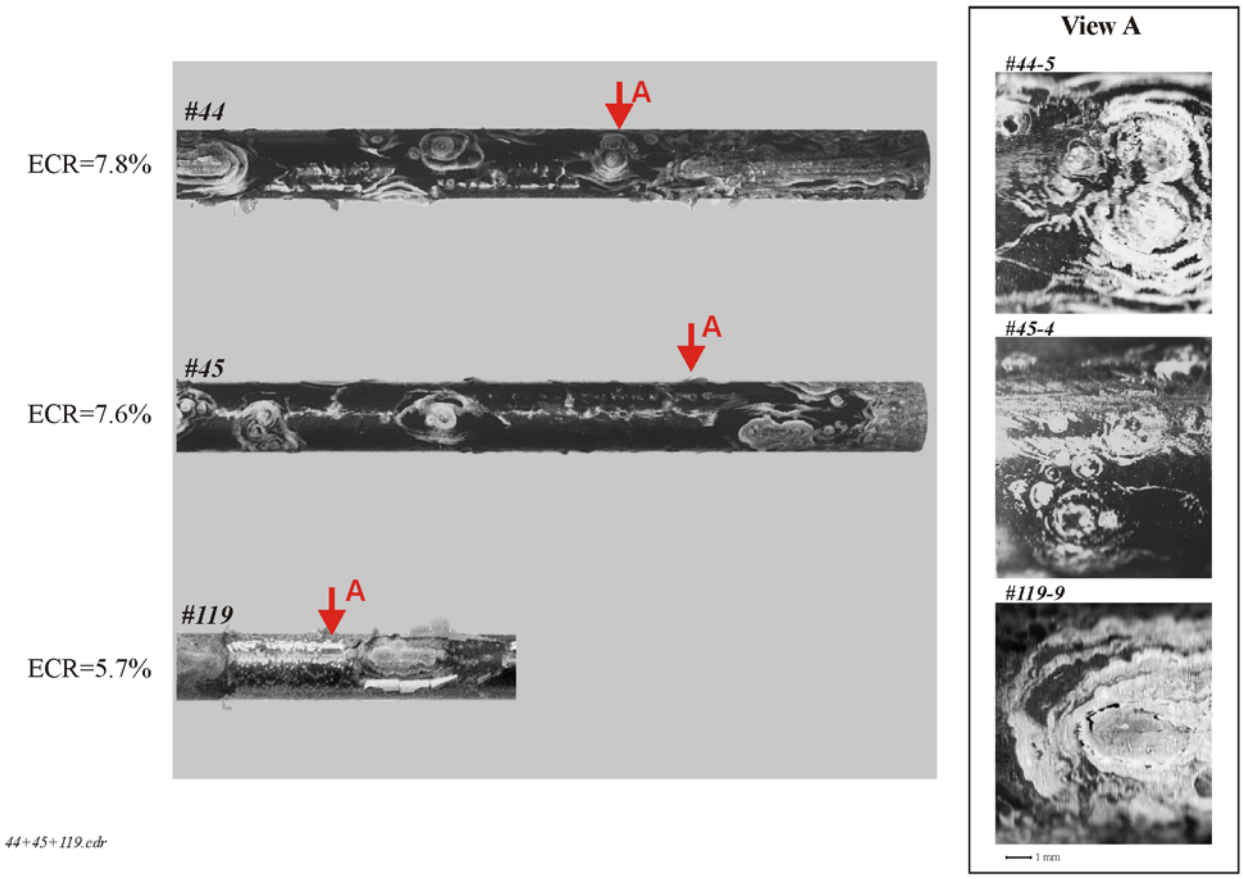

Fig. D-9. Appearance of E110 standard as-received tubes as a function of the ECR after a double-sided oxidation at 1000 C and F/F combination of heating and cooling rates

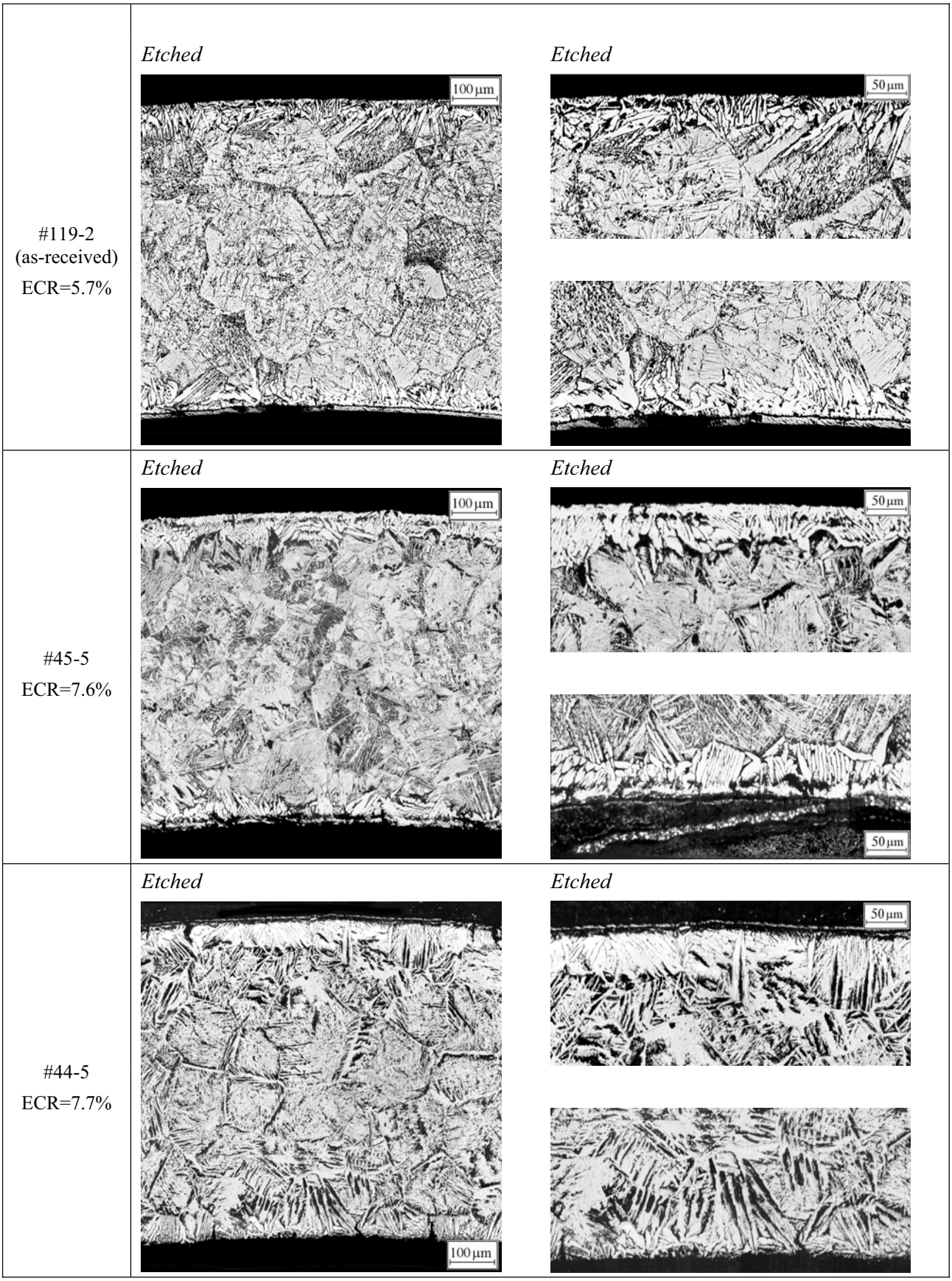

Fig. D-10. Microstructure of E110 standard as-received tubes after a double-sided oxidation at 1000°C and F/F combination of heating and cooling rates

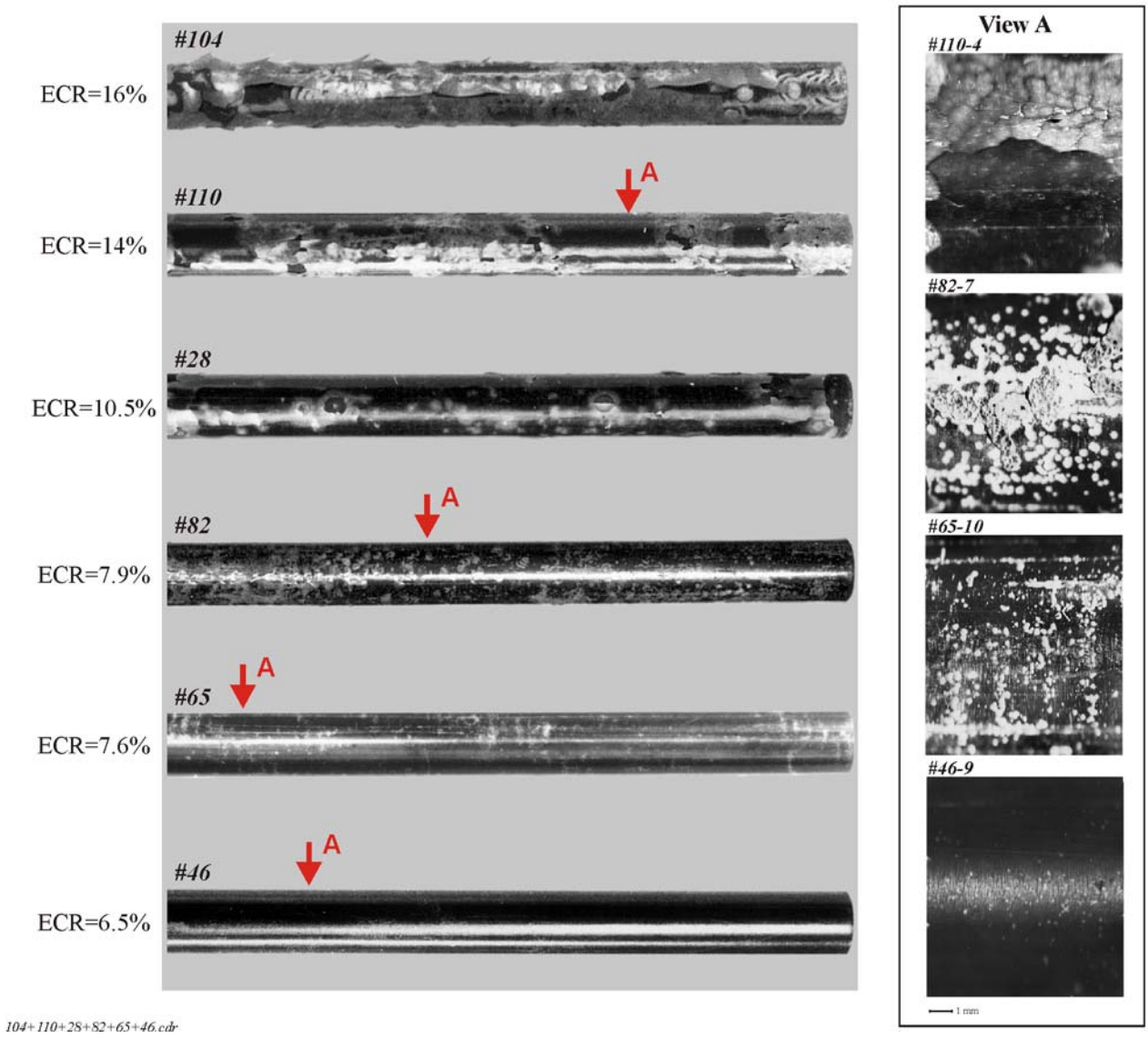

Fig. D-11. Appearance of E110 standard as-received tubes as a function of the ECR after a double-sided oxidation at 1100 C and F/F combination of heating and cooling rates

Etched

#46-5 ECR=6.5 %

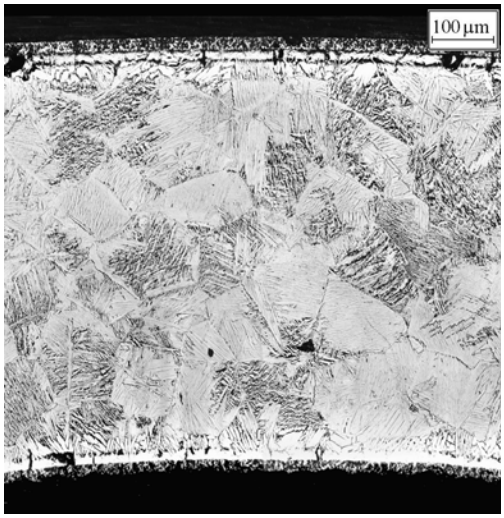

#65-5 ECR=7.6 %

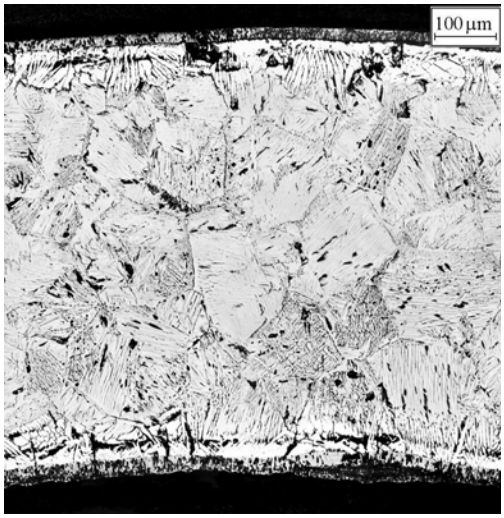

#41-5 ECR=8.2 %

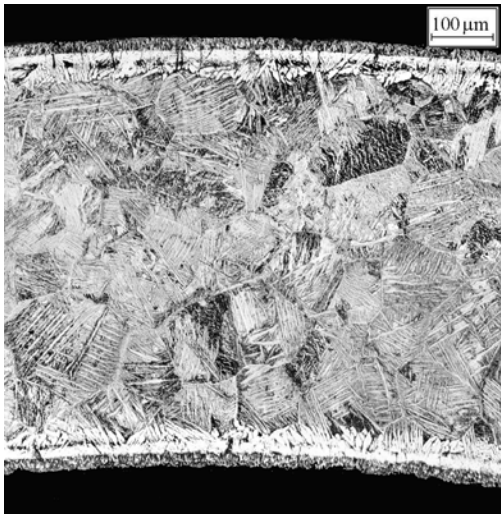

#30-5 ECR=8.9 %

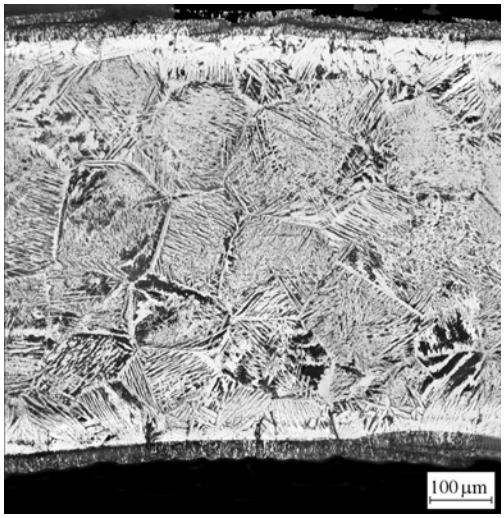

#68-5 ECR=10.0 %

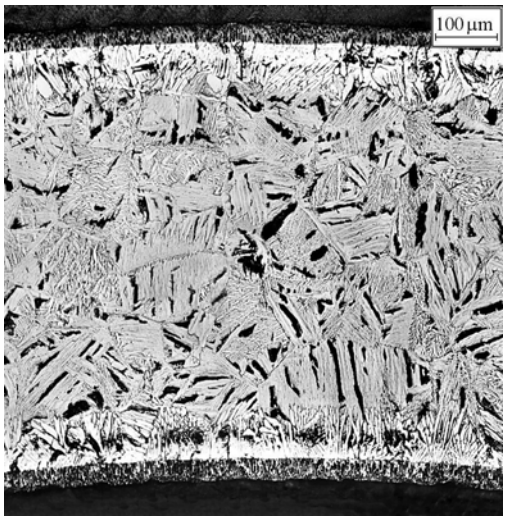

#110-5 ECR=14.0 %

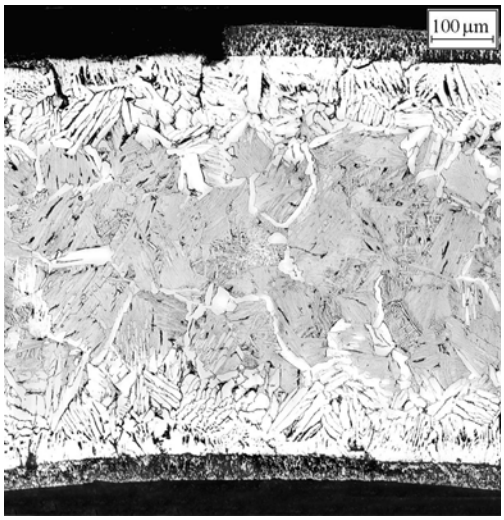

Fig. D-12. Microstructure of E110 standard as-received tubes after a double-sided oxidation at 1100 C and F/F combination of heating and cooling rates (ECR=6.5–14 %)

Sample	External surface (Etched)	Internal surface
#46-5 ECR=6.5 %	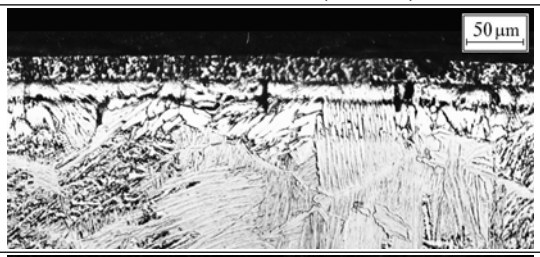	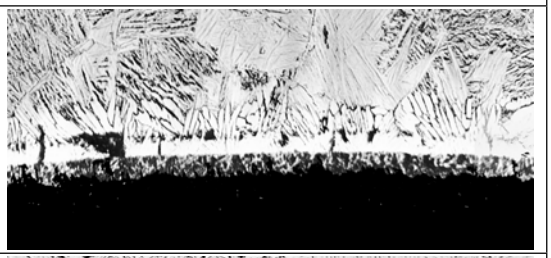
#65-5 ECR=7.6 %	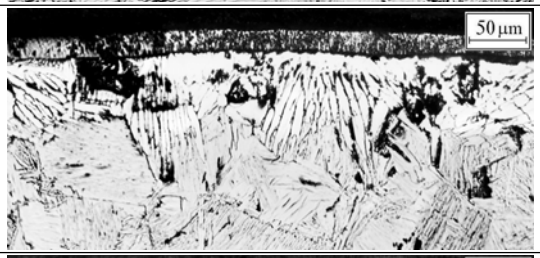	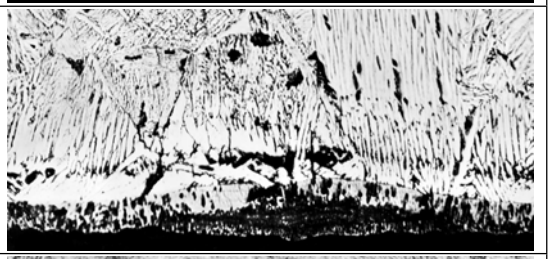
#81-5 ECR=8.1 %	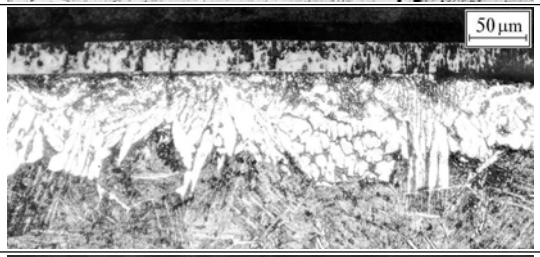	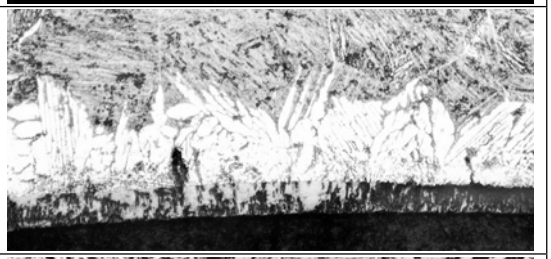
#30-5 ECR=8.9 %		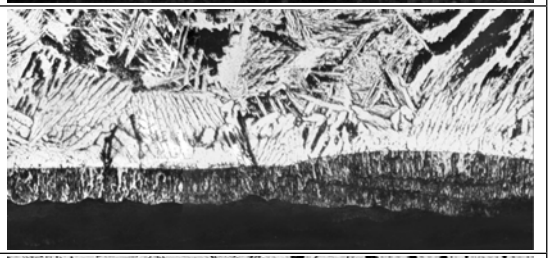
#68-5 ECR=10 %	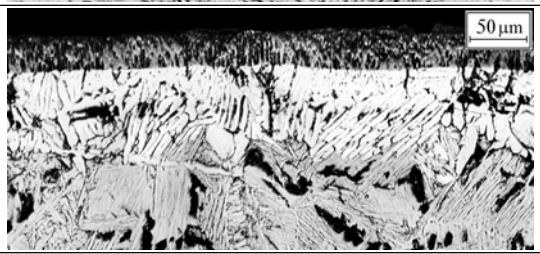	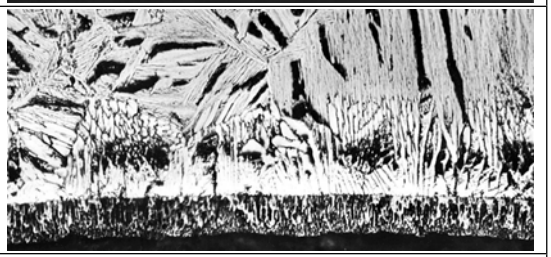
#110-5 ECR=14 %	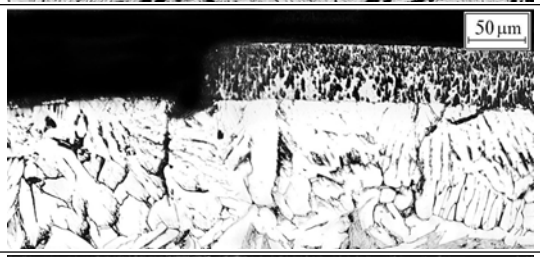	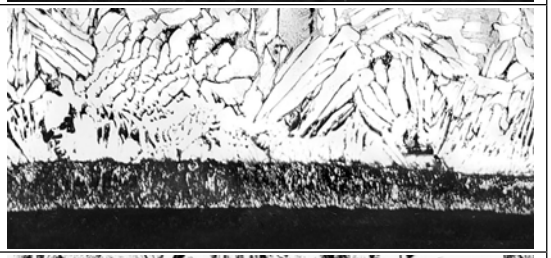
#104-5 ECR=16 %	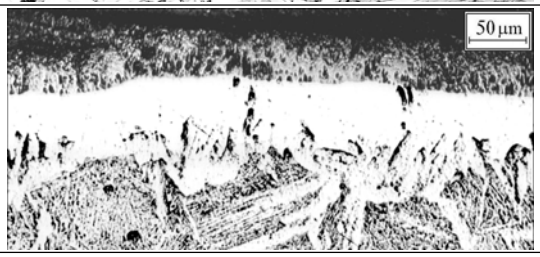	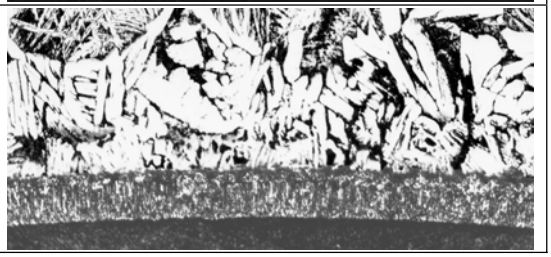

Fig. D-13. Microstructure of ZrO_2 and α-Zr(O) layers in E110 standard as-received tubes after a double-sided oxidation at 1100 C and F/F combination of heating and cooling rates

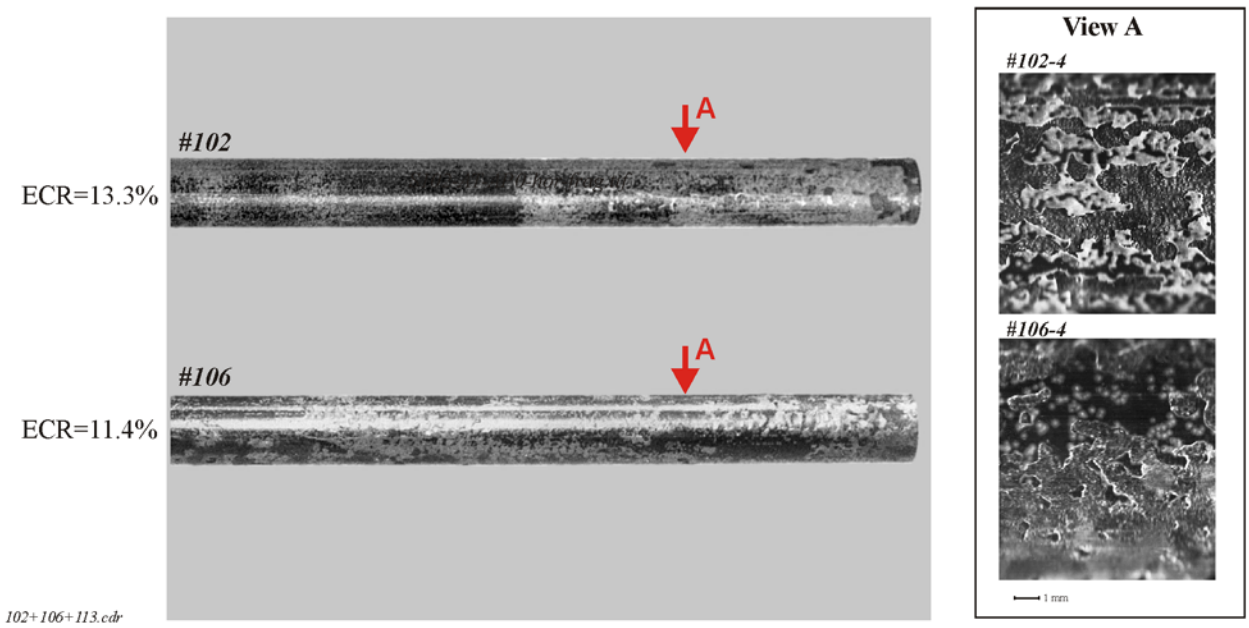

Fig. D-14. Appearance of E110 standard as-received tubes as a function of the ECR after a double-sided oxidation at 1200 C and F/F combination of heating and cooling rates

#106-4	ECR=11.5 %	#102-4	ECR=13.3 %
Etched 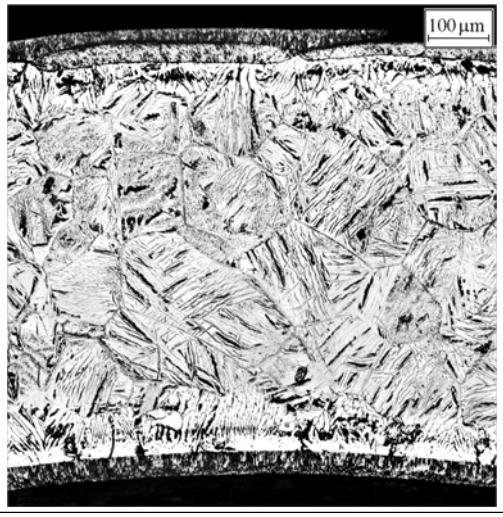		*Etched* 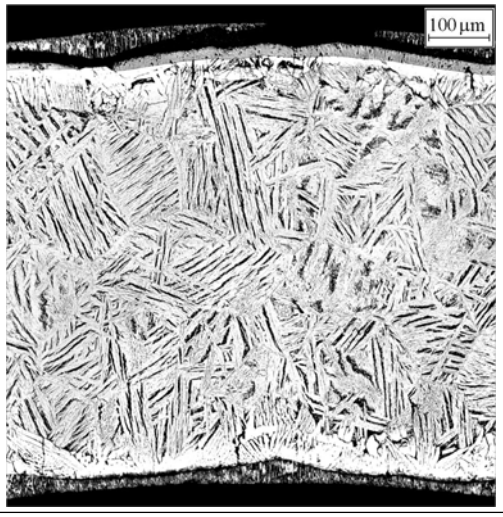	
Etched 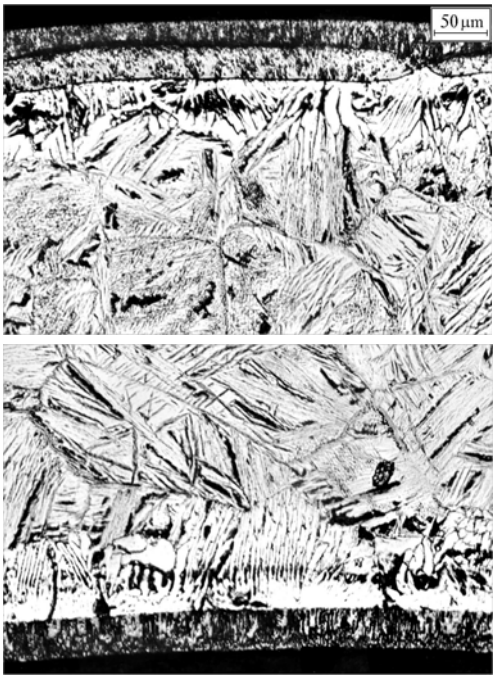		*Etched* 	

Fig. D-15. Microstructure of E110 standard as-received tubes after a double-sided oxidation at 1200°C and F/F combination of heating and cooling rates

APPENDIX E

Appearance and Microstructure of E110 Standard As-received Tubes after a Single-sided Oxidation at 1100 C and F/F Combination of Heating and Cooling Rates

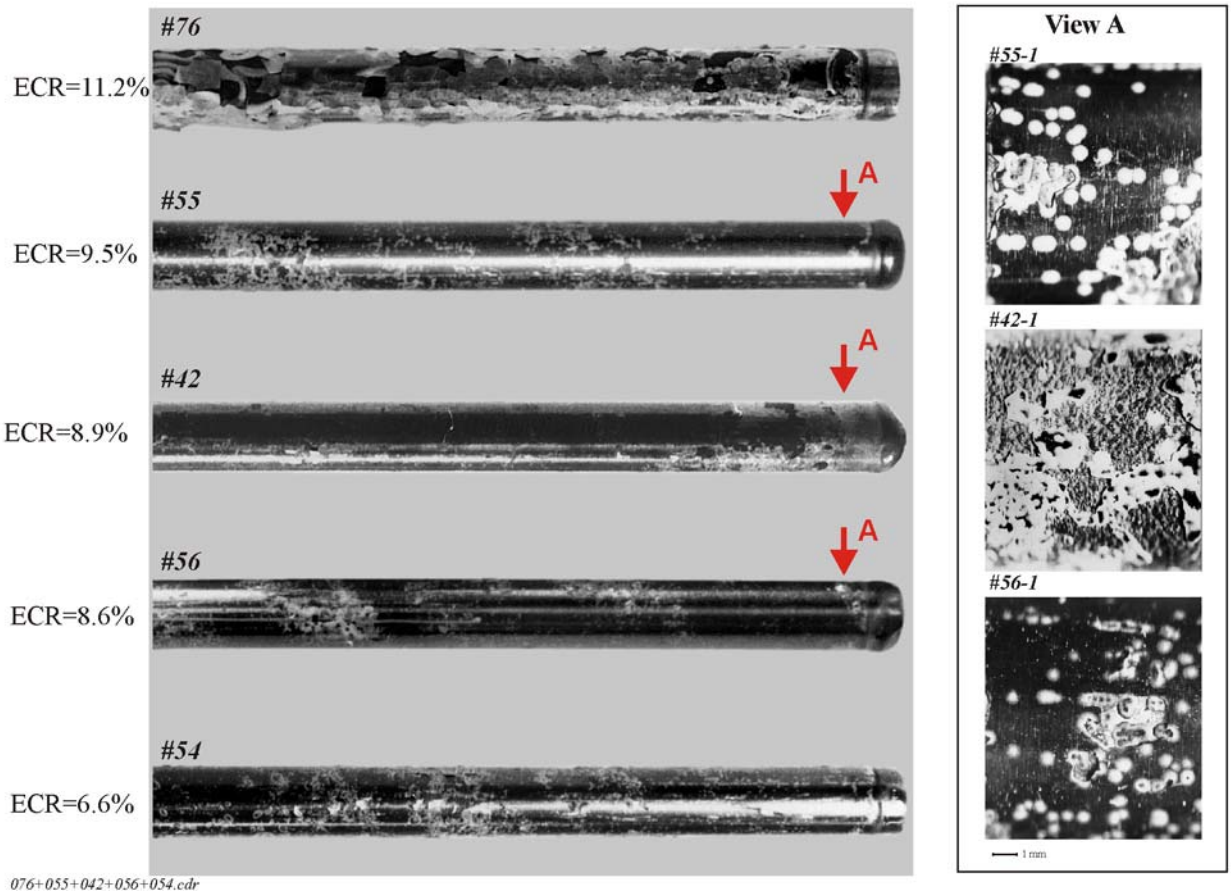

Fig. E.1. Appearance of E110 standard as-received tubes as a function of the ECR after single-sided oxidation at 1100 C and F/F combination of heating and cooling rates

#54-5	ECR=6.6 %	#42-5	ECR=8.9 %
Etched		Etched	

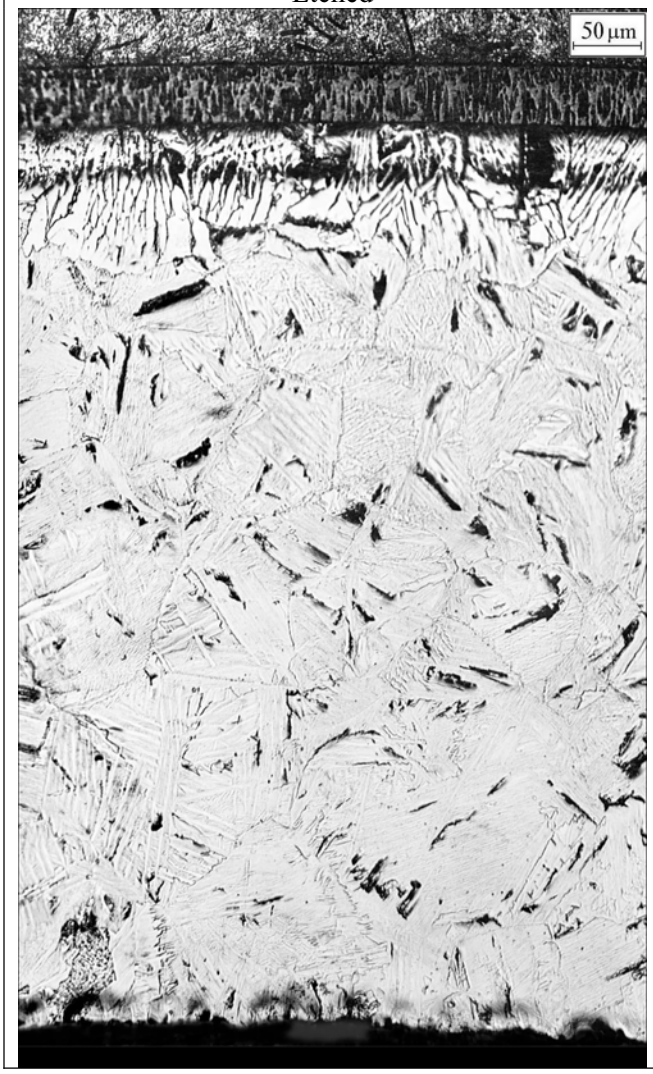

Fig. E.2. Microstructure of E110 standard as-received tubes after a single-sided oxidation at 1100 C and F/F combination of heating and cooling rates

APPENDIX F

Appearances and Microstructures of E635 Standard As-received Tubes after a Double-sided Oxidation at 1000, 1100 C and F/F Combination of Heating and Cooling Rates

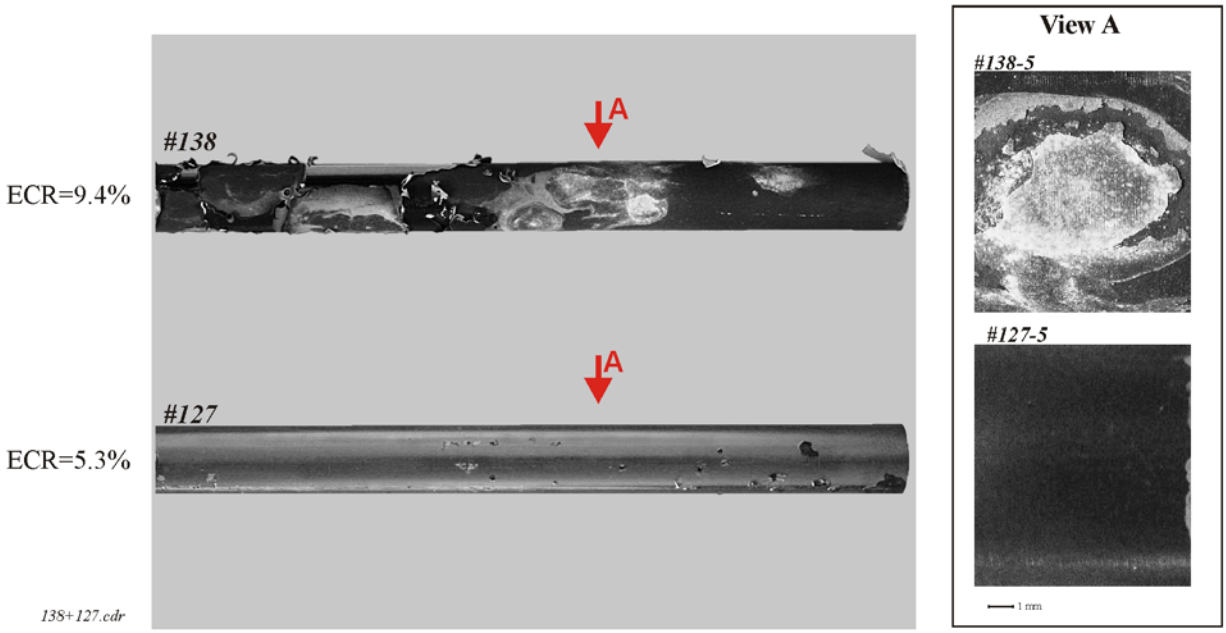

Fig. F-1. Appearance of E635 standard as-received tubes as a function of the ECR after a double-sided oxidation at 1000 C and F/F combination of heating and cooling rates

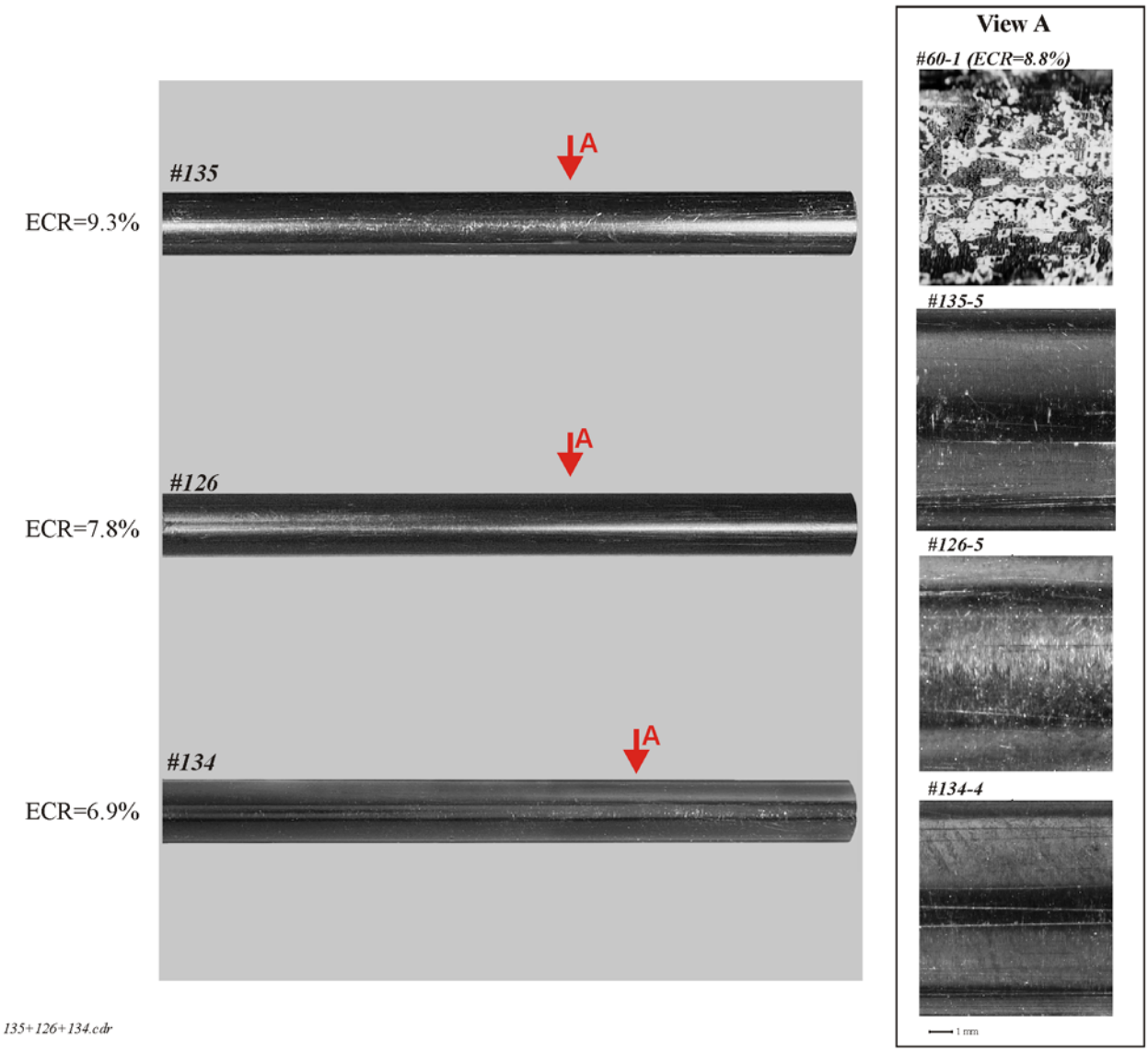

Fig. F-2. Appearance of E635 standard as-received tubes as a function of the ECR after a double-sided oxidation at 1100 C and F/F combination of heating and cooling rates

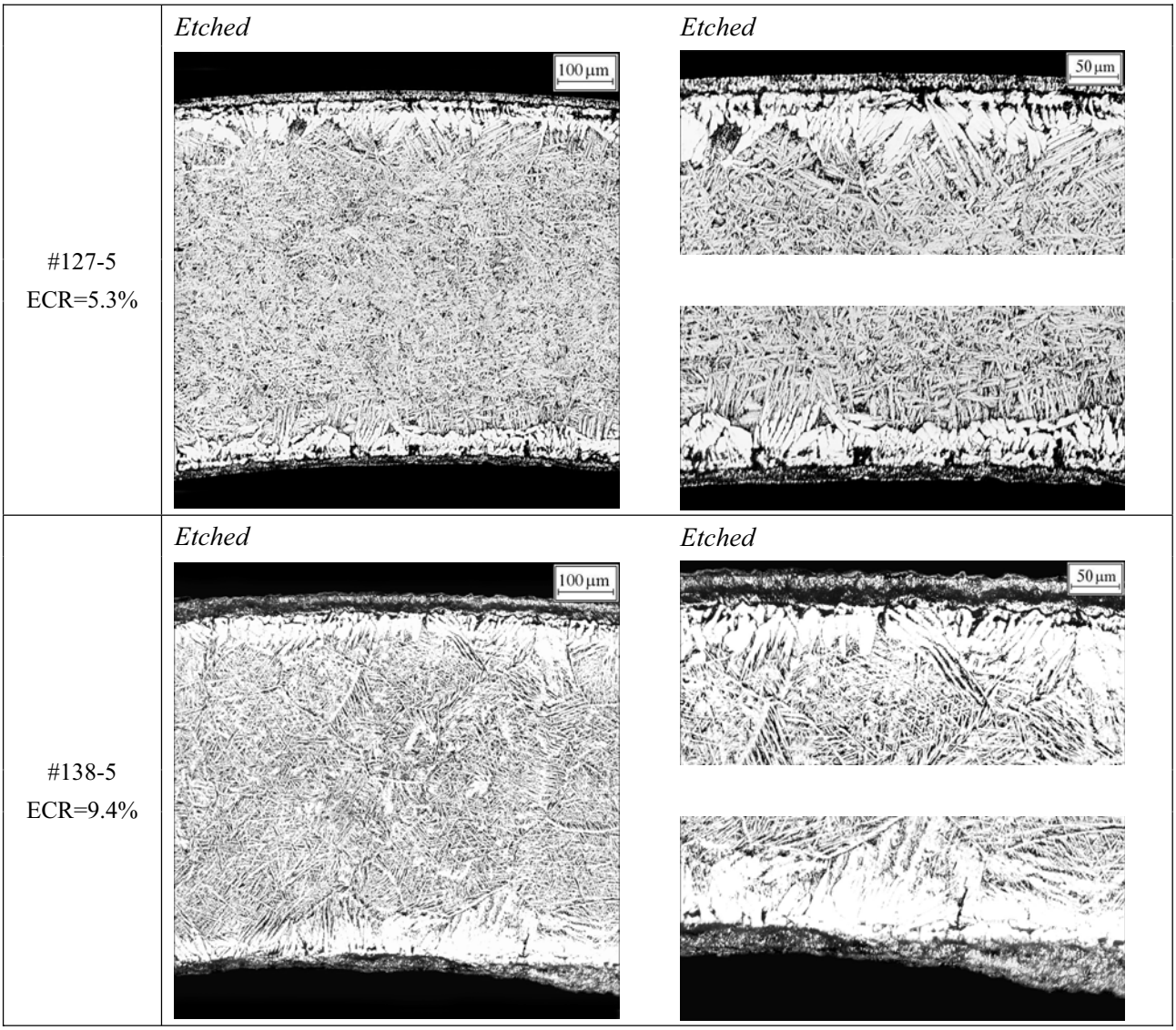

Fig. F-3. Microstructure of E635 standard as-received tubes after a double-sided oxidation at 1000 C and F/F combination of heating and cooling rates

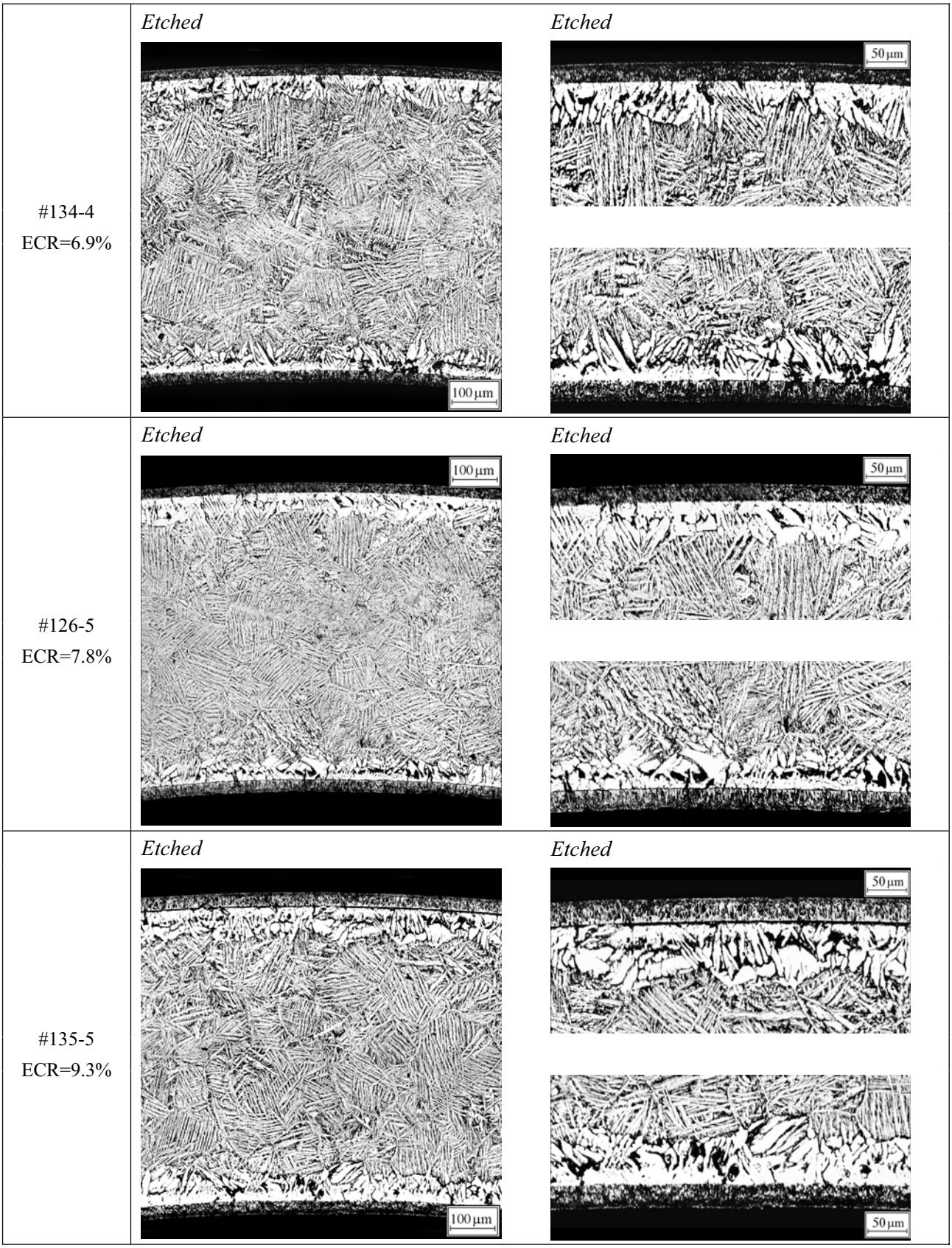

Fig. F-4. Microstructure of E635 standard as-received tubes after a double-sided oxidation at 1100 C and F/F combination of heating and cooling rates

APPENDIX G

Appearances and Microstructures of Zry-4 As-received Claddings after a Double-sided Oxidation at 1100 C and S/S, F/F Combinations of Heating and Cooling Rates

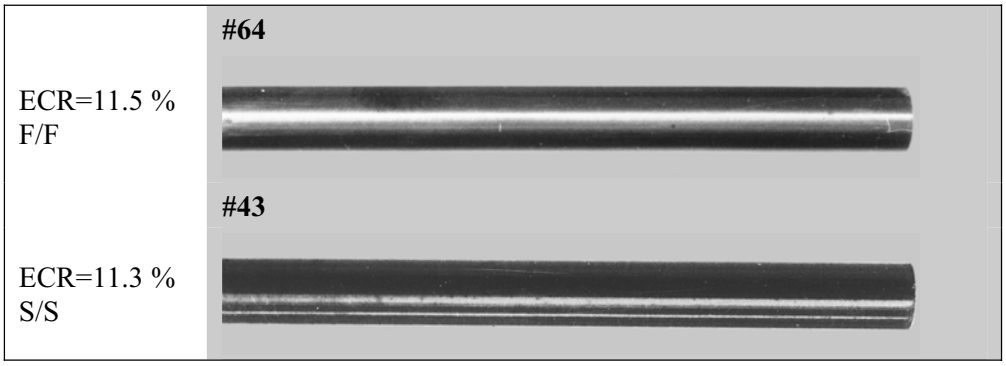

Fig. G-1. Appearance of Zry-4 as-received claddings after a double-sided oxidation at 1100 C and S/S, F/F combinations of heating and cooling rates

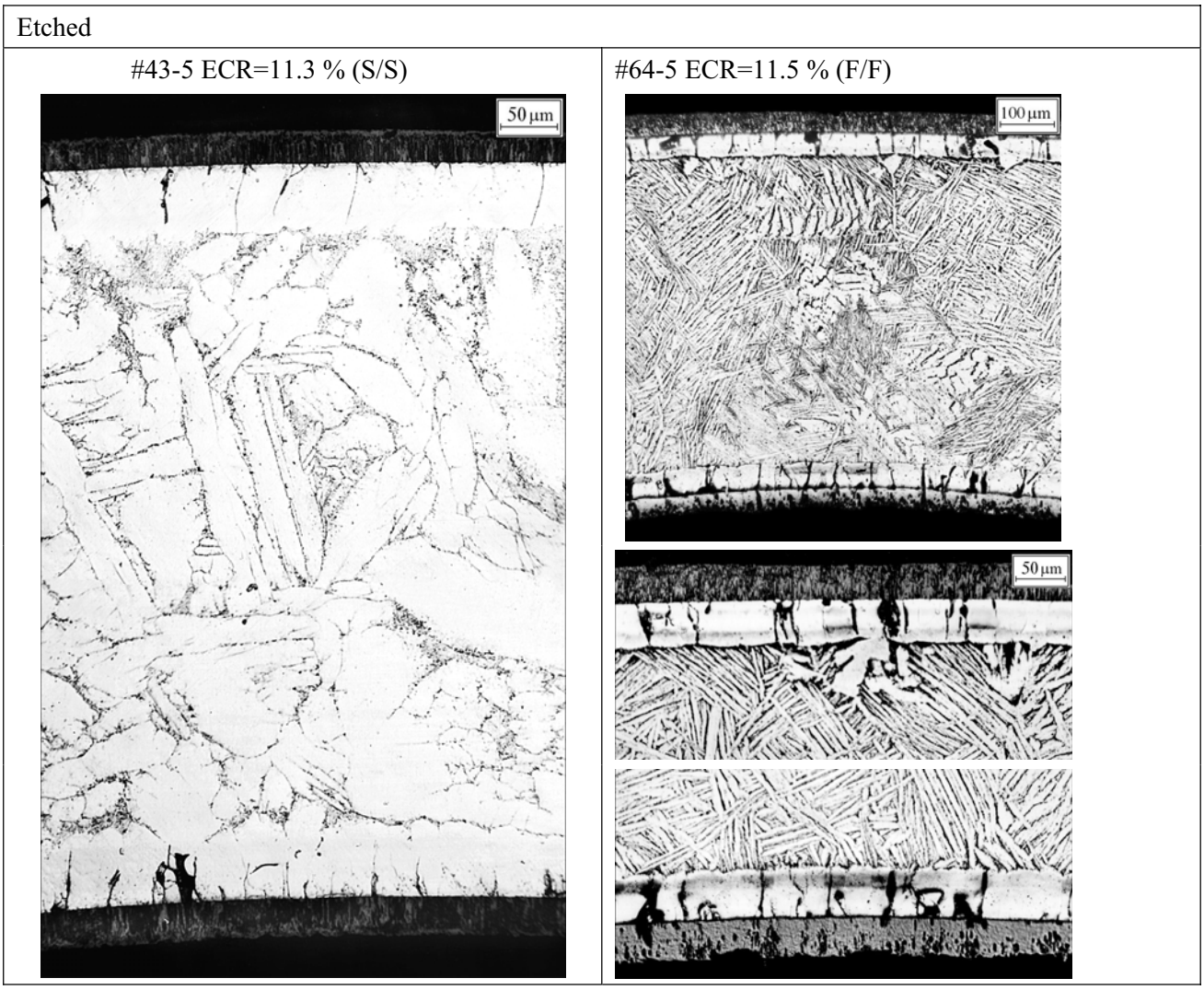

Fig. G-2. Microstructure of Zry-4 as-received claddings after a double-sided oxidation at 1100 C and S/S, F/F combinations of heating and cooling rates

APPENDIX H

Appearance and Microstructure of E110, E635 As-received Tubes Manufactured on the Basis of the Sponge Zr, $E110_{low\ Hf}$ As-received Tubes after a Double-sided Oxidation at 900, 1000, 1100, 1200 C and F/F Combination of Heating and Cooling Rates

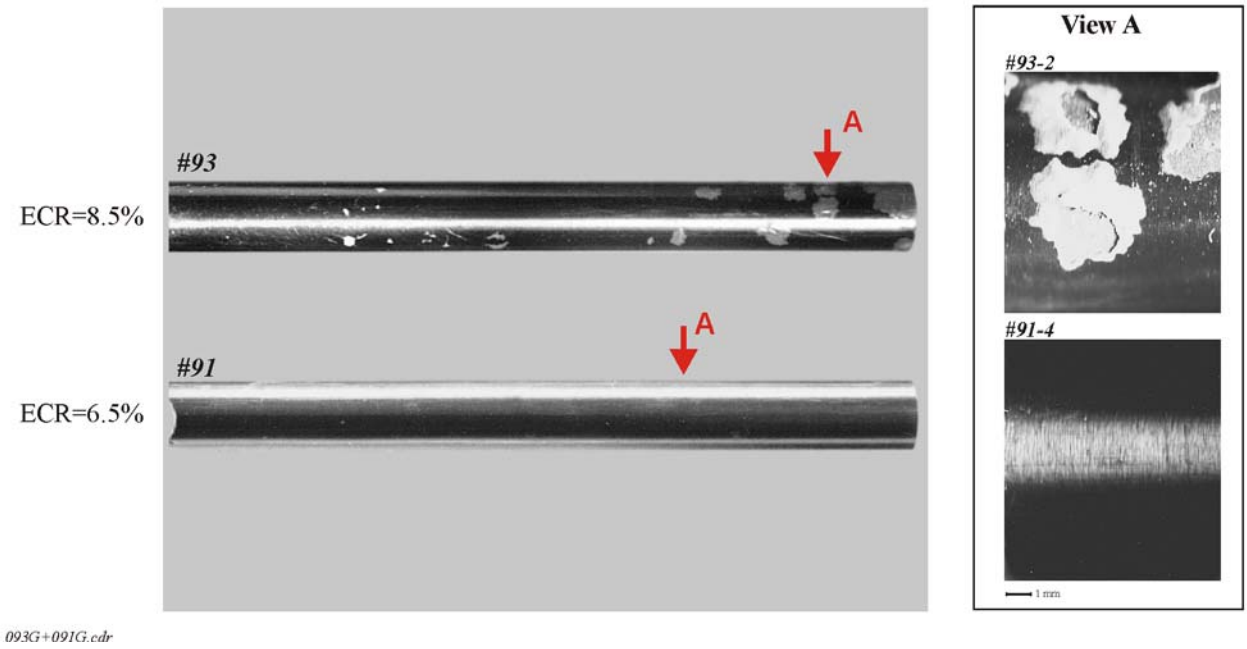

Fig. H-1. Appearance of $E110_{G(fr)}$ as-received tubes as a function of the ECR after a double-sided oxidation at 1000 C and F/F combination of heating and cooling rates

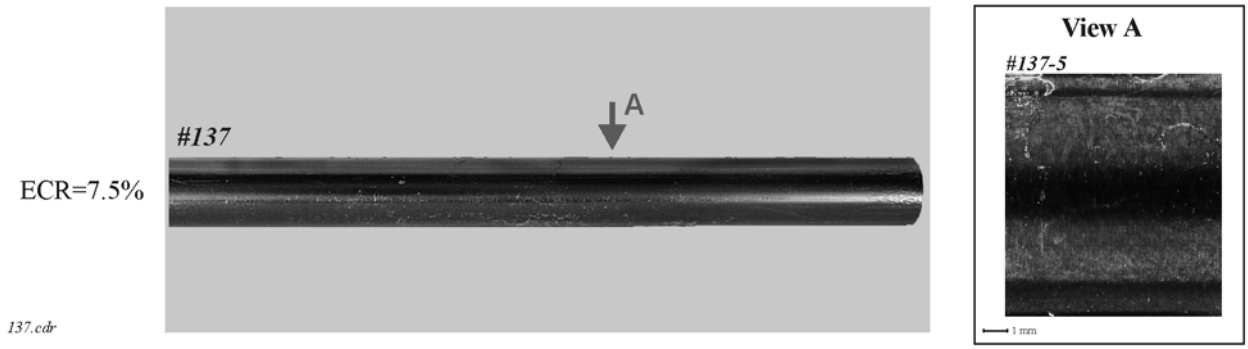

Fig. H-2. Appearance of $E110_{G(3ru)}$ as-received tubes as a function of the ECR after a double-sided oxidation at 900 C and F/F combination of heating and cooling rates

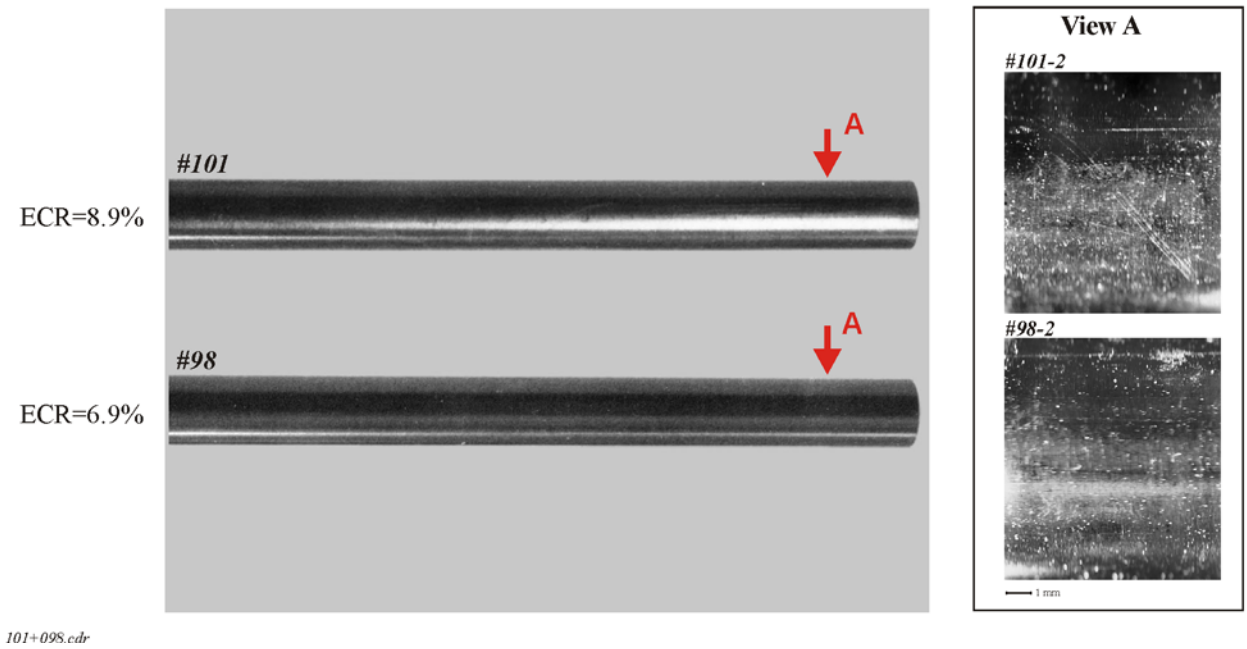

Fig. H-3. Appearance of E110$_{G(3ru)}$ as-received tubes as a function of the ECR after a double-sided oxidation at 1000 C and F/F combination of heating and cooling rates

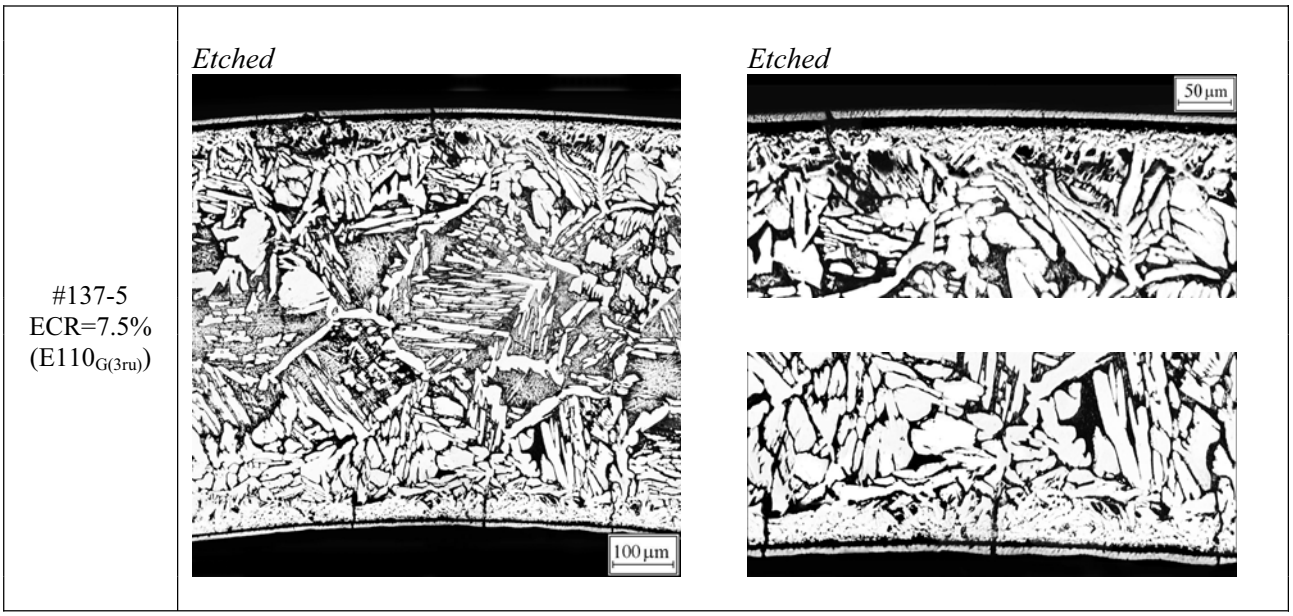

Fig. H-4. Microstructure of E110$_{G(3ru)}$ as-received tubes after a double-sided oxidation at 900°C and ECR=7.5 % (F/F combination of heating and cooling rates)

#98-4 ECR=6.9 %	$E110_{G(3ru)}$	#91-4 ECR=6.5 %	$E110_{G(fr)}$
Etched 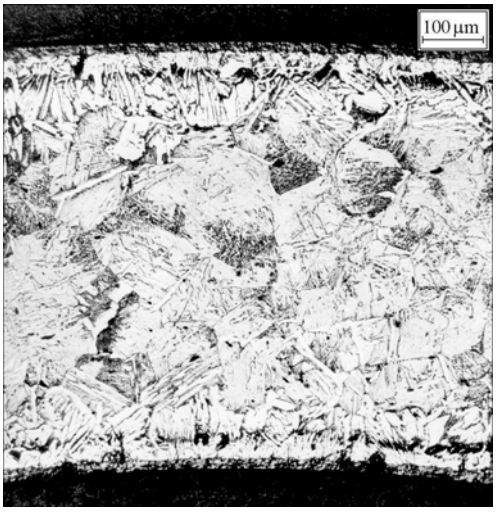 		*Etched* 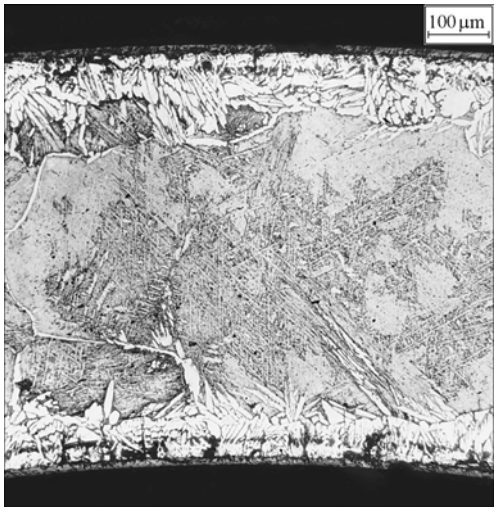 	
Etched  		*Etched*  	

Fig. H-5. Microstructure of $E110_{G(3ru)}$ and $E110_{G(fr)}$ as-received tubes after a double-sided oxidation at 1000°C and ECR=6.5–6.9 % (F/F combination of heating and cooling rates)

#101-4 ECR=8.9 %	$E110_{G(3ru)}$	#93-4 ECR=8.5 %	$E110_{G(fr)}$
Etched 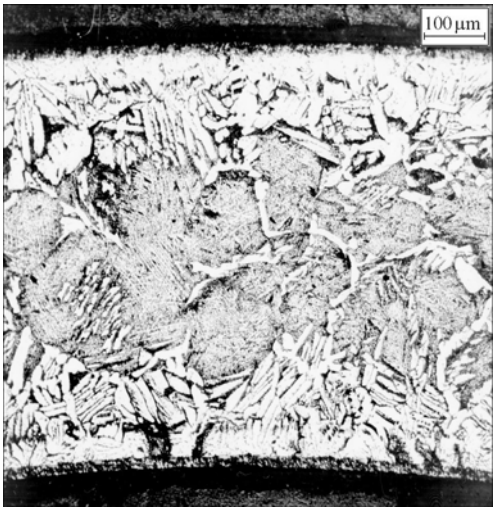 		*Etched* 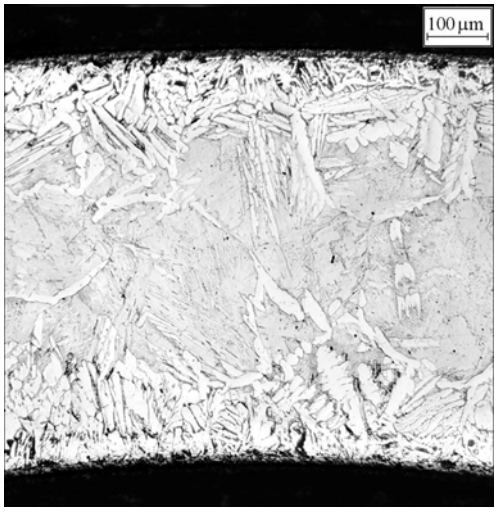 	
Etched 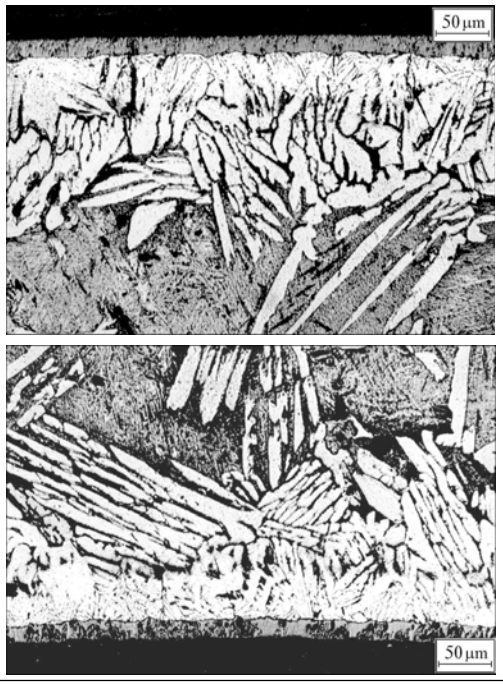 		*Etched* 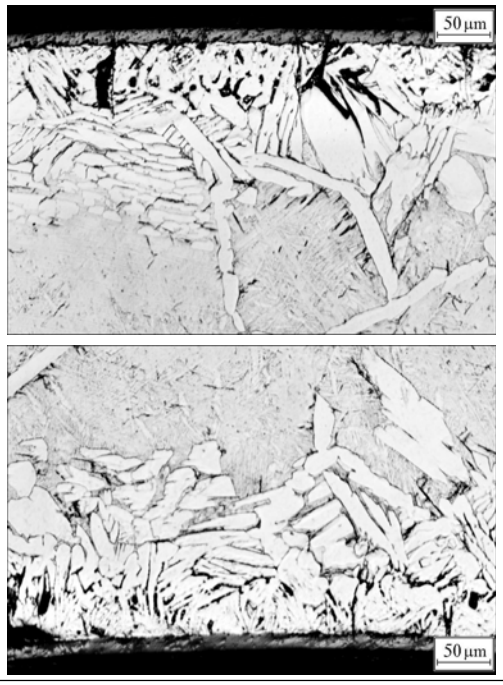 	

Fig. H-6. Microstructure of $E110_{G(3ru)}$ and $E110_{G(fr)}$ as-received tubes after a double-sided oxidation at 1000°C and ECR=8.5–8.9 % (F/F combination of heating and cooling rates)

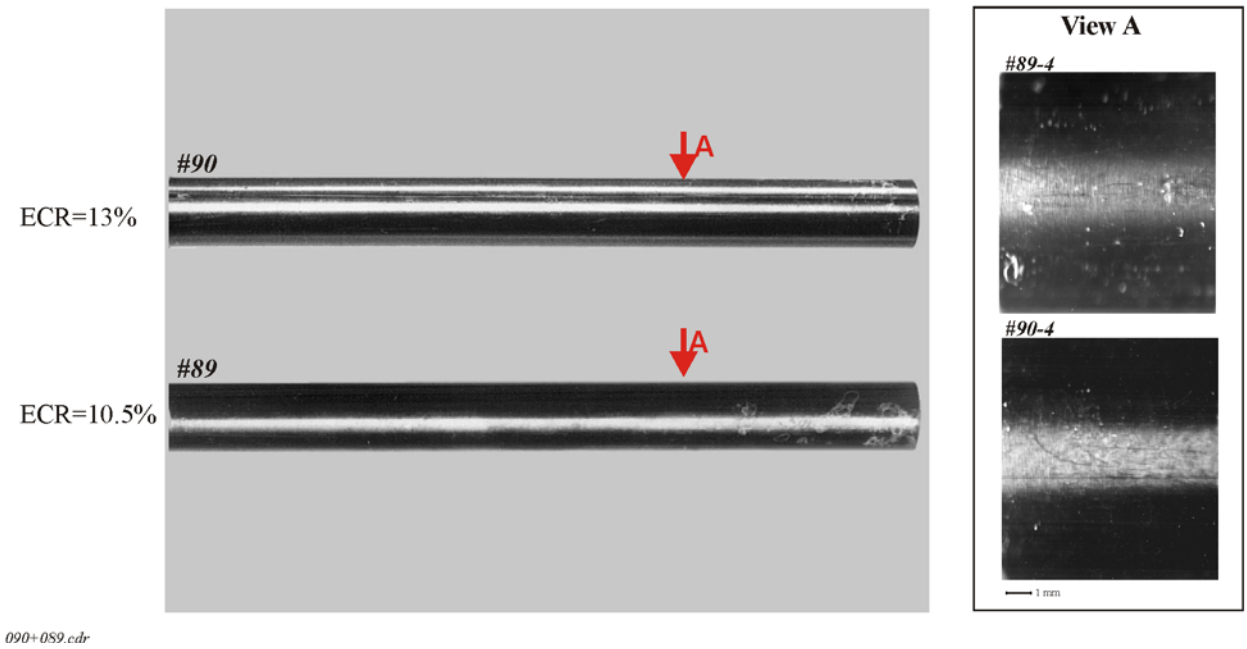

Fig. H-7. Appearance of $E110_{G(fr)}$ as-received tubes as a function of the ECR after a double-sided oxidation at 1100 C and F/F combination of heating and cooling rates

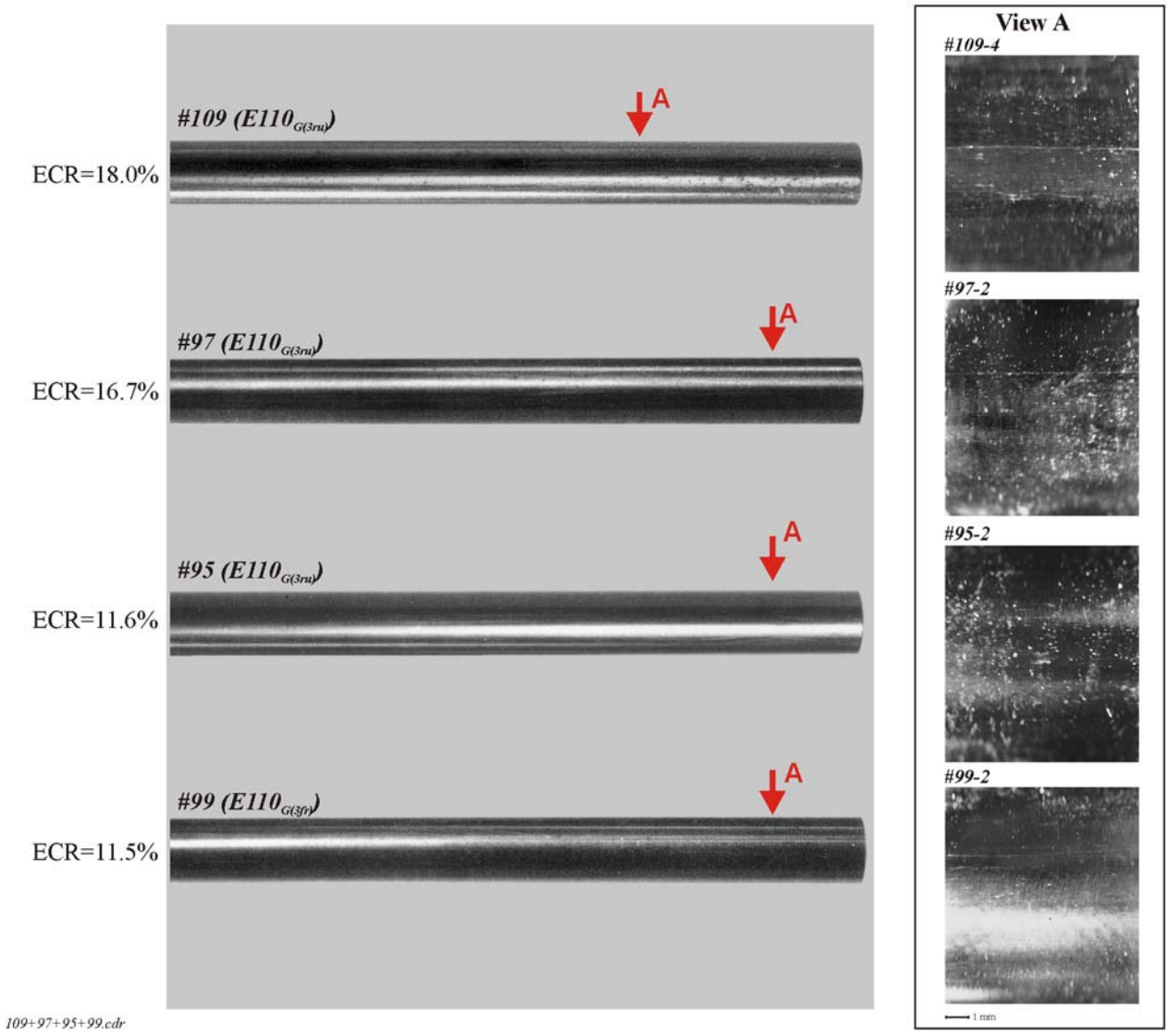

Fig. H-8. Appearance of $E110_{G(3ru)}$ and $E110_{G(3fr)}$ standard as-received tubes as a function of the ECR after a double-sided oxidation at 1100 C and F/F combination of heating and cooling rates

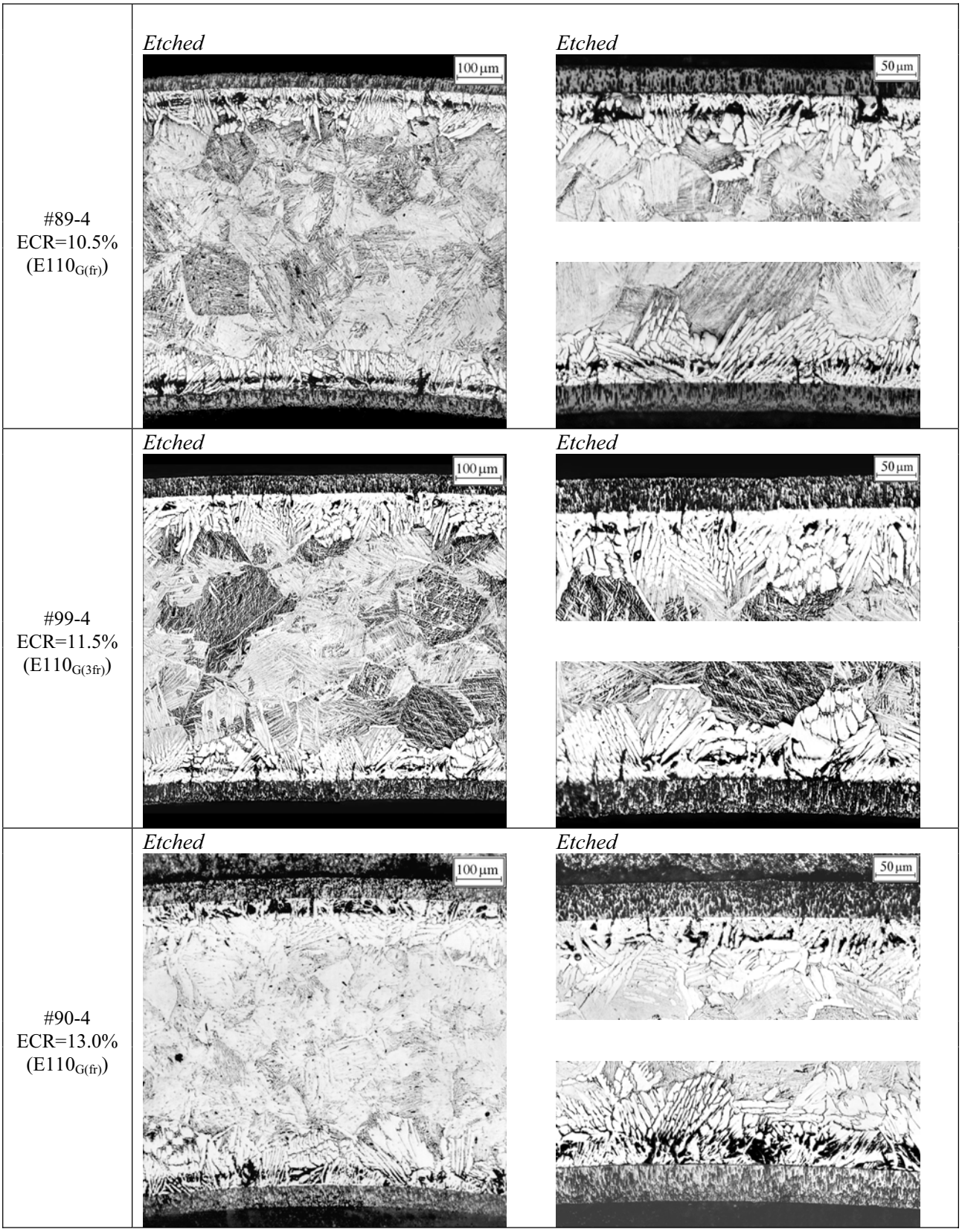

Fig. H-9. Microstructure of $E110_{G(fr)}$, $E110_{G(3fr)}$ as-received tubes after a double-sided oxidation at 1100°C and F/F combination of heating and cooling rates

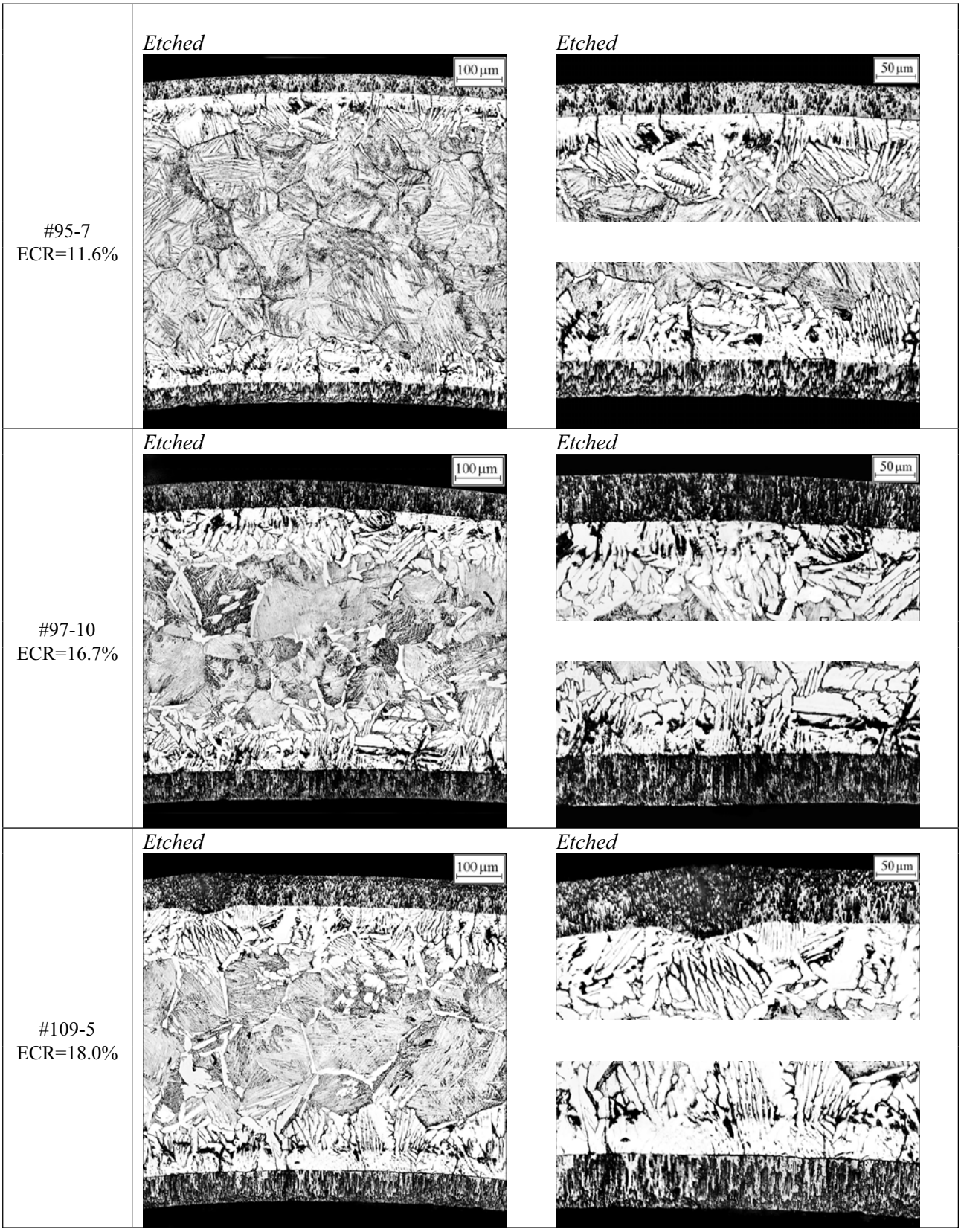

Fig. H-10. Microstructure of E110$_{G(3ru)}$ as-received tubes after a double-sided oxidation at 1100°C and F/F combination of heating and cooling rates

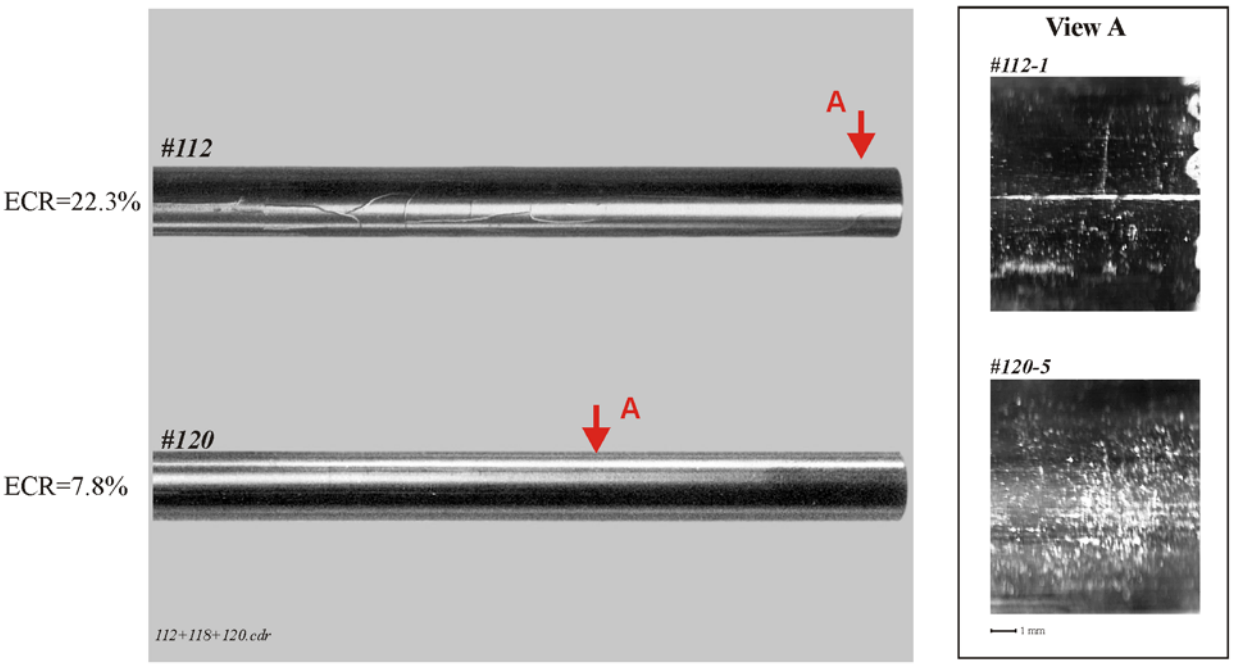

Fig. H-11. Appearance of E110$_{G(3ru)}$ as-received tubes as a function of the ECR after a double-sided oxidation at 1200 C and F/F combination of heating and cooling rates

#120-5 ECR=7.8 %		#112-2 ECR=23.5 %	
Etched 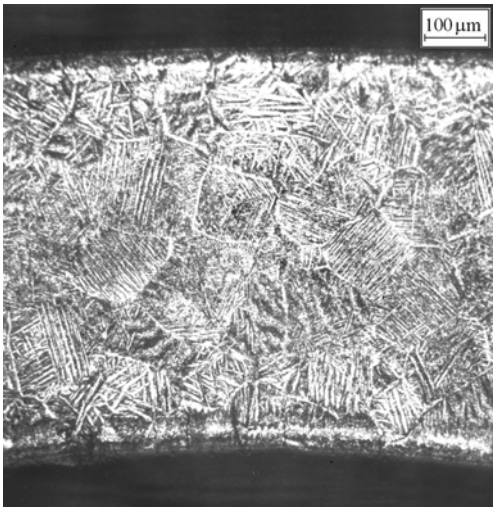		*Etched* 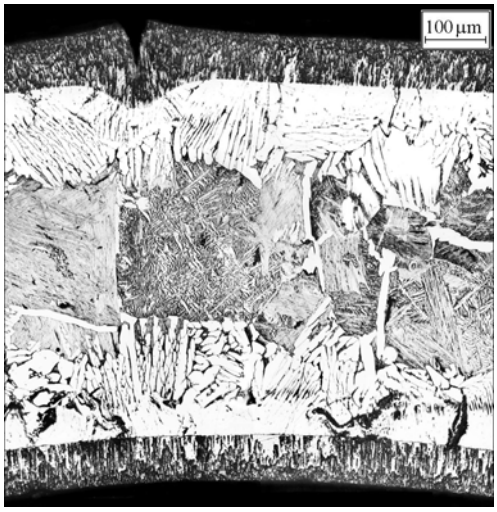	
Etched 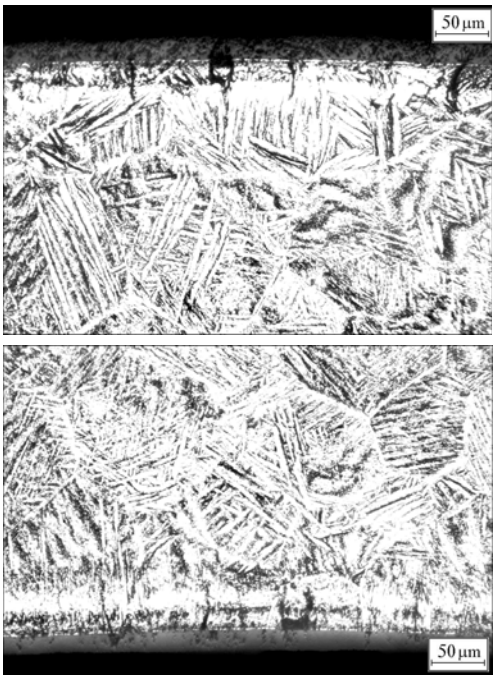		*Etched* 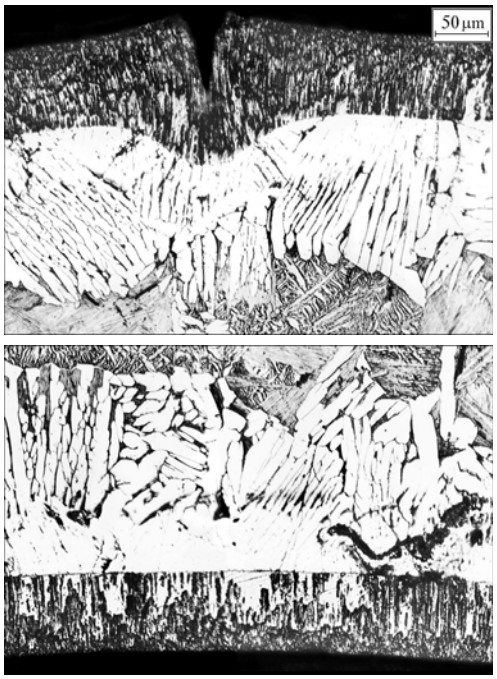	

Fig. H-12. Microstructure of E110$_{G(3ru)}$ as-received tubes after a double-sided oxidation at 1200°C and F/F combination of heating and cooling rates

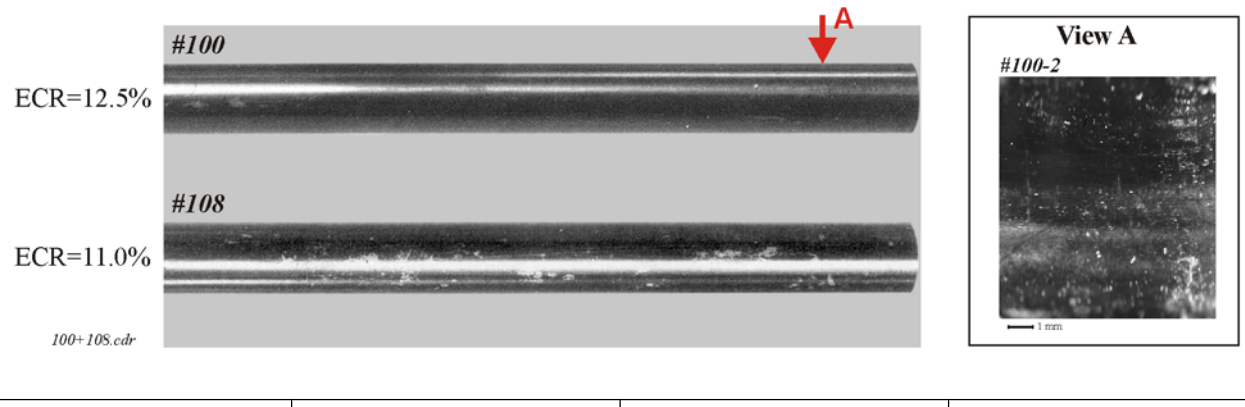

#108-4	ECR=11.0 %	#100-4	ECR=12.5 %
Etched		*Etched*	
Etched		*Etched*	

Fig. H-13. Appearance and microstructure of E635$_{G(fr)}$ as-received tubes after a double-sided oxidation at 1100°C and F/F combination of heating and cooling rates

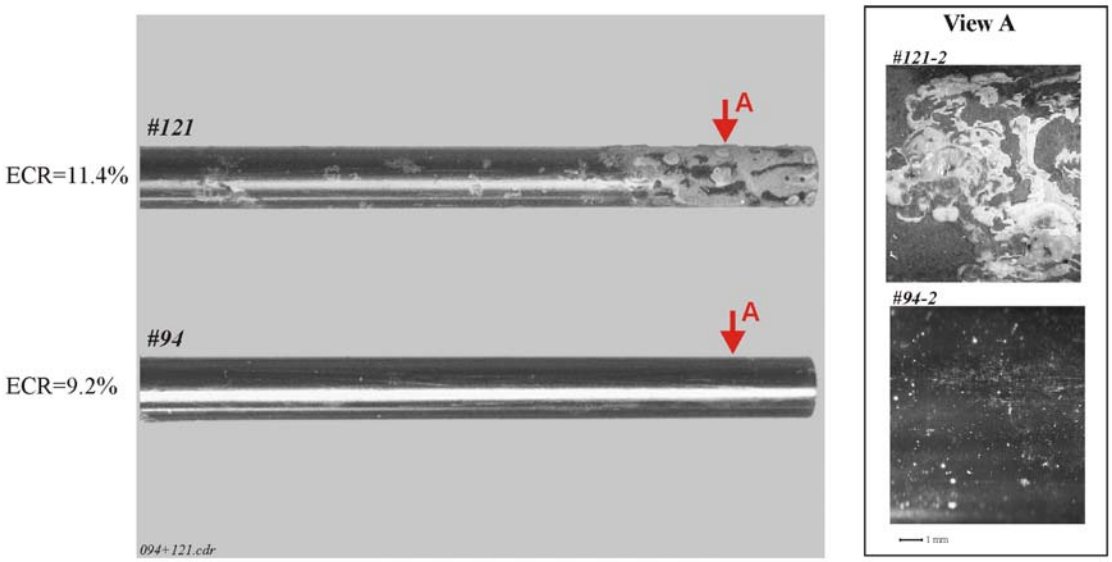

Fig. H-14. Appearance of E110$_{low\ Hf}$ as-received tubes after a double-sided oxidation at 1100 C and F/F combination of heating and cooling rates

#94-4	ECR=9.2 %	**#121-4**	ECR=11.4 %
Etched		Etched	

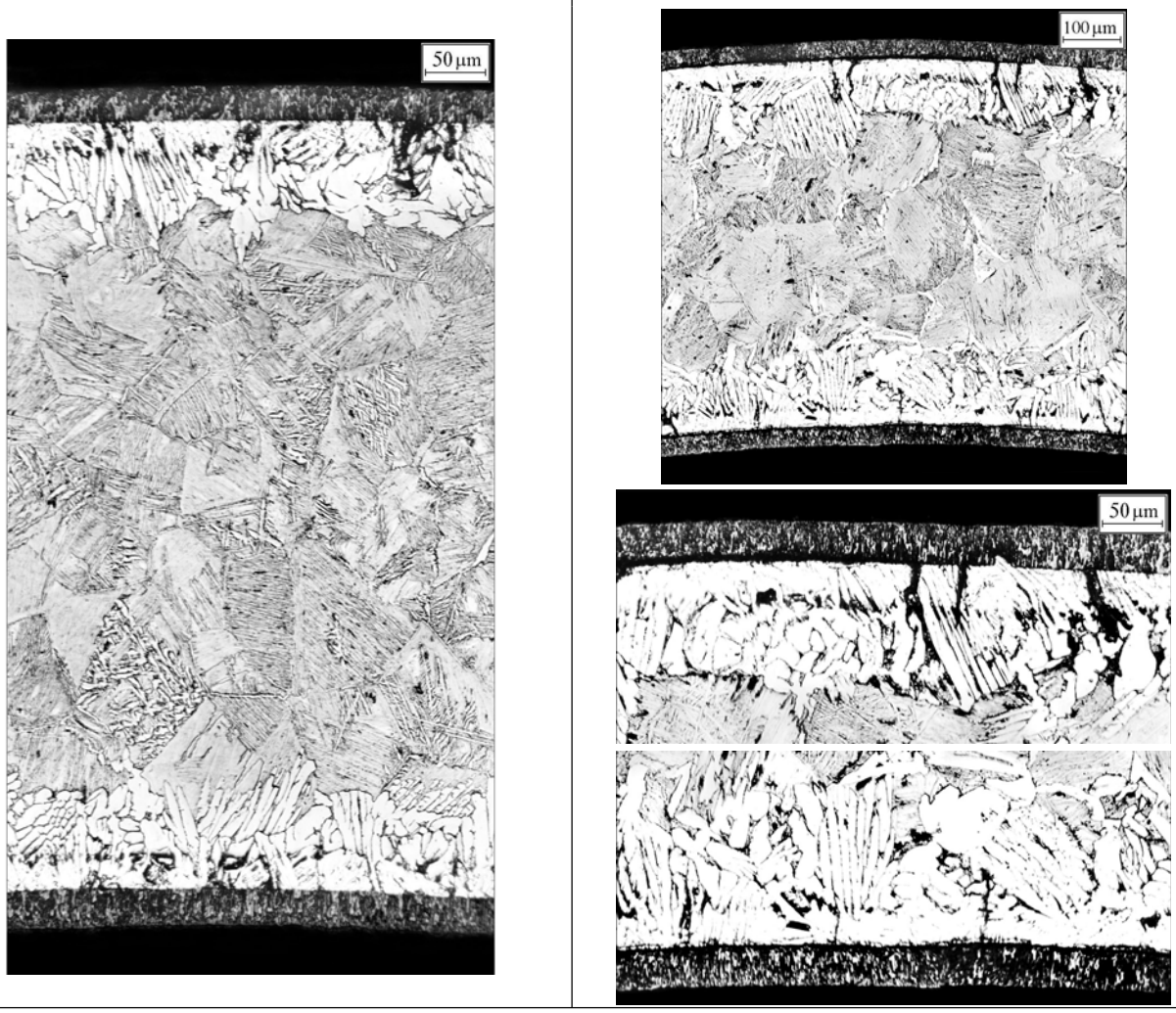

Fig. H-15. Microstructure of E110$_{low\ Hf}$ as-received tubes after a double-sided oxidation at 1100 C and F/F combination of heating and cooling rates

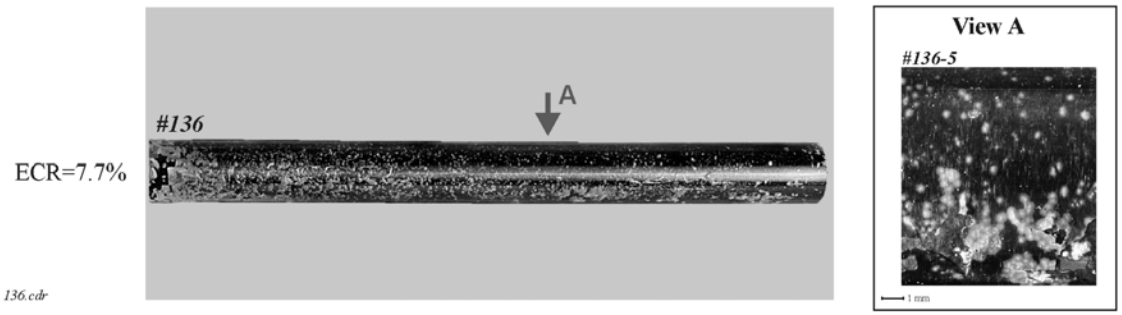

Fig. H-16. Appearance of $E110_m$ as-received machined/etched tubes after a double-sided oxidation at 1100 C and F/F combination of heating and cooling rates

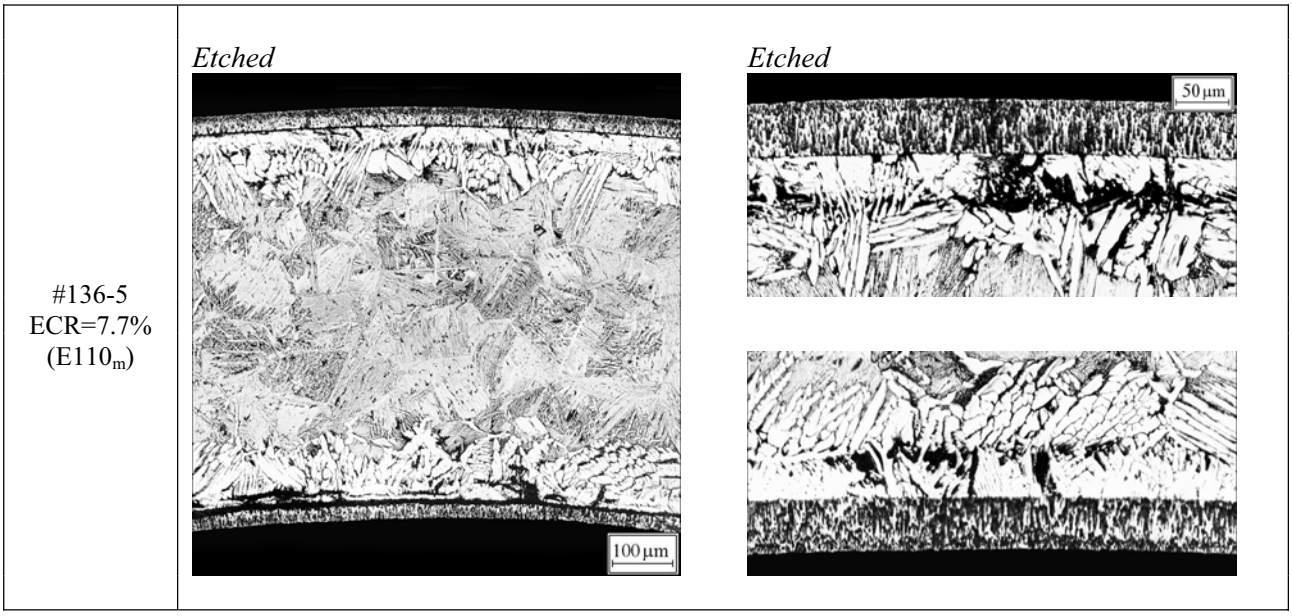

Fig. H-17. Microstructure of $E110_m$ as-received machined/etched tubes after a double-sided oxidation at 1100 C and F/F combination of heating and cooling rates

APPENDIX I

Appearance and Microstructure of E110 Commercial Irradiated Cladding after a Double-sided Oxidation at 1000, 1100, 1200 C and S/S, S/F, F/F Combinations of Heating and Cooling Rates

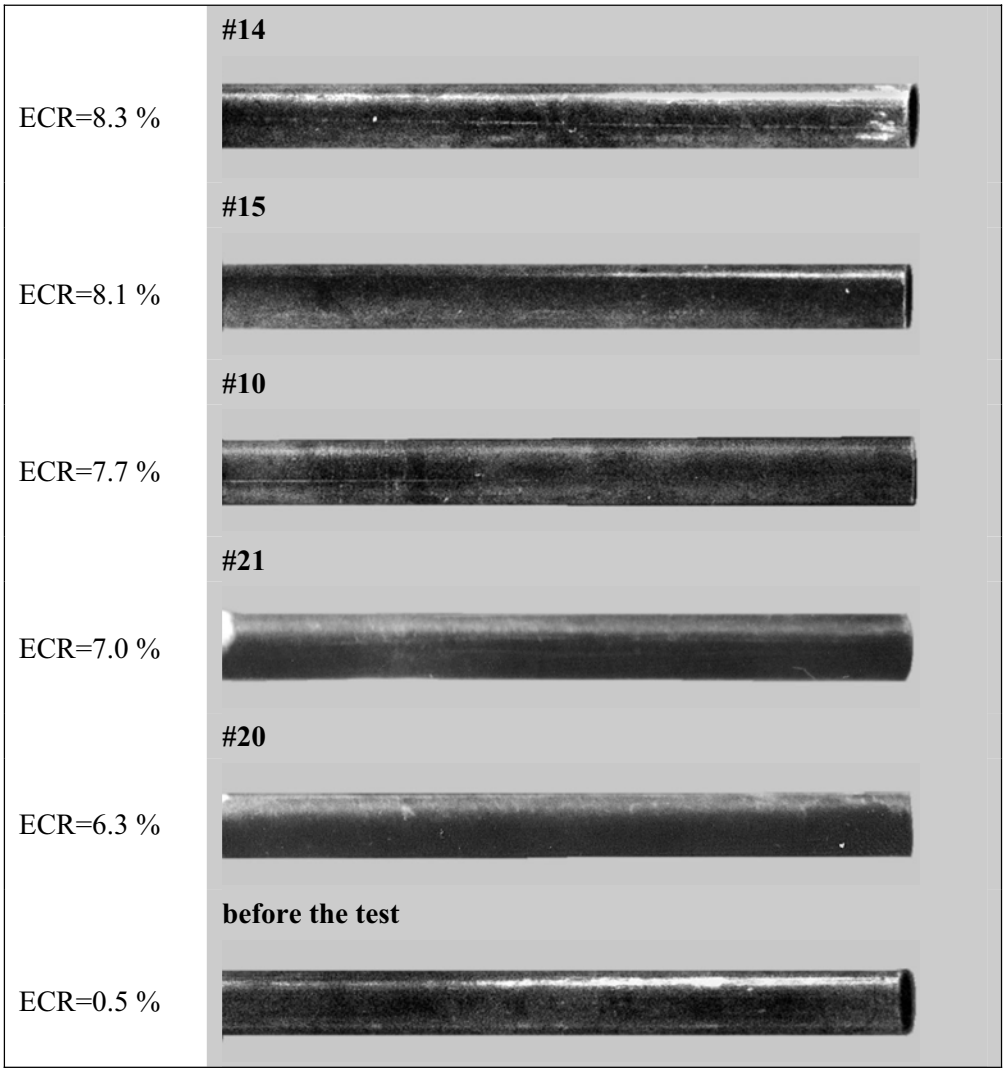

Fig. I-1. Appearance of E110 commercial irradiated claddings before and after a double-sided oxidation at 1100 C and F/F combination of heating and cooling rates

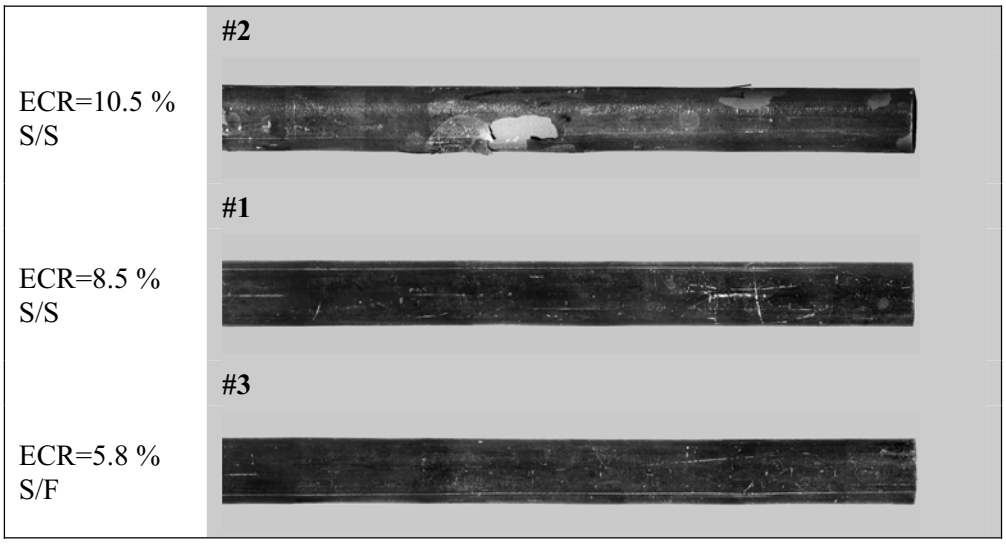

Fig. I-2. Appearance of E110 commercial irradiated claddings after a double-sided oxidation at 1100 C and S/S, S/F combinations of heating and cooling rates

Fig. I-3. Appearance of E110 commercial irradiated claddings after a double-sided oxidation at 1000 C, 1200 C and F/F combination of heating and cooling rates

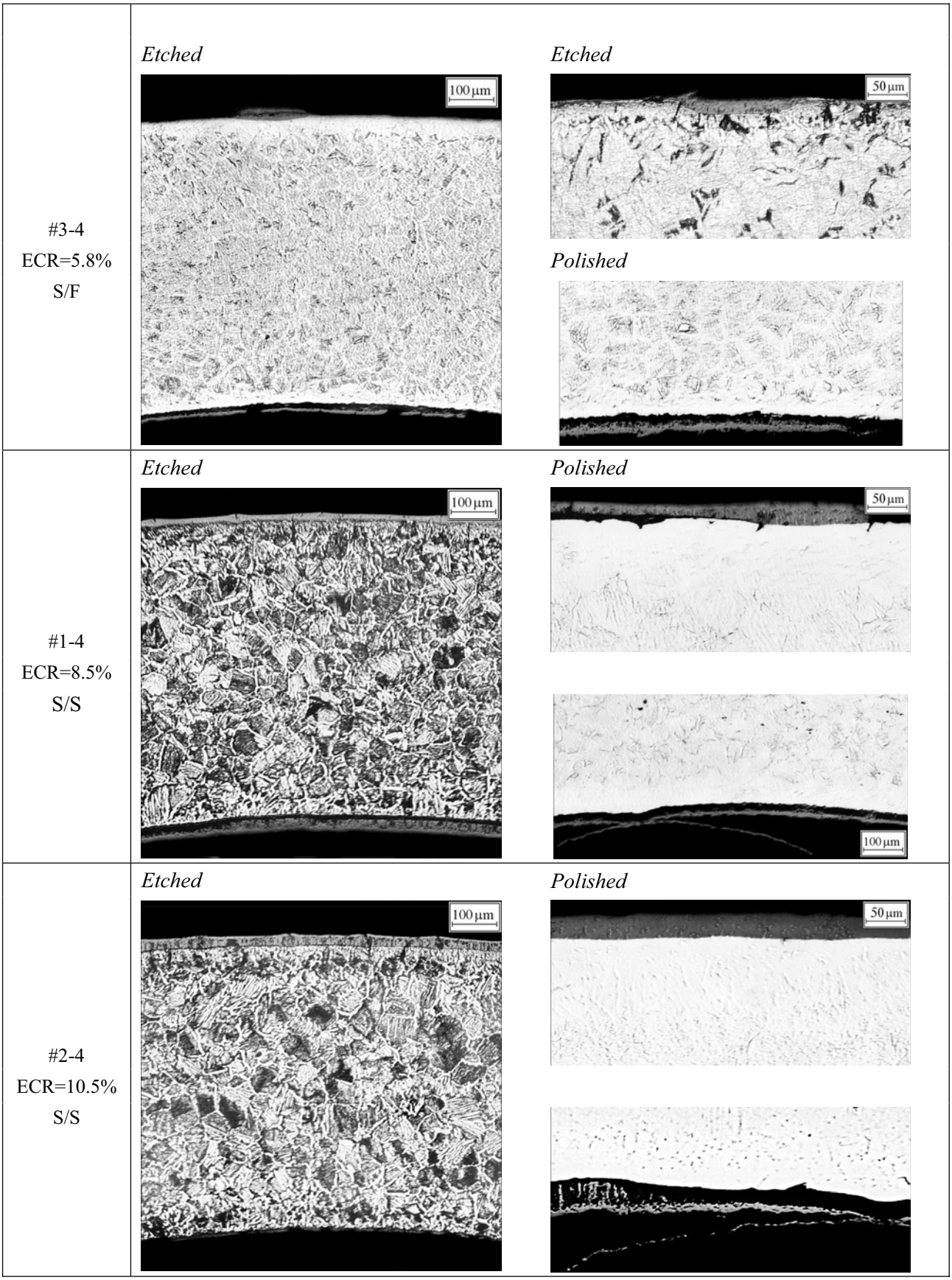

Fig. I-4. Microstructure of E110 commercial irradiated cladding after a double-sided oxidation at 1100 C and S/F, S/S combinations of heating and cooling rates

Etched

before the oxidation tests

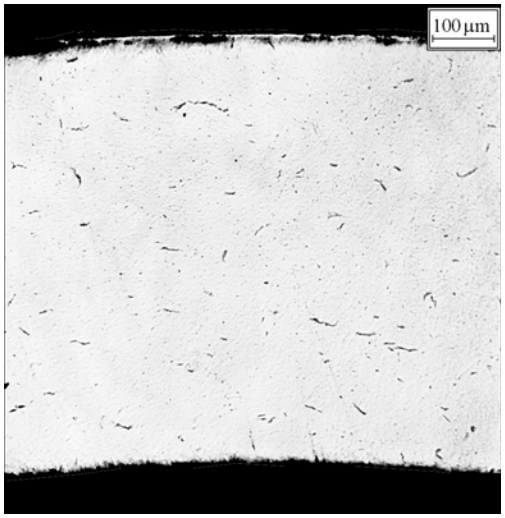

#20-4 ECR=6.3 %

#21-4 ECR=7.0 %

#10-4 ECR=7.7 %

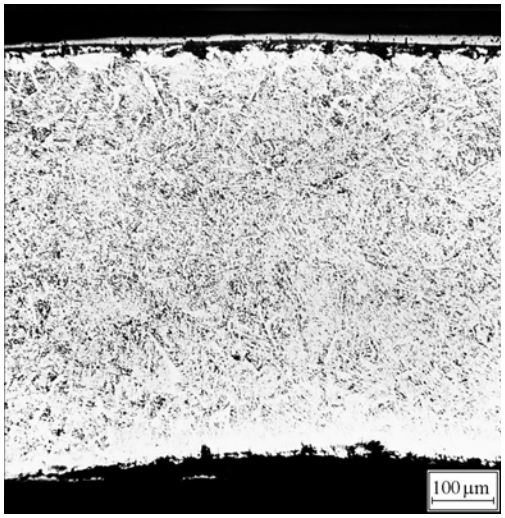

#15-4 ECR=8.1 %

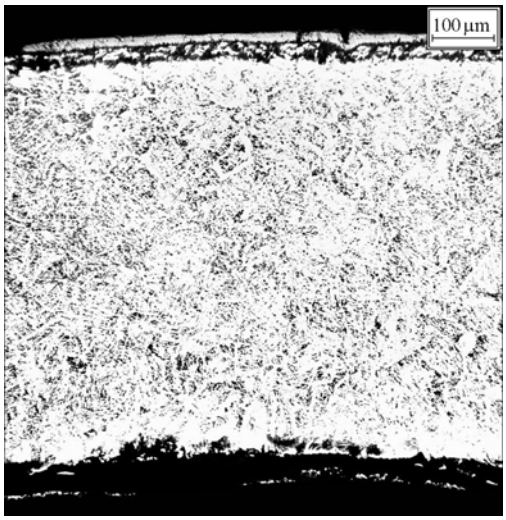

#14-4 ECR=8.3 %

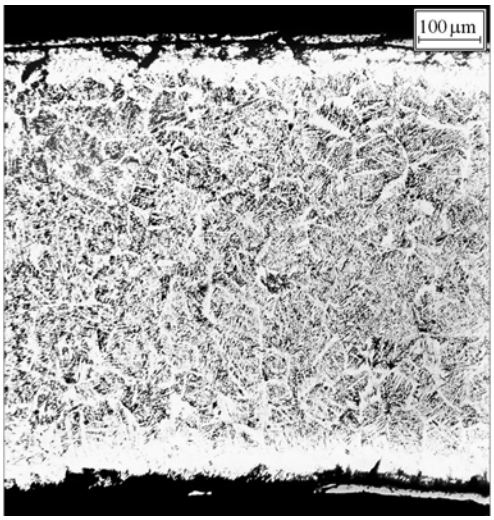

Fig. I-5. Microstructure of E110 commercial irradiated claddings before and after a double-sided oxidation at 1100 C and F/F combination of heating and cooling rates

Sample	External surface	Internal surface
Before oxidation tests (Polished)	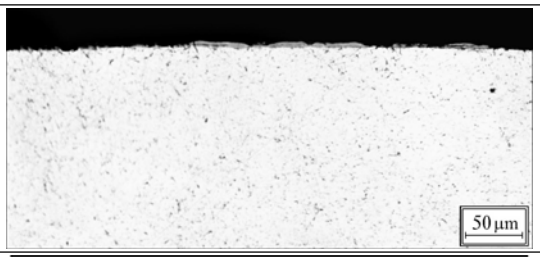	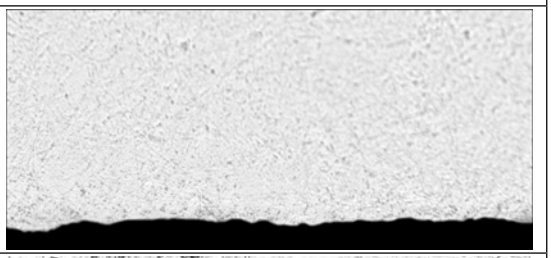
#20-4 ECR=6.3 % (Etched)	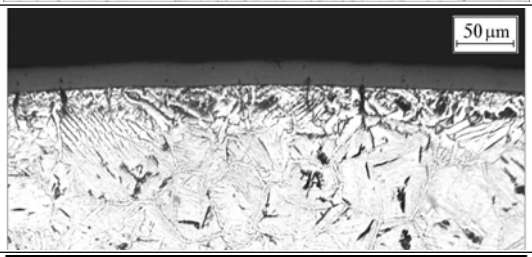	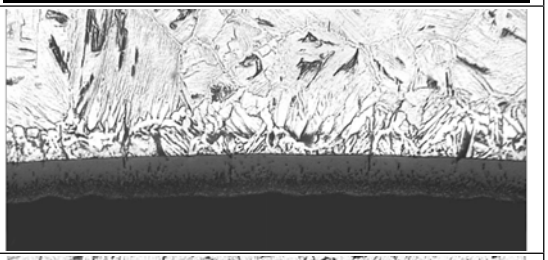
#21-4 ECR=7.0 % (Etched)	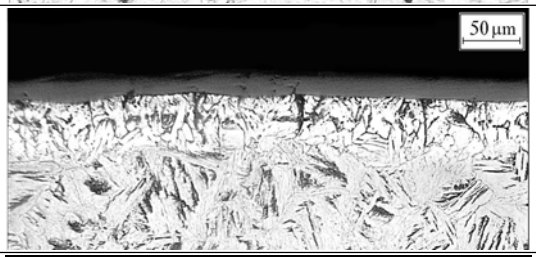	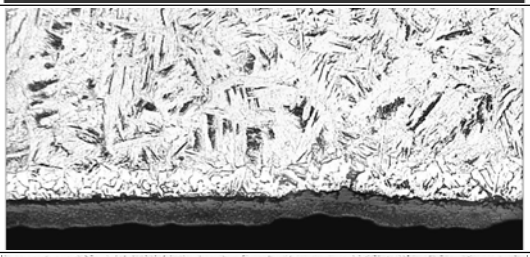
#10-4 ECR=7.7 % (Polished)	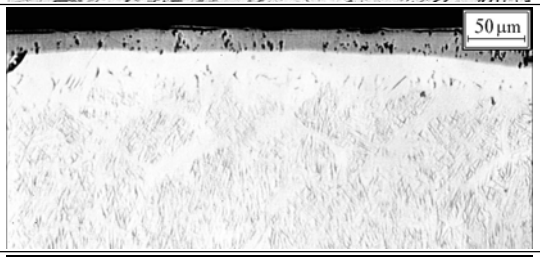	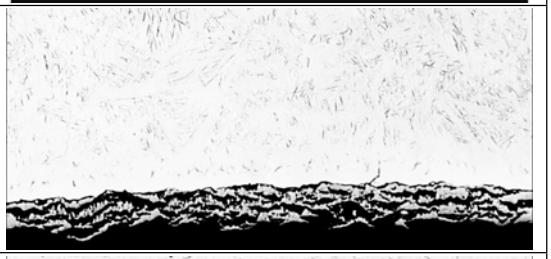
#15-4 ECR=8.1 % (Polished)	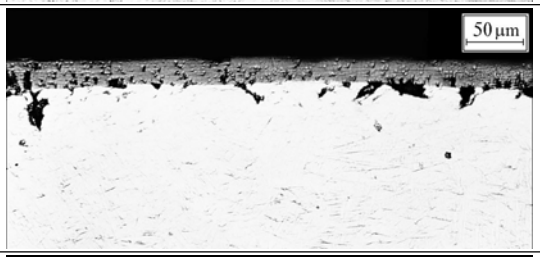	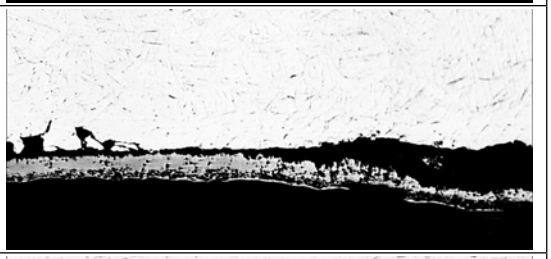
#14-4 ECR=8.3 % (Polished)		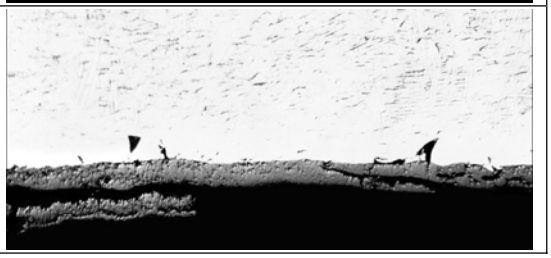

Fig. I-6. Microstructure of ZrO_2 and α-Zr(O) layers in E110 commercial irradiated cladding before and after a double-sided oxidation at 1100 C and F/F combination of heating and cooling rates

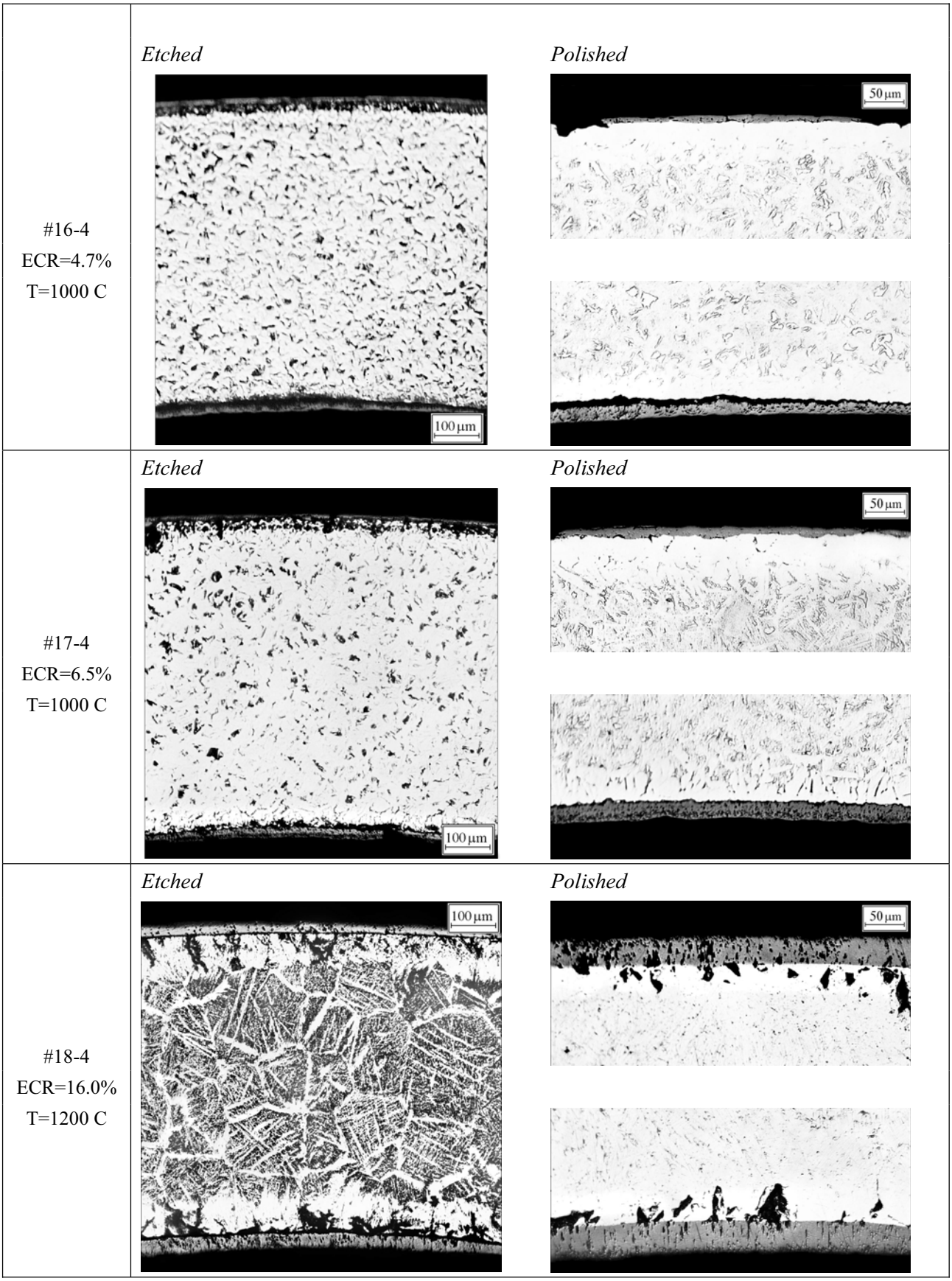

Fig. I-7. Microstructure of E110 commercial irradiated cladding after a double-sided oxidation at 1000°C, 1200 C and F/F combination of heating and cooling rates

NRC FORM 335
(9-2004)
NRCMD 3.7

U.S. NUCLEAR REGULATORY COMMISSION

BIBLIOGRAPHIC DATA SHEET

(See instructions on the reverse)

1. REPORT NUMBER
(Assigned by NRC, Add Vol., Supp., Rev., and Addendum Numbers, if any.)

NUREG/IA-0211

2. TITLE AND SUBTITLE

EXPERIMENTAL STUDY OF EMBRITTLEMENT OF ZR-1% NB VVER CLADDING UNDER LOCA RELEVANT CONDITIONS

3. DATE REPORT PUBLISHED

MONTH	YEAR
March	2005

4. FIN OR GRANT NUMBER

Y6789

5. AUTHOR(S)

L. Yegorova, K. Lioutov, N. Jouravkova, A. Konobeev
V. Smirnov, V. Chesanov, A. Goryachev

6. TYPE OF REPORT

IRSN 2005-194 NSI RRC KI 3188

7. PERIOD COVERED *(Inclusive Dates)*

8. PERFORMING ORGANIZATION - NAME AND ADDRESS *(If NRC, provide Division, Office or Region, U.S. Nuclear Regulatory Commission, and mailing address; if contractor, provide name and mailing address.)*

Nuclear Safety Institute of Russian Research Centre "Kurchatov Institute" Moscow, Russian Federation
State Research Centre "Research Institute of Atomic Reactors" Dimitrovgrad, Russian Federation

9. SPONSORING ORGANIZATION - NAME AND ADDRESS *(If NRC, type "Same as above"; if contractor, provide NRC Division, Office or Region, U.S. Nuclear Regulatory Commission, and mailing address.)*

Division of Systems Analysis and Regulatory Effectiveness
Office of Nuclear Regulatory Research
U.S. Nuclear Regulatory Commission
Washington, DC 20555-0001

10. SUPPLEMENTARY NOTES

11. ABSTRACT *(200 words or less)*

During 2001-2004, research was performed to develop test data on the embrittlement of niobium-bearing (Zr-1%Nb) cladding of the VVER type under loss-of-coolant accident (LOCA) conditions. Procedures were developed and validated to determine the zero ductility threshold. Pre-test and post-test examinations included weight gain and hydrogen content measurements, preparation of metallographic samples, and examination of samples using optical microscopy, scanning electron microscopy and transmission electron microscopy. Sensitivity of the zero ductility threshold to heating and cooling rates was determined. Oxidation kinetics and ductility threshold were measured for the standard E110 alloy, six variants with different impurities, Zircaloy, and irradiated E110. Oxidation temperatures were varied from 800-1200 C, and mechanical (ring compression) testing temperatures were varied from 20-300 C. It was concluded that (a) the current type of E110 cladding has an optimal microstructure, (b) oxidation and ductility of the oxidized cladding are very sensitive to microchemical composition and surface finish, (c) the use of sponge zirconium for fabrication of cladding tubes provides a significant reduction of the oxidation rate and an increase in the zero ductility threshold, and (d) additional improvement in oxidation and ductility can be achieved by polishing the cladding surface.

12. KEY WORDS/DESCRIPTORS *(List words or phrases that will assist researchers in locating the report.)*

Alloy
Cladding
E110
Hydrogen Content
Kurchatov Institute
Loss-of-Coolant Accident
Material Properties
Niobium
Oxidation
Ring Compression
Russian
Zirconium
Zircaloy

13. AVAILABILITY STATEMENT

unlimited

14. SECURITY CLASSIFICATION

(This Page)
unclassified

(This Report)
unclassified

15. NUMBER OF PAGES

16. PRICE

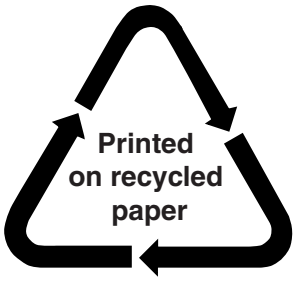

Federal Recycling Program